CSIC
Consejo Superior de Investigaciones Científicas
Instituto de Química Médica

UAM
Universidad Autónoma de Madrid
Facultad de Ciencias
Departamento de Química Orgánica

Contribución del Esqueleto de Cromenopirazol en la Modulación del Sistema Endocannabinoide

Memoria

Para optar al grado de Doctor en Ciencias Químicas
por la Universidad Autónoma de Madrid

Paula Morales Lázaro

Madrid 2015

Directora

Dra. Nadine Jagerovic

CSIC
Consejo Superior de Investigaciones Científicas
Instituto de Química Médica

UAM
Universidad Autonoma de Madrid
Facultad de Ciencias
Departamento de Química Orgánica

Exploring the Chromenopyrazole Scaffold for the Modulation of the Endocannabinoid System

Paula Morales Lázaro

Madrid 2015

Supervisor

Dr. Nadine Jagerovic

GOBIERNO DE ESPAÑA
MINISTERIO DE ECONOMÍA Y COMPETITIVIDAD

CSIC
CONSEJO SUPERIOR DE INVESTIGACIONES CIENTÍFICAS
Instituto de Química Médica

Dra. NADINE JAGEROVIC, Investigadora Científica del Consejo Superior de Investigaciones Científicas (CSIC)

CERTIFICA: Que el trabajo reflejado en la presente memoria, titulada "Contribución del Esqueleto de Cromenopirazol en la Modulación del Sistema Endocannabinoide" (*Exploring the Chromenopyrazole Scaffold in the Modulation of the Endocannabinoid System*) ha sido realizada en el Instituto de Química Médica del CSIC por Dña. PAULA MORALES LÁZARO y autoriza su presentación para que sea calificada como Tesis Doctoral.

Madrid, 5 de octubre de 2015

Fdo. Dra. Nadine Jagerovic

Acknowledgements/ Agradecimientos

La presente tesis doctoral ha sido realizada en el Instituto de Química Médica (IQM) del CSIC bajo la dirección de la Dra. Nadine Jagerovic, a quien agradezco tanta dedicación, paciencia y apoyo. Gracias por enseñarme tanto, por ayudarme a crecer en lo profesional y lo personal. *Merci beaucoup* ☺

Quiero expresar mi agradecimiento a la Prof. Pilar Goya por permitirme formar parte de su grupo de investigación, por sus buenos consejos y su apoyo a lo largo de estos años.

Al Prof. Javier Fernández Ruiz y a su grupo de investigación de la Universidad Complutense de Madrid, por hacerme sentir una más y enseñarme tanto sobre farmacología de cannabinoides. Agradecer especialmente a María Gómez Cañas por su disponibilidad, incondicional ayuda y amistad.

A la Prof. Cristina Sánchez y a su grupo de investigación de la Universidad Complutense de Madrid, por acogerme en su laboratorio y haberme permitido aprender mucho sobre el potencial antitumoral de los cannabinoides. A Sandra, por enseñarme y ayudarme en la realización de los experimentos en cáncer de mama.

Al Prof. Claudio Olea y a su grupo de investigación de la Universidad de Chile por la realización de los estudios de electroquímica.

A la Prof. Inés Díaz-Laviada y a su grupo de investigación de la Universidad de Alcalá de Henares por la realización de los estudios en cáncer de próstata.

Al Prof. Rafael Franco y a su grupo de investigación de la Universidad de Barcelona por la realización de los estudios de funcionalidad CB_2, por su disponibilidad, eficiencia y ayuda.

I would like to thank Prof. Patricia Reggio who hosted me in her lab at the University of North Carolina at Greensboro and guided me through the docking studies of chromenopyrazoles in the cannabinoid receptor models.

I would also like to thank Prof. Ruth Ross and Dr. Lauren Whyte for hosting me in her lab at the University of Toronto, for her guidance through the pharmacological evaluation of the GPR55 activity of the novel compounds.

Al personal especializado del IQM y del Centro de Química Orgánica Lora Tamayo (RMN, microanálisis, espectrometría de masas, HPLC), por su gran ayuda y eficiencia, que han agilizado enormemente el trabajo realizado durante todo este tiempo. A la Dra. Laura Lagartera y a Silvia Soto por la realización de los experimentos de SPR.

A la Prof. María Jesús Pérez Pérez, directora del IQM durante la realización de esta tesis, por la ayuda mostrada en todo momento. Al personal de gerencia y administración que ha pasado por el IQM durante estos años, especialmente a Pedro y a Nico por su gran ayuda y eficacia. A Javier Renau, por su incondicional colaboración en mis numerosas dudas informáticas.

Agradecer también al Dr. José Alemán de la Universidad Autónoma de Madrid su tutela y disponibilidad durante la realización de esta tesis.

Al Dr. Vicente Arán, por ser una fuente inagotable de conocimiento y buen humor.

No querría olvidarme de mis compañeros a lo largo de todos estos años, porque sin su amistad y colaboración estoy segura de que no hubiera sido posible sacar adelante esta tesis doctoral.

A mi familia y amigos, por el tiempo robado. A Diego, por estar siempre ahí.

Abstract

In the last decades, the endocannabinoid system (ECS) has emerged as a promising therapeutic target. The identification of the cannabinoid receptors CB_1R and CB_2R and their endogenous lipid ligands has triggered an exponential growth of studies exploring the role of the ECS in physiological and pathological processes. The potential of cannabinoids has been preclinically explored in the treatment of a wide variety of diseases such as cancer, bone-related disorders, neurodegenerative diseases, or metabolic syndromes among others. So far, however, the clinical use of synthetic and phyto-cannabinoids has been limited to pain, emesis and appetite due to their undesirable psychoactive properties. Thus, emerging strategies for exploiting cannabinoids as medicines need to be developed to overcome these side-effects. The dissertation focusses on three of these strategies: a) selective CB_2R ligands; b) multitarget cannabinoids for cancer therapy; c) compounds acting on a new additional therapeutic target of the ECS.

In this context, we propose to explore the chromenopyrazole scaffold for the development of novel modulators of the ECS.

a) Structural modifications of the chromenopyrazole scaffold led to the synthesis of new cannabinoids allowing fine-tuning of cannabinoid receptor affinity and activity. Structural features required for CB_1R/CB_2R affinity and selectivity were studied by molecular modeling. In addition, bivalent chromenopyrazoles were prepared in order to explore the CB_2R dimerization process.

b) Multifunctional chromenopyrazoles have been designed and synthesized for cancer therapy. This approach involved the antitumor properties of cannabinoids and the redox properties characterizing quinones. The antiproliferative activity of these new compounds was successfully explored *in vitro* and *in vivo* in breast and prostate cancer models.

c) Finally, the chromenopyrazole scaffold as modulator of the new target GPR55 has been explored. The design of two series of compounds followed by their synthesis was reported. Their ability to

activate GPR55 was measured through an innovative label-free cell impedance assay allowing the discovery of novel GPR55 partial agonists and antagonists.

To sum up, exploration of the chromenopyrazole as a versatile scaffold led to the identification of CB_2R selective ligands and bivalent ligands, multifunctional antitumor agents, and GPR55 modulators. These compounds represent promising pharmacological tools and drugs for further development.

Abbreviations and acronyms

Throughout this dissertation the standard abbreviations and acronyms recommended by *American Chemical Society* for Organic and Medicinal Chemistry fields, as reviewed in *Journal of Organic Chemistry* (http://pubs.acs.org/paragonplus/submission/joceah/joceah_abbreviations.pdf) and *Journal of Medicinal Chemistry* (http://pubs.acs.org/paragonplus/submission/jmcmar/jmcmar_abbreviations.pdf), have been utilized. Additionally, the following abbreviations and acronyms have been used:

Abn-CBD	Abnormal cannabidiol
AC	Adenylate cyclase
ACEA	Arachidonyl-2'-chloroethylamide
ACPA	Arachidonylcyclopropylamide
ADT	Androgen deprivation therapy
AEA	Anandamide
2-AG	2-Arachidonoylglycerol
2- AGE	Noladin ether
2-AGPI	2-Arachidonoyl-containing LPI species
AT	Anandamide transporter
ATF	Activating transcription factor
BTIB	(Bis(trifluoroacetoxy)iodo)benzene
Caco-2	Colorectal adenocarcinoma cell line colon carcinoma
CBD	Cannabidiol
CBN	Cannabinol
CBR	Cannabinoid receptor
CB_1R	Cannabinoid receptor type 1
CB_2R	Cannabinoid receptor type 2
ECS	Endocannabinoid system
FITC	Fluorescein isothiocyanate
Fk	Forskolin
HEK293	Human embryonic kidney cells
HER2	Human epidermal growth factor receptor 2
IBX	2-Iodoxybenzoic acid
JNK	c-Jun N-terminal kinase

LPI	Lysophosphatidylinositol
MAGL	Monoacylglycerol lipase
Met-AEA	(*R*)-(+)-Methanandamide
NADA	*N*-Arachidonoyl-dopamine
NFAT	Nuclear factor of activated T-cells
PI	Propidium iodide
PLC	Phospholipase C
RhoA	Ras homolog gene family, member A
ROCK	Rho-associated protein kinase
THC	Tetrahydrocannabinol
TIMP	Tissue inhibitors of metalloproteinases
TMH	Transmembrane helix
TNBC	Triple negative breast cancer
VEGF	Vascular endotelial growth factor

Index

Summary*

The endocannabinoid system (ECS) has shown to be of great importance in the regulation of numerous physiological and pathological processes. To date, two cannabinoid receptors, CB_1R and CB_2R, have been discovered and are found predominantly in the central nervous system (CB_1R) or the immune system (CB_2R) among other organs and tissues. Endogenous cannabinoid receptor ligands (endocannabinoids) and the enzymes involved in their synthesis, cell uptake and degradation have also been identified and are part of the ECS. Other G-coupled protein receptors such as GPR55 have also been proposed as potential member of the ECS. However, this categorization instigates strong debate due to the lack of pharmacological tools to fully determine GPR55 biological functions.

The potential of cannabinoid receptor ligands has been preclinically explored in the treatment of diverse symptoms and diseases such as pain, inflammation, metabolic syndromes, cancer, hypertension, bone-related disorders or neurodegenerative processes. The only cannabinoids on clinical use today are the phytocannabinoids tetrahydrocannabinol (Δ^9-THC) and cannabidiol (CBD), and the THC synthetic derivative nabilone, which are approved for pain, emesis and appetite disorders. Taking into account the fact that these compounds lack of CB_1R/CB_2R selectivity, identifying new synthetic cannabinoids is of great interest. These novel entities should be exempt of the undesirable psychotropic effects related to the activation of brain CB_1R to have greater opportunity to be explored as cannabinoid-based medicines.

In this context, we aimed to explore the chromenopyrazole scaffold (figure 1) as a privileged structure in drug discovery targeting the ECS. From that perspective, this research work has been structured in three different chapters regarding biological and chemical outcomes.

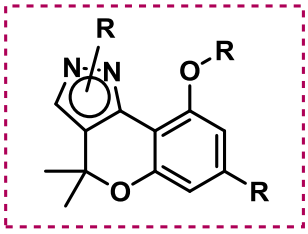

Figure 1. Chromenopyrazole scaffold general structure.

Chapter 1

Chromenopyrazoles were first identified in our research group as non-psychoactive CB_1R agonists with peripheral antinociceptive properties. However, CB_2Rs, mainly located in peripheral tissues, represent another promising drug target for the treatment of numerous diseases avoiding the psychotropic side effects characteristic of targeting CB_1R in the brain. Consequently, the main goal of this chapter was to optimize the structure modifications on the chromenopyrazole core in order to obtain CB_2R selective ligands. Thus, focusing on the pyrazole and the phenol substituents, novel series of chromenopyrazoles were synthesized in moderate to high yields using a route of four to six steps (figure 2). The affinity of these new compounds for the cannabinoid receptors CB_1R and CB_2R was evaluated measuring their ability to displace the radioligand [^{3}H]CP55940 from both receptors respectively transfected into HEK293 EBNA cells. Then, functional activity of the compounds with better CB_2R affinity profiles was tested by cAMP accumulation experiments, GTPγS binding assays and by an *in vitro* assay on BV-2 microglial cells. Docking studies using the active CB_1R^* and CB_2R^* models provided structural information related to ligand-receptor interactions and validating the experimental structure-activity relationships.

Among the series of chromenopyrazoles reported in this chapter, novel CB_2R selective and potent agonists have been identified, as well as CB_2R antagonists, and potent CB_1R/CB_2R agonists. Moreover, predicted pharmacokinetic properties of these newly synthesized CB_2R ligands calculated *in silico* using QikProp from Maestro Software clearly suggested their favorable druggability profiles.

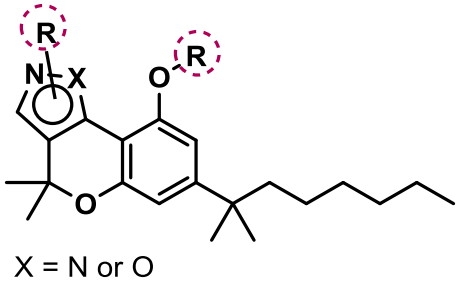

Figure 2. Fine-tuning of affinity and selectivity of chromenopyrazoles towards CB_2R was achieved by structural modifications at R-positions of the scaffold.

In order to explore the CB_2R homodimer process, the design of bivalent ligands was proposed (figure 3). In the last years growing evidence suggests that numerous GPCRs, cannabinoid receptors among them, may form hetero- and homodimers. This oligomerization interferes with the receptor function, activation and signal transduction. In this scenario, bivalent ligands, which consist of two pharmacophores connected by a spacer, have emerged in the last years as promising pharmacological entities and potential tools for the biological study of their respective dimeric receptors. Thus, a series of homobivalent chromenopyrazoles containing alkyl chains as spacers and their respective univalent 9-alkoxychromenopyrazole analogs were synthesized. Different alkyl chains (ten to sixteen methylenes) were introduced in order to investigate the influence of the spacer length on affinity and potency. Their ability to bind to the cannabinoid receptors was measured through radioligand assays. They show significant CB_2R affinity with full CB_2R selectivity over CB_1R. It is worthy to note that their corresponding univalent ligands did not display any affinity for neither CB_1R nor CB_2R, suggesting a possible interaction of both pharmacophores of the bivalent entities with CB_2R. Furthermore, these ligands showed agonism through cAMP functional assays using HEK293 cells stably expressing CB_2R for which the presence of CB_2R dimers has been confirmed. To our knowledge, this is the first time that fully CB_2R selective bivalent ligands are described.

Figure 3. Homobivalent chromenopyrazoles. DMH: 1,1 Dimethylheptyl.

In summary, within the first chapter, new selective CB_2R agonists and antagonists, as well as, the first fully CB_2R selective bivalent ligands have been identified.

Chapter 2

This chapter focused on a multitarget strategy applied to cancer therapy. Based on increasing evidence of cannabinoids antitumor properties and the well-known redox properties of quinones, we designed compounds with a structure that include both features. Thus, structural modification of the chromenopyrazole scaffold has been oriented towards this new approach. *Para* and *ortho*-chromenopyrazolediones were synthesized by regioselective oxidation of chromenopyrazoles. Their antitumor properties were evaluated *in vitro* and *in vivo* in different models of human cancers.

a) *Ortho*-chromenopyrazolediones (figure 4) showed affinity and selectivity for the CB_2R eliminating possible side psychotropic effect derived from the activity at the CB_1R in the brain. Concerning their antitumor activity, they decreased cell proliferation in human triple-negative breast cancer cell line (MDA-MB-231) using MTT assays. An additional important fact is their lack of significant cytotoxicity against normal human mammary epithelial cells (HMEC). Further mechanistic studies allowed us to determine that these antitumor effects were mediated through activation of CB_2R and through induction of oxidative stress. As confirmed by western blot analysis using active caspase-3 as biomarker, these compounds induced apoptosis in the aforementioned breast cancer cell line. The antiproliferative effect of the most potent derivative was reproduced *in vivo*. This cannabinoid-quinone induced significant reduction of tumor xenograft growth (MDA-MB-231) in nude mice.

Moreover, the lack of toxicity in different vital organs was further confirmed *in vivo* by histopathological analysis.

b) *Para*-chromenopyrazolediones (figure 4) exhibited CB_1R/CB_2R affinity in the submicromolar range. Some of these compounds were efficient against two prostate cancer cell lines, LNCaP and PC-3. This antiproliferative activity has been shown to involve oxidative stress, PPARγ activation, and CB_1R activation. In *in vivo* mice experiments, one of the compounds totally blocked the growth of the aggressive androgen-sensitive prostate cancer tumor.

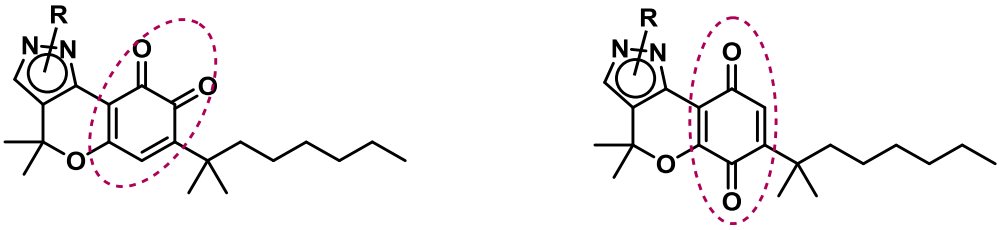

Figure 4. *Para* and *ortho*-chromenopyrazolediones.

In summary, within the second chapter, the discovery of a new class of anticancer cannabinoid-quinones with potential for the development of anticancer agents against hormone-sensitive prostate tumors and triple negative breast cancer has been reported.

Chapter 3

In the last chapter of this dissertation we focused our efforts in the identification of novel ligands of the putative cannabinoid receptor GPR55. The validity of the categorization of GPR55 as a cannabinoid member is still under debate mainly due to the lack of potent and selective agonists and antagonists. In this scenario, we designed and synthesized two different series of new chromenopyrazole derivatives (figure 5) on the basis of the structural features recently identified for GPR55 ligands.

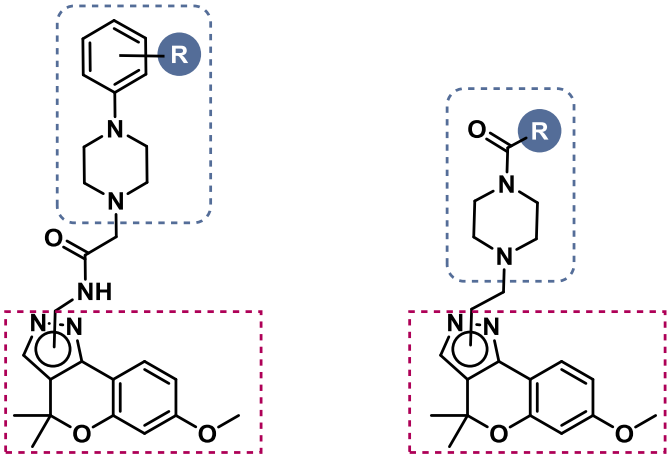

Figure 5. Phenylpiperazinyl-acetamidomethyl-chromenopyrazoles and acyl-piperazinyl-chromenopyrazoles.

Appraisal of GPR55 activity of the new synthesized compounds was accomplished by using an innovative cell-impedance, label-free based assay with HEK293 cells stably expressing human GPR55. The real-time impedance responses provide an integrative assessment of the cellular consequence to GPR55 stimulation taking into account the different possible signaling pathways.

Analysis of data obtained allowed potent GPR55 partial agonists to be identified (EC_{50} values in nanomolar range). Upon antagonist treatment, four of these GPR55 partial agonists significantly inhibited GPR55-mediated responses to lysophosphatidylinositol (LPI). In contrast to LPI, these compounds did not show off-target effects at concentrations up to 10 μM in this assay. Due to the relation of GPR55 with the endocannabinoid system, selectivity towards the classical cannabinoid receptors was investigated through CB_1R and CB_2R radioligand binding experiments. Some of the compounds exhibited GPR55 full selectivity. Additionally, one of the series displayed high affinity for CB_2R. It is worthy to note that none of the compounds bind to the CB_1R. Moreover, their predicted physicochemical parameters suggested a clear pharmacokinetic improvement compared to LPI.

In summary, within the third chapter, we have discovered a novel GPR55 chemotype that may serve to develop appropriate pharmacological tools or novel drugs to continue with the challenging goal of the validation of this receptor.

To conclude, medicinal chemistry efforts directed toward distinct strategies to obtain compounds acting on the endocannabinoid system (ECS) led to the discovery of a privileged scaffold, the chromenopyrazole.

*P.M. performed: **i**) the synthesis and characterization of the novel compounds and their *in silico* pharmacokinetic properties at Instituto de Química Médica (CSIC); **ii**) the binding studies, hosted by Prof. Javier Fernández-Ruiz, Facultad de Medicina, Universidad Complutense de Madrid (UCM); **iii**) the triple-negative breast cancer antiproliferative studies *in vitro* and *in vivo,* hosted by Prof. Cristina Sánchez, Facultad de Biología, UCM; **iv**) the molecular modeling, hosted by Prof Patricia Reggio, Department of Chemistry and Biochemistry, University of North Carolina at Greensboro (UNCG); **v**) the GPR55 cell-impedance assays, hosted by Prof. Ruth Ross, Department of Pharmacology and Toxicology, University of Toronto (UofT).
Other assays (SPR, electrochemistry, cAMP, GTPγS binding, BV-2 microglial cells, and all the antitumor evaluation in prostate cancer) have been performed by collaborators.

Resumen*

El sistema endocannabinoide ha mostrado tener gran relevancia en la regulación de numerosos procesos fisiológicos y patológicos. Hasta el momento se han identificado dos tipos de receptores cannabinoides: *tipo 1* (CB_1), predominantes en el sistema nervioso central, y *tipo 2* (CB_2), ubicados principalmente en el sistema inmune entre otros órganos y tejidos. Asimismo, se han identificado los ligandos endógenos de estos receptores y las enzimas implicadas en su síntesis, recaptación y degradación. Otros receptores acoplados a proteínas G, como GPR55, también se han propuesto como posibles miembros del sistema endocannabinoide. Sin embargo, esta categorización aún no ha sido confirmada debido a la falta de herramientas farmacológicas que permitan caracterizar apropiadamente las funciones biológicas de GPR55.

El potencial terapéutico de los ligandos cannabinoides ha sido evaluado a nivel preclínico para el tratamiento de numerosas enfermedades y síntomas como el dolor, la inflamación, el cáncer y la hipertensión, así como patologías metabólicas y neurodegenerativas. El problema fundamental asociado al tratamiento con cannabinoides radica en la imposibilidad actual de separar los efectos terapéuticos de la acción psicoactiva. Hoy en día, los únicos cannabinoides utilizados en la clínica son el tetrahidrocannabinol, su análogo sintético nabilona y el cannabidiol; se emplean para el tratamiento del dolor, la emesis y la mejora del apetito. Estos compuestos actúan sobre ambos receptores CB_1 y CB_2 provocando efectos psicoactivos asociados a la modulación del receptor CB_1 en el cerebro. Por tanto, es de gran interés la identificación de nuevos cannabinoides sintéticos con efectos secundarios reducidos.

En este contexto, nos propusimos explorar el potencial del esqueleto de cromenopirazol (figura 1) en el desarrollo de nuevas moléculas capaces de modular el sistema endocannabinoide. Para ello, este proyecto se ha estructurado en tres capítulos atendiendo a criterios químicos y farmacológicos.

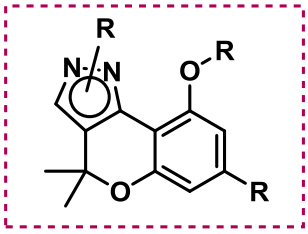

Figura 1. Estructura general del esqueleto de cromenopirazol.

Capítulo 1

Por analogía a fitocannabinoides como el cannabinol, en nuestro grupo de trabajo se diseñó y sintetizó previamente una familia de compuestos, denominados cromenopirazoles. Estas estructuras fueron caracterizadas como ligandos agonistas del receptor CB_1 y mostraron propiedades antinociceptivas en un modelo de analgesia periférica sin presentar psicoactividad.

El receptor CB_2, cuya activación no desencadena efectos psicotrópicos, representa una prometedora diana terapéutica para el tratamiento de diversas patologías. Por ello, este capítulo se centra en la optimización del esqueleto de cromenopirazol con el fin de desarrollar ligandos selectivos y potentes para este receptor. Con este objetivo se sintetizó una nueva serie de derivados modificando los sustituyentes del pirazol y el fenol (figura 2). La afinidad de los nuevos compuestos por los receptores CB_1 y CB_2 fue evaluada mediante ensayos de desplazamiento de radioligando. La funcionalidad de los compuestos que presentaron mejor perfil de afinidad y/o selectividad por el receptor CB_2 fue evaluada mediante ensayos de acumulación de AMP cíclico intracelular, GTPγS o experimentos en células BV-2 microgliales. A continuación, se llevaron a cabo estudios de modelización molecular usando modelos computacionales de receptores cannabinoides CB_1 y CB_2 activados (CB_1* y CB_2*). Estos estudios proporcionaron información estructural sobre las interacciones del complejo ligando-receptor, permitiendo validar las relaciones estructura-actividad obtenidas experimentalmente.

En este estudio se identificaron nuevos agonistas CB_2 potentes y selectivos. Asimismo, algunos de los compuestos de esta serie mostraron ser antagonistas CB_2 o potentes agonistas CB_1/CB_2. Por otro lado, estudios *in silico* llevados a cabo mediante el programa *QikProp* (*Maestro*) sugirieron un perfil farmacocinético favorable para los cromenopirazoles desarrollados en este capítulo.

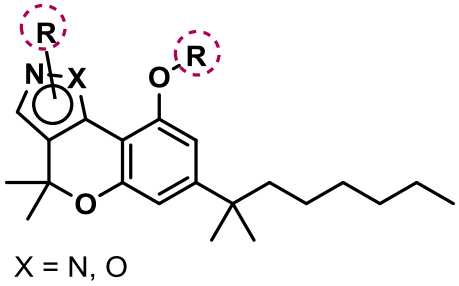

Figura 2. Modificaciones estructurales en las posiciones destacadas dieron lugar a derivados de cromenopirazol con afinidad por el receptor CB_2.

En los últimos años numerosos estudios han demostrado que determinados receptores acoplados a proteínas G, CB_1 y CB_2 entre ellos, existen como heterodímeros y homodímeros en condiciones fisiológicas y patológicas. Esta oligomerización puede modificar tanto la función del receptor como su activación por determinados compuestos. Con el fin de explorar la homodimerización del receptor CB_2, se propuso el diseño de ligandos bivalentes siguiendo el patrón estructural mostrado en la figura 3. Este tipo de ligandos están formados por dos unidades farmacofóricas unidas por un espaciador de una longitud determinada. En este contexto, se sintetizó una familia de cromenopirazoles bivalentes y sus respectivos análogos monovalentes 9-alcoxicromenopirazoles. En lo que se refiere al espaciador, se introdujeron cadenas alquílicas de distinta longitud (de diez a dieciséis metilenos) con el fin de estudiar la influencia del espaciador sobre la potencia y afinidad de las nuevas moléculas. Los compuestos bivalentes y sus análogos monovalentes fueron evaluados mediante ensayos de desplazamiento de radioligando para determinar sus afinidades por los receptores CB_1 y CB_2. Los derivados bivalentes mostraron ser ligandos selectivos del receptor CB_2 con afinidad en el rango submicromolar. Sin embargo, sus análogos monovalentes no presentaron afinidad por estos receptores. Estos resultados sugieren una posible interacción del segundo

farmacóforo con el receptor. Determinados ligandos bivalentes mostraron agonismo en ensayos de funcionalidad basados en la determinación de acumulación de AMPc en células HEK293 transfectadas con CB_2 y en la cuales se confirmó la extistencia de homodimeros CB_2.

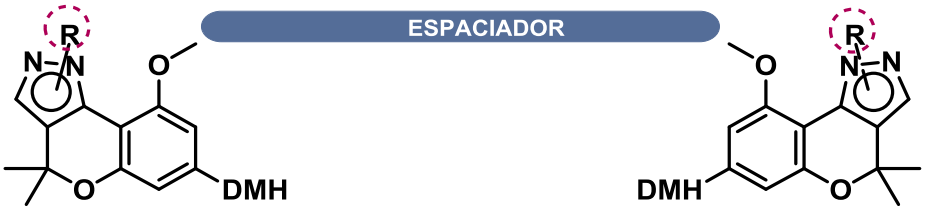

Figure 3. Estructura general de cromenopirazoles homobivalentes. DMH: 1,1 dimetilheptilo.

En resumen, a lo largo del primer capítulo de esta tesis doctoral se han identificado tanto agonistas CB_2 potentes como ligandos bivalentes selectivos para dicho receptor, todos ellos basados en la estrutura de cromenopirazol.

Capítulo 2

Existen múltiples procesos biológicos involucrados en la patogénesis del cáncer. Para abordar su tratamiento se suelen utilizar terapias combinadas. En este ámbito, resulta de especial interés el desarrollo de ligandos capaces de actuar sobre varias dianas terapéuticas implicadas en procesos neoplásicos. Debido al potencial antitumoral de las quinonas y a las propiedades anticancerosas de los cannabinoides, se llevó a cabo el diseño y la síntesis de nuevos compuestos basados en ambos motivos estructurales. En el segundo capítulo se presenta la síntesis de *para* y *orto*-cromenopirazoldionas mediante oxidación regioselectiva del esqueleto de partida. Su interacción con los receptores cannabinoides fue evaluada mediante ensayos de desplazamiento de radioligando. Por otro lado, las propiedades antitumorales de estas nuevas moléculas fueron evaluadas *in vitro* e *in vivo* en distintos modelos de cáncer.

a) *Orto*-cromenopirazoldionas (figura 4, izquierda): Estos compuestos mostraron afinidad y selectividad por el receptor CB_2 descartando así posibles efectos psicoactivos asociados a la activación de CB_1. Con respecto a su actividad antitumoral, las *orto*-cromenopirazoldionas fueron capaces de disminuir la proliferación de células humanas de cáncer de mama triple negativo (MDA-MB-231). Además, estos compuestos no presentaron citotoxicidad en células mamarias epiteliales normales (HMEC). Mediante distintos estudios *in vitro* se intentó profundizar en la determinación del mecanismo de acción antitumoral de estos compuestos. Estas moléculas actúan a través de la activación de receptores CB_2 y la generación de estrés oxidativo. El análisis mediante *western blot* de la activación de caspasa 3 permitió determinar que estos compuestos son capaces de inducir apoptosis en la mencionada línea celular MDA-MB-231. El derivado más potente de esta serie fue evaluado en un modelo *in vivo* de cáncer de mama triple negativo. Dicha quinona-cannabinoide fue capaz de reducir significativamente el crecimiento del tumor en ratones inmunodeprimidos. Además, mediante análisis histopatológicos de órganos vitales, se demostró que el compuesto no induce toxicidad en este modelo de la enfermedad.

b) *Para*-cromenopirazoldionas (figura 4, derecha): Estas nuevas moléculas presentaron afinidad por ambos receptores cannabinoides en el rango submicromolar. Asimismo, presentaron un marcado efecto antiproliferativo en líneas celulares derivadas de tumores humanos de próstata LNCaP y PC-3, dependiente e independiente de andrógenos respectivamente. En esta actividad antitumoral se demostró la implicación de los receptores CB_1, los receptores PPARγ y la generación de estrés oxidativo. Finalmente, se realizaron ensayos *in vivo* con una de las *para*-cromenopirazoldionas mostrando su capacidad para bloquear casi totalmente el crecimiento tumoral LNCaP y reducir significativamente el crecimiento de tumores PC-3.

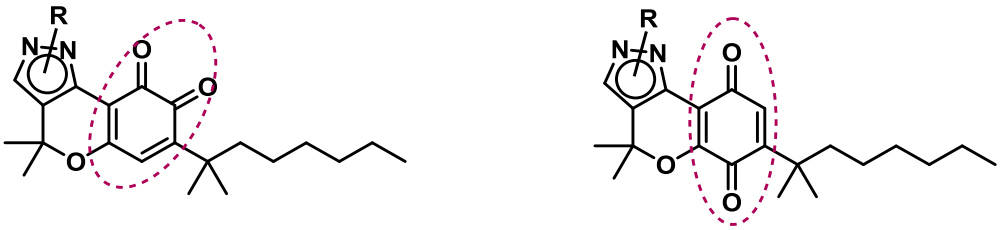

Figura 4. *Para* y *orto*-cromenopirazoldionas.

En resumen, en este segundo capítulo se ha descubierto un nuevo prototipo para el desarrollo de fármacos antitumorales con potencial aplicación para el tratamiento del cáncer de mama triple negativo y el cáncer de próstata.

Capítulo 3

En el último capítulo de esta tesis doctoral se aborda la búsqueda de nuevos ligandos del receptor GPR55. La falta de agonistas y antagonistas selectivos para este receptor ha dificultado su validación como miembro del sistema endocannabinoide. Por ello, se diseñaron y sintetizaron dos series de cromenopirazoles (figura 5) en base a requisitos estructurales recientemente identificados para ligandos de GPR55.

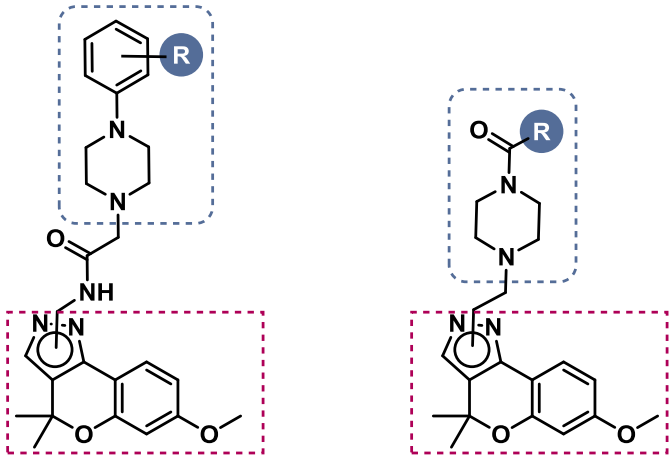

Figura 5. Fenilpiperazinil-acetamidometil-cromenopirazoles y acil-piperazinil-cromenopirazoles.

La actividad de los nuevos compuestos en el receptor GPR55 fue determinada mediante un novedoso estudio de impedancia celular en células HEK293 que expresan el receptor GPR55 de manera estable. Estos ensayos permiten obtener la respuesta celular integrada tras la estimulación del receptor en tiempo real, evitando así los problemas derivados del análisis de una sola vía de señalización. Estos estudios permitieron identificar potentes agonistas parciales de GPR55 (con concentraciones efectivas medias en el rango nanomolar). Del mismo modo, algunos de los compuestos de esta serie mostraron capacidad para inhibir el efecto del agonista endógeno lisofosfatidilinositol (LPI). Al contrario que LPI, los derivados de cromenopirazol no presentan efectos en células HEK293 normales a altas concentraciones.

Debido a la estrecha relación entre GPR55 y los receptores cannabinoides clásicos, se evaluó la unión de los nuevos compuestos a los receptores CB_1 y CB_2 mediante ensayos de desplazamiento de radioligando. Algunos de estos derivados no mostraron afinidad por CB_1 ni CB_2 siendo ligandos selectivos de GPR55 frente a receptores cannabinoides clásicos. Sin embargo, aunque ninguno de los compuestos se une al receptor CB_1, algunos sí presentaron afinidad por CB_2.

En resumen, en el tercer capítulo de esta tesis doctoral se ha descubierto un prototipo para el desarrollo de nuevos ligandos y herramientas farmacológicas del receptor GPR55.

A lo largo de esta tesis doctoral se ha identificado un nuevo esqueleto privilegiado para el desarrollo de moléculas capaces de modular el sistema endocannabinoide.

* La doctoranda (P.M.) ha llevado a cabo las siguientes tareas: **i**) síntesis y caracterización estructural de los nuevos compuestos y predicción *in silico* de sus propiedades farmacocinéticas en el Instituto de Química Médica (CSIC); **ii**) ensayos de unión a receptores CB_1 y CB_2 de los nuevos compuestos en el laboratorio del Prof. Javier Fernández-Ruiz, Facultad de Medicina, Universidad Complutense de Madrid (UCM); **iii**) ensayos *in vitro* e *in vivo* en cáncer de mama triple negativo en el laboratorio de la Prof. Cristina Sánchez, Facultad de Biología, UCM; **iv**) estudios de modelización molecular en el laboratorio de la Prof. Patricia Reggio, *Department of Chemistry and Biochemistry, University of North Carolina at Greensboro* (UNCG); **v**) ensayos de impedancia celular evaluando la capacidad de los nuevos compuestos para modular GPR55 en el laboratorio de la Prof. Ruth Ross, *Department of Pharmacology and Toxicology, University of Toronto* (UofT).
El resto de ensayos (SPR, electroquímica, funcionalidad mediante AMPc, GTPγS, células microgliales BV-2, así como la evaluación antitumoral en cáncer de próstata) han sido realizados por grupos de investigación colaboradores.

Chapter 1

Chromenopyrazoles: Novel Cannabinoid Receptor Modulators

Contents

1. Introduction

Cannabis sativa has been extensively employed by mankind throughout the history. The earliest recorded use of cannabis can be traced back to ancient China nearly five thousand years ago. It was used as a source of textiles and food, as well as for medicinal, religious and recreational purposes. From China, the use of cannabis spread across Asia and to the Middle East but it did not reach Europe until centuries later. Medicinally, cannabis was used in many cultures to treat diverse complaints including pain, convulsions, inflammation, asthma and lack of appetite.[1]

The decline of medicinal cannabis began in the early twentieth century mainly due to its spread consumption as a recreational psychoactive drug. This fact limited the research of cannabis therapeutic applications until the 1960s. The isolation and structural characterization of the main active constituent of *Cannabis sativa*, Δ^9–tetrahydrocannabinol (Δ^9–THC, figure 5), was reported in 1964 by Gaoni and Mechoulam.[2] Subsequent studies demonstrated the existence of a number of structurally related cannabinoids in the plant.

During the last decades, research in this field has remarkably accelerated. The discovery of specific receptors in the body and an entire endogenous cannabinoid system has led to the development of numerous synthetic cannabimimetic drugs and a better understanding of their physiological effects.

1.1 Endocannabinoid system (ECS)

Although cannabinoids have been used for medicinal purposes for centuries, their mechanism of action remained unclear until a couple of decades ago. In 1988, Devane *et al.*[3] identified specific binding sites in the brain (cannabinoid receptors, CBRs) that were activated by different phytocannabinoids. This discovery was followed by the cloning and expression of a complementary DNA that encodes for this receptor, which was consequently named as cannabinoid receptor type 1 (CB_1R).[4] In 1993, Munro *et al.*[5] isolated and cloned the second cannabinoid receptor, cannabinoid receptor type 2 (CB_2R), from the human promyelocytic cell line HL60. Furthermore, as

phytocannabinoids themselves do not exist in the brain, the existence of these receptors prompted research to identify the endogenous molecules able to activate them. Accordingly, Devane *et al.*[6] reported the isolation of anandamide [*N*-arachidonoylethanolamine (AEA), figure 3], a lipid neurotransmitter considered the first endocannabinoid identified. Later, 2-Arachidonoylglycerol (2-AG, figure 3) and several other endogenous molecules acting on CBRs have been discovered.[7,8]

In addition to the cannabinoid receptors and their endogenous ligands, the proteins responsible for the biosynthesis, inactivation and transport of endocannabinoids are also part of the ECS. The metabolizing enzymes fatty acid amide hydrolase (FAAH) and monoacylglycerol lipase (MAGL) as well the anandamide transporter (AT) have been extensively studied.[9–13]

Whether additional cannabinoid receptors are part of the ECS still instigates strong debate. Recent studies have shown that several cannabinoid ligands bind to the receptor GPR55[14] supporting the idea that it plays an important role in the ECS (this receptor will be extensively described in the third chapter of this dissertation). Furthermore, GPR18[15] (*N*-arachidonoyl glycine) and GPR119[16] have been suggested as putative cannabinoid receptors in different investigations. Moreover, there is extensive evidence indicating that ECS also interacts with a number of established non-CB_1, non-CB_2 GPCRs, ligand-gated ion channels, ion channels, and nuclear receptors.[17,18]

Cannabinoid receptors

CBRs belong to the superfamily of G-protein coupled receptors (GPCRs) and are single polypeptides with seven transmembrane α-helices, an extracellular, glycosylated *N*-terminus and an intracellular *C*-terminus.[19] CB_1R and CB_2R types possess 68% amino acid identity within their transmembrane regions but only 44% identity throughout the entire peptide. Despite this structural difference, many cannabinoid compounds display nearly equal affinity for both receptors.

CB_1R and CB_2R are membrane-bound proteins and therefore are extremely difficult to purify and crystalize. The lack of CBRs high-resolution crystal structure has hampered the progress in

understanding their three-dimensional structure; however, computational homology models have been developed to enable drug design.

Signaling pathways

The complexity of signaling pathways of GPCRs is extended to CBRs. Both CB_1R and CB_2R share some common signaling mechanisms that are schematically represented in figure 1. They are coupled to $G_{i/o}$ proteins, negatively to adenylyl cyclase (AC) and positively to mitogen-activated protein kinase (MAPK). Consequently, activation of these receptors causes inhibition of AC, thus inhibiting the conversion of ATP to cyclic AMP (cAMP). Reduction of cAMP levels affects phosphorylation by protein kinase A, which triggers modulation of ion channels and other second messengers such as intracellular calcium. Whereas AC inactivation is mediated by the α subunit of the $G_{i/o}$ protein,[4] the βγ subunit of this G-protein complex causes activation of extracellular signal-regulated kinase (ERK).[20] This enzyme in conjunction with other MAPKs such as c-Jun N-terminal kinase (JNK) and p38 are regulated by activation of CBRs. In spite of their common features, CB_1R and CB_2R differ in signaling mechanisms and tissue distribution (figure 2). For instance, modulation of voltage-dependent ion channels has been related to CB_1R activation.[17,21]

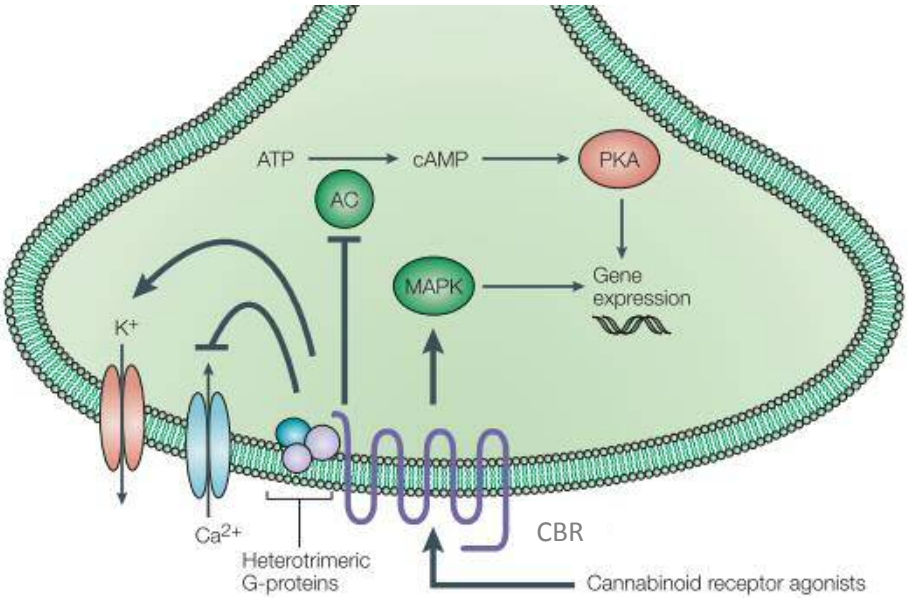

Figure 1. General overview of signaling pathways associated with CBRs activation by agonists. Extracted from Di Marzo *et al.*[22]

CB_1 Receptors

The CB_1R is among the most abundant and widely distributed GPCRs in the brain. CB_1Rs are mainly found on nerve cells in the brain, spinal cord and peripheral nervous system, but are also present in certain peripheral organs and tissues, among them endocrine glands, spleen, leukocytes, heart and parts of the reproductive, urinary and gastrointestinal tracts. CB_1R plays an important role in the physiology of the nervous system.[17] These receptors are highly expressed in regions of the brain, which are responsible for movement (basal ganglia, cerebellum), memory processing (hippocampus, cerebral cortex) and pain modulation (certain parts of the spinal cords, periaqueductal grey).[4,17,23] CB_1R modulates synaptic transmission by inhibiting calcium channels and possibly activating potassium channels on presynaptic terminals.[24] Based on these findings, it has been suggested that CB_1R agonists suppress neuronal excitability and play a role in regulating neurotransmitter release.[21,25]

CB_2 Receptors

The CB_2R is predominantly expressed within the immune system, however, its expression was further confirmed in the brain on microglia,[26] blood vessels,[26] and on some neurons.[27,28] Since CB_2Rs

are mainly located in immune cells, among them leukocytes, one of their main functions is the modulation of release of cytokines, which are responsible of inflammation and regulation of the immune system. Moreover, CB_2R regulates immune responses by regulating immune cell migration[29] and antigen presentation.[30]

Even though CB_2R has been widely studied for its immunomodulatory properties, it exhibits a valuable role in the CNS through microglial cells.[31] Interestingly, its activation does not trigger psychoactive effects, while activation of CB_1R clearly does. Thus, CB_2R represents a very promising target for the management of neurological disorders.

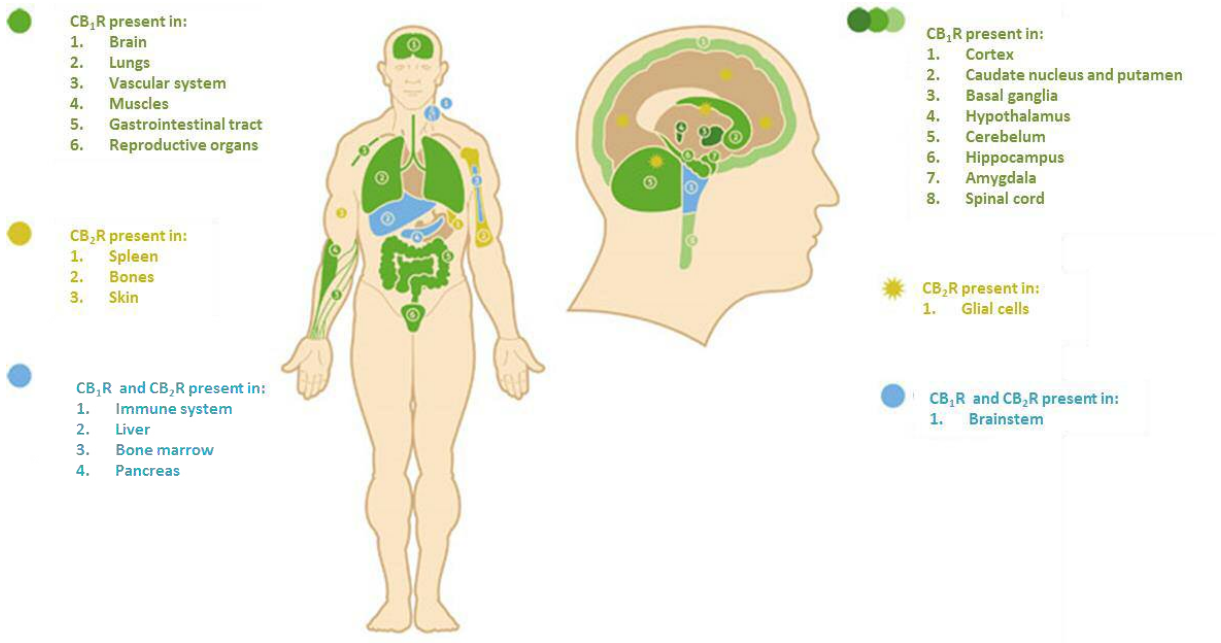

Figure 2. Tissue distribution of the human CB_1R and CB_2R receptors in the body. Extracted from Fundación Canna.[32]

Oligomerization of Cannabinoid Receptors

Recent studies have shown that GPCRs, can exist and function as dimers or higher order multimers.[33–35] Regarding CBRs, the presence of homodimers and heteromers in different tissues has been convincingly demonstrated over these last years.

For the CB_1R, heteromers have been shown to exist with serotonin,[36,37] angiotensin,[38] opioid,[39,40] GPR55,[41,42] orexin,[43,44] dopamine[45] and adenosine[46] receptors among others. Although CB_2R has

been less investigated, very recent research revealed that it forms heterodimers with CB_1R,[47] with the orphan receptor GPR55[48,49] and with HER2 (human epidermal growth factor receptor 2) receptors in cancer cells.[50] All these data concerning CBR heteromerization suggest that the ECS interacts in a significant manner with several other endogenous systems.

In what concerns cannabinoids receptor homodimerization, more data have been published on CB_1R homodimers than CB_2R counterparts. The presence of CB_1R homodimers has been confirmed in different biological tissues *in vivo* and *in vitro*.[51–55] Even if their functional role has not been properly determined, diverse pharmacological approaches have already been explored.[56–58] On the other hand, CB_2R homodimers have been evidenced[59–61] but not fully evaluated and their pharmacological potential has not been explored yet.

It is certain that homo- and heterodimerization affects the manner in which the CBRs respond to ligands. However, it remains a challenge to clearly identify what biological functions are impacted by these dimers and to develop drugs targeting them.

1.2 Cannabinoid ligands

Cannabinoid modulators can be classified attending to diverse criteria such as their biological activity, their nature or their chemical structure. Herein, cannabinergic ligands will be briefly categorized attending to the last criterion:

1.2.1 Endocannabinoids and related compounds

As aforementioned, the identification of cannabinoid receptors was followed by the detection of their endogenous ligands. These molecules, named endocannabinoids, are lipid neurotransmitters that mediate retrograde signal from postsynaptic neurons to presynaptic ones targeting CBRs.[62] Endocannabinoids comprise a family of polyunsaturated fatty acids that structurally differ from phytocannabinoids. Among the endocannabinoids identified so far are anandamide (*N*-arachidonoylethanolamide, AEA), 2-arachidonoylglycerol (2-AG), 2-arachidonylglyceryl ether

(noladin ether, 2-AGE), *O*-arachidonoyl ethanolamine (virodhamine), and *N*-arachidonoyl-dopamine (NADA) (figure 3).

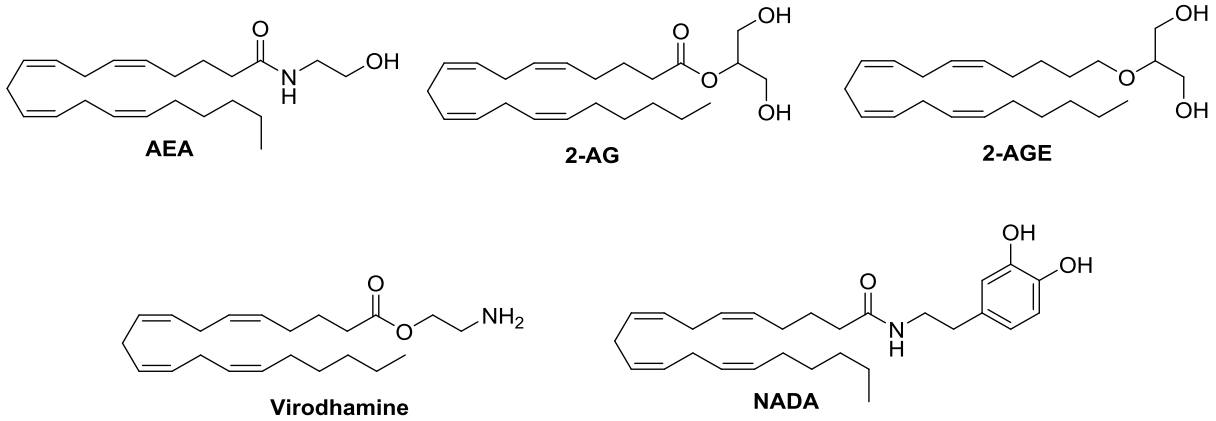

Figure 3. Structure of endocannabinoids: AEA, 2-AG, 2-AGE, virodhamine and NADA.

The first two discovered endocannabinoids, AEA and 2-AG, are more widely spread and have been more intensively evaluated.[25] AEA is a CB_1R/CB_2R partial agonist while 2-AG exhibit full agonism towards both receptors. In contrast to other brain chemical signals, which are stored in the nerve cells, endocannabinoids are synthesized "on demand" from membrane phospholipid precursors upon stimulation.[63,64] After release, they are rapidly deactivated by uptake into cells and metabolized by enzymatic hydrolysis by FAAH and MAGL.[13,65]

There is no doubt that this endogenous machinery presents a promising therapeutic potential, consequently, different drug discovery strategies have been explored. One of them considers amplifying the ECS tone by inhibiting the enzymes FAAH or MAGL, or the transporter AT. Another emerging strategy is based on positive allosteric modulation of CBRs that would enhance cannabimimetic activity of endocannabinoids. Development of synthetic endocannabinoid analogues that activate CBRs but are weak substrates for the metabolic enzymes has also been proposed as a promising approach.[66] Subsequently, diverse synthetic eicosanoids have been described in the last years. Structural modifications of AEA and 2-AG have reported on the polar head, the lipophilic pentyl tail and the arachidonoyl backbone. For instance, molecules such as ACEA (arachidonyl-2'-chloroethylamide) or ACPA (arachidonylcyclopropylamide)[67] (figure 4), AEA analogues with modified polar groups, led to compounds with increased CB_1R affinity. (*R*)-(+)-

Methanandamide (Met-AEA), another anandamide analogue alkylated at position 1, retains activity while providing a better enzymatic stability.

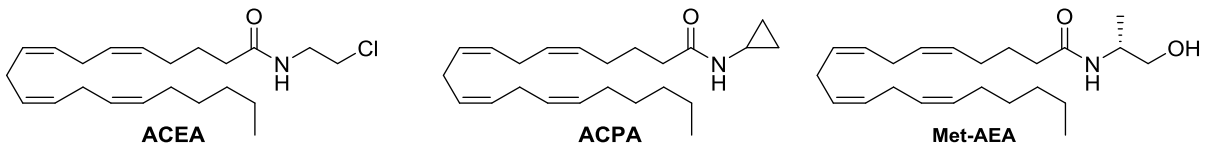

Figure 4. Structure of synthetic endocannabinoids derivatives ACEA, ACPA and (*R*)-methanandamide.

1.2.2 Phytocannabinoids and derivatives

To date over 80 cannabinoids, the so-called phytocannabinoids, have been isolated from the cannabis plant. Contrary to other naturally occurring drugs, such as opioids, nicotine, cocaine or caffeine, they do not contain nitrogen, and hence are not alkaloids. Most phytocannabinoids share common structural features that include a dibenzopyran ring and a hydrophobic alkyl chain. The most abundant cannabinoids in the plant are Δ^9-tetrahydrocannabinol (Δ^9-THC), cannabidiol (CBD), cannabinol (CBN), cannabigerol (CBG), and cannabichromene (CBC) (figure 5).

Phytocannabinoids show different affinity for CB_1R and CB_2R. Δ^9-THC binds to both receptors with similar potencies. This compound is largely responsible of the pharmacological properties as well as of the psychoactive effects associated with marijuana use. Other phytocannabinoids also contribute to the therapeutic effects of the plant, especially CBD, a non-psychoactive compound that demonstrated anti-inflammatory, analgesic, anti-anxiety and anti-tumor properties among others.[68]

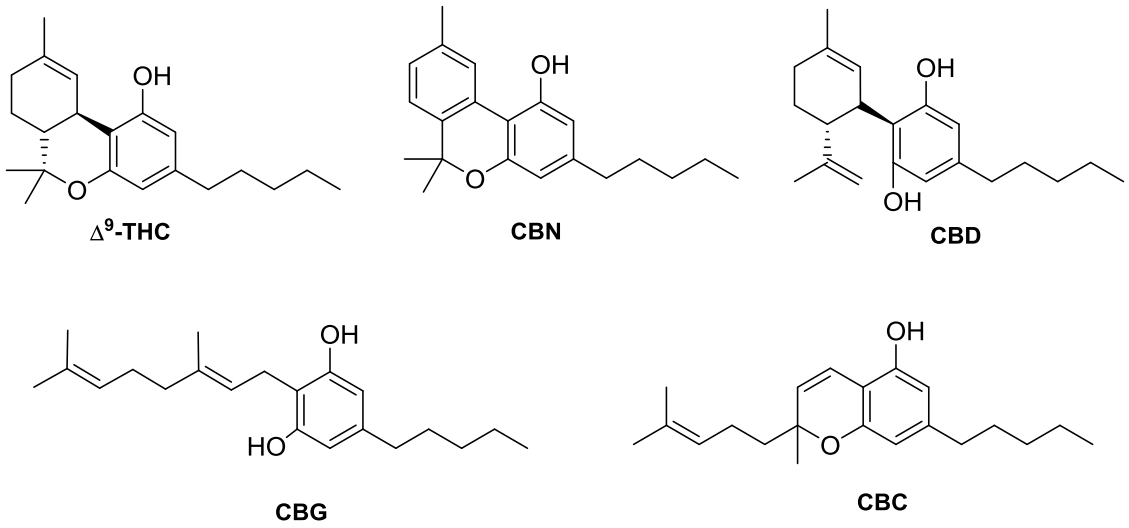

Figure 5. Structure of some plant cannabinoid ligands.

Numerous phytocannabinoid analogues and related derivatives have been synthesized. Consequently, SAR (structure-activity relationship) studies have helped to elucidate the structural requirements for cannabinoid activity. From a pharmacophoric point of view, different features of phytocannabinoid structures such as the alkyl lipophilic chain, the phenolic and the pyran ring have been explored leading to potent synthetic cannabinoid ligands. Some relevant and well-studied phytocannabinoid analogues are CP55,940, HU210, JWH133 and HU308 (figure 6). CP55,940, a very potent full agonist at both CB_1R and CB_2R, is currently used as a valuable experimental tool. Replacement of the methyl of Δ^9-THC by a hydroxymethyl group allowed the discovery of HU210, a very potent CB_1R/CB_2R agonist. In contrast, the deoxy and the methoxy-Δ^9-THC derivatives JWH133 and HU308 are CB_2R agonists with significant selectivity over CB_1R.[69] The only structural modification of Δ^9-THC that led to an approved drug is nabilone (figure 6). Its therapeutic potential will be discussed further in this dissertation

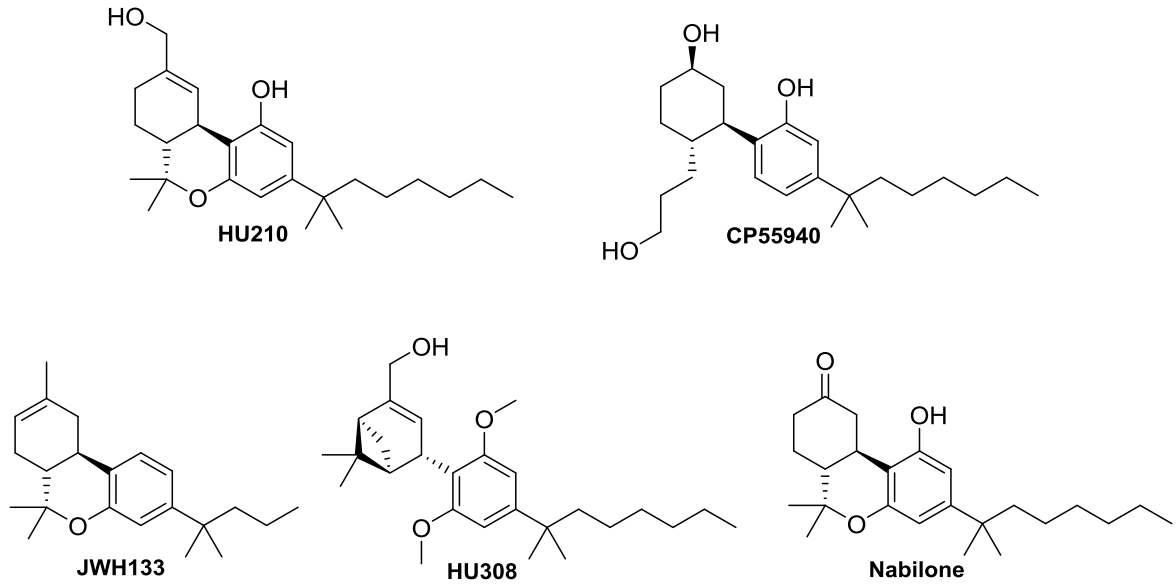

Figure 6. Structure of some phytocannabinoid synthetic derivatives.

1.2.3 Synthetic cannabinoids

The interest gained by the ECS as valuable target for drug discovery led to the synthesis of numerous cannabinoid ligands in the last years. Approaches for the development of novel cannabinergic drugs include selective activation or blockage of CB_1R or CB_2R.[70] These compounds are designed trying to improve the poor drug-like properties and to reduce the undesirable effects of phytocannabinoids. Other approaches include the inhibition of FAAH, MAGL or AT, as well as the design of ligands capable of modulating the ECS by binding to allosteric sites.[71,72] From a structural point of view, diverse cannabinoid scaffolds have been identified in the last decades, some of them will be briefly mentioned herein:

Aminoalkylindoles

In the early 1990´s aminoalkyindoles were identified as cannabinoid ligands.[73] These compounds are derivatives of pravadoline and were initially developed as non-steroidal anti-inflammatory drugs. Since they are not structurally related to phyto- or endocannabinoids, their identification was considered as a breakthrough in the field. Particularly, that of *R*-(+)-WIN55,212 (figure 7), a very potent CB_1R/CB_2R agonist which has been extensively used to investigate the endocannabinoid

system. SAR studies on the aminoalkylindole scaffold revealed that the morpholine and/or the benzomorpholino ring are not necessary to retain CBR activity. Remarkable members of this family are the naphthoylindole JWH015[74] (figure 7), a CB_1R/CB_2R agonist that displays certain selectivity towards CB_2R, and the iodoindole derivative AM630[75] (figure 7), a CB_2R inverse agonist and weak CB_1R partial agonist.

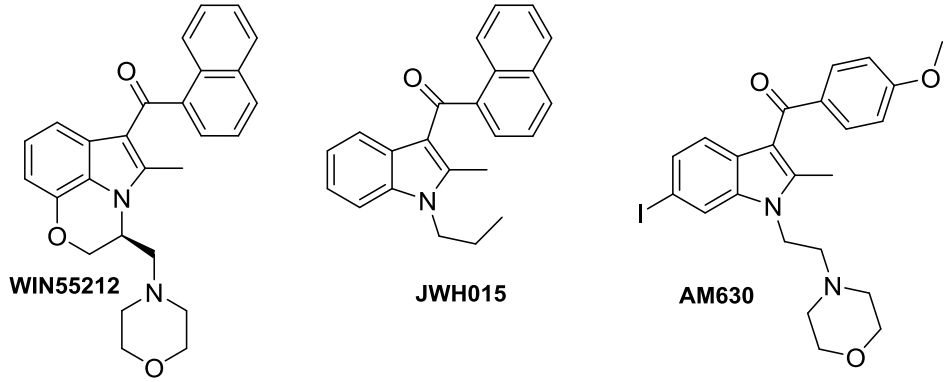

Figure 7. Aminoalkylindole cannabinoid ligands WIN55212, JWH015 and AM630.

Arylpyrazoles

The arylpyrazole scaffold was identified in 1994 by Sanofi with the discovery of SR141716A (rimonabant, figure 8). This compound is a potent CB_1R antagonist/inverse agonist which therapeutic potential has been deeply investigated and will be further discuss in this dissertation.[76]

Arylpyrazoles have been widely explored in the cannabinoid system becoming very relevant in the design of CB_1R or CB_2R inverse agonists or antagonists. SAR studies have revealed that for CB_1R binding affinity the pyrazole ring should be substituted at positions 1 and 5 with substituted phenyl moieties. Cannabinoids AM251[77] and AM281[78] (figure 8) are two representative CB_1R inverse agonists of this class. Moreover, a potent antiobesity derivative of SR141716A, the triazole LH21 (figure 8), was discovered in our research group.[79] Sanofi also discovered the first CB_2R antagonist, SR144528[80] (figure 8), an arylpyrazole that has been used as pharmacological tool in numerous *in vitro* and *in vivo* models.

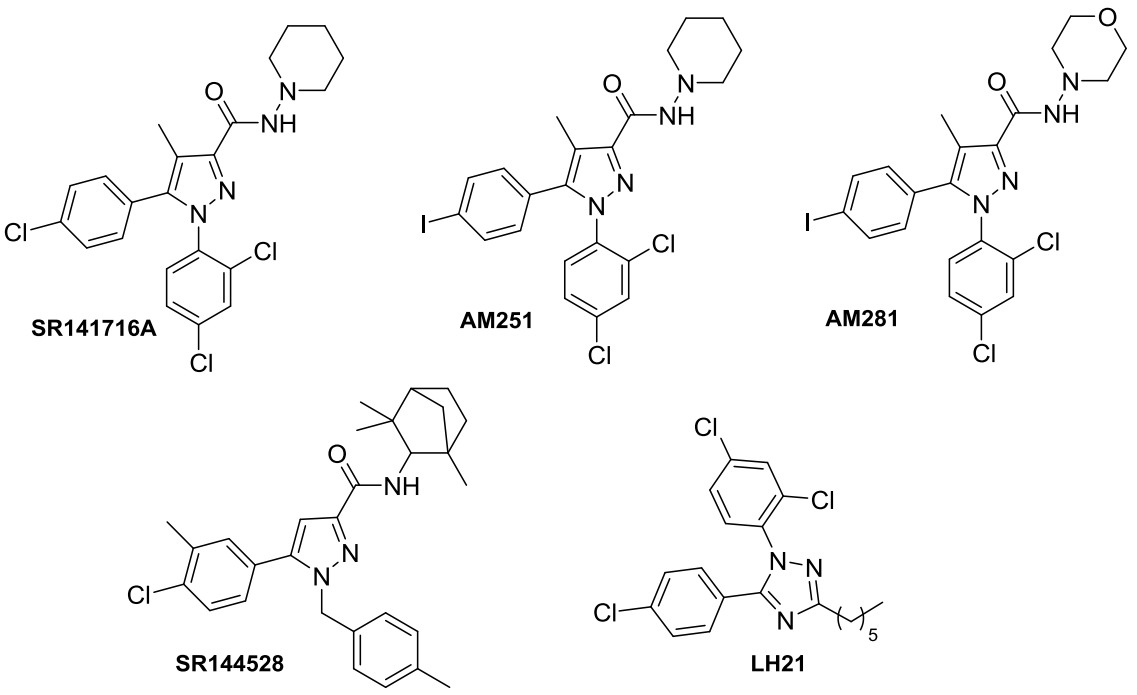

Figure 8. Arylpyrazoles SR141716A, AM251, AM281, SR144528, and LH21.

Indole-2-carboxamides

In the last years, allosteric modulation has emerged as a very attractive pharmacological approach in the cannabinoid field.[72] Allosteric modulators can provide mechanisms for fine-tuning the receptor response while reducing side effects.[81] From this perspective, 5-chloro-3-ethyl-*N*-(4-(piperidin-1-yl)-phenethyl)-1*H*-indole-2-carboxamide (ORG27569, figure 9) was identified as the prototypical allosteric modulator for the CB_1R.[82] ORG27569 is able to increase orthosteric CP55,940 binding affinity but decreases CP55,940 agonist efficacy in CB_1R Gα-mediated pathways assays.[83] SAR analysis of indole-2-carboxamides revealed the wide potential of this scaffold for developing CB_1R allosteric modulators.[84–87] For instance, a derivative developed by Kendall and coworkers[72,86,87] (LDK1258) exhibits an improved CB_1R allosteric profile.

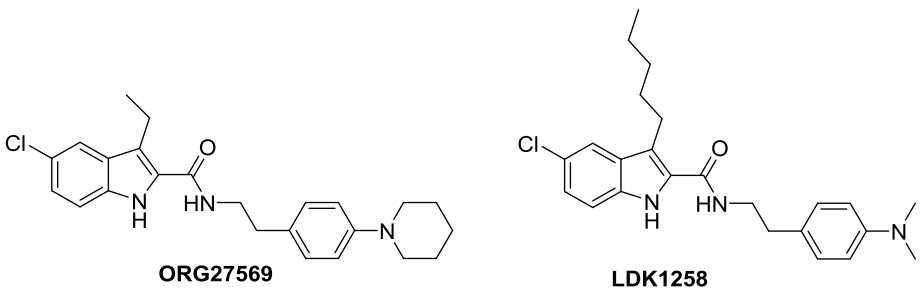

Figure 9. Indole-2-carboxamides ORG27569 and its derivative LDK1258.

Other cannabinergic ligands

Other classes of ligands that exhibit interesting cannabinoid activity have been identified in the last years. These compounds do not fall into the structural categories previously mentioned. For example, the company Eli Lilly developed the diarylbenzofuran[88] scaffold describing the ability of the novel compounds to act as selective CB_1R inverse agonists. Diarylmethyleneazetidine analogues have been reported by Aventis Pharma as CB_1R receptor antagonists. Furthermore, Bayer Healthcare identified the cannabinoid potential of the biaryl ether core reporting a potent CB_1R/CB_2R agonist (BAY38-7271)[89] and a CB_1R partial agonist (BAY59-3074).[90]

Recently, the CB_2R have centered much attention leading to the development of scaffolds such as 1,8-naphthyridine-3-carboxamides,[91,92] quinoline-2,4(1*H*,3*H*)-diones,[93] or triazolopyrimidine[94] derivatives which were described as CB_2R agonists displaying weak affinity towards CB_1R. Moreover, the pharmaceutical company Shionogi discovered the potential of the 3-carbamoyl-2-pyridone scaffold targeting the ECS.[95] In fact, the CB_1R/CB_2R dual agonist S-444823[96] and the CB_2R agonist S-777469[97] were characterized as antipruritic agents and were tested in late stage clinical trials for treating atopic dermatitis. Figure 10 illustrates different hit compounds commented herein. However, these are only representative examples of the research that is being done in this drug discovery field. Nonetheless, more efforts need to be done to identify better chemotypes especially with improved selectivity and druggability profile.

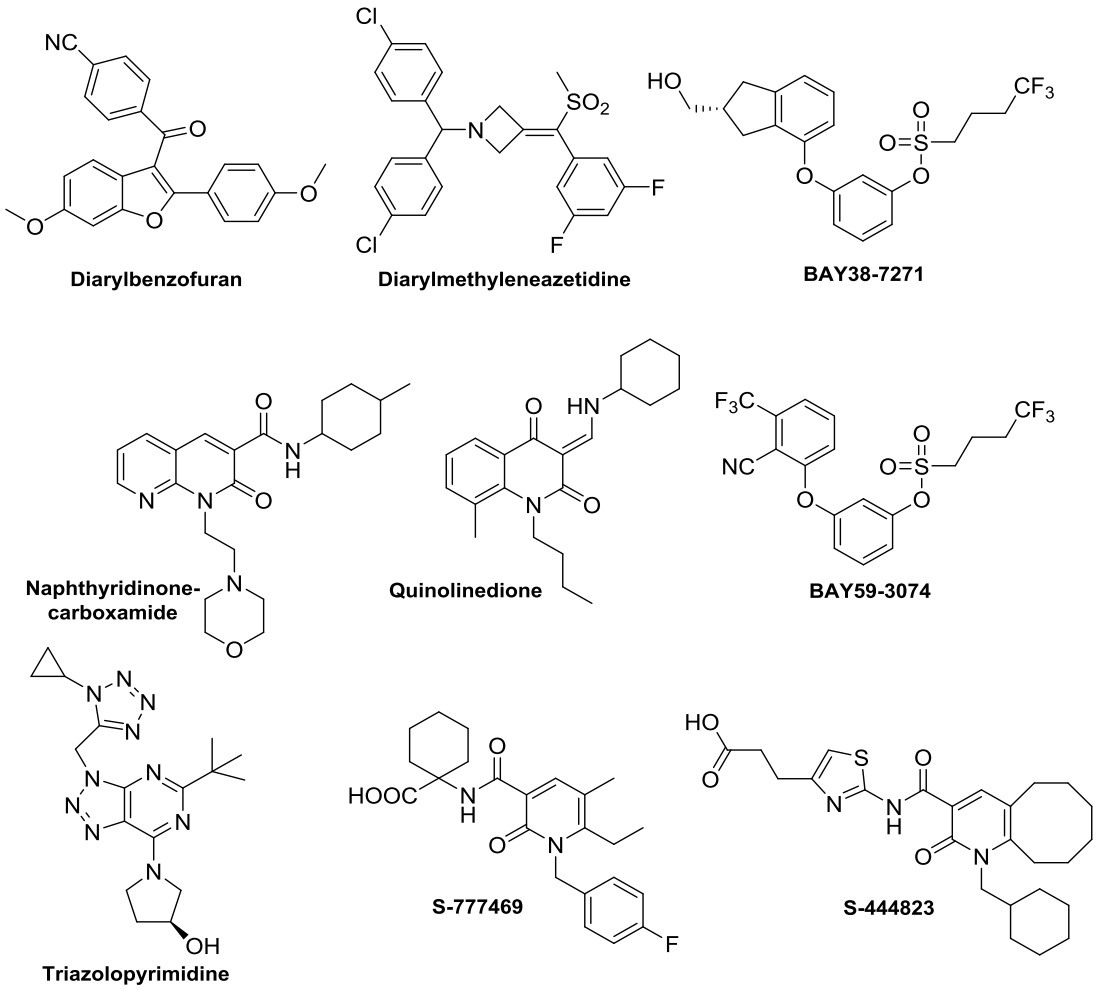

Figure 10. Representative ligands from novel cannabinergic scaffolds: diarylbenzofuran, diarylmethyleneazetidine, biaryl ethers (BAY38-7271 and BAY59-3074), 1,8-naphthyridin-2(1*H*)-one-3-carboxamide, quinoline-2,4(1*H*,3*H*)-dione, triazolopyrimidine and 3-carbamoyl-2-pyridones (S-777469 and S-444823).

1.3 Therapeutic perspectives

It is widely demonstrated that compounds targeting the ECS, particularly CB_1R and/or CB_2R, have therapeutic potential for the clinical management of an ever growing number of disorders.[98] These include inflammatory and neuropathic pain, neurological pathologies or cancer among others. However, just a few of these diseases can be treated with cannabinoid-based medicines nowadays. Marinol® (dronabinol, synthetic Δ^9-THC) and Cesamet® (nabilone, a THC synthetic analogue, figure 6) can be prescribed in several countries as antiemetic drugs for chemotherapy-induced nausea and vomiting,[99,100] and for anorexia[101] treatment in patients with AIDS. Sativex® (nabiximols, a

combination of Δ^9-THC and CBD, 1:1 ratio) is used for the symptomatic relief of neuropathic pain in adults suffering multiple sclerosis, and as an adjunctive analgesic treatment for adult cancer patients. Rimonabant (SR141716A, figure 8), a CB_1R antagonist/inverse agonist, was commercialized in 2006 as Acomplia® for the management of obesity.[102] Unfortunately, the beneficial effects were accompanied by a significantly increase of depression, anxiety, headache, and suicidal thoughts which forced its withdrawal from the market few years later.

Even though CB_1R/CB_2R agonists are currently in the forefront of clinical research[103] for different applications such as cancer and neuroprotection, there is an increasing interest in exploiting novel pharmacological strategies.[72] CB_2R selective agonists or peripherally restricted CB_1R/CB_2R agonists exhibit a promising therapeutic potential for treating various pathologies while avoiding the adverse psychotropic effects related to the modulation of CB_1R in the brain.[104] CB_1R and/or CB_2R antagonists or inverse agonist as well allosteric cannabinoid ligands are also emerging and may be useful in the treatment of certain diseases.[70,72] Nonetheless, more preclinical and specially clinical research needs to be done in this field.

Pain

The analgesic effects of phytocannabinoids have been known for centuries. Antinociceptive properties of cannabinoids are not surprising since CBRs are largely expressed in CNS areas which control pain modulation such as spinal dorsal horn and the dorsal root ganglion.[105] Consequently, the ECS represents a very interesting target for pain treatment.[106]

As already mentioned, CB_1R/CB_2R agonists are already in the clinic in certain countries for the treatment of neuropathic pain related to multiple sclerosis or cancer treatment. However, psychotropic effects due to central CB_1R activation are major limitations for advancing therapies. From this perspective, CB_2R selective agonists are potential candidates in the management of pain as revealed in a wide variety of *in vitro* and *in vivo* models of inflammatory, post-operative or neuropathic pain.[107] Furthermore, pharmacological strategies that enhance levels of

endocannabinoids by inhibiting enzymes controling endocannabinoid deactivation also exert antinociceptive activity.[106]

Cancer

Besides their well-established palliative effects on some cancer-associated symptoms, cannabimimetics have recently shown to produce antitumor activity in different models of cancer. *In vitro* and *in vivo* data revealed their ability to reduce tumor growth, and to inhibit angiogenesis, migration and metastasis.[100,108,109] Potential pharmacological approaches for cancer treatment involving the ECS will be further described in the second chapter of this dissertation.

Emesis, obesity and metabolic disorders

The ECS has widely demonstrated an important role in the regulation of metabolic physiological processes, specially in food intake, energy balance, glucose and lipid metabolism.[110,111] As previuosly mentioned, dronabinol and nabilone, are currently on the market for antiemetic purposes.

Based on the role of the endocannabinoids as orexigenic mediators, inhibition of CB_1R has been considered a new promising pharmacological approach for he treatment of obesity and metabolic syndrome. However, when the psychiatric side effects of rimonabant forced its withdrawal from the clinic, the development of CB_1R antagonist and inverse agonists significantly diminished.[112,113]

Compounds acting preferentially through CB_2R have shown their efficacy in a rat model of alcoholic hepatic steatosis by decreasing the liver/body weight ratio and hepatic triglyceride content.[114,115] Consequently, CB_2R ligands represent a potential new alternative for treatment of some metabolic disorders.

Neurodegenerative diseases

The wide expression of CBRs in the CNS suggests the involvement of the ECS in neurophysiological processes.[116] For this reason, this system was widely validated as an outstanding target for the treatment of numerous brain-related pathologies such as motor disorders,[117] adult and neonatal ischemia,[118] brain trauma,[119,120] epilepsy,[121–123] memory-related disorders,[124] or

neurodegeneration.[125,126] Cannabinoids exhibit neuroprotective effects, they participate in the regulation of neuronal homeostasis and survival what confers them the ability to inhibit events related to the progression of neurodegeneration such as excitotoxicity, oxidative stress, or neuroinflammation.[116,127] Different pharmacological studies provide evidence of their potential in the management of neurodegenerative diseases such as Parkinson´s disease,[128] Alzheimer´s disease,[129,130] amyotrophic lateral sclerosis,[131] Huntington's disease,[31,132] or multiple sclerosis.[133,134]

Although, CB_1R is the main receptor of the CNS, the presence of CB_2R in microglia and neuronal cells as well as its role in the immune system,[26–28] suggest the possibility to use CB_2R agonists to treat certain neurological conditions without psychotropic unwanted effects.[135,136] Alternative pharmacological approaches to achieve neuroprotection may be to enhance the endogenous cannabinoid tone or allosteric modulation of CBRs.[66,137] The non-psychoactive compound CBD have also attracted much attention in this field. Indeed, its anti-convulsive properties have recently encouraged different clinical trials in severe pediatric epilepsies such as Dravet syndrome and Lennox-Gastaut syndrome.[121]

Other applications

Aside from neurology, cancer and metabolism there seems to be a diverse range of possibilities for the therapeutic use of cannabinoids. The role of the ECS has been extensively studied in pathophysiological conditions such as gastrointestinal disorders,[138] atherosclerosis and certain other cardiovascular diseases.[139] Cannabinoids have also shown a promising potential in the management of bone-related diseases,[140] immune disorders,[141] drug addiction[142] or cerebral malaria.[143]

Preclinical evidence thoroughly confirmed that CBRs are outstanding targets for developing useful medications for numerous ailments. Nonetheless, a deeper understanding of its pharmacology as well as novel drugs and therapeutic approaches are needed to overcome their limitations. Additionally, there is a clear need for human clinical research to confirm their effectiveness in patients.

2. Background and aims

The separation of the therapeutic effects of cannabinoids from their psychotropic effects has been long pursued in the development of ECS modulators. In this sense, CB_2R, represents a promising target for the treatment of numerous disorders without serious undesired CNS side effects. In this context, the main purpose of this chapter is the synthesis, optimization and evaluation of selective CB_2R ligands.

Previous work in our research group led to the identification of a novel cannabinoid scaffold: the chromenopyrazole (figure 11, left). This new tricyclic structure was designed in analogy to the classical cannabinoid cannabinol, bearing a benzopyran moiety but exploring for the first time the contribution of a pyrazole ring in place of the CBN´s phenyl group. In this study, a series of chromenopyrazoles were described as non-psychoactive and selective CB_1R agonists with peripheral antinociceptive properties.[144] Different lipophilic side chains were studied at the pharmacophoric position 7 obtaining the best results for the 1,1-dimethylheptyl derivatives.

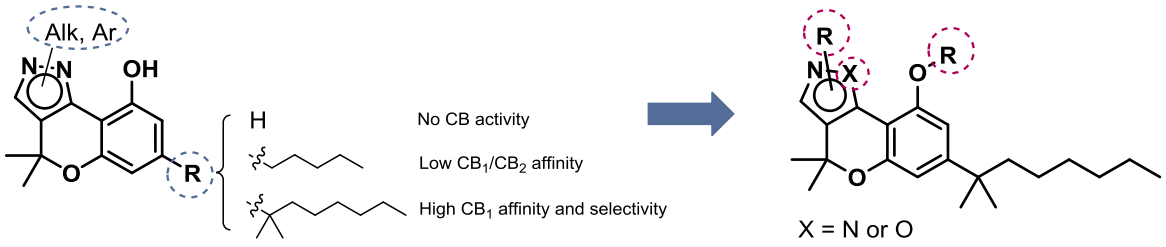

Figure 11. Structural modifications on the chromenopyrazole scaffold. On the left, results obtained in 2012;[144] on the right novel substitution patterns.

In an attempt to target the CB_2R, we proposed different structural modifications on the chromenopyrazole scaffold (figure 11, right) retaining the mentioned aliphatic chain. We decided to explore the conversion of the phenolic hydroxyl, a pharmacophoric moiety of classical cannabinoids, to different alkoxy groups in order to study the importance of this position in our heterocyclic core. Moreover, different pyrazole substituents as well as bioisosteric replacement of the pyrazole by an isoxazole have been explored for further fine-tuning of CBRs affinity and selectivity.

With these considerations in mind, the first part of this chapter is devoted to the identification of CB_2R ligands by exploring pharmacophoric features in the chromenopyrazole scaffold. Specifically, the aims of section 3.1 are:

- Synthesis and structural characterization of novel 7-(1,1-dimethylheptyl)-chromenopyrazole derivatives.[a]
- Evaluation of their affinity and activity at CB_1R and CB_2R.[b,c]
- Prediction of their pharmacokinetical profile by *in silico* approaches.[a]
- Molecular modeling investigation on the structural features required for CB_1R/CB_2R affinity and selectivity.[d]

Regarding the recent cannabinoid literature and the identification of different cannabinoid homo- and heterodimers in different tissues and cell lines, we proposed the synthesis of chromenopyrazole bivalent ligands as potential tools for the study of CB_2 homodimers. Previous findings in section 3.1 led to design these new structures. Accordingly, the specific aims of section 3.2 are as follows:

- Synthesis of homobivalent chromenopyrazoles and their corresponding monovalent analogues.[a]
- Evaluation of their affinity for CB_1R and CB_2R by radioligand binding assays.[b]
- Appraisal of their functionality in a cAMP screening.[c]

a) Performed by PM at Instituto de Química Médica (CSIC).
b) Performed in collaboration with Prof. Javier Fernández-Ruiz (Facultad de Medicina, UCM).
c) Performed in collaboration with Prof. Rafael Franco (Facultad de Farmacia, UB).
d) Performed by PM hosted by Prof. Patricia Reggio (Chemistry Department, University of North Carolina at Greensboro).

3. Results

3.1 From CB_1R towards CB_2R selectivity

3.1.1 Synthesis

Compounds **1.4**–**1.38** were synthesized following the synthetic route shown in scheme 1. Firstly, demethylation of the commercially available 5-(1,1-dimethylheptyl)-1,3-dimethoxybenzene with boron tribromide provided the desired resorcinol **1.1**. Chromanone **1.2** was obtained upon treatment of 5-(1,1-dimethylheptyl)-1,3-dihydroxybenzene (**1.1**) with 3,3-dimethylacrylic acid in presence of phosphorus pentoxide using methanesulfonic acid as solvent at 70 ºC. In order to deepen the study of this reaction, the influence of different 5-alkyl-substituted resorcinols on the formation of 2,2-dimethyl-chroman-4-ones was examined experimentally and theoretically. These data are reported in Appendix 1 of this dissertation.

Following with our synthetic route (scheme 1), 7-(1,1-dimethylheptyl)-5-hydroxy-3-(hydroxymethylen)-2,2-dimethylchroman-4-one (**1.3**) was obtained by α–formylation of **1.2** under microwave conditions using an excess of sodium hydride followed by the addition of ethyl formate. Then, condensation of the β-ketoaldehyde **1.3** with the appropriate hydrazine gave the corresponding 7-alkyl-1(2),4-dihydro-4,4-dimethylchromeno[4,3-c]pyrazol-9-oles **1.4**–**1.13**. Two regioisomers can be form, *N*1- and *N*2-substituted pyrazoles. As expected, with alkylhydrazines, both (*N*1/*N*2) regioisomers (**1.5a**, **1.5b**, **1.6a**, **1.6b**, **1.9a**, and **1.9b**) were isolated with different relative ratios. *N*2-Isomer was formed as the major compound with methylhydrazine, whereas, an approximate relative ratio of 1:1 was obtained for ethyl and hydroxyethyl regioisomers. In the case of the arylhydrazines, reaction with β-ketoaldehyde **1.3** resulted in the isolation of one isomer, corresponding to the *N*1-aryl-chromenopyrazole (**1.7**, **1.8**, **1.11** and **1.12**). This may be due to the fact that the substituted nitrogen of arylhydrazines is less nucleophilic.

Compound **1.10** was prepared by condensation of chromenopyrazole **1.4** with formaldehyde to obtain the hydroxymethylpyrazole derivative following the procedure previously reported.[145,146]

Although HPLC-MS analysis of the crude displayed both regioisomers, only the major one (*N*2-pyrazole) was properly isolated and characterized.

The synthesis of compounds **1.14–1.38** was achieved by alkylation of the phenolic oxygen of chromenopyrazoles **1.4–1.8** with the corresponding alkyl halide. Alkylation of **1.4** led to *N*-alkylated, and *N*-/*O*- alkylated subproducts that decreased the yield of the desired *O*-alkylated compounds.

To increase structural diversity at this position and expand the SAR study, derivatives with different R^2 substituents such as methyl, benzyl, hydroxypropoxy or bromopropoxy were synthesized.

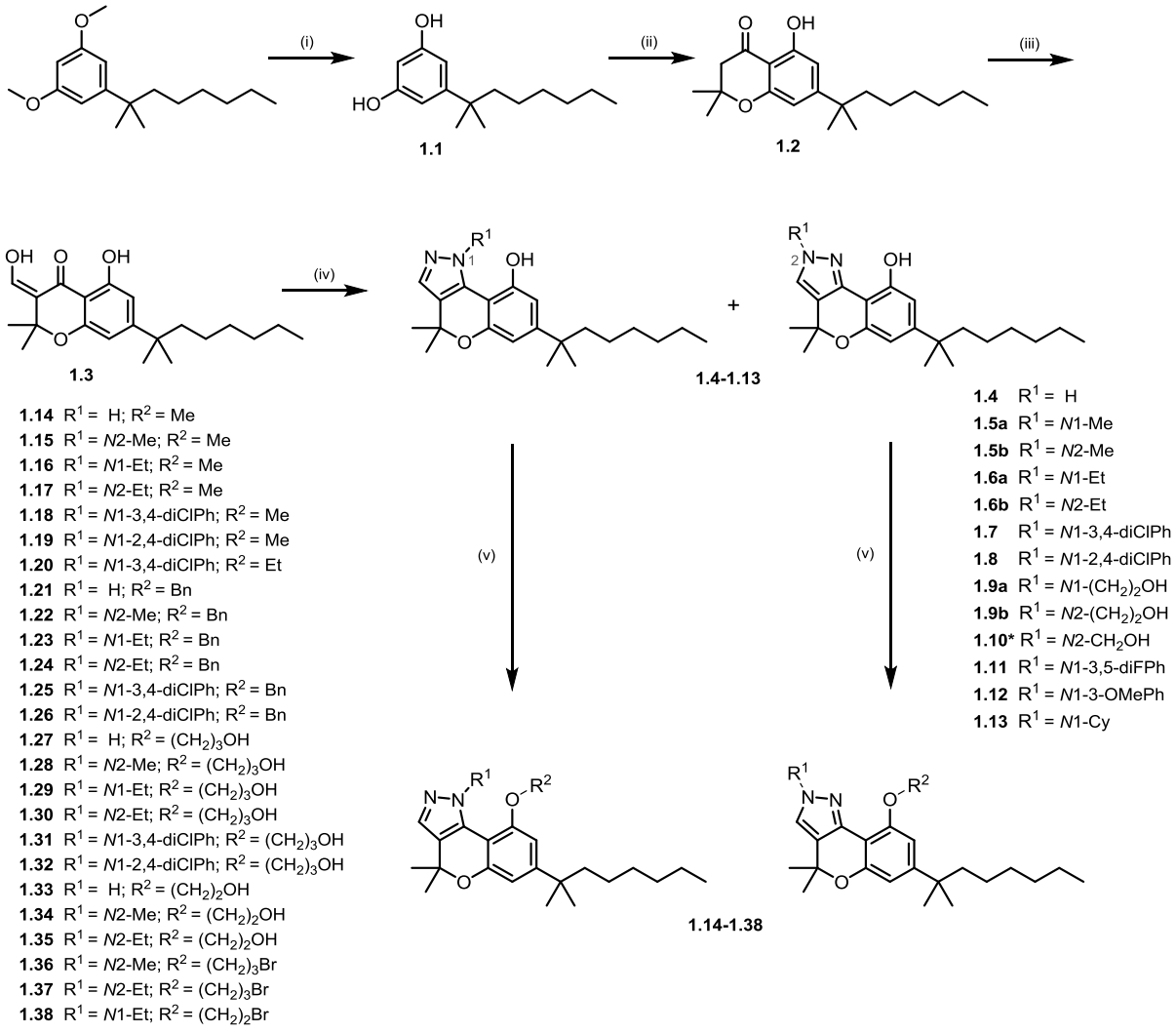

Scheme 1. Synthesis of chromenopyrazoles **1.14–1.38**. Reaction conditions: **(i)** BBr_3, CH_2Cl_2, overnight, 0 ºC-r.t., 92%; **(ii)** 3,3-dimethylacrylic acid, methanesulfonic acid, P_2O_5, 8 h, 70 ºC, 81%; **(iii)** a) NaH, THF, MW, 25 min, 45 ºC; b) ethyl formate, MW, 25 min, 45 ºC, 76%; **(iv)** corresponding hydrazine, EtOH, 1-4 h, 40 ºC, 2-82%; **(v)** a) NaH, THF, 10 min, b) 1-bromo or iodoalkane, 1-12 h, reflux, 22-96%. *****Compound **1.10** was synthesized by reaction of **1.4** with formaldehyde in EtOH, 5 h, reflux, 69%.

To explore the SAR of the phenol substitution, we decided to prepare two conformationally restricted etherified derivatives by incorporating a fourth ring. For that purpose, the pyrano-chromenopyrazoles **1.39** and **1.40** were synthesized as depicted in scheme 2. Alkoxychromenopyrazoles **1.29** and **1.30** were obtained by *O*-alkylation of **1.6a** and **1.6b** with 3-bromopropanol as previously detailed. Subsequent cyclodehydration with phosphorus pentoxide yielded the desired condensed cyclic ethers.

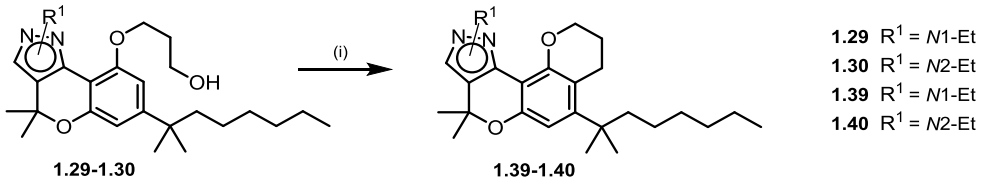

Scheme 2. Synthesis of pyrano-chromenopyrazoles **1.39** and **1.40.** Reaction conditions: **(i)** P_2O_5, toluene, 1 h, reflux, 52-87%.

Further exploration of our scaffold led us to the bioisosteric replacement of the pyrazole by an isoxazole moiety. For this purpose, condensation of β-diketone **1.3** to isoxazole **1.41** was efficiently achieved upon reaction with hydroxylamine hydrochloride under ethanol refluxing conditions. Phenolic alkylation of chromenoisoxazole **1.41** yielded methoxy (**1.42**) and hydroxypropoxy (**1.43**) derivatives. This reaction was performed following the procedure described for alkoxychromenopyrazoles.

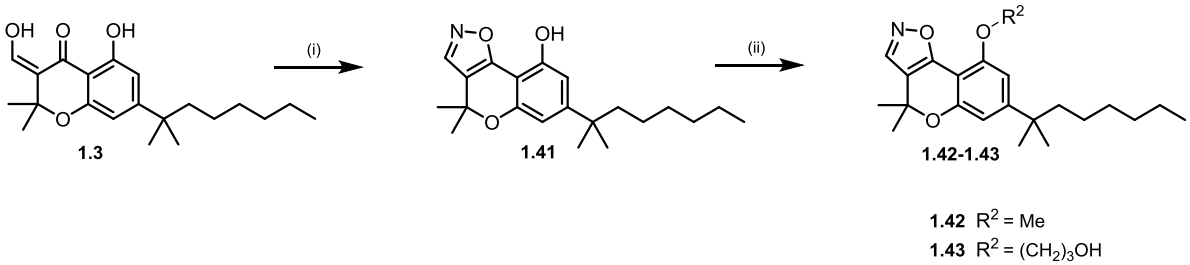

Scheme 3. Synthesis of chromenoisoxazoles **1.41–1.43**. Reaction conditions: **(i)** Hydroxylamine hydrochloride, ethanol, 45 min, reflux, 91%; **(ii)** a) NaH, THF, 10 min, 0 ºC; b) 1-bromo or iodoalkane, 1-3 h, reflux, 22-61%.

3.1.2 Cannabinoid binding studies

The synthesized compounds were evaluated *in vitro* for their ability to displace the radioligand [^{3}H]CP55,940 from human CB_1R (*h*CB_1R) and CB_2R (*h*CB_2R). As source of these receptors, commercial membrane preparations of HEK293 EBNA cells stably expressing each receptor type were used. Initially, compounds were screened at 40 μM. A complete dose–response curve was generated for compounds that displaced the radioligand over 70% in the preliminary screening. Table 1 lists the experimental binding affinities (K_i values) from the respective displacement curves for *h*CB_1R and *h*CB_2R.

As previously reported by us,[144] chromenopyrazoles **1.4** to **1.8** showed significant to high affinity and selectivity for CB_1R (K_i: 4.5–28.5 nM). These CB_1R chromenopyrazoles were characterized by a free phenol group. *N*-Methyl, or ethyl substitution of the pyrazole ring did not drastically changed CB_1R binding and selectivity. With respect to the novel substitutions that have been introduced on the pyrazole ring (**1.9**–**1.13**), the presence of hydroxyalkyl groups (**1.9a**, **1.9b** and **1.10**) resulted in loss of selectivity but with high to moderate affinity constants for both CBRs. The nature of the *N*-substituents clearly influenced the CBRs binding. Aromatic substituents such as 3,5-difluorophenyl or 4-methoxyphenyl (**1.11** and **1.12**) led to loss of affinity while the *N*1-cyclohexyl derivative **1.13** exhibited CB_2R selectivity.

Regarding the *O*-alkylated chromenopyrazoles, different features could be highlighted from our results. In general, the loss of the free phenolic group led to compounds displaying high to moderate CB_2R affinity with low or lack of CB_1R activity. Among the phenolic substituents (R^2), alkyl groups, in particular propanol, gave the best CB_2 selectivity ratios whereas bencyloxy-chromenopyrazoles caused a significant decrease in this percentage. It is interesting to note that the condensation of a 2,4*H*-pyran to the chromenopyrazoles structure (**1.39** and **1.40**) which was done for restricted conformational issues, elicited excellent CB_2R selectivity.

The pyrazole substitution also contributes to determine affinity and selectivity issues. As depicted in table 1, unsubstituted pyrazoles (**1.14**, **1.21**, **1.27** and **1.33**) revealed high affinity towards both

receptors regardless the nature of the phenol substitution. *N*-Aryl substitution (**1.18**, **1.19**, **1.25**, **1.26**, **1.31** and **1.32**) led to inactive derivatives while *N*-methyl or ethyl substituents (**1.15**–**1.17**, **1.22**–**1.24**, **1.28**–**1.30** and **1.34**–**1.38**) resulted in high to moderate CB_2R affinity and selectivity independently of the nature of the phenol substituent. These results suggest that CB_2Rs do not tolerate bulky aromatic substituents in the pyrazole ring.

In an effort to explore the chromenopyrazoles scaffold for cannabinoid activity, we proposed the bioisosteric replacement of the pyrazole by an isoxazole. This structural modification on the initial scaffold led to very potent cannabinoid ligands. Compound **1.41** exhibits high affinity for both CB_1R and CB_2R with K_i values in the low nanomolar range (CB_1R K_i: 15.4 nM; CB_2R K_i: 5.3 nM). The results obtained for *O*-alkylated chromenopyrazoles prompted us develop the alkoxy derivatives of chromenoisoxazole **1.41**. Replacement of the phenolic hydroxyl group with either a methoxy (**1.42**) or a hydroxypropoxy (**1.43**) group led to CB_2R selectivity. Chromenoisoxazole **1.42** is the most potent and selective ligand of our series, being over 3000-fold selective for CB_2R with an affinity constant of 12.8 nM.

Table 1. Binding affinity of chromenopyrazoles **1.4**–**1.43** and the reference cannabinoids SR141716, WIN55,212-2 for *h*CB_1R and *h*CB_2R.

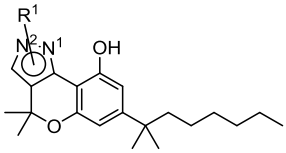

1.4–1.13

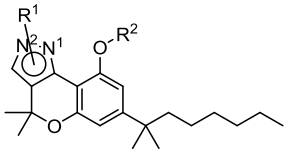

1.14–1.38

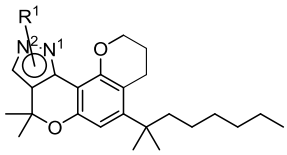

1.39–1.40

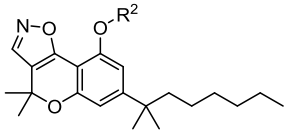

1.41–1.43

Compd	R^1	R^2	CB_1R K_i (nM)[a]	CB_2R K_i (nM)[a]	CB_1R Selectivity[b]	CB_2R Selectivity[c]
1.4	H	H	28.5 ± 23.7	>40000	>1428	-
1.5b	*N*2-Me	H	14.2 ± 2.9	>40000	>2816	-
1.6a	*N*1-Et	H	4.5 ± 0.6	>40000	>8888	-
1.6b	*N*2-Et	H	18.6 ± 2.9	>40000	>2150	-
1.7	*N*1-3,4-diClPh	H	514 ± 205	270	-	1.9
1.8	*N*1-2,4-diClPh	H	5.2 ± 4.3	>40000	>7692	-
1.9a	*N*1-$(CH_2)_2OH$	H	19.1 ± 8.9	366 ± 169	19.1	-
1.9b	*N*2-$(CH_2)_2OH$	H	54.4 ± 8.1	39.6 ± 7.1	-	1.4
1.10	*N*2-CH_2OH	H	218.1 ± 40.5	59.4 ± 31.2	-	3.7

1.11	*N*1-3,5-diFPh	H	>40000	>40000	-	-
1.12	*N*1-3-OMePh	H	6440 ± 655	562.0 ± 13.2	-	11.5
1.13	*N*1-Cy	H	1140 ± 190	53.7 ± 11.8	-	21.5
1.14	H	Me	272 ± 75	87.1 ± 10.6	-	3.1
1.15	*N*2-Me	Me	4159 ± 542	66.4 ± 13.29	-	62.6
1.16	*N*1-Et	Me	5040 ± 670	159.5 ± 31.2	-	31.6
1.17	*N*2-Et	Me	2930 ± 470	92.6 ± 17.1	-	31.8
1.18	*N*1-3,4-diClPh	Me	2324 ± 327	2256 ± 499	-	-
1.19	*N*1-2,4-diClPh	Me	1693 ± 239	1493 ± 272	-	-
1.20	*N*1-3,4-diClPh	Et	>40000	3545 ± 89	-	>11.3
1.21	H	Bn	22.4 ± 4.1	93.3 ± 29.5	4.2	-
1.22	*N*2-Me	Bn	702.4 ± 98.6	208.8 ± 39.5	-	3.3
1.23	*N*1-Et	Bn	613.7 ± 206.9	295.9 ± 53.6	-	2.0
1.24	*N*2-Et	Bn	671.3 ± 166.1	212.2 ± 49.4	-	3.1
1.25	*N*1-3,4-diClPh	Bn	>40000	3740 ± 297	-	>10.7
1.26	*N*1-2,4-diClPh	Bn	>40000	>40000	-	-
1.27	H	$(CH_2)_3OH$	450.4 ± 9.9	26.0 ± 7.1	-	17.3
1.28	*N*2-Me	$(CH_2)_3OH$	>40000	364.0 ± 68.9	-	>109.9
1.29	*N*1-Et	$(CH_2)_3OH$	1613 ± 284	440 ± 145	-	3.6
1.30	*N*2-Et	$(CH_2)_3OH$	>40000	97.4 ± 9.9	-	>410.7
1.31	*N*1-3,4-diClPh	$(CH_2)_3OH$	>40000	>40000	-	-
1.32	*N*1-2,4-diClPh	$(CH_2)_3OH$	>40000	>40000	-	-
1.33	H	$(CH_2)_2OH$	64.8 ± 18.0	3.6 ± 0.7	-	18
1.34	*N*2-Me	$(CH_2)_2OH$	1086 ± 198	39.8 ± 24.9	-	27.2
1.35	*N*2-Et	$(CH_2)_2OH$	6512 ± 714	210.6 ± 93.2	-	31.0
1.36	*N*2-Me	$(CH_2)_3Br$	1482 ± 221	77.3 ± 0.87	-	19.1
1.37	*N*2-Et	$(CH_2)_3Br$	657 ± 159	87.1 ± 14.2	-	7.5
1.38	*N*1-Et	$(CH_2)_2Br$	1331 ± 320	78.7 ± 11.3	-	16.9
1.39	*N*1-Et	-	>10000	563.8 ± 13.1	-	>17.7
1.40	*N*2-Et	-	>40000	121.6 ± 43.5	-	>330.5
1.41	-	H	15.4 ± 12.2	5.3 ± 0.8	-	2.9
1.42	-	Me	>40000	12.8 ± 2.4	-	>3125
1.43	-	$(CH_2)_3OH$	332.6 ± 143.9	65.5 ± 21.8	-	5.1
SR141716	-	-	7.3 ± 0.9	>40000	-	-
WIN55,212-2	-	-	45.6 ± 8.6	3.7 ± 0.2	-	-

[a]Values obtained from competition curves using [^{3}H]CP55940 as radioligand for *h*CB_1R and *h*CB_2R and are expressed as the mean ± SEM of at least three experiments. [b]$K_i(CB_1R)/K_i(CB_2R)$ selectivity ratio. [c]$K_i(CB_2R)/K_i(CB_1R)$ selectivity ratio.

Following the first aims of this chapter concerning the SARs of the chromenopyrazoles as cannabinoids, that were the exploration of the substitution on i) the phenol, ii) the pyrazole, and iii) replacement of pyrazole by isoxazole, some general conclusions can be featured.

i) The phenol substitution seems to play a crucial role in selectivity. CB_1R selective chromenopyrazoles bear a free hydroxyl phenolic group, whereas high CB_2R selectivity was achieved when the phenol was alkylated.

ii) The nature of the pyrazole substituent influences the affinity for CBRs. In general, alkyl groups showed better affinity for CB_1R and/or CB_2R compared to aryl substituents.

iii) The bioisosteric replacement of the pyrazole by an isoxazole resulted in cannabinoid ligands with affinity in the nanomolar range.

3.1.3 Functional assays

Although radioligand binding assays are widely used to determine the affinities of ligands for a receptor, they do not reveal information about how ligands modulate receptor activity. Thus, functional receptor assays are required in order to evaluate the properties of a ligand. Cannabinoid activity of certain chromenopyrazoles derivatives was evaluated through different functional experiments. Compounds were selected according to high CB_2 selectivity and/or affinity criteria.
Activity at CB_2R was appraised through cAMP accumulation experiments. To further assess functionality through a different outcome, GTPγS binding assays were performed. In addition, selected CB_2R ligands were evaluated using an *in vitro* assay on BV-2 microglial cells.

cAMP accumulation assay at CB_2R.

Adenosine 3',5'-cyclic monophosphate (cAMP) is the main second messenger in the signalling pathway for G_i protein-coupled receptors. The G_i activation induces the inhibition of the effector activity (adenylate cyclase), resulting in a decrease of intracellular cAMP concentration. Detection of

this reduction in cAMP production depends on the basal level of cAMP present within the cells. Using forskolin (Fk) to activate adenylate cyclase allows an easier detection of this inhibitory effect. Functional properties of our new molecules were investigated in cAMP assays using HEK293 cells stably expressing the human CB_2 receptor subtype.

Agonism. Effects of tested compounds on forskolin-stimulated cAMP levels were determined in a preliminary screening at two concentrations (at 200 nM and 1 μM). As CB_2 is a $G_{i/o}$-coupled receptor, its activation by agonists leads to inhibition of forskolin-stimulated cAMP accumulation, whereas inverse agonists may facilitate cAMP production and antagonists do not trigger changes in forskolin-stimulated cAMP levels.

Results obtained from this cAMP screening are depicted in figure 12. Molecules displaying high inhibition of forskolin-stimulated cAMP accumulation (**1.33** and **1.40**−**1.43**) or not showing effect (**1.15**, **1.30** and **1.34**) were selected for further pharmacological characterization. Compounds exhibiting slight inhibitory effect at both concentrations (**1.16**, **1.17**, **1.21**, **1.27**, **1.36** and **1.38**) were considered as potential partial or weak agonists in our screening.

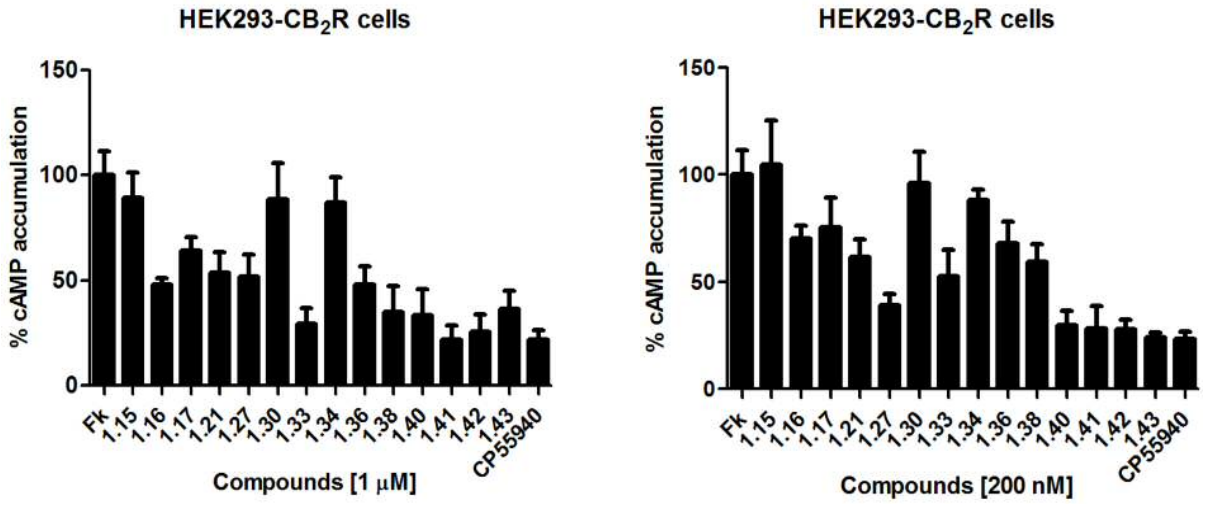

Figure 12. cAMP screening in HEK293 cells stably expressing the human CB_2R type. Results are expressed as percent of forskolin-stimulated cAMP accumulation at a concentration of 200 nM and 1 μM of our compounds and the reference cannabinoid CP55,940. All data result from at least three independent experiments, performed in triplicates.

The tested compounds were also screened in normal HEK293 cells at the same concentrations. As displayed in figure 13, the compounds, as well as the reference agonist CP55,940, did not exert effect in this cell line. These results confirm that the ability of certain chromenopyrazoles and chromenoisoxazoles to inhibit forskolin-stimulated cAMP accumulation was effectively mediated by CB_2R.

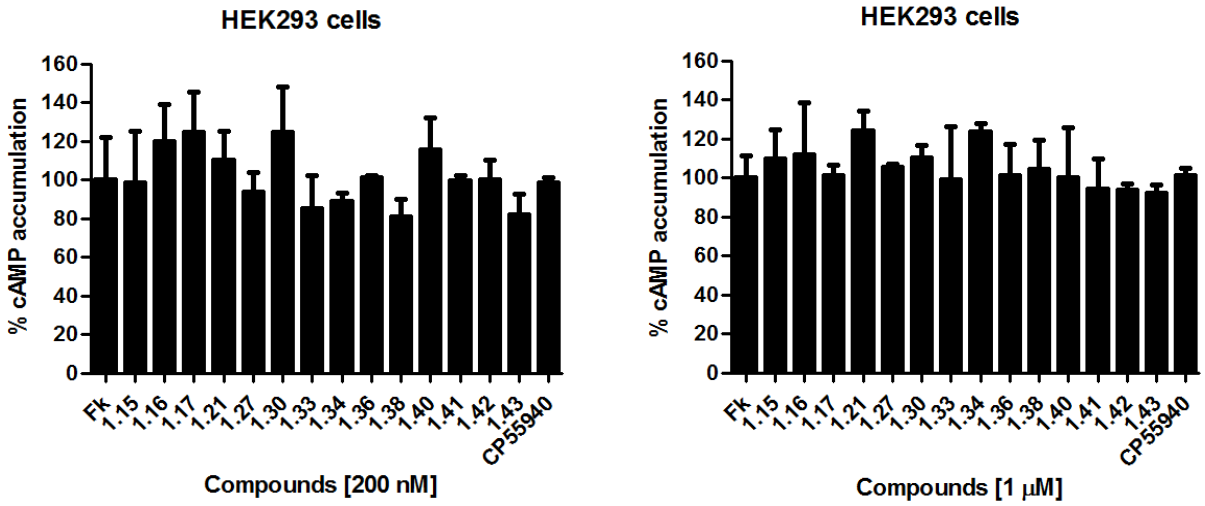

Figure 13. cAMP screening in normal HEK293 cells. Results are expressed as percent of forskolin-stimulated cAMP accumulation at a concentration of 200 nM and 1 μM of test compounds. All data result from at least three independent experiments, performed in triplicates.

For compounds with a good inhibitory effect in the aforementioned cAMP screening (**1.33** and **1.40**−**1.43**), full concentration−response curves were measured and EC_{50} and E_{max} values were determined. CB_2R-activation by **1.33** and **1.40**−**1.43** led to a dose-dependent inhibition of forskolin-stimulated cAMP increase. All these ligands are potent CB_2R agonists showing EC_{50} values in the nanomolar range (table 2). Results obtained for the well-known potent CB_1R/CB_2R agonist CP55,940 and the CB_2R selective agonist JWH133 are consistent with previously published data.[19] It is noteworthy that the most potent and efficacious ligand of our series is the chromenoisoxazole **1.42** (EC_{50} = 4.2 nM), which displays more CB_2R selectivity and potency than the reference cannabinoid agonists. This data highlight **1.42** as a potential lead compound for additional pharmacological development.

Table 2. Functional potencies of compounds **1.33**, **1.40**−**1.43** and the reference cannabinoids CP55,940 and JWH133 at CB_2 receptor determined by measuring the decrease in forskolin-stimulated cAMP levels in HEK293-CB_2R cells.

Compd	R^1	R^2	CB_2R cAMP assays	
			[a]EC_{50} (nM)	[b]E_{max} (%)
1.33	H	$(CH_2)_2OH$	21.6 ± 1.5	95 ± 6
1.40	*N*2-Et	-	25.5 ± 2.0	98 ± 11
1.41	-	H	134.0 ± 2.3	98 ± 9
1.42	-	Me	4.2 ± 1.5	101 ± 10
1.43	-	$(CH_2)_3OH$	14.0 ± 1.9	91± 10
CP55,940	-	-	8.3 ± 1.5	106 ± 9
JWH133	-	-	81.8 ± 1.7	98 ± 11

[a]EC_{50} values were calculated using nonlinear regression analysis. Data are expressed as the mean ± SEM of at least three independent experiments performed in triplicates. [b]Forskolin stimulated cAMP levels were normalized to 100%. E_{max} is the maximum inhibition of forskolin stimulated cAMP levels.

Antagonism. Compounds exhibiting no inhibition of forskolin-stimulated cAMP accumulation in the preliminary screening (**1.15**, **1.30** and **1.34**, figure 12), were subjected to further cAMP studies in HEK293 cells stably expressing CB_2R in order to confirm their functionality. Their effect on CP55,940-induced inhibition of cAMP accumulation was evaluated (figure 14).

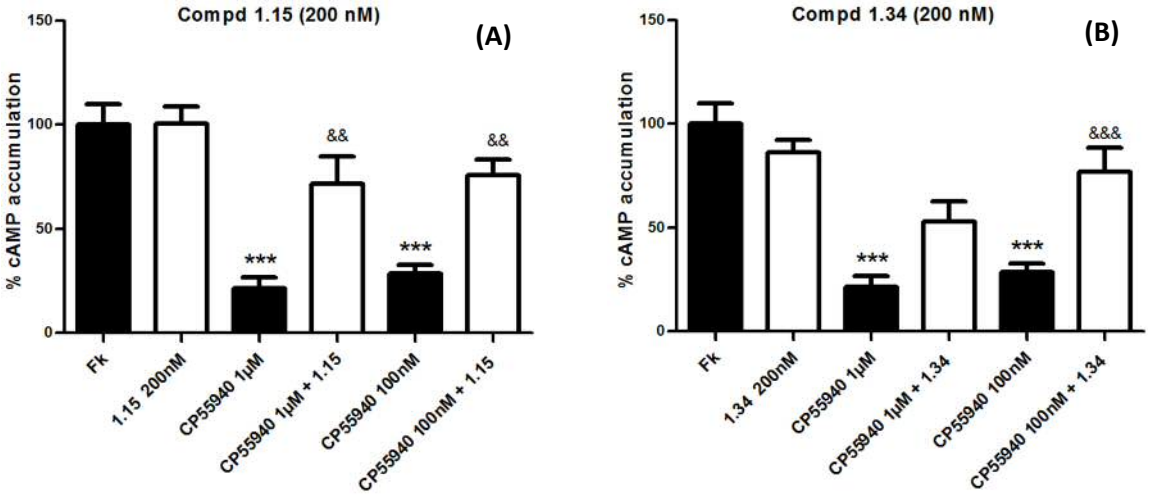

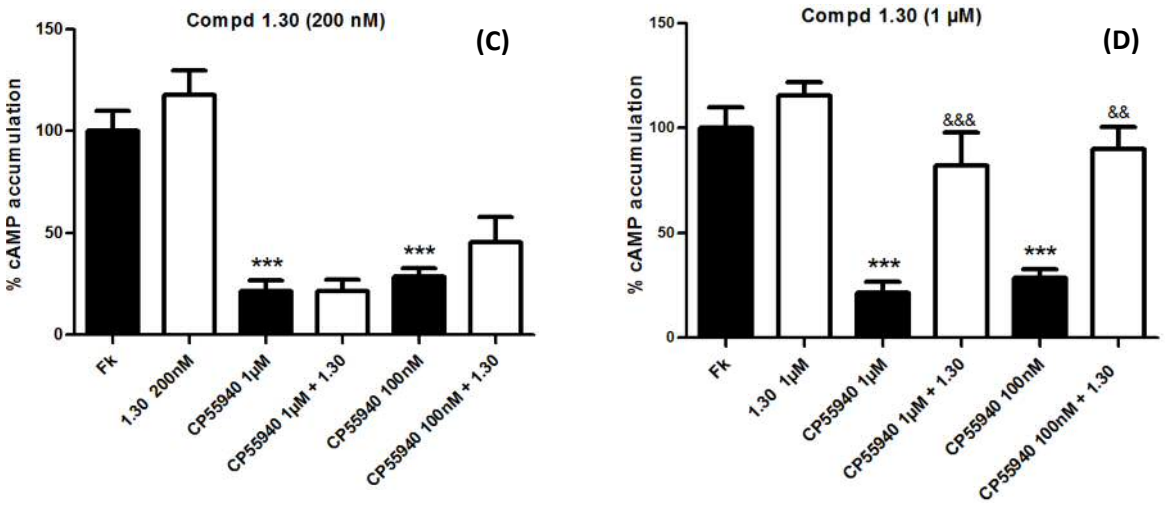

Figure 14. Effect of compounds **1.15**, **1.30** and **1.34** on CP55,940-induced inhibition of cAMP accumulation in HEK293-CB_2R cells. (A) Compound **1.15** at 200 nM; (B) Compound **1.34** at 200 nM; (C) Compound **1.30** at 200 nM; (D) Compound **1.30** at 1 µM. All data result from at least three independent experiments, performed in triplicates. Data were assessed by one-way analysis of variance ($F(5,43)=20.57$, $p<0.0001$ for compound **1.16**; $F(5,42)=17.92$, $p<0.0001$ for compound **1.34**; $F(5,33)=27.16$, $p<0.0001$ for compound **1.30** (C); $F(5,33)=22.03$, $p<0.0001$ for compound **1.30** (D); *$p<0.05$, **$p<0.01$,***$p<0.005$ compounds alone *versus* control (forskolin cAMP accumulation); &$p<0.05$, &&$p<0.01$, &&&$p<0.005$ CB_2 agonist *versus* CB_2 agonist + **1.15**, **1.30** or **1.34**).

As shown in figure 14, in the presence of **1.15** at 200 nM, the inhibitory activity of the reference CB_2 agonist was significantly decreased (at 100 nM and 1 µM). Likewise, 200 nM of **1.34** was found to antagonize the effect of CP55,940 (figure 14, B). At the same concentration, **1.30** did not show this capacity (figure 14, C), however, its administration at 1 µM was able to significantly reverse CP55,940-induced inhibition of cAMP. These data indicate that **1.15**, **1.30** and **1.34** are CB_2R antagonists through this functional readout being **1.15** and **1.34** more potent than **1.30**.

GTPγS binding assays: CB_1R and CB_2R

Activity of selected compounds was carried out by evaluating the coupling of CBR/G-protein, by using the radioligand [^{35}S]-GTPγS (guanosine 5'-O-[gamma-thio]triphosphate). When a GPCR is activated by agonist binding in the presence of GTPγS, it displaces GDP and the G protein is persistently activated. The extent of receptor activation is determined by the difference between basal [^{35}S]-GTPγS binding and binding in the presence of the compound.[147]

Functionality at CB_1R. Even though our main aim is to develop CB_2R selective ligands, the evaluation of compounds with good affinity towards CB_1R (**1.9b**, **1.21** and **1.41**) was considered of interest. GTPγS experiments have been performed in membranes extracted from HEK293 cells stably

expressing CB_1 receptors. Tested compounds present ability to stimulate CB_1R activation acting as agonists of this receptor with EC_{50} values in the nanomolar range (table 3). As reported by us in 2012,[144] the functional activity of CB_1 selective chromenopyrazoles **1.4**, **1.6a** and **1.6b** was evaluated on mouse *vas deferens*. These compounds inhibited the electrically evoked contractile response of this tissue exhibiting a full agonist profile. Therefore, all the CB_1R ligands from this series demonstrated ability to activate CB_1 regardless the functional outcome. Activity of **1.33** at CB_1R remains to be determined.

Table 2. [^{35}S]-GTPγS binding of compounds **1.9b**, **1.21** and **1.41** and the reference cannabinoid WIN55,212-2 for *h*CB_1R.

Compd	R^1	R^2	CB_1R GTPγS assays	
			[a]EC_{50} (nM)	[b]E_{max} (%)
1.9b	*N*1-$(CH_2)_2OH$	H	298.8 ± 54.2	97 ± 52
1.21	H	Bn	191.0 ± 90.8	234 ± 79
1.41	-	H	15.8 ± 8.6	196 ± 111
WIN55,212	-	-	44 ± 30	153 ± 70

[a]EC_{50} values were calculated using nonlinear regression analysis. Data are expressed as the mean ± SEM of at least three independent experiments, each one run in triplicates. [b]E_{max}: Maximal agonist effect, determined using nonlinear regression analysis.

Functionality at CB_2R. Functional properties of compounds **1.33**, **1.41**−**1.43** at CB_2R was further appraised through [^{35}S]-GTPγS binding assays in commercial CB_2R-containing membranes (see experimental section). Dose-response analyses of these new derivatives indicate that they act as full CB_2 agonists through this outcome (table 4). Even though, EC_{50} values are in the nanomolar range, potencies slightly vary from those obtained in cAMP experiments. As in the previous functional readout, chromenoisoxazole **1.42** stands out in GTPγS binding assays being the most potent and selective CB_2R ligand of this series.

Table 4. [^{35}S]-GTPγS binding of compounds **1.33**, **1.41**−**1.43** and the reference cannabinoid HU308 for *h*CB_2R.

Compd	R^1	R^2	CB_2R GTPγS assays	
			[a]EC_{50} (nM)	[b]E_{max} (%)
1.33	H	$(CH_2)_2OH$	95.1 ± 7.2	110 ± 17

1.41	-	H	50.2 ± 24.9	114 ± 37
1.42	-	Me	38.6 ± 6.7	98 ± 8
1.43	-	$(CH_2)_3OH$	539.6 ± 208.1	96 ± 15
HU308	-	-	64.5 ± 1.6	91 ± 7

[a]EC_{50} values were calculated using nonlinear regression analysis. Data are expressed as the mean ± SEM of at least three independent experiments, each one run in triplicates. [b]E_{max}: Maximal agonist effect, determined using nonlinear regression analysis.

Bioassay for CB_2R functionality on cultured cells.

In the course of our studies, activity of CB_2R chromenopyrazoles **1.15**, **1.30** and **1.34** have been also studied in a BV-2 murine microglial cell line. This cell line has been used extensively in research related to neurodegenerative disorders. However, in the present study, we used this cell line for evaluating the functionality of new compounds. The ability of our compounds to reduce lipopolysaccharide (LPS)-induced inflammatory responses in cultures was determined. CB_2R are highly expressed in this microglial cell line so the activation of this receptor results in a decrease of the intensity of the proinflammatory response.[148–150] This response is quantified by measuring the concentration of prostaglandin E2 (PGE2) using an ELISA immunoassay. CB_2R agonists will reduce the inflammatory response (by attenuating LPS-induced PGE2 release), whereas antagonists or inverse agonists of CB_2R reverse agonistic effects and may even increase the inflammatory response produced by LPS. Two well-known CB_2R ligands, the non-selective agonist WIN55,212-2, and the CB_2R selective antagonist/inverse agonist SR144528 were evaluated as reference. As depicted in figure 15, stimulation of BV-2 cells with LPS produced a great increase in PGE2 release which was completely reversed by co-incubation with WIN55,212-2. In addition, the effect of this agonist was completely blocked by SR144528 supporting the fact that PGE2 release is mediated through CB_2R activation.

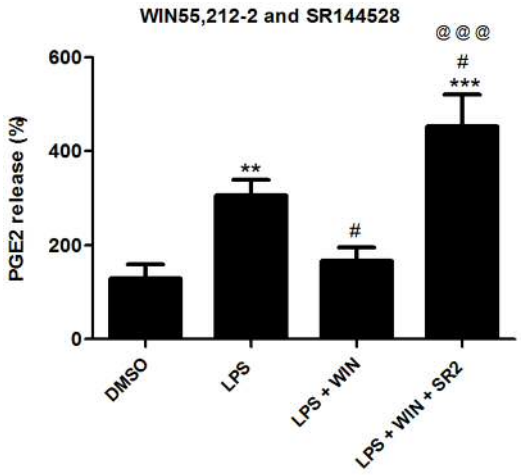

Figure 15. Effects of control ligands WIN55,212-2 (WIN) and SR144528 (SR2) on the LPS-induced release of PGE2 in cultured BV-2 cells. Data were assessed by one-way analysis of variance ($F(3,27) = 11.93$, $p<0.0001$; $^{*}p<0.05$, $^{**}p<0.01$,$^{***}p<0.005$ *versus* control (DMSO-exposed); $^{\#}p<0.05$, $^{\#\#}p<0.01$, $^{\#\#\#}p<0.005$ *versus* LPS; $^{@}p<0.05$, $^{@@}p<0.01$, $^{@@@}p<0.005$ *versus* LPS+WIN).

Chromenopyrazoles **1.30** and **1.34** did not reverse LPS-induced response (figure 15 D and F), however they were able to reverse the effect of WIN55,212-2 suggesting neutral antagonism at CB_2R (figure 16 C and E). In addition, **1.15** showed elevated PGE2 levels when combined with LPS (figure 16 B) suggesting inverse agonistic properties. These data are in agreement with the results obtained in the cAMP assays for compounds **1.30** and **1.34** (figure 14). Results obtained for **1.15** in the LPS-induced PGE2 and cAMP assays differ since **1.15** acted as inverse agonist/antagonist in the LPS assays whereas no inverse agonist was detected in cAMP tests. This variation can be attributed to different sources of CB_2R (BV-2 murine microglial cells and CB_2R-HEK293 EBNA cells).

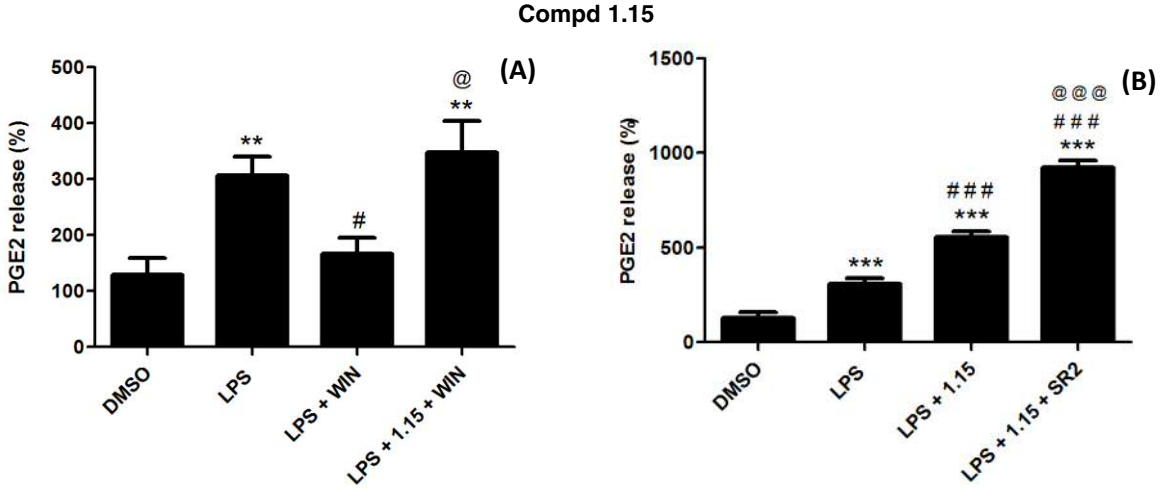

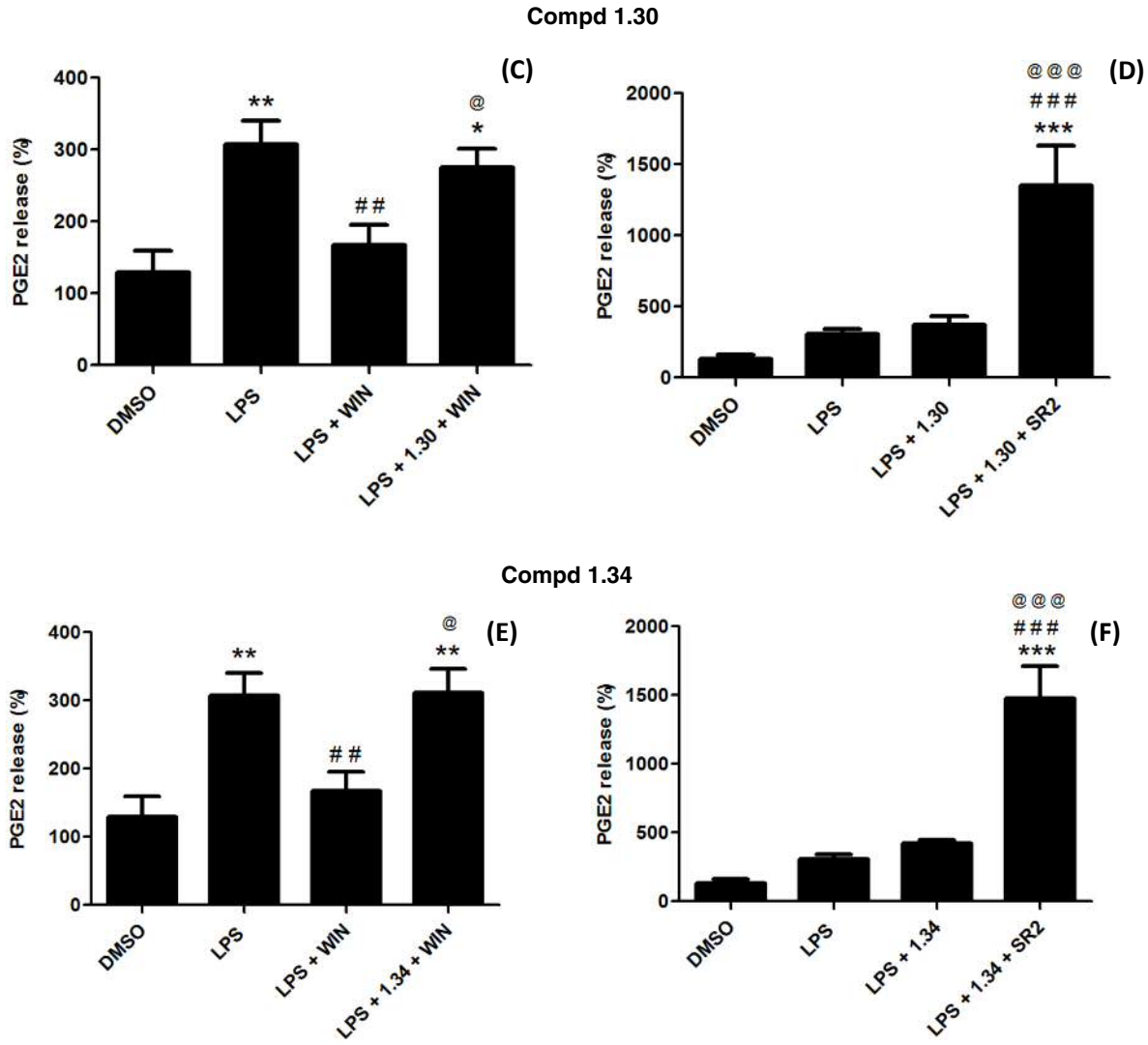

Figure 16. Effects of compounds **1.15**, **1.30** or **1.34**, combined with WIN55,212-2 and/or SR144528, on the LPS-induced release of PGE2 in cultured BV-2 cells. (A) Compound **1.15** and WIN; (B) Compound **1.15** and SR2; (C) Compound **1.30** and WIN; (D) Compound **1.30** and SR2; (E) Compound **1.34** and WIN; (F) Compound **1.34** and SR2. Data were assessed by one-way analysis of variance ($F(3,26)=8.03$, $p=0.0008$ for (A); $F(3,27)=104.20$, $p<0.0001$ for (B); $F(3,27)=7.94$, $p=0.0008$ for (C); $F(3,27)=18.15$, $p<0.0001$ for (D); $F(3,27)=8.43$, $p=0.0005$ for (E); $F(3,27)=30.81$, $p<0.0001$ for (F); $^{*}p<0.05$, $^{**}p<0.01$,$^{***}p<0.005$ *versus* controls (DMSO-exposed); $^{\#}p<0.05$, $^{\#\#}p<0.01$, $^{\#\#\#}p<0.005$ *versus* LPS; $^{@}p<0.05$, $^{@@}p<0.01$, $^{@@@}p<0.005$ *versus* WIN+LPS or compounds **1.15**, **1.30** or **1.34**+LPS)

To sum up, all these functional data indicate that we have discovered novel selective and potent agonists of the cannabinoid receptor CB_2R. This behaviour was demonstrated through different biochemical assays, including ligand-mediated GTPγS binding, forskolin-stimulated cAMP and competition binding experiments. Among this series CB_2R antagonists and potent CB_1R/CB_2R agonists were also identified.

3.1.4 Molecular modeling

As already mentioned, significant CBR affinity differences were observed among the chromenopyrazoles and isoxazoles described in this chapter. These data offered us the opportunity to explore the structural features required for CB_1R/CB_2R selectivity using molecular modeling approaches. Cannabinoid selectivity and structural patterns led us to select molecules **1.4**, **1.6b**, **1.17** and **1.41** for docking studies. The CB_1R chromenopyrazole **1.4** was compared with its isoxazole analog **1.41**, a potent non-selective CB_1R/CB_2R ligand. On the other hand, the CB_1R selective chromenopyrazole **1.6b** was studied in relation to its methoxy derivative **1.17**, which displays CB_2R selectivity.

Firstly, conformational analysis of **1.4**, **1.6b**, **1.17** and **1.41** was performed to determine the minimum energy conformers. In what concerns the *N*-H-chromenopyrazole **1.4**, two tautomers can exist, however, we only considered the tautomer displayed in figure 18. This consideration was based on our previous studies concerning annular tautomerism (OH···N and/or NH···O) of hydroxychromenopyrazoles, in which the tautomer OH···N was shown to be the predominant specie in solution.[151] Figure 18, illustrates the global minimum energy conformers of **1.4**, **1.6b**, **1.17** and **1.41**.

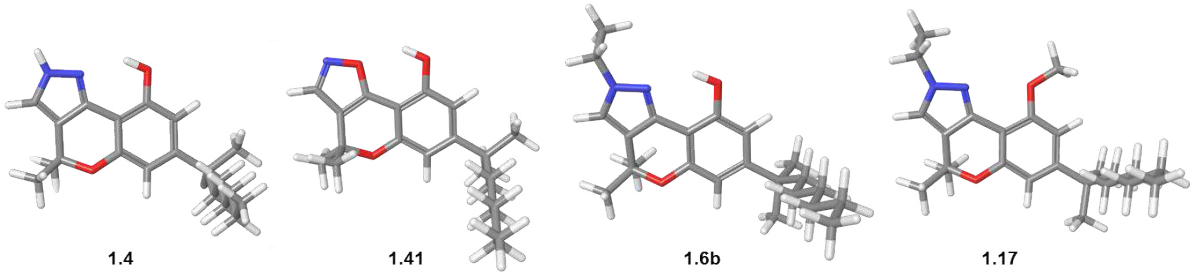

Figure 18. Minimum energy conformers of compounds **1.4**, **1.6b**, **1.17** and **1.41**.

Furthermore, we have calculated the electrostatic potential maps of minimum energy conformers of compounds **1.4**, **1.6b**, **1.17** and **1.41** (figure 19). The range of the electrostatic potential has been normalized to be the same for all of the analogues and is given in kJ/mol. The phenolic hydroxyl group revealed to be the most negative electrostatic potential region (in red) of compounds **1.4** and

1.6b. Chromenoisoxazole **1.41** showed two electron rich hot spots (in red) originated by the phenolic hydroxyl group and by the isoxazole nitrogen, this last one being the most electronegative region of the molecule. As expected, the *O*-methoxy chromenopyrazole **1.17** displayed a weaker electronegative region due to the low exposure of the free lone pair of electrons of the methylated phenolic oxygen.

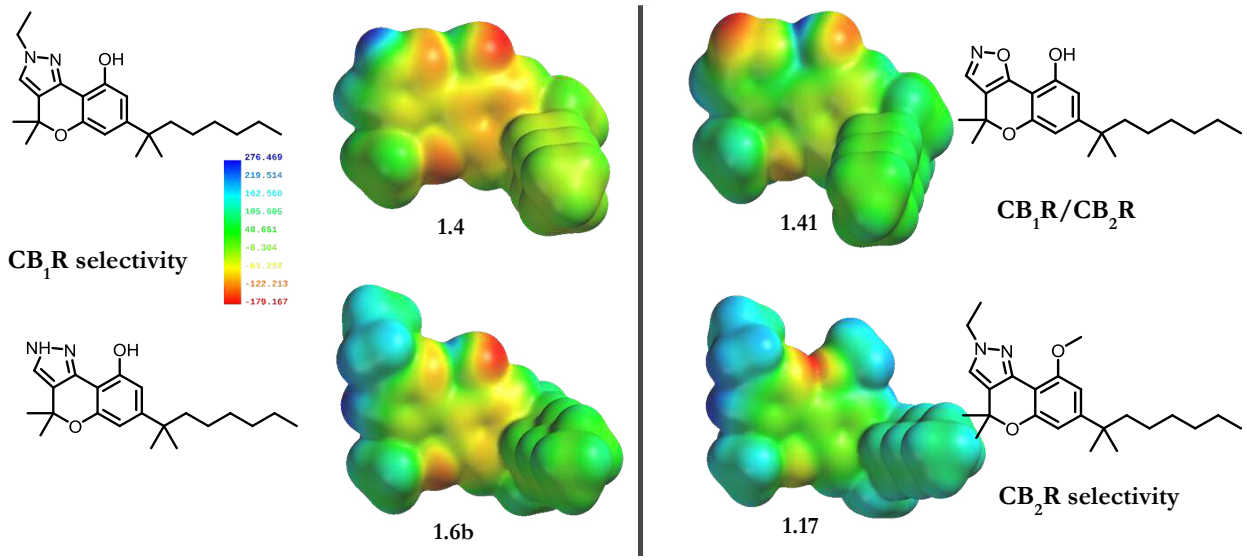

Figure 19. The molecular electrostatic potential maps of the minimum energy conformations of compounds **1.4**, **1.6b**, **1.17** and **1.41** are illustrated here. The electrostatic potential scale (in kJ/mol) is provided as a color scale. This scale is from blue (most electropositive) to red (most electronegative).

The global energy minima of **1.4**, **1.6b**, **1.17** and **1.41** were docked using a model of the active state (R*) of the cannabinoid receptors CB_1R and CB_2R.[152,153] These models include the extracellular and intracellular loops, the N-terminus (truncated in CB_1R) and the C-terminus, including the intracellular helix portion of each receptor, termed Helix 8. Cannabinoid receptor docking studies were performed in the same binding site described for HU210[154] in the CB_1R* model and for AM841[155,156] in the CB_2R* model.

*Chromenopyrazole **1.4**/CB_1R* docking studies.*

Lysine K3.28(192) was used as the primary interaction site for the phenolic hydroxyl group compound of **1.4**. The choice of this primary interaction is supported by the fact that mutation of this residue in CB_1R resulted in the loss of binding of classical, non-classical and endocannabinoids.

Thus, the lysine K3.28(192) is considered crucial for CB_1R binding of this class of ligand.[157] Figure 20 (left) presents docking results for **1.4** binding at CB_1R* from a cellular transmembrane view. As illustrated in this figure, the energy-minimized **1.4**/CB_1R* complex shows two main binding site anchoring interactions. The phenolic oxygen of **1.4** is engaged in hydrogen bond with K3.28(192) [hydrogen bond (N-O) distance = 2.75 Å and (N-H--O) angle = 151°]. The *N*1-pyrazole nitrogen establishes a hydrogen bond with serine S7.39(383)) [hydrogen bond (N-O) distance = 3.02 Å and (O-H--N) angle = 140°]. The ligand **1.4** exhibits the greatest pairwise interaction energy with K3.28(192) (-11.88 kcal/mol) and S7.39(383) (-10.88 kcal/mol) followed by significant interactions with C7.42(386) (-6.22 kcal/mol), D2.50(163) (-6.03 kcal/mol), L7.43(387) (-5.20 kcal/mol), N7.45(389) (-5.13 kcal/mol) and V3.32(196) (-4.40 kcal/mol). The energy difference between the initial **1.4** conformation and the final docked conformation in the energy-minimized complex was found to be 6.51 kcal/mol at the HF 6-31G* level. The overall interaction energy for **1.4** at CB_1R* was found to be -63.92 kcal/mol (see table A in the experimental section).

*Chromenoisoxazole **1.41**/CB_1R* docking studies.*

The docking of **1.41** in the CB_1R* receptor model revealed a similar occupation of the binding site with hydrogen bonds involving the lysine K3.28(192) [hydrogen bond (N-O) distance = 2.82 Å and (N-H--O) angle = 153°] and the serine S7.39(383) [hydrogen bond (N-O) distance = 2.77 Å and (O-H--N) angle = 130°] as key residues (figure 20, right). It is interesting to note that an additional hydrogen bond between the pyran oxygen and cysteine C7.42(386) was revealed in the **1.41**/CB_1R* complex [hydrogen bond (S-O) distance = 3.19 Å and (S-H-O) angle = 167°]. Comparing the energies involved in this complex, **1.41** displays the greatest pairwise interaction energy with K3.28(192) (-9.59 kcal/mol) and C7.42(386) (-7.39 kcal/mol). The interaction with S7.39(383) was found to be only -4.36 kcal/mol, indicating a weak hydrogen bond with the isoxazole nitrogen. Other favourable electrostatic and van der Waals interactions were found with D2.50(163) (-4.85 kcal/mol), L7.43(387) (-5.12 kcal/mol), N7.45(389) (-5.20 kcal/mol) and V3.32(196) (-4.30

kcal/mol). The energy difference between the initial **1.41** conformation and the final docked conformation in the energy-minimized complex was found to be 2.07 kcal/mol at the HF 6-31G* level. The overall interaction energy for **1.41** at CB_1R* was found to be -60.87 kcal/mol (see table B in the experimental section).

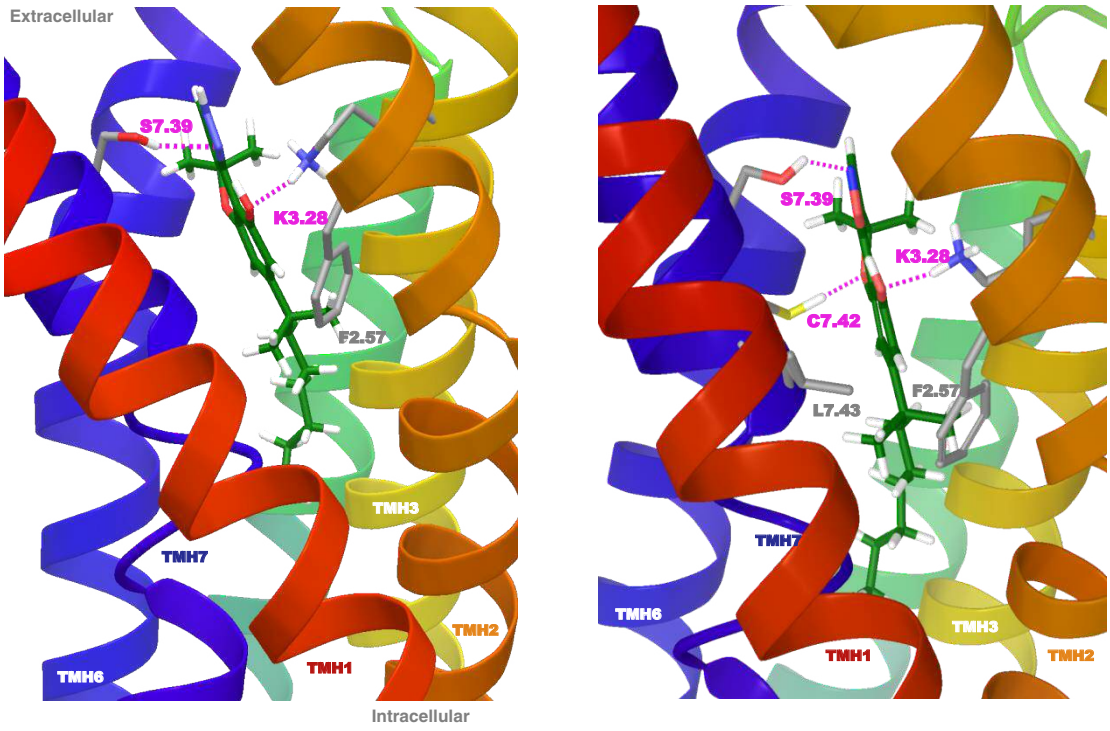

Figure 20. Binding site of **1.4** (left, in green) and **1.41** (right, in green) in the CB_1R* model. Hydrogen bonds are represented with magenta dashed lines.

*Chromenopyrazole **1.6b**/CB_1R* docking studies.*

As illustrated in figure 21 (left), the energy minimized **1.6b**/CB_1R* complex presents two hydrogen bonds with K3.28(192). The first involved K3.28(192) as hydrogen donor to the phenolic oxygen of **1.6b** [hydrogen bond (N-O) distance = 2.75 Å and (N-H--O) angle = 152°]. The second interaction involved K3.28(192) hydrogen bonding with the pyrazole *N*1 nitrogen [hydrogen bond (N-N) distance = 3.10 Å and (N-H--N) angle = 132°]. This pyrazole nitrogen also forms a hydrogen bond with S7.39(383) [hydrogen bond (N-O) distance = 3.15 Å and (O-H--N) angle =134°]. However, this interaction is weaker than the corresponding one in the **1.4**/CB_1R* complex. Chromenopyrazole **1.6b** displays its greatest pairwise interaction energy with K3.28(192) (-14.34

kcal/mol, mainly electrostatic energy), followed by N7.45(389) (-5.19 kcal/mol), L7.43(387) (-5.13 kcal/mol) and C7.42(386) (-4.76 kcal/mol) which are predominantly van der Waals energy. Moreover, the complex exhibits significant interactions with V3.32(196) (-4.72 kcal/mol) and D2.50(163) (-4.70 kcal/mol). The energy difference between the initially docked **1.6b** conformation and the final conformation in the energy-minimized complex was found to be 5.13 kcal/mol at the HF 6-31G* level. The overall interaction energy for **1.6b**/CB_1R* complex was found to be -59.92 kcal/mol (see table C in the experimental section).

*Chromenopyrazole **1.17**/CB_1R* docking studies.*

Compound **1.17** was also docked in the CB_1R* model at the same binding site. However, consistent with its poor affinity for CB_1R, it was unable to form any hydrogen bond with any residue of the receptor. Furthermore, the methoxy group shows a steric overlap with phenylalanine F2.57(170) and leucine L7.43(387) as illustrated in figure 21 (right). In this model, the hydrogen bond between the phenolic oxygen of **1.17** and K3.28(192) does not take place due to the low accessibility of the lone pairs of electrons. As demonstrated for other tricyclic cannabinoids, this electronic density is crucial for ligand-CB_1R[157,158] and explains the low affinity for this receptor displayed by **1.17**.

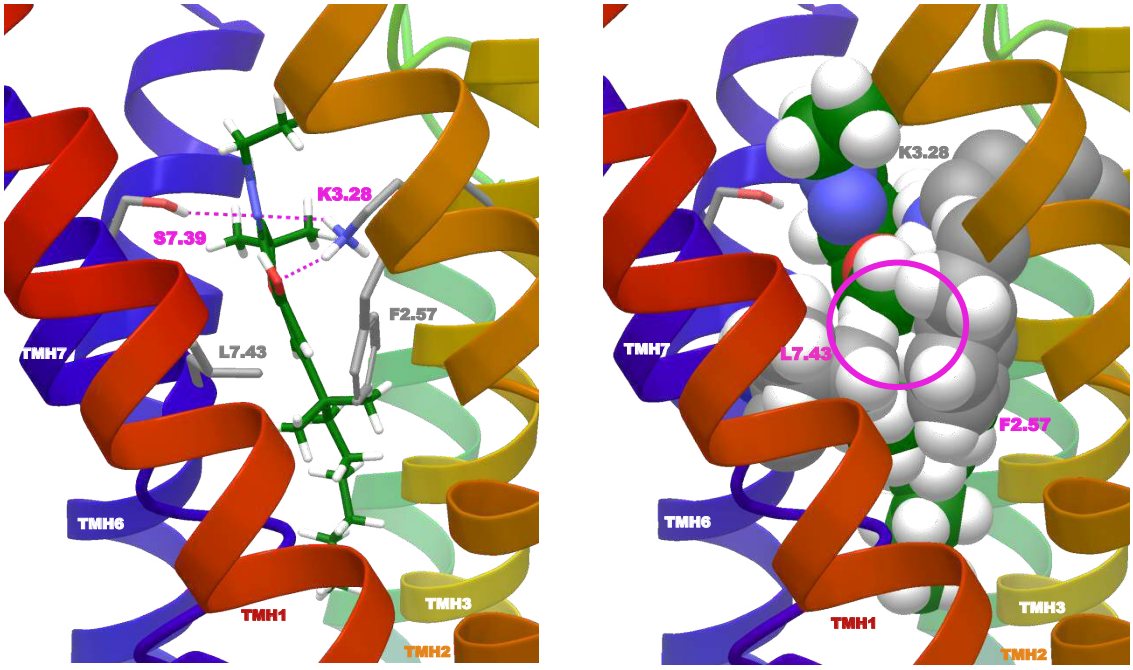

Figure 21. Binding site of **1.6b** (left, in green) in the CB_1R^* model. Hydrogen bonds are represented with magenta dashed lines. Structure of **1.17** (right, in green) superimposed on the **1.6b**-CB_1R^* complex. The magenta circle indicates van der Waals steric overlap with F2.57 and L7.43 in the CB_1R^* binding site.

*Chromenopyrazole **1.4**/CB_2R^* docking studies.*

After exploring the docking of compound **1.4** in the CB_1R^* model, we studied the potential interactions of this chromenopyrazole in the previously reported advanced CB_2R^* model[153,156,159] at the AM841 binding site.[156] The CB_2R^* model contains a salt bridge between the aspartic acid D275 in the EC-3 loop and lysine K3.28(109). Docking studies of **1.4** revealed a steric clash between the pyrazole moiety of the structure and the lysine involved in the ionic lock as illustrated in figure 22 (left). These results are in agreement with the experimental pharmacological data (K_i (CB_2R) > 40 μM).

*Chromenoisoxazole **1.41**/CB_2R^* docking studies.*

Compound **1.41** was also docked in the previous CB_2R^* model at the same binding site. As illustrated in figure 22 (right), the energy minimized **1.41**/CB_2R^* complex presents two main interactions, a hydrogen bond between the isoxazole nitrogen and K3.28(109) [hydrogen bond (N-O) distance = 2.86 Å and (N-H--O) angle = 157°] and a hydrogen bond involving the phenolic oxygen of **1.41** and S6.58(268) [hydrogen bond (O-O) distance = 2.63 Å and (O-H--O) angle = 170°]. Chromenoisoxazole **1.41** displays its greatest pairwise interaction energy with K3.28(109) (-10.33 kcal/mol) and S6.58(268) (-7.84 kcal/mol). The complex also establishes significant interactions (mainly van der Waals energy) with V3.32(113) (-6.26 kcal/mol) followed by S7.39(285) (-4.78 kcal/mol), L7.43(289) (-3.52 kcal/mol) C7.42(288) (-3.13 kcal/mol) and M6.55(265) (-3.11 kcal/mol). Phenylalanines F3.25(106) and F7.35(281) as well as the residues involved in the ionic lock (K3.28 and D275) define the top of the binding site for this ligand. The energy difference between the initial **1.41** conformation and the final docked conformation in the energy-minimized complex was found to be 2.56 kcal/mol at the HF 6-31G* level. The overall interaction energy for **1.41**/CB_2R^* complex was found to be -60.25 kcal/mol (see table D in the experimental section). Comparing the docking studies of chromenoisoxazole **1.41** with the corresponding

chromenopyrazole **1.4** in the CB_2R^* model, there is a clear difference. The hydrogen of the pyrazole moiety unables the lysine involved in the ionic lock to interact with the heterocycle, whereas the isoxazole nitrogen does not exhibit steric overlapping. Thus, these modeling features corroborate the experimental binding affinities obtained for both compounds.

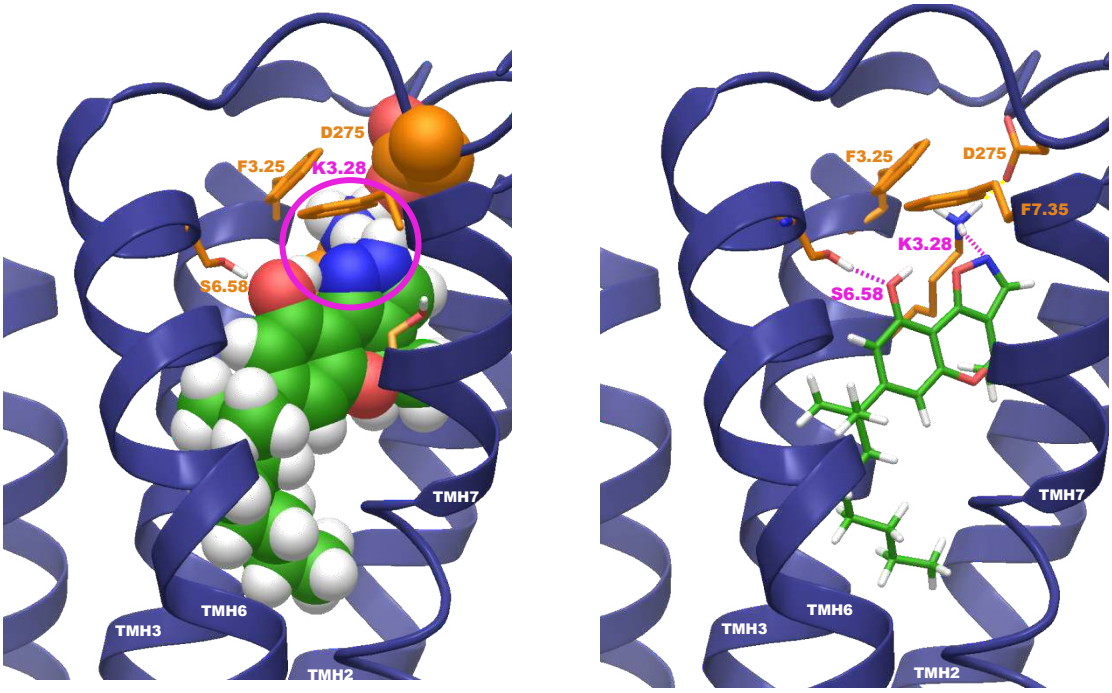

Figure 22. Binding site of **1.41** (right, in green) in the CB_2R^* model. Hydrogen bonds are represented with magenta dashed lines. Structure of **1.4** (left, in green) was superimposed on the **1.41**-CB_2R^* complex. The magenta circle indicates van der Waals steric overlap with K3.28 which forms a salt bridge with D275 in the CB_2R^* binding site.

*Chromenopyrazole **1.6b**/CB_2R^* docking studies.*

As previously shown in the **1.4**/CB_2R^* complex (figure 22, left), chromenopyrazole **1.6b** exhibits a steric clash between the pyrazole moiety of the structure and the ionic lock formed by aspartic acid D275 and lysine K3.28(109). Moreover, as shown in figure 23, a major steric overlap with phenylalanine F7.35(281) is displayed. These findings likely explain the lack of affinity of chromenopyrazole **1.6b** for CB_2R.

*Chromenopyrazole **1.17**/CB_2R^* docking studies.*

Docking studies of the methoxy derivative **1.17** performed in the CB_1R^* model clearly showed a lack of affinity towards this receptor type. Here, we docked **1.17** in the CB_2R^* model. Figure 23 (right)

illustrates the energy-minimized **1.17**/CB_2R* complex. Compound **1.17** displays similar occupation of the binding site but it adopts a different orientation than the free phenolic hydroxyl ligands **1.4**, **1.41**, and **1.6b**. This orientation enables serine S6.58(268) to form a hydrogen bond with the pyran oxygen [hydrogen bond (O-O) distance = 3.21 Å and (O-H--O) angle = 110°]. Compound **1.17** exhibits the greatest pairwise interaction energy with S6.58(268) (-5.55 kcal/mol) and D275 (-6.79 kcal/mol) which are mainly constituted by electrostatic energy. Significant van der Waals interactions are established between the ligand and the following residues: S7.39(285) (-6.17 kcal/mol), F3.36(117) (-4.85 kcal/mol), V3.32(113) (-4.41 kcal/mol), C7.42(288) (-3.88 kcal/mol) and M6.55(265) (-3.07 kcal/mol). The energy difference between the initial **1.17** conformation and the final docked conformer in the energy-minimized complex was found to be 2.79 kcal/mol at the HF 6-31G* level. The overall interaction energy for **1.17**/CB_2R* complex was found to be -53.82 kcal/mol (table E, experimental section). The overall energy of this complex is higher than in the **1.41**/CB_2R* complex what explains the affinity differences obtained by radioligand binding experiments.

Docking studies of other methoxy chromenopyrazoles were performed within the same binding site in the CB_2R* model achieving similar results.

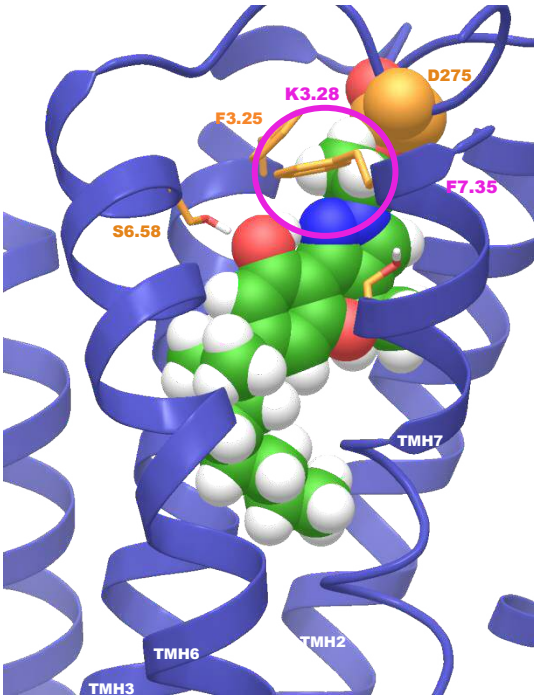

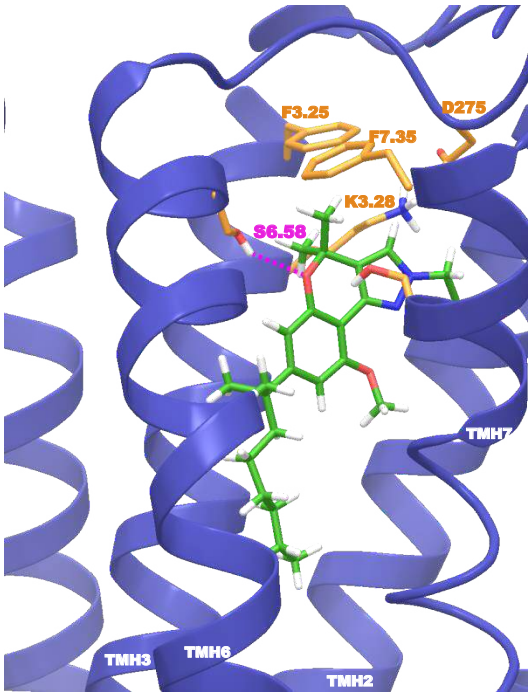

Figure 23. Binding site of **1.17** (right, in green) in the CB_2R* model. Hydrogen bonds are represented with magenta dashed lines. Structure of **1.6b** (left, in green) was superimposed on the **1.41**-CB_2R* complex. The magenta circle indicates van der Waals steric overlap with K3.28 and F7.35. K3.28 and D275 form a salt bridge with in the CB_2R* binding site. K3.28 is facing the molecule as in the **1.41**-CB_2R* complex but is hidden by the molecule from this perspective, while F7.35 is not displayed as van der Waals volume to facilitate the view.

From these CB_2R complexes we can see the importance of serine S6.58(268) in the binding site as already revealed by the AM851/CB_2R* complex.[156] Pei and coworkers suggested that for the binding of AM841, the conserved residue K3.28(109) appears to play little role in ligand-CB_2R interaction.[156] However, in our docking studies, in the **1.41**/CB_2R* complex, K3.28(109) establishes a hydrogen bond with the isoxazole nitrogen. The importance of this residue was previously observed in the recently reported study of 1,8-naphthyridin-2(1*H*)-one-3-carboxamides,[91] which exhibits a hydrogen bond with K3.28(109) in the CB_2R active model.

Taking all these data together we can highlight key molecular features involved in the determination of CB_1R and/or CB_2R binding of our compounds. Docking studies suggests that the presence of the pyrazole or isoxazole moiety as well as the phenolic oxygen play a crucial role in affinity and selectivity.

For CB_1R affinity, the phenolic lone pair have to be available to bind with K3.28(192), as in phenols **1.4**, **1.6b** and **1.41**, otherwise the affinity for the type 1 cannabinoid receptor is very low. *O*-alkylation of the initial phenolic hydroxyl of our scaffold led to less potent but selective CB_2R ligands (as in **1.17**). This fact might be due to the different orientation and low accessibility of the lone pair of electrons of the phenolic oxygen, essential for CB_1R interaction. The steric hindrance generated by the *O*-substituent in the CB_1R binding site impacts their affinity towards this receptor; however, it clearly enables CB_2R activity. Substituted phenols align in the proper orientation in the CB_2R binding site leading to an interaction of S6.58(268) with the ligand pyran oxygen. The different orientation of cannabinoids attending to these structural modifications in the phenol was studied with Δ^8-THC and Me-Δ^8-THC by Makriyannis and collaborators.[71,160,161] Our results are consistent with the SAR of classical cannabinoids. Several studies have demonstrated that the conversion of the

C-1 phenolic hydroxyl of a classical cannabinoid, such as THC, to a methoxy group resulted in a CB_2R-selective ligand.[162–165]

These observations may help to further explain affinities and selectivities of other compounds from our series. For instance, in the case of the *N*1-cyclohexyl chromenopyrazole **1.13**, the decrease in CB_1R affinity might be due to the low exposure of the phenolic oxygen electrons as a consequence of the steric volume created by the pyrazole substituent.

Furthermore, these structural studies encouraged us to synthesize novel derivatives. At this point, we had only synthesized **1.41** of the isoxazole series. It is why, based on the above considerations, we underwent the synthesis of the *O*-methylated isoxazole **1.42** leading to a CB_2R selective and potent ligand.

3.1.5 ADME properties

In silico physicochemical parameters

Due to the high percentage of drug development failures associated to deficient ADME (absorption, distribution, metabolism, and excretion) properties, characterization of drug candidate compounds in this field gets increasingly important. Thus, it is necessary to obtain data at early stages of the discovery process. After administration, a drug is first carried through the blood stream by absorption, permeation and transport processes. Then, the distribution is crucial for the drug to reach a specific target in organ or tissue. Finally, the active drug is eliminated by metabolic processes and excreted.

Pharmacokinetic properties of the newly synthesized CB_2R ligands and of well-known cannabinoids such as Δ^9-THC or CP55,940 have been calculated *in silico* using QikProp from Maestro Software. This program calculates a set of 34 physicochemical descriptors based on the global minimum energy conformer of each molecule. The rationale behind *in silico* approaches are the relatively lower cost and the time factor involved, when compared to experimental procedures.[166,167]

The predicted data for these new compounds indicated that Lipinski and Jorgensen pharmacokinetics rules are followed (table 5).[168,169] As displayed in table 5, the prediction of blood-brain barrier permeability, human oral absorption and potassium channel characteristic of long QT syndrome suggests favorable druggability profile for all the chromenopyrazole derivatives. However, not all of them present aqueous solubility values within the ranges predicted by QikProp for 95% of known oral drugs. For instance, chromenopyrazoles bearing a bromoalkyl or a pyrano group (**1.36**−**1.40**) displayed high lipophilicity *in silico* values. Solubility issues are widely known for cannabinoids pharmacology because of their lipophilic nature.[170,171] It is worth mentioning that chromenoisoxazoles and certain chromenopyrazoles displayed an improved solubility profile compared to classical cannabinoids such as Δ^9-THC or CBN.

Thus, taking all pharmacological and ADME prediction data into consideration, the highly selective and potent CB_2R agonist **1.42** may serve as lead structure for further optimizing this novel class of CB_2R ligands not only with regard to potency but also regarding physicochemical properties.

Table 5. Physicochemical descriptors calculated by QikProp 3.5 integrated in Maestro (Schrödinger, LLC, New York, USA)

Compd	QPlogS[a]	QlogBB[b]	QPlogHERG[c]	QPPCaco[d]	%Human oral absorption GI[e]
1.13	-7.51	-0.20	-5.22	4875	100
1.14	-5.90	-0.43	-5.03	2902	100
1.15	-6.24	-0.02	-5.21	7394	100
1.16	-6.82	-0.10	-5.09	6647	100
1.17	-6.53	-0.01	-5.36	8211	100
1.27	-6.13	-1.13	-5.01	1117	100
1.28	-6.45	-0.71	-5.20	2864	100
1.29	-6.91	-0.52	-4.70	4414	100
1.30	-6.70	-0.69	-5.25	3348	100
1.33	-5.88	-0.84	-5.01	1838	100
1.34	-6.13	-0.19	-5.08	7112	100
1.35	-6.44	-0.18	-5.19	8327	100
1.36	-8.50	-0.03	-5.20	7495	100
1.37	-8.87	-0.01	-5.31	8810	100
1.38	-8.61	-0.02	-4.81	6647	100
1.39	-7.45	-0.06	-4.73	6357	100

1.40	-7.18	0.06	-5.24	8465	100
1.41	-5.64	-0.82	-4.92	1230	100
1.42	-5.31	-0.15	-4.77	4505	100
1.43	-5.90	-0.76	-5.11	2435	100
CBD	-6.01	-0.44	-4.8	2693	100
CBN	-6.50	-0.12	-5.21	4261	100
CP55,940	-6.10	-1.51	-5.20	642	100
THC	-6.65	-0.09	-4.84	4564	100

[a]Predicted aqueous solubility [-6.5/0.5]; [b]Predicted log of the brain/blood partition coefficient [-3.0/1.2]; [c]HERG K^+ Channel Blockage (log IC_{50}) [concern below -5]; [d]Apparent Caco-2 cell permeability in nm/s [<25 poor, >500 excellent]; [e]Human Oral Absorption in GI [<25% is poor]; [range of 95% of drugs].

Binding to plasma proteins: SPR-biosensor analysis

An important factor in this ADME process is the interaction with soluble proteins in plasma. In fact, the affinity of a drug toward plasma proteins directly affects bioavailability, tissue distribution, metabolism, clearance and toxicity. Accumulation of lipophilic drugs such as cannabinoids occurs in body fat resulting in higher concentration in fat than in plasma.[171] However, the binding of these drugs to the plasma proteins is important for their distribution and transport to their biological targets. High concentrations of drugs in plasma will allow penetration in highly vascularized tissues. In this context, it was interesting to get information on the interactions between our chromenopyrazoles and the main plasma proteins. Human Serum Albumin (HSA) and α_1-acid glycoprotein (AGP) are the most relevant plasma proteins playing critical roles in transporting drugs, metabolites and endogenous ligands.[172–174] Therefore, binding towards HSA and AGP of representative CB_2R ligands has been tested using surface plasmon resonance (SPR). Even though a wide variety of experimental assays have been used for this purpose,[175,176] SPR has recently emerged as a very efficient method for measuring drug-plasma proteins binding.[177] SPR is an optical technique utilized for detecting binding of a mobile molecule (cannabinoids) to a molecule immobilized on a thin metal film (HSA or AGP). SPR technology is based on a biosensor system characterized by label-free detection and real-time data acquisition.[178–180] Detection of refractive

index allows the detection of mass differences due to biomolecular interactions around the chip surface. The response signal is reported as resonance unit (RU).

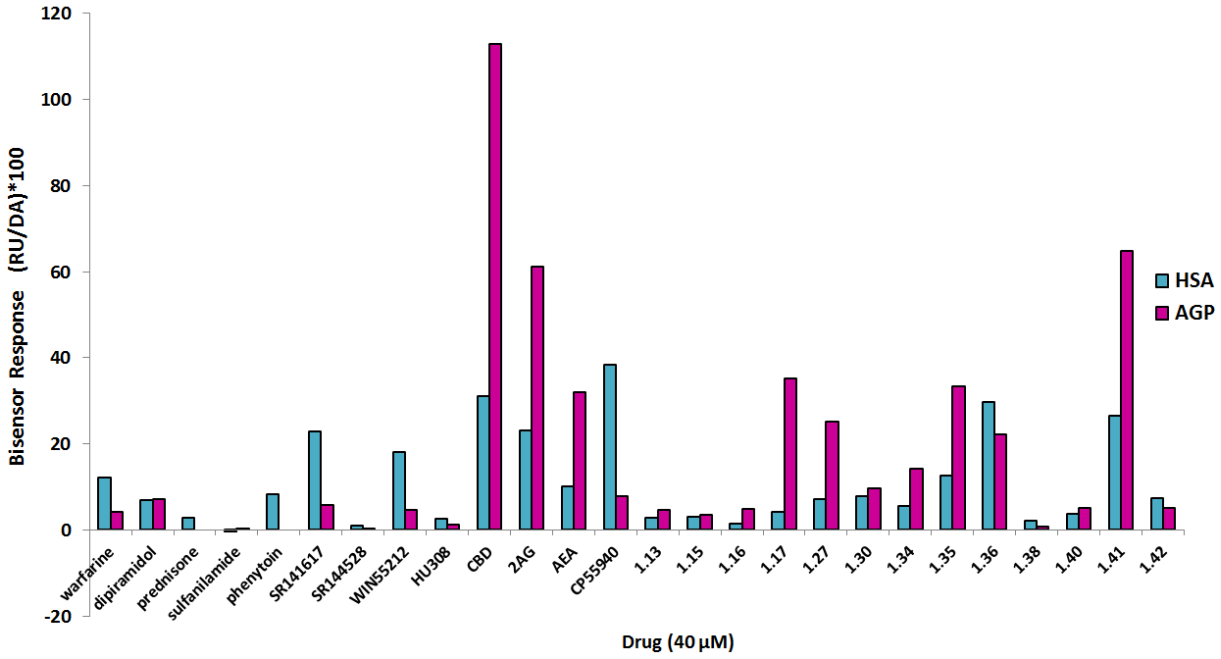

Figure 17. Plot of HSA binding levels determined by SPR for chromenopyrazoles (**1.13**, **1.15**−**1.17**, **1.27**, **1.30**, **1.34**−**1.36**, **1.38** and **1.40**−**1.42**), cannabinoids SR141617, SR144528, WIN55212, HU308, CBD, 2AG, AEA and CP55,940 and the reference compounds (warfarin, dipiramidol, phenytoin, prednisone, sulfanilamide, and phenytoin) at 40 µM.

In the present study, binding to HSA and AGP was determined by SPR–biosensor binding experiments using previously reported protocols.[181] Drugs with different binding levels to HSA and AGP [Warfarin (HSA>AGP), phenytoin (HSA specific), dipiramidol (HSA=AGP), prednisone (HSA specific), and sulfanilamide (negative control for HSA/AGP] were used as controls. As this experiments had not been previously reported in the literature for cannabinoids, different reference cannabinoid ligands (SR141617, SR144528, WIN55212, HU308, CBD, 2AG, AEA and CP55940) were also assessed for comparison. A representative set of chromenopyrazoles (**1.13**, **1.15**−**1.17**, **1.27**, **1.30**, **1.34**−**1.36**, **1.38** and **1.40**−**1.42**) and reference compounds were evaluated for binding to HSA and AGP. The results are summarized in figure 17. Binding levels over 50 RU/Da indicate nonspecific interactions with HSA or AGP.

First of all, the binding responses collected for the reference HSA and AGP ligands (warfarin, phenytoin, dipiramidol, prednisone, and sulphanilamide) agreed with the well documented binding properties of these reference compounds.

The tested reference cannabinoid ligands CBD, 2AG, and AEA showed very high binding levels to the plasma protein AGP, whereas CBD, 2AG, and CP55940 bound particularly to HSA. These high affinities are probably due to unspecific interactions. It has to be kept in mind that in general cannabinoids are very lipophilic compounds. SR141617 and WN55212-2 have a similar profile in this test with higher binding to HAS than AGP. Curiously, SR144528 and HU308 did not show significant affinity for both plasma proteins. Albeit no clear conclusion is attained from these results, intermediate to high plasma protein binding levels are coherent with the results observed regarding tissue and plasma *in vivo* distribution of cannabinoids[171] Tested chromenopyrazoles **1.13**, **1.15**, **1.16**, **1.38**, **1.40** and **1.42** exhibited medium HSA and AGP binding levels suggesting a satisfactory free drug concentration in plasma. Compounds **1.17**, **1.27**, **1.35**, **1.36** and **1.41** showed very high plasma protein binding that could be interesting for potential *in vivo* retard effect.

For certain compounds, further SPR studies were attempted but the complexity of their binding kinetic sensograms did not lead to clear data. A possible multi binding sites occupancy of HSA or AGP has been suggested but the experimental and theoretical kinetic curves did not corroborate this fact. Direct analysis of interactions between cannabinoids and plasma proteins are difficult to interpret since most of cannabinoids are very lipophilic compounds producing unspecific binding.

3.2 Bivalent ligands for CB_2Rs

As commented in the introduction of this chapter, many GPCRs, cannabinoid receptors among them, can form physiologically interacting homo- or heterodimers.[36,47,49,52] This oligomerization may affect receptor's function, signal transduction or their interaction with drugs. The physiological relevance of such dimerization has not yet been fully established for CBRs whereas implication of some GPCRs homo- and heterodimers in different pathologies has already been reported in the literature.[35,182]

Within this field, bivalent ligands have emerged as promising new pharmacological entities and potential tools for the biological study of their respective dimeric receptors.[34,35,183–185] Despite the challenges arising from their synthesis,[184] bivalent ligands can exhibit enhanced activity and selectivity over their respective corresponding parent ligands[185] offering unique strategies in drug development.

Bivalent ligands have been synthesized and evaluated for several GPCRs. Opioid,[186,187] dopamine[188,189] or histamine[190] are some of the receptors for which a bivalent compound provided higher activity than their monomer counterparts. CB_1R homobivalent[56–58] and heterobivalent[191–193] ligands have been extensively reported and explored. However, in what concerns CB_2Rs, there is only a very recent study in which the first bivalent compounds for have been designed and synthesized.[194] Unfortunately, these molecules have largely lost activity and selectivity compared to the benzimidazole monomer.[195] Thus, the functionality of the parent compound was CB_2R agonist whereas the corresponding bivalent molecules showed to be weak antagonists/inverse agonists of CB_1R and CB_2R. Subsequently, the purpose of the following research is the identification of potential homobivalent ligands able to selectively activate CB_2 receptors.

3.2.1 Design

The bivalent ligand approach consists of bridging two pharmacophores in a single entity. In our case, the search of homobivalent ligands for CB_2 receptors requires two identical recognition units covalently linked by the appropriate spacer.

The first step for this design is the election of a CB_2 selective pharmacophore as well as a suitable connecting position to place the linker without significantly disturbing CBR affinity and selectivity. The results observed on SAR in section **3.1** led us to choose the chromenopyrazole scaffold as monomer for this study. Position 9 of our heterocycle was chosen as attachment point for the linker regarding the previous data attained after phenolic alkylation. As methyl and ethyl pyrazole substituents furnished the best CB_2 selectivity ratios in the monomeric chromenopyrazole series, they were selected for this bivalent approach (figure 24).

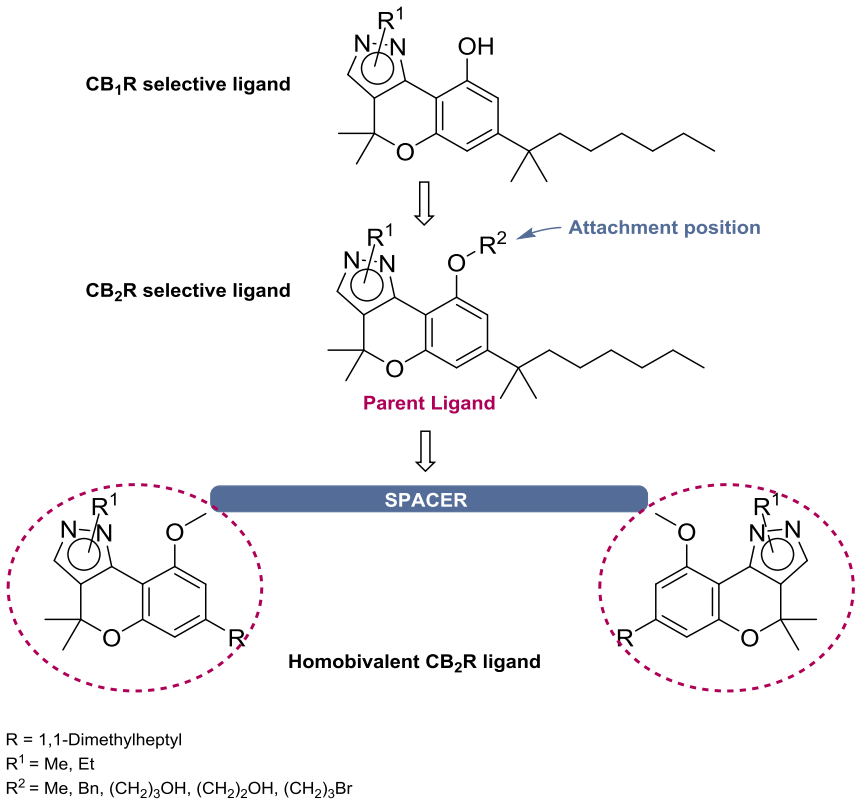

Figure 24. Design of potential homobivalent ligands for CB_2 cannabinoid receptors.

The lack of a theoretical or crystallographic structure for the dimeric CB_2R complicates the selection of an appropriate spacer.[196] The nature and the length of the linker is relevant and in most of cases crucial for biological activity.[184,185] As reported for GPCRs bivalent ligands, optimal chain length varies from 5 to 8 atoms, which was the case for dopamine receptors,[188,189] to 20 atoms, as described for H_2 histamine receptor.[190]

Since there were no previous data on bivalent ligands for CB_2R, the closest information is related to CB_1R. Studies for CB_1-μ opioid heteromers showed interesting data *in vivo* for a chain length of 20 atoms.[193] In what concerns CB_1-CB_1 receptors, suitable spacers seem to be shorter. The work performed by Thomas and coworkers[56] indicated that the optimal chain length for CB_1R homobivalent ligands is 15 atoms, while a study performed in our group revealed peak results for a 7 atoms linker.[58]

Hydrophobic alkyl spacers were selected for our new CB_2-CB_2 compounds regarding the lack of affinity obtained with hydrophilic chains (polyethylene glycol or small peptide chains) for CB_1R bivalent ligands.[56,57,197]

In a first approximation, alkyl chains containing from 10 to 16 methylenes have been considered as linkers. Additionally, the corresponding univalent compounds, 9-alkoxychromenopyrazoles, will be synthesized and evaluated in order to compare with their bivalent counterparts.

3.2.2 Synthesis

Bivalent chromenopyrazoles and their univalent analogs were synthesized as depicted in scheme 4 starting from chromenopyrazoles **1.5b**, **1.6a** and **1.6b** (synthetic route described in section **3.1.1**). Preparation of 9-alkoxychromenopyrazoles (**1.44**−**1.55**) was achieved in high yields by deprotonation of the hydroxyl group with sodium hydride, followed by rapid addition of an excess of the appropriate 1-bromoalkane. For the formation of the bivalent compounds **1.56**−**1.67**, the alkylation of the corresponding chromenopyrazoles with 0.5 equivalents of the desired dibromoalkane was not as easy as that of their univalent counterparts. Different bases were tested,

and finally cesium carbonate was selected and used under inert atmosphere. Thus, the desired bivalent compounds (**1.56−1.67**) were achieved with moderate yields.

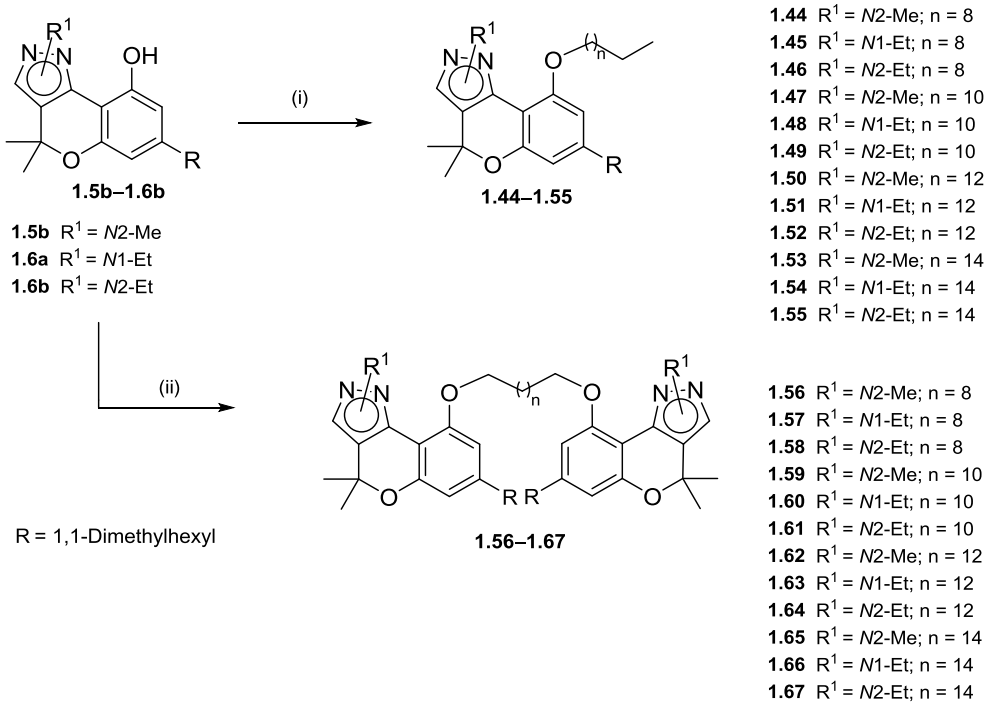

Scheme 4. Synthesis of 9-alkoxychromenopyrazoles **1.44−1.55** and bivalent chromenopyrazoles **1.56−1.67**. Reagents and conditions: **(i)** a) NaH, anhydrous THF, 10 min, b) 1-bromoalkane, reflux, 2-12 h, 32-90%; **(ii)** a) Cs_2CO_3, anhydrous THF, 10 min, b) 1,(n+2)-dibromoalkane, reflux, 8-72 h, 17-59%.

3.2.3 Cannabinoid binding studies

Previous radioligand binding experiments revealed the ability of starting compounds **1.5b**, **1.6a** and **1.6b** to selectively bind to CB_1R with high affinity in the nanomolar range.[144] The newly synthesized uni- and bivalent chromenopyrazole derivatives were evaluated by using the same procedure (section **3.1.2**).

As displayed in table 6, monovalent compounds **1.44−1.55**, did not exhibit affinity towards CB_1R nor CB_2R. These results contrast with the CB_2R affinity values obtained for chromenopyrazoles bearing a methoxy, bencyloxy or hydroxypropoxy groups (**1.14−1.38**). These observations allow us to conclude that elongation of the alkyl phenolic substituent at position 9 prevents CB_2R binding.

In what concerns the bivalent compounds (**1.56**−**1.67**), most of them are CB_2R selective ligands displaying moderate affinity for this receptor but lacking of activity for CB_1R type. The bivalent derivatives **1.57**, **1.60**, **1.61**, **1.63** and **1.64** showed affinity in the submicromolar range for CB_2R whereas **1.56**, **1.58**, **1.59**, **1.62** and **1.65**−**1.67** bind weakly to this receptor. These binding data suggest that the optimal linker length for this series is from 12 to 14 methylenes. The ethyl pyrazole substituent seems to be preferred among this series regardless the *N*1 or *N*2 position.

It is worthy to note that bivalent ligands display an improved CB_2R binding profile compared to their univalent counterparts. These results are in agreement with the currently observed data for other GPCR bivalent ligands. However, to confirm how the presence of two pharmacophoric units affects CB_2 affinity needs to be further explored.

Table 6. Binding affinity of alkoxychromenopyrazoles (**1.44**−**1.55**) and bivalent chromenopyrazoles (**1.56**−**1.67**) for *h*CB_1 and *h*CB_2 cannabinoid receptors.

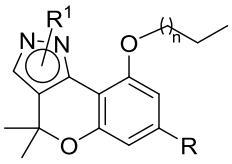

1.44–1.55

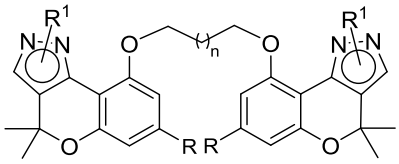

1.56–1.67

Compd	R^1	n[b]	CB_1 K_i [μM][a]	CB_2 K_i [μM][a]
1.44	*N*2-Me	8	>40	>40
1.45	*N*1-Et	8	>40	>40
1.46	*N*2-Et	8	>40	>40
1.47	*N*2-Me	10	>40	32.3 ± 8.4
1.48	*N*1-Et	10	>40	>40
1.49	*N*2-Et	10	>40	>40
1.50	*N*2-Me	12	>40	>40
1.51	*N*1-Et	12	>40	>40
1.52	*N*2-Et	12	>40	>40
1.53	*N*2-Me	14	>40	>40
1.54	*N*1-Et	14	>40	>40
1.55	*N*2-Et	14	>40	>40
1.56	*N*2-Me	8	>40	3.47 ± 1.06
1.57	*N*1-Et	8	>40	0.91 ± 0.19
1.58	*N*2-Et	8	>40	5.82 ± 1.46

1.59	*N*2-Me	10	>40	10.21 ± 4.70
1.60	*N*1-Et	10	>40	0.42 ± 0.14
1.61	*N*2-Et	10	>40	0.35 ± 0.02
1.62	*N*2-Me	12	>40	2.58 ± 0.18
1.63	*N*1-Et	12	>40	0.84 ± 0.15
1.64	*N*2-Et	12	>40	0.28 ± 0.06
1.65	*N*2-Me	14	>40	17.4 ± 5.2
1.66	*N*1-Et	14	>40	>40
1.67	*N*2-Et	14	>40	2.12 ± 0.21

[a]Values obtained from competition curves using [^{3}H]CP55940 as radioligand for *h*CB_1 and *h*CB_2 cannabinoid receptors and are expressed as the mean ± SEM of at least three experiments. [b]n represents the total length of the 9-alkoxy chain.

3.2.4 Functional assays

Functional properties of our new molecules were investigated by cAMP assays using HEK293 cells stably expressing the human CB_2R. Bivalent chromenopyrazoles showing submicromolar CB_2R affinity (**1.57**, **1.60**, **1.61**, **1.63** and **1.64**) were selected for appraisal. Likewise, their corresponding univalent derivatives (**1.45**, **1.48**, **1.49**, **1.51** and **1.52**) were evaluated for comparison.

Effects of compounds on forskolin-stimulated cAMP levels were determined in a preliminary screening at 200 nM. As shown in figure 25, compounds **1.57**, **1.60** and **1.64** inhibit cAMP accumulation at tested concentration, what indicates their ability-to activate this $G_{i/o}$-protein coupled receptor. Interestingly and according to binding data, the monovalent analogs did not significantly trigger changes in forskolin-stimulated cAMP levels. Unexpectedly, the univalent compound **1.49** facilitated cAMP production suggesting an inverse agonist profile.

In addition, cAMP assays were performed in non-transfected HEK293 cells at the same concentration (200 nM). As displayed in figure 25, both series, monovalent and bivalent, as well as the reference agonist CP55,940, did not exert effect in this cell line. Therefore, these experiments allowed us to confirm that the results obtained in HEK293-CB_2 cells were fully mediated by CB_2R.

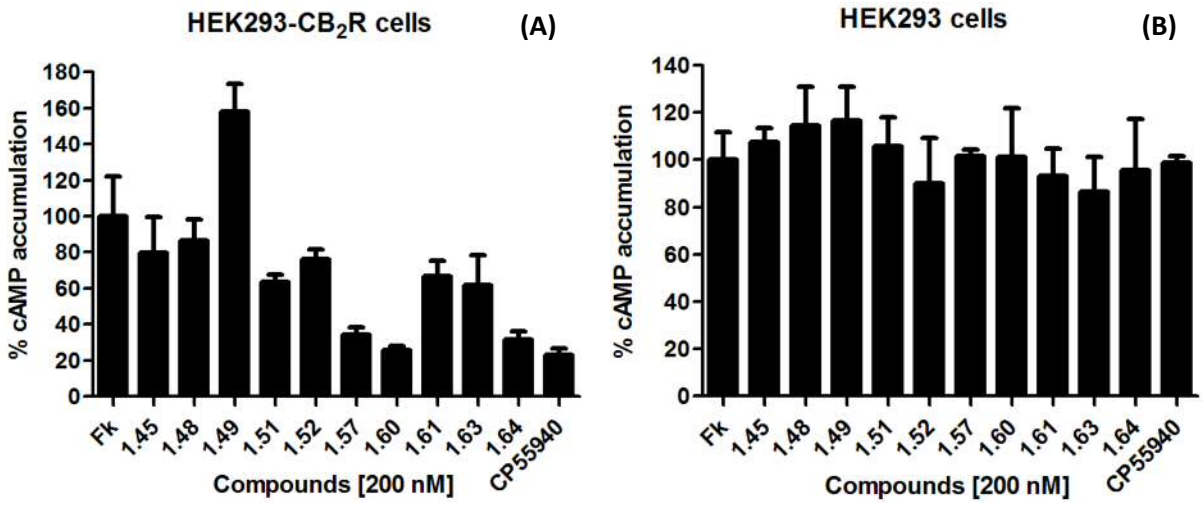

Figure 25. cAMP screening of novel compounds in HEK293 cells stably expressing the human CB_2 receptor subtype (A) and normal HEK293 cells (B). Results are expressed as percent of forskolin-stimulated cAMP accumulation at a concentration of 200 nM of our compounds and the reference cannabinoid CP55,940. All data result from at least three independent experiments, performed in triplicates.

Dose-response curves of bivalent chromenopyrazoles **1.57**, **1.60** and **1.64** were performed to determine their activity at CB_2R. As display in table 7, these compounds are CB_2R selective agonists exhibiting potency and efficacy in the nanomolar range.

Table 7. Functional potencies of compounds **1.57**, **1.60** and **1.64** and the reference cannabinoids CP55,940 and JWH133 at CB_2 receptor determined by measuring the decrease in forskolin-stimulated cAMP levels in HEK293-CB_2R cells.

Compd	R^1	n	CB_2 cAMP assays	
			[a]EC_{50} (nM)	[b]E_{max} (%)
1.57	*N*1-Et	8	85.8 ± 22.1	124 ± 15
1.60	*N*1-Et	10	43.2 ± 21.6	133 ± 14
1.64	*N*2-Et	12	501.2 ± 22.8	98 ± 8
CP55,940	-	-	8.3 ± 1.5	106 ± 9
JWH133	-	-	81.8 ± 1.7	98 ± 11

[a]EC_{50} values were calculated using nonlinear regression analysis. Data are expressed as the mean ± SEM of at least three independent experiments performed in triplicates. [b]Forskolin stimulated cAMP levels were normalized to 100%. E_{max} is the maximum inhibition of forskolin stimulated cAMP levels.

Results attained from this study indicate that for the chromenopyrazole scaffold, bivalency has a positive effect on CB_2 receptor activity. Moreover, in this cell line, CB_2-CB_2 dimers have been recently identified by our collaborators (Rafael Franco and Gemma Navarro, University of Barcelona). By employing FRET and BRET techniques they have demonstrated the presence of

these homodimers in HEK293 cells stably expressing the human CB_2R (data not published yet). Nonetheless, it remains to be determined if the activity of our bivalent ligands is due to the interaction with homodimers or if both pharmacophores bind to monomeric CB_2 receptors.

4. Discussion and conclusions

From CB_1R towards CB_2R selectivity

The implication of CBRs in a variety of physiopathological processes highlights their potential in the management of a broad range of diseases. Since CB_1R is associated with psychotropic effects when acting on the CNS, the therapeutic applications of CB_1R ligands or non-selective cannabinoids are limited. Therefore, different strategies, such as the use of peripherally restricted CB_1R or selective CB_2R ligands, need to be developed. Previous work in our research group allowed the discovery of new non-psychoactive CB_1R ligands with peripheral analgesic properties.[144] Using this scaffold, we proposed different structural modifications attempting to develop novel CB_2R selective ligands. Our optimization efforts kept the 1,1-dimethylheptyl group as the lipophilic chain necessary for activity and focused on surveying the pyrazole and phenol substitutions, on a conformational restricted analogue, and on replacing the pyrazole core of the scaffold by an isoxazole. The compounds were prepared following a 4- to 6- steps synthesis in moderate to high yields.

The pharmacological profile of the synthesized compounds was evaluated by radioligand binding assays for CBRs affinity, and by forskolin-stimulated cAMP and GTPγS binding experiments for functionality at CBRs.

Interestingly, fine-tuning of affinity and selectivity was achieved. In terms of receptor selectivity, phenol substitution played a key role. CB_2R selectivity was achieved when the phenol of the chromenopyrazoles was alkylated (**1.15**–**1.17**, **1.22**–**1.24**, **1.28**–**1.30**, and **1.34**–**1.38**), whereas unsubstituted phenols (**1.4**–**1.8**) led to CB_1R selective compounds. An interesting finding is the bioisosteric replacement of the pyrazole by an isoxazole that resulted in the most potent and selective CB_2R ligand (**1.42**). The affinity of the chromenopyrazoles derivatives for CBRs depended on the nature of the pyrazole substitution but not on its *N*1 or *N*2 position. In general, the alkyl groups showed better affinity for CB_1R or/and CB_2R compared to aryl substituents (except **1.8**). The conformational restricted strategy (**1.38**, **1.40**) did not improve CBR affinity.

At functional level, most of the tested CB_2R ligands revealed to be agonists being the chromenopyrazoles **1.33** and the chromenoisoxazoles **1.40**−**1.43** the most potent compounds. Three of the CB_2R ligands (**1.15**, **1.30** and **1.34**) showed antagonistic properties.

Structural modifications on the phenolic hydroxyl group of classical cannabinoids leading to partial CB_2R selectivity have been reported.[162–165] However, to our knowledge, there is no molecular model that rationally explains the structural features and the interactions triggering this selectivity in the cannabinoid receptor models. Given the interesting results obtained for the novel chromenopyrazoles and chromenoisoxazoles, exploration of the binding site interactions was conducted through docking studies of selected derivatives (**1.4**, **1.41**, **1.17**, and **1.6b**) in CB_1R and CB_2R active state molecular models. These studies confirmed that the phenolic lone pair (**1.4**, **1.6b** and **1.41**) is crucial for binding affinity to CB_1R* through lysine K3.28(192) main interaction, whereas, *O*-methylation (**1.17**) generates steric hindrance in this receptor type. Regarding the CB_2R*/ligand complexes, serine S6.58(268) seems to play an important role in the binding site of our compounds. Previous studies suggested the interaction of this serine in the AM851/CB_2R* binding pocket.[156] Furthermore, in the **1.41**/CB_2R* complex we propose that the isoxazole nitrogen establishes a hydrogen bond with lysine K3.28(109). The importance of this residue has also been recently confirmed in parallel studies performed in Patricia Reggio's group on 1,8-naphthyridin-2(1*H*)-one-3-carboxamides.[91] Therefore, the different ligand-receptor interactions that have been studied provide detailed structural information identifying the key molecular features required for CB_1R and/or CB_2R affinity and selectivity.

In silico predicted pharmacokinetic (ADME) properties suggest favorable druggability profile for the new CB_2R ligands. Moreover, chromenoisoxazoles and certain chromenopyrazoles displayed improved solubility profile compared to classical cannabinoids such as Δ^9-THC or CBN.

Other pharmacokinetic parameters that have been evaluated by SPR–biosensor binding experiments concerned interactions between cannabinoids and plasma proteins HSA and AGP. However, direct interactions analysis of the tested compounds along with reference cannabinoids were difficult to

interpret since most of cannabinoids are very lipophilic compounds and produced unspecific binding.

Despite the research efforts currently directed to the development of CB_2R selective ligands, most of these compounds exhibit CB_1R mediated side effects at high doses. Consequently, the fully selective and potent CB_2R agonist **1.42** discovered herein is a very interesting lead compound for further research. In fact, this chromenoisoxazole has shown a neuroprotective profile in an in *in vitro* neuroinflammatory model realized in M213 neurons.[198] The isoxazole **1.42** is currently being studied in an *in vivo* model of Huntington´s disease generated by stereotaxic lesions with malonate. Preliminary magnetic resonance imaging (MRI) analysis shows that **1.42** administration decreased the striatal lesion volume caused by malonate. Overall, the chromenoisoxazole **1.42** that does not cause CB_1R-mediated psychotropic effects has a promising neuroprotective profile. Therefore, **1.42** could be useful for those neurodegenerative pathologies in which the activation of CB_2R may have therapeutic value.

Bivelent ligands for CB_2Rs

Continuing with our research project and regarding the increasing experimental data suggesting the importance of CBRs dimers, we decided to design a series of CB_2R homobivalent ligands as the second aim of this chapter. CB_2R homodimers have been identified in different tissues; however, they have not been properly described, characterized and their pharmacological potential has not been explored. In this scenario, bivalent compounds may serve as pharmacological tools to study CB_2R dimerization as well as its functional significance. Thus, following with the chromenopyrazole scaffold, molecules in which two pharmacophoric entities are linked by alkyl chains (10 to 16 methylenes) through the phenolic positions were synthesized. Their respective univalent 9-alkoxychromenopyrazole analogs were prepared to study the influence of bivalency on binding studies. Homobivalent compounds displayed CB_2R affinity with total selectivity over CB_1R being the 12 and 14-atoms linkers optimal for binding. It is worthy to note that their corresponding univalent analogues did not display affinity for CB_1R or CB_2R suggesting a possible interaction of both

pharmacophores with CB_2R. Thus, the second pharmacophore unit seems to play a role in the binding that needs to be determined. At that point, two binding modes could be considered. The bivalent ligand can interact with the two orthosteric binding sites of two adjacent protomers simultaneously or it can target the orthosteric and an allosteric binding sites of the same receptor.[184] Both modes of binding evoke positive cooperativity.

Functional cAMP experiments confirmed that the CB_2R bivalent ligands (**1.57**, **1.60** and **1.64**) are able to activate CB_2R. Additionally, the presence of CB_2R homodimers in the *h*CB_2R-HEK293 cells used for functional assays has been confirmed by FRET and BRET techniques. This data might support the hypothesis of an interaction of a bivalent ligand with two orthosteric binding sites of two adjacent protomers. Of course, this needs to be confirmed by additional and complementary experiments. To our knowledge, these are the first homobivalent ligands able to selectively activate CB_2R. Albeit more research is clearly needed to study their mechanism, these novel compounds might be helpful tools for designing bivalent probes to investigate CB_2R homodimers as well as to explore new options in drug development.

Taking all these data together, in this chapter we showed that the chromenopyrazole heterocycle represents a versatile cannabinoid scaffold with a high potential for the development of CB_2R ligands.

5. Experimental section

Chemistry

General methods and materials. Reagents and solvents were purchased from Sigma-Aldrich Co., Fluorochem, Acros Organics, Manchester Organics and Lab-Scan and were used without further purification or drying. Silica gel 60 F254 (0.2 mm) thin layer plates were purchased from Merck GmbH. Microwave assisted organic synthesis was performed using the microwave reactor Biotage Initiator. Products were purified using flash column chromatography (Merck Silica gel 60, 230-400 mesh) or medium pressure chromatography using Biotage Isolera One with pre-packed silica gel columns (Biotage SNAP cartridges). The compounds were characterized by a combination of NMR experiments, HPLC-MS, high-resolution mass spectrometry (HRMS) and elemental analysis. HPLC-MS analysis was performed on a Waters 2695 HPLC system equipped with a photodiode array 2996 coupled to Micromass ZQ 2000 mass spectrometer (ESI-MS), using a reverse-phase column SunFireTM (C-18, 4.6 x 50 mm, 3.5 μm) in a 10 min gradient A: CH_3CN/0.1% formic acid, B: H_2O/0.1% formic acid visualizing at λ = 254 nm. Flow rate was 1 mL/min. Elemental analyses of the compounds were performed using a LECO CHNS-932 apparatus. Deviations of the elemental analysis results from the calculated are within ± 0.4%. The purity of compounds **1.44**−**1.67** was determined by LC coupled to HRMS. The experiments were performed in a LC-MS hybrid quadrupole/time of flight (QTOF) analyzer equipped with an Agilent 1200 LC coupled to an Agilent 6500 Accurate Mass (1-2 ppm mass accuracy) using electrospray ionization in the positive mode (ESI^+). ^1H, ^{13}C, HSQC and HMBC-NMR spectra were recorded on a Bruker 300 (300 and 75 MHz), or a Varian 500 (500 and 126 MHz) at 25 °C. Samples were prepared as solutions in deuterated solvent and referenced to internal non-deuterated solvent peak. Chemical shifts were expressed in ppm (δ) downfield of tetramethylsilane. Coupling constants are given in hertzs (Hz). Melting points were measured on a MP 70 Mettler Toledo apparatus.

5-(1,1-Dimethylheptyl)-1,3-dihydroxybenzene (1.1).[199]

To a solution of 5-(1,1-dimethylheptyl)-1,3-dimethoxybenzene (0.45 g, 1.90 mmol) in dry CH_2Cl_2 (9 mL) was added boron tribromide (1M in CH_2Cl_2) (19 mL, 19 mmol) at 0 °C under nitrogen atmosphere. The reaction mixture was allowed to warm to room temperature and was stirred overnight. After reaction completion, MeOH was carefully added (until pH = 7). The solvent was removed under vacuum and the crude was purified by chromatography on silica gel (EtOAc) to afford the title compound as a white solid (0.37 g, 92%); mp: 88–91 ºC (98 ºC);[199] ^{1}H-NMR (300

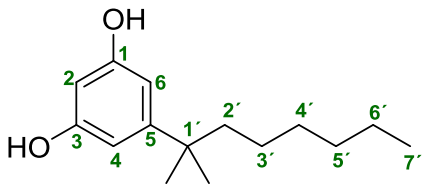

MHz, $CDCl_3$) δ: 6.35–6.45 (m, 2H, 4-H), 6.16–6.11 (m, 1H, 2-H), 4.65–4.62 (br s, 2H, OH), 1.45–1.50 (m, 2H, 2´-H), 1.22 (s, 6H, $C(CH_3)_2$), 1.21–1.10 (m, 6H, 3´-H, 4´-H, 5´-H,), 1.03–0.99 (br s, 2H, 6´-H), 0.84 ppm (t, J = 6.5 Hz, 3H, CH_3); ^{13}C-NMR (75 MHz, $CDCl_3$) δ: 163.2 (3-C), 154.0 (5-C), 111.2 (4-C), 101.3 (2-C)), 45.0 (2´-C), 35.3, 31.1, 23.9 (3´-C, 4´-C, 5´-C) , 29.8 (8´-C), 25.1 (6´-C), 14.8 ppm (7´-C); HPLC-MS: [A, 80→95%], t_R: 1.19 min, (96%); MS (ES^+, *m/z*) 237 $[M+H]^+$; Anal. calcd. for $C_{15}H_{24}O_2$: C 76.23, H 10.24, found: C 76.11, H 10.18.

7-(1,1-Dimethylheptyl)-5-hydroxy-2,2-dimethylchroman-4-one (1.2).

5-(1,1-Dimethylheptyl)resorcinol (2.50 g, 10.59 mmol) and 3,3-dimethylacrylic acid (1.59 g, 15.88 mmol) both dissolved in methanesulfonic acid (16 mL, 0.24 mmol) were added to P_2O_5 (1.20 g, 8.81

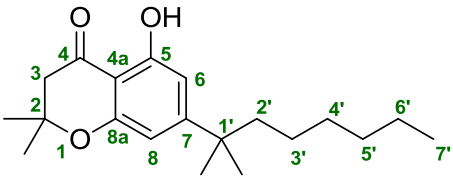

mmol) under nitrogen atmosphere. Then, the reaction mixture was stirred 8 h at 70 ºC. Afterwards, water was added (50 mL) and the product was extracted with EtOAc (3 x 50 mL). The combined organic layers were dried over $MgSO_4$. The organic solvent was evaporated under reduced pressure and the crude was purified by column chromatography on silica gel (hexane/EtOAc, 5:1), obtaining the desired compound as a pale yellow solid (2.77 g, 81%), mp: 50–52 ºC (lit: oil); ^{1}H-NMR (300 MHz, $CDCl_3$) δ: 11.53 (s, 1H, OH), 6.45 (d, J = 1.6 Hz, 1H, 6-H), 6.37 (d, J = 1.6 Hz, 1H, 8-H), 2.71 (s, 2H, 3-H), 1.60–1.49 (m, 2H, 2'-H), 1.47 (s, 6H, $OC(CH_3)_2$), 1.22 (s, 6H, $C(CH_3)_2$), 1.23–1.17 (m, 6H, 3'-H, 4'-H, 5'-H), 1.11–0.94 (m, 2H, 6'-H) 0.84 ppm (t, J = 6.6 Hz,

3H, 7'-H); ^{13}C-NMR (75 MHz, $CDCl_3$) δ: 197.4 (4-C), 162.6 (7-C), 161.3 (5-C), 159.5 (8a-C), 106.6 (6-C), 105.7 (8-C), 105.3 (4a-C), 78.9 (2-C), 48.1 (3-C), 44.0 (2'-C), 38.7 (1'-C), 31.7, 29.9, 22.6 (3'-C, 4'-C, 5'-C), 28.4 ($C(CH_3)_2$), 26.7 ($OC(CH_3)_2$), 24.6 (6'-C), 14.0 ppm (7'-C); HPLC-MS: [A, 80→95%], t_R: 4.94 min, (95%); MS (ES^+, *m/z*) 319 $[M + H]^+$; Anal. calcd. for $C_{20}H_{30}O_3$: C 75.43, H 9.50, found: C 75.52, H 9.64.

7-(1,1-Dimethylheptyl)-5-hydroxy-3-hydrodymethylene-2,2-dimethylchroman-4-one (1.3).

A solution of **1.2** (0.40 g, 1.25 mmol) in anhydrous THF (8 mL) was added to a vial containing dry sodium hydride (0.30 g, 12.57 mmol) under nitrogen atmosphere. The mixture was irradiated under microwave at 45 ºC for 25 minutes. Subsequently, ethyl formate (2.88 mL, 37.70 mmol) was added to the sealed vial and it was irradiated under microwave at 45 ºC for 25 minutes. Water was added and the product was extracted with EtOAc (3 x 5 mL). The combined organic layers were dried over $MgSO_4$ and the solvent was evaporated under reduced pressure. The crude was purified by column chromatography on silica gel (hexane/EtOAc, 4:1), to afford compound **1.3** as a yellow oil (0.33 g, 76%); ^{1}H-NMR (300 MHz, $CDCl_3$) δ: 13.49 (d, *J* = 11.7 Hz, 1H, CHO*H*), 11.28 (s, 1H, 5-OH), 7.34 (d, *J* = 11.7 Hz, 1H, C*H*OH), 6.47 (d, *J* = 1.6 Hz, 1H, 6-H), 6.36 (d, *J* = 1.6 Hz, 1H, 8-H), 1.58 (s, 6H, $OC(CH_3)_2$), 1.56–1.46 (m, 2H, 2'-H), 1.22 (s, 6H, $C(CH_3)_2$), 1.14–1.28 (m**,** 6H, 3'-H, 4'-H, 5'-H), 1.10–1.04 (m, 2H, 6'-H), 0.84 ppm (t, *J* = 6.5 Hz, 3H, 7'-H); ^{13}C-NMR (75 MHz, $CDCl_3$) δ: 189.4 (4-C), 162.7 (7-C), 161.6 (5-C), 161.5 (CHOH), 158.7 (8a-C), 114.4 (3-C), 107.4 (6-C), 106.2 (8-C), 104.9 (4a-C), 78.3 (2-C), 44.4 (2'-C), 38.8 (1'-C), 31.7, 29.9, 22.6 (3'-C, 4'-C, 5'-C), 28.4 ($C(CH_3)_2$), 28.2 ($OC(CH_3)_2$), 24.6 (6'-C), 14.1 ppm (7'-C); HPLC-MS: [A, 80→95%], t_R: 2.88 min, (97%); MS (ES^+, *m/z*) 347 $[M + H]^+$; Anal. calcd. for $C_{21}H_{30}O_4$: C 72.80, H 8.73, found: C 73.07, H 8.64.

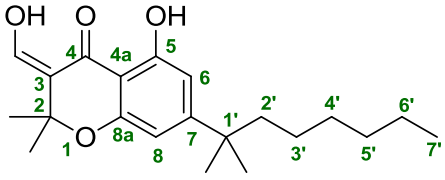

7-(1,1-Dimethylheptyl)-2,4-dihydro-4,4-dimethylchromeno[4,3-*c*]pyrazol-9-ol (1.4).

A solution of **1.3** (0.50 g, 1.44 mmol) and anhydrous hydrazine (0.11 mL, 3.61 mmol) in EtOH (9 mL) was stirred during 4 h at 40 ºC. The solvent was evaporated under reduced pressure and the crude was purified by column chromatography on silica gel (hexane/EtOAc, 2:1) to furnish **1.4** as a yellow oil (0.40 g, 81%); ^{1}H-NMR (300 MHz, $CDCl_3$) δ: 7.32–7.29 (br s, 1H, NH), 6.58 (d, *J* = 1.5 Hz, 1H, 6-H), 6.51 (d, *J* = 1.5 Hz, 8-H), 6.48 (s, 1H, 3-H), 1.63 (s, 6H, $OC(CH_3)_2$), 1.58-1.52 (m, 2H, 2´-H), 1.25 (s, 6H, $C(CH_3)_2$), 1.18 (s, 6H, 3´-H, 4´-H, 5´-H), 1.12–1.05 (m, 2H, 6´-H), 0.83 ppm (t, *J* = 6.7 Hz, 3H, 7´-H); ^{13}C-NMR (75 MHz, $CDCl_3$) δ: 153.7 (9-C), 153.5 (5a-C), 153.4 (7-C), 144.1 (9b-C), 129.1 (3-C), 123.4 (3a-C), 106.8 (8-C), 106.5 (6-C), 101.7 (9a-C), 77.0 ($OC(CH_3)_2$), 44.9 (2´-C), 38.4 ($C(CH_3)_2$), 32.2, 30.4, 30.0 (3´-C, 4´-C, 5´-C), 29.3 ($C(CH_3)_2$), 25.0 ($OC(CH_3)_2$), 23.1 (6´-C), 14.5 ppm (7´-C); HPLC-MS: [A, 80→95%], t_R: 3.80 min, (98%); MS (ES^+, *m/z*) 343 $[M+H]^+$; Anal. calcd. for $C_{21}H_{30}N_2O_2$: C 73.65, H 8.83, found: C 74.01, H, 8.59.

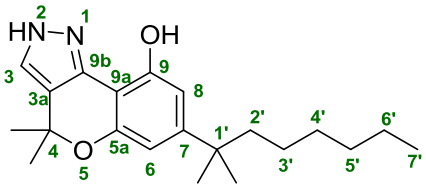

7-(1,1-Dimethylheptyl)-1,4-dihydro-1,4,4-trimethylchromeno[4,3-*c*]pyrazol-9-ol (1.5a) and 7-(1,1-dimethylheptyl)-2,4-dihydro-2,4,4-trimethylchromeno[4,3-*c*]pyrazol-9-ol (1.5b).

Compounds **1.5a** and **1.5b** were obtained from **1.3** (1.19 g, 3.40 mmol) using methylhydrazine (0.63 g, 13.60 mmol) and following the procedure described for **1.4**. Column chromatography on silica gel (hexane/EtOAc, 3:1) afforded both regioisomers. Compound **1.5a** was obtained as a yellow solid (24 mg, 2%), mp: 93–95 ºC; ^{1}H-NMR (300 MHz, $CDCl_3$) δ: 7.68–7.64 (br s, 1H, OH), 7.32 (s, 1H, 3-H), 6.61 (d, *J* = 1.8 Hz, 1H, 8-H), 6.50 (d, *J*= 1.8 Hz, 1H, 6-H), 4.18 (s, 3H, NCH_3), 1.57 (s, 6H, $OC(CH_3)_2$), 1.49–1.45 (m, 2H, 2'-H), 1.24 (s, 6H, $C(CH_3)_2$), 1.18-1.12 (m, 6H, 4'-H, 5'-H, 6'-H), 1.05–1.01 (m, 2H, 3'-H), 0.83 ppm (t, *J* = 6.4 Hz, 3H, 7'-H); ^{13}C-NMR (75 MHz, $CDCl_3$) δ: 154.2 (9-C), 152.8 (7-C), 150.7 (5a-C), 133.3 (9b-C), 131.6 (3-C), 123.1 (3a-C), 108.6 (8-C), 107.5 (6-C), 102.7 (9a-C), 76.5 ($OC(CH_3)_2$), 44.4 (NCH_3), 41.0 (2'-C), 37.8 ($C(CH_3)_2$), 31.8, 30.0, 22.6 (3'-C, 4'-C, 5'-C), 28.7 ($C(CH_3)_2$), 27.3

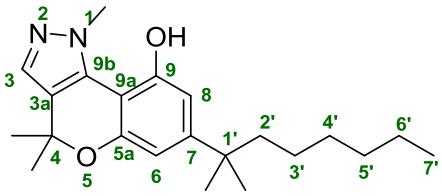

($OC(CH_3)_2$), 24.6 (6'-C), 14.1 ppm (7'-C); HPLC-MS: [A, 80→95%], t_R: 2.63 min, (98%); MS (ES^+, *m/z*) 357 $[M + H]^+$.

Compound **1.5b** was obtained as a yellow oil (0.90 g, 74%); ^{1}H-NMR (300 MHz, $CDCl_3$) δ: 8.24 (s, 1H, OH), 7.09 (s, 1H, 3-H), 6.58 (d, *J* = 1.7 Hz, 1H, 8-H), 6.48 (d, *J* = 1.7 Hz, 1H, 6-H), 3.89 (s, 3H, NCH_3), 1.60 (s, 6H, $OC(CH_3)_2$), 1.59–1.46 (m, 2H, 2'-H), 1.25 (s, 6H, $C(CH_3)_2$), 1.21–1.15 (m, 6H, 3'-H, 4'-H, '-H), 1.11–1.03 (m, 2H, 6'-H), 0.83 ppm (t, *J* = 6.7 Hz, 3H, 7'-H); ^{13}C-NMR (75 MHz, $CDCl_3$) δ: 153.2 (9-C), 152.8 (7-C), 152.6 (5a-C), 142.5 (9b-C), 124.0 (3-C), 120.3 (3a-C), 106.5 (6-C), 106.3 (8-C), 101.2 (9a-C), 76.6 ($OC(CH_3)_2$), 45.5 (NCH_3), 38.8 (2'-C), 38.0 ($C(CH_3)_2$), 31.8, 30.0, 22.6 (3'-C, 4'-C, 5'-C), 29.7 ($OC(CH_3)_2$), 28.9 ($C(CH_3)_2$), 24.6 (6'-C), 14.0 ppm (7'-C); HPLC-MS: [A, 80→95%], t_R: 5.19 min, (99%); MS (ES^+, *m/z*) 357 $[M + H]^+$; Anal. calcd. for $C_{22}H_{32}N_2O_2$: C 74.12, H 9.05, found: C 74.30, H, 9.38.

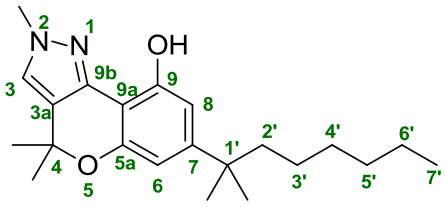

7-(1,1-Dimethylheptyl)-1-ethyl-1,4-dihydro-4,4-dimethylchromeno[4,3-*c*]pyrazol-9-ol (1.6a) and 7-(1,1-dimethylheptyl)-2-ethyl-2,4-dihydro-4,4-dimethylchromeno[4,3-*c*]pyrazol-9-ol (1.6b).

Prepared from **1.3** (0.80 g, 2.31 mmol) and ethylhydrazine oxalate (1.21 g, 8.09 mmol) by following the procedure described for **1.4**. Column chromatography on silica gel (hexane/EtOAc, 2:1) allowed isolation of the two isomers. Compound **1.6a** was obtained as a pale-yellow solid (0.42 g, 52%), mp: 129–131 ºC; ^{1}H-NMR (300 MHz, $CDCl_3$) δ: 8.37–8.31 (br s, 1H, OH), 7.39 (s, 1H, 3-H), 6.61 (d, *J* = 1.7 Hz, 1H, 8-H), 6.55 (d, *J*= 1.7 Hz, 1H, 6-H), 4.68 (q, *J* = 7.0 Hz, 2H, NCH_2CH_3), 1.58 (s, 6H, $OC(CH_3)_2$), 1.52 (m, 2H, 2'-H), 1.45 (t, *J* = 7.0 Hz, 3H, NCH_2CH_3), 1.24 (s, 6H, $C(CH_3)_2$), 1.21–1.12 (m, 6H, 3'-H, 4'-H, 5'-H), 1.08–1.03 (m, 2H, 6'-H), 0.83 ppm (t, *J* = 6.6 Hz, 3H, 7'-H); ^{13}C-NMR (75 MHz, $CDCl_3$) δ: 154.3 (9-C), 152.7 (7-C), 151.7 (5a-C), 132.7 (9b-C), 131.8 (3-C), 123.0 (3a-C), 108.5 (8-C), 107.5 (6-C), 102.8 (9a-C), 76.3

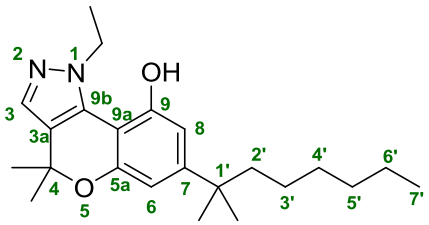

($OC(CH_3)_2$), 48.0 (NCH_2CH_3), 44.4 (2'-C), 37.8 ($C(CH_3)_2$), 31.7, 30.0, 22.6 (3'-C, 4'-C, 5'-C), 28.6 ($C(CH_3)_2$), 27.3 ($OC(CH_3)_2$), 24.6 (6'-C), 16.0 (NCH_2CH_3), 14.0 ppm (7'-C); HPLC-MS: [A, 80→95%], t_R: 2.88 min, (98%); MS (ES^+, *m/z*) 371 $[M + H]^+$; Anal. calcd for $C_{23}H_{34}N_2O_2$: C 74.55, H 9.25, found: C 74.63, H 9.19.

Compound **1.6b** was obtained as a yellow oil (0.23 g, 28%); ^{1}H-NMR (300 MHz, $CDCl_3$) δ: 8.32 (s, 1H, OH), 7.16 (s, 1H, 3-H), 6.57 (d, *J* = 1.7 Hz, 1H, 8-H), 6.48 (d, *J* = 1.6 Hz, 1H, 6-H), 4.16 (q, *J* = 7.2 Hz, 2H, NCH_2CH_3), 1.61 (s, 6H, $OC(CH_3)_2$), 1.59–1.54 (m, 2H, 2'-H), 1.51 (t, *J* = 7.2 Hz, 3H, NCH_2CH_3), 1.25 (s, 6H, $C(CH_3)_2$), 1.20–1.16 (m, 6H, 3'-H, 4'-H, 5'-H), 1.12–0.99 (m, 2H, 6'-H), 0.83 ppm (t, *J* = 6.8 Hz, 3H, 7'-H); ^{13}C-NMR (75 MHz, $CDCl_3$) δ: 153.2 (9-C), 152.8 (7-C), 152.5 (5a-C), 142.3 (9b-C), 122.4 (3-C), 119.9 (3a-C), 106.5 (6-C), 106.3 (8-C), 101.3 (9a-C), 76.8 ($OC(CH_3)_2$), 47.0 (NCH_2CH_3), 44.5 (2'-C), 38.0 ($C(CH_3)_2$), 31.8, 30.0, 22.7 (3'-C, 4'-C, 5'-C), 29.7 ($OC(CH_3)_2$), 28.9 ($C(CH_3)_2$), 24.6 (6'-C), 15.5 (NCH_2CH_3), 14.1 ppm (7'-C); HPLC-MS: [A, 80→95%], t_R: 5.84 min, (97%); MS (ES^+, *m/z*) 371 $[M + H]^+$; Anal. calcd for $C_{23}H_{34}N_2O_2$: C 74.55, H 9.25, found: C 74.23, H 9.41.

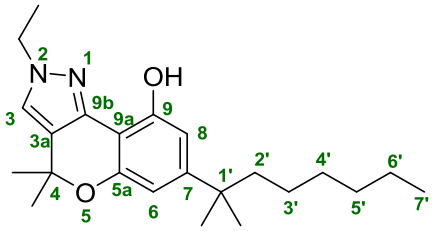

1-(3,4-Dichlorophenyl)-7-(1,1-dimethylheptyl)-1,4-dihydro-4,4-dimethylchromeno[4,3-*c*]pyrazol-9-ol (1.7).

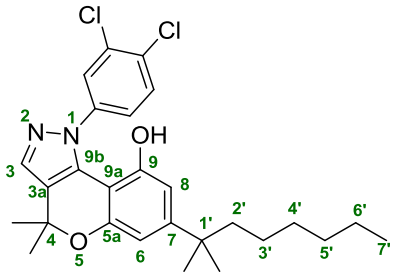

Prepared from **1.3** (17 mg, 0.05 mmol) and 3,4-dichlorophenylhydrazine hydrochloride (10 mg, 0.05 mmol) following the procedure described for **1.4**. Column chromatography on silica gel (hexane/EtOAc, 2:1) afforded **1.7** as an orange solid (9 mg, 40%); mp: 124–126 ºC; ^{1}H-NMR (300 MHz, $CDCl_3$) δ: 7.65 (d, *J* = 2.3 Hz, 1H, 2-H_{Ph}), 7.50 (s, 1H, 3-H), 7.43 (d, *J* = 8.5 Hz, 1H, 5-H_{Ph}), 7.25 (dd, *J* = 2.3 Hz, *J* = 8.5 Hz, 1H, 6-H_{Ph}), 6.66 (d, *J* = 1.6 Hz, 1H, 6-H), 6.24 (d, *J* = 1.6 Hz, 1H, 8-H), 1.68 (s, 6H, $OC(CH_3)_2$), 1.60–1.54 (m, 2H, 2´-H), 1.22 (s, 6H, $C(CH_3)_2$), 1.20–1.09 (m, 6H, 3´-H, 4´-H and 5´-H), 1.08–1.02 (m, 2H, 6´-H), 0.84 ppm (t, *J* = 6.5 Hz, 3H, 7´-H); ^{13}C-NMR (75

MHz, $CDCl_3$) δ: 154.6 (9-C), 154.0 (5a-C), 150.0 (7-C), 142.3 (1-C_{Ph}), 135.3 (3-C), 133.2 (3-C_{Ph}), 132.2 (9b-C), 130.4 (4-C_{Ph}), 126.5 (5-C_{Ph}), 125.4 (2-C_{Ph}), 123.9 (6-C_{Ph}), 122.7 (3a-C), 109.6 (6-C), 108.0 (8-C), 102.4 (9a-C), 76.2 (O*C*(CH_3)$_2$), 44.7 (2´-C), 38.3 (*C*(CH_3)$_2$), 32.1, 30.3, 25.0 (3´-C, 4´-C, 5´-C), 28.9 (C(*C*H_3)$_2$), 27.7 (OC(*C*H_3)$_2$, 23.0 (6´-C), 14.5 ppm (7´-C); HPLC-MS: [A, 80%→95%], t_R: 5.35 min, (98%); MS (ES^+, *m/z*) 487 $[M+H]^+$; Anal. calcd for $C_{27}H_{32}Cl_2N_2O_2$: C 66.53, H 6.62, found: C 66.30, H 6.58.

1-(2,4-Dichlorophenyl)-7-(1,1-dimethylheptyl)-1,4-dihydro-4,4-dimethylchromeno[4,3-*c*]pyrazol-9-ol (1.8).

Prepared from **1.3** (50 mg, 0.16 mmol) and 2,4-dichlorophenylhydrazine hydrochloride (0.13 g, 0.63 mmol) following the procedure described for **1.4**. Column chromatography on silica gel (hexane/EtOAc, 2:1) afforded **1.8** as an orange oil (52 mg, 75%); ^{1}H-NMR (300 MHz, $CDCl_3$) δ: 7.43 (s, 1H, 3-H), 7.39 (d, *J* = 2.2 Hz, 1H, 3-H_{Ph}), 7.27 (dd, *J* = 2.2 Hz, *J* = 8.7 Hz, 1H, 5-H_{Ph}), 7.21 (d, *J* = 8.7 Hz, 1H, 6-H_{Ph}), 6.56 (d, *J* = 1.6 Hz, 1H, 6-H), 6.12 (d, *J* = 1.6 Hz, 1H, 8-H), 1.64 (s, 6H, OC(CH_3)$_2$), 1.46–1.41 (m, 2H, 2´-H), 1.16–1.08 (m, 12H, 3´-H, 4´-H, 5´-H, C(CH_3)$_2$), 1.12–0.98 (m, 2H, 6´-H), 0.82 ppm (t, *J* = 6.9 Hz, 3H, 7´-H); ^{13}C-NMR (75 MHz, $CDCl_3$) δ: 154.3 (9-C), 153.6 (5a-C), 151.3 (7-C), 140.3 (1-C_{Ph}), 135.3 (2-C_{Ph}), 135.0 (4-C_{Ph}) , 134.4 (3-C), 133.0 (9b-C), 129.8 (3-C_{Ph}), 129.6 (5-C_{Ph}), 127.3 (6-C_{Ph}), 123.4 (3a-C), 108.8 (6-C), 107.6 (8-C), 102.6 (9a-C), 77.6 (O*C*(CH_3)$_2$), 44.7 (2´-C), 39.1 (*C*(CH_3)$_2$), 32.1 , 30.3, 24.9 (3´-C, 4´-C, 5´-C), 28.9 (C(*C*H_3)$_2$), 28.0 (OC(*C*H_3)$_2$), 23.0 (6´-C), 14.5 ppm (7´-C); HPLC-MS: [A, 80→95%], t_R: 4.70 min, (99%); MS (ES^+, *m/z*) 487 $[M+H]^+$. Anal. calcd for $C_{27}H_{32}Cl_2N_2O_2$: C 66.53, H 6.62, found: C 66.91, H 6.41.

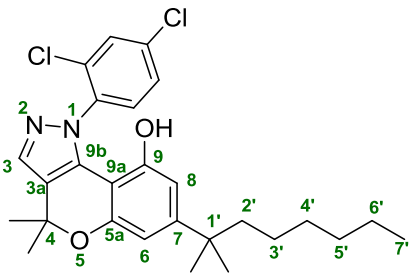

7-(1,1-Dimethylheptyl)-1,4-dihydro-1-(2-hydroxyethyl)-4,4-dimethylchromeno[4,3-*c*]pyrazol-9-ol (1.9a) and 7-(1,1-dimethylheptyl)-2,4-dihydro-2-(2-hydroxyethyl)-4,4-dimethylchromeno[4,3-*c*]pyrazol-9-ol (1.9b).

Prepared from **1.3** (40 mg, 0.11 mmol) and 2-hydroxyethylhydrazine (15.64 µL, 0.23 mmol) by following the procedure described for **1.4**. Column chromatography on silica gel (hexane/EtOAc, 2:3) allowed isolation of the two isomers. Compound **1.9a** was obtained as a white oil (10 mg, 23%); ^{1}H-NMR (300 MHz, $CDCl_3$) δ: 8.15 (s, 1H, 9-OH), 7.30 (s, 1H, 3-H), 6.62 (d, *J* = 1.6 Hz, 1H, 8-H), 6.53 (d, *J* = 1.6 Hz, 1H, 6-H), 4.29 (t, *J* = 5.7 Hz, 2H, NCH_2CH_2OH), 4.10–4.03 (m, 2H, NCH_2CH_2OH), 1.65 (s, 6H, $OC(CH_3)_2$), 1.62–1.52 (m, 2H, 2'-H), 1.28 (s, 6H, $C(CH_3)_2$), 1.25–1.17 (m, 6H, 3'-H, 4'-H, 5'-H), 1.16–1.00 (m, 2H, 6'-H), 0.87 ppm (t, *J* = 6.6 Hz, 3H, 7'-H); ^{13}C-NMR (75

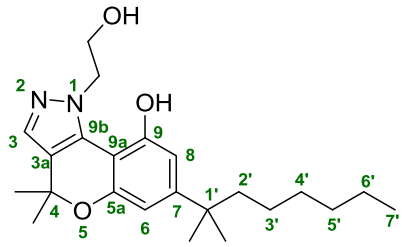

MHz, $CDCl_3$) δ: 152.9 (9-C), 152.6 (7-C), 152.4 (5a-C), 143.0 (9b-C), 124.2 (3-C), 120.0 (3a-C), 106.4 (8-C), 106.1 (6-C), 100.8 (9a-C), 76.1 ($OC(CH_3)_2$), 61.4 (NCH_2CH_2OH), 54.0 (NCH_2CH_2OH), 44.2 (2'-C), 37.8 ($C(CH_3)_2$), 31.5, 29.7, 24.4 (3'-C, 4'-C, 5´-H), 29.3 ($C(CH_3)_2$), 28.6 ($OC(CH_3)_2$), 22.4 (6'-C), 13.8 ppm (7'-C); HPLC-MS: [A, 70→95%], t_R: 5.11 min, (95%); MS (ES^+, *m/z*) 387 $[M + H]^+$; Anal. calcd for $C_{23}H_{34}N_2O_3$: C 71.47, H 8.87, found: C 71.19, H 9.04.

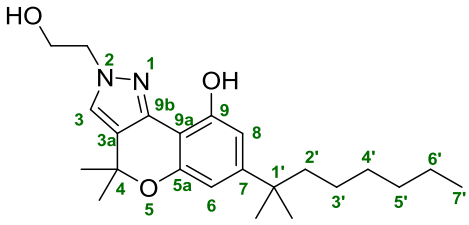

Compound **1.9b** was obtained as a yellow solid (22 mg, 50%), mp: 93–95 ºC; ^{1}H-NMR (300 MHz, $CDCl_3$) δ: 7.38 (s, 1H, 3-H), 6.63 (d, *J* = 1.8 Hz, 1H, 8-H), 6.50 (d, *J* = 1.9 Hz, 1H, 6-H), 4.63 (t, *J* = 5.0 Hz, 2H, NCH_2CH_2OH), 4.12 (t, *J* = 5.0 Hz, 2H, NCH_2CH_2OH), 1.57 (s, 6H, $OC(CH_3)_2$), 1.25 (s, 6H, $C(CH_3)_2$), 1.21–1.16 (m, 8H, 2´-H, 3'-H, 4'-H, 5'-H), 1.13–1.00 (m, 2H, 6'-H), 0.83 ppm (t, *J* = 6.5 Hz, 3H, 7'-H); ^{13}C-NMR (75 MHz, $CDCl_3$) δ: 154.4 (9-C), 153.4 (7-C), 150.4 (5a-C), 149.9 (9b-C), 133.7 (3-C), 123.3 (3a-C), 109.3 (6-C), 108.8 (8-C), 102.9 (9a-C), 76.8 ($OC(CH_3)_2$), 62.1 (NCH_2CH_2OH), 53.5 (NCH_2CH_2OH), 44.6 (2'-C), 38.0 ($C(CH_3)_2$), 32.0, 30.2, 25.9 (3'-C, 4'-C, 5´-H), 28.9 ($OC(CH_3)_2$), 27.5 ($C(CH_3)_2$), 22.9 (6'-C), 14.3 ppm (7'-C); HPLC-MS: [A, 70→95%], t_R: 3.93 min, (99%); MS (ES^+, *m/z*) 387 $[M + H]^+$; Anal. calcd for $C_{23}H_{34}N_2O_3$: C 71.47, H 8.87, found: C 71.62, H 8.96.

7-(1,1-Dimethylheptyl)-2,4-dihydro-2-hydroxymethyl-4,4-dimethylchromeno[4,3-*c*]pyrazol-9-ol (1.10).

Formaldehyde (37% in water, 13 μL, 0.17 mmol) was added to chromenopyrazole **1.4** (20 mg, 0.05 mmol) dissolved in ethanol (2 mL). The mixture was heated under reflux for 5 h and then cooled down to room temperature. After evaporation of the solvent under reduced pressure, the crude was purified by chromatography on silica gel (hexane/EtOAc, 1:1). Although HPLC-MS of the crude displayed both regioisomers, only the major one (*N*2-pyrazole) was properly isolated and characterized. Compound **1.10** was obtained as a white solid (14 mg, 69%) mp: 90-92 ºC; ^{1}H-NMR (300 MHz, $CDCl_3$) δ: 7.35 (s, 1H, 3-H), 6.59 (d, *J* = 1.6 Hz, 1H, 8-H), 6.51 (d, *J* = 1.6 Hz, 1H, 6-H), 5.30 (s, 2H, NC*H*$_2$OH), 1.64 (s, 6H, OC(CH$_3$)$_2$), 1.61–1.49 (m, 2H, 2´-H), 1.25 (s, 6H, C(CH$_3$)$_2$), 1.23–0.94 (m, 6H, 3'-H, 4'-H, 5'-H), 0.81 ppm (t, *J* = 4.8 Hz, 3H, 7'-H); ^{13}C-NMR (75 MHz, $CDCl_3$) δ: 151.7 (9-C), 150.6 (7-C), 149.1 (5a-C), 148.2 (9b-C), 127.0 (3-C), 124.7 (3a-C), 110.1 (6-C), 109.3 (8-C), 104.9 (9a-C), 75.4 (O*C*(CH$_3$)$_2$), 65.8 (NCH$_2$OH), 43.2 (2'-C), 39.5 (*C*(CH$_3$)$_2$), 32.5, 31.6, 25.5 (3'-C, 4´-C, 5'-C), 28.9 (OC(*C*H$_3$)$_2$), 27.4 (C(*C*H$_3$)$_2$), 23.7 (6'-C), 14.7 ppm (7'-C); HPLC-MS: [A, 80→95%], t_R: 3.42 min, (96%); MS (ES$^+$, *m*/*z*) 373 [M + H]$^+$; Anal. calcd for $C_{22}H_{32}N_2O_3$: C 70.94, H 8.66, found: C 71.12, H 8.93.

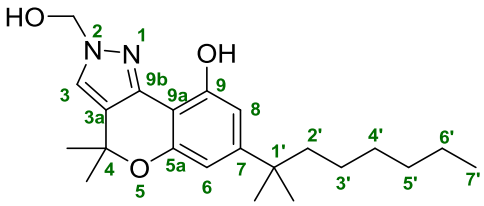

1-(3,5-Difluorophenyl)-7-(1,1-dimethylheptyl)-1,4-dihydro-4,4-dimethylchromeno[4,3-*c*]pyrazol-9-ol (1.11).

Prepared from **1.3** (30 mg, 0.08 mmol) and 3,5-difluorophenylhydrazine hydrochloride (62 mg, 0.34 mmol) following the procedure described for **1.4**. Column chromatography on silica gel (hexane/EtOAc, 3:1) afforded **1.11** as a yellow oil (32 mg, 82%); ^{1}H-NMR (300 MHz, $CDCl_3$) δ: 7.55 (s, 1H, 3-H), 7.10–6.98 (m, 3H, 2-H$_{Ph}$, 4-H$_{Ph}$, 6-H$_{Ph}$), 6.65 (d, *J* = 1.9 Hz, 1H, 6-H), 6.70 (d, *J* = 1.9 Hz, 1H, 8-H), 1.62 (s, 6H, OC(CH$_3$)$_2$), 1.49–1.43 (m, 2H, 2´-H), 1.26 (s, 6H, C(CH$_3$)$_2$), 1.19–1.08 (s, 8H, 3´-H, 4´-H, 5´-H, 6´-

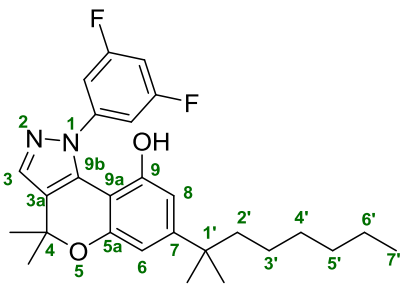

H), 0.93–0.85 ppm (m, 3H, 7´-H); ^{13}C-NMR (75 MHz, $CDCl_3$) δ: 155.2 (9-C), 154.0 (5a-C), 152.6 (7-C), 141.7 (1-C_{Ph}), 136.3 (3-C), 135.7 (3-C_{Ph}) , 135.4 (3-C_{Ph}), 134.2 (9b-C), 130.1, 128.7, 126.0 (2-C_{Ph}, 4-C_{Ph}, 6-C_{Ph}), 122.9 (3a-C), 109.3 (6-C), 108.1 (8-C), 103.9 (9a-C), 75.6 (O*C*$(CH_3)_2$), 44.0 (2´-C), 38.8 (*C*$(CH_3)_2$), 32.6, 31.0, 25.7, 23.2 (3´-C, 4´-C, 5´-C, 6´-C), 28.7 (C(*C*$H_3)_2$), 27.4 (OC(*C*$H_3)_2$), 15.1 ppm (7´-C); HPLC-MS: [A, 80%→95%], t_R: 4.22 min, (99%); MS (ES^+, *m/z*) 455 $[M+H]^+$; Anal. calcd for $C_{27}H_{32}F_2N_2O_2$: C 71.34, H 7.10, found: C 71.02, H 6.95.

7-(1,1-dimethylheptyl)-1,4-dihydro-1-(3-methoxyphenyl)-4,4-dimethylchromeno[4,3-*c*]pyrazol-9-ol (1.12).

Prepared from **1.3** (80 mg, 0.23 mmol) and 3-methoxyphenylhydrazine hydrochloride (0.16 g, 0.92 mmol) following the procedure described for **1.4**. Column chromatography on silica gel (hexane/EtOAc, 3:1) afforded **1.12** as a yellow oil (48 mg, 47%); ^{1}H-NMR (300 MHz, $CDCl_3$) δ: 7.47 (s, 1H, 3-H), 7.32 (t, *J* = 7.5 Hz, 1H, 5-H_{Ph}), 7.27 (t, *J* = 1.7 Hz, 1H, 2-H_{Ph}), 7.18–7.13 (m, 1H, 6-H_{Ph}), 7.01– 6.96 (m, 1H, 4-H_{Ph}), 6.60 (d, *J* = 1.8 Hz, 1H, 6-H), 6.53 (d, *J* = 1.8 Hz, 1H, 8-H), 3.75 (s, 3H, OCH_3), 1.63 (s, 6H, OC$(CH_3)_2$), 1.60–1.52 (m, 2H, 2´-H), 1.31–1.20 (m, 12H, 3´-H, 4´-H, 5´-H, C$(CH_3)_2$), 1.16–1.09 (m, 2H, 6´-H), 0.89–0.79 ppm (m, 3H, 7´-H); ^{13}C-NMR (75 MHz, $CDCl_3$) δ: 156.1 (9-C), 154.1 (3-C_{Ph}), 150.9 (5a-C), 141.2 (7-C), 138.2 (1-C_{Ph}), 136.2 (3-C), 133.4 (9b-C), 130.2 (5-C_{Ph}), 113.4 (6-C_{Ph}), 122.3 (4-C_{Ph}), 120.3 (3a-C), 109.0 (2-C_{Ph}), 108.6 (6-C), 105.0 (8-C), 103.4 (9a-C), 75.0 (O*C*$(CH_3)_2$), 56.3 (OCH_3), 44.8 (2´-C), 38.7 (*C*$(CH_3)_2$), 31.7, 30.2, 26.1 (3´-C, 4´-C, 5´-C), 28.9 (C(*C*$H_3)_2$), 27.6 (OC(*C*$H_3)_2$), 23.0 (6´-C), 14.3 ppm (7´-C); HPLC-MS: [A, 80→95%], t_R: 3.81 min, (94%); MS (ES^+, *m/z*) 449 $[M+H]^+$. Anal. calcd for $C_{28}H_{36}N_2O_3$: C 74.97, H 8.09, found: C 75.06, H 7.78.

1-Cyclohexyl-7-(1,1-dimethylheptyl)-1,4-dihydro-4,4-dimethylchromeno[4,3-*c*]pyrazol-9-ol (1.13).

Prepared from **1.3** (93 mg, 0.27 mmol) and cyclohexylhydrazine hydrochloride (0.12 g, 0.80 mmol) by following the procedure described for **1.4**. Column chromatography on silica gel (hexane/EtOAc, 2:1) afforded compound **1.13** as a pale-yellow solid (39 mg, 35%), mp: 98–100 ºC; ^{1}H-NMR (300 MHz, $CDCl_3$) δ: 7.38 (s, 1H, 3-H), 6.62 (d, J = 1.7 Hz, 1H, 6-H), 6.57 (d, J = 1.7 Hz, 1H, 8-H), 4.61–4.52 (m, 1H, H_a), 1.86–1.80 (m, 4H, H_b and H_f), 1.76–1.69 (m, 6H, H_c, H_d, H_e), 1.64 (s, 6H, $OC(CH_3)_2$), 1.49–1.44 (m, 2H, 2´-H), 1.24 (s, 6H, $C(CH_3)_2$), 1.19–1.08 (m, 8H, 3'-H, 4'-H, 5'-H, 6´-H), 0.92–0.86 ppm (m, 3H, 7´-H); ^{13}C-NMR (75 MHz, $CDCl_3$) δ: 152.8 (9-C), 151.6 (7-C), 149.9 (5a-C), 134.8 (9b-C), 130.6 (3-C), 125.3 (3a-C), 109.3 (8-C), 106.1 (6-C), 103.2 (9a-C), 75.7 ($OC(CH_3)_2$), 50.3 (C_a), 43.1 (2'-C), 38.2 ($C(CH_3)_2$), 32.6 (C_b, C_f), 31.6, 31.0, 24.0, 22.8 (3'-C, 4'-C, 5'-C, 6´-C), 28.9 ($C(CH_3)_2$), 27.7 ($OC(CH_3)_2$), 26.9, 26.3 (C_c, C_d,C_e), 14.7 ppm (7'-C); HPLC-MS: [A, 80→95%], t_R: 5.02 min, (97%); MS (ES^+, m/z) 426 $[M + H]^+$; Anal. calcd for $C_{27}H_{40}N_2O_2$: C 76.37, H 9.50, found: C 76.11, H 9.74.

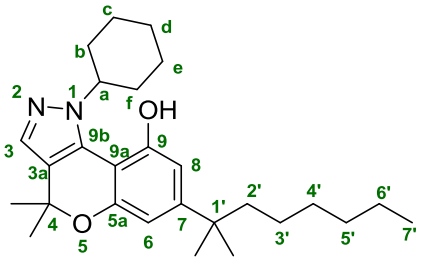

7-(1,1-Dimethylheptyl)-2,4-dihydro-9-methoxy-4,4-dimethylchromeno[4,3-*c*]pyrazole (1.14).

A solution of **1.4** (50 mg, 0.14 mmol) in anhydrous THF (3 mL) was added dropwise to a precooled suspension of sodium hydride (5.2 mg, 0.22 mmol) in anhydrous THF (1 mL) under nitrogen atmosphere. The resulting yellow solution was stirred for 10 minutes at room temperature. Then, iodomethane (27 μL, 0.43 mmol) was rapidly added. The reaction mixture was refluxed for 1 hour. The crude was diluted with diethyl ether, filtered and concentrated in vacuo. Column chromatography on silica gel (hexane/EtOAc, 3:1) afforded **1.14** as a yellow oil (21 mg, 40%); ^{1}H-NMR (300 MHz, $CDCl_3$) δ: 8.13–8.09 (br s, 1H, NH), 7.31 (d, J = 1.5 Hz, 1H, 6-H), 7.19 (d, J = 1.5 Hz, 8-H), 6.74 (s, 1H, 3-H), 3.95 (s, 3H, OCH_3), 1.69–1.60 (br s, 6H, $OC(CH_3)_2$), 1.60–1.56 (m, 2H, 2´-H), 1.39 (s, 6H, $C(CH_3)_2$), 1.25–1.22 (m, 6H, 3´-H, 4´-H, 5´-H), 1.17–1.08 (m, 2H, 6´-H), 0.81 ppm (t, J = 6.7 Hz, 3H, 7´-H); ^{13}C-NMR (75 MHz,

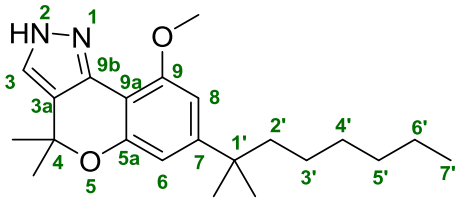

$CDCl_3$) δ: 157.0 (9-C), 155.4 (5a-C), 154.1 (7-C), 143.2 (9b-C), 125.6 (3-C), 120.1 (3a-C), 108.0 (8-C), 107.5 (6-C), 102.3 (9a-C), 76.8 (O*C*(CH_3)$_2$), 49.6 (OCH_3), 43.7 (2´-C), 40.2 (*C*(CH_3)$_2$), 37.2, 34.7, 24.6 (3´-C, 4´-C, 5´-C), 29.1 (C(*C*H_3)$_2$), 28.3 (OC(*C*H_3)$_2$), 22.7 (6´-C), 15.1 ppm (7´-C); HPLC-MS: [A, 80%→95%], t_R: 5.41 min, (97%); MS (ES^+, *m/z*) 357 $[M+H]^+$; Anal. calcd. for $C_{22}H_{32}N_2O_2$: C 74.12, H 9.05, found: C 74.35, H, 8.87.

7-(1,1-Dimethylheptyl)-2,4-dihydro-9-methoxy-2,4,4-trimethylchromeno[4,3-*c*]pyrazole (1.15).

Prepared from **1.5b** (25 mg, 0.07 mmol), sodium hydride (2.5 mg, 0.10 mmol) and iodomethane (13 μL, 0.21 mmol) following the procedure described for **1.14**. Column chromatography on silica gel (hexane/EtOAc, 2:1) afforded **1.15** as a white solid (17 mg, 68%); mp: 85–87 ºC; ^{1}H-NMR (300 MHz, $CDCl_3$) δ: 7.63 (s, 1H, 3-H), 6.91 (d, *J* = 1.8 Hz, 1H, 6-H), 6.76 (d, *J* = 1.8 Hz, 1H, 8-H), 4.02 (s, 3H, NCH_3), 3.90 (s, 3H, OCH_3), 1.59 (s, 6H, OC(CH_3)$_2$), 1.45–1.36 (m, 2H, 2´-H), 1.30 (s, 6H, C(CH_3)$_2$), 1.2–1.13 (m, 6H, 3´-H, 4´-H, 5´-H), 1.10–1.03 (m, 2H, 6´-H), 0.87 ppm (t, *J* = 7.0 Hz, 3H, 7´-H); ^{13}C-NMR (75 MHz, $CDCl_3$) δ: 153.2 (9-C), 152.6 (5a-C), 151.8 (7-C), 142.1 (9b-C), 124.3 (3-C), 122.0 (3a-C), 109.5 (6-C), 105.7 (8-C), 103.1 (9a-C), 76.2 (O*C*(CH_3)$_2$), 57.0 (OCH_3), 45.3 (NCH_3), 39.2 (2´-C), 37.8 (*C*(CH_3)$_2$), 32.0, 31.3, 25.3 (3´-C, 4´-C, 5´-C), 29.5 (C(*C*H_3)$_2$), 27.8 (OC(*C*H_3)$_2$), 23.5 (6´-C), 13.8 ppm (7´-C); HPLC-MS: [A, 80%→95%], t_R: 3.58 min, (99%); MS (ES^+, *m/z*) 371 $[M+H]^+$; Anal. calcd. for $C_{23}H_{34}N_2O_2$: C 74.55, H 9.25, found: C 74.89, H, 8.96.

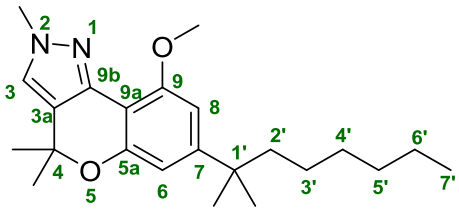

7-(1,1-Dimethylheptyl)-1-ethyl-1,4-dihydro-9-methoxy-4,4-dimethylchromeno[4,3-*c*]pyrazole (1.16).

Prepared from **1.6a** (25 mg, 0.067 mmol), sodium hydride (2.5 mg, 0.1 mmol) and iodomethane (12 μL, 0.20 mmol) following the procedure previously described for **1.14**. Column chromatography on silica gel (hexane/EtOAc, 3:1) afforded **1.16** as a white solid (13 mg, 52%); mp: 90–91 ºC; ^{1}H-NMR (300 MHz, $CDCl_3$) δ: 7.34 (s, 1H, 3-H), 6.70 (d, *J* = 1.5 Hz, 2H, 6-H), 6.52 (d, *J* = 1.5 Hz, 1H, 8-H),

4.42 (q, J = 7.9 Hz, 2H, NCH_2CH$_3$), 3.81 (s, 3H, OCH$_3$), 1.60 (s, 6H, OC(CH$_3$)$_2$), 1.54-1.50 (m, 2H, 2´-H), 1.45 (t, J = 7.9 Hz, 3H, NCH$_2$CH_3), 1.31 (s, 6H, C(CH_3)$_2$), 1.24–1.19 (br s, 8H, 3´-H, 4´-H, 5´-H, 6´-H), 0.86 ppm (t, J = 8.0 Hz, 3H, 7´-H); ^{13}C-NMR (75 MHz, CDCl$_3$) δ: 153.0 (9-C), 152.6 (5a-C), 150.4 (7-C), 132.3 (3-C), 131.7 (9b-C), 121.9 (3a-C), 109.0 (8-C), 105.3 (6-C), 101.1 (9a-C), 76.8 (OC(CH$_3$)$_2$), 54.5 (OCH$_3$), 49.6 (NCH$_2$CH$_3$), 43.9 (2´-C), 38.4 (C(CH$_3$)$_2$), 31.8, 30.5, 26.0 (3´-C, 4´-C, 5´-C), 28.7 (C(CH$_3$)$_2$), 26.9 (OC(CH$_3$)$_2$), 22.9 (6´-C), 15.8 (NCH$_2$CH$_3$), 14.6 ppm (7´-C); HPLC-MS: [A, 15% - 95%], t_R: 5.81 min, (98%); MS (ES$^+$, m/z) 385 [M+H]$^+$; Anal. calcd. for $C_{24}H_{36}N_2O_2$: C 74.96, H 9.44, found: C 74.57, H 9.25.

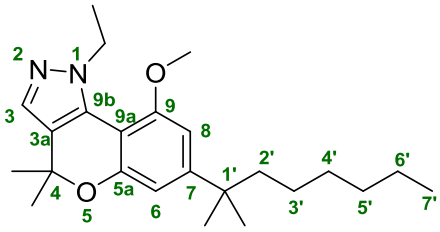

7-(1,1-Dimethylheptyl)-2-ethyl-2,4-dihydro-9-methoxy-4,4-dimethylchromeno[4,3-*c*]pyrazole (1.17).

Prepared from **1.6b** (25 mg, 0.07 mmol), sodium hydride (2.5 mg, 0.1 mmol) and iodomethane (12 μL, 0.20 mmol) following the procedure described for **1.14**. Column chromatography on silica gel (hexane/EtOAc, 1:1) afforded **1.17** as a white solid (20 mg, 77%); mp: 87–88 ºC; ^{1}H-NMR (300 MHz, CDCl$_3$) δ: 7.09 (s, 1H, 3-H), 6.50 (d, J = 1.3 Hz, 8-H), 6.37 (s, 1H, J = 1.3 Hz, 6-H), 4.19 (q, 2H, J = 7.2 Hz, NCH_2CH$_3$), 3.90 (s, 3H, OCH$_3$), 1.64 (s, 6H, OC(CH$_3$)$_2$), 1.57–1.54 (br s, 2H, 2´-H), 1.53 (t, 3H, J = 7.6 Hz, NCH$_2$CH_3), 1.27 (s, 6H, C(CH$_3$)$_2$), 1.20–1.11 (m, 6H, 3´-H, 4´-H, 5´-H), 1.09–1.04 (br s, 2H, 6´-H), 0.83 ppm (t, J = 7.8 Hz, 3H, 7´-H); ^{13}C-NMR (75 MHz, CDCl$_3$) δ: 155.3 (9-C), 154.0 (5a-C), 153.8 (7-C), 143.7 (9b-C), 128.2 (3-C), 126.1 (3a-C), 107.4 (6-C), 106.8 (8-C), 103.7 (9a-C), 78.0 (OC(CH$_3$)$_2$), 56.8 (OCH$_3$), 47.3 (NCH$_2$CH$_3$), 45.7 (2´-C), 39.0 (C(CH$_3$)$_2$), 32.3, 31.1, 25.7 (3´-C, 4´-C, 5´-C), 29.1 (C(CH$_3$)$_2$), 27.4 (OC(CH$_3$)$_2$), 23.3 (6´-C), 16.2 (NCH$_2$CH$_3$), 14.0 ppm (7´-C); HPLC-MS: [A, 80% - 95%], t_R: 3.95 min, (99%); MS (ES$^+$, m/z) 385 [M+H]$^+$; Anal. calcd. for $C_{24}H_{36}N_2O_2$: C 74.96, H 9.44, found: C 75.02, H 9.18.

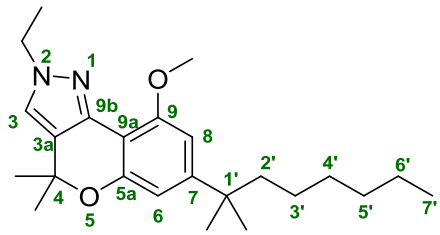

1-(3,4-Dichlorophenyl)-7-(1,1-dimethylheptyl)-1,4-dihydro-9-methoxy-4,4-dimethylchromeno[4,3-*c*]pyrazole (1.18).

Prepared from **1.7** (27 mg, 0.05 mmol), sodium hydride (2 mg, 0.08 mmol) and iodomethane (10 μL, 0.16 mmol) following the procedure previously described for **1.14**. Column chromatography on silica gel (hexane/EtOAc, 1:1) afforded **1.18** as a yellow oil (11 mg, 47%); ^{1}H-NMR (300 MHz, $CDCl_3$) δ: 7.81 (d, J = 1.9 Hz, 1H, 2-H_{Ph}), 7.72 (s, 1H, 3-H), 7.49 (d, J = 7.8 Hz, 1H, 5-H_{Ph}), 7.37 (dd, J = 7.8 Hz, J = 1.9 Hz, 1H, 6-H_{Ph}), 6.74 (d, J = 1.4 Hz, 1H, 6-H), 6.30 (d, J = 1.4 Hz, 1H, 8-H), 3.28 (s, 3H, OCH_3), 1.72 (s, 6H, $OC(CH_3)_2$), 1.68–1.60 (m, 2H, 2´-H), 1.39 (s, 6H, $C(CH_3)_2$), 1.27–1.18 (m, 6H, 3´-H, 4´-H, 5´-H), 1.12–1.08 (br s, 2H, 6´-H), 0.91 ppm (t, J = 7.1 Hz, 3H, 7´-H); ^{13}C-NMR (75 MHz, $CDCl_3$) δ: 154.2 (9-C), 153.8 (5a-C), 152.1 (7-C), 143.1 (1-C_{Ph}), 135.7 (3-C), 134.2 (3-C_{Ph}), 132.6 (9b-C), 130.8 (4-C_{Ph}), 126.3 (5-C_{Ph}), 125.9 (2-C_{Ph}), 124.0 (6-C_{Ph}), 120.1 (3a-C), 109.3 (6-C), 108.4 (8-C), 103.5 (9a-C), 76.1 ($OC(CH_3)_2$), 54.9 (OCH_3), 43.5 (2´-C), 39.0 ($C(CH_3)_2$), 33.9, 32.3, 26.8 (3´-C, 4´-C, 5´-C), 28.3 ($C(CH_3)_2$), 27.1 ($OC(CH_3)_2$, 22.7 (6´-C), 14.0 ppm (7´-C); HPLC-MS: [A, 80%→95%], t_R: 11.13 min, (95%); MS (ES^+, m/z) 501 $[M+H]^+$; Anal. calcd. for $C_{28}H_{34}Cl_2N_2O_2$: C 67.06, H 6.83, found: C 66.79, H 6.55.

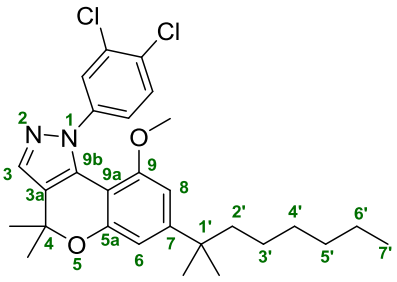

1-(2,4-Dichlorophenyl)-7-(1,1-dimethylheptyl)-1,4-dihydro-9-methoxy-4,4-dimethylchromeno[4,3-*c*]pyrazole (1.19).

Prepared from **1.8** (26 mg, 0.05 mmol), sodium hydride (2 mg, 0.08 mmol) and iodomethane (10 μL, 0.16 mmol) following the procedure previously described. Column chromatography on silica gel (hexane/EtOAc, 1:1) afforded **1.19** as a orange oil (12 mg, 50%); ^{1}H-NMR (300 MHz, $CDCl_3$) δ: 7.51 (s, 1H, 3-H), 7.47 (d, J = 2.0 Hz, 1H, 3-H_{Ph}), 7.35 (dd, J = 2.0 Hz, J = 8.1 Hz, 1H, 5- H_{Ph}), 7.38 (d, J = 8.1 Hz, 1H, 6-H_{Ph}), 6.60 (d, J = 1.7 Hz, 1H, 6-H), 6.28 (d, J = 1.7 Hz, 1H, 8-H), 3.21 (s, 3H, OCH_3), 1.59 (s, 6H,

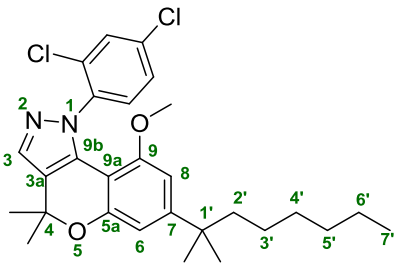

$OC(CH_3)_2$), 1.52-1.46 (m, 2H, 2´-H), 1.30 (s, 6H, $C(CH_3)_2$), 1.19–1.07 (m, 6H, 3´-H, 4´-H, 5´-H), 1.07–1.02 (br s, 2H, 6´-H), 0.79 ppm (t, *J* = 7.0 Hz, 3H, 7´-H); ^{13}C-NMR (75 MHz, $CDCl_3$) δ: 157.0 (9-C), 156.3 (5a-C), 155.8 (7-C), 141.7 (1-C_{Ph}), 136.1 (2-C_{Ph}), 135.5 (4-C_{Ph}), 133.9 (3-C), 131.2 (9b-C), 130.8 (3-C_{Ph}), 129.7 (5-C_{Ph}), 128.3 (6-C_{Ph}), 122.9 (3a-C), 109.7 (6-C), 105.2 (8-C), 103.1 (9a-C), 77.4 ($OC(CH_3)_2$), 56.0 (OCH_3), 43.6 (2´-C), 38.5 ($C(CH_3)_2$), 33.1 , 31.7, 26.4 (3´-C, 4´-C, 5´-C), 29.2 ($C(CH_3)_2$), 27.9 ($OC(CH_3)_2$), 24.3 (6´-C), 13.9 ppm (7´-C); HPLC-MS: [A, 80%→95%], t_R: 9.17 min, (98%); MS (ES^+, *m/z*) 501 $[M+H]^+$; Anal. calcd. for $C_{28}H_{34}Cl_2N_2O_2$: C 67.06, H 6.83, found: C 66.85, H 7.02.

1-(3,4-Dichlorophenyl)-7-(1,1-dimethylheptyl)-9-ethoxy-1,4-dihydro-4,4-dimethylchromeno[4,3-*c*]pyrazole (1.20).

Prepared from **1.7** (20 mg, 0.04 mmol), sodium hydride (1.5 mg, 0.06 mmol) and iodoethane (10 μL, 0.12 mmol) following the procedure previously described for **1.14**. Column chromatography on silica gel (hexane/EtOAc, 3:1) afforded **1.20** as a yellow oil (8 mg, 39%); ^{1}H-NMR (300 MHz, $CDCl_3$) δ: 7.75 (d, *J* = 1.5 Hz, 1H, 2-H_{Ph}), 7.63 (s, 1H, 3-H), 7.41 (d, *J* = 7.2 Hz, 1H, 5-H_{Ph}), 7.29 (dd, *J* = 7.2 Hz, *J* = 1.5 Hz, 1H, 6-H_{Ph}), 6.60 (d, *J* = 1.6 Hz, 1H, 6-H), 6.41 (d, *J* = 1.6 Hz, 1H, 8-H), 3.72 (q, *J* = 7.3 Hz, 2H, OCH_2CH_3), 1.67 (s, 6H, $OC(CH_3)_2$), 1.55–1.49 (m, 2H, 2´-H), 1.34 (s, 6H, $C(CH_3)_2$), 1.29–1.20 (m, 6H, 3´-H, 4´-H, 5´-H), 1.16–1.13 (br s, 2H, 6´-H), 1.01 (t, *J* = 7.3 Hz, 3H, OCH_2CH_3), 0.85 ppm (t, *J* = 6.9 Hz, 3H, 7´-H); ^{13}C-NMR (75 MHz, $CDCl_3$) δ: 155.4 (9-C), 154.7 (5a-C), 153.5 (7-C), 142.9 (1-C_{Ph}), 134.6 (3-C), 133.1 (3-C_{Ph}), 131.8 (9b-C), 130.6 (4-C_{Ph}), 127.1 (5-C_{Ph}), 126.6 (2- C_{Ph}), 123.1 (6-C_{Ph}), 110.2 (6-C), 106.4 (8-C), 105.8 (9a-C), 76.0 ($OC(CH_3)_2$),63.2 (OCH_3), 44.7 (2´-C), 39.8 ($C(CH_3)_2$), 33.7, 32.0, 27.5 (3´-C, 4´-C, 5´-C), 30.6 ($C(CH_3)_2$), 28.2 ($OC(CH_3)_2$, 23.0 (6´-C), 14.2 (OCH_2CH_3), 13.9 ppm (7´-C); HPLC-MS: [iso 95% - 5%], t_R: 5.57 min, (95%); MS (ES^+, *m/z*) 515 $[M+H]^+$; Anal. calcd. for $C_{29}H_{36}Cl_2N_2O_2$: C 67.57, H 7.04, found: C 67.23, H 6.89.

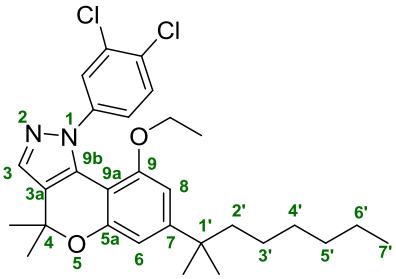

General procedure for the synthesis of alkoxychromenopyrazoles 1.21−1.38

A solution of the corresponding chromenopyrazole (1 eq) in anhydrous THF (1-5 mL) was added dropwise to a precooled suspension of sodium hydride (1.1−2.5 eq) in anhydrous THF (0.5-2 mL) under nitrogen atmosphere. The resulting solution was stirred for 10 minutes at room temperature. The corresponding alkyl halide (3-5 eq) was rapidly added, the reaction mixture was refluxed for 1-12 hours. The crude was dissolved in EtOAc, washed with water and extracted three times with EtOAc. The organic layers were combined and dried over $MgSO_4$. After removal of the solvent under vacuum, the crude was purified by chromatography on silica gel. The chromatography eluents and yields are indicated below for each reaction.

9-Benzyloxy-2,4-dihydro-7-(1,1-dimethylheptyl)-4,4-dimethylchromeno[4,3-*c*]pyrazole (1.21). Prepared from **1.4** (10 mg, 0.03 mmol), sodium hydride (1.20 mg, 0.04 mmol) and benzyl bromide (10 μL, 0.09 mmol). Column chromatography on silica gel (hexane/EtOAc, 3:1) afforded the title compound. Compound **1.21** was obtained as a yellow solid (5 mg, 41%); mp: 110–112 ºC; ^{1}H-NMR (300 MHz, $CDCl_3$) δ: 7.55–7.29 (m, 5H, 2-H_{Bn}, 3-H_{Bn}, 4-H_{Bn}, 5-H_{Bn}, 6-H_{Bn}), 7.16 (s, 1H, 3-H), 6.62 (d, J = 1.5 Hz, 1H, 6-H), 6.57 (d, J = 1.5 Hz, 1H, 8-H), 5.18 (s, 2H, OCH_2), 1.64 (s, 6H, $OC(CH_3)_2$), 1.58–1.48 (m, 2H, 2´-H), 1.25 (s, 6H, $C(CH_3)_2$), 1.22–1.12 (m, 6H, 3´-H, 4´-H, 5´-H), 1.12–0.96 (m, 2H, 6´-H), 0.90–0.79 ppm (m, 3H, 7´-H); ^{13}C-NMR (75 MHz, $CDCl_3$) δ: 157.0 (9-C), 155.2 (5a-C), 153.7 (7-C), 142.5 (9b-C), 139.6 (1-C_{Bn}), 134.8 (3-C), 129.3, 128.1, 127.5 (2-C_{Bn}, 3-C_{Bn}, 4-C_{Bn}, 5-C_{Bn}, 6-C_{Bn}), 124.3 (3a-C), 111.4 (6-C), 108.6 (8-C), 106.3 (9a-C), 75.7 ($OC(CH_3)_2$), 71.3 (OCH_2), 43.1 (2´-C), 39.4 ($C(CH_3)_2$), 32.8, 30.6, 25.8 (3´-C, 4´-C, 5´-C), 28.2 ($C(CH_3)_2$), 27.3 ($OC(CH_3)_2$), 23.9 (6´-C), 15.1 ppm (7´-C); ppm (7´-C); HPLC-MS: [iso 95% - 5%], t_R: 2.25 min, (95%); MS (ES^+, m/z) 433 $[M+H]^+$; Anal. calcd. for $C_{28}H_{36}N_2O_2$: C 77.74, H 8.39, found: C 77.92, H, 8.16.

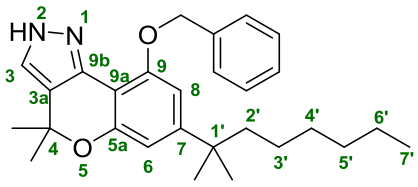

9-Benzyloxy-7-(1,1-dimethylheptyl)-2,4-dihydro-2,4,4-trimethylchromeno[4,3-*c*]pyrazole (1.22).

Prepared from **1.5b** (10 mg, 0.03 mmol), sodium hydride (1.10 mg, 0.04 mmol) and benzyl bromide (10 μL, 0.09 mmol) following the procedure previously described. Column chromatography on silica gel (hexane/EtOAc, 2:1) afforded the title compound as a pale yellow oil (12 mg, 96%); ^{1}H-NMR

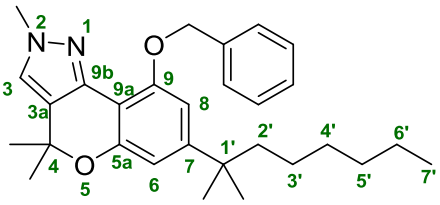

(300 MHz, $CDCl_3$) δ: 7.71 (d, J = 7.0 Hz, 2H, 2-H_{Bn}, 6-H_{Bn}), 7.41–7.36 (m, 2H, 3-H_{Bn}, 5-H_{Bn}), 7.31–7.26 (m, 1H, 4-H_{Bn}), 7.11 (s, 1H, 3-H), 6.58 (d, J = 1.3 Hz, 1H, 6-H), 6.50 (d, J = 1.3 Hz, 1H, 8-H), 5.92 (s, 2H, OCH_2), 3.98 (s, 3H, NCH_3), 1.56 (s, 6H, $OC(CH_3)_2$), 1.50–1.44 (m, 2H, 2´-H), 1.22 (s, 6H, $C(CH_3)_2$), 1.16–1.11 (m, 6H, 3´-H, 4´-H, 5´-H), 1.05–0.99 (br s, 2H, 6´-H), 0.81 ppm (t, J = 8.0 Hz, 3H, 7´-H); ^{13}C-NMR (75 MHz, $CDCl_3$) δ: 154.3 (9-C), 153.8 (5a-C), 151.2 (7-C), 141.0 (9b-C), 137.8 (1-C_{Bn}), 128.1 (3-C_{Bn}, 5-C_{Bn}), 127.1 (4-C_{Bn}), 126.9 (2-C_{Bn}, 6-C_{Bn}), 123.2 (3-C), 122.1 (3a-C), 108.9 (6-C), 105.7 (8-C), 104.9 (9a-C), 75.5 ($OC(CH_3)_2$), 70.6 (OCH_2), 44.5 (NCH_3), 39.0 (2´-C), 37.9 ($C(CH_3)_2$), 31.7, 29.8, 24.5 (3´-C, 4´-C, 5´-C), 28.9 ($C(CH_3)_2$), 28.7 ($OC(CH_3)_2$), 22.5 (6´-C), 14.0 ppm (7´-C); HPLC-MS: [iso 95% - 5%], t_R: 2.47 min, (100%); MS (ES^+, m/z) 447 $[M+H]^+$; Anal. calcd. for $C_{29}H_{38}N_2O_2$: C 77.99, H 8.58, found: C 77.65, H, 8.81.

9-Benzyloxy-7-(1,1-dimethylheptyl)-1-ethyl-1,4-dihydro-4,4-dimethylchromeno[4,3-*c*]pyrazole (1.23).

Prepared from **1.6a** (20 mg, 0.05 mmol), sodium hydride (1.9 mg, 0.08 mmol) and benzyl bromide

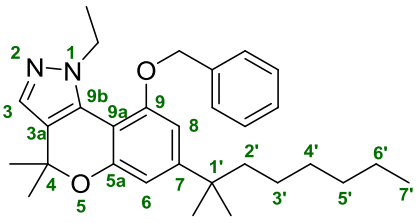

(19 μL, 0.16 mmol) following the general procedure. Column chromatography on silica gel (hexane/EtOAc, 2:1) afforded **1.23** as a yellow oil (14 mg, 70%); ^{1}H-NMR (300 MHz, $CDCl_3$) δ: 7.78 (d, J = 7.1 Hz, 2H, 2-H_{Bn}, 6-H_{Bn}), 7.49–7.45 (m, 2H, 3-H_{Bn}, 5-H_{Bn}), 7.38–7.33 (m, 1H, 4-H_{Bn}), 7.30 (s, 1H, 3-H), 6.58 (d, J = 1.9 Hz, 1H, 6-H), 6.50 (d, J = 1.9 Hz, 1H, 8-H), 5.45 (s, 2H, OCH_2), 4.38 (q, J = 7.5 Hz, 2H, NCH_2CH_3), 1.63 (s, 6H, $OC(CH_3)_2$), 1.59-1.55 (br s, 2H, 2´-H), 1.49 (t, 3H, J = 7.5 Hz, NCH_2CH_3), 1.29 (s, 6H, $C(CH_3)_2$), 1.22–1.13 (m, 6H, 3´-H, 4´-H, 5´-H), 1.10–1.02 (m, 2H, 6´-H), 0.90 ppm (t, J = 6.7 Hz, 3H, 7´-H); ^{13}C-NMR (75 MHz,

$CDCl_3$) δ: 152.5 (9-C), 151.9 (5a-C), 150.6 (7-C), 141.0 (9b-C), 138.5 (1-C_{Bn}), 129.2 (3-C_{Bn}, 5-C_{Bn}), 127.0 (4-C_{Bn}), 125.3 (2-C_{Bn}, 6-C_{Bn}), 123.1 (3-C), 121.9 (3a-C), 108.1 (6-C), 106.5 (8-C), 103.9 (9a-C), 74.9 (O*C*$(CH_3)_2$), 71.5 (OCH_2), 48.3 (N*C*H_2CH_3), 45.8 (2´-C), 39.4 (*C*$(CH_3)_2$), 32.1, 30.8, 25.6 (3´-C, 4´-C, 5´-C), 29.3 (C(*C*$H_3)_2$), 28.1 (OC(*C*$H_3)_2$), 23.0 (6´-C), 14.9 (NCH$_2$*C*H_3), 13.7 ppm (7´-C); HPLC-MS: [iso 95% - 5%], t_R: 3.28 min, (96%); MS (ES^+, *m/z*) 461 $[M+H]^+$; Anal. calcd. for for $C_{30}H_{40}N_2O_2$: C 78.22, H 8.75, found: C 77.98, H 9.06.

9-Benzyloxy-7-(1,1-dimethylheptyl)-2-ethyl-2,4-dihydro-4,4-dimethylchromeno[4,3-*c*]pyrazole (1.24).

Prepared from **1.6b** (14 mg, 0.04 mmol), sodium hydride (1.50 mg, 0.05 mmol) and benzyl bromide (13 μL, 0.11 mmol) following the procedure previously described. Column chromatography on silica gel (hexane/EtOAc, 3:1) afforded the title compound as a white oil (14 mg, 81%); ^{1}H-NMR (300 MHz, $CDCl_3$) δ: 7.76 (d, *J* = 7.1 Hz, 2H, 2-H_{Bn}, 6-H_{Bn}), 7.40–7.37 (m, 2H, 3-H_{Bn}, 5-H_{Bn}), 7.32–7.27 (m, 1H, 4-H_{Bn}), 7.15 (s, 1H, 3-H), 6.60 (d, *J* = 1.7 Hz, 1H, 6-H), 6.59 (d, *J* = 1.7 Hz, 1H, 8-H), 5.28 (s, 2H, OCH_2), 4.24 (q, *J* = 7.3 Hz, 2H, N*C*H_2CH_3), 1.63–1.58 (m, 11H, OC$(CH_3)_2$, 2´-H, NCH$_2$CH_3), 1.25 (s, 6H, C$(CH_3)_2$), 1.20–1.07 (m, 6H, 3´-H, 4´-H, 5´-H), 1.08–0.91 (m, 2H, 6´-H), 0.83 ppm (t, *J* = 6.9 Hz, 3H, 7´-H); ^{13}C-NMR (75 MHz, $CDCl_3$) δ: 154.4 (9-C), 153.8 (5a-C), 151.1 (7-C), 140.8 (9b-C), 137.9 (1-C_{Bn}), 128.1 (3-C_{Bn}, 5-C_{Bn}), 127.1 (4-C_{Bn}), 126.9 (2-C_{Bn}, 6-C_{Bn}), 121.7 (3-C), 121.0 (3a-C), 109.0 (6-C), 105.9 (8-C), 104.7 (9a-C), 75.6 (O*C*$(CH_3)_2$), 70.5 (OCH_2), 47.1 (N*C*H_2CH_3), 44.6 (2´-C), 38.0 (*C*$(CH_3)_2$), 31.7, 29.9, 24.6 (3´-C, 4´-C, 5´-C), 28.9 (C(*C*$H_3)_2$), 27.8 (OC(*C*$H_3)_2$), 22.6 (6´-C), 15.4 (NCH$_2$*C*H_3), 14.1 ppm (7´-C); HPLC-MS: [iso 95% - 5%], t_R: 2.67 min, (99%); MS (ES^+, *m/z*) 461 $[M+H]^+$; Anal. calcd. for $C_{30}H_{40}N_2O_2$: C 78.22, H 8.75, found: C 78.50, H 8.97.

9-Benzyoxy-1-(3,4-dichlorophenyl)-7-(1,1-dimethylheptyl)-1,4-dihydro-4,4-dimethylchromeno[4,3-*c*]pyrazole (1.25).

Prepared from **1.7** (15 mg, 0.03 mmol), sodium hydride (1.20 mg, 0.04 mmol) and benzyl bromide (11 μL, 0.09 mmol) following the procedure previously described. Column chromatography on silica gel (hexane/EtOAc, 3:1) afforded the title compound as a pale yellow oil (13 mg, 75%); ^{1}H-NMR (300 MHz, $CDCl_3$) δ: 7.44 (s, 1H, 3-H), 7.32–7.19 and 7.12–6.95 (m and m, 4H and 4H, 2-H_{Bn}, 3-H_{Bn}, 4-H_{Bn}, 5-H_{Bn}, 6-H_{Bn}, 2-H_{Ph}, 5-H_{Ph}, 6-H_{Ph}), 6.66 (d, J = 1.6 Hz, 1H, 6-H), 6.44 (d, J = 1.6 Hz, 1H, 8-H), 4.53 (s, 2H, OCH_2), 1.55 (s, 8H, $OC(CH_3)_2$, 2´-H), 1.20 (s, 6H, $C(CH_3)_2$), 1.14–1.10 (m, 6H, 3´-H, 4´-H, 5´-H), 1.07–0.88 (m, 2H, 6´-H), 0.83–0.72 ppm (m, 3H, 7´-H); ^{13}C-NMR (75 MHz, $CDCl_3$) δ: 154.0 (9-C), 153.3 (5a-C), 152.9 (7-C), 142.0 (9b-C), 135.5 (3-C), 134.9, 132.5, 131.7, 130.2, 129.4, 128.4, 128.2, 128.0, 127.8, 127.6, 127.4, 125.2 (1-C_{Bn}, 2-C_{Bn}, 3-C_{Bn}, 4-C_{Bn}, 5-C_{Bn}, 6-C_{Bn}, 1-C_{Ph}, 2-C_{Ph}, 3-C_{Ph}, 4-C_{Ph}, 5-C_{Ph}, 6-C_{Ph}), 124.7 (3a-C), 122.2 (9a-C), 109.6 (6-C), 103.6 (8-C), 76.2 ($OC(CH_3)_2$), 70.0 (OCH_2), 44.4 (2´-C), 38.2 ($C(CH_3)_2$), 31.7, 29.9, 24.6 (3´-C, 4´-C, 5´-C), 28.7($C(CH_3)_2$), 27.2 ($OC(CH_3)_2$), 22.6 (6´-C), 14.1 ppm (7´-C); HPLC-MS: [iso 95% - 5%], t_R: 6.44 min, (94%); MS (ES^+, m/z) 577 $[M+H]^+$; Anal. calcd. for $C_{34}H_{38}Cl_2N_2O_2$: C 70.70, H 6.63, found: C 70.82, H 6.57.

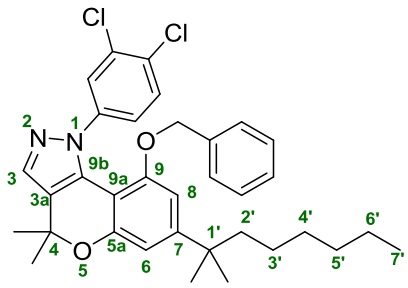

9-Benzyloxy-1-(2,4-dichlorophenyl)-7-(1,1-dimethylheptyl)-1,4-dihydro-4,4-dimethyl-9-methoxychromeno[4,3-*c*]pyrazole (1.26).

Prepared from **1.8** (18 mg, 0.04 mmol), sodium hydride (1.40 mg, 0.05 mmol) and benzyl bromide (13 μL, 0.11 mmol) following the procedure previously described. Column chromatography on silica gel (hexane/EtOAc, 3:1) afforded the title compound as an orange oil (13 mg, 61%); ^{1}H-NMR (300 MHz, $CDCl_3$) δ: 7.55 (s, 1H, 3-H), 7.36–7.27 (m, 4H, 2-H_{Bn}, 3-H_{Bn}, 5-H_{Bn}, 6-H_{Bn}), 7.15 (d, J = 2.3 Hz, 1H, 3-H_{Ph}), 7.13–7.02 (m, 2H, 6-H_{Ph}, 4-H_{Bn}), 6.97 (dd, J = 8.5, 2.3 Hz, 1H, 5-H_{Ph}), 6.65 (d, J = 1.6 Hz, 1H, 6-H), 6.35 (d, J = 1.6 Hz, 1H, 8-H), 4.53 (s, 2H, OCH_2), 1.64 (s, 6H, $OC(CH_3)_2$), 1.52–1.36 (m, 2H, 2´-H), 1.22 (s, 6H, $C(CH_3)_2$), 1.20–1.09 (m, 6H, 3´-H, 4´-H, 5´-H), 1.03–0.89 (m, 2H, 6´-H), 0.88–0.79 ppm

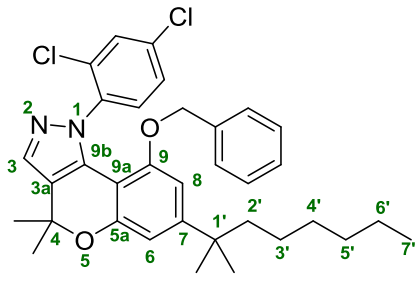

(m, 3H, 7´-H); ^{13}C-NMR (75 MHz, $CDCl_3$) δ: 154.1 (9-C), 153.7 (5a-C), 153.3 (7-C), 140.3 (9b-C), 136.8 (3-C), 135.2, 134.8, 133.9, 131.7, 131.7, 129.8, 128.9, 128.8, 128.5, 128.3, 127.7, 127.1 (1-C_{Bn}, 2-C_{Bn}, 3-C_{Bn}, 4-C_{Bn}, 5-C_{Bn}, 6-C_{Bn}, 1-C_{Ph}, 2-C_{Ph}, 3-C_{Ph}, 4-C_{Ph}, 5-C_{Ph}, 6-C_{Ph}), 123.7 (9a-C), 109.7 (6-C), 104.2 (8-C), 77.6 (O*C*$(CH_3)_2$), 70.6 (OCH_2), 44.8 (2´-C), 38.5 (*C*$(CH_3)_2$), 32.1, 30.2, 24.9 (3´-C, 4´-C, 5´-C), 29.1 (C(*C*$H_3)_2$), 27.9 (OC(*C*$H_3)_2$), 23.0 (6´-C), 14.5 ppm (7´-C); HPLC-MS: [iso 95% - 5%], t_R: 4.12 min, (94%); MS (ES^+, *m/z*) 577 $[M+H]^+$; Anal. calcd. for $C_{34}H_{38}Cl_2N_2O_2$: C 70.70, H 6.63, found: C 70.95, H 6.49.

7-(1,1-Dimethylheptyl)-2,4-dihydro-9-(3-hydroxypropoxy)-4,4-dimethylchromeno[4,3-*c*]pyrazole (1.27).

Prepared from **1.4** (0.10 g, 0.29 mmol), sodium hydride (14 mg, 0.58 mmol) and 3-bromo-1-propanol (0.19 mL, 1.46 mmol). Column chromatography on silica gel (hexane/EtOAc, 1:1) afforded the title compound as a white solid (55 mg, 47%); mp: 82–84 ºC; ^{1}H-NMR (300 MHz, $CDCl_3$) δ: 8.28–8.21 (br s, 1H, NH), 7.18 (s, 1H, 3-H), 6.58 (d, *J* = 1.6 Hz, 1H, 6-H), 6.49 (d, *J* = 1.6 Hz, 1H, 8-H), 4.29 (t, *J* = 6.5 Hz, 2H, O*C*$H_2CH_2CH_2OH$), 3.67 (t, *J* = 6.3 Hz, 2H, $OCH_2CH_2CH_2OH$), 2.13 (p, *J* = 6.3 Hz, 2H, $OCH_2CH_2CH_2OH$), 1.61 (s, 6H, OC$(CH_3)_2$), 1.59–1.45

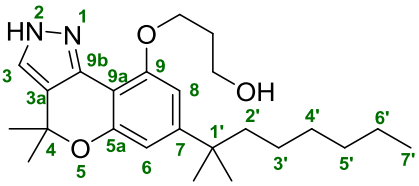

(m, 2H, 2´-H), 1.25 (s, 6H, C$(CH_3)_2$), 1.22–1.12 (m, 8H, 3´-H, 4´-H, 5´-H, 6´-H), 0.83 ppm (t, *J* = 6.7 Hz, 3H, 7´-H); ^{13}C-NMR (75 MHz, $CDCl_3$) δ: 153.8 (9-C), 153.2 (5a-C), 152.9 (7-C), 142.5 (9b-C), 123.8 (3-C), 120.0 (3a-C), 106.6 (6-C), 106.4 (8-C), 101.1 (9a-C), 76.6 (O*C*$(CH_3)_2$), 59.3 ($OCH_2CH_2CH_2OH$), 48.8 ($OCH_2CH_2CH_2OH$), 44.5 (2´-C), 38.0 (*C*$(CH_3)_2$), 32.7 ($OCH_2CH_2CH_2OH$), 31.8, 30.0, 24.6, 22.6 (3´-C, 4´-C, 5´-C, 6´-C), 29.7 (C(*C*$H_3)_2$), 28.9 (OC(*C*$H_3)_2$), 14.1 ppm (7´-C); HPLC-MS: [A, 80%→95%], t_R: 3.85 min, (97%); MS (ES^+, *m/z*) 401 $[M+H]^+$; Anal. calcd. for $C_{24}H_{36}N_2O_3$: C 71.96, H 9.06, found: C 72.23, H, 9.10.

7-(1,1-Dimethylheptyl)-2,4-dihydro-9-(3-hydroxypropoxy)-2,4,4-trimethylchromeno[4,3-*c*]pyrazole (1.28).

Prepared from **1.5b** (30 mg, 0.08 mmol), sodium hydride (3 mg, 0.12 mmol) and 3-bromo-1-propanol (51 μL, 0.37 mmol) following the procedure previously described. Column chromatography on silica gel (hexane/EtOAc, 1:1) afforded the title compound as a pale orange oil (20 mg, 59%); ^{1}H-NMR (300 MHz, $CDCl_3$) δ: 7.01 (s, 1H, 3-H), 6.52 (d, *J* = 1.6 Hz, 1H, 6-H), 6.45 (d, *J* = 1.6 Hz, 1H, 8-H), 4.18 (t, *J* = 6.5 Hz, 2H, $OCH_2CH_2CH_2OH$), 4.01 (s, 3H, NCH_3), 3.86–3.80 (m, 2H, $OCH_2CH_2CH_2OH$), 2.13–1.96 (m, 2H, $OCH_2CH_2CH_2OH$), 1.52 (s, 6H, $OC(CH_3)_2$), 1.42–1.38 (m, 2H, 2´-H), 1.19 (s, 6H, $C(CH_3)_2$), 1.16–0.92 (m, 8H, 3´-H, 4´-H, 5´-H, 6´-H), 0.77 ppm (t, *J* = 6.6 Hz, 3H, 7´-H); ^{13}C-NMR (75 MHz, $CDCl_3$) δ: 153.6 (9-C), 152.7 (5a-C), 150.8 (7-C), 139.5 (9b-C), 122.6 (3-C), 120.5 (3a-C), 109.2 (6-C), 107.6 (8-C), 101.3 (9a-C), 74.8 ($OC(CH_3)_2$), 59.5 ($OCH_2CH_2CH_2OH$), 50.1 ($OCH_2CH_2CH_2OH$), 45.3 (NCH_3), 39.5 (2´-C), 37.6 ($C(CH_3)_2$), 32.8 ($OCH_2CH_2CH_2OH$), 31.5, 30.9, 24.6, 22.6 (3´-C, 4´-C, 5´-C, 6´-C), 29.4 ($C(CH_3)_2$), 28.9 ($OC(CH_3)_2$), 13.0 ppm (7´-C); HPLC-MS: [A, 80%→95%], t_R: 4.07 min, (93%); MS (ES^+, *m/z*) 415 $[M+H]^+$; Anal. calcd. for $C_{25}H_{38}N_2O_2$: C 72.43, H 9.24, found: C 72.12, H 8.98.

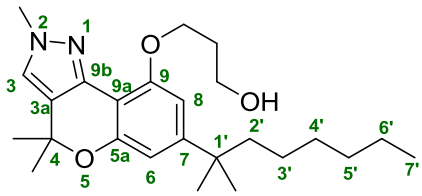

7-(1,1-Dimethylheptyl)-1-ethyl-1,4-dihydro-9-(3-hydroxypropoxy)-4,4-dimethylchromeno[4,3-*c*]pyrazole (1.29).

Prepared from **1.6a** (56 mg, 0.15 mmol), sodium hydride (9 mg, 0.38 mmol) and 3-bromo-1-propanol (0.10 mL, 0.75 mmol) following the general procedure. Column chromatography on silica gel (hexane/EtOAc, 1:1) afforded **1.29** as a yellow solid (31 mg, 48%); mp: 91–93 ºC; ^{1}H-NMR (300 MHz, $CDCl_3$) δ: 7.37 (s, 1H, 3-H), 6.60 (d, *J* = 1.8 Hz, 1H, 6-H), 6.57 (d, *J* = 1.8 Hz, 1H, 8-H), 4.40–4.33 (m, 2H, $OCH_2CH_2CH_2OH$), 4.07–3.89 (m, 2H, NCH_2CH_3), 3.62–3.51 (m, 2H, $OCH_2CH_2CH_2OH$), 2.11 (p, *J* = 6.4 Hz, 2H, $OCH_2CH_2CH_2OH$), 1.55 (s, 6H, $OC(CH_3)_2$), 1.50 (t, *J* = 7.0 Hz, 3H, NCH_2CH_3), 1.41–1.36 (m, 2H, 2´-H), 1.24 (s, 6H, $C(CH_3)_2$), 1.12–0.98 (m, 8H, 3´-H, 4´-H,

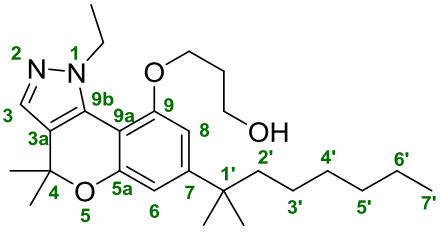

5´-H, 6´-H), 0.85 ppm (t, J = 6.6 Hz, 3H, 7´-H); ^{13}C-NMR (75 MHz, $CDCl_3$) δ: 154.8 (9-C), 153.5 (5a-C), 151.6 (7-C), 141.4 (9b-C), 131.6 (3-C), 124.5 (3a-C), 110.3 (6-C), 107.9 (8-C), 102.6 (9a-C), 75.0 (O*C*$(CH_3)_2$), 63.2 (O*C*$H_2CH_2CH_2OH$), 57.6 (OCH_2CH_2*C*H_2OH), 46.5 (N*C*H_2CH_3), 44.7 (2´-C), 38.0 (*C*$(CH_3)_2$), 32.6 (OCH_2*C*H_2CH_2OH), 30.9, 29.6, 24.5, 21.7 (3´-C, 4´-C, 5´-C, 6´-C), 29.2 (C(*C*$H_3)_2$), 28.1 (OC(*C*$H_3)_2$), 15.0 (NCH_2*C*H_3), 14.1 ppm (7´-C); HPLC-MS: [A, 80%→95%], t_R: 3.42 min, (99%); MS (ES^+, m/z) 429 $[M+H]^+$; Anal. calcd. for for $C_{26}H_{40}N_2O_3$: C 72.86, H 9.41, found: C 72.75, H 9.63.

7-(1,1-Dimethylheptyl)-2-ethyl-2,4-dihydro-9-(3-hydroxypropoxy)-4,4-dimethylchromeno[4,3-*c*]pyrazole (1.30).

Prepared from **1.6b** (25 mg, 0.07 mmol), sodium hydride (2.40 mg, 0.10 mmol) and 3-bromo-1-propanol (28 μL, 0.20 mmol) following the procedure previously described. Column chromatography on silica gel (hexane/EtOAc, 1:1) afforded the title compound as a yellow gummy solid (22 mg, 76%); ^{1}H-NMR (300 MHz, $CDCl_3$) δ: 7.13 (s, 1H, 3-H), 6.58 (d, J = 1.6 Hz, 1H, 6-H), 6.52 (d, J = 1.6 Hz, 1H, 8-H), 4.31–4.25 (m, 2H, O*C*$H_2CH_2CH_2OH$), 4.09–3.98 (m, 2H, N*C*H_2CH_3), 3.66–3.45 (m, 2H, OCH_2CH_2*C*H_2OH), 2.14–2.10 (m, 2H, OCH_2*C*H_2CH_2OH), 1.59 (s, 6H, OC$(CH_3)_2$), 1.51 (t, J = 7.2 Hz, 3H, NCH_2*C*H_3), 1.46–1.42 (m, 2H, 2´-H), 1.26 (s, 6H, C$(CH_3)_2$), 1.22–0.96 (m, 8H, 3´-H, 4´-H, 5´-H, 6´-H), 0.87–0.79 ppm (m, 3H, 7´-H); ^{13}C-NMR (75 MHz, $CDCl_3$) δ: 153.5 (9-C), 152.8 (5a-C), 150.9 (7-C), 139.2 (9b-C), 120.8 (3-C), 120.3 (3a-C), 109.0 (6-C), 107.6 (8-C), 101.3 (9a-C), 74.8 (O*C*$(CH_3)_2$), 65.3 (O*C*$H_2CH_2CH_2OH$), 60.8 (OCH_2CH_2*C*H_2OH), 46.0 (N*C*H_2CH_3), 43.5 (2´-C), 37.1 (*C*$(CH_3)_2$), 31.5 (OCH_2*C*H_2CH_2OH), 30.7, 28.9, 23.6, 21.6 (3´-C, 4´-C, 5´-C, 6´-C), 28.1 (C(*C*$H_3)_2$), 27.8 (OC(*C*$H_3)_2$), 14.7 (NCH_2*C*H_3), 13.0 ppm (7´-C); HPLC-MS: [A, 80%→95%], t_R: 4.63 min, (96%); MS (ES^+, m/z) 429 $[M+H]^+$; Anal. calcd. for for $C_{26}H_{40}N_2O_3$: C 72.86, H 9.41, found: C 72.88, H 9.19.

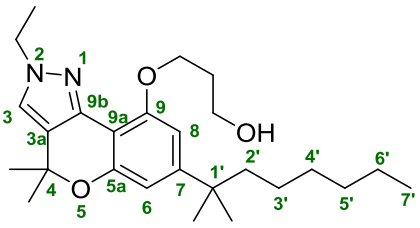

1-(3,4-Dichlorophenyl)-7-(1,1-dimethylheptyl)-1,4-dihydro-9-(3-hydroxypropoxy)-4,4-dimethylchromeno[4,3-*c*]pyrazole (1.31).

Prepared from **1.7** (20 mg, 0.04 mmol), sodium hydride (2.50 mg, 0.10 mmol) and 3-bromo-1-propanol (28 μL, 0.20 mmol) following the procedure previously described. Column chromatography on silica gel (hexane/EtOAc, 1:1) afforded the title compound as a yellow oil (9 mg, 40%); ^{1}H-NMR (300 MHz, $CDCl_3$) δ: 7.97 (d, *J* = 2.5 Hz, 1H, 2- H_{Ph}), 7.71 (dd, *J* = 7.8, 2.5 Hz, 1H, 6-H_{Ph}), 7.49 (d, *J* = 7.8 Hz, 1H, 5- H_{Ph}), 7.47 (s, 1H, 3-H), 6.62 (d, *J* = 1.7 Hz, 1H, 6-H), 6.60 (d, *J* = 1.7 Hz, 1H, 8-H), 4.12 (t, *J* = 6.2 Hz, 2H, OC*H*$_2$CH$_2$CH$_2$OH), 3.88 (t, *J* = 6.2 Hz, 2H, OCH$_2$CH$_2$C*H*$_2$OH), 2.09 (p, *J* = 6.2 Hz, 2H, OCH$_2$C*H*$_2$CH$_2$OH), 1.65 (s, 6H, OC(CH$_3$)$_2$), 1.60–1.40 (m, 2H, 2´-H), 1.22 (s, 6H, C(CH$_3$)$_2$), 1.20–0.94 (m, 8H, 3´-H, 4´-H, 5´-H, 6´-H), 0.83–0.72 ppm (m, 3H, 7´-H); ^{13}C-NMR (75 MHz, $CDCl_3$) δ: 155.2 (9-C), 153.9 (5a-C), 152.5 (7-C), 140.7 (1-C_{Ph}), 139.7 (9b-C), 136.0 (3-C_{Ph}), 130.3 (3-C), 129.6 (4-C_{Ph}), 127.4 (5-C_{Ph}), 125.3 (2-C_{Ph}), 124.1 (6-C_{Ph}), 121.6 (3a-C), 110.7 (6-C), 108.5 (8-C), 102.3 (9a-C), 75.1 (O*C*(CH$_3$)$_2$), 67.9 (O*C*H$_2$CH$_2$CH$_2$OH), 62.1 (OCH$_2$CH$_2$*C*H$_2$OH), 44.6 (2´-C), 38.2 (*C*(CH$_3$)$_2$), 31.7 (OCH$_2$*C*H$_2$CH$_2$OH), 30.9, 29.1, 24.0, 21.3 (3´-C, 4´-C, 5´-C, 6´-C), 28.6 (C(*C*H$_3$)$_2$), 27.9 (OC(*C*H$_3$)$_2$), 14.3 ppm (7´-C); HPLC-MS: [A, 80%→95%], t_R: 4.58 min, (93%); MS (ES$^+$, *m*/*z*) 545 [M+H]$^+$; Anal. calcd. for $C_{30}H_{38}Cl_2N_2O_3$: C 66.05, H 7.02, found: C 65.81, H 7.13.

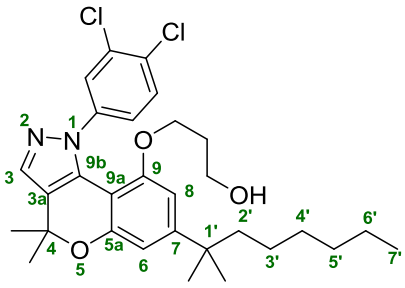

1-(2,4-Dichlorophenyl)-7-(1,1-dimethylheptyl)-1,4-dihydro-9-(3-hydroxypropoxy)-4,4-dimethyl-9-methoxychromeno[4,3-*c*]pyrazole (1.32).

Prepared from **1.8** (51 mg, 0.10 mmol), sodium hydride (5 mg, 0.21 mmol) and 3-bromo-1-propanol (71 μL, 0.52 mmol) following the procedure previously described. Column chromatography on silica gel (hexane/EtOAc, 1:1) afforded the title compound as a yellow gummy solid (18 mg, 31%); ^{1}H-NMR (300 MHz, $CDCl_3$) δ: 7.57 (s, 1H, 3-H), 7.51 (d, *J* = 1.8 Hz, 1H, 3-H_{Ph}), 7.25–7 .18 (m, 2H, 5- H_{Ph}, 6-H_{Ph}), 6.66 (d, *J* = 1.6 Hz, 1H, 6-H), 6.40 (d, *J* = 1.6 Hz, 1H, 8-H), 3.82–3.60 (m, 2H, OC*H*$_2$CH$_2$CH$_2$OH), 3.56 (t, *J* = 6.0 Hz, 2H, OCH$_2$CH$_2$C*H*$_2$OH), 1.90–1.85 (m, 2H, OCH$_2$C*H*$_2$CH$_2$OH), 1.63 (s, 6H, OC(CH$_3$)$_2$), 1.57–

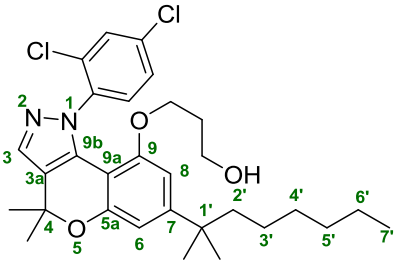

1.46 (m, 2H, 2´-H), 1.24 (s, 6H, $C(CH_3)_2$), 1.22–0.96 (m, 8H, 3´-H, 4´-H, 5´-H, 6´-H), 0.84 ppm (t, *J* = 6.6 Hz, 3H, 7´-H); ^{13}C-NMR (75 MHz, $CDCl_3$) δ: 153.6 (9-C), 153.3 (5a-C), 153.2 (7-C), 140.0 (1-C_{Ph}), 134.8 (9b-C), 134.4 (2-C_{Ph}), 133.5 (4-C_{Ph}), 131.1 (3-C), 129.6 (3-C_{Ph}), 128.6 (5-C_{Ph}), 127.0 (6-C_{Ph}), 123.5 (3a-C), 109.1 (6-C), 103.7 (8-C), 103.0 (9a-C), 76.5 ($OC(CH_3)_2$), 64.9 ($OCH_2CH_2CH_2OH$), 59.4 ($OCH_2CH_2CH_2OH$), 44.3 (2´-C), 38.1 ($C(CH_3)_2$), 31.6 ($OCH_2CH_2CH_2OH$), 31.0, 29.8, 24.5, 22.5 (3´-C, 4´-C, 5´-C, 6´-C), 28.5 ($C(CH_3)_2$), 27.3 ($C(CH_3)_2$), 14.0 ppm (7´-C); HPLC-MS: [A, 80%→95%], t_R: 4.72 min, (96%); MS (ES^+, *m/z*) 545 $[M+H]^+$; Anal. calcd. for $C_{30}H_{38}Cl_2N_2O_3$: C 66.05, H 7.02, found: C 66.26, H 6.97.

7-(1,1-Dimethylheptyl)-2,4-dihydro-9-(2-hydroxyethoxy)-4,4-dimethylchromeno[4,3-*c*]pyrazole (1.33).

Prepared from **1.4** (20 mg, 0.06 mmol), sodium hydride (2 mg, 0.08 mmol) and 2-bromoetanol (20 μL, 0.29 mmol). Column chromatography on silica gel (hexane/EtOAc, 1:1) afforded the title compound as a white solid (12 mg, 54%); mp: 85–87 ºC; ^{1}H-NMR (300 MHz, $CDCl_3$) δ: 7.34 (s, 1H, 3-H), 6.60 (d, *J* = 1.7 Hz, 1H, 6-H), 6.52 (d, *J* = 1.7 Hz, 1H, 8-H), 4.19–4.07 (m, 2H, OCH_2CH_2OH), 3.56–3.45 (m, 2H, OCH_2CH_2OH), 1.64 (s, 6H, $OC(CH_3)_2$), 1.60–1.48 (m, 2H, 2´-H), 1.25 (s, 6H, $C(CH_3)_2$), 1.23–0.97 (m, 8H, 3´-H, 4´-H, 5´-H, 6´-H), 0.88–0.79 ppm (m, 3H, 7´-H); ^{13}C-NMR (75 MHz, $CDCl_3$) δ: 155.2 (9-C), 154.1 (5a-C), 152.6 (7-C), 141.3 (9b-C), 124.9 (3-C), 121.9 (3a-C), 109.3 (6-C), 106.6 (8-C), 102.7 (9a-C), 74.8 ($OC(CH_3)_2$), 60.1 (OCH_2CH_2OH), 51.4 (OCH_2CH_2OH), 43.2 (2´-C), 37.7 ($C(CH_3)_2$), 32.0, 31.4, 25.7, 22.3 (3´-C, 4´-C, 5´-C, 6´-C), 29.8 ($C(CH_3)_2$), 27.9 ($OC(CH_3)_2$), 15.0 ppm (7´-C); HPLC-MS: [A, 80%→95%], t_R: 3.45 min, (93%); MS (ES^+, *m/z*) 387 $[M+H]^+$; Anal. calcd. for $C_{23}H_{34}N_2O_3$: C 71.47, H 8.87, found: C 71.80, H, 8.64.

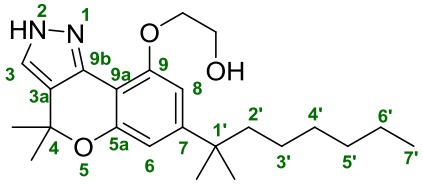

7-(1,1-Dimethylheptyl)-2,4-dihydro-9-(2-hydroxyethoxy)-2,4,4-trimethylchromeno[4,3-*c*]pyrazole (1.34).

Prepared from **1.5b** (20 mg, 0.05 mmol), sodium hydride (2 mg, 0.08 mmol) and 2-bromoetanol (16 μL, 0.22 mmol) following the procedure previously described. Column chromatography on silica gel (hexane/EtOAc, 1:2) afforded the title compound as a pale yellow oil (16 mg, 73%); ^{1}H-NMR (300 MHz, $CDCl_3$) δ: 7.19 (s, 1H, 3-H), 6.59 (d, *J* = 1.8 Hz, 1H, 6-H), 6.51 (d, *J* = 1.8 Hz, 1H, 8-H), 4.30–4.25 (m, 2H, OCH_2CH_2OH), 4.05 (s, 3H, NCH_3), 3.81–3.74 (m, 2H, OCH_2CH_2OH), 1.60 (s, 6H, $OC(CH_3)_2$), 1.40–1.35 (m, 2H, 2´-H), 1.21 (s, 6H, $C(CH_3)_2$), 1.12–0.89 (m, 8H, 3´-H, 4´-H, 5´-H, 6´-H), 0.81 ppm (t, *J* = 6.9 Hz, 3H, 7´-H); ^{13}C-NMR (75 MHz, $CDCl_3$) δ: 154.1 (9-C), 153.5 (5a-C), 152.3 (7-C), 140.5 (9b-C), 123.8 (3-C), 121.4 (3a-C), 111.2 (6-C), 108.5 (8-C), 103.6 (9a-C), 76.0 ($OC(CH_3)_2$), 64.3 (OCH_2CH_2OH), 59.2 (OCH_2CH_2OH), 40.6 (NCH_3), 39.0 (2´-C), 38.1 ($C(CH_3)_2$), 32.1, 30.8, 25.7, 21.3 (3´-C, 4´-C, 5´-C, 6´-C), 29.7 ($C(CH_3)_2$), 28.0 ($OC(CH_3)_2$), 14.7 ppm (7´-C); HPLC-MS: [A, 80%→95%], t_R: 3.41 min, (99%); MS (ES^+, *m/z*) 401 $[M+H]^+$; Anal. calcd. for $C_{24}H_{36}N_2O_3$: C 71.96, H 9.06, found: C 71.67, H, 8.84.

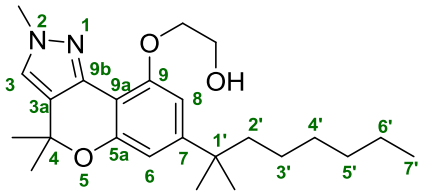

7-(1,1-Dimethylheptyl)-2-ethyl-2,4-dihydro-9-(2-hydroxyethoxy)-4,4-dimethylchromeno[4,3-*c*]pyrazole (1.35).

Prepared from **1.6b** (25 mg, 0.07 mmol), sodium hydride (4 mg, 0.16 mmol) and 2-bromoetanol (23 μL, 0.33 mmol) following the procedure previously described. Column chromatography on silica gel (hexane/EtOAc, 1:1) afforded the title compound as a white oil (13 mg, 48%); ^{1}H-NMR (300 MHz, $CDCl_3$) δ: 7.22 (s, 1H, 3-H), 6.61 (d, *J* = 1.8 Hz, 1H, 6-H), 6.57 (d, *J* = 1.8 Hz, 1H, 8-H), 4.30–4.23 (m, 2H, OCH_2CH_2OH), 3.95 (q, *J* = 7.1 Hz, 2H, NCH_2CH_3), 3.63–3.59 (m, 2H, OCH_2CH_2OH), 1.62 (s, 6H, $OC(CH_3)_2$), 1.54 (t, *J* = 7.1 Hz, 3H, NCH_2CH_3), 1.40–1.33 (br s, 2H, 2´-H), 1.28 (s, 6H, $C(CH_3)_2$), 1.23–0.91 (m, 8H, 3´-H, 4´-H, 5´-H, 6´-H), 0.88–0.81 ppm (m, 3H, 7´-H); ^{13}C-NMR (75 MHz, $CDCl_3$) δ: 155.2 (9-C), 153.7 (5a-C), 151.8 (7-C), 140.3 (9b-C), 124.6 (3-C), 121.5 (3a-C), 110.2 (6-C), 108.6 (8-C), 102.4 (9a-C), 75.1

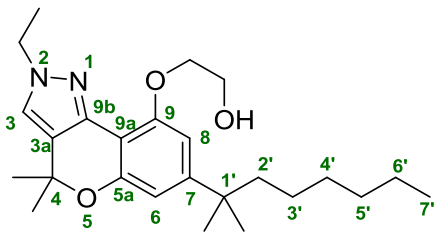

(O*C*(CH$_3$)$_2$), 68.5 (O*C*H$_2$CH$_2$OH), 61.3 (OCH$_2$*C*H$_2$OH), 47.3 (N*C*H$_2$CH$_3$), 42.9 (2´-C), 37.7 (*C*(CH$_3$)$_2$), 31.7, 30.2, 25.3, 22.5 (3´-C, 4´-C, 5´-C, 6´-C), 29.2 (C(*C*H$_3$)$_2$), 28.3 (OC(*C*H$_3$)$_2$), 15.2 (NCH$_2$*C*H$_3$), 14.3 ppm (7´-C); HPLC-MS: [A, 80%→95%], t_R: 5.22 min, (92%); MS (ES$^+$, *m/z*) 415 [M+H]$^+$; Anal. calcd. for $C_{25}H_{38}N_2O_3$: C 72.43, H 9.24, found: C 72.60, H 9.08.

9-(3-Bromopropoxy)-7-(1,1-dimethylheptyl)-2,4-dihydro-2,4,4-trimethylchromeno[4,3-*c*]pyrazole (1.36).

Prepared from **1.5b** (43 mg, 0.12 mmol), sodium hydride (4 mg, 0.18 mmol) and 1,3-dibromopropane (61 μL, 0.60 mmol) following the procedure previously described. Column chromatography on silica gel (hexane/EtOAc, 3:1) afforded the title compound as a white solid (27 mg, 47%); mp: 96–98 ºC; ^{1}H-NMR (300 MHz, CDCl$_3$) δ: 7.49 (s, 1H, 3-H), 6.73 (d, *J* = 1.8 Hz, 1H, 6-H), 6.68 (d, *J* = 1.8 Hz, 1H, 8-H), 4.34 (t, *J* = 6.3 Hz, 2H, OC*H*$_2$CH$_2$CH$_2$Br), 4.07 (s, 3H, NCH$_3$), 3.87 (t, *J* = 6.3 Hz, 2H, OCH$_2$CH$_2$C*H*$_2$Br), 2.49 (p, *J* = 6.3 Hz, 2H, OCH$_2$C*H*$_2$CH$_2$Br), 1.60 (s, 6H, OC(CH$_3$)$_2$), 1.58–1.46 (m, 2H, 2´-H), 1.27 (s, 6H, C(CH$_3$)$_2$), 1.24–0.94 (m, 8H, 3´-H, 4´-H, 5´-H, 6´-H), 0.90–0.77 ppm (m, 3H, 7´-H); ^{13}C-NMR (75 MHz, CDCl$_3$) δ: 153.0 (9-C), 152.5 (5a-C), 151.3 (7-C), 141.0 (9b-C), 124.7 (3-C), 121.8 (3a-C), 109.9 (6-C), 108.5 (8-C), 103.2 (9a-C), 75.1 (O*C*(CH$_3$)$_2$), 62.3 (O*C*H$_2$CH$_2$CH$_2$Br), 46.7 (NCH$_3$), 38.6 (2´-C), 37.3 (*C*(CH$_3$)$_2$), 33.1 (OCH$_2$CH$_2$*C*H$_2$Br), 31.7 (OCH$_2$*C*H$_2$CH$_2$Br), 30.8, 30.1, 25.6, 21.3 (3´-C, 4´-C, 5´-C, 6´-C), 29.7 (C(*C*H$_3$)$_2$), 28.1 (OC(*C*H$_3$)$_2$), 14.0 ppm (7´-C); HPLC-MS: [A, 80%→95%], t_R: 5.55 min, (96%); MS (ES$^+$, *m/z*) 477 [M+H]$^+$; Anal. calcd. for $C_{25}H_{37}BrN_2O_2$: C 62.89, H 7.81, found: C 63.05, H 7.72.

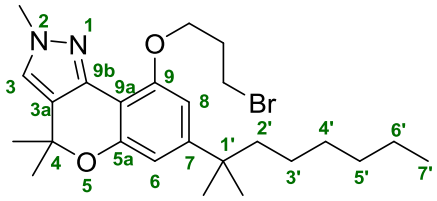

9-(3-Bromopropoxy)-7-(1,1-dimethylheptyl)-2-ethyl-2,4-dihydro-4,4-dimethylchromeno[4,3-*c*]pyrazole (1.37).

Prepared from **1.6b** (20 mg, 0.05 mmol), sodium hydride (2 mg, 0.08 mmol) and 1,3-dibromopropane (27 μL, 0.27 mmol) following the procedure previously described. Column chromatography on silica gel (hexane/EtOAc, 3:1) afforded the title compound as a yellow oil (15 mg, 55%); ^{1}H-NMR (300 MHz, CDCl$_3$) δ: 7.21 (s, 1H, 3-H), 6.62 (d, *J* = 1.7 Hz, 1H, 6-H), 6.56 (d, *J*

= 1.7 Hz, 1H, 8-H), 4.29–4.16 (m, 2H, OC*H*$_2$CH$_2$CH$_2$Br), 4.11 (q, 2H, *J* = 7.0 Hz, NC*H*$_2$CH$_3$), 3.52–3.47 (m, 2H, OCH$_2$CH$_2$C*H*$_2$Br), 2.12–2.04 (m, 2H, OCH$_2$C*H*$_2$CH$_2$Br), 1.65 (s, 6H, OC(CH$_3$)$_2$),

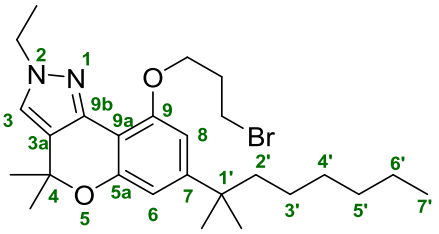

1.60 (t, *J* = 7.0 Hz, 3H, NCH$_2$C*H*$_3$), 1.40–1.34 (m, 2H, 2´-H), 1.29 (s, 6H, C(CH$_3$)$_2$), 1.23–0.98 (m, 8H, 3´-H, 4´-H, 5´-H, 6´-H), 0.86 ppm (t, *J* = 7.1 Hz, 3H, 7´-H); ^{13}C-NMR (75 MHz, CDCl$_3$) δ: 152.9 (9-C), 152.1 (5a-C), 150.3 (7-C), 138.4 (9b-C), 121.7 (3-C), 120.1 (3a-C), 108.3 (6-C), 106.5 (8-C), 101.8 (9a-C), 75.3 (O*C*(CH$_3$)$_2$), 65.2 (O*C*H$_2$CH$_2$CH$_2$Br), 45.9 (N*C*H$_2$CH$_3$), 44.1 (2´-C), 38.0 (*C*(CH$_3$)$_2$), 32.7 (OCH$_2$CH$_2$*C*H$_2$Br), 31.9 (OCH$_2$*C*H$_2$CH$_2$Br), 31.0, 29.8, 24.2, 21.6 (3´-C, 4´-C, 5´-C, 6´-C), 28.7 (C(*C*H$_3$)$_2$), 27.5 (OC(*C*H$_3$)$_2$), 14.8 (NCH$_2$*C*H$_3$), 13.5 ppm (7´-C); HPLC-MS: [A, 80%→95%], t_R: 5.14 min, (95%); MS (ES$^+$, *m/z*) 491 [M+H]$^+$; Anal. calcd. for $C_{26}H_{39}BrN_2O_2$: C 63.54, H 8.00, found: C 63.87, H 8.12.

9-(2-Bromoethoxy)-7-(1,1-dimethylheptyl)-1-ethyl-1,4-dihydro-4,4-dimethylchromeno[4,3-*c*]pyrazole (1.38).

Prepared from **1.6a** (20 mg, 0.05 mmol), sodium hydride (2 mg, 0.08 mmol) and 1,2-dibromoethane (23 μL, 0.27 mmol) following the general procedure. Column chromatography on silica gel

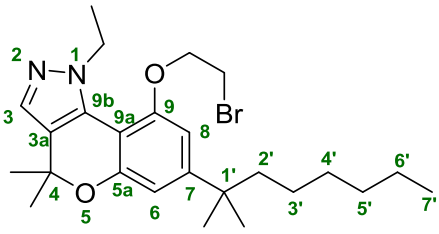

(hexane/EtOAc, 2:1) afforded **1.38** as a yellow oil (16 mg, 64%); ^{1}H-NMR (300 MHz, CDCl$_3$) δ: 7.29 (s, 1H, 3-H), 6.69 (d, *J* = 1.5 Hz, 1H, 6-H), 6.61 (d, *J* = 1.5 Hz, 1H, 8-H), 4.38–4.31 (m, 2H, OC*H*$_2$CH$_2$Br), 4.03 (q, *J* = 7.5 Hz, 2H, NC*H*$_2$CH$_3$), 3.71–3.62 (m, 2H, OCH$_2$C*H*$_2$Br), 1.56 (s, 6H, OC(CH$_3$)$_2$), 1.53 (t, *J* = 7.5 Hz, 3H, NCH$_2$C*H*$_3$), 1.50–1.42 (m, 2H, 2´-H), 1.27 (s, 6H, C(CH$_3$)$_2$), 1.17–1.04 (m, 8H, 3´-H, 4´-H, 5´-H, 6´-H), 0.88 ppm (t, *J* = 6.6 Hz, 3H, 7´-H); ^{13}C-NMR (75 MHz, CDCl$_3$) δ: 155.3 (9-C), 154.0 (5a-C), 152.5 (7-C), 142.6 (9b-C), 133.7 (3-C), 124.8 (3a-C), 109.9 (6-C), 108.1 (8-C), 103.5 (9a-C), 76.2 (O*C*(CH$_3$)$_2$), 64.7 (O*C*H$_2$CH$_2$Br), 45.9 (N*C*H$_2$CH$_3$), 43.8 (2´-C), 37.5 (*C*(CH$_3$)$_2$), 31.2 (OCH$_2$*C*H$_2$Br), 30.3, 29.7, 25.7, 22.3 (3´-C, 4´-C, 5´-C, 6´-C), 29.0 (C(*C*H$_3$)$_2$), 27.7 (OC(*C*H$_3$)$_2$), 15.2 (NCH$_2$*C*H$_3$),

14.0 ppm (7´-C); HPLC-MS: [A, 80%→95%], t_R: 5.64 min, (95%); MS (ES^+, *m/z*) 477 $[M+H]^+$; Anal. calcd. for $C_{25}H_{37}BrN_2O_2$: C 62.89, H 7.81, found: C 62.61, H 8.03.

7-(1,1-Dimethylheptyl)-1-ethyl-1,4,9,10-tetrahydro-4,4-dimethyl-8*H*-pyrano[2',3':5,6]chromeno[4,3-*c*]pyrazole (1.39).

Compound **1.29** (25 mg, 0.06 mmol) in 1.5 mL of dry toluene was added to a stirred suspension of P_20_5 (16 mg, 0.12 mmol) in 2 mL of dry toluene under nitrogen atmosphere and the mixture was refluxed for 1 hour. After completion, the reaction mixture was cooled to room temperature and filtered. The filtrate was diluted with EtOAc and washed with NaOH (0.1 N), water, brine and extracted three times with EtOAc. The combined organic layers were dried over $MgSO_4$ and the solvent was removed under vacuum. Column chromatography on silica gel (hexane/EtOAc, 4:1) afforded **1.39** as a yellow oil (20 mg, 87%); ^{1}H-NMR (300 MHz, $CDCl_3$) δ: 7.39 (s, 1H, 3-H), 6.59 (s, 1H, 6-H), 4.41–4.32 (m, 2H, $OCH_2CH_2CH_2$), 4.21–4.16 (m, 2H, NCH_2CH_3), 2.84–2.78 (m, 2H, $OCH_2CH_2CH_2$), 2.09–2.01 (m, 2H, $OCH_2CH_2CH_2$), 1.61 (s, 6H, $OC(CH_3)_2$), 1.56 (t, *J* = 6.7 Hz, 3H, NCH_2CH_3), 1.45–1.40 (m, 2H, 2´-H), 1.27 (s, 6H, $C(CH_3)_2$), 1.10–0.96 (m, 8H, 3´-H, 4´-H, 5´-H, 6´-H), 0.85–0.79 ppm (m, 3H, 7´-H); ^{13}C-NMR (75 MHz, $CDCl_3$) δ: 153.9 (11a-C), 152.8 (5a-C), 152.0 (7-C), 142.5 (11c-C), 132.3 (3-C), 128.0 (3a-C), 109.6 (7a-C), 108.3 (6-C), 103.5 (11b-C), 74.9 ($OC(CH_3)_2$), 63.7 ($OCH_2CH_2CH_2$), 46.1 (NCH_2CH_3), 43.4 (2´-C), 37.7 ($C(CH_3)_2$), 32.0, 31.3, 29.4, 24.6, 23.9, 21.2 (3´-C, 4´-C, 5´-C, 6´-C, $OCH_2CH_2CH_2$), 29.0 ($C(CH_3)_2$), 28.5 ($OC(CH_3)_2$), 15.4 (NCH_2CH_3), 14.1 ppm (7´-C); HPLC-MS: [A, 80%→95%], t_R: 5.82 min, (95%); MS (ES^+, *m/z*) 411 $[M+H]^+$; Anal. calcd. for $C_{26}H_{38}N_2O_2$: C 76.06, H 9.33, found: C 75.82, H 9.08.

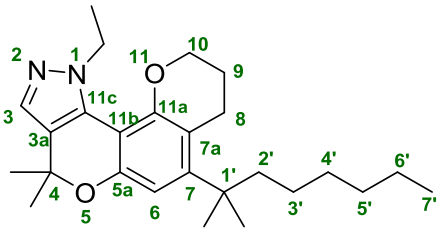

7-(1,1-Dimethylheptyl)-2-ethyl-2,4,9,10-tetrahydro-4,4-dimethyl-8*H*-pyrano[2',3':5,6]chromeno[4,3-*c*]pyrazole (1.40).

Prepared from **1.30** (71 mg, 0.16 mmol), and P_20_5 (46 mg, 0.33 mmol) following the procedure previously described for **1.39**. Column chromatography on silica gel (hexane/EtOAc, 4:1) afforded

the title compound as a pale yellow oil (23 mg, 52%); ^{1}H-NMR (300 MHz, $CDCl_3$) δ: 7.20 (s, 1H, 3-H), 6.61 (s, 1H, 6-H), 4.31–4.27 (m, 2H, OCH_2CH$_2$CH$_2$), 4.20–4.16 (m, 2H, NCH_2CH$_3$), 2.72–2.69 (m, 2H, OCH$_2$CH$_2$CH_2), 2.11–2.04 (m, 2H, OCH$_2$CH_2CH$_2$), 1.67 (s, 6H, OC(CH$_3$)$_2$), 1.52 (t, J = 7.0 Hz, 3H, NCH$_2$CH_3), 1.50–1.46 (m, 2H, 2´-H), 1.26 (s, 6H, C(CH$_3$)$_2$), 1.15–0.99 (m, 8H, 3´-H, 4´-H, 5´-H, 6´-H), 0.84 ppm (t, J = 6.9 Hz, 3H, 7´-H); ^{13}C-NMR (75 MHz, $CDCl_3$) δ: 154.0 (11a-C), 153.7 (5a-C), 152.5 (7-C), 140.9 (11c-C), 122.3 (3-C), 119.6 (3a-C), 108.8 (7a-C), 108.1 (6-C), 104.2 (11b-C), 75.3 (O*C*(CH$_3$)$_2$), 65.0 (O*C*H$_2$CH$_2$CH$_2$), 45.9 (N*C*H$_2$CH$_3$), 44.1 (2´-C), 38.2 (*C*(CH$_3$)$_2$), 31.4, 30.8, 29.5, 24.9, 24.0, 22.6 (3´-C, 4´-C, 5´-C, 6´-C, OCH$_2$*C*H$_2$*C*H$_2$), 29.1 (C(*C*H$_3$)$_2$), 28.7 (OC(*C*H$_3$)$_2$), 14.9 (NCH$_2$*C*H$_3$), 13.8 ppm (7´-C); HPLC-MS: [A, 80%→95%], t_R: 5.07 min, (98%); MS (ES$^+$, *m/z*) 411 [M+H]$^+$; Anal. calcd. for $C_{26}H_{38}N_2O_2$: C 76.06, H 9.33, found: C 76.35, H 8.99.

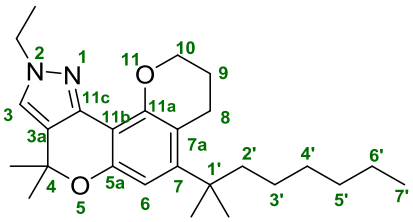

7-(1,1-Dimethylheptyl)-4,4-dimethyl-4*H*-chromeno[3,4-*d*]isoxazol-9-ol (1.41).

A solution of 7-(1,1-dimethylheptyl)-5-hydroxy-3-hydroxymethylene-2,2-dimethylchroman-4-one (**1.3**) (0.12 g, 0.35 mmol) and hydroxylamine hydrochloride (49 mg, 0.71 mmol) in ethanol (4 mL) was refluxed for 45 minutes. After cooling the mixture, the crude was filtered and washed with cold ethanol. After removal of the solvent, the crude was purified by chromatography on silica gel (hexane/EtOAc, 2:1) to obtain **1.41** as a pale yellow solid (0.11 g; 91%); mp: 109-111 ºC; ^{1}H-NMR (300 MHz, $CDCl_3$) δ: 8.12 (s, 1H, 3-H), 6.57 (d, J = 1.6 Hz, 1H, 8-H), 6.55 (d, J = 1.4 Hz, 6-H), 1.64 (s, 6H, OC(CH$_3$)$_2$), 1.59–1.47 (m, 2H, 2´-H), 1.24 (s, 6H, C(CH$_3$)$_2$), 1.17–1.09 (br s, 8H, 3´-H, 4´-H, 5´-H, 6´-H), 0.82 ppm (t, J = 7.0 Hz, 3H, 7´-H); ^{13}C-NMR (75 MHz, $CDCl_3$) δ: 160.2 (9-C), 156.6 (9b-C), 153.6 (5a-C), 151.7 (7-C), 145.4 (3-C), 119.4 (9a-C), 109.5 (8-C), 108.1 (6-C), 105.9 (3a-C), 78.0 (O*C*(CH$_3$)$_2$), 44.5 (2´-C), 38.5 (*C*(CH$_3$)$_2$), 31.9, 30.1, 24.8 (3´-C, 4´-C, 5´-C), 29.2 (C(*C*H$_3$)$_2$), 28.9 (OC(*C*H$_3$)$_2$), 22.9 (6´-C), 14.3 ppm (7´-C);

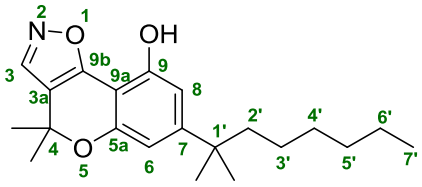

HPLC-MS: [A, 80%→95%], t_R: 2.77 min, (99%); MS (ES^+, m/z) 344 $[M+H]^+$; Anal. calcd. for $C_{21}H_{29}NO_3$: C 73.44, H 8.51, found: C 73.81, H, 8.59.

7-(1,1-Dimethylheptyl)-9-methoxy-4,4-dimethyl-4*H*-chromeno[3,4-*d*]isoxazole (1.42).

Prepared from **1.41** (30 mg, 0.09 mmol), sodium hydride (3 mg, 0.13 mmol), and iodomethane (16 μL, 0.26 mmol) following the procedure described for **1.14**. Column chromatography on silica gel (hexane/EtOAc, 2:1) afforded **1.42** as a yellow oil (19 mg, 61%); ^{1}H-NMR (300 MHz, $CDCl_3$) δ: 8.10 (s, 1H, 3-H), 6.47 (d, J = 1.6 Hz, 1H, 8-H), 6.35 (d, J = 1.6 Hz, 1H, 6-H), 3.59 (s, 3H, OCH_3), 1.77 (s, 6H, $OC(CH_3)_2$), 1.54– 1.31 (m, 2H, 2´-H), 1.26 (s, 6H, $C(CH_3)_2$), 1.17–0.98 (m, 8H, 3´-H, 4´-H, 5´-H, 6´-H), 0.83–0.78 ppm (m, 3H, 7´-H); ^{13}C-NMR (75 MHz, $CDCl_3$) δ: 165.6 (9-C), 162.2 (9b-C), 157.8 (5a-C), 153.5 (7-C), 150.1 (3-C), 118.0 (9a-C), 108.3 (8-C), 106.5 (6-C), 103.0 (3a-C), 76.7 ($OC(CH_3)_2$), 52.2 (OCH_3), 44.3 (2´-C), 39.4 ($C(CH_3)_2$), 32.1, 30.3, 24.8, 23.6 (3´-C, 4´-C, 5´- C, 6´-C), 28.7 ($C(CH_3)_2$), 26.0 ($OC(CH_3)_2$), 14.6 ppm (7´-C); HPLC-MS: [A, 80%→95%], t_R: 4.97 min, (98%); MS (ES^+, m/z) 358 $[M+H]^+$; Anal. calcd. for $C_{22}H_{31}NO_3$: C 73.92, H 8.74, found: C 74.11, H, 8.95.

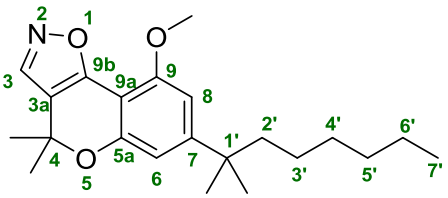

7-(1,1-Dimethylheptyl)-9-(3-hydroxypropoxy)-4,4-dimethyl-4*H*-chromeno[3,4-*d*]isoxazole (1.43).

Prepared from **1.41** (50 mg, 0.14 mmol), sodium hydride (7 mg, 0.29 mmol) and 3-bromo-1-propanol (99 μL, 0.72 mmol) as described for compounds **1.21**−**1.38**. Column chromatography on silica gel (hexane/EtOAc, 2:1) afforded the title compound. Compound **1.43** was obtained as a yellow oil (13 mg, 22%); ^{1}H-NMR (300 MHz, $CDCl_3$) δ: 8.11 (s, 1H, 3-H), 6.69 (d, J = 1.6 Hz, 1H, 8-H), 6.58 (d, J = 1.6 Hz, 1H, 6-H), 4.15 (t, J = 7.1 Hz, 2H, $OCH_2CH_2CH_2OH$), 3.78 (t, J = 4.7 Hz, 2H, $OCH_2CH_2CH_2OH$), 2.11–2.09 (m, 2H, $OCH_2CH_2CH_2OH$), 1.65 (s, 6H, $OC(CH_3)_2$), 1.61–1.57 (m 2H, 2´-H), 1.51 (s, 6H, $C(CH_3)_2$), 1.23–1.14 (m, 8H, 3´-H, 4´-H, 5´-H, 6´-H), 0.86–0.80 ppm (m, 3H, 7´-H); ^{13}C-NMR (75 MHz, $CDCl_3$) δ:

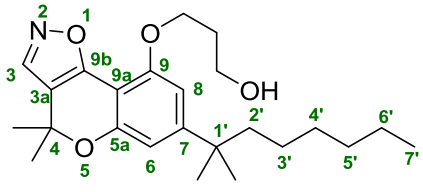

160.5 (9-C), 155.7 (9b-C), 154.0 (5a-C), 150.9 (7-C), 143.5 (3-C), 120.6 (9a-C), 108.9 (8-C), 106.3 (6-C), 105.8 (3a-C), 75.0 ($OC(CH_3)_2$), 66.3 ($OCH_2CH_2CH_2OH$), 62.8 ($OCH_2CH_2CH_2OH$), 44.3 (2´-C), 40.1 ($OCH_2CH_2CH_2OH$), 38.3 ($C(CH_3)_2$), 32.7, 31.5, 23.9, 22.6 (3´-C, 4´-C, 5´-C, 6´-C), 28.3 ($C(CH_3)_2$), 27.1 ($OC(CH_3)_2$), 14.7 ppm (7´-C); HPLC-MS: [A, 80%→95%], t_R: 2.96 min, (95%); MS (ES^+, *m/z*) 402 $[M+H]^+$; Anal. calcd. for $C_{24}H_{35}NO_4$: C 71.79, H 8.79, found: C 72.06, H, 8.55.

General procedure for the synthesis of alkoxychromenopyrazoles 1.44−1.55

The corresponding chromenopyrazole (1eq) was dissolved in anhydrous THF (1-5 mL); the solution was added over sodium hydride (1.5-3 eq) under nitrogen atmosphere. After 10 minutes stirring at room temperature, an excess of the corresponding 1-bromoalkane (5-10 eq) was rapidly added to the solution and the mixture was refluxed (2-12 h). After completion of the reaction (determined by TLC), the mixture was dissolved in EtOAc, washed with water and extracted three times with EtOAc. The combined organic layers were dried over $MgSO_4$ and the solvent was removed under vacuum. The crude was purified by gradient flash column chromatography with hexane and EtOAc performed on a Biotage Isolera One.

9-Decyloxy-7-(1,1-dimethylheptyl)-2,4-dihydro-2,4,4-trimethylchromeno[4,3-*c*]pyrazole (1.44).

1.44 was prepared from **1.5b** (20 mg, 0.056 mmol), sodium hydride (3.3 mg, 0.14 mmol) and 1-bromodecane (81 µL, 0.39 mmol). A pale-yellow oil was obtained (18 mg, 66%). ^{1}H-NMR (500 MHz, $CDCl_3$) δ: 7.07 (s, 1H, 3-H), 6.56 (d, *J* = 1.7 Hz, 1H, 8-H), 6.53 (d, *J* = 1.7 Hz, 1H, 6-H), 4.10 (t, *J* = 7.1 Hz, 2H, 1”-H), 3.92 (s, 3H, NCH_3), 1.92 (p, *J* =7.1 Hz, 2H, 2”-H), 1.62–1.50 (br s, 10H, $OC(CH_3)_2$, *alkyl chain*), 1.42–1.39 (m, 2H, 2’-H), 1.35–1.22 (m, 18H, $C(CH_3)_2$, *alkyl chain*), 1.21–1.12 (m, 4H, *alkyl chain*), 1.10–0.96 (m, 2H, 3’-H), 0.88 (t, *J* = 6.8 Hz, 3H, 12”-H), 0.83 ppm (t, *J* = 7.2 Hz, 3H, 7’-H); ^{13}C-NMR (126 MHz, $CDCl_3$) δ: 155.0 (9-C), 153.7 (7-C), 151.1 (5a-C), 141.3 (9b-C), 123.1 (3-C), 122.1 (3a-C), 108.4 (8-C), 105.4 (6-C), 103.9 (9a-C), 75.4 ($OC(CH_3)_2$), 69.0 (1”-C), 44.5 (NCH_3), 39.0 (2’-C), 38.0 ($C(CH_3)_2$), 32.8, 31.9, 31.8, 29.9, 29.7, 29.6,

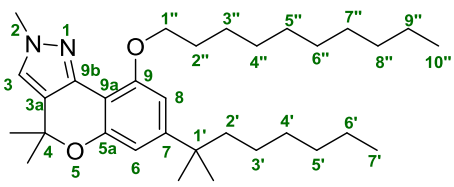

29.5, 29.4, 25.9, 22.7 and 22.6 (*alkyl chain*), 28.9 (OC(CH_3)$_2$), 28.8 (C(CH_3)$_2$), 24.5 (3'-C), 14.1 (7'-C), 14.0 ppm (10"-C); HRMS calcd for $C_{32}H_{53}N_2O_2$ $[M+H]^+$: 497.4102, found: 497.4106.

9-Decyloxy-7-(1,1-dimethylheptyl)-1-ethyl-1,4-dihydro-4,4-dimethylchromeno[4,3-*c*]pyrazole (1.45).

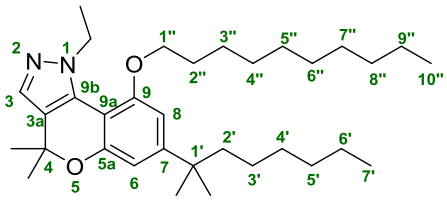

1.45 was prepared from **1.6a** (14 mg, 0.038 mmol), sodium hydride (2 mg, 0.95 mmol) and 1-bromodecane (55 µL, 0.27 mmol). A white oil was obtained (12 mg, 62%). ^{1}H-NMR (500 MHz, $CDCl_3$) δ: 7.32 (s, 1H, 3-H), 6.66 (d, *J* = 1.7 Hz, 1H, 8-H), 6.54 (d, *J* = 1.7 Hz, 1H, 6-H), 4.53 (q, *J* = 7.2 Hz, 2H, NCH_2CH$_3$), 4.08 (t, *J* = 7.0 Hz, 2H, 1"-H), 1.85 (p, *J* = 7.0 Hz, 2H, 2"-H), 1.55 (s, 6H, OC(CH_3)$_2$), 1.48–1.40 (m, 2H, 2'-H), 1.38 (t, *J* = 7.2 Hz, 3H, NCH$_2$CH_3), 1.33–1.21 (m, 20H, *alkyl chain*), 1.22–1.15 (m, 6H, C(CH_3)$_2$), 1.11–1.04 (m, 2H, 3'-H), 0.88 (t, *J* = 6.8 Hz, 3H, 10"-H), 0.84 ppm (t, *J* = 7.0 Hz, 3H, 7'-H); ^{13}C-NMR (126 MHz, $CDCl_3$) δ: 153.9 (9-C), 153.4 (7-C), 152.1 (5a-C), 132.2 (9b-C), 132.0 (3-C), 123.2 (3a-C), 109.5 (6-C), 104.6 (8-C), 103.7 (9a-C), 76.4 (O*C*(CH$_3$)$_2$), 69.0 (1"-C), 47.9 (N*C*H$_2$CH$_3$), 44.4 (2'-C), 38.0 (*C*(CH$_3$)$_2$), 31.9, 31.7, 29.9, 29.54, 29.52, 29.4, 29.3, 29.2, 26.1, 22.7 and 22.6 (*alkyl chain*), 28.7 (C(*C*H$_3$)$_2$), 27.2 (OC(*C*H$_3$)$_2$), 24.6 (3'-C), 15.5 (NCH$_2$*C*H$_3$), 14.1 (7'-C), 14.0 ppm (10"-C); HRMS calcd for $C_{33}H_{55}N_2O_2$ $[M+H]^+$: 511.4258, found: 511.4260.

9-Decyloxy-7-(1,1-dimethylheptyl)-2-ethyl-2,4-dihydro-4,4-dimethylchromeno[4,3-*c*]pyrazole (1.46).

Compound **1.46** was prepared from **1.6b** (18 mg, 0.048 mmol), sodium hydride (2.9 mg, 0.12 mmol) and 1-bromodecane (70 µL, 0.34 mmol). A pale-yellow oil was obtained (18 mg, 75%). ^{1}H-NMR (500 MHz, $CDCl_3$) δ: 7.11 (s, 1H, 3-H), 6.56 (d, *J* = 1.7 Hz, 1H, 8-H), 6.52 (d, *J* = 1.7 Hz, 1H, 6-H), 4.19 (q, *J* = 7.3 Hz, 2H, NCH_2CH$_3$), 4.09 (t, *J* = 6.6 Hz, 2H, 1"-H), 1.91 (p, *J* = 6.6 Hz, 2H, 2"-H), 1.58 (s, 6H, OC(CH_3)$_2$), 1.52 (t, *J* = 7.3 Hz, 3H, NCH$_2$CH_3), 1.43–1.33 (m, 2H, 2'-H), 1.32 – 1.22 (br s, 20H, C(CH_3)$_2$, *alkyl chain*), 1.19–1.13 (m, 6H, *alkyl chain*), 1.09–0.97 (m, 2H, 3'-H), 0.87 (t, *J* = 6.8, 3H, 10"-H), 0.83 ppm (t, *J* = 7.0 Hz, 3H, 7'-H); ^{13}C-NMR (126 MHz, $CDCl_3$) δ: 155.0 (9-C), 153.7

(7-C), 151.0 (5a-C), 140.9 (9b-C), 121.7 (3-C), 121.3 (3a-C), 108.4 (6-C), 105.6 (8-C), 103.9 (9a-C),

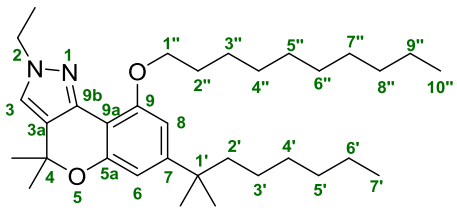

75.5 (O*C*$(CH_3)_2$), 68.9 (1”-C), 47.0 (N*C*H_2CH_3), 44.6 (2’-C), 37.9 (*C*$(CH_3)_2$), 31.9, 31.7, 29.9, 29.7, 29.6, 29.5, 29.3, 26.1, 22.7 and 22.6 (*alkyl chain*), 28.9 (OC(*C*$H_3)_2$), 28.8 (C(*C*$H_3)_2$), 24.6 (3’-C), 15.4 (NCH$_2$*C*H_3), 14.1 (7’-C), 14.0 ppm (10”-C); HRMS calcd for $C_{33}H_{55}N_2O_2$ $[M+H]^+$: 511.4258, found: 511.4277.

7-(1,1-Dimethylheptyl)-9-dodecyloxy-2,4-dihydro-2,4,4-trimethylchromeno[4,3-*c*]pyrazole (1.47).

Compound **1.47** was prepared from **1.5b** (30 mg, 0.084 mmol), sodium hydride (5 mg, 0.21 mmol)

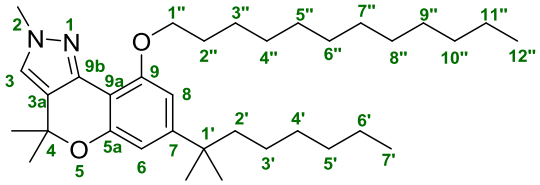

and 1-bromododecane (0.14 mL, 0.59 mmol). A yellow oil was obtained (14 mg, 32%). ^{1}H-NMR (500 MHz, $CDCl_3$) δ: 7.08 (s, 1H, 3-H), 6.56 (d, *J* = 1.6 Hz, 1H, 8-H), 6.53 (d, *J* = 1.6 Hz, 1H, 6-H), 4.10 (t, *J* = 6.9 Hz, 2H, 1”-H), 3.92 (s, 3H, NCH_3), 1.92 (p, *J* =7.0 Hz, 2H, 2”-H), 1.58–1.56 (br s, 8H, *alkyl chain*), 1.55 (s, 6H, OC$(CH_3)_2$), 1-40–1.36 (m, 2H, 2’-H), 1.30–1.24 (br s, 18H, C$(CH_3)_2$, *alkyl chain*), 1.24–1.14 (m, 4H, *alkyl chain*), 1.08–1.01 (m, 2H, 3’-H), 0.88 (t, *J* = 6.9 Hz, 3H, 12”-H), 0.83 ppm (t, *J* = 7.0 Hz, 3H, 7’-H); ^{13}C-NMR (126 MHz, $CDCl_3$) δ: 155.1 (9-C), 153.8 (7-C), 151.2 (5a-C), 141.3 (9b-C), 123.1 (3-C), 122.1 (3a-C), 108.4 (8-C), 106.3 (6-C), 103.9 (9a-C), 75.4 (O*C*$(CH_3)_2$), 69.0 (1”-C), 44.6 (NCH_3), 39.1 (2’-C), 38.0 (*C*$(CH_3)_2$), 31.9, 31.8, 30.0, 29.72, 29.70, 29.66, 29.65, 29.58, 29.38, 29.37, 26.0, 22.7 and 22.6 (*alkyl chain*), 28.9 (OC(*C*$H_3)_2$), 28.8 (C(*C*$H_3)_2$), 24.6 (3’-C), 14.1 (7’-C), 14.0 ppm (12”-C); HRMS calcd for $C_{34}H_{57}N_2O_2$ $[M+H]^+$: 525.4415, found: 525.4414.

7-(1,1-Dimethylheptyl)-9-dodecyloxy-1-ethyl-1,4-dihydro-4,4-dimethylchromeno[4,3-*c*]pyrazole (1.48).

1.48 was prepared from **1.6a** (30 mg, 0.08 mmol), sodium hydride (6 mg, 0.24 mmol) and 1-bromododecane (0.19 mL, 0.81 mmol). A yellow oil was obtained (17 mg, 39%). ^{1}H-NMR (500 MHz, $CDCl_3$) δ: 7.32 (s, 1H, 3-H), 6.66 (d, *J* = 1.7 Hz, 1H, 8-H), 6.54 (d, *J* = 1.7 Hz, 1H, 6-H), 4.53

(q, J = 7.2 Hz, 2H, NCH_2CH$_3$), 4.08 (t, J = 7.0 Hz, 2H, 1”-H), 1.85 (p, J = 7.2 Hz, 2H, 2”-H), 1.59–

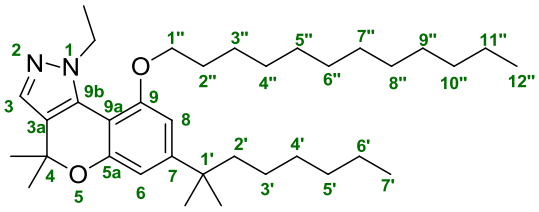

1.51 (m, 10H, OC(CH$_3$)$_2$, *alkyl chain*), 1.46–1.40 (m, 2H, 2’-H), 1.38 (t, J = 7.2 Hz, 3H, NCH$_2$CH_3), 1.28 - 1.26 (br s, 10H, *alkyl chain*), 1.26–1.25 (br s, 12H, C(CH$_3$)$_2$, *alkyl chain*), 1.21–1.18 (m, 4H, *alkyl chain*), 1.10–1.03 (m, 2H, 3’-H), 0.88 (t, J = 6.9 Hz, 3H, 12”-H), 0.84 ppm (t, J = 6.8 Hz, 3H, 7’-H); ^{13}C-NMR (126 MHz, CDCl$_3$) δ: 153.9 (9-C), 153.4 (7-C), 152.2 (5a-C), 132.2 (9b-C), 132.1 (3-C), 123.3 (3a-C), 109.5 (6-C), 104.6 (8-C), 103.7 (9a-C), 76.4 (OC(CH$_3$)$_2$), 69.0 (1”-C), 47.9 (NCH$_2$CH$_3$), 44.4 (2’-C), 38.0 (C(CH$_3$)$_2$), 31.9, 31.7, 29.9, 29.7, 29.6, 29.58, 29.56, 29.46, 29.3, 29.2, 26.1, 22.7 and 22.6 (*alkyl chain*), 28.8 (C(CH$_3$)$_2$), 27.2 (OC(CH$_3$)$_2$), 24.6 (3’-C), 15.5 (NCH$_2$$CH_3$), 14.1 (7’-C), 14.0 ppm (12”-C); HRMS calcd for C$_{35}$H$_{59}$N$_2$O$_2$ [M+H]$^+$: 539.4571, found: 539.4556.

7-(1,1-Dimethylheptyl)-9-dodecyloxy-2-ethyl-2,4-dihydro-4,4-dimethylchromeno[4,3-*c*]pyrazole (1.49).

Compound **1.49** was prepared from **1.6b** (42 mg, 0.11 mmol), sodium hydride (7 mg, 0.28 mmol) and 1-bromododecane (0.19 mL, 0.79 mmol). A yellow oil was obtained (45 mg, 74%). ^{1}H-NMR

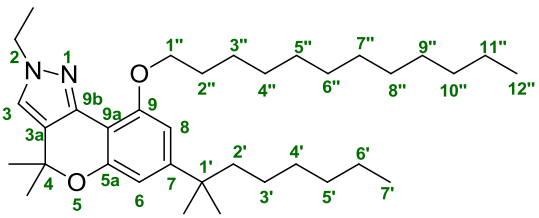

(500 MHz, CDCl$_3$) δ: 7.11 (s, 1H, 3-H), 6.56 (d, J = 1.6 Hz, 1H, 8-H), 6.52 (d, J = 1.6 Hz, 1H, 6-H), 4.19 (q, J = 7.3 Hz, 2H, NCH_2CH$_3$), 4.09 (t, J = 6.6 Hz, 2H, 1”-H), 1.91 (p, J = 6.6 Hz, 2H, 2”-H), 1.62 (p, J = 7.1 Hz, 2H, *alkyl chain*), 1.58 (s, 6H, OC(CH$_3$)$_2$), 1.53 (t, J = 7.3 Hz, 3H, NCH$_2$CH_3), 1.43–1.35 (m, 2H, 2’-H), 1.27–1.25 (br s, 22H, C(CH$_3$)$_2$, *alkyl chain*), 1.19 – 1.14 (m, 6H, *alkyl chain*), 1.07 – 1.00 (m, 2H, 3’-H), 0.88 (t, J = 7.1, 3H, 12”-H), 0.83 ppm (t, J = 7.0 Hz, 3H, 7’-H); ^{13}C-NMR (126 MHz, CDCl$_3$) δ: 155.1 (9-C), 153.7 (7-C), 151.0 (5a-C), 140.9 (9b-C), 121.8 (3-C), 121.4 (3a-C), 108.4 (6-C), 105.6 (8-C), 104.0 (9a-C), 75.5 (OC(CH$_3$)$_2$), 67.0 (1”-C), 47.0 (NCH$_2$CH$_3$), 44.6 (2’-C), 38.0 (C(CH$_3$)$_2$), 31.9, 31.8, 30.0, 29.72, 29.71, 29.68, 29.65, 29.64, 29.5, 29.4, 26.1, 22.7 and 22.6 (*alkyl*

chain), 28.9 (OC(*C*H$_3$)$_2$), 28.8 (C(*C*H$_3$)$_2$), 24.6 (3'-C), 15.4 (NCH$_2$*C*H$_3$), 14.1 (7'-C), 14.0 ppm (12"-C); HRMS calcd for $C_{35}H_{59}N_2O_2$ $[M+H]^+$: 539.4571, found: 539.4578.

7-(1,1-Dimethylheptyl)-2,4-dihydro-9-tetradecyloxy-2,4,4-trimethylchromeno[4,3-*c*]pyrazole (1.50)

Compound **1.50** was prepared from **1.5b** (28 mg, 0.078 mmol), sodium hydride (4.7 mg, 0.19 mmol) and 1-bromotetradecane (0.15 mL, 0.52 mmol). A yellow oil was obtained (32 mg, 74%). ^{1}H-NMR

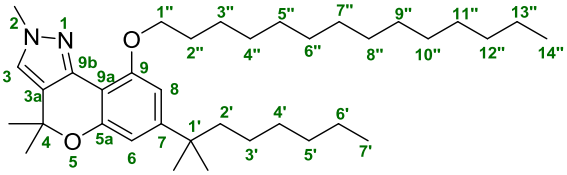

(500 MHz, $CDCl_3$) δ: 7.07 (s, 1H, 3-H), 6.56 (d, *J* = 1.7 Hz, 1H, 8-H), 6.53 (d, *J* = 1.7 Hz, 1H, 6-H), 4.10 (t, *J* = 6.8 Hz, 2H, 1"-H), 3.91 (s, 3H, NCH$_3$), 1.92 (p, *J* =6.8 Hz, 2H, 2"-H), 1.57–1.54 (br s, 12H, OC(CH$_3$)$_2$, *alkyl chain*), 1.42–1.36 (m, 2H, 2'-H), 1.31–1.23 (m, 22H, C(CH$_3$)$_2$, *alkyl chain*), 1.20–1.15 (m, 6H, *alkyl chain*), 1.09–1.00 (m, 2H, 3'-H), 0.88 (t, *J* = 6.7 Hz, 3H, 14"-H), 0.83 ppm (t, *J* = 6.8 Hz, 3H, 7'-H); ^{13}C-NMR (126 MHz, $CDCl_3$) δ: 155.0 (9-C), 153.7 (7-C), 151.1 (5a-C), 141.2 (9b-C), 123.1 (3-C), 122.1 (3a-C), 108.4 (8-C), 105.4 (6-C), 103.8 (9a-C), 75.3 (O*C*(CH$_3$)$_2$), 69.0 (1"-C), 44.5 (NCH$_3$), 39.0 (2'-C), 37.9 (*C*(CH$_3$)$_2$), 31.9, 31.7, 29.9, 29.7, 29.69, 29.63, 29.60, 29.5, 29.4, 29.3, 26.0, 22.7 and 22.6 (*alkyl chain*), 28.9 (OC(*C*H$_3$)$_2$), 28.8 (C(*C*H$_3$)$_2$), 24.5 (3'-C), 14.1 (7'-C), 14.0 ppm (14"-C); HRMS calcd for $C_{36}H_{61}N_2O_2$ $[M+H]^+$: 553.4728, found: 553.4736.

7-(1,1-Dimethylheptyl)-1-ethyl-1,4-dihydro-4,4-dimethyl-9-tetradecyloxychromeno[4,3-*c*]pyrazole (1.51)

Compound **1.51** was prepared from **1.6a** (16.5 mg, 0.045 mmol), sodium hydride (3 mg, 0.11 mmol) and 1-bromotetradecane (94 μL, 0.32 mmol). A yellow oil was obtained (19 mg, 75%). ^{1}H-NMR

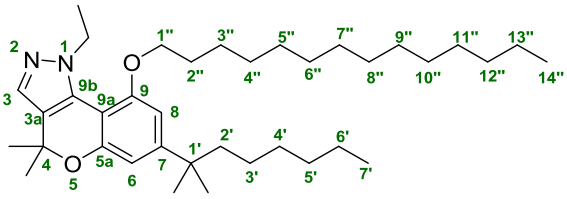

(500 MHz, $CDCl_3$) δ: 7.32 (s, 1H, 3-H), 6.66 (d, *J* = 1.7 Hz, 1H, 8-H), 6.54 (d, *J* = 1.7 Hz, 1H, 6-H), 4.53 (q, *J* = 7.2 Hz, 2H, NC*H*$_2$CH$_3$), 4.08 (t, *J* = 7.0 Hz, 2H, 1"-H), 1.85 (p, *J* = 7.0 Hz, 2H, 2"-H), 1.55 (s, 6H, OC(CH$_3$)$_2$), 1.47–1.40 (m, 2H, 2'-H), 1.38 (t, *J* = 7.2 Hz, 3H, NCH$_2$C*H*$_3$), 1.28 (s, 6H, C(CH$_3$)$_2$), 1.27–1.24 (m, 22H, *alkyl chain*), 1.23–1.16

(m, 6H, *alkyl chain*), 1.11–1.03 (m, 2H, 3'-H), 0.88 (t, *J* = 6.8 Hz, 3H, 14"-H), 0.84 ppm (t, *J* = 7.2 Hz, 3H, 7'-H); ^{13}C-NMR (126 MHz, $CDCl_3$) δ: 153.9 (9-C), 153.4 (7-C), 152.1 (5a-C), 132.2 (9b-C), 132.0 (3-C), 123.2 (3a-C), 109.5 (6-C), 104.6 (8-C), 103.7 (9a-C), 76.3 (O*C*$(CH_3)_2$), 69.0 (1"-C), 47.9 (N*C*H_2CH_3), 44.4 (2'-C), 38.0 (*C*$(CH_3)_2$), 31.9, 31.7, 29.9, 29.7, 29.63, 29.58, 29.55, 29.4, 29.3, 29.2, 26.1, 22.7 and 22.6 (*alkyl chain*), 28.7(C(*C*$H_3)_2$), 27.2 (OC(*C*$H_3)_2$), 24.6 (3'-C), 15.5 (NCH$_2$*C*H_3), 14.1 (7'-C), 14.0 ppm (14"-C); HRMS calcd for $C_{37}H_{63}N_2O_2$ $[M+H]^+$: 567.4884, found: 567.4898.

7-(1,1-Dimethylheptyl)-2-ethyl-2,4-dihydro-4,4-dimethyl-9-tetradecyloxychromeno[4,3-*c*]pyrazole (1.52)

Compound **1.52** was prepared from **1.6b** (23 mg, 0.06 mmol), sodium hydride (3.7 mg, 0.15 mmol) and 1-bromotetradecane (0.13 mL, 0.43 mmol). A yellow oil was obtained (23 mg, 66%). ^{1}H-NMR

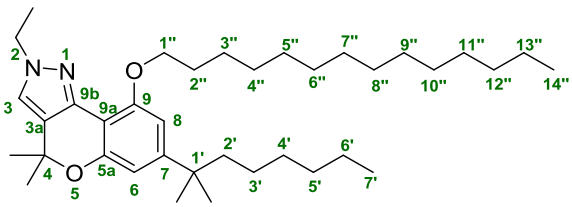

(500 MHz, $CDCl_3$) δ: 7.11 (s, 1H, 3-H), 6.56 (d, *J* = 1.7 Hz, 1H, 8-H), 6.52 (d, *J* = 1.7 Hz, 1H, 6-H), 4.19 (q, *J* = 7.3 Hz, 2H, NC*H*$_2$CH$_3$), 4.09 (t, *J* = 6.7 Hz, 2H, 1"-H), 1.92 (p, *J* = 6.7 Hz, 2H, 2"-H), 1.58 (s, 6H, OC$(CH_3)_2$), 1.53 (t, *J* = 7.3 Hz, 3H, NCH$_2$C*H*$_3$), 1.45–1.32 (m, 8H, 2'-H, *alkyl chain*), 1.26–1.24 (br s, 22H, C$(CH_3)_2$, *alkyl chain*), 1.20–1.13 (m, 6H, *alkyl chain*), 1.08–1.00 (m, 2H, 3'-H), 0.88 (t, *J* = 6.7, 3H, 14"-H), 0.83 ppm (t, *J* = 7.0 Hz, 3H, 7'-H); ^{13}C-NMR (126 MHz, $CDCl_3$) δ: 155.0 (9-C), 153.7 (7-C), 151.0 (5a), 140.9 (9b-C), 121.7 (3-C), 121.3 (3a-C), 108.4 (6-C), 105.5 (8-C), 103.9 (9a-C), 75.4 (O*C*$(CH_3)_2$), 68.9 (1"-C), 47.0 (N*C*H_2CH_3), 44.6 (2'-C), 37.9 (*C*$(CH_3)_2$), 31.9, 31.7, 29.9, 29.71, 29.70, 29.65, 29.63, 29.5, 29.4, 22.7 and 22.6 (*alkyl chain*), 28.9 (OC(*C*$H_3)_2$), 28.8 (C(*C*$H_3)_2$), 24.5 (3'-C), 15.4 (NCH$_2$*C*H_3), 14.1 (7'-C), 14.0 ppm (14"-C); HRMS calcd for $C_{37}H_{63}N_2O_2$ $[M+H]^+$: 567.4884, found: 567.4899.

7-(1,1-Dimethylheptyl)-9-hexadecyloxy-2,4-dihydro-2,4,4-trimethylchromeno[4,3-*c*]pyrazole (1.53)

Compound **1.53** was prepared from **1.5b** (50 mg, 0.14 mmol), sodium hydride (5 mg, 0.21 mmol) and 1-bromohexadecane (0.21 mL, 0.7 mmol). A pale-yellow oil was obtained (73 mg, 90%). ^{1}H-

NMR (500 MHz, $CDCl_3$) δ: 7.07 (s, 1H, 3-H), 6.56 (d, *J* = 1.6, 1H, 8-H), 6.53 (d, *J* = 1.6 Hz, 1H, 6-H), 4.10 (t, *J* = 6.8 Hz, 2H, 1”-H), 3.92 (s, 3H, NCH_3), 1.92 (p, *J* = 6.9 Hz, 2H, 2”-H), 1.57 (s, 6H, $OC(CH_3)_2$), 1.56–1.54 (br s, 12H, *alkyl chain*), 1.41–1.36 (m, 2H, 2’-H), 1.27–1.24 (m, 22H, $C(CH_3)_2$, *alkyl chain*), 1.17 (m, 4H, *alkyl chain*), 1.08 – 1.01 (m, 2H, 3’-H), 0.88 (t, *J* = 7.0, 3H, 16”-H), 0.83 ppm (t, *J* = 7.0, 3H, 7’-H); ^{13}C-NMR (126 MHz, $CDCl_3$) δ: 155.1 (9-C), 153.8 (7-C), 151.1 (5a-C), 141.3 (9b-C), 123.1 (3-C), 122.1 (3a-C), 108.4 (6-C), 105.5 (8-C), 103.9 (9a-C), 75.4 ($OC(CH_3)_2$), 69.0 (1”-C), 44.6 (NCH_3), 39.0 (2’-C), 38.0 ($C(CH_3)_2$), 31.9, 31.8, 30.0, 29.71, 29.66, 29.59, 29.38, 29.36, 26.0, 22.7 and 22.6 (*alkyl chain*), 28.9 ($OC(CH_3)_2$), 28.8 ($C(CH_3)_2$), 24.6 (3’-C), 14.1 (7’-C), 14.0 ppm (16”-C); HRMS calcd for $C_{38}H_{65}N_2O_2$ $[M+H]^+$: 581.5041, found: 581.5045.

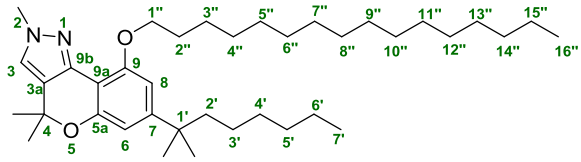

7-(1,1-Dimethylheptyl)-1-ethyl-9-hexadecyloxy-1,4-dihydro-4,4-dimethylchromeno[4,3-*c*]pyrazole (1.54).

Compound **1.54** was prepared from **1.6a** (50 mg, 0.14 mmol), sodium hydride (10 mg, 0.41 mol) and 1-bromohexadecane (0.21 mL, 1.4 mmol). A orange oil was obtained (46 mg, 57%). ^{1}H-NMR (500 MHz, $CDCl_3$) δ: 7.32 (s, 1H, 3-H), 6.66 (d, *J* = 1.7 Hz, 1H, 8-H), 6.54 (d, *J* = 1.7 Hz, 1H, 6-H), 4.53 (q, *J* = 7.2 Hz, 2H, NCH_2CH_3), 4.08 (t, *J* = 7.0 Hz, 2H, 1”-H), 1.85 (p, *J* = 7.1 Hz, 2H, 2”-H), 1.55 (s, 6H, $OC(CH_3)_2$), 1.46–1.41 (m, 2H, 2’-H), 1.38 (t, *J* = 7.2 Hz, 3H, NCH_2CH_3), 1.27 (s, 6H, $C(CH_3)_2$), 1.26–1.25 (br s, 24H, *alkyl chain*), 1.22–1.18 (m, 8H, *alkyl chain*), 1.11–1.03 (m, 2H, 3’-H), 0.87 (t, *J* = 6.8 Hz, 3H, 16”-H), 0.83 ppm (t, *J* = 6.6 Hz, 3H, 7’-H); ^{13}C-NMR (126 MHz, $CDCl_3$) δ: 153.9 (9-C), 153.4 (7-C), 152.1 (5a-C), 132.2 (9b-C), 132.0 (3-C), 123.3 (3a-C), 109.5 (6-C), 104.6 (8-C), 103.7 (9a-C), 76.4 ($OC(CH_3)_2$), 69.0 (1”-C), 47.9 (NCH_2CH_3), 44.4 (2’-C), 38.0 ($C(CH_3)_2$), 31.9, 31.7, 29.9, 29.69, 29.65, 29.59, 29.56, 29.5, 29.4, 29.2, 26.1, 22.7 and 22.6 (*alkyl chain*), 28.8 ($C(CH_3)_2$),

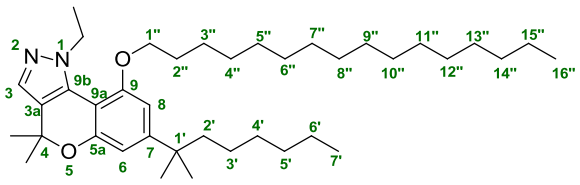

27.2 ($OC(CH_3)_2$), 24.6 (3'-C), 15.5 (NCH_2CH_3), 14.1 (7'-C), 14.0 ppm (16"-C); HRMS calcd for $C_{39}H_{67}N_2O_2$ $[M+H]^+$: 595.5197, found: 595.5213.

7-(1,1-Dimethylheptyl)-2-ethyl-9-hexadecyloxy-2,4-dihydro-4,4-dimethylchromeno[4,3-*c*]pyrazole (1.55).

Compound **1.55** was prepared from **1.6b** (45 mg, 0.12 mmol), sodium hydride (9 mg, 0.36 mmol) and 1-bromohexadecane (0.26 mL, 0.85 mmol). A orange oil was obtained (31 mg, 43%). ^{1}H-NMR (500 MHz, $CDCl_3$) δ: 7.11 (s, 1H, 3-H), 6.55 (d, *J* = 1.6 Hz, 1H, 8-H), 6.52 (d, *J* = 1.6 Hz, 1H, 6-H), 4.19 (q, *J* = 7.3 Hz, 2H, NCH_2CH_3), 4.09 (t, *J* = 6.8 Hz, 2H, 1"-H), 1.91 (p, *J* = 6.8 Hz, 2H, 2"-H), 1.65–1.59 (m, 2H, *alkyl chain*), 1.58 (s, 6H, $OC(CH_3)_2$), 1.52 (t, *J* = 7.3 Hz, 3H, NCH_2CH_3), 1.42–1.34 (m, 2H, 2'-H), 1.27–1.25 (br s, 30H, $C(CH_3)_2$, *alkyl chain*), 1.22–1.10 (m, 6H, *alkyl chain*), 1.04–1.00 (m, 2H, 3'-H), 0.88 (t, *J* = 7.0 Hz, 3H, 16"-H), 0.83 ppm (t, *J* = 7.0 Hz, 3H, 7'-H); ^{13}C-NMR (126 MHz, $CDCl_3$) δ: 155.1 (9-C), 153.7 (7-C), 151.0 (5a-C), 140.9 (9b-C), 121.8 (3-C), 121.4 (3a-C), 108.4 (6-C), 105.6 (8-C), 104.0 (9a-C), 75.5 ($OC(CH_3)_2$), 69.0 (1"-C), 47.0 (NCH_2CH_3), 44.6 (2'-C), 38.0 ($C(CH_3)_2$), 31.9, 31.8, 30.0, 29.73, 29.71, 29.69, 29.66, 29.65, 29.5, 29.4, 26.1, 22.7 and 22.6 (*alkyl chain*), 28.9 ($OC(CH_3)_2$), 28.8 ($C(CH_3)_2$), 24.6 (3'-C), 15.4 (NCH_2CH_3), 14.1 (7'-C), 14.0 ppm (16"-C); HRMS calcd for $C_{39}H_{67}N_2O_2$ $[M+H]^+$: 595.5197, found: 595.5203.

General procedure the synthesis of bivalent chromenopyrazoles 1.56−1.67

A solution of the corresponding chromenopyrazole (1 eq) in anhydrous THF (1-5 mL) was added to a Kimax® vial containing Cs_2CO_3 (10 eq) under nitrogen atmosphere. After 10 minutes stirring, the correspondent dibromoalkane (0.5 eq) was added. The mixture was heated at reflux temperature for 8-72 hours. Then, the mixture was dissolved in EtOAc, washed with water and extracted three times with EtOAc. The organic layers were combined and dried over $MgSO_4$, filtered and the solvent was evaporated under reduced pressure. The crude was purified by gradient flash column chromatography with hexane and EtOAc performed on a Biotage Isolera One.

1,10-Bis[(7-(1,1-dimethylheptyl)-2,4-dihydro-2,4,4-trimethylchromeno[4,3-*c*]pyrazol-9-yl)oxy]decane (1.56).

Compound **1.56** was prepared from **1.5b** (28 mg, 0.08 mmol), Cs_2CO_3 (0.25 g, 0.78 mmol) and 1,10-dibromodecane (11 mg, 0.039 mmol). A yellow oil was obtained (6 mg, 18%). ^{1}H-NMR (500 MHz, $CDCl_3$) δ: 7.07 (s, 2H, 3-H), 6.56 (d, *J* = 1.7 Hz, 2H, 8-H), 6.53 (d, *J* = 1.7 Hz, 2H, 6-H), 4.10 (t, *J* = 6.8 Hz, 4H, 1”-H), 3.91 (s, 6H, NCH_3), 1.92 (p, *J* = 6.9 Hz, 4H, 2”-H), 1.63–1.49 (m, 24H, $OC(CH_3)_2$, *alkyl chain*), 1.42–1.38 (m, 8H, 2’-H, *alkyl chain*), 1.26 (s, 12H, $C(CH_3)_2$), 1.23–1.13 (m, 12H, *alkyl chain*), 1.08–1.00 (m, 4H, 3’-H), 0.83 ppm (t, *J* = 7.0 Hz, 6H, 7’-H); ^{13}C-NMR (126 MHz, $CDCl_3$) δ: 155.1 (9-C), 153.8 (7-C), 151.2 (5a-C), 141.2 (9b-C), 123.2 (3-C), 122.1 (3a-C), 108.4 (8-C), 105.4 (6-C), 103.9 (9a-C), 75.4 ($OC(CH_3)_2$), 69.0 (1”-C), 44.6 (NCH_3), 39.0 (2’-C), 38.0 ($C(CH_3)_2$), 31.7, 29.9, 29.66, 29.61, 29.4, 26.0 and 22.6 (*alkyl chain*), 28.9 ($OC(CH_3)_2$), 28.8 ($C(CH_3)_2$), 24.6 (3’-C), 14.1 ppm (7’-C); HRMS calcd for $C_{54}H_{83}N_4O_4$ $[M+H]^+$: 851.6409, found: 851.6392.

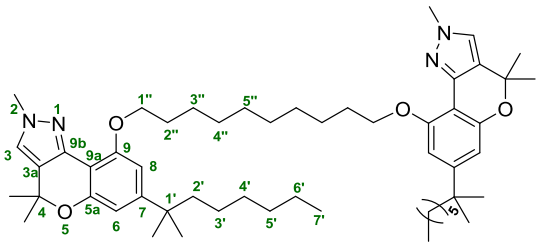

1,10-Bis[(7-(1,1-dimethylheptyl)-1-ethyl-1,4-dihydro-4,4-dimethylchromeno[4,3-*c*]pyrazol-9-yl)oxy]decane (1.57).

Compound **1.57** was prepared from **1.6a** (23 mg, 0.062 mmol), Cs_2CO_3 (0.20 g, 0.62 mmol) and 1,10-dibromodecane (9.0 mg, 0.03 mmol). A yellow oil was obtained (12 mg, 44%). ^{1}H-NMR (500 MHz, $CDCl_3$) δ: 7.32 (s, 2H, 3-H), 6.66 (d, *J* = 1.7 Hz, 2H, 8-H), 6.54 (d, *J* = 1.7 Hz, 2H, 6-H), 4.53 (q, *J* = 7.2 Hz, 4H, NCH_2CH_3), 4.08 (t, *J* = 7.1 Hz, 4H, 1”-H), 1.85 (p, *J* = 7.1 Hz, 4H, 2”-H), 1.54–1.57 (br s, 24H, $OC(CH_3)_2$, *alkyl chain*), 1.48–1.40 (m, 4H, 2’-H), 1.37 (t, *J* = 7.2 Hz, 6H, NCH_2CH_3), 1.33–1.29 (m, 8H, *alkyl chain*), 1.27–1.25 (br s, 12H, $C(CH_3)_2$), 1.23–1.15 (m, 4H, *alkyl chain*), 1.13–1.02 (m, 4H, 3’-H), 0.82 ppm (t, *J* = 7.0 Hz, 6H, 7’-H); ^{13}C-NMR (126 MHz, $CDCl_3$) δ: 153.9 (9-C), 153.4 (7-C), 152.1 (5a-C), 132.2 (9b-C), 132.0 (3-C), 123.3 (3a-C), 109.5 (6-C), 104.6 (8-C), 103.6 (9a-C), 76.4

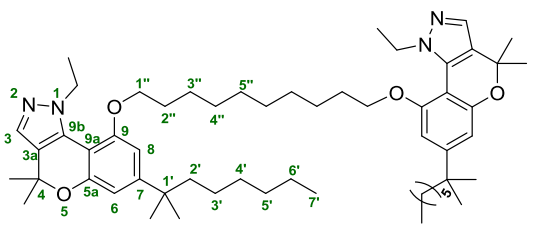

(O*C*(CH_3)$_2$), 69.0 (1”-C), 47.9 (N*C*H_2CH$_3$), 44.4 (2’-C), 38.0 (*C*(CH_3)$_2$), 31.7, 29.9, 29.50, 29.47, 29.2, 26.1 and 22.6 (*alkyl chain*), 28.7 (C(*C*H_3)$_2$), 27.2 (OC(*C*H_3)$_2$), 24.6 (3’-C), 15.5 (NCH$_2$*C*H_3), 14.1 ppm (7’-C); HRMS calcd for $C_{56}H_{87}N_4O_4$ $[M+H]^+$: 879.6722, found: 879.6704.

1,10-Bis[(7-(1,1-dimethylheptyl)-2-ethyl-2,4-dihydro-4,4-dimethylchromeno[4,3-*c*]pyrazol-9-yl)oxy]decane (1.58).

Compound **1.58** was prepared from **1.6b** (29 mg, 0.079 mmol), Cs_2CO_3 (0.26 g, 0.79 mmol) and 1,10-dibromodecane (11.6 mg, 0.04 mmol). A yellow oil was obtained (10 mg, 29%). ^{1}H-NMR (500 MHz, $CDCl_3$) δ: 7.26 (s, 2H, 3-H), 6.56 (d, *J* = 1.7 Hz, 2H, 8-H), 6.52 (d, *J* = 1.7 Hz, 2H, 6-H), 4.18 (q, *J* = 7.3 Hz, 4H, NC*H*$_2$CH$_3$), 4.09 (t, *J* = 6.6 Hz, 4H, 1”-H), 1.91 (p, *J* = 6.6 Hz, 4H, 2”-H), 1.57 – 1.55 (br s, 26H, OC(CH$_3$)$_2$), 1.51 (t, *J* = 7.3 Hz, 6H, NCH$_2$C*H*$_3$), 1.42–1.33 (m, 8H, 2’-H, *alkyl chain*), 1.26 (s, 12H, C(CH$_3$)$_2$), 1.21–1.13 (m, 6H, *alkyl chain*), 1.09–0.98 (m, 4H, 3’-H), 0.83 ppm (t, *J* = 7.0 Hz, 6H, 7’-H); ^{13}C-NMR (126 MHz, $CDCl_3$) δ: 155.1 (9-C), 153.7 (7-C), 151.0 (5a-C), 140.9 (9b-C), 121.7 (3-C), 121.4 (3a-C), 108.5 (6-C), 105.6 (8-C), 103.9 (9a-C), 75.5 (O*C*(CH_3)$_2$), 68.9 (1”-C), 47.0 (N*C*H$_2$CH$_3$), 44.6 (2’-C), 38.0 (*C*(CH_3)$_2$), 31.7, 30.0, 29.73, 29.69, 29.5, 26.1 and 22.6 (*alkyl chain*), 28.9 (OC(*C*H_3)$_2$), 28.8 (C(*C*H_3)$_2$), 24.5 (3’-C), 15.4 (NCH$_2$*C*H_3), 14.1 ppm (7’-C); HRMS calcd for $C_{56}H_{87}N_4O_4$ $[M+H]^+$: 879.6722, found: 879.6736.

1,12-Bis[(7-(1,1-dimethylheptyl)-2,4-dihydro-2,4,4-trimethylchromeno[4,3-*c*]pyrazol-9-yl)oxy]dodecane (1.59).

Compound **1.59** was prepared from **1.5b** (25 mg, 0.07 mmol), Cs_2CO_3 (0.23 g, 0.70 mmol) and 1,12-dibromododecane (11.1 mg, 0.03 mmol). A pale-yellow oil was isolated (9 mg, 29%). ^{1}H-NMR (500 MHz, $CDCl_3$) δ: 7.07 (s, 2H, 3-H), 6.56 (d, *J* = 1.6 Hz, 2H, 8-H), 6.53 (d, *J* = 1.6 Hz, 2H, 6-H), 4.10 (t, *J* = 6.8 Hz, 4H, 1”-H), 3.91 (s, 6H, NCH$_3$), 1.92 (p, *J* = 6.8 Hz, 4H, 2”-H), 1.60–1.51 (m, 28H, OC(CH$_3$)$_2$, *alkyl chain*), 1.41–1.29 (m, 4H, 2’-H), 1.26 (s, 12H, C(CH$_3$)$_2$), 1.23–1.14 (m, 12H, *alkyl chain*), 1.10–0.97 (m, 4H, 3’-H), 0.83 ppm (t, *J* = 6.9 Hz, 6H, 7’-H); ^{13}C-NMR (126 MHz, $CDCl_3$) δ:

155.1 (9-C), 153.8 (7-C), 151.2 (5a-C), 141.3 (9b-C), 123.2 (3-C), 122.1 (3a-C), 108.4 (8-C), 105.4 (6-C), 103.9 (9a-C), 75.4 ($OC(CH_3)_2$), 69.0 (1"-C), 44.6 (NCH_3), 39.1 (2'-C), 38.0 ($C(CH_3)_2$), 31.7, 30.0, 29.72, 29.70, 29.6, 29.4, 26.0 and 22.6 (*alkyl chain*), 28.9 ($OC(CH_3)_2$), 28.8 ($C(CH_3)_2$), 24.6 (3'-C), 14.1 ppm (7'-C); HRMS calcd for $C_{56}H_{87}N_4O_4$ $[M+H]^+$: 879.6722, found: 879.6697.

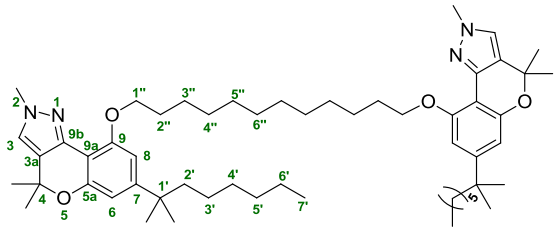

1,12-Bis[(7-(1,1-dimethylheptyl)-1-ethyl-1,4-dihydro-4,4-dimethylchromeno[4,3-*c*]pyrazol-9-yl)oxy]dodecane (1.60).

Compound **1.60** was prepared from **1.6a** (25 mg, 0.07 mmol), Cs_2CO_3 (0.22 g, 0.68 mmol) and 1,12-dibromododecane (10.7 mg, 0.03 mmol). A white oil was obtained (10 mg, 32%). ^{1}H-NMR (500 MHz, $CDCl_3$) δ: 7.32 (s, 2H, 3-H), 6.66 (d, *J* = 1.7, 2H, 8-H), 6.54 (d, *J* = 1.7 Hz, 2H, 6-H), 4.53 (q, *J* = 7.2 Hz, 4H, NCH_2CH_3), 4.08 (t, *J* = 7.0 Hz, 4H, 1"-H), 1.85 (p, *J* = 6.9 Hz, 4H, 2"-H), 1.60–1.52 (m, 20H, $OC(CH_3)_2$, *alkyl chain*), 1.47–1.40 (m, 4H, 2'-H), 1.38 (t, *J* = 7.2 Hz, 6H, NCH_2CH_3), 1.29–1.26 (br s, 20H, $C(CH_3)_2$, *alkyl chain*), 1.24–1.17 (m, 12H, *alkyl chain*), 1.11–1.04 (m, 4H, 3'-H), 0.83 ppm (t, *J* = 6.9 Hz, 6H, 7'-H); ^{13}C-NMR (126 MHz, $CDCl_3$) δ: 153.9 (9-C), 153.4 (7-C), 152.2 (5a-C), 132.2 (9b-C), 132.0 (3-C), 123.3 (3a-C), 109.5 (6-C), 104.6 (8-C), 103.6 (9a-C), 76.4 ($OC(CH_3)_2$), 69.0 (1"-C), 47.9 (NCH_2CH_3), 44.4 (2'-C), 38.0 ($C(CH_3)_2$), 31.7, 30.9, 29.9, 29.6, 29.5, 29.2, 26.1 and 22.6 (*alkyl chain*), 28.8 ($C(CH_3)_2$), 27.2 ($OC(CH_3)_2$), 24.6 (3'-C), 15.5 (NCH_2CH_3), 14.1 ppm (7'-C); HRMS calcd for $C_{58}H_{91}N_4O_4$ $[M+H]^+$: 907.7035, found: 907.7042.

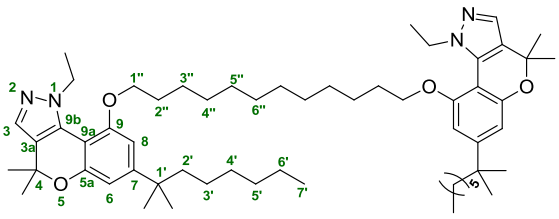

1,12-Bis[(7-(1,1-dimethylheptyl)-2-ethyl-2,4-dihydro-4,4-dimethylchromeno[4,3-*c*]pyrazol-9-yl)oxy]dodecane (1.61).

Compound **1.61** was prepared from **1.6b** (52 mg, 0.14 mmol), Cs_2CO_3 (0.46 g, 1.40 mmol) and 1,12-dibromododecane (22.10 mg, 0.07 mmol). A yellow oil was isolated (11 mg, 18%). ^{1}H-NMR (500 MHz, $CDCl_3$) δ: 7.11 (s, 2H, 3-H), 6.56 (d, *J* = 1.6 Hz, 2H, 8-H), 6.52 (d, *J* = 1.6 Hz, 2H, 6-H), 4.18

(q, J = 7.3 Hz, 4H, NCH_2CH$_3$), 4.09 (t, J = 6.6 Hz, 4H, 1"-H), 1.96–1.89 (m, 4H, 2"-H), 1.65–1.59 (m, 4H, *alkyl chain*), 1.57 (s, 12H, OC(CH_3)$_2$), 1.52 (t, J = 7.3 Hz, 6H, NCH$_2$CH_3), 1.41–1.28 (m, 20H, 2'-H, *alkyl chain*), 1.26 (s, 12H, C(CH_3)$_2$), 1.20–1.13 (m, 8H, *alkyl chain*), 1.06–1.01 (m, 4H, 3'-H), 0.83 ppm (t, J = 7.0 Hz, 6H, 7'-H); ^{13}C-NMR (126 MHz, CDCl$_3$) δ:155.1 (9-C), 153.7 (7-C), 151.0 (5a-C), 140.9 (9b-C), 121.8 (3-C), 121.4 (3a-C), 108.5 (6-C), 105.6 (8-C), 103.9 (9a-C), 75.5 (O*C*(CH$_3$)$_2$), 69.0 (1"-C), 47.0 (N*C*H$_2$CH$_3$), 44.6 (2'-C), 38.0 (*C*(CH$_3$)$_2$), 31.8, 30.0, 29.8, 29.7, 29.5, 26.1, 24.6 and 22.6 (*alkyl chain*), 28.9 (OC(*C*H$_3$)$_2$), 28.8 (C(*C*H$_3$)$_2$), 15.4 (NCH$_2$*C*H$_3$), 14.1 ppm (7'-C); HRMS calcd for $C_{58}H_{91}N_4O_4$ [M+H]$^+$: 907.7035, found: 907.7031.

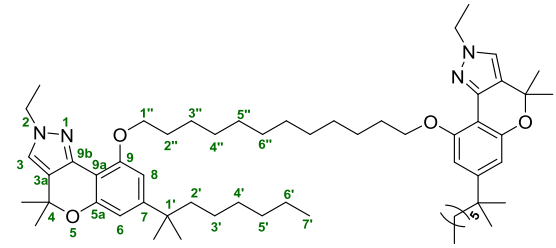

1,14-Bis[(7-(1,1-dimethylheptyl)-2,4-dihydro-2,4,4-trimethylchromeno[4,3-*c*]pyrazol-9-yl)oxy]tetradecane (1.62).

Compound **1.62** was prepared from **1.5b** (20 mg, 0.056 mmol), Cs_2CO_3 (0.18 g, 0.56 mmol) and 1,14-dibromotetradecane (9.9 mg, 0.028 mmol). A white oil was obtained (11 mg, 43%). ^{1}H-NMR (500 MHz, CDCl$_3$) δ: 7.07 (s, 2H, 3-H), 6.56 (d, J = 1.7 Hz, 2H, 8-H), 6.53 (d, J = 1.7 Hz, 2H, 6-H), 4.10 (t, J = 6.8 Hz, 4H, 1"-H), 3.91 (s, 6H, NCH$_3$), 1.94 (p, J = 6.8 Hz, 4H, 2"-H), 1.59–1.55 (m, 24H, OC(CH$_3$)$_2$, *alkyl chain*), 1.38–1.34 (m, 10H, *alkyl chain*), 1.26 (s, 12H, C(CH$_3$)$_2$), 1.20–1.16 (m, 14H, *alkyl chain*), 1.07–1.03 (m, 4H, 3'-H), 0.83 ppm (t, J = 6.9 Hz, 6H, 7'-H); ^{13}C-NMR (126 MHz, CDCl$_3$) δ: 155.1 (9-C), 153.8 (7-C), 151.2 (5a-C), 141.3 (9b-C), 123.1 (3-C), 122.1 (3a-C), 108.4 (8-C), 105.5 (6-C), 103.9 (9a-C), 75.4 (O*C*(CH$_3$)$_2$), 69.0 (1"-C), 44.6 (NCH$_3$), 39.0 (2'-C), 38.0 (*C*(CH$_3$)$_2$), 31.7, 30.0, 29.8, 29.72, 29.70, 29.6, 29.4, 26.0 and 22.6 (*alkyl chain*), 28.9 (OC(*C*H$_3$)$_2$), 28.8 (C(*C*H$_3$)$_2$), 24.6 (3'-C), 14.1 ppm (7'-C); HRMS calcd for $C_{58}H_{91}N_4O_4$ [M+H]$^+$: 907.7034, found: 907.7017.

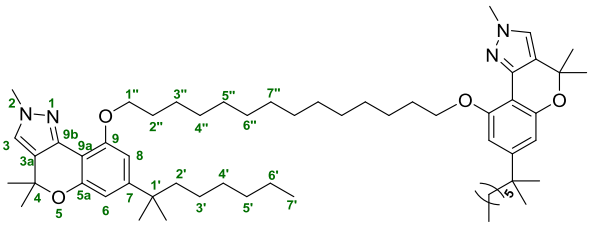

1,14-Bis[(7-(1,1-dimethylheptyl)-1-ethyl-1,4-dihydro-4,4-dimethylchromeno[4,3-*c*]pyrazol-9-yl)oxy]tetradecane (1.63).

Compound **1.63** was prepared from **1.6a** (18 mg, 0.048 mmol), Cs_2CO_3 (0.15 g, 0.48 mmol) and 1,14-dibromotetradecane (8.6 mg, 0.024 mmol). A pale-yellow oil was obtained (9 mg, 39%). ^{1}H-NMR (500 MHz, $CDCl_3$) δ: 7.32 (s, 2H, 3-H), 6.66 (d, *J* = 1.7 Hz, 2H, 8-H), 6.54 (d, *J* = 1.7 Hz, 2H, 6-H), 4.53 (q, *J* = 7.2 Hz, 4H, NCH_2CH_3), 4.08 (t, *J* = 7.0 Hz, 4H, 1"-H), 1.85 (p, *J* = 7.0 Hz, 4H, 2"-H), 1.59–1.53 (m, 22H, $OC(CH_3)_2$, *alkyl chain*), 1.48–1.42 (m, 4H, 2'-H), 1.37 (t, *J* = 7.2 Hz, 6H, NCH_2CH_3), 1.27 (s, 24H, $C(CH_3)_2$, *alkyl chain*), 1.22–1.17 (m, 10H, *alkyl chain*), 1.12–1.06 (m, 4H, 3'-H), 0.83 ppm (t, *J* = 6.9 Hz, 6H, 7'-H); ^{13}C-NMR (126 MHz, $CDCl_3$) δ: 153.9 (9-C), 153.4 (7-C), 152.1 (5a-C), 132.2 (9b-C), 132.0 (3-C), 123.3 (3a-C), 109.5 (6-C), 104.6 (8-C), 103.7 (9a-C), 76.4 ($OC(CH_3)_2$), 69.0 (1"-C), 47.9 (NCH_2CH_3), 44.4 (2'-C), 38.0 ($C(CH_3)_2$), 31.7, 29.9, 29.7, 29.6, 29.57, 29.50, 29.2, 26.1 and 22.6 (*alkyl chain*), 28.8 ($C(CH_3)_2$), 27.2 ($OC(CH_3)_2$), 24.6 (3'-C), 15.5 (NCH_2CH_3), 14.1 ppm (7'-C); HRMS calcd for $C_{60}H_{95}N_4O_4$ $[M+H]^+$: 935.7347, found: 935.7360.

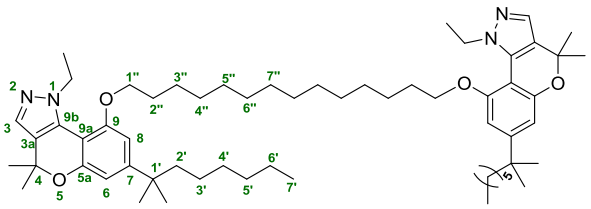

1,14-Bis[(7-(1,1-dimethylheptyl)-2-ethyl-2,4-dihydro-4,4-dimethylchromeno[4,3-*c*]pyrazol-9-yl)oxy]tetradecane (1.64).

Compound **1.64** was prepared from **1.6b** (20 mg, 0.054 mmol), Cs_2CO_3 (0.17 g, 0.54 mmol) and 1,14-dibromotetradecane (9.6 mg, 0.027 mmol). A yellow oil was obtained (15 mg, 59%). ^{1}H-NMR (500 MHz, $CDCl_3$) δ: 7.10 (s, 2H, 3-H), 6.56 (d, *J* = 1.6 Hz, 2H, 8-H), 6.51 (d, *J* = 1.6 Hz, 2H, 6-H), 4.18 (q, *J* = 7.3 Hz, 4H, NCH_2CH_3), 4.09 (t, *J* = 6.6 Hz, 4H, 1"-H), 1.90 (q, *J* = 7.2, 6.8 Hz, 4H, 2"-H), 1.60–1.55 (m, 26H, $OC(CH_3)_2$, *alkyl chain*), 1.52 (t, *J* = 7.3 Hz, 6H, NCH_2CH_3), 1.33–1.22 (br s, 12H, $C(CH_3)_2$), 1.22–1.11 (m, 22H, *alkyl chain*), 1.06–1.00 (m, 4H, 3'-H), 0.83 ppm (t, *J* = 6.7 Hz, 6H, 7'-H); ^{13}C-NMR (126 MHz, $CDCl_3$) δ: 155.1 (9-C), 153.8 (7-C), 151.0 (5a-C), 140.9 (9b-C), 121.8 (3-C), 121.4 (3a-C), 108.5 (6-C), 105.6 (8-C), 104.0 (9a-C), 75.5 ($OC(CH_3)_2$), 69.0 (1"-C), 47.0 (NCH_2CH_3), 44.6 (2'-C), 38.0 ($C(CH_3)_2$), 31.8, 30.0, 29.74, 29.72, 29.69, 29.5, 26.1 and 22.6 (*alkyl*

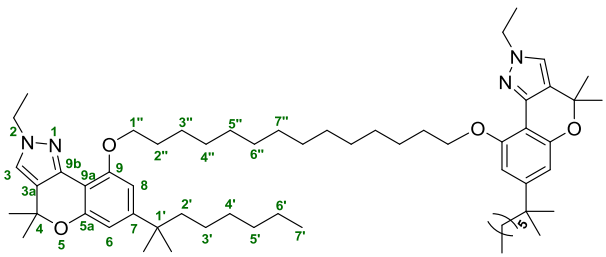

chain), 29.0 (OC(*C*H$_3$)$_2$), 28.9 (C(*C*H$_3$)$_2$), 24.6 (3'-C), 15.4 (NCH$_2$*C*H$_3$), 14.1 ppm (7'-C); HRMS calcd for $C_{60}H_{95}N_4O_4$ $[M+H]^+$: 935.7347, found: 935.7359.

1,16-Bis[(7-(1,1-dimethylheptyl)-2,4-dihydro-2,4,4-trimethylchromeno[4,3-*c*]pyrazol-9-yl)oxy]hexadecane (1.65).

Compound **1.65** was prepared from **1.5b** (35 mg, 0.098 mmol), Cs_2CO_3 (0.32 g, 0.98 mmol) and 1,16-dibromohexadecane (18 mg, 0.049 mmol). A yellow oil was isolated (20 mg, 44%). ^{1}H-NMR

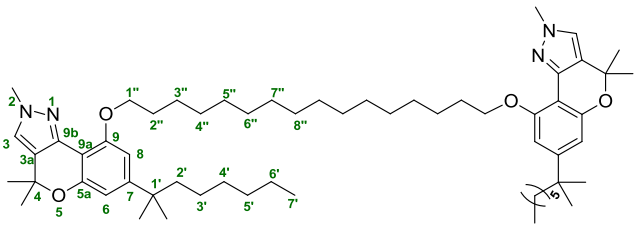

(500 MHz, $CDCl_3$) δ: 7.07 (s, 2H, 3-H), 6.56 (d, *J* = 1.7 Hz, 2H, 8-H), 6.53 (d, *J* = 1.7 Hz, 2H, 6-H), 4.10 (t, *J* = 6.8 Hz, 4H, 1"-H), 3.91 (s, 6H, NCH_3), 1.92 (p, *J* = 7.9 Hz, 4H, 2"-H), 1.61–1.50 (m, 24H, OC(CH$_3$)$_2$, *alkyl chain*), 1.41–1.36 (m, 4H, 2'-H), 1.28–1.24 (br s, 24H, C(CH$_3$)$_2$, *alkyl chain*), 1.21–1.14 (m, 12H, *alkyl chain*), 1.09–0.99 (m, 4H, 3'-H), 0.83 ppm (t, *J* = 6.9 Hz, 6H, 7'-H); ^{13}C-NMR (126 MHz, $CDCl_3$) δ: 155.1 (9-C), 153.8 (7-C), 151.1 (5a-C), 141.3 (9b-C), 123.1 (3-C), 122.1 (3a-C), 108.4 (8-C), 105.5 (6-C), 103.9 (9a-C), 75.4 (O*C*(CH$_3$)$_2$), 69.0 (1"-C), 44.6 (NCH_3), 39.0 (2'-C), 38.0 (*C*(CH$_3$)$_2$), 31.7, 30.0, 29.75, 29.73, 29.70, 29.66, 29.60, 29.4, 26.0 and 22.6 (*alkyl chain*), 28.9 (OC(*C*H$_3$)$_2$), 28.8 (C(*C*H$_3$)$_2$), 24.6 (3'-C), 14.1 ppm (7'-C); HRMS calcd for $C_{60}H_{95}N_4O_4$ $[M+H]^+$: 935.7348, found: 935.7336.

1,16-Bis[(7-(1,1-dimethylheptyl)-1-ethyl-1,4-dihydro-4,4-dimethylchromeno[4,3-*c*]pyrazol-9-yl)oxy]hexadecane (1.66).

Compound **1.66** was prepared from **1.6a** (35 mg, 0.095 mmol), Cs_2CO_3 (0.31 g, 0.95 mmol) and 1,16-dibromohexadecane (17.5 mg, 0.048 mmol). A orange oil was isolated (8 mg, 17%). ^{1}H-NMR

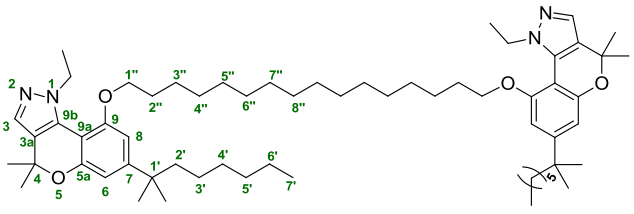

(500 MHz, $CDCl_3$) δ: 7.33 (s, 2H, 3-H), 6.66 (d, *J* = 1.8 Hz, 2H, 8-H), 6.54 (d, *J* = 1.8 Hz, 2H, 6-H), 4.54 (q, *J* = 7.2 Hz, 4H, NC*H*$_2$CH$_3$), 4.08 (t, *J* = 7.0 Hz, 4H, 1"-H), 1.85 (p, *J* = 7.2 Hz, 4H, 2"-H), 1.53–1.58 (br s, 20H, OC(CH$_3$)$_2$, *alkyl chain*), 1.46–1.42 (m, 4H, 2'-H), 1.38 (t, *J* = 7.2

Hz, 6H, NCH_2CH_3), 1.30–1.23 (m, 28H, $C(CH_3)_2$, *alkyl chain*), 1.22–1.17 (m, 12H, *alkyl chain*), 1.11–1.03 (m, 4H, 3'-H), 0.84 ppm (t, *J* = 6.8 Hz, 6H, 7'-H); ^{13}C-NMR (126 MHz, $CDCl_3$) δ: 153.9 (9-C), 153.4 (7-C), 152.2 (5a-C), 132.1 (9b-C), 132.1 (3-C), 123.3 (3a-C), 109.5 (6-C), 104.6 (8-C), 103.7 (9a-C), 76.3 ($OC(CH_3)_2$), 69.0 (1"-C), 47.9 (NCH_2CH_3), 44.4 (2'-C), 38.1 ($C(CH_3)_2$), 31.7, 29.9, 29.70, 29.67, 29.62, 29.58, 29.49, 29.2, 26.1 and 22.6 (*alkyl chain*), 28.8 ($C(CH_3)_2$), 27.2 ($OC(CH_3)_2$), 24.6 (3'-C), 15.5 (NCH_2CH_3), 14.1 ppm (7'-C); HRMS calcd for $C_{62}H_{99}N_4O_4$ $[M+H]^+$: 963.7661, found: 963.7635.

1,16-Bis[(7-(1,1-dimethylheptyl)-2-ethyl-2,4-dihydro-4,4-dimethylchromeno[4,3-*c*]pyrazol-9-yl)oxy]hexadecane (1.67).

Compound **1.67** was prepared from **1.6b** (19 mg, 0.051 mmol), Cs_2CO_3 (0.17 g, 0.51 mmol) and 1,16-dibromohexadecane (9.4 mg, 0.025 mmol). A yellow oil was isolated (7 mg, 29%). ^{1}H-NMR (500 MHz, $CDCl_3$) δ: 7.11 (s, 2H, 3-H), 6.56 (d, *J* = 1.6 Hz, 2H, 8-H), 6.52 (d, *J* = 1.6 Hz, 2H, 6-H),

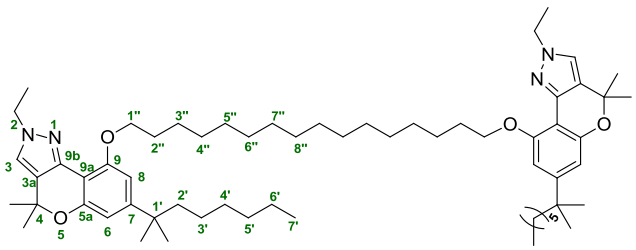

4.19 (q, *J* = 7.3 Hz, 4H, NCH_2CH_3), 4.09 (t, *J* = 6.6 Hz, 4H, 1"-H), 1.91 (p, *J* = 7.3 Hz, 4H, 2"-H), 1.64–1.59 (m, 8H, *alkyl chain*), 1.57 (s, 12H, $OC(CH_3)_2$), 1.52 (t, *J* = 7.3 Hz, 6H, NCH_2CH_3), 1.42–1.34 (m, 4H, 2"-H), 1.28–1.25 (br s, 28H, $C(CH_3)_2$, *alkyl chain*), 1.23–1.13 (m, 12H, *alkyl chain*), 1.08–1.00 (m, 4H, 3"-H), 0.83 ppm (t, *J* = 7.0 Hz, 6H, 7'-H); ^{13}C-NMR (126 MHz, $CDCl_3$) δ: 155.1 (9-C), 153.8 (7-C), 151.0 (5aC), 140.9 (9b-C), 121.7 (3-C), 121.4 (3a-C), 108.4 (6-C), 105.5 (8-C), 104.0 (9a-C), 75.5 ($OC(CH_3)_2$), 69.0 (1"-C), 47.0 (NCH_2CH_3), 44.6 (2'-C), 38.0 ($C(CH_3)_2$), 31.8, 30.0, 29.8, 29.74, 29.71, 29.66, 29.5, 26.1 and 22.6 (*alkyl chain*), 28.9 ($OC(CH_3)_2$), 28.8 ($C(CH_3)_2$), 24.6 (3'-C), 15.5 (NCH_2CH_3), 14.1 ppm (7'-C); HRMS calcd for $C_{62}H_{99}N_4O_4$ $[M+H]^+$: 963.7661, found: 963.7691.

Pharmacological assays

Cannabinoid binding experiments. Membranes from transfected cells with human CB_1 or CB_2 expressed cannabinoid receptors (RBHCB1M400UA and RBXCB2M400UA) were supplied by Perkin-Elmer Life and Analytical Sciences (Boston, MA). The protein concentration for the CB_1 receptor membranes was 8.0 mg/mL, whereas for the CB_2 receptor membranes was 4.0 mg/mL or 3.6 mg/mL depending on the batch. The commercial membranes were diluted (approximatively 1:20) with the binding buffer (50 mM TrisCl, 5 mM $MgCl_2.H_2O$, 2.5 mM EDTA, 0.5 mg/mL BSA and pH = 7.4 for CB_1 binding; 50 mM TrisCl, 5 mM $MgCl_2.H_2O$, 2.5 mM EGTA, 1 mg/mL BSA and pH = 7.5 for CB_2 binding). The final membrane protein concentration was 0.4 mg/mL of incubation volume and 0.2 mg/mL of incubation volume for the CB_1 and the CB_2 receptor assays, respectively. The radioligand used was [^{3}H]-CP55940 (PerkinElmer) at a concentration of membrane K_D x 0.8 nm, and the final volume was 200 μL for CB_1 binding and was 600 μL for CB_2 binding. 96-Well plates and the tubes necessary for the experiment were previously siliconized with Sigmacote (Sigma).

Membranes were resuspended in the corresponding buffer and were incubated with the radioligand and each compound (10^{-4}-10^{-11} M) for 90 min at 30 ºC. Non-specific binding was determined with 10 μM WIN55212-2 and 100 % binding of the radioligand to the membrane was determined by its incubation with membrane without any compound. Filtration was performed by a Harvester® filtermate (Perkin-Elmer) with Filtermat A GF/C filters pretreated with polyethylenimine 0.05%. After filtering, the filter was washed nine times with binding buffer, dried and a melt-on scintillation sheet (Meltilex™ A, Perkin Elmer) was melted onto it. Then, radioactivity was quantified by a liquid scintillation spectrophotometer (Wallac MicroBeta Trilux, Perkin-Elmer). Competition binding data were analyzed by using GraphPad Prism program and K_i values are expressed as mean ± SEM of at least three experiments performed in triplicate for each point.

cAMP accumulation assay. cAMP accumulation in HEK293 cells stably expressing CB_2 receptor was performed using the HTRF-cAMP dynamic kit (CisBio, France) according to manufacturer's

instructions. Briefly, cells were treated with the indicated ligands for 10 min, incubated in lysis buffer (20 mM Tris, 1% Triton X-100, pH 7.5) for 30 min and dispensed in white 384-well microplates at a density of 30,000 cells per well. The cellular lysates were incubated for 60 min at room temperature containing HTRF assay reagents, and time-resolved Förster´s resonance energy transfer (FRET) signals were measured after excitation at 320 nm using the Envision 2104 Multilabel Reader (PerkinElmer). Data analysis was made based on the fluorescence ratio emitted by the labelled cAMP probe (665 nm) over the light emitted by the europium cryptate-labelled anti-cAMP antibody (620 nm). A standard curve was used to calculate cAMP concentration. Forskolin stimulated cAMP levels were normalized to 100%. Data was analyzed by using GraphPad Prism program using nonlinear regression analysis. EC_{50} and E_{max} values are expressed as mean ± SEM of at least three experiments performed in triplicates and were calculated.

[^{35}S]-GTPγS binding assays.

Protocol for CB_1 receptors:

Cell culture: HEK293-CB_1 cells were grown to confluence under 5% CO_2 in Dulbecco's Modified Eagle's Medium (Lonza) containing 10% fetal bovine serum (Sigma), 1X Penicillin-Streptomycin-Amphotericin B antibiotics (Lonza), and ultraglutamine 2 mM (Lonza).

Membrane preparation: Cells were washed twice with ice-cold phosphate-buffer saline, detached from flasks by incubation with lifting buffer (glucose 5.6 mM, KCl 5 mM, HEPES 5 mM, NaCl 137 mM and EGTA 1 mM, pH 7.4) and collected by centrifugation (500xg). The cells were resuspended in ice-cold lysis buffer ($MgSO_4$ 0.2 mM, KH_2PO_4 0.38 mM , Na_2HPO_4 0.61 mM , pH 7.4) and homogenized using a glass-PTFE homogenizer. Crude membranes were isolated by centrifugation for 20 min at 20,000xg. The resulting membrane pellets were resuspended in 50 mM Tris-HCl buffer (pH 7.4) and stored at -80 ºC in aliquots of 0.8 mg/ml protein determined for Bio-Rad DC™ Protein Assay. All procedures were performed at 4°C.

Agonist-Stimulated [^{35}S]GTPγS Binding: Cannabinoid agonist stimulation of [^{35}S]GTPγS binding was determined using several concentrations of compounds from 10^{-4} to 10^{-11} M, incubated with

HEK293-CB_1 membranes (20 μg/well) for 60 min at 30°C in assay buffer (100 mM NaCl, 50 mM Tris-HCl, 5 mM $MgCl_2$, 1 mM EGTA, 1 mM DTT, 50 μM GDP, 10 mU/ml adenosine deaminase and 1 mg/ml BSA, pH 7.4) containing 0.1 nM [^{35}S]GTPγS (Perkinelmer). Nonspecific binding was determined in the presence of 10 μM GTPγS. 96-Well plates and the tubes necessary for the experiment were previously siliconized with Sigmacote (Sigma).

Experiments were terminated by rapid filtration performed by a Harvester filtermate (PerkineElmer) with Filtermat A GF/C filters. After filtering, the filter was washed nine times with filtration buffer (50mMTris-HCl and 1 mg/ml BSA, pH 7.4), dried and a melt-on scintillation sheet (Meltilex™ A, Perkin Elmer) was melted onto it. Then, radioactivity was quantified by a liquid scintillation spectrophotometer (Wallac MicroBeta Trilux, PerkineElmer). Data were analyzed by nonlinear regression analysis of sigmoidal dose-response curves using GraphPad Prism 5.01 (GraphPad, San Diego, CA). EC_{50} values are expressed as mean SEM of at least three experiments performed in triplicate for each point.

Protocol for CB_2 receptors:

[^{35}S]-GTPγS binding analyses were carried out for compounds **1.33** and **1.41−1.43** using CB_2R-containing membranes (HTS020M2, Eurofins Discovery Services). To this end, membranes (5 μg/well) were permeabilized by addition of saponin (Sigma-Aldrich), then mixed with 0.3 nM [^{35}S]-GTPγS (Perkin-Elmer) and 10 μM GDP (Sigma-Aldrich) in 20 mM HEPES (Sigma-Aldrich) buffer containing 100 mM NaCl (Merck) and 10 mM $MgCl_2$ (Merck), at pH 7.4. 30 nM CP55,940 (Sigma-Aldrich) and increasing concentrations of compound **1.33** and **1.41−1.43** (from 10^{-11} to 10^{-5} M) were added in a final volume of 100 μl and incubated for 30 min at 30 °C. The non-specific signal was measured with 10 μM GTPγS (Sigma-Aldrich). All 96-well plates and the tubes necessary for the experiment were previously silanized with Sigmacote (Sigma-Aldrich). The reaction was terminated by rapid vacuum filtration with a filter mate Harvester apparatus (Perkin-Elmer) through Filtermat A GF/C filters. The filters were washed nine times with ice-cold filtration buffer (10 mM sodium phosphate, pH 7.4), and bound radioactivity was measured with a 1450 LSC & Luminiscence

counter Wallac MicroBeta TriLux (Perkin-Elmer). [^{35}S]-GTPγS binding data were analyzed to determine the EC_{50} and E_{max} values by using an iterative curve-fitting procedure with the GraphPad Prism version 5.02 (GraphPad Software Inc.). EC_{50} and E_{max} values are expressed as mean ± SEM of at least three experiments performed in triplicate for each point.

Functional activity for CB_2 receptors on cultured cells. The functional activity of the new compounds for CB_2R was evaluated in cultured BV-2 cells, a mouse microglial cell line. Cells were plated at a density of $5x10^5$ cells per well in 12-well culture plates previously coated with 15 μg/ml Poly-L-ornithine (Sigma), and incubated overnight in Dulbecco's Modified Eagle's Medium (DMEM, Lonza) supplemented with 10% fetal bovine serum (FBS, Lonza), 2 mM Ultraglutamine and antibiotics (Lonza) in a humidified atmosphere of 5% CO_2 at 37 ºC. One hour before treatment, medium was replaced with DMEM supplemented with 1 % FBS, 2 mM Ultraglutamine and antibiotics. Cells were treated for 16 hours with 1 μg/ml Lipopolysaccharides (LPS from Escherichia coli 055:B5, Sigma), alone or in combination with the investigated compound, used at a concentration 10-fold the K_i obtained in binding studies. 10 μM WIN55,212-2 (Sigma) and 10 μM SR144528 (Santa Cruz Biotechnology) were used as reference compounds because of their capabitilily to either activate or block the CB_2R, respectively. Media were then removed and used for the determination of PGE2 release using the ELISA kit DetectX® Prostaglandin E2 (Arbor Assays).

SPR–biosensor measurements of plasma proteins binding.

Surface plasmon resonance (SPR) experiments were performed at 25 ºC with a Biacore X–100 apparatus (GE Healthcare, Biacore AB, Uppsala, Sweden).

Immobilization of human serum albumin (HSA). Essentially fatty acid and globulin free HSA (Sigma-Aldrich) was used without further purification. A stock solution was prepared in phosphate buffered saline (PBS, pH 7.4) and stored at -20 ºC. Immediately prior to use, this solution was diluted to a concentration of 100 μg/mL in 10 mM sodium acetate, pH 5.0. HSA was immobilized

on CM5 sensor chips (Biacore) by the use of amine-coupling chemistry. The surface was blocked by 7-min injection with 1 M ethanolamine, pH 8.0. The immobilization level ranged between 9000 and 10000 RU.

Immobilization of α_1-acid glycoprotein (AGP). AGP (99% purity) was from Sigma-Aldrich Sweden AB, Stockholm, Sweden. The protein was modified before immobilization in order to allow coupling via thiol groups. PDEA-AGP was synthesized by dissolving 1 mg of AGP and 3 mg of 2-(2-pyridinyldithio)ethanolamine hydrochloride (PDEA) in 1.0 mL of 0.1 M 2-(4-morpholino)-ethanesulfonic buffer (MES), pH 5.0. The solution was incubated for 10 min at room temperature after addition of 50 μL of 1-ethyl-3-(3-dimethylaminopropyl)carbodiimide hydrochloride (EDC). The modified protein was separated from PDEA by applying it to a NAP 10 column (Amersham Biosciences, Uppsala, Sweden) and eluting with 1.25 mL of protein with 0.01 M citrate buffer, pH 3.6, resulting also in an appropriate buffer exchange. The modification reaction was believed to be quantitative, resulting in approximately 800 μg/mL final concentration of the modified protein. Aliquots of PDEA-AGP were stored at -20 °C and diluted to 270 μg/mL in 0.01 M citrate buffer, pH 3.6, immediately before immobilization. Immobilization of the PDEA-modified AGP was performed at 25 °C. The carboxymethyl-modified dextrane polymer of the CM5 sensor chip was activated with a 2-min injection of a 1:1 mixture of 0.2 M 1-ethyl-3-(3-dimethylaminopropyl)carbodiimide hydrochloride (EDC) and 0.05 M *N*-hydroxysuccinimide (NHS). Disulfide bridges were introduced on the sensor surface by injection of 40 mM cystamine dihydrochloride in 0.1 M sodium borate, pH 8.5, for 3 min. Disulfides were reduced to free thiol groups by injection of 0.1 M dithioerythrithol (DTE) in 0.1 M sodium borate, pH 8.5, for 3 min. PDEA-modified AGP was then injected for 26 min. Excess reactive groups were deactivated by a 4 min injection of 20 mM 2-(2-pyridinyldithio)ethanolamine and 1 M NaCl in 0.1 sodium acetate, pH 4.3 (PDEA-NaCl). The immobilization level achieved varied from 6000-7000 RU.

Ranking experiments. Control drugs (warfarin, dipiramidol, prednisone, phenytoin, and sulfanilamide), the well-known cannabinoids SR141617, SR144528, CP55940, HU308, CBD, 2-AG

and AEA, and chromenopyrazoles were prepared as 10 mM stock solutions in 100% dimethyl sulfoxide (DMSO). The stock solutions were diluted in PBS containing DMSO to reach a final concentration of 40 μM in PBS containing 3% DMSO. Binding studies were perfomed at a flow rate of 90 μL/min and 40 s association and 60 s dissociation times. Regeneration was not required between injections cycles. To clean the flow system, an extra wash with 50% DMSO was performed between each injection. Binding responses were corrected for solvent (DMSO bulk differences) by using the software available on the Biacore X-100. Several measurements of warfarin binding to HSA were carried out over the course of the experiment as a mean of control of the HSA binding efficiency throughout the assay. The dose-response curves were obtained by plotting the RU/Da*100 against the drug concentrations. At working concentration (40 μM), all of the compounds gave measurable responses. For HSA positive controls were used ranking from warfarin to prednisone and AGP controls were used ranking from warfarin to dipiramidol. Sulfanilamide was used as a negative control for both proteins.

***In silico* ADME calculations.**

A set of 34 physico-chemical descriptors was computed using QikProp version 3.5 integrated in Maestro (Schrödinger, LLC, New York, USA). The QikProp descriptors are shown in table 5. The 3D conformations used in the calculation of QikProp descriptors were generated using the program Spartan ´08 (Wave function, Inc., Irvine CA) as follows: the structure of each molecule was built from the fragment library available in the program. Then, *ab initio* energy minimizations of each structure at the Hartree-Fock 6-31G* level were performed. A conformational search was next implemented using Molecular Mechanics (Monte Carlo method) followed by a minimization of the energy of each conformer calculated at the Hartree-Fock 6-31G* level. The global minimum energy conformer of each compound was used as input for ADME studies with QikProp.

Molecular modeling

Amino acid numbering. The numbering scheme for Class A GPCRs suggested by Ballesteros and Weinstein[200] was employed here. In this numbering system, the label 0.50 is assigned to the most highly conserved Class A residue in each transmembrane helix (TMH). This number is preceded by the TMH number and followed in parenthesis by the sequence number. All other residues in a TMH are numbered relative to this residue.

Conformational analysis of the compounds. Global minimum energy conformations of **1.4**, **1.6b**, **1.17** and **1.41** were determined with Spartan ´08 (Wave function, Inc., Irvine CA) as follows: the structure of each molecule was built from the fragment library available in the program. Then, *ab initio* energy minimizations of each structure at the Hartree-Fock 6-31G* level were performed. A conformational search was next implemented using Molecular Mechanics (Monte Carlo method) followed by a minimization of the energy of each conformer calculated at the Hartree-Fock 6-31G* level. For this search, selected bonds were allowed to rotate: C-O bond in the phenolic ring, the first two C-C bonds of the dimethylheptyl chain, and the N-C bond in the ethyl substituent of the pyrazole. Representative conformers according to their geometry were selected for *ab initio* energy minimization (HF 6-31G*). The global minimum energy conformer of each compound was used as input for receptor docking studies.

Electrostatic Potential Map Calculation. The electrostatic potential density surface was calculated using Spartan ´08 (Wave function, Inc., Irvine CA). The electrostatic potential energy was calculated using the Hartree-Fock method at the 6-31G* level of theory and was mapped on the 0.002 isodensity surface of each molecule. The surface was color-coded according to the potential, with electron rich regions colored red and electron poor regions colored blue.

CB_1^* and CB_2R^* models. The models used for these docking studies were developed by Patricia Reggio and coworkers.[153] These models are based on the crystal structure of the class A GPCR, rhodopsin.[201] Complete details on the generation of the activated state models were published and properly described by them in the literature.[153,154,202,203]

Docking studies. Minimum energy conformers of each ligand were selected for the initial docking. Binding site anchoring interactions within the receptor for each ligand were based on earlier published docking studies for HU210[154] and for AM-841.[155,156] Initial steric clashes were removed manually with interactive graphics. The energy of the ligand-CBR* TMH bundle complex was minimized using the OPLS2005 force field in Macromodel (version 9.1, Schrödinger, LLC, New York, NY). An 8.0-Å extended nonbonded cutoff (updated every 10 steps), a 20.0- Å electrostatic cutoff, and a 4.0-Å hydrogen bond cutoff were used in each stage of the calculation. All residues except D2.50(163), K3.28(192) and D6.58(366) (CB_1 model), and D2.50(79), K3.28 (109) and D275 (CB_2 model), were neutralized during the minimization. C alpha atom restraints (100 kcal/mol) for all C alpha atoms were applied, and the full bundle was energy minimized until an energy gradient of 0.1 kcal/mol was reached. The C alpha atom restraints were then reduced in steps to 50 kcal/mol, and 0 kcal/mol (no restraints) until an energy gradient of 0.1 kcal/mol was achieved at each step. To allow the loops to adjust in their proper environment, atoms of the TMH regions were frozen, and the bundle was re-minimized in water solvent to 0.1 kcal/mol gradient with loop residues fully charged.

Energy expense assessments for docked ligands. To calculate the energy difference between the global minimum energy conformer of each compound and its final conformation after energy minimization of the ligand-receptor complex, rotatable bonds in the global minimum energy conformation were driven to their corresponding value in the final docked conformation and the single point energy of the resultant structure was calculated at the HF 6-31G* level using Jaguar (version 9.1, Schrodinger, LLC, New York, NY).

Assessment of Pairwise Interaction Energies. After defining the atoms of each ligand as one group (group 1) and the atoms corresponding to a residue that lines the binding site in the final ligand-CB R* complex as another group (group 2), Macromodel (version 9.1, Schrödinger, LLC, New York, NY) was used to output the pairwise interaction energy (coulombic and Van der Waals) for a given pair of atoms. The pairs corresponding to group 1 (ligand) and group 2 (residue of

interest) were then summed to yield the interaction energy between the ligand and that residue. Total interaction energy for each ligand with the cannabinoid receptor was calculated by summing the pairwise interaction energies for all residues in the binding site of that ligand and adding to this sum, the conformational energy expense for the ligand.

Additional Information:

Pairwise interaction energies for **1.4**, **1.6b** and **1.41** at CB_1R^* model.

Table A. 1.4/CB_1R^* Complex

Residue	VdW (kcal/mol)	Electrostatic (kcal/mol)	Total Energy (kcal/mol)
L2.46	-1.54	-0.02	-1.56
D2.50	-3.04	-2.99	-6.03
G2.53	-0.10	0.01	-0.09
F2.57	-2.44	-0.40	-2.84
F2.64	-0.47	-0.18	-0.65
K3.28	-1.06	-9.96	-11.02
L3.29	-0.86	-0.01	-0.87
G3.31	-0.28	-0.04	-0.32
V3.32	-4.34	-0.06	-4.40
S3.35	-2.87	0.30	-2.57
F3.36	-3.04	0.12	-2.92
A3.38	-0.12	0.04	-0.08
S3.39	-1.06	0.21	-0.85
V3.40	0.00	0.00	0.00
L3.43	-0.08	0.01	-0.07
L6.44	-0.18	0.01	-0.17
C6.47	-0.24	0.04	-0.20
P6.50	-0.39	-0.10	-0.49
L6.51	-2.33	-0.03	-2.36
I6.54	-2.20	0.20	-2.00
M6.55	-0.15	0.04	-0.11
F7.35	0.00	0.00	0.00
C7.38	0.00	0.00	0.00
S7.39	0.87	-11.75	-10.88
M7.40	-0.29	-0.02	-0.31
C7.42	-5.42	-0.80	-6.22
L7.43	-5.32	0.12	-5.20
L7.44	-0.41	-0.06	-0.47
N7.45	-5.01	-0.12	-5.13
S7.46	-1.67	0.32	-1.35
N7.49	-1.44	0.24	-1.20
S7.46	-1.67	0.32	-1.35
N7.49	-1.44	0.24	-1.20
P7.50	-0.07	0.02	-0.05

Conf Expense	6.51
Grand Total	**-63.92**

Table B. 1.41/CB_1R^* Complex

Residue	VdW (kcal/mol)	Electrostatic (kcal/mol)	Total Energy (kcal/mol)
C7.42	-5.55	-1.85	-7.39
K3.28	-1.85	-7.74	-9.59
S7.39	-0.78	-3.58	-4.36
V3.32	-4.20	-0.10	-4.30
S7.46	-1.69	0.24	-1.44
F2.57	-1.91	0.05	-1.86
N7.45	-5.12	-0.08	-5.20
S3.39	-0.92	0.05	-0.87
L7.43	-4.69	-0.43	-5.12
L6.51	-2.35	-0.09	-2.44
I6.54	-2.15	0.35	-1.80
F3.36	-3.37	0.14	-3.23
L2.46	-1.14	0.01	-1.13
S3.35	-2.76	0.12	-2.64
N7.49	-1.06	0.13	-0.93
L3.29	-1.38	0.08	-1.30
F2.64	-0.99	-0.45	-1.44
D2.50	-3.04	-1.81	-4.85
P6.50	-0.49	-0.20	-0.69
C6.47	-0.37	0.00	-0.38
F7.35	-0.38	-0.03	-0.41
S2.60	-0.39	0.08	-0.31
L7.44	-0.44	0.00	-0.44
M6.55	-0.18	0.05	-0.12
L6.44	-0.12	-0.01	-0.13
G3.31	-0.26	-0.04	-0.30
C7.38	-0.29	0.03	-0.26
G2.53	-0.09	0.09	-0.01
Conf Expense			2.07
Grand Total			**-60.87**

Table C. 1.6b/CB_1R^* Complex

Residue	VdW (kcal/mol)	Electrostatic (kcal/mol)	Total Energy (kcal/mol)
S1.39	0.00	0.00	0.00
T1.46	0.00	0.00	0.00
L2.46	-1.23	0.02	-1.21
D2.50	-3.17	-1.53	-4.70
G2.53	-0.11	0.11	0.00
F2.57	-2.24	0.20	-2.04
S2.60	-0.47	-0.06	-0.53
F2.61	0.00	0.00	0.00
F2.64	-1.20	0.11	-1.09

K3.28	-0.80	-13.54	-14.34
L3.29	-1.34	0.14	-1.20
G3.31	-0.23	-0.07	-0.30
V3.32	-4.56	-0.16	-4.72
S3.35	-2.64	0.09	-2.55
F3.36	-3.37	0.12	-3.25
S3.39	-0.94	0.05	-0.89
L3.43	-0.05	0.01	-0.04
L6.44	-0.14	0.00	-0.14
C6.47	-0.30	0.02	-0.28
P6.50	-0.37	-0.19	-0.56
L6.51	-2.72	-0.19	-2.91
I6.54	-2.11	0.23	-1.88
M6.55	-0.32	0.04	-0.28
D6.58	-0.13	-0.04	-0.17
F7.35	-0.17	0.05	-0.12
C7.38	0.00	0.00	0.00
S7.39	-2.40	-1.16	-3.56
M7.40	0.00	0.00	0.00
C7.42	-4.42	-0.34	-4.76
L7.43	-4.55	-0.58	-5.13
L7.44	-0.44	0.00	-0.44
N7.45	-5.01	-0.18	-5.19
S7.46	-1.57	0.16	-1.41
T7.47	-0.08	0.00	-0.08
N7.49	-1.37	0.14	-1.23
P7.50	-0.06	0.01	-0.05
Conf Expense			5.13
Grand Total			**-59.92**

Pairwise interaction energies for **1.41** and **1.17** at CB_2R^* model.

Table D. 1.41/CB_2R^* Complex

Residue	VdW (kcal/mol)	Electrostatic (kcal/mol)	Total Energy (kcal/mol)
S6.58	1.26	-9.10	-7.84
K3.28	-2.31	-8.02	-10.33
V6.51	-2.98	0.08	-2.90
N7.45	-2.29	0.25	-2.04
V3.32	-6.00	-0.26	-6.26
F3.36	-2.53	0.15	-2.38
F7.35	-2.33	-0.29	-2.62
L6.54	-3.08	0.35	-2.74
S7.46	-0.85	0.11	-0.74
L7.43	-3.46	-0.06	-3.52
F2.57	-1.41	0.16	-1.26
S7.39	-4.89	0.10	-4.78
M6.55	-3.24	0.13	-3.11
C7.42	-2.97	-0.16	-3.13
S2.60	-0.91	0.21	-0.70
T3.35	-1.23	0.12	-1.11

M7.40	-2.36	-0.04	-2.40
F3.25	-1.01	0.12	-0.90
I3.29	-1.85	-0.22	-2.07
T3.33	-0.96	-0.11	-1.08
F2.64	-0.41	0.05	-0.36
D275	-0.95	1.51	0.56
W5.43	-0.25	0.04	-0.21
F2.61	-0.19	0.05	-0.15
I7.44	-0.25	0.00	-0.25
P6.50	-0.16	0.01	-0.14
C7.38	-0.28	-0.07	-0.36
Conf Expense			2.56
Grand Total			**-60.25**

Table E. 1.17/CB_2R^* Complex

Residue	VdW (kcal/mol)	Electrostatic (kcal/mol)	Total Energy (kcal/mol)
S6.58	-1.89	-3.66	-5.55
S2.60	-0.95	0.13	-0.82
V6.51	-2.97	0.06	-2.91
V3.32	-4.16	-0.24	-4.41
I3.29	-1.37	0.11	-1.27
L6.54	-2.48	0.16	-2.32
F7.35	-1.36	0.23	-1.14
K3.28	-3.14	3.27	0.13
N7.45	-2.26	0.13	-2.13
F2.57	-2.15	-0.27	-2.43
F3.25	-1.86	0.07	-1.79
M6.55	-3.10	0.04	-3.07
D275	-1.37	-5.42	-6.79
F3.36	-4.84	-0.01	-4.85
C7.42	-3.68	-0.20	-3.88
S7.39	-5.64	-0.53	-6.17
M7.40	-2.40	0.33	-2.08
L7.43	-1.47	-0.16	-1.62
S3.39	-0.80	-0.01	-0.81
T3.35	-0.65	0.00	-0.65
F2.61	-0.20	-0.04	-0.24
V2.56	-0.42	-0.13	-0.55
S7.46	-0.25	0.05	-0.20
N7.49	-0.07	0.06	-0.01
V3.40	-0.13	0.01	-0.11
A7.36	-0.35	0.13	-0.22
L6.44	-0.13	-0.01	-0.14
T3.33	-0.23	-0.04	-0.28
S274	-0.15	-0.06	-0.21
F2.64	-0.12	0.09	-0.02
A2.53	-0.10	0.09	-0.01
T272	-0.11	0.15	0.04
T6.61	-0.06	-0.04	-0.10

Conf Expense	2.79
Grand Total	**-53.82**

6. References

(1) Mechoulam, R.; Hanuš, L. A Historical Overview of Chemical Research on Cannabinoids. *Chem. Phys. Lipids* **2000**, *108*, 1–13.

(2) Gaoni, Y.; Mechoulam, R. Isolation, Structure, and Partial Synthesis of an Active Constituent of Hashish. *J. Am. Chem. Soc.* **1964**, *86*, 1646–1647.

(3) Devane, W. A.; Dysarz, F. A.; Johnson, M. R.; Melvin, L. S.; Howlett, A. C. Determination and Characterization of a Cannabinoid Receptor in Rat Brain. *Mol. Pharmacol.* **1988**, *34*, 605–613.

(4) Matsuda, L. A.; Lolait, S. J.; Brownstein, M. J.; Young, A. C.; Bonner, T. I. Structure of a Cannabinoid Receptor and Functional Expression of the Cloned cDNA. *Nature* **1990**, *346*, 561–564.

(5) Munro, S.; Thomas, K. L.; Abu-Shaar, M. Molecular Characterization of a Peripheral Receptor for Cannabinoids. *Nature* **1993**, *365*, 61–65.

(6) Devane, W.; Hanus, L.; Breuer, A.; Pertwee, R.; Stevenson, L.; Griffin, G.; Gibson, D.; Mandelbaum, A.; Etinger, A.; Mechoulam, R. Isolation and Structure of a Brain Constituent That Binds to the Cannabinoid Receptor. *Science (80-.).* **1992**, *258*, 1946–1949.

(7) Sugiura, T.; Kondo, S.; Sukagawa, A.; Nakane, S.; Shinoda, A.; Itoh, K.; Yamashita, A.; Waku, K. 2-Arachidonoylgylcerol: A Possible Endogenous Cannabinoid Receptor Ligand in Brain. *Biochem. Biophys. Res. Commun.* **1995**, *215*, 89–97.

(8) Mechoulam, R.; Hanuš, L. O.; Pertwee, R.; Howlett, A. C. Early Phytocannabinoid Chemistry to Endocannabinoids and Beyond. *Nat. Rev. Neurosci.* **2014**, *15*, 757–764.

(9) Mechoulam, R.; Ben-Shabat, S.; Hanus, L.; Ligumsky, M.; Kaminski, N. E.; Schatz, a R.; Gopher, a; Almog, S.; Martin, B. R.; Compton, D. R. Identification of an Endogenous 2-Monoglyceride, Present in Canine Gut, That Binds to Cannabinoid Receptors. *Biochem. Pharmacol.* **1995**, *50*, 83–90.

(10) Mechoulam, R.; Ben Shabat, S.; Hanus, L.; Fride, E.; Vogel, Z.; Bayewitch, M.; Sulcova, A. E. Endogenous Cannabinoid Ligands--Chemical and Biological Studies. *J. Lipid Mediat. Cell Signal.* **1996**, *14*, 45–49.

(11) Fu, J.; Bottegoni, G.; Sasso, O.; Bertorelli, R.; Rocchia, W.; Masetti, M.; Guijarro, A.; Lodola, A.; Armirotti, A.; Garau, G.; Bandiera, T.; Reggiani, A.; Mor, M.; Cavalli, A.; Piomelli, D. A Catalytically Silent FAAH-1 Variant Drives Anandamide Transport in Neurons. *Nat. Neurosci.* **2011**, *15*, 64–69.

(12) Marsicano, G.; Chaouloff, F. Moving Bliss: A New Anandamide Transporter. *Nat. Neurosci.* **2011**, *15*, 5–6.

(13) Beltramo, M.; Stella, N.; Calignano, a; Lin, S. Y.; Makriyannis, a; Piomelli, D. Functional Role of High-Affinity Anandamide Transport, as Revealed by Selective Inhibition. *Science* **1997**, *277*, 1094–1097.

(14) Pertwee, R. G. GPR55: A New Member of the Cannabinoid Receptor Clan? *Br. J. Pharmacol.* **2007**, *152*, 984–986.

(15) McHugh, D.; Hu, S. S. J.; Rimmerman, N.; Juknat, A.; Vogel, Z.; Walker, J. M.; Bradshaw, H. B. N-Arachidonoyl Glycine, an Abundant Endogenous Lipid, Potently Drives Directed Cellular Migration through GPR18, the Putative Abnormal Cannabidiol Receptor. *BMC Neurosci.* **2010**, *11*, 44–56.

(16) Brown, A. J. Novel Cannabinoid Receptors. *Br. J. Pharmacol.* **2007**, *152*, 567–575.

(17) Demuth, D. G.; Molleman, A. Cannabinoid Signalling. *Life Sci.* **2006**, *78*, 549–563.

(18) Pertwee, R. G.; Howlett, A. C.; Abood, M. E.; Alexander, S. P. H.; Marzo, V. Di; Elphick, M. R.; Greasley, P. J.; Hansen, H. S.; Kunos, G. International Union of Basic and Clinical Pharmacology . LXXIX . Cannabinoid Receptors and Their Ligands : Beyond CB 1 and CB 2. *Pharmacol Rev* **2010**, *62*, 588–631.

(19) Howlett, a C.; Barth, F.; Bonner, T. I.; Cabral, G.; Casellas, P.; Devane, W. a; Felder, C. C.; Herkenham, M.; Mackie, K.; Martin, B. R.; Mechoulam, R.; Pertwee, R. G. International Union of Pharmacology. XXVII. Classification of Cannabinoid Receptors. *Pharmacol. Rev.* **2002**, *54*, 161–202.

(20) Shoemaker, J. L.; Ruckle, M. B.; Mayeux, P. R.; Prather, P. L. Agonist-Directed Trafficking of Response by Endocannabinoids Acting at CB2 Receptors. *J. Pharmacol. Exp. Ther.* **2005**, *315*, 828–838.

(21) Turu, G.; Hunyady, L. Signal Transduction of the CB1 Cannabinoid Receptor. *J. Mol. Endocrinol.* **2010**, *44*, 75–85.

(22) Di Marzo, V.; Bifulco, M.; De Petrocellis, L. The Endocannabinoid System and Its Therapeutic Exploitation. *Nat. Rev. Drug Discov.* **2004**, *3*, 771–784.

(23) Abood, M. E.; Martin, B. R. Neurobiology of Marijuana Abuse. *Trends Pharmacol. Sci.* **1992**, *13*, 201–206.

(24) Mackie, K.; Lai, Y.; Westenbroek, R.; Mitchell, R. Cannabinoids Activate an Inwardly Rectifying Potassium Conductance and Inhibit Q-Type Calcium Currents in AtT20 Cells Transfected with Rat Brain Cannabinoid Receptor. *J. Neurosci.* **1995**, *15*, 6552–6561.

(25) Basavarajappa, B. S. Neuropharmacology of the Endocannabinoid Signaling System-Molecular Mechanisms, Biological Actions and Synaptic Plasticity. *Curr. Neuropharmacol.* **2007**, *5*, 81–97.

(26) Ashton, J. C.; Friberg, D.; Darlington, C. L.; Smith, P. F. Expression of the Cannabinoid CB2 Receptor in the Rat Cerebellum: An Immunohistochemical Study. *Neurosci. Lett.* **2006**, *396*, 113–116.

(27) Gong, J.-P.; Onaivi, E. S.; Ishiguro, H.; Liu, Q.-R.; Tagliaferro, P. A.; Brusco, A.; Uhl, G. R. Cannabinoid CB2 Receptors: Immunohistochemical Localization in Rat Brain. *Brain Res.* **2006**, *1071*, 10–23.

(28) Van Sickle, M. D.; Duncan, M.; Kingsley, P. J.; Mouihate, A.; Urbani, P.; Mackie, K.; Stella, N.; Makriyannis, A.; Piomelli, D.; Davison, J. S.; Marnett, L. J.; Di Marzo, V.; Pittman, Q. J.; Patel, K. D.; Sharkey, K. A. Identification and Functional Characterization of Brainstem Cannabinoid CB2 Receptors. *Science* **2005**, *310*, 329–332.

(29) Miller, a M.; Stella, N. CB2 Receptor-Mediated Migration of Immune Cells: It Can Go Either Way. *Br. J. Pharmacol.* **2008**, *153*, 299–308.

(30) Buckley, N. E.; McCoy, K. L.; Mezey, É.; Bonner, T.; Zimmer, A.; Felder, C. C.; Glass, M.; Zimmer, A. Immunomodulation by Cannabinoids Is Absent in Mice Deficient for the Cannabinoid CB2 Receptor. *Eur. J. Pharmacol.* **2000**, *396*, 141–149.

(31) Palazuelos, J.; Aguado, T.; Pazos, M. R.; Julien, B.; Carrasco, C.; Resel, E.; Sagredo, O.; Benito, C.; Romero, J.; Azcoitia, I.; Fernández-Ruiz, J.; Guzmán, M.; Galve-Roperh, I. Microglial CB2

Cannabinoid Receptors Are Neuroprotective in Huntington's Disease Excitotoxicity. *Brain* **2009**, *132*, 3152–3164.

(32) The Endocannabinoid System | Fundación CANNA: laboratorio de pruebas de cannabis http://www.fundacion-canna.es/en/endocannabinoid-system (accessed Sep 1, 2015).

(33) Vischer, H. F.; Castro, M.; Pin, J.-P. G Protein-Coupled Receptor Multimers: A Question Still Open Despite the Use of Novel Approaches. *Mol. Pharmacol.* **2015**, *88*, 561–571.

(34) Ferré, S. The GPCR Heterotetramer: Challenging Classical Pharmacology. *Trends Pharmacol. Sci.* **2015**, *36*, 145–152.

(35) Ferré, S.; Casadó, V.; Devi, L. a; Filizola, M.; Jockers, R.; Lohse, M. J.; Milligan, G.; Pin, J.-P.; Guitart, X. G Protein-Coupled Receptor Oligomerization Revisited: Functional and Pharmacological Perspectives. *Pharmacol. Rev.* **2014**, *66*, 413–434.

(36) Viñals, X.; Moreno, E.; Lanfumey, L.; Cordomí, A.; Pastor, A.; de La Torre, R.; Gasperini, P.; Navarro, G.; Howell, L. a.; Pardo, L.; Lluís, C.; Canela, E. I.; McCormick, P. J.; Maldonado, R.; Robledo, P. Cognitive Impairment Induced by Delta9-Tetrahydrocannabinol Occurs through Heteromers between Cannabinoid CB1 and Serotonin 5-HT2A Receptors. *PLOS Biol.* **2015**, *13*, e1002194.

(37) Pazos, M. R.; Mohammed, N.; Lafuente, H.; Santos, M.; Martínez-Pinilla, E.; Moreno, E.; Valdizan, E.; Romero, J.; Pazos, A.; Franco, R.; Hillard, C. J.; Alvarez, F. J.; Martínez-Orgado, J. Mechanisms of Cannabidiol Neuroprotection in Hypoxic-Ischemic Newborn Pigs: Role of 5HT(1A) and CB2 Receptors. *Neuropharmacology* **2013**, *71*, 282–291.

(38) Rozenfeld, R.; Gupta, A.; Gagnidze, K.; Lim, M. P.; Gomes, I.; Lee-Ramos, D.; Nieto, N.; Devi, L. A. AT1R-CB1R Heteromerization Reveals a New Mechanism for the Pathogenic Properties of Angiotensin II. *EMBO J.* **2011**, *30*, 2350–2363.

(39) Hojo, M.; Sudo, Y.; Ando, Y.; Minami, K.; Takada, M.; Matsubara, T.; Kanaide, M.; Taniyama, K.; Sumikawa, K.; Uezono, Y. Mu-Opioid Receptor Forms a Functional Heterodimer with Cannabinoid CB1 Receptor: Electrophysiological and FRET Assay Analysis. *J. Pharmacol. Sci.* **2008**, *108*, 308–319.

(40) Bushlin, I.; Gupta, A.; Stockton, S. D.; Miller, L. K.; Devi, L. a. Dimerization with Cannabinoid Receptors Allosterically Modulates Delta Opioid Receptor Activity during Neuropathic Pain. *PLoS One* **2012**, *7*, e49789.

(41) Kargl, J.; Balenga, N.; Parzmair, G. P.; Brown, A. J.; Heinemann, A.; Waldhoer, M. The Cannabinoid Receptor CB1 Modulates the Signaling Properties of the Lysophosphatidylinositol Receptor GPR55. *J. Biol. Chem.* **2012**, *287*, 44234–44248.

(42) Martínez-Pinilla, E.; Reyes-Resina, I.; Oñatibia-Astibia, a.; Zamarbide, M.; Ricobaraza, a.; Navarro, G.; Moreno, E.; Dopeso-Reyes, I. G.; Sierra, S.; Rico, a. J.; Roda, E.; Lanciego, J. L.; Franco, R. CB1 and GPR55 Receptors Are Co-Expressed and Form Heteromers in Rat and Monkey Striatum. *Exp. Neurol.* **2014**, *261*, 44–52.

(43) Ward, R. J.; Pediani, J. D.; Milligan, G. Heteromultimerization of Cannabinoid CB(1) Receptor and Orexin OX(1) Receptor Generates a Unique Complex in Which Both Protomers Are Regulated by Orexin A. *J. Biol. Chem.* **2011**, *286*, 37414–37428.

(44) Jäntti, M. H.; Mandrika, I.; Kukkonen, J. P. Human Orexin/hypocretin Receptors Form Constitutive Homo- and Heteromeric Complexes with Each Other and with Human CB1 Cannabinoid Receptors. *Biochem. Biophys. Res. Commun.* **2014**, *445*, 486–490.

(45) Akirav, I.; Fattore, L. Cannabinoid CB1 and Dopamine D1 Receptors Partnership in the Modulation of Emotional Neural Processing. *Front. Behav. Neurosci.* **2011**, *5*, 1–2.

(46) Bonaventura, J.; Rico, A. J.; Moreno, E.; Sierra, S.; Sánchez, M.; Luquin, N.; Farré, D.; Müller, C. E.; Martínez-Pinilla, E.; Cortés, A.; Mallol, J.; Armentero, M.-T.; Pinna, A.; Canela, E. I.; Lluís, C.; McCormick, P. J.; Lanciego, J. L.; Casadó, V.; Franco, R. L-DOPA-Treatment in Primates Disrupts the Expression of A2A Adenosine-CB1 Cannabinoid-D2 Dopamine Receptor Heteromers in the Caudate Nucleus. *Neuropharmacology* **2013**, 1–12.

(47) Callén, L.; Moreno, E.; Barroso-Chinea, P.; Moreno-Delgado, D.; Cortés, A.; Mallol, J.; Casadó, V.; Lanciego, J. L.; Franco, R.; Lluis, C.; Canela, E. I.; McCormick, P. J. Cannabinoid Receptors CB1 and CB2 Form Functional Heteromers in Brain. *J. Biol. Chem.* **2012**, *287*, 20851–20865.

(48) Balenga, N. A.; Martínez-Pinilla, E.; Kargl, J.; Schröder, R.; Peinhaupt, M.; Platzer, W.; Bálint, Z.; Zamarbide, M.; Dopeso-Reyes, I.; Ricobaraza, A.; Pérez-Ortiz, J. M.; Kostenis, E.; Waldhoer, M.; Heinemann, A.; Franco, R. Heteromerization of GPR55 and Cannabinoid CB2 Receptors Modulates Signaling. *Br. J. Pharmacol.* **2014**, *171*, 5387–5406.

(49) Moreno, E.; Andradas, C.; Medrano, M.; Caffarel, M. M.; Pérez-Gómez, E.; Blasco-Benito, S.; Gómez-Cañas, M.; Pazos, M. R.; Irving, A. J.; Lluís, C.; Canela, E. I.; Fernández-Ruiz, J.; Guzmán, M.; McCormick, P. J.; Sánchez, C. Targeting CB2-GPR55 Receptor Heteromers Modulates Cancer Cell Signaling. *J. Biol. Chem.* **2014**, *289*, 21960–21972.

(50) Perez-Gomez, E.; Andradas, C.; Blasco-Benito, S.; Caffarel, M. M.; Garcia-Taboada, E.; Villa-Morales, M.; Moreno, E.; Hamann, S.; Martin-Villar, E.; Flores, J. M.; Wenners, A.; Alkatout, I.; Klapper, W.; Rocken, C.; Bronsert, P.; Stickeler, E.; Staebler, A.; Bauer, M.; Arnold, N.; Soriano, J.; Perez-Martinez, M.; Megias, D.; Moreno-Bueno, G.; Ortega-Gutierrez, S.; Artola, M.; Vazquez-Villa, H.; Quintanilla, M.; Fernandez-Piqueras, J.; Canela, E. I.; McCormick, P. J.; Guzman, M.; Sanchez, C. Role of Cannabinoid Receptor CB2 in HER2 Pro-Oncogenic Signaling in Breast Cancer. *JNCI J. Natl. Cancer Inst.* **2015**, *107*, djv077.

(51) Wager-Miller, J.; Westenbroek, R.; Mackie, K. Dimerization of G Protein-Coupled Receptors: CB1 Cannabinoid Receptors as an Example. *Chem. Phys. Lipids* **2002**, *121*, 83–89.

(52) Mackie, K. Cannabinoid Receptor Homo- and Heterodimerization. *Life Sci.* **2005**, *77*, 1667–1673.

(53) Xu, W.; Filppula, S.; Mercier, R.; Yaddanapudi, S.; Pavlopoulos, S.; Cai, J.; Pierce, W. M.; Makriyannis, A. Purification and Mass Spectroscopic Analysis of Human CB1 Cannabinoid Receptor Functionally Expressed Using the Baculovirus System. *J. Pept. Res.* **2005**, *66*, 138–150.

(54) Katona, I.; Rancz, E. a; Acsady, L.; Ledent, C.; Mackie, K.; Hajos, N.; Freund, T. F. Distribution of CB1 Cannabinoid Receptors in the Amygdala and Their Role in the Control of GABAergic Transmission. *J. Neurosci.* **2001**, *21*, 9506–9518.

(55) Hájos, N.; Katona, I.; Naiem, S. S.; Mackie, K.; Ledent, C.; Mody, I.; Freund, T. F. Cannabinoids Inhibit Hippocampal GABAergic Transmission and Network Oscillations. *Eur. J. Neurosci.* **2000**, *12*, 3239–3249.

(56) Zhang, Y.; Gilliam, A.; Maitra, R.; Damaj, M. I.; Tajuba, J. M.; Seltzman, H. H.; Thomas, B. F. Synthesis and Biological Evaluation of Bivalent Ligands for the Cannabinoid 1 Receptor. *J. Med. Chem.* **2010**, *53*, 7048–7060.

(57) Huang, G.; Pemp, D.; Stadtmüller, P.; Nimczick, M.; Heilmann, J.; Decker, M. Design, Synthesis and in Vitro Evaluation of Novel Uni- and Bivalent Ligands for the Cannabinoid Receptor Type 1 with Variation of Spacer Length and Structure. *Bioorg. Med. Chem. Lett.* **2014**, *24*, 4209–4214.

(58) Fernández-Fernández, C.; Decara, J.; Bermúdez-Silva, F. J.; Sánchez, E.; Morales, P.; Gómez-Cañas, M.; Gómez-Ruíz, M.; Callado, L. F.; Goya, P.; Rodríguez de Fonseca, F.; Martín, M. I.; Fernández-Ruíz, J.; Meana, J. J.; Jagerovic, N. Description of a Bivalent Cannabinoid Ligand with Hypophagic Properties. *Arch. Pharm. (Weinheim).* **2013**, *346*, 171–179.

(59) Filppula, S.; Yaddanapudi, S.; Mercier, R.; Xu, W.; Pavlopoulos, S.; Cai, J.; Pierce, W. M.; Makriyannis, A. Purification and Mass Spectroscopic Analysis of Human CB2 Cannabinoid Receptor Functionally Expressed Using the Baculovirus System. *J. Pept. Res.* **2005**, *66*, 138–150.

(60) Zvonok, N.; Yaddanapudi, S.; Williams, J.; Dai, S.; Dong, K.; Rejtar, T.; Karger, B. L.; Makriyannis, A. Comprehensive Proteomic Mass Spectrometric Characterization of Human Cannabinoid CB2 Receptor. *J. Proteome Res.* **2007**, *6*, 2068–2079.

(61) Singh, J.; Song, Z.-H.; Reggio, P. H. Structure of a Cannabinoid Receptor Subtype 2 Homodimer Determined by Cysteine and Homobifunctional Crosslinking Experiments Combined with Computational Studies. *Biophys. J.* **2012**, *102*, 244a.

(62) Wilson, R. I.; Nicoll, R. a. Endogenous Cannabinoids Mediate Retrograde Signalling at Hippocampal Synapses. *Nature* **2001**, *410*, 588–592.

(63) Di Marzo, V.; Fontana, A.; Cadas, H.; Schinelli, S.; Cimino, G.; Schwartz, J. C.; Piomelli, D. Formation and Inactivation of Endogenous Cannabinoid Anandamide in Central Neurons. *Nature* **1994**, *372*, 686–691.

(64) Stella, N.; Schweitzer, P.; Piomelli, D. A Second Endogenous Cannabinoid That Modulates Long-Term Potentiation. *Nature* **1997**, *388*, 773–778.

(65) Cravatt, B. F.; Giang, D. K.; Mayfield, S. P.; Boger, D. L.; Lerner, R. A.; Gilula, N. B. Molecular Characterization of an Enzyme That Degrades Neuromodulatory Fatty-Acid Amides. *Nature* **1996**, *384*, 83–87.

(66) Pertwee, R. G. The Therapeutic Potential of Drugs That Target Cannabinoid Receptors or Modulate the Tissue Levels or Actions of Endocannabinoids. *AAPS J.* **2005**, *7*, E625–E654.

(67) Hillard, C. J.; Manna, S.; Greenberg, M. J.; DiCamelli, R.; Ross, R. a; Stevenson, L. a; Murphy, V.; Pertwee, R. G.; Campbell, W. B. Synthesis and Characterization of Potent and Selective Agonists of the Neuronal Cannabinoid Receptor (CB1). *J. Pharmacol. Exp. Ther.* **1999**, *289*, 1427–1433.

(68) Mechoulam, R.; Peters, M.; Murillo-Rodriguez, E.; Hanus, L. O. Cannabidiol--Recent Advances. *Chem. Biodivers.* **2007**, *4*, 1678–1692.

(69) Huffman, J. W. The Search for Selective Ligands for the CB2 Receptor. *Curr. Pharm. Des.* **2000**, *6*, 1323–1337.

(70) Vemuri, V. K.; Makriyannis, A. Medicinal Chemistry of Cannabinoids. *Clin. Pharmacol. Ther.* **2015**, *97*, 553–558.

(71) Makriyannis, A. 2012 Division of Medicinal Chemistry Award Address. Trekking the Cannabinoid Road: A Personal Perspective. *J. Med. Chem.* **2014**, *57*, 3891–3911.

(72) Picone, R. P.; Kendall, D. Minireview: From the Bench, Toward the Clinic: Therapeutic Opportunities for Cannabinoid Receptor Modulation. *Mol. Endocrinol.* **2015**, *29*, 801–813.

(73) D'Ambra, T. E.; Estep, K. G.; Bell, M. R.; Eissenstat, M. A.; Josef, K. A.; Ward, S. J.; Haycock, D. A.; Baizman, E. R.; Casiano, F. M. Conformationally Restrained Analogs of Pravadoline: Nanomolar Potent, Enantioselective, (aminoalkyl)indole Agonists of the Cannabinoid Receptor. *J. Med. Chem.* **1992**, *35*, 124–135.

(74) Murataeva, N.; Mackie, K.; Straiker, A. The CB2-Preferring Agonist JWH015 Also Potently and Efficaciously Activates CB1 in Autaptic Hippocampal Neurons. *Pharmacol. Res.* **2012**, *66*, 437–442.

(75) Ross, R. A.; Brockie, H. C.; Stevenson, L. A.; Murphy, V. L.; Templeton, F.; Makriyannis, A.; Pertwee, R. G. Agonist-Inverse Agonist Characterization at CB1 and CB2 Cannabinoid Receptors of L759633, L759656, and AM630. *Br. J. Pharmacol.* **1999**, *126*, 665–672.

(76) Rinaldi-Carmona, M.; Barth, F.; Héaulme, M.; Shire, D.; Calandra, B.; Congy, C.; Martinez, S.; Maruani, J.; Néliat, G.; Caput, D. SR141716A, a Potent and Selective Antagonist of the Brain Cannabinoid Receptor. *FEBS Lett.* **1994**, *350*, 240–244.

(77) Lan, R.; Liu, Q.; Fan, P.; Lin, S.; Fernando, S. R.; McCallion, D.; Pertwee, R.; Makriyannis, A. Structure-Activity Relationships of Pyrazole Derivatives as Cannabinoid Receptor Antagonists. *J. Med. Chem.* **1999**, *42*, 769–776.

(78) Lan, R.; Gatley, J.; Lu, Q.; Fan, P.; Fernando, S. R.; Volkow, N. D.; Pertwee, R.; Makriyannis, a. Design and Synthesis of the CB1 Selective Cannabinoid Antagonist AM281: A Potential Human SPECT Ligand. *AAPS PharmSci* **1999**, *1*, E4.

(79) Pavon, F. J.; Bilbao, A.; Hernández-Folgado, L.; Cippitelli, A.; Jagerovic, N.; Abellán, G.; Rodríguez-Franco, M. I.; Serrano, A.; Macias, M.; Gómez, R.; Navarro, M.; Goya, P.; Rodríguez de Fonseca, F. Antiobesity Effects of the Novel in Vivo Neutral Cannabinoid Receptor Antagonist 5-(4-Chlorophenyl)-1-(2,4-Dichlorophenyl)-3-Hexyl-1H-1,2,4-Triazole – LH 21. *Neuropharmacology* **2006**, *51*, 358–366.

(80) Rinaldi-Carmona, M.; Barth, F.; Millan, J.; Derocq, J.-M.; Casellas, P.; Congy, C.; Oustric, D.; Sarran, M.; Bouaboula, M.; Calandra, B.; Portier, M.; Shire, D.; Breliére, J.; Le Fur, G. SR 144528 , the First Potent and Selective Antagonist of the CB2 Cannabinoid Receptor. **1998**, *284*, 644–650.

(81) Wootten, D.; Christopoulos, A.; Sexton, P. M. Emerging Paradigms in GPCR Allostery: Implications for Drug Discovery. *Nat. Rev. Drug Discov.* **2013**, *12*, 630–644.

(82) Price, M. R.; Baillie, G. L.; Thomas, A.; Stevenson, L. a; Easson, M.; Goodwin, R.; Mclean, A.; Mcintosh, L.; Goodwin, G.; Walker, G.; Westwood, P.; Marrs, J.; Thomson, F.; Cowley, P.; Christopoulos, A.; Pertwee, R. G.; Ross, R. A. Allosteric Modulation of the Cannabinoid CB 1 Receptor. *Mol. Pharmacol.* **2005**, *68*, 1484–1495.

(83) Baillie, G. L.; Horswill, J. G.; Anavi-Goffer, S.; Reggio, P. H.; Bolognini, D.; Abood, M. E.; McAllister, S.; Strange, P. G.; Stephens, G. J.; Pertwee, R. G.; Ross, R. a. CB(1) Receptor Allosteric Modulators Display Both Agonist and Signaling Pathway Specificity. *Mol. Pharmacol.* **2013**, *83*, 322–338.

(84) Piscitelli, F.; Ligresti, A.; La Regina, G.; Coluccia, A.; Morera, L.; Allarà, M.; Novellino, E.; Di Marzo, V.; Silvestri, R. Indole-2-Carboxamides as Allosteric Modulators of the Cannabinoid CB(1) Receptor. *J. Med. Chem.* **2012**, *55*, 5627–5631.

(85) Nguyen, T.; German, N.; Decker, A. M.; Li, J.-X.; Wiley, J. L.; Thomas, B. F.; Kenakin, T. P.; Zhang, Y. Structure–activity Relationships of Substituted 1H-Indole-2-Carboxamides as CB1 Receptor Allosteric Modulators. *Bioorg. Med. Chem.* **2015**, *23*, 2195–2203.

(86) Mahmoud, M. M.; Ali, H. I.; Ahn, K. H.; Damaraju, A.; Samala, S.; Pulipati, V. K.; Kolluru, S.; Kendall, D. a; Lu, D. Structure − Activity Relationship Study of Indole-2-Carboxamides Identi Fi Es a Potent Allosteric Modulator for the Cannabinoid Receptor 1 (CB1). *J. Med. Chem.* **2013**, *56*, 7965–7975.

(87) Khurana, L.; Ali, H. I.; Olszewska, T.; Ahn, K. H.; Damaraju, A.; Kendall, D. a.; Lu, D. Optimization of Chemical Functionalities of Indole-2-Carboxamides to Improve Allosteric Parameters for the Cannabinoid Receptor 1 (CB1). *J. Med. Chem.* **2014**, *57*, 3040–3052.

(88) Culliman, G.; Kennan, F.; Koppel, G. Cannabinoid Receptor Antagonists. US5596106A, 1997.

(89) De Vry, J.; Jentzsch, K. R. Discriminative Stimulus Effects of BAY 38-7271, a Novel Cannabinoid Receptor Agonist. *Eur. J. Pharmacol.* **2002**, *457*, 147–152.

(90) De Vry, J.; Denzer, D.; Reissmueller, E.; Eijckenboom, M.; Heil, M.; Meier, H.; Mauler, F. 3-[2-Cyano-3-(trifluoromethyl)phenoxy]phenyl-4,4,4-Trifluoro-1-Butanesulfonate (BAY 59-3074): A Novel Cannabinoid Cb1/Cb2 Receptor Partial Agonist with Antihyperalgesic and Antiallodynic Effects. *J. Pharmacol. Exp. Ther.* **2004**, *310*, 620–632.

(91) Lucchesi, V.; Hurst, D. P.; Shore, D. M.; Bertini, S.; Ehrmann, B. M.; Allarà, M.; Lawrence, L.; Ligresti, A.; Minutolo, F.; Saccomanni, G.; Sharir, H.; Macchia, M.; Di Marzo, V.; Abood, M. E.; Reggio, P. H.; Manera, C. CB2-Selective Cannabinoid Receptor Ligands: Synthesis, Pharmacological Evaluation, and Molecular Modeling Investigation of 1,8-Naphthyridin-2(1H)-One-3-Carboxamides. *J. Med. Chem.* **2014**, *57*, 8777–8791.

(92) Manera, C.; Benetti, V.; Castelli, M. P.; Cavallini, T.; Lazzarotti, S.; Pibiri, F.; Saccomanni, G.; Tuccinardi, T.; Vannacci, A.; Martinelli, A.; Ferrarini, P. L.; Farmaceutiche, S. Design , Synthesis , and Biological Evaluation of New 1 , 8-Naphthyridin-4 (1H) -on-3-Carboxamide and Quinolin-4 (1H) -on-3-Carboxamide Derivatives as CB 2 Selective Agonists. *Society* **2006**, *4*, 5947–5957.

(93) Han, S.; Zhang, F.-F.; Qian, H.-Y.; Chen, L.-L.; Pu, J.-B.; Xie, X.; Chen, J.-Z. Development of Quinoline-2,4(1 H ,3 H)-Diones as Potent and Selective Ligands of the Cannabinoid Type 2 Receptor. *J. Med. Chem.* **2015**, *58*, 5751–5769.

(94) Nettekoven, M.; Adam, J.-M.; Bendels, S.; Bissantz, C.; Fingerle, J.; Grether, U.; Grüner, S.; Guba, W.; Kimbara, A.; Ottaviani, G.; Püllmann, B.; Rogers-Evans, M.; Röver, S.; Rothenhäusler, B.; Schmitt, S.; Schuler, F.; Schulz-Gasch, T.; Ullmer, C. Novel Triazolopyrimidine-Derived Cannabinoid Receptor 2 Agonists As Potential Treatment for Inflammatory Kidney Diseases. *ChemMedChem* **2015**.

(95) Odan, M.; Ishizuka, N.; Hiramatsu, Y.; Inagaki, M.; Hashizume, H.; Fujii, Y.; Mitsumori, S.; Morioka, Y.; Soga, M.; Deguchi, M.; Yasui, K.; Arimura, A. CB 1/2 Dual Agonists with 3-Carbamoyl 2-Pyridone Derivatives as Antipruritics: Reduction of CNS Side Effects by Introducing Polar Functional Groups. *Bioorganic Med. Chem. Lett.* **2012**, *22*, 2894–2897.

(96) Odan, M.; Ishizuka, N.; Hiramatsu, Y.; Inagaki, M.; Hashizume, H.; Fujii, Y.; Mitsumori, S.; Morioka, Y.; Soga, M.; Deguchi, M.; Yasui, K.; Arimura, A. Discovery of S-444823, a Potent CB1/CB2 Dual Agonist as an Antipruritic Agent. *Bioorganic Med. Chem. Lett.* **2012**, *22*, 2898–2901.

(97) Odan, M.; Ishizuka, N.; Hiramatsu, Y.; Inagaki, M.; Hashizume, H.; Fujii, Y.; Mitsumori, S.; Morioka, Y.; Soga, M.; Deguchi, M.; Yasui, K.; Arimura, A. Discovery of S-777469: An Orally Available CB2 Agonist as an Antipruritic Agent. *Bioorganic Med. Chem. Lett.* **2012**, *22*, 2803–2806.

(98) Pertwee, R. G. Emerging Strategies for Exploiting Cannabinoid Receptor Agonists as Medicines. *Br. J. Pharmacol.* **2009**, *156*, 397–411.

(99) Sharkey, K. a; Darmani, N. a; Parker, L. a. Regulation of Nausea and Vomiting by Cannabinoids and the Endocannabinoid System. *Eur. J. Pharmacol.* **2014**, *722*, 134–146.

(100) Abrams, D. I.; Guzman, M. Cannabis in Cancer Care. *Clin. Pharmacol. Ther.* **2015**, *97*, 575–586.

(101) Scherma, M.; Satta, V.; Fratta, W.; Fadda, P. The Endocannabinoid System: Anorexia Nervosa and Binge Eating Disorder. In *Cannabinoids in Neurologic and Mental Disease*; Elsevier, 2015; pp. 389–413.

(102) Després, J.-P.; Lemieux, I.; Alméras, N. Contribution of CB1 Blockade to the Management of High-Risk Abdominal Obesity. *Int. J. Obes. (Lond).* **2006**, *30 Suppl 1*, S44–S52.

(103) Clinical Trials Cannabinoids https://clinicaltrials.gov/ct2/results?term=cannabinoids&pg=1 (accessed Sep 28, 2015).

(104) Dhopeshwarkar, A.; Mackie, K. CB2 Cannabinoid Receptors as a Therapeutic Target - What Does the Future Hold? *Mol. Pharmacol.* **2014**, *86*, 430–437.

(105) Martin, W. J.; Patrick, S. L.; Coffin, P. O.; Tsou, K.; Walker, J. M. An Examination of the Central Sites of Action of Cannabinoid-Induced Antinociception in the Rat. *Life Sci.* **1995**, *56*, 2103–2109.

(106) Guindon, J.; Hohmann, A. G. The Endocannabinoid System and Pain. *CNS Neurol. Disord. Drug Targets* **2009**, *8*, 403–421.

(107) Guindon, J.; Hohmann, A. G. Cannabinoid CB2 Receptors: A Therapeutic Target for the Treatment of Inflammatory and Neuropathic Pain. *Br. J. Pharmacol.* **2008**, *153*, 319–334.

(108) Velasco, G.; Hernández-Tiedra, S.; Dávila, D.; Lorente, M. The Use of Cannabinoids as Anticancer Agents. *Prog. Neuropsychopharmacol. Biol. Psychiatry* **2016**, *64*, 259–266.

(109) Velasco, G.; Sánchez, C.; Guzmán, M. Towards the Use of Cannabinoids as Antitumour Agents. *Nat. Rev. Cancer* **2012**, *12*, 436–444.

(110) Williams, C. M.; Whalley, B. J.; McCabe, C. Cannabinoids and Appetite (dys)regulation. In *Cannabinoids in Neurologic and Mental Disease*; Fattore, L., Ed.; Elsevier, 2015; pp. 315–339.

(111) Scherma, M.; Fattore, L.; Paola Castelli, M.; Fratta, W.; Fadda, P. The Role of the Endocannabinoid System in Eating Disorders: Neurochemical and Behavioural Preclinical Evidence. *Curr. Pharm. Des.* **2014**, *20*, 2089–2099.

(112) Sharma, M. K.; Murumkar, P. R.; Barmade, M. A.; Giridhar, R.; Yadav, M. R. A Comprehensive Patents Review on Cannabinoid 1 Receptor Antagonists as Antiobesity Agents. *Expert Opin. Ther. Pat.* **2015**, 1–24.

(113) Silvestri, C.; Di Marzo, V. Second Generation CB1 Receptor Blockers and Other Inhibitors of Peripheral Endocannabinoid Overactivity and the Rationale of Their Use against Metabolic Disorders. *Expert Opin. Investig. Drugs* **2012**, *21*, 1309–1322.

(114) Lotersztajn, S.; Teixeira-Clerc, F.; Julien, B.; Deveaux, V.; Ichigotani, Y.; Manin, S.; Tran-Van-Nhieu, J.; Karsak, M.; Zimmer, a; Mallat, a. CB2 Receptors as New Therapeutic Targets for Liver Diseases. *Br. J. Pharmacol.* **2008**, *153*, 286–289.

(115) Lotersztajn, S.; Teixeira-Clerc, F.; Mallat, A.; Louvet, A. Selective CB2 Receptor Agonists for Use in the Prevention or Treatment of Alcoholic Liver Disease. WO/2011/009883, January 2011.

(116) Gowran, A.; Noonan, J.; Campbell, V. a. The Multiplicity of Action of Cannabinoids: Implications for Treating Neurodegeneration. *CNS Neurosci. Ther.* **2011**, *17*, 637–644.

(117) Fernández-Ruiz, J. The Endocannabinoid System as a Target for the Treatment of Motor Dysfunction. *Br. J. Pharmacol.* **2009**, *156*, 1029–1040.

(118) Fernández-López, D.; Lizasoain, I.; Moro, M. A.; Martínez-Orgado, J. Cannabinoids: Well-Suited Candidates for the Treatment of Perinatal Brain Injury. *Brain Sci.* **2013**, *3*, 1043–1059.

(119) Fernández-Ruiz, J.; Moro, M. a.; Martínez-Orgado, J. Cannabinoids in Neurodegenerative Disorders and Stroke/Brain Trauma: From Preclinical Models to Clinical Applications. *Neurotherapeutics* **2015**, [Epub ahead of print].

(120) Osuna-Zazuetal, M. A.; Ponce-Gómez, J. A.; Pérez-Neri, I. Neuroprotective Mechanisms of Cannabinoids in Brain Ischemia and Neurodegenerative Disorders. *Invest. Clin.* **2015**, *56*, 188–200.

(121) Devinsky, O.; Cilio, M. R.; Cross, H.; Fernandez-Ruiz, J.; French, J.; Hill, C.; Katz, R.; Di Marzo, V.; Jutras-Aswad, D.; Notcutt, W. G.; Martinez-Orgado, J.; Robson, P. J.; Rohrback, B. G.; Thiele, E.; Whalley, B.; Friedman, D. Cannabidiol: Pharmacology and Potential Therapeutic Role in Epilepsy and Other Neuropsychiatric Disorders. *Epilepsia* **2014**, *55*, 791–802.

(122) Hill, A.; Hill, T.; Whalley, B. The Development of Cannabinoid Based Therapies for Epilepsy. In *Endocannabinoids : Molecular, Pharmacological, Behavioral and Clinical Features.*; Murillo-Rodríguez, E., Ed.; 2013; pp. 164–204.

(123) Rosenberg, E. C.; Tsien, R. W.; Whalley, B. J.; Devinsky, O. Cannabinoids and Epilepsy. *Neurotherapeutics* **2015**, [Epub ahead of print].

(124) Marsicano, G.; Lafenêtre, P. Roles of the Endocannabinoid System in Learning and Memory. *Curr. Top. Behav. Neurosci.* **2009**, *1*, 201–230.

(125) Fernández-Ruiz, J.; Hernández, M.; García-Movellán, Y. Cannabinoids and the Brain: New Hopes for New Therapies. In *Cannabinoids*; Di Marzo, V., Ed.; John Wiley & Sons, Ltd: Chichester, UK, 2014; pp. 175–218.

(126) Fernández-Ruiz, J.; Romero, J.; Ramos, J. A. Endocannabinoids and Neurodegenerative Disorders: Parkinson's Disease, Huntington's Chorea, Alzheimer's Disease, and Others. In *Endocannabinoids*; Pertwee, R. G., Ed.; Handbook of Experimental Pharmacology; Springer International Publishing: Cham, 2015; Vol. 231, pp. 233–259.

(127) Fernández-Ruiz, J.; García, C.; Sagredo, O.; Gómez-Ruiz, M.; de Lago, E. The Endocannabinoid System as a Target for the Treatment of Neuronal Damage. *Expert Opin. Ther. Targets* **2010**, *14*, 387–404.

(128) Gómez-Gálvez, Y.; Palomo-Garo, C.; Fernández-Ruiz, J.; García, C. Potential of the Cannabinoid CB2 Receptor as a Pharmacological Target against Inflammation in Parkinson's Disease. *Prog. Neuro-Psychopharmacology Biol. Psychiatry* **2015**, *64*, 200–208.

(129) Bisogno, T.; Di Marzo, V. The Role of the Endocannabinoid System in Alzheimers Disease: Facts and Hypotheses. *Curr. Pharm. Des.* **2008**, *14*, 2299–2305.

(130) Liu, C. S.; Chau, S. a.; Ruthirakuhan, M.; Lanctôt, K. L.; Herrmann, N. Cannabinoids for the Treatment of Agitation and Aggression in Alzheimer's Disease. *CNS Drugs* **2015**, *8*, 615–623.

(131) De Lago, E.; Moreno-Martet, M.; Espejo-Porras, F.; Fernández-Ruiz, J. Endocannabinoids and Amyotrophic Lateral Sclerosis. In *Cannabinoids in Neurologic and Mental Disease*; Fattore, L., Ed.; Elsevier, 2015; pp. 99–123.

(132) Sagredo, O.; Ruth Pazos, M.; Valdeolivas, S.; Fernandez-Ruiz, J. Cannabinoids: Novel Medicines for the Treatment of Huntingtons Disease. *Recent Pat. CNS Drug Discov.* **2012**, *7*, 41–48.

(133) De Lago, E.; Moreno-Martet, M.; Cabranes, A.; Ramos, J. a.; Fernández-Ruiz, J. Cannabinoids Ameliorate Disease Progression in a Model of Multiple Sclerosis in Mice, Acting Preferentially through CB 1 Receptor-Mediated Anti-Inflammatory Effects. *Neuropharmacology* **2012**, *62*, 2298–2307.

(134) Pertwee, R. G. Cannabinoids and Multiple Sclerosis. *Mol. Neurobiol.* **2007**, *36*, 45–59.

(135) Onaivi, E. S.; Ishiguro, H.; Liu, Q.-R. Future Perspectives: Cannabinoid CB2 Receptor Ligands and Their Therapeutic Potential in Mental Diseases. In *Cannabinoids in Neurologic and Mental Disease*; Elsevier, 2015; pp. 425–444.

(136) Chung, E. S.; Bok, E.; Chung, Y. C.; Baik, H. H.; Jin, B. K. Cannabinoids Prevent Lipopolysaccharide-Induced Neurodegeneration in the Rat Substantia Nigra in Vivo through Inhibition of Microglial Activation and NADPH Oxidase. *Brain Res.* **2012**, *1451*, 110–116.

(137) Hwang, J.; Adamson, C.; Butler, D.; Janero, D. R.; Makriyannis, A.; Bahr, B. a. Enhancement of Endocannabinoid Signaling by Fatty Acid Amide Hydrolase Inhibition: A Neuroprotective Therapeutic Modality. *Life Sci.* **2010**, *86*, 615–623.

(138) Izzo, A. a.; Sharkey, K. a. Cannabinoids and the Gut: New Developments and Emerging Concepts. *Pharmacol. Ther.* **2010**, *126*, 21–38.

(139) Stanley, C.; O'Sullivan, S. E. Vascular Targets for Cannabinoids: Animal and Human Studies. *Br. J. Pharmacol.* **2014**, *171*, 1361–1378.

(140) Whyte, L. S.; Ford, L.; Ridge, S. a.; Cameron, G. a.; Rogers, M. J.; Ross, R. a. Cannabinoids and Bone: Endocannabinoids Modulate Human Osteoclast Function in Vitro. *Br. J. Pharmacol.* **2012**, *165*, 2584–2597.

(141) Cabral, G. A.; Rogers, T. J.; Lichtman, A. H. Turning Over a New Leaf: Cannabinoid and Endocannabinoid Modulation of Immune Function. *J. Neuroimmune Pharmacol.* **2015**, *10*, 193–203.

(142) De Luca, M. A.; Fattore, L. Cannabinoids and Drug Addiction. In *Cannabinoids in Neurologic and Mental Disease*; Fattore, L., Ed.; Elsevier, 2015; pp. 289–313.

(143) De Campos, A. C.; Brant, F.; Miranda, A. S.; Machado, F. S.; Teixeira, A. L. Cannabidiol Increases Survival and Promotes Rescue of Cognitive Function in a Murine Model of Cerebral Malaria. *Neuroscience* **2015**, *289*, 166–180.

(144) Cumella, J.; Hernández-Folgado, L.; Girón, R.; Sánchez, E.; Morales, P.; Hurst, D. P.; Gómez-Cañas, M.; Gómez-Ruiz, M.; Pinto, D. C. G. a; Goya, P.; Reggio, P. H.; Martin, M. I.; Fernández-Ruiz, J.; Silva, A. M. S.; Jagerovic, N. Chromenopyrazoles: Non-Psychoactive and Selective CB1 Cannabinoid Agonists with Peripheral Antinociceptive Properties. *ChemMedChem* **2012**, *7*, 452–463.

(145) Marion, R.; Zaarour, M.; Qachachi, N. a.; Saleh, N. M.; Justaud, F.; Floner, D.; Lavastre, O.; Geneste, F. Characterization and Catechole Oxidase Activity of a Family of Copper Complexes Coordinated by Tripodal Pyrazole-Based Ligands. *J. Inorg. Biochem.* **2011**, *105*, 1391–1397.

(146) Juliá, S.; Martínez-Martorell, C.; Elguero, J. A Selective Synthesis of Unsymmetrical 1,1'-Methylenebisdiazoles by Solid-Liquid Phase Transfer Catalysis. *Heterocycles* **1986**, *24*, 2233–2237.

(147) Yao, B.; Mackie, K. Behavioral Neurobiology of the Endocannabinoid System. *Curr. Top. Behav. Neurosci. 1,* **2009**, *1*, 87–110.

(148) Puffenbarger, R. A.; Boothe, A. C.; Cabral, G. A. Cannabinoids Inhibit LPS-Inducible Cytokine mRNA Expression in Rat Microglial Cells. *Glia* **2000**, *29*, 58–69.

(149) Maresz, K.; Carrier, E. J.; Ponomarev, E. D.; Hillard, C. J.; Dittel, B. N. Modulation of the Cannabinoid CB2 Receptor in Microglial Cells in Response to Inflammatory Stimuli. *J. Neurochem.* **2005**, *95*, 437–445.

(150) Oh, Y. T.; Lee, J. Y.; Lee, J.; Lee, J. H.; Kim, J. E.; Ha, J.; Kang, I. Oleamide Suppresses Lipopolysaccharide-Induced Expression of iNOS and COX-2 through Inhibition of NF-kB Activation in BV2 Murine Microglial Cells. *Neurosci. Lett.* **2010**, *474*, 148–153.

(151) Hernandez-Folgado, L.; Cumella, J. M.; Morales, P.; Alkorta, I.; Elguero, J.; Jagerovic, N. Tautomerism of Hydroxychromenopyrazoles. *J. Mol. Struct.* **2012**, *1015*, 162–165.

(152) Reggio, P. H. Cannabinoid Receptors and Their Ligands: Ligand-Ligand and Ligand-Receptor Modeling Approaches. *Handb. Exp. Pharmacol.* **2005**, 247–281.

(153) Hurst, D. P.; Grossfield, A.; Lynch, D. L.; Feller, S.; Romo, T. D.; Gawrisch, K.; Pitman, M. C.; Reggio, P. H. A Lipid Pathway for Ligand Binding Is Necessary for a Cannabinoid G Protein-Coupled Receptor. *J. Biol. Chem.* **2010**, *285*, 17954–17964.

(154) Kapur, A.; Hurst, D. P.; Fleischer, D.; Whitnell, R.; Thakur, G. a; Makriyannis, A.; Reggio, P. H.; Abood, M. E. Mutation Studies of Ser7.39 and Ser2.60 in the Human CB1 Cannabinoid Receptor: Evidence for a Serine-Induced Bend in CB1 Transmembrane Helix 7. *Mol. Pharmacol.* **2007**, *71*, 1512–1524.

(155) Nebane, N. M.; Hurst, D. P.; Carrasquer, C. a.; Qiao, Z.; Reggio, P. H.; Song, Z. H. Residues Accessible in the Binding-Site Crevice of Transmembrane Helix 6 of the CB2 Cannabinoid Receptor. *Biochemistry* **2008**, *47*, 13811–13821.

(156) Pei, Y.; Mercier, R. W.; Anday, J. K.; Thakur, G. a.; Zvonok, A. M.; Hurst, D.; Reggio, P. H.; Janero, D. R.; Makriyannis, A. Ligand-Binding Architecture of Human CB2 Cannabinoid Receptor: Evidence for Receptor Subtype-Specific Binding Motif and Modeling GPCR Activation. *Chem. Biol.* **2008**, *15*, 1207–1219.

(157) Song, Z. H.; Bonner, T. I. A Lysine Residue of the Cannabinoid Receptor Is Critical for Receptor Recognition by Several Agonists but Not WIN55212-2. *Mol. Pharmacol.* **1996**, *49*, 891–896.

(158) Hurst, D. P.; Lynch, D. L.; Barnett-Norris, J.; Hyatt, S. M.; Seltzman, H. H.; Zhong, M.; Song, Z.-H.; Nie, J.; Lewis, D.; Reggio, P. H. N-(piperidin-1-Yl)-5-(4-Chlorophenyl)-1-(2,4-Dichlorophenyl)-4-Methyl-1H-Pyrazole-3-Carboxamide (SR141716A) Interaction with LYS 3.28(192) Is Crucial for Its Inverse Agonism at the Cannabinoid CB1 Receptor. *Mol. Pharmacol.* **2002**, *62*, 1274–1287.

(159) Zhang, R.; Hurst, D. P.; Barnett-Norris, J.; Reggio, P. H.; Song, Z.-H. Cysteine 2.59(89) in the Second Transmembrane Domain of Human CB2 Receptor Is Accessible within the Ligand Binding Crevice: Evidence for Possible CB2 Deviation from a Rhodopsin Template. *Mol. Pharmacol.* **2005**, *68*, 69–83.

(160) Guo, J.; Pavlopoulos, S.; Tian, X.; Lu, D.; Nikas, S. P.; Yang, D.-P.; Makriyannis, A. Conformational Study of Lipophilic Ligands in Phospholipid Model Membrane Systems by Solution NMR. *J. Med. Chem.* **2003**, *46*, 4838–4846.

(161) Yang, D. P.; Mavromoustakos, T.; Beshah, K.; Makriyannis, a. Amphipathic Interactions of Cannabinoids with Membranes. A Comparison between Delta 8-THC and Its O-Methyl Analog Using Differential Scanning Calorimetry, X-Ray Diffraction and Solid State 2H-NMR. *Biochim. Biophys. Acta* **1992**, *1103*, 25–36.

(162) Razdan, R. K. Structure–Activity Relationships of Classical Cannabinoids. In *The Cannabinoid Receptors*; Reggio, P. H., Ed.; Humana Press: Totowa, NJ, 2009; pp. 3–19.

(163) Huffman, J. W.; Hepburn, S. a.; Reggio, P. H.; Hurst, D. P.; Wiley, J. L.; Martin, B. R. Synthesis and Pharmacology of 1-Methoxy Analogs of CP-47,497. *Bioorganic Med. Chem.* **2010**, *18*, 5475–5482.

(164) Huffman, J. W.; Bushell, S. M.; Miller, J. R. a; Wiley, J. L.; Martin, B. R. 1-Methoxy-, 1-Deoxy-11-Hydroxy- and 11-Hydroxy-1-Methoxy-Δ8-Tetrahydrocannabinols: New Selective Ligands for the CB2 Receptor. *Bioorganic Med. Chem.* **2002**, *10*, 4119–4129.

(165) Gareau, Y.; Dufresne, C.; Gallant, M.; Rochette, C.; Sawyer, N.; Slipelz, D. M.; Weech, P. K.; Metters, K. M.; Labelle, M.; Frosst, M. Structure Activity Relationships of Tetrahydrocannabinol Analogues on Human Cannabinoid Receptors. **1996**, *6*, 189–194.

(166) Ekins, S.; Waller, C. L.; Swaan, P. W.; Cruciani, G.; Wrighton, S. a; Wikel, J. H. Progress in Predicting Human ADME Parameters in Silico. *J. Pharmacol. Toxicol. Methods* **2001**, *44*, 251–272.

(167) Van de Waterbeemd, H.; Gifford, E. ADMET in Silico Modelling: Towards Prediction Paradise? *Nat. Rev. Drug Discov.* **2003**, *2*, 192–204.

(168) Jorgensen, W. L.; Duffy, E. M. Prediction of Drug Solubility from Structure. *Adv. Drug Deliv. Rev.* **2002**, *54*, 355–366.

(169) Lipinski, C. A. Drug-like Properties and the Causes of Poor Solubility and Poor Permeability. *J. Pharmacol. Toxicol. Methods* **2001**, *44*, 235–249.

(170) Huestis, M. A. Human Cannabinoid Pharmacokinetics. *Chem. Biodivers.* **2009**, *4*, 1770–1804.

(171) Grotenhermen, F. Pharmacokinetics and Pharmacodynamics of Cannabinoids. *Clin. Pharmacokinet.* **2003**, *42*, 327–360.

(172) Bertucci, C.; Domenici, E. Reversible and Covalent Binding of Drugs to Human Serum Albumin: Methodological Approaches and Physiological Relevance. *Curr. Med. Chem.* **2002**, *9*, 1463–1481.

(173) Ghuman, J.; Zunszain, P. a.; Petitpas, I.; Bhattacharya, A. a.; Otagiri, M.; Curry, S. Structural Basis of the Drug-Binding Specificity of Human Serum Albumin. *J. Mol. Biol.* **2005**, *353*, 38–52.

(174) Fanali, G.; Di Masi, A.; Trezza, V.; Marino, M.; Fasano, M.; Ascenzi, P. Human Serum Albumin: From Bench to Bedside. *Mol. Aspects Med.* **2012**, *33*, 209–290.

(175) Beaudry, F.; Coutu, M.; Brown, N. K. Determination of Drug-Plasma Protein Binding Using Human Serum Albumin Chromatographic Column and Multiple Linear Regression Model. *Biomed. Chromatogr.* **1999**, *13*, 401–406.

(176) Buchholz, L.; Cai, C.-H.; Andress, L.; Cleton, A.; Brodfuehrer, J.; Cohen, L. Evaluation of the Human Serum Albumin Column as a Discovery Screening Tool for Plasma Protein Binding. *Eur. J. Pharm. Sci.* **2002**, *15*, 209–215.

(177) Frostell-Karlsson, A.; Remaeus, A.; Roos, H.; Andersson, K.; Borg, P.; Halamainen, M.; Karlsson, R. Biosensor Analysis of the Interaction between Immobilized Human Serum Albumin and Drug Compounds for Prediction of Human Serum Albumin Binding Levels. *J. Med. Chem.* **2000**, 1986–1992.

(178) Cooper, M. a. Optical Biosensors in Drug Discovery. *Nat. Rev. Drug Discov.* **2002**, *1*, 515–528.

(179) McDonnell, J. M. Surface Plasmon Resonance: Towards an Understanding of the Mechanisms of Biological Molecular Recognition. *Curr. Opin. Chem. Biol.* **2001**, *5*, 572–577.

(180) Patching, S. G. Surface Plasmon Resonance Spectroscopy for Characterisation of Membrane Protein–ligand Interactions and Its Potential for Drug Discovery. *Biochim. Biophys. Acta - Biomembr.* **2014**, *1838*, 43–55.

(181) Rich, R. L.; Day, Y. S.; Morton, T. a; Myszka, D. G. High-Resolution and High-Throughput Protocols for Measuring Drug/human Serum Albumin Interactions Using BIACORE. *Anal. Biochem.* **2001**, *296*, 197–207.

(182) Brugarolas, M.; Navarro, G.; Martínez-Pinilla, E.; Angelats, E.; Casadó, V.; Lanciego, J. L.; Franco, R. G-Protein-Coupled Receptor Heteromers as Key Players in the Molecular Architecture of the Central Nervous System. *CNS Neurosci. Ther.* **2014**, *20*, 703–709.

(183) Franco, R.; Martínez-Pinilla, E.; Ricobaraza, A.; McCormick, P. J. Challenges in the Development of Heteromer-GPCR-Based Drugs. *Prog. Mol. Biol. Transl. Sci.* **2013**, *117*, 143–162.

(184) Hiller, C.; Kühhorn, J.; Gmeiner, P. Class A G-Protein-Coupled Receptor (GPCR) Dimers and Bivalent Ligands. *J. Med. Chem.* **2013**, *56*, 6542–6559.

(185) Shonberg, J.; Scammells, P. J.; Capuano, B. Design Strategies for Bivalent Ligands Targeting GPCRs. *ChemMedChem* **2011**, *6*, 963–974.

(186) Fulton, B. S.; Knapp, B. L.; Bidlack, J. M.; Neumeyer, J. L. Effect of Linker Substitution on the Binding of Butorphan Univalent and Bivalent Ligands to Opioid Receptors. *Bioorg. Med. Chem. Lett.* **2010**, *20*, 1507–1509.

(187) Zhang, B.; Zhang, T.; Sromek, A. W.; Scrimale, T.; Bidlack, J. M.; Neumeyer, J. L. Synthesis and Binding Affinity of Novel Mono- and Bivalent Morphinan Ligands for K, M, and Δ Opioid Receptors. *Bioorg. Med. Chem.* **2011**, *19*, 2808–2816.

(188) Gogoi, S.; Biswas, S.; Modi, G.; Antonio, T.; Reith, M. E. A.; Dutta, A. K. Novel Bivalent Ligands for D2/D3 Dopamine Receptors: Signi Fi Cant Cooperative Gain in D2 A Ffi Nity and Potency. *ACS Med. Chem. Lett.* **2012**, *3*, 991–996.

(189) Huber, D.; Löber, S.; Hübner, H.; Gmeiner, P. Bivalent Molecular Probes for Dopamine D2-like Receptors. *Bioorg. Med. Chem.* **2012**, *20*, 455–466.

(190) Birnkammer, T.; Spickenreither, A.; Brunskole, I.; Lopuch, M.; Kagermeier, N.; Bernhardt, G.; Dove, S.; Seifert, R.; Elz, S.; Buschauer, A. The Bivalent Ligand Approach Leads to Highly Potent and Selective Acylguanidine-Type Histamine H Receptor Agonists. *J. Med. Chem.* **2012**, *55*, 1147–1160.

(191) Perrey, D. A.; Gilmour, B. P.; Thomas, B. F.; Zhang, Y. Toward the Development of Bivalent Ligand Probes of Cannabinoid CB1 and Orexin OX1 Receptor Heterodimers. *ACS Med. Chem. Lett.* **2014**, *5*, 634–638.

(192) Fernández-Fernández, C.; Callado, L. F.; Girón, R.; Sánchez, E.; Erdozain, A. M.; López-Moreno, J. A.; Morales, P.; Rodríguez de Fonseca, F.; Fernández-Ruiz, J.; Goya, P.; Meana, J. J.; Martín, M. I.; Jagerovic, N. Combining Rimonabant and Fentanyl in a Single Entity: Preparation and Pharmacological Results. *Drug Des. Devel. Ther.* **2014**, *8*, 263–277.

(193) Le Naour, M.; Akgün, E.; Yekkirala, A.; Lunzer, M. M.; Powers, M. D.; Kalyuzhny, A. E.; Portoghese, P. S. Bivalent Ligands That Target M Opioid (MOP) and cannabinoid1 (CB1) Receptors Are Potent Analgesics Devoid of Tolerance. *J. Med. Chem.* **2013**, *56*, 5505–5513.

(194) Nimczick, M.; Pemp, D.; Darras, F. H.; Chen, X.; Heilmann, J.; Decker, M. Synthesis and Biological Evaluation of Bivalent Cannabinoid Receptor Ligands Based on hCB2R Selective Benzimidazoles Reveal Unexpected Intrinsic Properties. *Bioorg. Med. Chem.* **2014**, *22*, 3938–3946.

(195) Pagé, D.; Balaux, E.; Boisvert, L.; Liu, Z.; Milburn, C.; Tremblay, M.; Wei, Z.; Woo, S.; Luo, X.; Cheng, Y.-X.; Yang, H.; Srivastava, S.; Zhou, F.; Brown, W.; Tomaszewski, M.; Walpole, C.; Hodzic, L.; St-Onge, S.; Godbout, C.; Salois, D.; Payza, K.; Payza, K. Novel Benzimidazole Derivatives as Selective CB2 Agonists. *Bioorg. Med. Chem. Lett.* **2008**, *18*, 3695–3700.

(196) Shonberg, J.; Kling, R. C.; Gmeiner, P.; Löber, S. GPCR Crystal Structures: Medicinal Chemistry in the Pocket. *Bioorg. Med. Chem.* **2014**, *23*, 3880–3906.

(197) Nimczick, M.; Decker, M. New Approaches in the Design and Development of Cannabinoid Receptor Ligands: Multifunctional and Bivalent Compounds. *ChemMedChem* **2015**, *10*, 773–786.

(198) Gomez-Cañas, M.; Morales, P.; García-Toscano, L.; Navarrete, C.; Goya, P.; García-Arencibia, M.; Muñoz, E.; Fernández-Ruiz, J.; Jagerovic, N.; Pazos, M. R. Biological Chracterization of PM226, a Chromenoisoxazole, as a Selective CB2 Receptor Agonist with Neuroprotective Profile. In *XVI Annual Meeting of the Spanish Cannabinoid Research Society (SEIC)*; Granada, 2015.

(199) Dominianni, S. J.; Ryan, C. W.; DeArmitt, C. W. Synthesis of 5-(tert-Alkyl)resorcinols. *J. Org. Chem.* **1977**, *42*, 344–346.

(200) Ballesteros, J. a.; Weinstein, H. Integrated Methods for the Construction of Three-Dimensional Models and Computational Probing of Structure-Function Relations in G Protein-Coupled Receptors. In *Methods in Neurosciences*; Stuart, C. S., Ed.; San Diego, CA, 1995; Vol. 25, pp. 366–428.

(201) Palczewski, K. Crystal Structure of Rhodopsin: A G Protein-Coupled Receptor. *Science (80-.).* **2000**, *289*, 739–745.

(202) Reggio, P. H. Computational Methods in Drug Design: Modeling G Protein-Coupled Receptor Monomers, Dimers, and Oligomers. *AAPS J.* **2006**, *8*, E322–E336.

(203) Mnpotra, J. S.; Qiao, Z.; Cai, J.; Lynch, D. L.; Grossfield, A.; Leioatts, N.; Hurst, D. P.; Pitman, M. C.; Song, Z.-H.; Reggio, P. H. Structural Basis of G Protein-Coupled Receptor-Gi Protein Interaction: Formation of the Cannabinoid CB2 Receptor-Gi Protein Complex. *J. Biol. Chem.* **2014**, *289*, 20259–20272.

Chapter 2

Chromenopyrazolediones: New Antitumor Cannabinoid-Quinones

Contents

1. Introduction

Cancer is one of the most common diseases and a leading cause of death worldwide. Its incidence has grown in the past decades, and studies from the World Health Organization point to an incessant increase in the coming years.[1] Cancer is a complex multifactorial physiopathology that triggers dysregulation of diverse cellular systems. The development of new effective and safe antitumor treatments that improve the aggressive current therapies remains an unmet clinical need. In this scenario, the endocannabinoid system emerges as a promising anticancer target involved in the modulation of the main hallmarks of this disease.

1.1 Cannabinoids and cancer

So far, studies on cannabinoids as antitumor agents have been mainly focused on understanding the mechanism of action of well-known compounds such as Δ^9-THC, Δ^8-THC or CBD. However, few novel cannabinoids with antitumor properties have been reported in the literature. In this section we will provide a general biological perspective of the potential of cannabinoids in cancer pathology.

1.1.1 Palliative effects

Cannabis has long been known to limit or prevent nausea and vomiting, lack of appetite and pain. For this reason, cannabinoids have been successfully used in the treatment of some of the unwanted side effects caused by cancer chemotherapy.[2]

In the middle 1980´s, dronabinol (Marinol®) and nabilone (Cesamet®) were approved for the management of chemotherapy-induced nausea and emesis.[3] Nowadays, they are only prescribed in some countries after conventional anti-emetics fail.[4]

Even though the best-established palliative effect of cannabinoids in cancer patients is the control of nausea and vomiting, these compounds are also appetite stimulants and pain inhibitors. Research from different groups demonstrates that THC and other cannabinoids have a stimulatory effect on

appetite and increase food intake in animals. Moreover, phase III trials confirmed the orexigenic effect of THC in the treatment of cancer anorexia.[5–7]

The effectiveness of cannabinoids in alleviating pain associated with cancer has been widely evidenced. Cannabinoids inhibit pain in animal models of acute and chronic allodynia, hyperalgesia or spontaneous pain by inhibiting nociceptive neurotransmission.[8,9] Different clinical trials support that THC and other synthetic derivatives have similar analgesic potency to codeine, a moderate opioid analgesic, emphasizing their relevance in the management of cancer pain.[10–12] In several countries, Sativex® (Δ^9-THC and CBD) is prescribed as an adjunctive analgesic treatment for adult patients with advanced cancer.[13]

Chemotherapy-induced peripheral neuropathies can also be attenuated by treatment with certain cannabinoid compounds as demonstrated in different rodent models of neurotoxicity.[14] Indeed, direct agonists such as WIN55,212, alleviates mechanical and cold allodynia in models of paclitaxel,[15] vincristine[16] and cisplatin[17]-evoked neuropathy. Several research groups highlight the role of CB_2R modulators in the treatment of chemotherapy-induced peripheral neuropathy because of their ability to prevent microglial activation.[18,19] In addition, CBD has shown ability to protect against doxorubicin-induced cardiomyopathy[20] and cisplatin-induced nephrotoxicity.[21]

Cannabinoid palliative effects have been properly validated, nonetheless, further studies are required to establish personalized medicine. Distinct treatment approaches are needed for the prevention of these undesired cancer-induced effects depending on the patients' genetic and the types of cancer involved.

1.1.2 Antitumor properties

Besides their aforementioned palliative potential, cannabinoids have exhibited antitumor effects in numerous *in vitro* and *in vivo* experimental models of cancer.[22–24]Antiproliferative properties of cannabis compounds were first identified four decades ago. Munson *et al.*[25] demonstrated that oral administration of Δ^9-THC, Δ^8-THC or CBN inhibited the growth of Lewis lung-adenocarcinoma in

mice. Despite the importance of these findings, it took more than two decades before the potential antitumor properties associated with these molecules were further explored. Since the late 1990s, an emerging body of investigation has demonstrated that cannabinoids can reduce tumor growth and progression on a wide range of cancer cells in culture and in nude mice tumor xenografts (for instance: lung carcinomas, gliomas, thyroid epitheliomas, skin carcinomas and lymphomas).[23,26–30] Cannabinoids are able to modulate different cellular signaling pathways implicated in cancer cell proliferation, migration or death. The mechanisms through which pharmacological stimulation of cannabinoid receptors impact tumor growth are quite complex and the understanding of these processes remain incomplete.[23] In fact, the signaling pathways implicated in the activation of the endocannabinoid system may differ depending on specific cancers and/or experimental models. Great efforts are currently being done to further elucidate these anticancer effects.[31] Even though most studies reveal that cannabinoids promote anti-cancer effects, few reports have proposed that under certain conditions, cannabinoid treatment can induce tumor-promoting effects.[32,33]

Endocannabinoid system upregulation in cancer

The biological role of the endocannabinoid system in cancer physiopathology is far from being completely understood. The ECS is generally upregulated in neoplasms compared with non-tumor tissue.[23,26,34,35] These observations may be tumor type-specific so further research is needed to understand the regulation of cannabinoid receptor expression in cancer.[22,34] In distinct types of tumors, such as glioblastoma,[36] estrogen receptor-negative breast tumors[37] and in 91% of ErbB2-positive breast tumors,[38] a remarkable increase of CB_2R levels has been detected. Other specific tumors are instead accompanied by overexpression of the CB_1R, such as gastric carcinoma[39] and rhabdomyosarcoma.[40] Likewise, increased expression of both receptors has been reported in hepatocellular carcinoma,[41] mantle cell lymphoma,[42] acute myeloid leukemia,[43] malignant astrocytomas,[44] and human pancreatic cancer.[45] AEA and 2-AG endocannabinoid tones differ significantly between normal cells and several types of tumor.[46]

It is clear that dysregulation of the endocannabinoid system plays an important role in the physiopathology of cancer.[24,26] Few studies have suggested that its over-activation could induce tumorigenesis[34] and could be related to tumor aggressiveness.[47,48] But the majority of them suggest that pharmacological activation of the endocannabinoid system induces cell death and reduces tumor proliferation.[23,29] Bifulco[49] suggested a biphasic action on cannabinoid receptors: low concentrations of endocannabinoid (nanomolar range) lead to pro-proliferative activity, while, high doses (micromolar range) of exogenous cannabinoids contribute to antiproliferative and pro-apoptotic effects. Another explanation has been suggested by Andradas,[50] who proposed that GPR55 participates in the proliferative effect of THC on cancer cells as produced by low concentrations of the cannabinoid. This putative cannabinoid receptor is also upregulated in a wide variety of human cancers conferring a proliferative action on cancer cells from different origins, including gliomas, breast adenocarcinoma and squamous skin cell carcinoma, both *in vitro* and *in vivo*.[51–54] Therefore, GPR55 has emerged as a promising therapeutic target in oncology and as a new cancer biomarker with possible prognostic value.[55] In addition, very recent findings reveal that GPR55-CB_2R heterodimers are expressed in cancer cells and human tumors which indicates the existence of new potential therapeutic approaches.[56,57]

Albeit further research is required to clarify the complex role of the ECS in this pathology, it is clear that cannabinoid-based pharmacotherapies have a remarkable therapeutic potential in the control of cancer.

Potential mechanisms of antitumor action

The activation of cannabinoid receptors on cancer cells modulates signaling pathways implicated in cell proliferation and survival. Even though the underlying mechanisms are not totally unraveled, there is significant evidence for the involvement of at least four mechanisms: direct inhibition of transformed-cell growth through the suppression of mitogenic signal, induction of apoptosis, inhibition of tumor angiogenesis and metastasis (figure 1).

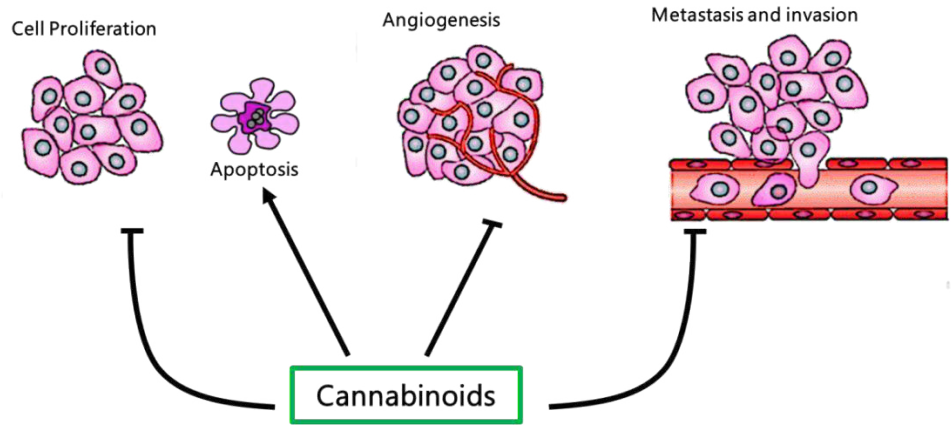

Figure 1. Mechanisms of cannabinoid antitumor action: Inhibition of cancer cell proliferation, induction of apoptosis, blockade of tumor angiogenesis, metastasization and invasiveness. Figure based on Velasco *et al.*[26]

Antiproliferative and pro-apoptotic effects. Cannabinoids impair uncontrolled cancer cell growth by inducing cell death through apoptosis and inhibition of cancer cell proliferation. Various signaling pathways are associated with these anticancer effects.

Activation of either CB_1R or CB_2R induces *de novo* synthesis of the pro-apoptotic sphingolipid ceramide. Synthesis of ceramide occurs via activation of the enzyme ceramide synthase and leads to the activation of an extracellular regulated kinase (ERK) signaling cascade. This process promotes cell cycle arrest and apoptosis.[26,27,45,58,59] In line with this proposal, up-regulation of the stress-regulated protein p8, an essential mediator of cannabinoid induced-apoptosis, is dependent on *de novo*-synthesized ceramide. This transcriptional regulator, together with several of its downstream targets such as the endoplasmic reticulum (ER) stress-related transcription factors ATF4 and CHOP, as well as the pseudokinase tribbles-homologue 3 (TRIB3) are implicated in the control of tumorigenesis and tumor progression.[26] This cascade of events trigger the interaction of TRIB3 with the serine-threonine kinase Akt,[60] leading to the inhibition of the Akt–mammalian target of rapamycin complex 1 (mTORC1) axis, and the subsequent induction of autophagy.[61] As acutely demonstrated in glioma animal models, the stimulation of autophagy mediates apoptosis after cannabinoid treatment.[61] Therefore, the ceramide accumulation and the activation of the ER-stress related pathway, induce cell death by apoptosis and stimulation of autophagy.[62,63] However,

additional mechanisms may cooperate with the p8-mediated autophagy pathway to induce cancer cell death. It has been suggested that the antiproliferative activity of cannabinoids may involve induction of cyclin kinase inhibitor (p27/KIP1) that modulates regulatory molecules of the cell cycle (cyclins, cdks) resulting in cell cycle arrest and apoptosis.[29,64,65]

Up-regulation of the p53 protein is also a factor to take into account in this process. This alteration may induce an increase of the pro-apoptotic BCL-2 proteins leading to the activation of caspases, which play an essential role in triggering apoptosis.[64] Likewise, CB_1R ligands have pro-apoptotic properties, in part, through inhibition of the Ras protein (p21ras) which is involved in inducing DNA synthesis.[66] Nonetheless, there are still many unraveled sides on death pathways activated by cannabinoids as well as on the different contribution of apoptosis and autophagy in cell death depending on the tumor system.

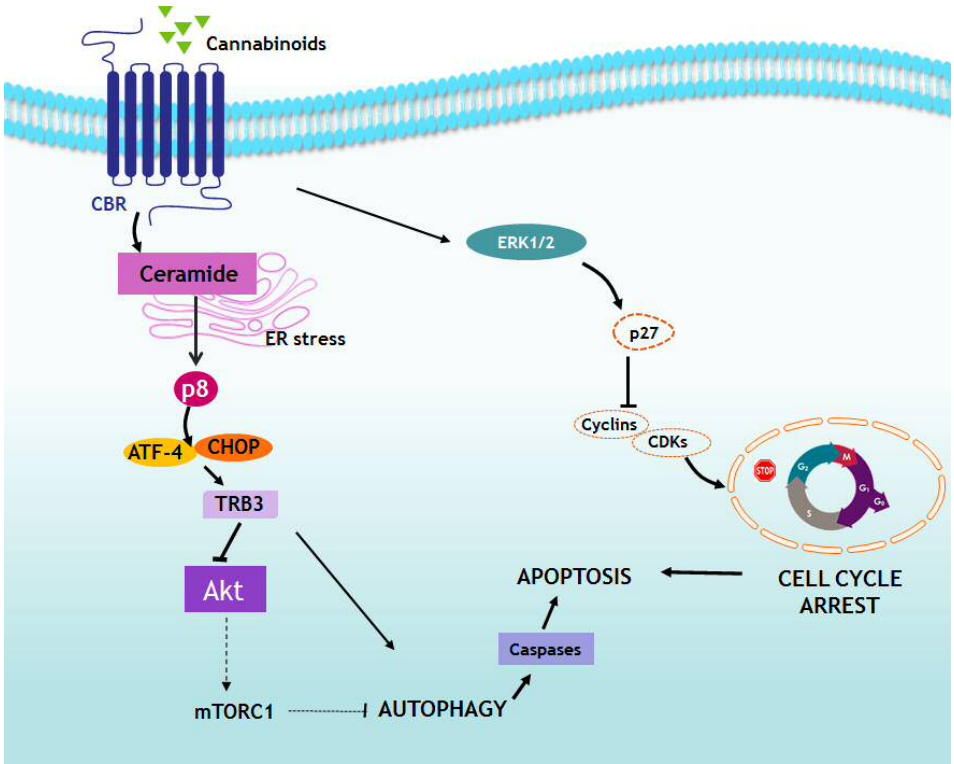

Figure 2. Schematic representation of the signaling pathways through which cannabinoids impact apoptosis and proliferation. Figure based on SEIC´s website.[67]

Effects on tumor invasion, metastasis and angiogenesis. Tumors induce blood vessel growth by secreting various growth factors that promote capillary development and neoplasm expansion. This key process in cancer progression, known as angiogenesis, can be blocked by the administration of certain cannabinoids.[68] The activation of cannabinoid receptors in cancer cells have resulted in the suppression of the vascular endothelial growth factor (VEGF) pathway which is an inducer of angiogenesis. Different elements of this cascade, such as the main ligand (VEGF) and the active forms of its main receptors (VEGFR1 and VEGFR2), are down-regulated after cannabinoid treatment of skin carcinomas,[69] gliomas[59,68] and thyroid carcinomas.[70] This inhibition of angiogenesis is also associated with a reduced expression of pro-angiogenic cytokine. Besides its anti-angiogenic action, cannabinoids may also confer anti-migrative, anti-adhesive, anti-invasive, and anti-metastatic properties.[71] In animal models of induced and spontaneous metastasis the administration of cannabinoids reduced the formation of distant tumor masses. Likewise, cannabinoids can inhibit adhesion, migration and invasiveness of lung (Δ^9-THC, Met-AEA),[72,73] glioma (Δ^9-THC),[74] cervical (Δ^9-THC, Met-AEA),[73] and breast (AEA, JWH-133, WIN-55,212)[75,76] cancer cells in culture. These effects are due to the modulation of matrix metalloproteinase 2 and its inhibitors. Matrix metalloproteinases (MMPs) are a family of proteolytic extracellular enzymes that play a crucial role in tumor invasion allowing tissue breakdown and remodeling during angiogenesis and metastasis. Tissue inhibitors of MMPs (TIMPs), and in particular TIMP-1, can inhibit the proteolytic activity of MMPs and suppress vascular tumor growth and angiogenesis in xenograft animal models.[77] For instance, in a cervical cancer cell line, Met-AEA as well as Δ^9-THC and CBD inhibited the invasive properties of these cells via increased expression of TIMP-1.[73,78,79] Blázquez *et al.*[74] reported that a decrease of MMP-2 expression in glioma cells can lead to inhibition of cell invasion after treatment with Δ^9-THC. They showed that ceramide biosynthesis and expression of the stress protein p8 are also involved in this process. Furthermore, THC and CBD have been shown to promote the expression of the intercellular adhesion molecule 1 (ICAM-1) on lung cancer cells as part of their anti-invasive and antimetastatic action.[80]

All these data suggest that cannabinoids are potent inhibitors of both cancer growth and spreading. Nonetheless, the potential development of cannabinoids as antitumor drugs has been restricted due to their psychoactive properties.

Towards clinical antitumor application

Nowadays, cannabinoids are only prescribed for palliative purposes, however, the promising preclinical data aforementioned is increasingly raising its potential in the treatment of tumor progression itself. Indeed, the anticancer properties of cannabinoids are beginning to be clinically evaluated. A few years ago, Guzmán *et al.*[81] developed the first clinical study to investigate the antitumor capacity of a cannabinoid receptor agonist on tumor growth activity. In this phase I pilot trial, they studied the effects of intratumoral administration of Δ^9-THC on nine patients with glioblastoma multiforme, who had failed surgical therapy and radiotherapy and exhibited clear evidence of tumor progression. The results obtained in this study suggested that cannabinoid treatment reduced tumor growth rate. Interestingly, intracranial Δ^9-THC administration was found to be safe and did not result in obvious psychoactive effects. Furthermore, combinational therapies of cannabinoids with other anticancer drugs, such as temozolomide or gemcitabine, are emerging as promising antitumor strategies.[82,83] Actually, there is an ongoing phase I clinical trial in which patients with recurrent glioblastoma are treated with a combination of Sativex® and temozolomide (benchmark agent for the management of these brain tumors) to evaluate a possible enhanced antitumor activity. Nonetheless, more extensive clinical studies are needed to extract significant conclusions that reinforce the potential utility of cannabinoids as anticancer therapeutics.

1.1.3 A focus on breast and prostate cancer

In this dissertation, we will focus on the activity of new cannabinoid-quinones in triple negative breast cancer and prostate tumors. Therefore, the following section briefly summarizes the current knowledge of these two types of cancers in relation to the endocannabinoid system.

Triple Negative Breast Cancer (TNBC)

Breast cancer is the most common malignant disease and the second leading cause of cancer death among Western women.[84] Despite recent advances in earlier detection and adjuvant systemic therapies, mortality rates remain very high due to the emergence of refractory tumors associated with multidrug resistance.

According to immunopathological criteria, there are three main breast cancer subtypes: hormone receptor-positive, HER2-positive (human epidermal growth factor receptor 2) and triple-negative tumors. Triple-negative breast cancers (TNBC) are defined by the absence of immunohistochemical expression of estrogen, progesterone, and HER2 receptors. Although this molecular subtype of breast cancer accounts for a low percentage of all breast tumors, it represents a disproportionate number of deaths.[85] TNBC show aggressive clinical behavior, this fact, along with the lack of available targeted therapies leave these patients with a very poor prognosis.[85–88] Chemotherapy with its well-known side effects is currently used as systemic treatment for this cancer.[89] For that reason, the discovery of new targets and drugs for the treatment of this disease is an urgent and essential clinical challenge. In this context, the therapeutic potential of cannabinoids has been recently explored as a new hope for TNBC patients.[90,91]

Recent evidence suggests that cannabinoid receptors are overexpressed in human breast cancer biopsies.[35,38,92] Further insights into the endocannabinoid upregulation have demonstrated a correlation between CB_2R expression and tumor aggressiveness in triple-negative breast cancer cells.[35] The putative novel cannabinoid receptor GPR55 is also highly expressed in these carcinomas.[93] Consequently, the ECS represents a promising target for the treatment of TNBC.

Prostate Cancer

Prostate cancer is the second most common cancer worldwide for males. The rates have increased in recent years as its detection has improved in the younger men and as life expectancy is longer.[94] Even though most prostate cancers grow slowly, aggressive cases are also detected. These oncogenic

cells may metastasize to other parts of the body such as bones and lymph nodes.[95] Therefore, there are extensive ongoing efforts to develop new therapeutic strategies to treat prostate cancer.[96]

The basis of medical treatment for advanced prostate cancer is androgen deprivation therapy (ADT), intended to lower testosterone levels. However, the reduction of clinical symptoms and tumor growth is accompanied by systemic consequences of testosterone deficiency such as osteoporosis, gynecomastia, anemia and insulin resistance among others.[97,98] Androgen deprivation is associated with a gradual transition of prostate cancer cells through a spectrum of androgen dependence, androgen sensitivity, and ultimately androgen independence. Too often the appearance of hormone refractory cancer cells eventually leads to the recurrence of cancer which turns to a hormone-independent state. This type of prostate cancer has a more aggressive phenotype and is unresponsive to further hormonal therapy whereby prognosis is very poor. Therefore, to find a treatment which could reduce or block both types of prostate cancer would be a very good challenge to move forward.

The expression of cannabinoid receptors has also been studied in prostate cancer tissue. It was demonstrated that CB_1R expression is upregulated in these neoplasms.[99] Indeed, high CB_1R immunoreactivity score in prostate cancer tissue is associated with prostate cancer severity and outcome.[100] Moreover, expression of FAAH[47] and GPR55[101] is demonstrated in some prostate carcinoma cell lines. In line with these observations, different endocannabinoids or cannabis-like compounds were evaluated exhibiting their ability to inhibit prostate cancer cell proliferation and produce apoptosis through cannabinoid receptor mechanisms.[102] The dysregulation of this system correlates with prostate cancer grade and progression. Therefore, the ECS represents a new potential therapeutic target for prostate cancer.[103,104]

1.2 Antitumor quinones

Quinones are a class of natural and synthetic compounds that possess numerous physiological and therapeutic effects.[105] Nowadays cytotoxic quinones represent an important group of antineoplastic

drugs. Antitumor properties of quinones have been widely reported and are still the focus of much research.[106,107] Quinones are formed by a common basic structural pattern: an *ortho* or a *para* substituted dione conjugated either to an aromatic nucleus or to a condensed polycyclic system. Their mode of action is related to their structure. Therefore, cytotoxic activity of quinoid derivatives can be accounted for their fast redox cycling potential and Michael acceptor properties.[108–110] Even though their mechanism of action is not completely understood, several mechanisms have been suggested. Most investigations propose different combinations of DNA intercalation,[111] topoisomerase inhibition,[112] DNA alkylation,[113,114] and induction of reactive oxygen species (ROS)[115] depending on the compound structural features.

Many of the drugs clinically approved or still in clinical trials against cancer are quinone-related compounds (figure 3). The quinoid moiety is present in anthracyclines which are among the most used anticancer drugs ever developed.[106] Daunorubicin (Cerubidine®) and doxorubicin (Adriamycin®), the most prominent members of this class of antitumor agents, are clinically used in the therapy of solid cancers as well as hematological malignancies.[116] Likewise, mitoxantrone (Novantrone®), a dihydroxyanthracenedione, is approved for the treatment of certain types of neoplasms such as metastatic breast cancer, acute myeloid leukemia, and non-Hodgkin's lymphoma.[117] Bioreductive alkylating agents such as mitomycin C and its derivatives also display remarkable antitumor effects. Mitomycin C, a potent DNA crosslinker, is a FDA approved drug for the treatment of solid tumors.[118,119]

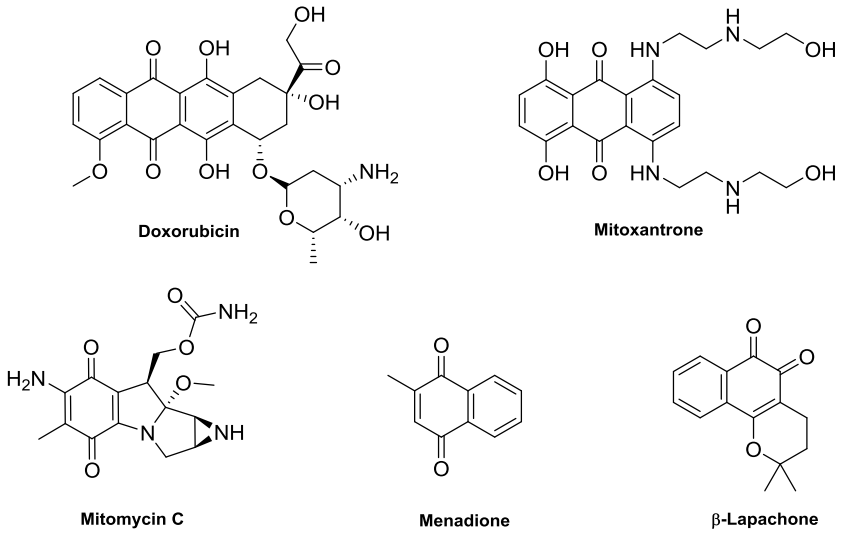

Figure 3. Some examples of quinoid compounds with antitumor activity.

Many other quinoid compounds are currently in advanced clinical phases. For instance, menadione, a potential antineoplastic agent for the treatment of prostate cancer.[120] This naphthoquinone is a prototypical redox cycling molecule that induces death through ROS-mediated pathways.[121] β-lapachone, an ortho naphthoquinone, originally isolated from a tree, is also being evaluated for its cancer growth inhibitory properties in diverse tumors.[106] Even though in many cases the antitumor mechanisms remain uncertain, it is unquestionable that the presence of the quinone moiety is exceptionally remarkable in the development of new anticancer drugs.

Despite the fact that quinones have been extensively studied as antitumor agents, there are only three with a cannabinoid-related structure. Few years ago, Kogan *et al.*[122] reported the antitumoral activity of quinone derivatives of phytocannabinoid compounds [cannabidiol (HU-331), Δ^8-THC (HU-336) and cannabinol (HU-345) (figure 4)]. Their biological activity was attributed to their quinone structure[123,124] independently of their cannabinoid character, since they do not bind to cannabinoid receptors.

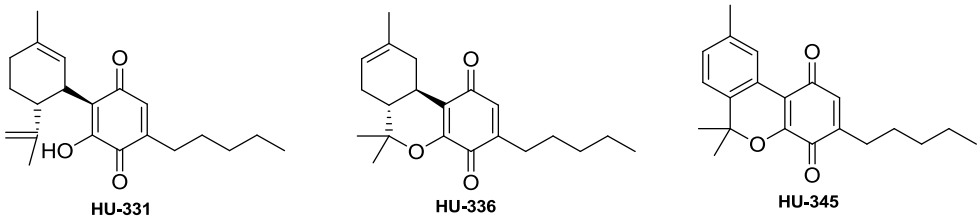

Figure 4. Quinones related to cannabinoids

The most effective, HU-331, reduced growth of human colon carcinoma HT-29 cells in nude mice. The mechanism of action of HU-331 is poorly understood. HU-311 does not promote cell death via cell cycle arrest. Recent studies[125] indicate that HU-311 inhibits the ATPase function of human topoisomerase IIα. The other cannabinoid-structure related quinone, HU-336, inhibits angiogenesis by inducing apoptosis of vascular endothelial cells. Consequently, anticancer quinone directly acting on the cannabinoid system has not been described so far.

2. Aims

A large diversity of biological signaling-pathways are implicated in the pathogenesis of cancer. Appropriate treatment of neoplasms often depends on pharmaceutical intervention at multiple pathways using combinations of different drugs. In this context, targeting different anticancer modes of action in a single molecule is a significant challenge.[126–128] Our interest in cannabinoid ligands and antiproliferative agents has prompted us to design molecules which structure includes cannabinoid quinone features. Taking into account these targets, we propose structural modifications of the chromenopyrazole scaffold, previously described in chapter 1, introducing the quinone moiety (figure 5). Subsequently, the specific aims of this chapter are:

- Synthesis of quinones from chromenopyrazoles.[a]
- Determination of electrochemical parameters of novel compounds.[b]
- Analysis of *in silico* drug-like properties of chromenopyrazolediones.[a]
- Evaluation of their ability to bind to CB_1R and CB_2R.[c]
- Assessment of their potential antitumor properties in different human cancer cell lines.[d]
- Elucidation of their mechanism of action.[d]
- Appraisal of the antitumor activity *in vivo* of the best derivatives.[d]

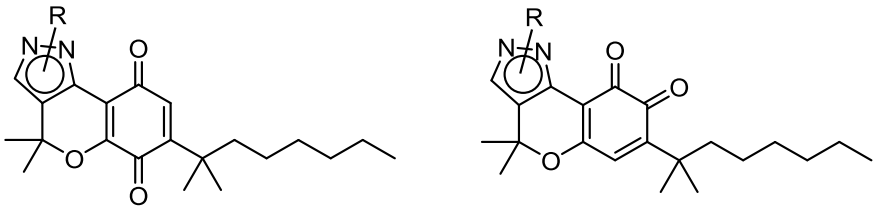

Figure 5. Proposed structures: chromenopyrazolediones.

a) Performed by PM at Instituto de Química Médica (CSIC).
b) Performed in collaboration with Prof. Claudio Olea (Facultad de Ciencias Químicas, Universidad de Chile).
c) Performed by PM hosted by Prof. Javier Fernández-Ruiz (Facultad de Medicina, UCM).
d) *Breast cancer studies*: performed by PM hosted by Prof. Cristina Sánchez (Facultad de Biología, UCM). *Prostate cancer studies*: Performed in collaboration with Prof. Inés Díaz-Laviada (Facultad de Medicina, Universidad de Alcalá de Henares).

3. Results

3.1 Chemistry

The initial 7-(1',1'-dimethylheptyl)-dihydro-4,4-dimethylchromeno[4,3-*c*]pyrazol-9-ols (**1.4–1.6)** were synthesized following the procedure described in the previous chapter.[129] The regio-controlled oxidation of the starting chromenopyrazoles to the corresponding 1,2- or 1,4-quinones was achived by reaction under mild conditions with hypervalent iodine reagents.[130] Reaction with *bis*(trifluoro-acetoxy)iodobenzene (BTIB) yielded the *para*-quinone derivatives[131,132] **2.1–2.3**, whereas regiospecific oxidation with *o*-iodoxybenzoic acid (IBX) furnished the *ortho* analogues **2.4–2.6**. Only few methods have been reported for the preparation of *ortho*-quinones by oxidation of phenols. In 2002, Pettus[133] described the use of IBX as a regioselective oxidant of phenols. Since then, IBX-mediated oxidations have been extended to polyaromatic *ortho*-quinones.[134,135] Scheme 1 outlines the synthesis of the *para* and *ortho* chromenopyrazolediones **2.1–2.6**. The 7-(1',1'-dimethylheptyl)-dihydro-4,4-dimethylchromeno [4,3-*c*]pyrazol-6,9 and 8,9-diones **2.1–2.6** were obtained in moderate to low yields.

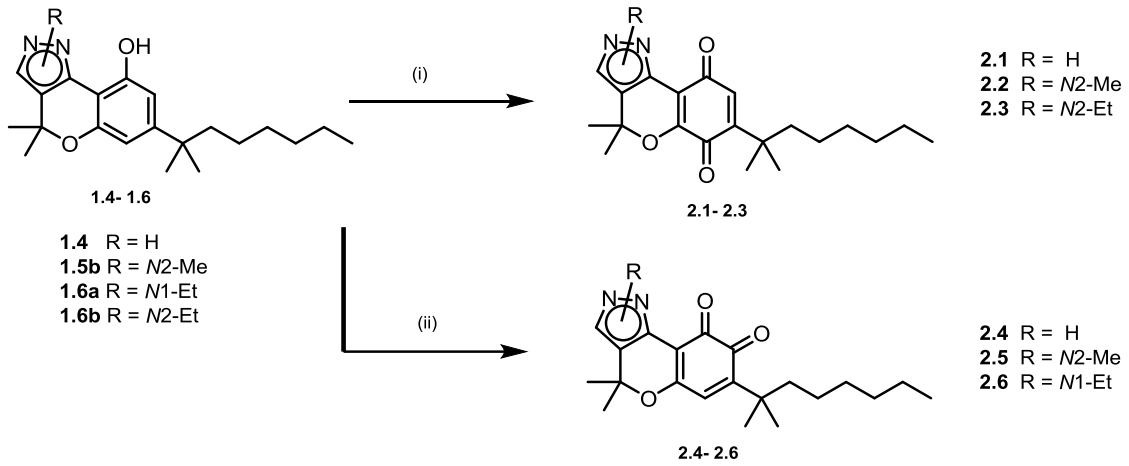

Scheme 1. Oxidation of chromenopyrazoles to the corresponding quinone derivatives **2.1–2.6**. Reaction conditions: **(i)** [*bis*(trifluoro-acetoxy)iodo]benzene, MeCN/ H_2O (6:1), 15 min, room temperature, 21-36%; **(ii)** *o*-iodoxybenzoic acid, DMF, 30 min, room temperature, 24-30%.

3.2 Electrochemistry

Since most of the biological functions of quinones are associated with their redox activity, the electrochemical properties of 7-(1',1'-dimethylheptyl)-1,4-dihydro-4,4-dimethylchromen[4,3-c]pyrazol-6,9-dione (**2.1**) and 7-(1',1'-dimethylheptyl)-2-ethyl-2,4-dihydro-4,4-dimethylchromen[4,3-c]pyrazol-6,9-dione (**2.3**), as examples, have been studied by cyclic voltammetry. Table 1 lists the values of the electrochemical parameters for **2.1** and **2.3**.

Table 1. Cyclic voltammetric parameters of **2.1** and **2.3** *vs.* saturated calomel electrode at 2.0 V/s

Compd	$E_{pc\ I}$ (mV)	$E_{pa\ I}$ (mV)	$E_{1/2}$ (mV)	I_{pa}/I_{pc}	$E_{pc\ II}$ (mV)
2.1	-0.512	-0.422	-0.467	0.54	-1.263
2.3	-0.590	-0.527	-0.559	0.65	-1.141

Chromenopyrazolediones **2.1** and **2.3** displayed comparable voltammetric behavior, showing two well-defined reduction waves in DMSO. The first wave for both quinones studied corresponded to a cuasi-reversible one-electron transfer. The reverse scan showed the anodic counterpart of the reduction waves (compound **2.1**, figure 6). According to the standard reversibility criteria, this couple corresponds to a cuasi-reversible diffusion-controlled one-electron transfer. It is attributable to the reduction of quinone to semiquinone that involves a stable anion radical at room temperature. The second couple is irreversible over the whole range of sweep rates used (0.1 at 2.0 V/s). We can attribute this wave to the production of a hydroquinone derivative.

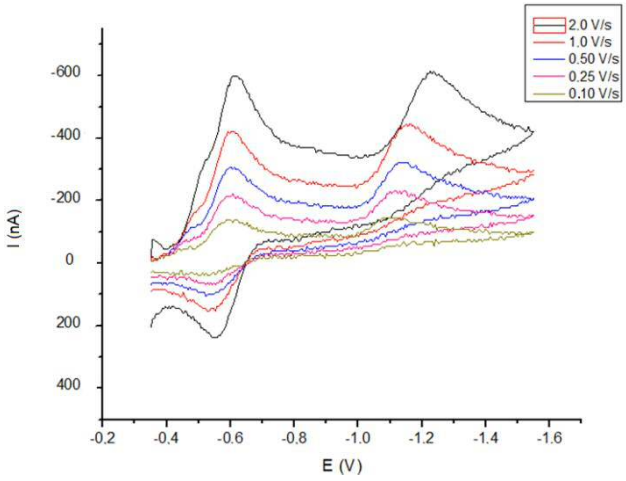

Figure 6. Cyclic voltammetric curves of 1 mM **2.1** sweep rates ranging from 0.1 to 2 V/s in 100% DMSO with 0.1M TBAP.

Electron spin resonance (ESR) experiments were carried out in order to correlate the cytotoxicity to the formation of radicals. The semiquinone free radicals were prepared in situ by electrochemical reductions in DMSO, applying a potential corresponding to the first wave for **2.1** or **2.3** obtained from the cyclic voltammetric experiments. The interpretation of the ESR spectra by means of a simulation process has led to the determination of the coupling constants for all the magnetic nuclei, confirmed by theoretical calculations. The ESR spectrum of **2.1** was analyzed and simulated in terms of one doublet from hydrogen nuclei of the quinone moiety; the hyperfine constant was 2.635 gauss. Figure 7 shows the ESR experimental and simulation spectra. Similar hyperfine pattern was found for **2.3** with hydrogen hyperfine constant value of 2.925 gauss.

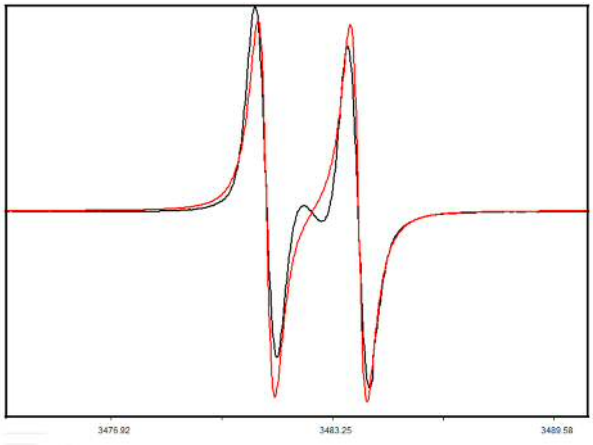

Figure 7. ESR experimental and simulated spectrum of **2.1** in DMSO.

3.3 Cannabinoid binding studies

The binding affinity of the chromenopyrazolediones **2.1**–**2.6** was determined through radioligand competition experiments. The ability of compounds **2.1**–**2.6** to displace [^{3}H]CP55940 from human CB_1R or CB_2R transfected into HEK293 EBNA cells was assessed. Standard cannabinoid ligand WIN55,212 was also tested for appraisal with the new derivatives. Initially, the compounds were screened at a concentration of 40 μM. The affinity constant (K_i) of compounds able to displace the

radioligand by more than 70% was determined from concentration−effect curves. The experimental binding affinities of **2.1**–**2.6** and WIN55,212 are reported in table 2. First of all, it is noteworthy that chromenopyrazolediones are the first cannabinoid structure-related quinones able to bind to the cannabinoid receptors. As already commented in the introduction, quinones related to cannabinoid structure reported so far do not have affinity for the cannabinoid receptors.[122]

Para-chromenopyrazolediones **2.1**–**2.3** display affinity for both receptors in the low micromolar range. Interestingly, **2.1** showed significant affinity in the nanomolar range for both CB_1 and CB_2 receptors. Besides, *ortho*-quinones **2.4**–**2.6** are fully selective towards CB_2R with affinity in the submicromolar range. Their lack of affinity for the CB_1R (higher than 40 μM) eliminates any psychotropic side effect that would be derived from activation of central CB_1R.

Table 2. Binding affinity of chromenopyrazolediones **2.1–2.6** and the reference cannabinoid WIN55,212 for *h*CB_1R and *h*CB_2R cannabinoid receptors.

Compd	CB_1R K_i (nM)[a]	CB_2R K_i (nM)[a]
2.1	324 ± 235	134 ± 21
2.2	14180 ± 5638	672 ± 191
2.3	8520 ± 3891	3665 ± 878
2.4	> 40000	398 ± 49
2.5	> 40000	597 ± 77
2.6	> 40000	529 ± 26
WIN55,212	45.6 ± 8.6	3.7 ± 0.2

[a]Values obtained from competition curves using [^{3}H]CP55940 as radioligand for *h*CB_1R and *h*CB_2R and are expressed as the mean ± SEM of at least three experiments.

3.4 *In silico* ADME properties

Inappropriate absorption, distribution, metabolism, and excretion are among the main determinants of drug development failures. Therefore, they should be considered at early stages of the drug discovery process. Nowadays, *in silico* approaches are widely accepted because of their fast and precise predictive potential.[136,137]

Pharmacokinetic properties of compounds **2.1** to **2.6** were predicted using QikProp on each global minimum energy conformer. As presented in table 3, chromenopyrazolediones follow Lipinski and Jorgensen pharmacokinetics rules.[138,139] As highlighted in the previous chapter, due to their lipophilic nature, solubility of cannabinoids is a great challenge. Interestingly, the cannabinoid-quinones described herein display adequate solubility values. Almost all the predicted properties of the tested compounds are within the ranges predicted by QikProp for 95% of known oral drugs (table 3). These data indicate that chromenopyrazolediones present a satisfactory druggability profile.

Table 3. Physicochemical descriptors of compounds **2.1–2.6** calculated by QikProp 3.5 integrated in Maestro (Schrödinger, LLC, New York, USA).

Compd	QPlogS[a]	QlogBB[b]	QPlogHERG[c]	QPPCaco[d]	%Human oral absorption GI[e]
2.1	-5.15	-1.01	-4.69	666	100
2.2	-5.36	-0.62	-4.90	1701	100
2.3	-5.78	-0.63	-5.23	1985	100
2.4	-5.35	-1.09	-4.90	611	100
2.5	-5.62	-0.69	-5.11	1562	100
2.6	-5.99	-0.65	-5.03	1976	100

[a]Predicted aqueous solubility [-6.5/0.5]; [b]Predicted log of the brain/blood partition coefficient [-3.0/1.2]; [c]HERG K^+ Channel Blockage (log IC_{50}) [concern below -5]; [d]Apparent Caco-2 cell permeability in nm/s [<25 poor, >500 excellent]; [e]Human Oral Absorption in GI [<25% is poor]; [range of 95% of drugs].

3.5 Cannabinoid-quinones for TNBC therapy

As previously mentioned, triple-negative breast neoplasms do not respond to endocrine therapy or other available targeted agents. Consequently, there is an evident need to develop effective anticancer agents with novel scaffolds or new mechanisms of action for the management of this disease. In this context, we decided to evaluate the antiproliferative activity of the novel cannabinoid-quinones in models of this highly aggressive breast cancer.

3.5.1 Antiproliferative properties *in vitro*

The antiproliferative activity of chromenopyrazolediones **2.1**–**2.6** was assessed against a human derived triple-negative breast cancer cell line, MDA-MB-231. Cell cultures were treated with different doses of **2.1**–**2.6** for 48 h, and cell viability was analyzed by colorimetric measurements using 3-(4,5-dimethylthiazol-2-yl)-2,5-diphenyltetrazolium bromide (MTT). As shown in figure 8, tested cannabinoid-quinones displayed growth inhibitory effects on triple-negative MDA-MB-231 breast cancer cells, with low micromolar IC_{50} values (table 4).

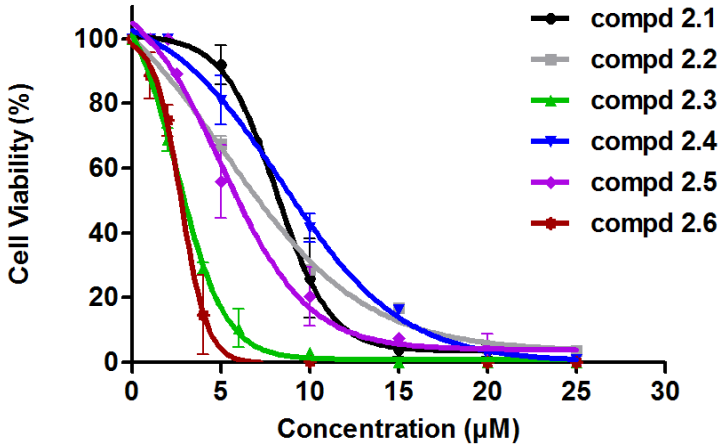

Figure 8. Dose-response curves of antiproliferative effect of chromenopyrazolediones **2.1**–**2.6** against the human breast cancer cell line MDA-MB-231.

Compounds **2.3** and **2.6** are the most potent inhibitors of cell proliferation with IC_{50} constants of 2.5 and 2.8 μM respectively (table 4). Regarding its antiproliferative capacity and its CB_2R selective profile, compound **2.6** was selected for additional investigations.

Table 4. Half-maximum inhibitory concentrations (IC_{50}) values for compounds **2.1**-**2.6**.

Compd	IC_{50} (μM)[a]
2.1	8.2 ± 1.1
2.2	5.8 ± 0.9
2.3	2.5 ± 0.1
2.4	8.5 ± 0.4

2.5	5.0 ± 0.8
2.6	2.8 ± 0.5

[a]Values are the mean ± SEM of three independent experiments performed in triplicate.

Triple-negative breast cancer is a very heterogeneous disease, not only on the molecular level, but also from a clinical point of view.[140,141] In fact, at least six different subtypes of this pathology have been already identified.[142] Therefore, the cytotoxicity of the selected compound **2.6** has been evaluated on three additional TNBC cell lines (SUM149, SUM159, and MDA-MB-468). As shown on figure 9, these TNBC cell lines were sensitive to compound **2.6**, with IC_{50} values of 4.6, 4.1 and 17.3 μM respectively.

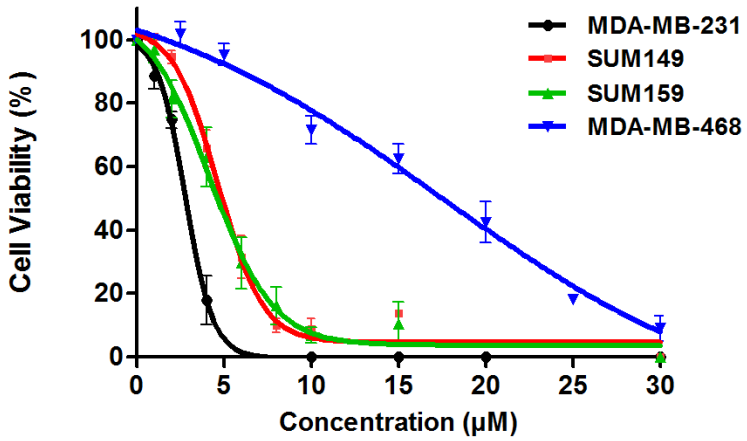

Figure 9. Dose-response curves of antiproliferative effect of chromenopyrazoledione **2.6** against the TNBC cell lines MDA-MB-231, SUM149, SUM159, and MDA-MB-468.

Citotoxicity on normal Human Mammary Epithelial.

Selective toxicity for cancer versus non-cancer cells is one of the main challenges of anticancer therapies. For that reason, we examined the growth inhibitory activity of compound **2.6** against human mammary epithelial cells (HMEC).

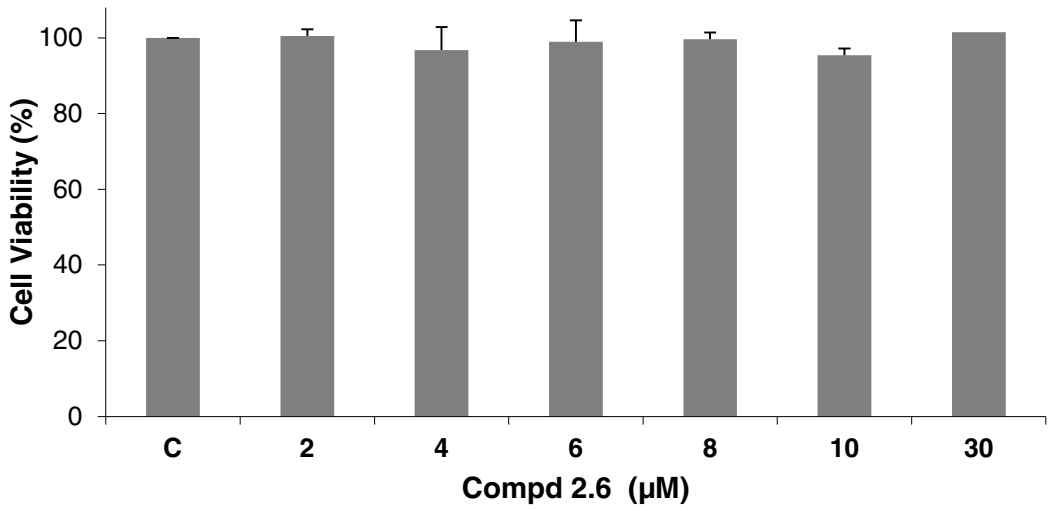

Figure 10. Effects of compound **2.6** on normal human mammary epithelial cell (HMEC) proliferation. HMECs were treated with increasing concentrations of the drug. Cell viability was determined 48 h after treatment. Values are the mean ± SEM of three independent experiments performed in duplicate.

At concentrations up to 10 times its IC_{50} value, chromenopyrazoledione **2.6** did not display antiproliferative activity in this non-transformed mammary epithelial cell line (figure 10). Therefore, compound **2.6** demonstrates effective inhibition of triple-negative breast cancer cell growth without affecting the proliferation of their non-transformed counterparts. This selective toxicity towards cancer cells versus non-transformed HMECs was previously observed in phytocannabinoids such as Δ^9-THC.[35,143]

In what concerns the selectivity of quinones toward cancer cells, it has been reported that quinones affect cancer cells in higher extent than healthy cells.[115,144] This selectivity could be explained by the fact that cancer cells have increased endogenous ROS levels compared with normal cells due to their accelerated metabolism.

3.5.2 Mechanism of action

With the aim of further appraising the antitumor mechanism of cannabinoid quinone **2.6**, we studied the effect of selective inhibitors, alone or in combination with the compound, on cell

viability. MDA-MB-231 cells were pre-incubated for 1h with the CB_1R antagonist SR141716 (SR1), the CB_2R antagonist SR144528 (SR2), the GPR55 antagonist CID16020046 (CID), and the antioxidant α-tocopherol (Toc). Afterward, these cells were challenged with compound **2.6** for 48 h at IC_{50} concentration (2.8 μM). As presented in figure 11, any of the inhibitors (SR1, SR2, CID, Toc) has any effect on MDA-MB-231 cell viability by themselves. Interestingly, SR2 and α-Toc were able to significantly prevent the inhibition of cell viability induced by **2.6**, indicating that activation of the CB_2R and generation of reactive oxygen species (ROS) were involved in the antiproliferative action of compound **2.6**. Conversely, neither SR1 nor CID altered the effect of chromenopyrazoledione **2.6** on cell viability, suggesting that neither CB_1R nor GPR55 are targets of this compound. These results support our initial design that was the combination of CB_2R activity with ROS production in a single anticancer agent.

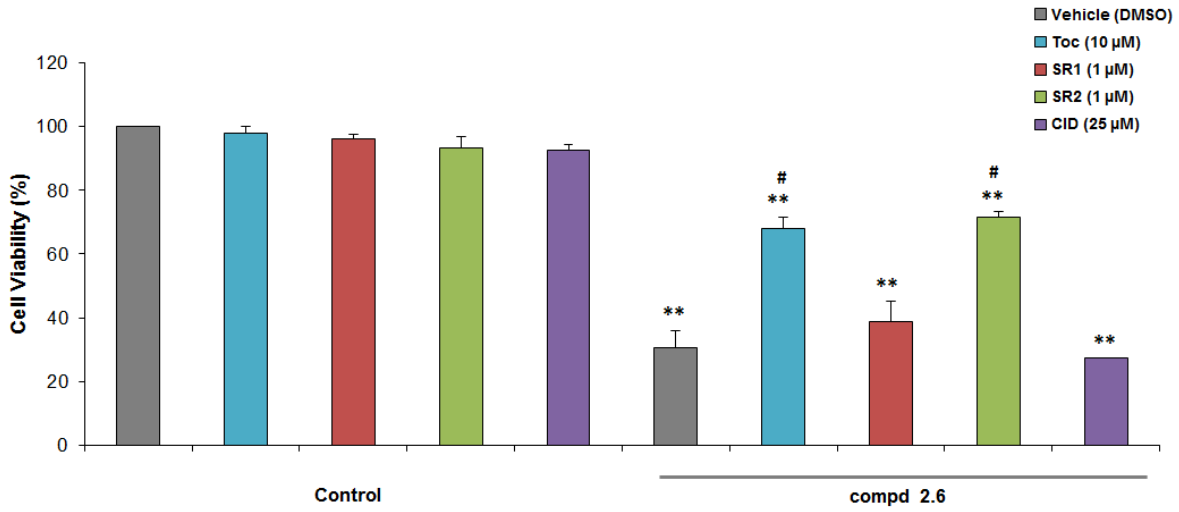

Figure 11. Molecular mechanisms involved in the growth inhibitory activity of compound **2.6**. MDA-MB-231 cell viability was determined by the MTT test. CB_1R selective antagonist: SR141716 (SR1); CB_2R selective antagonist: SR144528 (SR2); GPR55-selective antagonist: CID16020046 (CID); antioxidant: α-tocopherol (α-Toc). Results represent the mean ± SEM of three different experiments performed in triplicate. Data were assessed by two-way analysis of variance followed by the Student-Newman-Keuls (* $p < 0.05$ and ** $p < 0.01$ vs vehicle-treated cells; # $p < 0.05$ versus the compound alone).

In order to evaluate the cellular mechanism underlying this antiproliferative effect, the involvement of caspase-3 was assessed in MDA-MB-231 cells. Caspases are crucial mediators of mammalian cell death and caspase-3 is an apoptosis related cysteine peptidase responsible for apoptosis execution.

Western blots offer an efficient way of detecting caspase-3 activation.[145] Thus, western immunoblotting analysis was performed following a 48 h treatment of cells with IC_{50} dose of **2.6**. Figure 12 illustrates the procaspase-3 cleavage into caspase-3 which confirms the proapoptotic effect of cannabinoid-quinone **2.6** on this triple-negative breast cancer cell line.

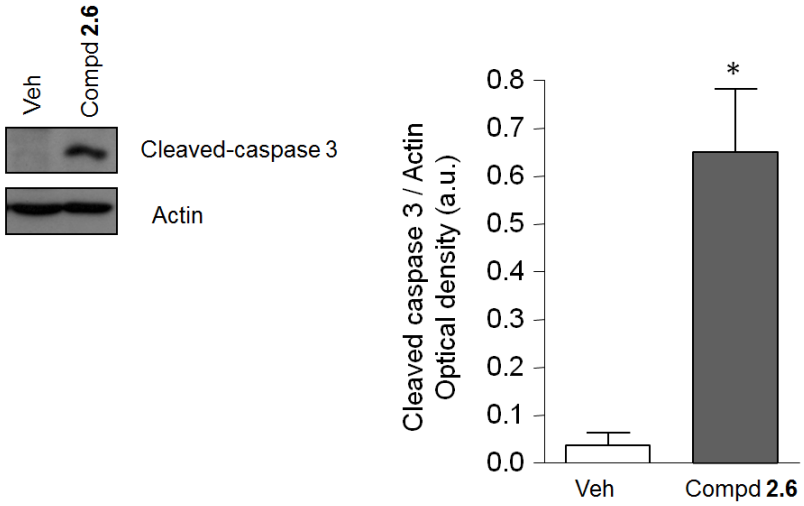

Figure 12. Analysis of caspase-3 protein expression. Western blot analysis of caspase 3 after 48 h exposure to compound **2.6** at IC_{50} concentration in MDA-MB-231 cells. The graph represents the densimetric analysis of protein levels. The optical density is relative to control cells set as 1. n = 3. Data were assessed by the Student's t-test (*p<0.05 *vs* vehicle-treated cells).

3.5.3 Antitumor activity *in vivo*

On the basis of its potent antiproliferative effect and its low toxicity in HMEC cells, compound **2.6** was selected for *in vivo* studies. To evaluate its capacity to inhibit TNBC growth, tumor xenografts were generated in nude mice by subcutaneous inoculation of MDA-MB-231 human breast adenocarcinoma cells. Mice were treated intraperitoneally three times a week during four weeks with vehicle or 2 mg/kg of compound **2.6**. As shown in figure 13, chromenopyrazoledione **2.6** was able to effectively reduce the growth of triple-negative xenografts in this animal model. Volume and weight of final tumors was significantly lower in all **2.6**-treated mice.

To assess the *in vivo* toxicity of compound **2.6**, organ histopathology was assessed in tumor-bearing mice post-treatment and without treatment (vehicle). Microscopic examination of tissues was performed as blind study to the identity of animals. Interestingly, the histopathological analysis of

animal organs (liver, spleen, lung, heart, ileum, colon, fundus, antrum, kidney, and duodenum) showed no sign of toxicity in these animals (data not shown).

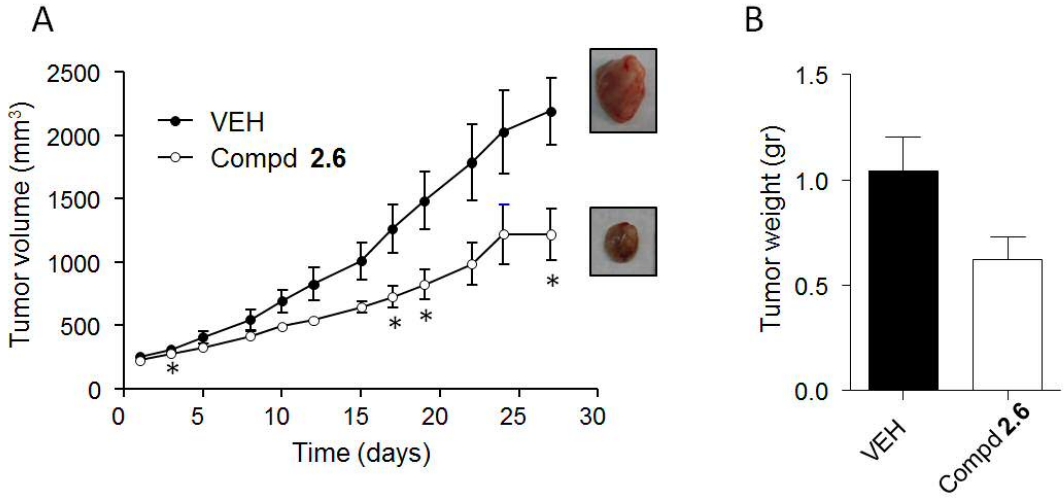

Figure 13. Compound **2.6** reduces tumor growth *in vivo*. (A) Effect of intraperitoneal administration of **2.6** on the growth of tumor xenografts generated in nude mice by injection of MDA-MB-231 human breast adenocarcinoma cells (mean ± SEM). Images show representative vehicle- and compound **2.6**-treated tumors. (B) Effect of **2.6** administration on tumor weight. Data were assessed by two-way (with repeated measures) analysis of variance followed by the Student-Newman-Keuls (*p<0.05 vs. vehicle-treated tumors).

In view of these data, we have identified compound **2.6** as a new promising anticancer drug candidate with potent antitumor activity *in vitro* and *in vivo* in triple-negative breast cancer.

3.6 Cannabinoid-quinones for prostate cancer treatment

Experimental evidence shows that the endocannabinoid system is dysregulated in prostate tumors. In particular, the level of expression of CB_1Rs in prostate cancer cells differs from non-malignant cells.[103] Thus, due to the significant role of these receptors in prostate cancer,[100,146,147] CB_1R agonists should provide a new therapeutic approach for this type of cancer. Among the series of chromenopyrazolediones **2.1**–**2.6**, the CB_1R ligands **2.1**–**2.3** were selected for their evaluation in androgen-dependent (LNCaP) and androgen-refractory (PC-3) prostate cancer-derived cell lines.

3.6.1 Antiproliferative properties *in vitro*

The antiproliferative effect of chromenopyrazolediones **2.1**–**2.3** was evaluated against the cancer cell lines LNCaP and PC-3. LNCaP is an androgen-dependent prostate cancer-derived cell line and PC-3

is an androgen-refractory prostate cancer-derived cell line. Increasing doses of **2.1–2.3** were added to cell cultures for 48h and cell viability was analyzed by colorimetric measurements using MTT as a dye. As showed in figure 14, all the tested cannabinoid-quinones are effective in prostate cancer cells, being **2.1** the most potent with an IC_{50} of 15 μM for prostate cancer LNCaP and PC-3 cells. Therefore, the chromenopyrazoledione **2.1** was selected for following investigations in these cancer cells.

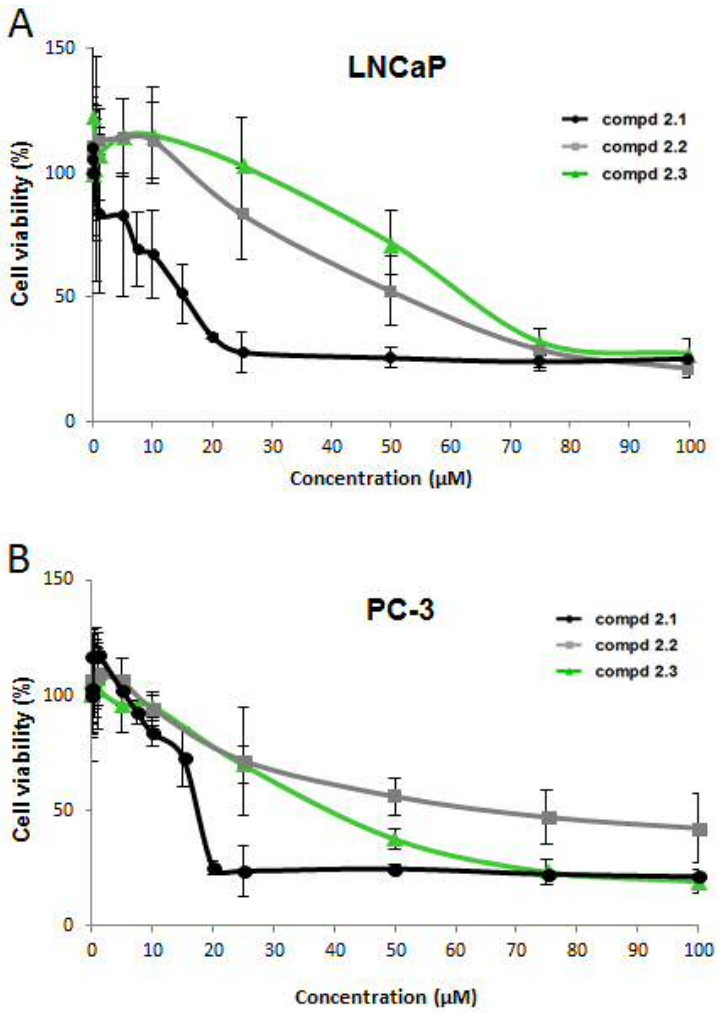

Figure 14. Chromenopyrazolediones **2.1–2.3** decrease human cancer cell viability. Human prostate cancer LNCaP (A) and PC-3 (B) cells were incubated for 48 h with increasing doses of the tested compounds. Cell viability was determined by MTT. Data are the mean ± SD of two different experiments performed in triplicate.

3.6.2 Mechanism of action

To study the effect of the chromenopyrazoledione **2.1** on the cell cycle of prostate cells, flow cytometry analysis were carried out. Results shown in figure 15 demonstrate that **2.1** increased the amount of cells in the sub G_0/G_1 phase of the cell cycle. This result suggests that **2.1** induces growth arrest and cell death.

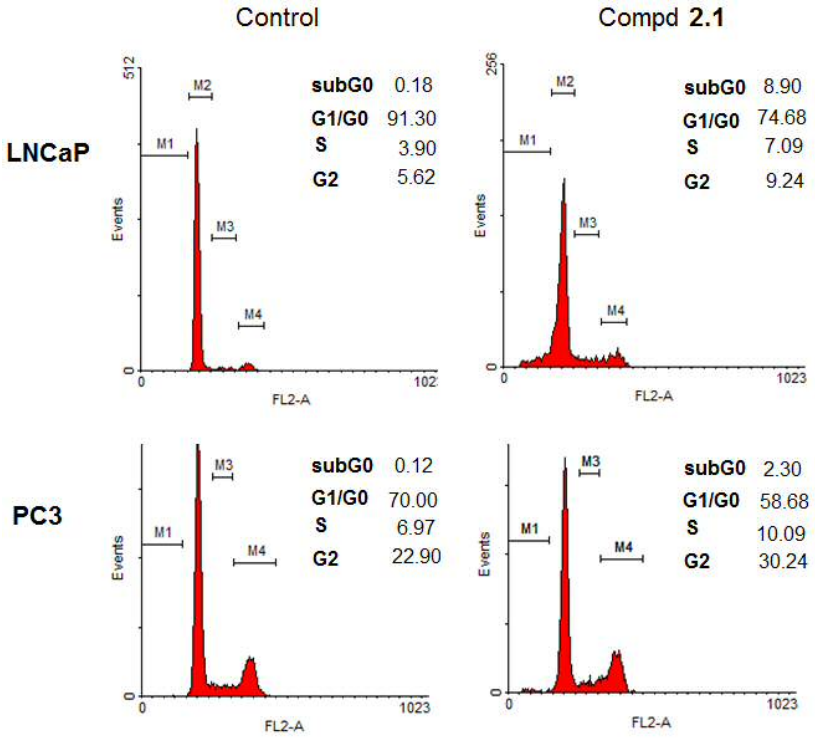

Figure 15. Chromenopyrazoledione **2.1** induces cell cycle arrest in human prostate cancer cells. Cell cycle analysis of human prostate LNCaP and PC-3 cells treated with the IC_{50} (15 μM) of **2.1** for 24 h. Cells were stained with IP and analyzed by flow cytometry. Figure is representative of other two performed in duplicate.

In order to quantify the percentage of apoptotic cells after drug treatment, LNCaP and PC-3 cells were stained with Annexin V-FITC/PI. Annexin V-FITC is a fluorescent conjugate (fluorescein isothiocyanate) of annexin, a protein with high affinity for cell membrane phosphatidyl serine located on the surface of cells undergoing apoptosis. Detection was then analysed by flow cytometry. Results showed that the rate of late apoptotic cells (figure 16: Annexin V-FITC positive/PI positive, upper right quadrant) in **2.1**-treated cells was statistically increased compared to the control cells. Early apoptotic cells (Annexin V-FITC positive/PI negative) were nearly 6 % in

LNCaP cells and nearly 4% in PC-3 cells. These findings indicate that **2.1** induces a significant percentage of apoptosis in prostate cancer cells being more efficient in promoting apoptosis in the androgen-sensitive LNCaP cell line.

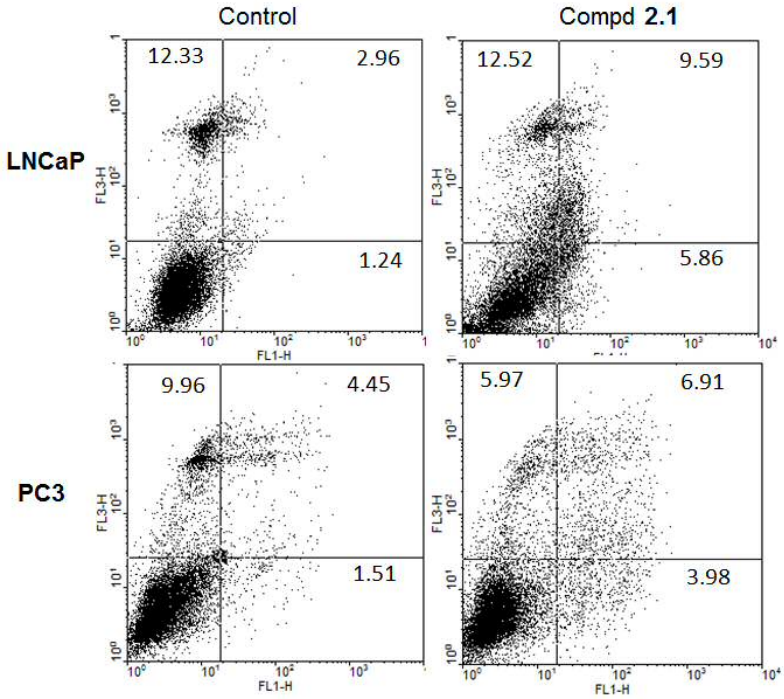

Figure 16. Chromenopyrazoledione **2.1** induces apoptosis in human prostate cancer cells. Evaluation of apoptosis by annexin V-FITC/PI staining followed by flow cytometric analysis. Representative plots of annexin V-FITC/PI staining of LNCaP or PC-3 cells cultured in the presence of the IC_{50} (15 μM) of **2.1** for 24 h are shown. Data showing the percentage of late apoptotic cells (upper right quadrant) are the mean ± SD of three different experiments performed in duplicate.

With the purpose of further studying the underlying molecular mechanism of **2.1**-induced prostate cell death, cell viability was assayed in presence of cannabinoid antagonists and antioxidant. A peroxisome proliferator-activated receptor gamma (PPARγ) antagonist was also tested since involvement of PPARγ receptor in the cannabinoid-induced inhibition of prostate cancer cells growth have been suggested.[148]

The CB_1R antagonist SR141716 (SR1, also named rimonabant), the CB_2 antagonist SR144528 (SR2), the antioxidant *N*-acetylcysteine (NAC), and the PPARγ antagonist GW 9662 were tested against LNCaP cells to confirm that they do not have any effect on the cellular viability by themselves.

Moreover, LNCaP cells pre-treated with SR1, SR2, NAC, or GW 9662 (1h before addition of our compound) were challenged with **2.1** (IC_{50} dose) and incubated for 48h. MTT cell viability assays showed that the CB_1R antagonist as well as the PPARγ antagonist and the antioxidant were able to significantly reduce the inhibition of cell viability induced by **2.1** (figure 17). These results indicate that chromenopyrazoledione **2.1** inhibits cell viability through a mechanism involving oxidative stress, PPARγ receptors and partially CB_1Rs. It is noteworthy that only SR1 and not SR2 prevent the antiproliferative effect of **2.1** in LNCaP cells albeit **2.1** exhibits higher affinity for CB_2R than for CB_1R. This fact might be due to a low expression of CB_2R in LNCaP cells as previously observed in this type of cancer.[146] The antioxidant NAC did not only prevent **2.1**-induced cell death but also slightly increased cell viability.

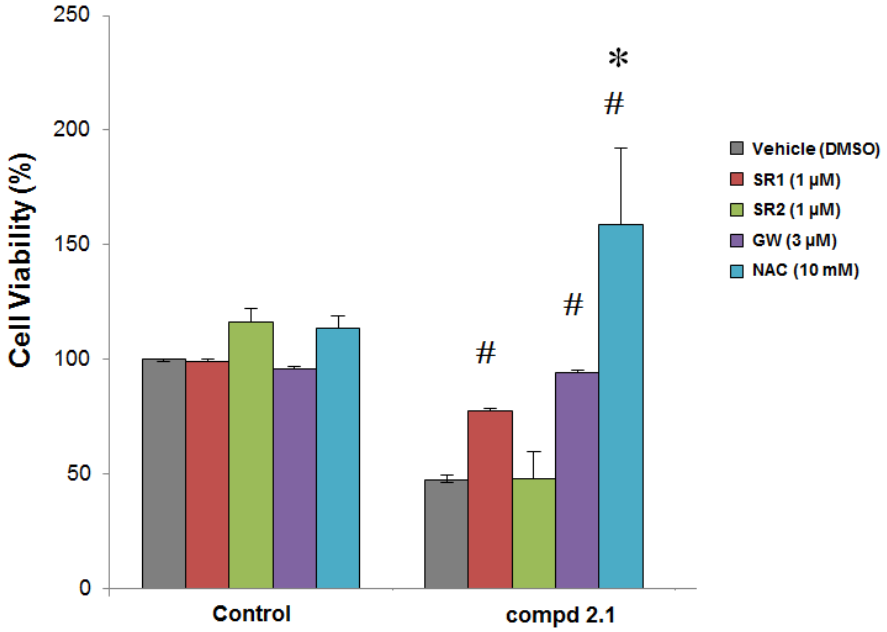

Figure 17. Signalling pathways involved in antiproliferative effect produced by compound **2.1**. LNCaP cells were incubated for 48 h with vehicle (control) or with **2.1** at IC_{50} dose (15 µM) in presence or not of different inhibitors (CB_1R antagonist, SR1; CB_2R antagonist, SR2; PPARγ antagonist, GW9662; and the antioxidant N-acetylcysteine NAC). Cell viability was determined by MTT. Results represent the mean ± SEM of four different experiments performed in duplicate. *p≤ 0,05 compared with Student's test *vs* NAC treated cells and #p≤ 0,05 compared with Student's test *vs* the compound alone.

3.6.3 Antitumor activity *in vivo*

To investigate the ability of compound **2.1** to inhibit prostate tumor growth *in vivo*, tumor xenografts were generated by subcutaneous inoculation of LNCaP or PC-3 cells in nude mice. Mice were daily treated with vehicle (control), or 2 mg/kg of **2.1** intraperitoneally administered for 15 days. As shown in figure 18, treatment with **2.1** almost completely blocked the growth of LNCaP tumors whereas it inhibited the growth of PC-3 tumors by 40 %. The final tumor volume was smaller in all **2.1**-treated mice.

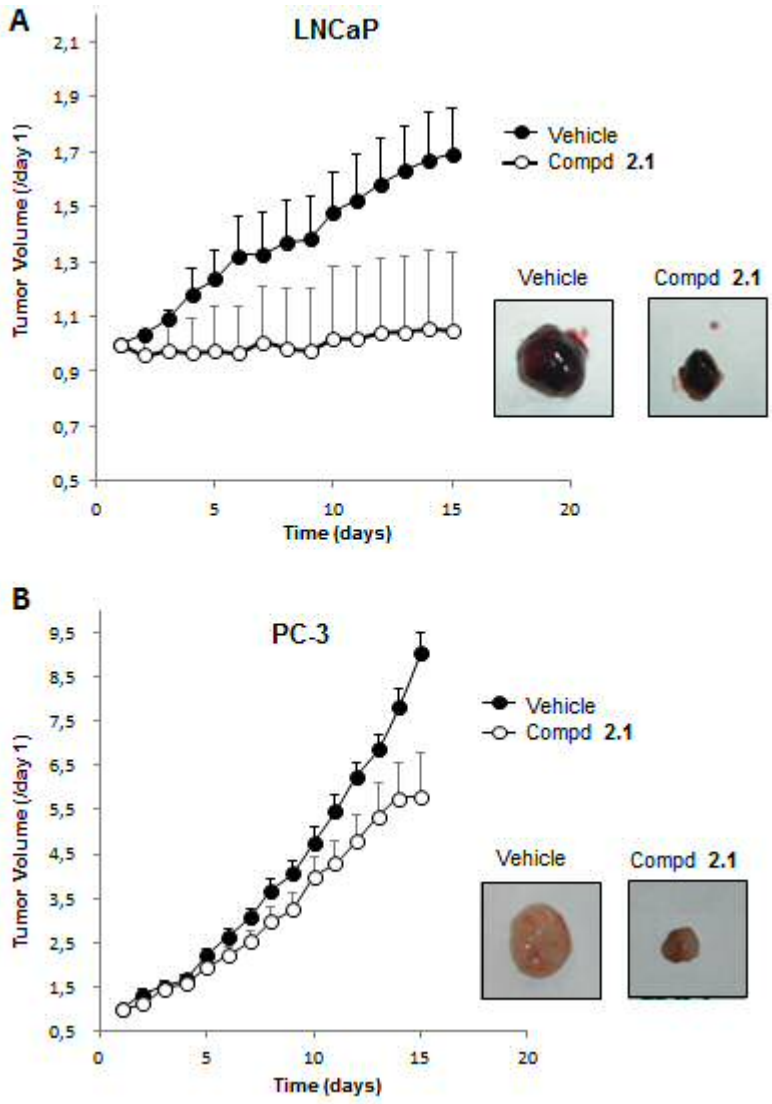

Figure 18. *In vivo* antitumoral effect of compound **2.1**. Athymic nude mice were injected s.c. in the right flank with either LNCaP (A) or PC-3 (B) cells and four weeks later (day 0) treated during 15 days with vehicle (control) or 2 mg/kg of **2.1**. Treatments were administered intraperitoneally every day. Tumor growth curves are represented in the graph. Results represent the mean ± SEM of eight mice in each group. A representative dissected tumor after the treatment is shown on the right.

4. Discussion and conclusions

Cancer treatment is among the most promising therapeutic uses for cannabinoids.[26] Numerous pharmacological and biochemical studies exert their antitumor actions in different cell and animal models of cancer[31,102,149,150] However, as commented in the introduction of this chapter, only a pilot clinical trial has been reported so far,[81] whereas a few more are presently in progress.

Since cancer is a complex multifactorial physiopathology triggered by dysregulation of diverse cellular systems, successful cancer treatments should involve the modulation of multiple signalling pathways using combinations of different agents with different mechanisms of action[126,128] Within this context, we associated the cytotoxic potential of quinones with the antiproliferative properties of cannabinoids in a single molecule.

Due to the versatility of the chromenopyrazole scaffold for cannabinoid ligands, as previously reported in chapter 1, we next explored its quinone derivatives as dual acting anticancer agents. Thus, *para*- and *ortho*-chromenopyrazolediones (**2.1–2.6**) were prepared by regioselective oxidation of the corresponding chromenopyrazoles with the appropriate hypervalent iodine reagent. These compounds were able to bind to cannabinoid receptors which make them the first quinones related to cannabinoid structure as cannabinoid ligands. Indeed, the cannabinoid-quinones reported in the literature which derive from oxidation of phytocannabinoids, were not able to modulate CB_1R or CB_2R.[122] Moreover, *ortho*-quinones (**2.4**-**2.6**) revealed fully selectivity for the *h*CB_2R. Thus, they are devoid of the centrally mediated CB_1R effects related to psychotropic activity. This full CB_2 receptor selectivity represents a high value for potential clinical application. Regarding the *para*-quinone chromenopyrazoles (**2.1**-**2.3**), they showed to be mixed CB_1R/CB_2R ligands with moderate but significant affinity for both receptor types.

To reduce the risk of late-stage failure, *in silico* approaches[136,137] of absorption, distribution, metabolism, and excretion (ADME) gave predictive properties of these cannabinoid-quinones.

Thus, the physicochemical descriptors calculated for compounds **2.1**-**2.6** suggest a satisfactory druggability profile.

We focussed the antitumor activity studies on two types of cancer, triple negative breast cancer and prostate cancer. In what concerns breast cancer, all the *para*- and *ortho*-quinone cannabinoids (**2.1**-**2.6**) displayed potent antiproliferative effects on triple-negative MDA-MB-231 breast cancer cells as the same extent than Δ^9-THC (IC_{50} = 5 μM) in the same cell line.[35]. However, *ortho*-quinone derivatives have the advantage of lacking CB_1R-mediated psychotropic effects. It is why we further concentrated our studies on the most potent of the *ortho*-quinone series, compound **2.6**. Considering that triple negative breast cancer as most of breast cancer types, is heterogeneous, the selected compound was tested in other three different triple negative cell lines (SUM149, SUM159 and MDA-MB-468) for which it showed antiproliferative profiles.

We next oriented our research on validating the proposed cannabinoid/ROS concept by studying the mechanism of action of compound **2.6**. Indeed, the antiproliferative effect of **2.6** has been shown to be mediated by CB_2R activation and through the induction of oxidative stress. We also proved that the putative cannabinoid receptor GPR55,[93,151,152] highly expressed in the triple-negative MDA-MB-231 cell line, was not involved in compound **2.6** antitumor action.

Two other concerns needed to be taken into consideration as it is done for most of antitumor agents: the selectivity for breast cancer cells *versus* normal breast cells and the cellular mechanism underlying this antiproliferative effect. Interestingly, compound **2.6** decreased the viability of breast cancer cells and did not affect normal mammary epithelial cell viability. This selectivity could be due to the cannabinoid or the ROS nature of the compound. The selective toxicity of cannabinoids towards cancer cells *versus* their non-transformed counterparts was previously observed in phytocannabinoids such as Δ^9-THC.[35,143] In what concerns the quinone nature of the compound, quinones are well-known to act as reactive oxygen species (ROS) and might cause damage to cancer cells but also to normal cells. On the one hand, modulation of oxidative stress is considered an anticancer strategy. Since the redox status of cancer cells differs from normal cells, tumor cells are

more sensitive to oxidative stress than normal cells. On the other hand, high ROS levels might be detrimental for normal cells as reviewed recently by Gorrini *et al.*[115] In our system, compound **2.6** proved to be very efficient in reducing the viability of cancer cells in a concentration range that did not affect the viability of non-transformed cells.

The antitumor effect of **2.6** was reproduced *in vivo* in tumor xenografts (MDA-MB-231) upon 4 weeks of treatment (2 mg/kg). The lack of toxicity of compound **2.6** observed in cells was further confirmed *in vivo* by histological analysis of different organs such as liver, spleens or heart after treatment.

From these data and concerning triple negative breast cancer, we can conclude that cannabinoid-quinone **2.6** showed encouraging efficacy in this proof-of-concept study.[153,154]

The other target that we considered for our quinones is prostate cancer. As commented earlier, the CB_1R plays a major role in prostate cancer process; it is why we selected the mixed CB_1R/CB_2R *para*-chromenopyrazolediones **2.1**-**2.3** for these studies. In cell viability assays, compounds **2.1**-**2.3** exerted antiproliferative effects in androgen-dependent (LNCaP) and androgen-refractory (PC-3) prostate cancer cell lines, chromenopyrazole **2.1** displaying the highest efficiency and potency in both lines. Compound **2.1** induced cell death through apoptosis as studied by flow cytometry, being more efficient in the androgen-sensitive LNCaP cell line. At molecular mechanistic level, cytotoxicity of **2.1** has been shown to be mediated through cannabinoid receptor TYPE 1 and oxidative stress. In addition to CB_1R and ROS pathways, participation of PPARγ receptor in this underlying mechanism has been explored, since involvement of PPARγ receptor in the cannabinoid-induced inhibition of prostate cancer cells growth has been recently reported.[148,155,156] It was then no surprising that PPARγ receptors had been found to be involved in the mechanism of action of the *para*-quinone cannabinoid **2.1**.

The *in vivo* studies of the *para*-quinone cannabinoid **2.1** corroborate the results obtained *in vitro*. Treatment with **2.1** (2 mg/kg) totally inhibited the growth of androgen-dependent prostate cancer (LNCaP) tumor compared with control. In relation to androgen-refractory prostate cancer (PC-3),

the tumor size decreased significantly after treatment with **2.1**. Cytotoxicity has not been evaluated on this compound, however concentrations used in our *in vivo* study are similar to those used with cannabidiol derived quinone[124] and far from the doses capable to produce toxicity.[157] Concerning our studies focussed on prostate cancer target, we can conclude that the cannabinoid-quinone **2.1** provides experimental arguments to the cannabinoid/ROS proof-of-concept.[158,159]

In conclusion, the studies reported in this chapter provide evidence supporting that quinones derived from chromenopyrazole exert remarkable antiproliferative properties *in vitro* and *in vivo* through cannabinoid receptor pathway and ROS production. We showed that the selected *ortho*-chromenopyrazoledione **2.6** induces triple-negative breast cancer cell death by apoptosis via CB_2R activation and ROS production, and lacks of toxic effects. We also report a potent anticancer agent (**2.1**) with *in vitro* and *in vivo* activity against hormone-sensitive prostate cancer triggering apoptosis through a mechanism that involves oxidative stress, CB_1R and PPARγ.

Both cannabinoid-quinones are good candidates for further development as new anticancer drugs.

5. Experimental section

Chemistry:

General methods and materials. All commercially available reagents and solvents were used without further purification. Products were purified using flash column chromatography (Merck Silica gel 60, 230-400 mesh). The purity of the compounds as determined by HPLC-MS and elemental analyses is > 95%. HPLC-MS analysis was performed on a Waters 2695 HPLC system equipped with a photodiode array 2996 coupled to Micromass ZQ 2000 mass spectrometer (ESI-MS), using a reverse-phase column SunFire™ (C-18, 4.6 x 50 mm, 3.5 μm) in gradient A: CH_3CN/0.1% formic acid, B: H_2O/0.1% formic acid visualizing at λ = 254 nm. Flow rate was 1 mL/min. Elemental analyses of the compounds were performed using a LECO CHNS-932 apparatus. Deviations of the elemental analysis results from the calculated are within ± 0.4%. ^1H, ^{13}C, HSQC and HMBC-NMR spectra were recorded on a Bruker 300 (300 and 75 MHz) at 25 °C. Samples were prepared as solutions in deuterated solvent and referenced to internal non-deuterated solvent peak. Chemical shifts were expressed in ppm (δ) downfield of tetramethylsilane. Coupling constants are given in hertzs (Hz). Melting points were measured on a MP 70 Mettler Toledo apparatus. Chromenopyrazoles **1.4–1.6** were prepared according to procedures described in chapter 1.

7-(1,1-Dimethylheptyl)-1,4-dihydro-4,4-dimethylchromeno[4,3-*c*]pyrazol-6,9-dione (2.1). To a solution of 7-(1,1-dimethylheptyl)-1,4-dihydro-4,4-dimethylchromeno[4,3-*c*]pyrazol-9-ol (**1.4**) (130 mg, 0.38 mmol) in MeCN/ H_2O (6:1, 2.5 mL) a solution of BTIB (490 mg, 1.14 mmol) in 2 mL of MeCN/ H_2O (6:1) was added dropwise. The reaction mixture was stirred at room temperature for 15 min, neutralized with aqueous $NaHCO_3$ satured solution, and extracted with diethyl ether. The organic layer was washed with H_2O, dried over $MgSO_4$ and concentrated. Column chromatography on silica gel (hexane/EtOAc, 1:2) afforded the title compound as a red solid (29

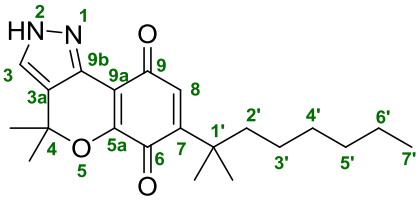

mg, 21%); mp: 85–86 ºC; ^{1}H-NMR (300 MHz, $CDCl_3$) δ: 8.41 (br s, 1H, NH), 7.40 (s, 1H, 3-H), 6.69 (s, 1H, 8-H), 1.59–1.57 (br s, 6H, $OC(CH_3)_2$), 1.55–1.48 (m, 2H, 2´-H), 1.30 (s, 6H, $C(CH_3)_2$), 1.27–1.23 (m, 6H, 3´-H, 4´-H and 5´-H), 1.19–1.12 (br s, 2H, 6´H), 0.86–0.82 ppm (m, 3H, 7´-H); ^{13}C-NMR (75 MHz, $CDCl_3$) δ: 184.1 (6-C), 180.9 (9-C), 160.2 (5a-C), 161.2 (7-C), 137.8 (9b-C), 132.0 (8-C), 130.4 (9a-C), 129.5 (3-C), 113.8 (3a-C), 78.6 ($OC(CH_3)_2$), 43.3 (2´-C), 30.9 (1´-C), 29.6, 28.7 y 27.4 (3´-C, 4´-C and 5´-C); 25.1 ($C(CH_3)_2$), 23.2 ($OC(CH_3)_2$), 21.8 (6´-C), 14.0 ppm (7´-C); HPLC-MS: [A, 70%→100%], t_R: 3.37 min (98%), MS (ES^+, m/z) 357 $[M+H]^+$; Anal. Calcd. for $C_{21}H_{28}N_2O_3$: C 70.76%, H 7.92%, found: C 71.03%, H 8.24%.

7-(1,1-Dimethylheptyl)-2,4-dihydro-2,4,4-trimethylchromeno[4,3-*c*]pyrazol-6,9-dione (2.2). Prepared from 7-(1,1-dimethylheptyl)-2,4-dihydro-2,4,4-trimethylchromeno[4,3-*c*]pyrazol-9-ol (**1.5b**) (35 mg, 0.1 mmol) and BTIB (129 mg, 0.3 mmol) by following the procedure described for **2.1**. Column chromatography on silica gel (hexane/EtOAc, 1:4) afforded **2.2** as a red solid (12 mg, 33%); mp: 89–90 ºC; ^{1}H-NMR (300 MHz, $CDCl_3$) δ: 7.36 (s, 1H, 3-H), 6.61 (s, 1H, 8-H), 3.95 (s, 3H, NCH_3), 1.84 (s, 6H, $OC(CH_3)_2$), 1.70–1.65 (br s, 2H, 2´-H), 1.33 (s, 6H, $C(CH_3)_2$), 1.26–1.20 (br s, 6H, 3´-H, 4´-H and 5´-H), 1.16–1.13 (m, 2H, 6´H), 0.85 ppm (t, J = 6,9 Hz, 3H, 7´-H); ^{13}C-NMR (75 MHz, $CDCl_3$) δ: 186.2 (6-C), 181.4 (9-C), 160.2 (5a-C), 155.0 (7-C), 139.6 (9b-C), 135.4 (8-C), 129.3 (9a-C), 126.9 (3-C), 115.7 (3a-C), 81.5 ($OC(CH_3)_2$), 43.0 (NCH_3), 40.9 (2´-C), 31.7 (1´-C), 30.8, 29.3 and 28.1 (3´-C, 4´-C and 5´-C), 27.5 ($C(CH_3)_2$), 23.4 ($OC(CH_3)_2$), 22.9 (6´-C), 14.6 ppm (7´-C); HPLC-MS: [A, 80%→100%], t_R: 2.43 min (99%), MS (ES^+, m/z) 371 $[M+H]^+$; Anal. Calcd. for $C_{22}H_{30}N_2O_3$: C 71.32%, H 8.16%, found: C 70.98%, H 8.31%.

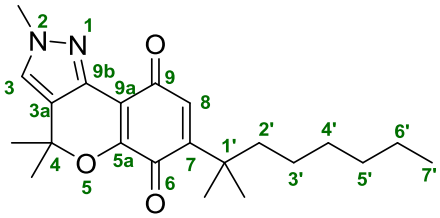

7-(1,1-Dimethylheptyl)-2-ethyl-2,4-dihydro-4,4-dimethylchromeno[4,3-*c*]pyrazol-6,9-dione (2.3). Prepared from 7-(1,1-dimethylheptyl)-2-ethyl-2,4-dihydro-4,4-dimethylchromeno[4,3-*c*]pyrazol-9-ol (**1.6b**) (61 mg, 0.16 mmol) and BTIB (212 mg, 0.49 mmol) by following the procedure described for **2.1**. Column chromatography on silica gel (hexane/EtOAc, 2:3) afforded **2.3** as a red

solid (22 mg, 36%); mp: 83–84 ºC; ^{1}H-NMR (300 MHz, $CDCl_3$) δ: 7.15 (s, 1H, 3-H), 6.50 (s, 1H, 8-H), 4.28 (q, J = 7.4 Hz, 2H, NCH_2CH_3), 1.72 (s, 6H, $OC(CH_3)_2$), 1.61–1.52 (m, 2H, 2´-H), 1.49 (t, J = 7.4 Hz, 3H, NCH_2CH_3), 1.30 (s, 6H, $C(CH_3)_2$), 1.23–1.10 (m, 8H, 3´-H, 4´-H, 5´-H and 6´-H), 0.89 ppm (t, J = 6.9 Hz, 3H, 7´-H); ^{13}C-NMR (75 MHz, $CDCl_3$) δ: 183.4 (6-C), 180.5 (9-C), 152.4 (5a-C), 151.4 (7-C), 137.2 (9b-C), 133.1 (8-C), 122.1 (3-C), 120.9 (3a-C), 110.6 (9a-C), 79.9 ($OC(CH_3)_2$), 46.6 (NCH_2CH_3), 39.7 (2´-C), 37.6 (1´-C), 31.6, 29.7 and 28.7 (3´-C, 4´-C and 5´-C), 26.6 ($OC(CH_3)_2$), 24.1 ($C(CH_3)_2$), 21.5 (6´-C), 14.6 (NCH_2CH_3), 13.0 ppm (7´-C); HPLC-MS: [A, 70%→100%], t_R: 3.86 min (96%), MS (ES^+, m/z) 385 $[M+H]^+$; Anal. Calcd. for $C_{23}H_{32}N_2O_3$: C 71.84%, H 8.39%, found: C 72.01%, H 8.62%.

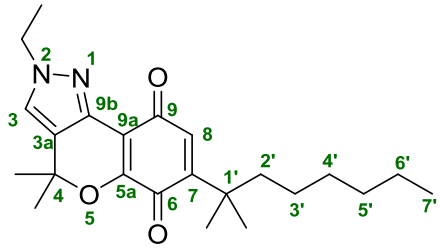

7-(1,1-Dimethylheptyl)-1,4-dihydro-4,4-dimethylchromeno[4,3-*c*]pyrazol-8,9-dione (2.4). To a solution of 7-(1,1-dimethylheptyl)-1,4-dihydro-4,4-dimethylchromeno[4,3-*c*]pyrazol-9-ol (**1.4**) (30 mg, 0.08 mmol) dissolved in DMF (1.5 mL) was added solid IBX (36 mg, 0.13 mmol), and the resulting mixture was stirred at room temperature for 30 min. The mixture was then extracted with EtOAc, washed with water and brine. The solvent was removed under vacuum. The resulting residue was purified by chromatography on a silica gel column (hexane/EtOAc, 2:1) to furnish the title compound as a red solid (9 mg, 29% yield); mp: 89–90 ºC; ^{1}H-NMR (300 MHz, $CDCl_3$) δ: 8.03–7.98 (br s, 1H, NH), 7.66 (s, 1H, 3-H), 7.12 (s, 1H, 6-H), 1.65 (s, 6H, $OC(CH_3)_2$), 1.51–1.49 (m, 2H, 2´-H), 1.37 (s, 6H, $C(CH_3)_2$), 1.29–1.27 (m, 6H, 3´-H, 4´-H, 5´-H), 1.21–1.18 (m, 2H, 6´H), 0.84 ppm (t, J = 7.1 Hz, 3H, 7´-H); ^{13}C-NMR (75 MHz, $CDCl_3$) δ: 180.1 (9-C), 179.6 (8-C), 164.4 (5*a*-C), 163.8 (7-C), 142.0 (6-C), 138.5 (9*b*-C), 131.5 (3-C), 130.3 (3*a*-C), 110.9 (9*a*-C), 79.7 ($OC(CH_3)_2$), 45.9 (2´-C), 31.2 (1´-C), 30.0, 29.3 y 28.1 (3´-C, 4´-C and 5´-C); 25.8 ($C(CH_3)_2$), 24.9 ($OC(CH_3)_2$), 22.5 (6´-C), 13.6 ppm (7´-C); HPLC-MS: [A, 80% →100%], t_R: 2.03 min (99%), MS (ES^+, m/z) 357 $[M+H]^+$. Anal. Calcd. for $C_{21}H_{28}N_2O_3$: C 70.76%, H 7.92%, found: C 70.41%, H 7.57%.

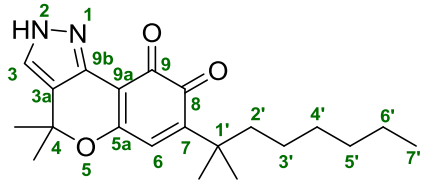

7-(1,1-Dimethylheptyl)-2,4-dihydro-2,4,4-trimethylchromeno[4,3-*c*]pyrazol-8,9-dione (2.5). Prepared from 7-(1,1-dimethylheptyl)-2,4-dihydro-2,4,4-trimethylchromeno[4,3-*c*]pyrazol-9-ol (**1.5b**) (45 mg, 0.12 mmol) and IBX (53 mg, 0.18 mmol) by following the procedure described for **2.4**. Column chromatography on silica gel (hexane/EtOAc, 1:1) afforded **2.5** as a red solid (11 mg, 24%); mp: 85–86 ºC; ^{1}H-NMR (300 MHz, $CDCl_3$) δ: 7.28 (s, 1H, 3-H), 6.73 (s, 1H, 6-H), 3.89 (s, 3H, NCH_3), 1.64 (s, 6H, $OC(CH_3)_2$), 1.57–1.55 (br s, 2H, 2´-H), 1.29 (s, 6H, $C(CH_3)_2$), 1.22–1.18 (m, 6H, 3´-H, 4´-H, 5´-H), 1.10–1.03 (m, 2H, 6´H), 0.81 ppm (t, J = 7.0 Hz, 3H, 7´-H); ^{13}C-NMR (75 MHz, $CDCl_3$) δ: 182.3 (9-C), 180.6 (8-C), 165.1 (5*a*-C), 160.3 (7-C), 139.8 (9*b*-C), 137.0 (6-C), 132.2 (3-C), 129.9 (3*a*-C), 113.8 (9*a*-C), 83.0 ($OC(CH_3)_2$), 42.3 (NCH_3), 41.0 (2´-C), 33.1 (1´-C), 32.0, 30.9 and 29.6 (3´-C, 4´-C and 5´-C), 28.1 ($C(CH_3)_2$), 22.9 ($OC(CH_3)_2$), 21.8 (6´-C), 14.1 ppm (7´-C); HPLC/MS: [A, 80%→100%], t_R: 2.07 min (96%), MS (ES^+, m/z) 371 $[M+H]^+$. Anal. Calcd. For $C_{22}H_{30}N_2O_3$: C 71.32%, H 8.16%, found: C 71.19%, H 7.82%.

7-(1,1-Dimethylheptyl)-1-ethyl-1,4-dihydro-4,4-dimethylchromeno[4,3-*c*]pyrazol-8,9-dione (2.6). Prepared from 7-(1,1-dimethylheptyl)-1-ethyl-1,4-dihydro-4,4-dimethylchromeno[4,3-*c*]pyrazol-9-ol (**1.6a**) (20 mg, 0.05 mmol) and IBX (22 mg, 0.08 mmol) by following the procedure described for **2.4**. Column chromatography on silica gel (hexanes/EtOAc, 4:1) afforded **2.6** as a red solid (6 mg, 30%); mp: 94–95 ºC; ^{1}H- NMR (300 MHz, $CDCl_3$) δ: 7.49 (s, 1H, 3-H), 7.11 (s, 1H, 6-H), 4.04 (q, J = 7.1 Hz, 2H, NCH_2CH_3), 1.49 (s, 6H, $OC(CH_3)_2$), 1.35 (t, J = 7.1 Hz, 3H, NCH_2CH_3), 1.30–1.26 (m, 2H, 2´-H), 1.22 (s, 6H, $C(CH_3)_2$), 1.19–1.16 (m, 6H, 3´-H, 4´-H, 5´-H), 1.03–1.01 (br s, 2H, 6´-H), 0.87 ppm (t, J = 6.9 Hz, 3H, 7´-H); ^{13}C-NMR (75 MHz, $CDCl_3$) δ: 182.9 (9-C), 181.0 (8-C), 161.5 (5*a*-C), 159.3 (7-C), 138.2 (9*b*-C), 135.9 (6-C), 131.0 (3-C), 129.7 (3*a*-C), 112.3 (9*a*-C), 80.1 ($OC(CH_3)_2$), 47.1 (NCH_2CH_3), 40.6 (2´-C), 35.3 (1´-C), 31.1, 29.8 and 28.5 (3´-C, 4´-C and 5´-C), 27.0 ($OC(CH_3)_2$),

25.3 (C(CH_3)$_2$), 22.1 (6´-C), 14.9 (NCH$_2$$CH_3$), 13.7 ppm (7´-C); HPLC-MS: [A, 80%→100%], t_R: 3.97 min (98%), MS (ES$^+$, m/z) 385 [M+H]$^+$. Anal. Calcd. for $C_{23}H_{32}N_2O$: C 71.84%, H 8.39%, found: C 71.93%, H 8.06%.

Electrochemistry:

Cyclic voltammetry. DMSO (spectroscopy grade) was obtained from Aldrich. Tetrabuthylammonium perchlorate (TBAP), used as supporting electrolyte, was obtained from Fluka. Cyclic voltammetry was carried out using a Metrohm 693 VA instrument with a 694 VA Stand convertor and a 693 VA Processor, in DMSO (ca. 1.0×10−3 mol L−1), under a nitrogen atmosphere at room temperature, with TBAP (ca. 0.1 mol L−1), using a three-electrode cell. A mercury-dropping electrode was used as the working electrode, a platinum wire as the auxiliary electrode, and saturated calomel as the reference electrode.

ESR spectroscopy. ESR spectra were recorded in the X band (9.7 GHz) using a Bruker ECS 106 spectrometer with a rectangular cavity and 50 kHz field modulation. The nitro radicals were generated by electrolytic reduction *in situ* under the same conditions of temperature, atmosphere and concentrations stated at the voltammetric experiment. Simulations of the spectra were made using the Simfonia Version 1.25 software. The hyperfine splitting constants were estimated to be accurate within 0.05 G.

In silico ADME calculations:

A set of 34 physico-chemical descriptors was computed using QikProp version 3.5 integrated in Maestro (Schrödinger, LLC, New York, USA). The QikProp descriptors are shown in table 3. The 3D conformations used in the calculation of QikProp descriptors were generated using the program Spartan ´08 (Wave function, Inc., Irvine CA) as follows: the structure of each molecule was built from the fragment library available in the program. Then, *ab initio* energy minimizations of each structure at the Hartree-Fock 6-31G* level were performed. A conformational search was next implemented using Molecular Mechanics (Monte Carlo method) followed by a minimization of the

energy of each conformer calculated at the Hartree-Fock 6-31G* level. The global minimum energy conformer of each compound was used as input for ADME studies with QikProp.

Pharmacological assays:

Cannabinoid binding experiments. Membranes from transfected cells with human CB_1 or CB_2 expressed cannabinoid receptors (RBHCB1M400UA and RBXCB2M400UA) were supplied by Perkin-Elmer Life and Analytical Sciences (Boston, MA). The protein concentration for the CB_1R membranes was 8.0 mg/mL, whereas for the CB_2R membranes was 4.0 mg/mL or 3.6 mg/mL depending on the batch. The commercial membranes were diluted (approximatively 1:20) with the binding buffer (50 mM TrisCl, 5 mM $MgCl_2.H_2O$, 2.5 mM EDTA, 0.5 mg/mL BSA and pH = 7.4 for CB_1 binding; 50 mM TrisCl, 5 mM $MgCl_2.H_2O$, 2.5 mM EGTA, 1 mg/mL BSA and pH = 7.5 for CB_2 binding). The final membrane protein concentration was 0.4 mg/mL of incubation volume and 0.2 mg/mL of incubation volume for the CB_1R and the CB_2R assays, respectively. The radioligand used was [^{3}H]-CP55940 (PerkinElmer) at a concentration of membrane K_D x 0.8 nm, and the final volume was 200 μL for CB_1R binding and was 600 μL for CB_2R binding. 96-Well plates and the tubes necessary for the experiment were previously siliconized with Sigmacote (Sigma).

Membranes were resuspended in the corresponding buffer and were incubated with the radioligand and each compound (10^{-4}-10^{-11} M) for 90 min at 30 ºC. Non-specific binding was determined with 10 μM WIN55,212 and 100 % binding of the radioligand to the membrane was determined by its incubation with membrane without any compound. Filtration was performed by a Harvester® filtermate (Perkin-Elmer) with Filtermat A GF/C filters pretreated with polyethylenimine 0.05%. After filtering, the filter was washed nine times with binding buffer, dried and a melt-on scintillation sheet (Meltilex™ A, Perkin Elmer) was melted onto it. Then, radioactivity was quantified by a liquid scintillation spectrophotometer (Wallac MicroBeta Trilux, Perkin-Elmer). Competition binding data were analyzed by using GraphPad Prism program and K_i values are expressed as mean ± SD of at least three experiments performed in triplicate for each point.

***In vitro* antiproliferative assays**:

Cell culture and viability. The cell lines used in this work were obtained from the American Type Culture Collection (ATCC, Manasas, VA, USA). Prostate LNCaP (ATCC CRL-1740) and PC-3 cells (ATCC CRL-1435) (Rockville, MD, USA) were routinely grown in RPMI 1640 supplemented with 10% fetal calf serum, 100 U/mL penicillin G, 100 μg/mL streptomycin, and 0.25 μg/mL amphotericin B (Invitrogen, Paisley, UK). MDA-MB-231 cells were obtained from the American Type Culture Collection (ATCC; Manassas, VA) and maintained in DMEM supplemented with 10% fetal bovine serum (FBS), 5 units/mL penicillin, and 5 mg/mL streptomycin. SUM149, SUM159, and MDA-MD-468 cells were kindly donated by Dr. Moreno-Bueno (Instituto de Investigaciones Biomédicas Alberto Sols, Madrid, Spain). SUM149 and SUM159 cells were maintained in Ham's F-12 medium with 5% FBS, 5 μg/mL insulin, and 0.5 μg/mL hydrocortisone. MDA-MD-468 was maintained in DMEM with 10% FBS. Human mammary epithelial cells (HMEC) were obtained from Cambrex and grown in mammary epithelial growth medium (Cambrex, East Rutherford, NJ) according to the manufacturer's instructions. In all cell types, low cell passages (between 10 and 20) were used. Experiments were done when cell monolayers were 80% confluent. Cannabinoid ligands were prepared in DMSO. Control incubations had the corresponding DMSO content (considered as 100% of cell viability). Cells were cultured at a density of 5000 cells/cm^2 in a 24-well plate. They were transferred to a serum-free medium or a 0.5% FBS medium (HMEC) at least 6 h before treatment with the compounds at concentrations ranging from 0 to 25 μM (or 0 to 100 μM, depending on the experiment) for 48 h. When indicated, cells were pre-incubated with the antagonists or the antioxidants for 1 h before treatment with the corresponding cannabinoid-quinone (at IC_{50} concentration). Finally, the MTT reduction assay was carried out to evaluate the effects of the different compounds on cell viability and to determine the IC_{50}. Briefly, cells were incubated for 2 h at 37ºC with 0.3 mg/mL of 3-(4,5-dimethylthiazol-2-yl)-2,5-diphenyltetrazolium bromide (MTT, Sigma, St Louis, MO, USA) and then were solubilized with 100 μl isopropanol.

Absorbance at 570 nm was measured with a plate spectrophotometer (ELX 800 Bio-Tek Instruments, INC).

Western Blot Analysis. MDA-MB-231 human breast cancer cells were treated with DMSO (vehicle), or compound **2.1** for two days. Cells were then harvested and lysed. Protein concentrations were quantified by the Bradford method with bovine serum albumin as the standard. Equal amounts of total cellular protein extract (25 μg) were separated by electrophoresis in SDS−polyacrylamide gels (12%) and transferred to PVDF membranes. After blocking with 5% nonfat milk, membranes were incubated at 4°C with the desired primary antibodies overnight at the following dilutions: anti-caspase-3 (1:500 Cell Signaling), and β-actin (1:5000; Sigma). Subsequently, membranes were incubated with appropriate secondary antibodies. Luminograms were obtained with an enhanced chemiluminescence detection kit (Amersham Life Sciences, Arlington Heights, IL) and densitometric analysis was performed with Quantity One software (Bio-Rad, Hercules, CA, USA).

Flow cytometry. Flow cytometry was used to detect apoptotic cells and the distribution of cell cycle. After being cultivated with medium alone or medium containing the indicated stimuli, 10^5 cells in 35 mm culture dish were harvested in tripsin, fixed in 70% ethanol and stained with 0.05 mg/mL Propidium iodide (PI) plus 0.2 mg/mL RNAse to indicate relative DNA content. The sub-G1 peak (DNA content less than 2 N) and cell cycle distribution were measured with FACScan flow cytometer (Beckton Dickinson, CA, Costa Rica). To analyze apoptosis by Anexin V staining, the cells were washed twice with PBS and incubated in 0.5 mL of Binding Buffer (10 mM HEPES pH 7.4, 150 mM NaCl, 2.5 mM $CaCl_2$, 1 mM $MgCl_2$, and 4% BSA), with **4** μg/mL Annexin V-FITC for 15 min. Cells were then washed in PBS and resuspended in Binding Buffer with 0.6 μg/mL iodure propidium, (Calbiochem, USA). 20000 cells of each sample were analyzed by flow cytometry in a FACScan (Beckton Dickinson, CA, Costa Rica).

***In vivo* antitumor assays:**

TNBC xenografts. All procedures involving animals were performed with the approval of the Complutense University Animal Experimentation Committee according to European official regulations. Tumors were induced in nude mice by subcutaneous injection of 5 x10^6 MDA-MB-231 human breast adenocarcinoma cells in PBS. When tumors reached an average size of 200 mm^3, animals were randomly assigned to different groups. At this point, animals started to receive vehicle or compound **2.6** (2 mg/kg/d) in 100 μl of sesame oil thrice a week by intraperitoneal injection. Tumors were routinely measured with an external caliper, and volume was calculated as $(4\pi/3) \times (\text{width}/2)^2 \times (\text{length}/2)$. After 4 weeks of treatment, animals were sacrificed. Tumors were excised, weighted and snap frozen for further analysis. Organs (liver, spleen, heart and lungs) were also collected and fixed in 4% PFA for histopathological analysis by H&E staining.

Prostate cancer xenografts. Athymic nude (nu/nu) (BALB/cOlaHsd-Foxn1^{nu}) five week-old male mice were obtained from Harlan Iberica Laboratory (Barcelona, Spain) and maintained under specific pathogen-free conditions with the approval of the Institutional Ethical Research Committee of Alcala University. All animal studies were conducted in accordance with the Spanish institutional regulation for the housing, care and use of experimental animals and met the European Community directives regulating animal research. Recommendations made by the United Kingdom co-ordinating Committee on Cancer Research (UKCCCR) have been kept carefully. To study the *in vivo* antitumor activity of **2.1,** prostate tumors were induced in athymic mice nu/nu (BALB/cOlaHsd-Foxn1^{nu}). Mice were injected subcutaneously in the right flank with 10 x 10^6 LNCaP or PC-3 cells in 0.1 mL of PBS + 0.5% BSA. Two weeks after transplantation, tumors had grown to an average volume of 150 mm^3. Mice were then divided into different experimental groups of 8 animals each, which were treated with 2.0 mg/kg of compound **2.1** intraperitoneally injected. The injection was repeated every day and treatment was continued for 15 days. Tumor volumes were monitored every day using calliper measurements and were calculated by the formula: $(4\pi/3)$x (w/2)2x (l/2). At the end of the treatment the animals were sacrificed and xenografted tumors were weighted and frozen.

6. References

(1) Jemal, A.; Bray, F.; Center, M. M.; Ferlay, J.; Ward, E.; Forman, D. Global Cancer Statistics. *CA. Cancer J. Clin.* **2011**, *61*, 69–90.

(2) Abrams, D. I.; Guzman, M. Cannabis in Cancer Care. *Clin. Pharmacol. Ther.* **2015**, *97*, 575–586.

(3) Tramèr, M. R.; Carroll, D.; Campbell, F. a; Reynolds, D. J.; Moore, R. a; McQuay, H. J. Cannabinoids for Control of Chemotherapy Induced Nausea and Vomiting: Quantitative Systematic Review. *Br. Med. J.* **2001**, *323*, 16–21.

(4) Sharkey, K. a; Darmani, N. a; Parker, L. a. Regulation of Nausea and Vomiting by Cannabinoids and the Endocannabinoid System. *Eur. J. Pharmacol.* **2014**, *722*, 134–146.

(5) Berry, E. M.; Mechoulam, R. Tetrahydrocannabinol and Endocannabinoids in Feeding and Appetite. *Pharmacol. Ther.* **2002**, *95*, 185–190.

(6) Jatoi, A.; Windschitl, H. E.; Loprinzi, C. L.; Sloan, J. A.; Dakhil, S. R.; Mailliard, J. A.; Pundaleeka, S.; Kardinal, C. G.; Fitch, T. R.; Krook, J. E.; Novotny, P. J.; Christensen, B. Dronabinol versus Megestrol Acetate versus Combination Therapy for Cancer-Associated Anorexia: A North Central Cancer Treatment Group Study. *J. Clin. Oncol.* **2002**, *20*, 567–573.

(7) Walsh, D.; Nelson, K. A.; Mahmoud, F. A. Established and Potential Therapeutic Applications of Cannabinoids in Oncology. *Support. Care Cancer* **2003**, *11*, 137–143.

(8) Walker, J. M.; Huang, S. M. Cannabinoid Analgesia. *Pharmacol. Ther.* **2002**, *95*, 127–135.

(9) Pertwee, R. G. Cannabinoid Receptors and Pain. *Prog. Neurobiol.* **2001**, *63*, 569–611.

(10) Mantyh, P. W.; Clohisy, D. R.; Koltzenburg, M.; Hunt, S. P. Molecular Mechanisms of Cancer Pain. *Nat. Rev. Cancer* **2002**, *2*, 201–209.

(11) Campbell, F. A.; Tramèr, M. R.; Carroll, D.; Reynolds, D. J.; Moore, R. A.; McQuay, H. J. Are Cannabinoids an Effective and Safe Treatment Option in the Management of Pain? A Qualitative Systematic Review. *BMJ* **2001**, *323*, 13–16.

(12) Iversen, L.; Chapman, V. Cannabinoids: A Real Prospect for Pain Relief? *Curr. Opin. Pharmacol.* **2002**, *2*, 50–55.

(13) Pertwee, R. G. Emerging Strategies for Exploiting Cannabinoid Receptor Agonists as Medicines. *Br. J. Pharmacol.* **2009**, *156*, 397–411.

(14) Guindon, J.; Lai, Y.; Takacs, S. M.; Bradshaw, H. B.; Hohmann, A. G. Alterations in Endocannabinoid Tone Following Chemotherapy- Induced Peripheral Neuropathy: Effects of Endocannabinoid Deactivation Inhibitors Targeting Fatty-Acid Amide Hydrolase and Monoacylglycerol Lipase in Comparison to Reference Analgesics Following. *Pharmacol. Res.* **2014**, *67*, 94–109.

(15) Pascual, D.; Goicoechea, C.; Suardíaz, M.; Martín, M. I. A Cannabinoid Agonist, WIN 55,212-2, Reduces Neuropathic Nociception Induced by Paclitaxel in Rats. *Pain* **2005**, *118*, 23–34.

(16) Rahn, E. J.; Makriyannis, A.; Hohmann, A. G. Activation of Cannabinoid CB1 and CB2 Receptors Suppresses Neuropathic Nociception Evoked by the Chemotherapeutic Agent Vincristine in Rats. *Br. J. Pharmacol.* **2007**, *152*, 765–777.

(17) Vera, G.; Chiarlone, A.; Cabezos, P. A.; Pascual, D.; Martín, M. I.; Abalo, R. WIN 55,212-2 Prevents Mechanical Allodynia but Not Alterations in Feeding Behaviour Induced by Chronic Cisplatin in the Rat. *Life Sci.* **2007**, *81*, 468–479.

(18) Naguib, M.; Xu, J. J.; Diaz, P.; Brown, D. L.; Cogdell, D.; Bie, B.; Hu, J.; Craig, S.; Hittelman, W. N. Prevention of Paclitaxel-Induced Neuropathy through Activation of the Central Cannabinoid Type 2 Receptor System. *Anesth. Analg.* **2012**, *114*, 1104–1120.

(19) Rahn, E. J.; Zvonok, A. M.; Thakur, G. a; Khanolkar, A. D.; Makriyannis, A.; Hohmann, A. G. Selective Activation of Cannabinoid CB2 Receptors Suppresses Neuropathic Nociception Induced by Treatment with the Chemotherapeutic Agent Paclitaxel in Rats. *J. Pharmacol. Exp. Ther.* **2008**, *327*, 584–591.

(20) Hao, E.; Mukhopadhyay, P.; Cao, Z.; Erdélyi, K.; Holovac, E.; Liaudet, L.; Lee, W.-S.; Haskó, G.; Mechoulam, R.; Pacher, P. Cannabidiol Protects against Doxorubicin-Induced Cardiomyopathy by Modulating Mitochondrial Function and Biogenesis. *Mol. Med.* **2015**, *21*, 38–45.

(21) Pan, H.; Mukhopadhyay, P.; Rajesh, M.; Patel, V.; Mukhopadhyay, B.; Gao, B.; Haskó, G.; Pacher, P. Cannabidiol Attenuates Cisplatin-Induced Nephrotoxicity by Decreasing Oxidative/nitrosative Stress, Inflammation, and Cell Death. *J. Pharmacol. Exp. Ther.* **2009**, *328*, 708–714.

(22) Velasco, G.; Hernández-Tiedra, S.; Dávila, D.; Lorente, M. The Use of Cannabinoids as Anticancer Agents. *Prog. Neuropsychopharmacol. Biol. Psychiatry* **2016**, *64*, 259–266.

(23) Guzmán, M. Cannabinoids: Potential Anticancer Agents. *Nat. Rev. Cancer* **2003**, *3*, 745–755.

(24) Chakravarti, B.; Ravi, J.; Ganju, R. K. Cannabinoids as Therapeutic Agents in Cancer : Current Status and Future Implications. *Oncotarget* **2014**, *5*, 5852–5872.

(25) Munson, A. E.; Harris, L. S.; Friedman, M. A.; Dewey, W. L.; Carchman, R. A. Antineoplastic Activity of Cannabinoids. *J. Natl. Cancer Inst.* **1975**, *55*, 597–602.

(26) Velasco, G.; Sánchez, C.; Guzmán, M. Towards the Use of Cannabinoids as Antitumour Agents. *Nat. Rev. Cancer* **2012**, *12*, 436–444.

(27) Galve-Roperh, I.; Sánchez, C.; Cortés, M. L.; Gómez del Pulgar, T.; Izquierdo, M.; Guzmán, M. Anti-Tumoral Action of Cannabinoids: Involvement of Sustained Ceramide Accumulation and Extracellular Signal-Regulated Kinase Activation. *Nat. Med.* **2000**, *6*, 313–319.

(28) Carracedo, A.; Gironella, M.; Lorente, M.; Garcia, S.; Guzmán, M.; Velasco, G.; Iovanna, J. L. Cannabinoids Induce Apoptosis of Pancreatic Tumor Cells via Endoplasmic Reticulum Stress-Related Genes. *Cancer Res.* **2006**, *66*, 6748–6755.

(29) Sarfaraz, S.; Adhami, V. M.; Syed, D. N.; Afaq, F.; Mukhtar, H. Cannabinoids for Cancer Treatment: Progress and Promise. *Cancer Res.* **2008**, *68*, 339–342.

(30) Guzmán, M.; Sánchez, C.; Galve-Roperh, I. Cannabinoids and Cell Fate. *Pharmacol. Ther.* **2002**, *95*, 175–184.

(31) Chakravarti, B.; Ravi, J.; Ganju, R. K. Cannabinoids as Therapeutic Agents in Cancer: Current Status and Future Implications. *Oncotarget* **2014**, *5*, 5852–5872.

(32) Cudaback, E.; Marrs, W.; Moeller, T.; Stella, N. The Expression Level of CB1 and CB2 Receptors Determines Their Efficacy at Inducing Apoptosis in Astrocytomas. *PLoS One* **2010**, *5*, e8702.

(33) Hart, S.; Fischer, O. M.; Ullrich, A. Cannabinoids Induce Cancer Cell Proliferation via Tumor Necrosis Factor -Converting Enzyme (TACE/ADAM17)-Mediated Transactivation of the Epidermal Growth Factor Receptor. *Cancer Res.* **2004**, *64*, 1943–1950.

(34) Malfitano, A. M.; Ciaglia, E.; Gangemi, G.; Gazzerro, P.; Laezza, C.; Bifulco, M. Update on the Endocannabinoid System as an Anticancer Target. *Expert Opin. Ther. Targets* **2011**, *15*, 297–308.

(35) Caffarel, M. M.; Sarrió, D.; Palacios, J.; Guzmán, M.; Sánchez, C. Delta9-Tetrahydrocannabinol Inhibits Cell Cycle Progression in Human Breast Cancer Cells through Cdc2 Regulation. *Cancer Res.* **2006**, *66*, 6615–6621.

(36) Schley, M.; Ständer, S.; Kerner, J.; Vajkoczy, P.; Schüpfer, G.; Dusch, M.; Schmelz, M.; Konrad, C. Predominant CB2 Receptor Expression in Endothelial Cells of Glioblastoma in Humans. *Brain Res. Bull.* **2009**, *79*, 333–337.

(37) Qamri, Z.; Preet, A.; Nasser, M. W.; Bass, C. E.; Leone, G.; Barsky, S. H.; Ganju, R. K. Synthetic Cannabinoid Receptor Agonists Inhibit Tumor Growth and Metastasis of Breast Cancer. *Mol. Cancer Ther.* **2009**, *8*, 3117–3129.

(38) Caffarel, M. M.; Andradas, C.; Mira, E.; Pérez-Gómez, E.; Cerutti, C.; Moreno-Bueno, G.; Flores, J. M.; García-Real, I.; Palacios, J.; Mañes, S.; Guzmán, M.; Sánchez, C. Cannabinoids Reduce ErbB2-Driven Breast Cancer Progression through Akt Inhibition. *Mol. Cancer* **2010**, *9*, 196–206.

(39) Miyato, H.; Kitayama, J.; Yamashita, H.; Souma, D.; Asakage, M.; Yamada, J.; Nagawa, H. Pharmacological Synergism between Cannabinoids and Paclitaxel in Gastric Cancer Cell Lines. *J. Surg. Res.* **2009**, *155*, 40–47.

(40) Oesch, S.; Walter, D.; Wachtel, M.; Pretre, K.; Salazar, M.; Guzmán, M.; Velasco, G.; Schäfer, B. W. Cannabinoid Receptor 1 Is a Potential Drug Target for Treatment of Translocation-Positive Rhabdomyosarcoma. *Mol. Cancer Ther.* **2009**, *8*, 1838–1845.

(41) Giuliano, M.; Pellerito, O.; Portanova, P.; Calvaruso, G.; Santulli, A.; De Blasio, A.; Vento, R.; Tesoriere, G. Apoptosis Induced in HepG2 Cells by the Synthetic Cannabinoid WIN: Involvement of the Transcription Factor PPARgamma. *Biochimie* **2009**, *91*, 457–465.

(42) Gustafsson, K.; Wang, X.; Severa, D.; Eriksson, M.; Kimby, E.; Merup, M.; Christensson, B.; Flygare, J.; Sander, B. Expression of Cannabinoid Receptors Type 1 and Type 2 in Non-Hodgkin Lymphoma: Growth Inhibition by Receptor Activation. *Int. J. Cancer.* **2008**, *123*, 1025–1033.

(43) Joseph, J.; Niggemann, B.; Zaenker, K. S.; Entschladen, F. Anandamide Is an Endogenous Inhibitor for the Migration of Tumor Cells and T Lymphocytes. *Cancer Immunol. Immunother.* **2004**, *53*, 723–728.

(44) Stella, N. Cannabinoid and Cannabinoid-like Receptors in Microglia, Astrocytes, and Astrocytomas. *Glia* **2010**, *58*, 1017–1030.

(45) Carracedo, A.; Gironella, M.; Lorente, M.; Garcia, S.; Guzmán, M.; Velasco, G.; Iovanna, J. L. Cannabinoids Induce Apoptosis of Pancreatic Tumor Cells via Endoplasmic Reticulum Stress-Related Genes. *Cancer Res.* **2006**, *66*, 6748–6755.

(46) Bifulco, M.; Laezza, C.; Pisanti, S.; Gazzerro, P. Cannabinoids and Cancer: Pros and Cons of an Antitumour Strategy. *Br. J. Pharmacol.* **2006**, *148*, 123–135.

(47) Thors, L.; Bergh, A.; Persson, E.; Hammarsten, P.; Stattin, P.; Egevad, L.; Granfors, T.; Fowler, C. J. Fatty Acid Amide Hydrolase in Prostate Cancer: Association with Disease Severity and Outcome, CB1 Receptor Expression and Regulation by IL-4. *PLoS One* **2010**, *5*, e12275.

(48) Nomura, D. K.; Long, J. Z.; Niessen, S.; Hoover, H. S.; Ng, S.-W.; Cravatt, B. F. Monoacylglycerol Lipase Regulates a Fatty Acid Network That Promotes Cancer Pathogenesis. *Cell* **2010**, *140*, 49–61.

(49) Pisanti, S.; Picardi, P.; D'Alessandro, A.; Laezza, C.; Bifulco, M. The Endocannabinoid Signaling System in Cancer. *Trends Pharmacol. Sci.* **2013**, *34*, 273–282.

(50) Andradas, C. Papel Del Receptor Huérfano GPR55 En La Fisiopatología Del Cáncer: Implicación En La Proliferación E Invasión de Células Tumorales, Universidad Complutense de Madrid, 2013.

(51) Oka, S.; Kimura, S.; Toshida, T.; Ota, R.; Yamashita, A.; Sugiura, T. Lysophosphatidylinositol Induces Rapid Phosphorylation of p38 Mitogen-Activated Protein Kinase and Activating Transcription Factor 2 in HEK293 Cells Expressing GPR55 and IM-9 Lymphoblastoid Cells. *J. Biochem.* **2010**, *147*, 671–678.

(52) Pérez-Gómez, E.; Andradas, C.; Flores, J. M.; Quintanilla, M.; Paramio, J. M.; Guzmán, M.; Sánchez, C. The Orphan Receptor GPR55 Drives Skin Carcinogenesis and Is Upregulated in Human Squamous Cell Carcinomas. *Oncogene* **2013**, *32*, 2534–2542.

(53) Andradas, C.; Caffarel, M. M.; Pérez-Gómez, E.; Salazar, M.; Lorente, M.; Velasco, G.; Guzmán, M.; Sánchez, C. The Orphan G Protein-Coupled Receptor GPR55 Promotes Cancer Cell Proliferation via ERK. *Oncogene* **2011**, *30*, 245–252.

(54) Leyva-Illades, D.; Demorrow, S. Orphan G Protein Receptor GPR55 as an Emerging Target in Cancer Therapy and Management. *Cancer Manag. Res.* **2013**, *5*, 147–155.

(55) Henstridge, C. M.; Balenga, N. a B.; Kargl, J.; Andradas, C.; Brown, A. J.; Irving, A.; Sanchez, C.; Waldhoer, M. Minireview: Recent Developments in the Physiology and Pathology of the Lysophosphatidylinositol-Sensitive Receptor GPR55. *Mol. Endocrinol.* **2011**, *25*, 1835–1848.

(56) Balenga, N. A.; Martínez-Pinilla, E.; Kargl, J.; Schröder, R.; Peinhaupt, M.; Platzer, W.; Bálint, Z.; Zamarbide, M.; Dopeso-Reyes, I.; Ricobaraza, A.; Pérez-Ortiz, J. M.; Kostenis, E.; Waldhoer, M.; Heinemann, A.; Franco, R. Heteromerization of GPR55 and Cannabinoid CB2 Receptors Modulates Signaling. *Br. J. Pharmacol.* **2014**, *171*, 5387–5406.

(57) Moreno, E.; Andradas, C.; Medrano, M.; Caffarel, M. M.; Pérez-Gómez, E.; Blasco-Benito, S.; Gómez-Cañas, M.; Pazos, M. R.; Irving, A. J.; Lluís, C.; Canela, E. I.; Fernández-Ruiz, J.; Guzmán, M.; McCormick, P. J.; Sánchez, C. Targeting CB2-GPR55 Receptor Heteromers Modulates Cancer Cell Signaling. *J. Biol. Chem.* **2014**, *289*, 21960–21972.

(58) Sanchez, C.; Rueda, D.; Segui, B.; Galve-Roperh, I.; Levade, T.; Guzman, M. The CB1 Cannabinoid Receptor of Astrocytes Is Coupled to Sphingomyelin Hydrolysis through the Adaptor Protein Fan. *Mol. Pharmacol.* **2001**, *59*, 955–959.

(59) Blázquez, C.; González-Feria, L.; Alvarez, L.; Haro, A.; Casanova, M. L.; Guzmán, M. Cannabinoids Inhibit the Vascular Endothelial Growth Factor Pathway in Gliomas. *Cancer Res.* **2004**, *64*, 5617–5623.

(60) Du, K.; Herzig, S.; Kulkarni, R. N.; Montminy, M. TRB3: A Tribbles Homolog That Inhibits Akt/PKB Activation by Insulin in Liver. *Science* **2003**, *300*, 1574–1577.

(61) Salazar, M.; Carracedo, A.; Salanueva, I. J.; Hernández-Tiedra, S.; Lorente, M.; Egia, A.; Vázquez, P.; Blázquez, C.; Torres, S.; García, S.; Nowak, J.; Fimia, G. M.; Piacentini, M.; Cecconi, F.; Pandolfi, P. P.; González-Feria, L.; Iovanna, J. L.; Guzmán, M.; Boya, P.; Velasco, G. Cannabinoid Action Induces Autophagy-Mediated Cell Death through Stimulation of ER Stress in Human Glioma Cells. *J. Clin. Invest.* **2009**, *119*, 1359–1372.

(62) Mizushima, N.; Levine, B.; Cuervo, A. M.; Klionsky, D. J. Autophagy Fights Disease through Cellular Self-Digestion. *Nature* **2008**, *451*, 1069–1075.

(63) Verfaillie, T.; Salazar, M.; Velasco, G.; Agostinis, P. Linking ER Stress to Autophagy: Potential Implications for Cancer Therapy. *Int. J. Cell Biol.* **2010**, *2010*, 930509.

(64) Sarfaraz, S.; Afaq, F.; Adhami, V. M.; Malik, A.; Mukhtar, H. Cannabinoid Receptor Agonist-Induced Apoptosis of Human Prostate Cancer Cells LNCaP Proceeds through Sustained Activation of ERK1/2 Leading to G1 Cell Cycle Arrest. *J. Biol. Chem.* **2006**, *281*, 39480–39491.

(65) Kogan, N. M. Cannabinoids and Cancer. *Mini Rev. Med. Chem.* **2005**, *5*, 941–952.

(66) Bifulco, M.; Laezza, C.; Portella, G.; Vitale, M.; Orlando, P.; De Petrocellis, L.; Di Marzo, V. Control by the Endogenous Cannabinoid System of Ras Oncogene-Dependent Tumor Growth. *FASEB J.* **2001**, *15*, 2745–2747.

(67) SEIC http://www.seic.es/wp-content/uploads/2013/11/30mecantitum08.pdf (accessed Oct 8, 2015).

(68) Blázquez, C.; Casanova, M. L.; Planas, A.; Gómez Del Pulgar, T.; Villanueva, C.; Fernández-Aceñero, M. J.; Aragonés, J.; Huffman, J. W.; Jorcano, J. L.; Guzmán, M. Inhibition of Tumor Angiogenesis by Cannabinoids. *FASEB J.* **2003**, *17*, 529–531.

(69) Casanova, M. L.; Blázquez, C.; Martínez-Palacio, J.; Villanueva, C.; Fernández-Aceñero, M. J.; Huffman, J. W.; Jorcano, J. L.; Guzmán, M. Inhibition of Skin Tumor Growth and Angiogenesis in Vivo by Activation of Cannabinoid Receptors. *J. Clin. Invest.* **2003**, *111*, 43–50.

(70) Portella, G.; Laezza, C.; Laccetti, P.; De Petrocellis, L.; Di Marzo, V.; Bifulco, M. Inhibitory Effects of Cannabinoid CB1 Receptor Stimulation on Tumor Growth and Metastatic Spreading: Actions on Signals Involved in Angiogenesis and Metastasis. *FASEB J.* **2003**, *17*, 1771–1773.

(71) Freimuth, N.; Ramer, R.; Hinz, B. Antitumorigenic Effects of Cannabinoids beyond Apoptosis. *J. Pharmacol. Exp. Ther.* **2010**, *332*, 336–344.

(72) Preet, A.; Ganju, R. K.; Groopman, J. E. Delta9-Tetrahydrocannabinol Inhibits Epithelial Growth Factor-Induced Lung Cancer Cell Migration in Vitro as Well as Its Growth and Metastasis in Vivo. *Oncogene* **2008**, *27*, 339–346.

(73) Ramer, R.; Hinz, B. Inhibition of Cancer Cell Invasion by Cannabinoids via Increased Expression of Tissue Inhibitor of Matrix Metalloproteinases-1. *J. Natl. Cancer Inst.* **2008**, *100*, 59–69.

(74) Blázquez, C.; Salazar, M.; Carracedo, A.; Lorente, M.; Egia, A.; González-Feria, L.; Haro, A.; Velasco, G.; Guzmán, M. Cannabinoids Inhibit Glioma Cell Invasion by down-Regulating Matrix Metalloproteinase-2 Expression. *Cancer Res.* **2008**, *68*, 1945–1952.

(75) Qamri, Z.; Preet, A.; Nasser, M. W.; Bass, C. E.; Leone, G.; Barsky, S. H.; Ganju, R. K. Synthetic Cannabinoid Receptor Agonists Inhibit Tumor Growth and Metastasis of Breast Cancer. *Mol. Cancer Ther.* **2009**, *8*, 3117–3129.

(76) Grimaldi, C.; Pisanti, S.; Laezza, C.; Malfitano, A. M.; Santoro, A.; Vitale, M.; Caruso, M. G.; Notarnicola, M.; Iacuzzo, I.; Portella, G.; Di Marzo, V.; Bifulco, M. Anandamide Inhibits Adhesion and Migration of Breast Cancer Cells. *Exp. Cell Res.* **2006**, *312*, 363–373.

(77) Zacchigna, S.; Zentilin, L.; Morini, M.; Dell'Eva, R.; Noonan, D. M.; Albini, A.; Giacca, M. AAV-Mediated Gene Transfer of Tissue Inhibitor of Metalloproteinases-1 Inhibits Vascular Tumor Growth and Angiogenesis in Vivo. *Cancer Gene Ther.* **2004**, *11*, 73–80.

(78) Ramer, R.; Merkord, J.; Rohde, H.; Hinz, B. Cannabidiol Inhibits Cancer Cell Invasion via Upregulation of Tissue Inhibitor of Matrix Metalloproteinases-1. *Biochem. Pharmacol.* **2010**, *79*, 955–966.

(79) Ramer, R.; Fischer, S.; Haustein, M.; Manda, K.; Hinz, B. Cannabinoids Inhibit Angiogenic Capacities of Endothelial Cells via Release of Tissue Inhibitor of Matrix Metalloproteinases-1 from Lung Cancer Cells. *Biochem. Pharmacol.* **2014**, *91*, 202–216.

(80) Haustein, M.; Ramer, R.; Linnebacher, M.; Manda, K.; Hinz, B. Cannabonoids Increase Lung Cancer Cell Lysis by Lymphokine-Activated Killer Cells via Upregulation of ICAM-1. *Biochem. Pharmacol.* **2014**, *92*, 312–325.

(81) Guzmán, M.; Duarte, M. J.; Blázquez, C.; Ravina, J.; Rosa, M. C.; Galve-Roperh, I.; Sánchez, C.; Velasco, G.; González-Feria, L. A Pilot Clinical Study of Delta9-Tetrahydrocannabinol in Patients with Recurrent Glioblastoma Multiforme. *Br. J. Cancer* **2006**, *95*, 197–203.

(82) Donadelli, M.; Dando, I.; Zaniboni, T.; Costanzo, C.; Dalla Pozza, E.; Scupoli, M. T.; Scarpa, A.; Zappavigna, S.; Marra, M.; Abbruzzese, A.; Bifulco, M.; Caraglia, M.; Palmieri, M. Gemcitabine/cannabinoid Combination Triggers Autophagy in Pancreatic Cancer Cells through a ROS-Mediated Mechanism. *Cell Death Dis.* **2011**, *2*, e152.

(83) Torres, S.; Lorente, M.; Rodríguez-Fornés, F.; Hernández-Tiedra, S.; Salazar, M.; García-Taboada, E.; Barcia, J.; Guzmán, M.; Velasco, G. A Combined Preclinical Therapy of Cannabinoids and Temozolomide against Glioma. *Mol. Cancer Ther.* **2011**, *10*, 90–103.

(84) Siegel, R. L.; Miller, K. D.; Jemal, A. Cancer Statistics, 2015. *CA. Cancer J. Clin.* **2015**, *65*, 5–29.

(85) Abramson, V. G.; Lehmann, B. D.; Ballinger, T. J.; Pietenpol, J. a. Subtyping of Triple-Negative Breast Cancer: Implications for Therapy. *Cancer* **2014**, 1–9.

(86) Hoeferlin, L. A.; E.Chalfant, C. E.; Park, M. A. Challenges in the Treatment of Triple Negative and HER2- Overexpressing Breast Cancer. *J Surg Sci* **2014**, *1*, 3–7.

(87) Foulkes, W. D.; Smith, I. E.; Reis-Filho, J. S. Triple-Negative Breast Cancer. *N. Engl. J. Med.* **2010**, *363*, 1938–1948.

(88) Hudis, C. A.; Gianni, L. Triple-Negative Breast Cancer: An Unmet Medical Need. *Oncologist* **2011**, *16*, 1–11.

(89) Wahba, H. A.; El-hadaad, H. A. Current Approaches in Treatment of Triple-Negative Breast Cancer Treatment Modalities of TNBC. *Cancer Biol Med* **2015**, 106–116.

(90) Shrivastava, A.; Kuzontkoski, P. M.; Groopman, J. E.; Prasad, A. Cannabidiol Induces Programmed Cell Death in Breast Cancer Cells by Coordinating the Cross-Talk between Apoptosis and Autophagy. *Mol. Cancer Ther.* **2011**, *10*, 1161–1172.

(91) Caffarel, M. M.; Andradas, C.; Pérez-Gómez, E.; Guzmán, M.; Sánchez, C. Cannabinoids: A New Hope for Breast Cancer Therapy? *Cancer Treat. Rev.* **2012**, *38*, 911–918.

(92) Perez-Gomez, E.; Andradas, C.; Blasco-Benito, S.; Caffarel, M. M.; Garcia-Taboada, E.; Villa-Morales, M.; Moreno, E.; Hamann, S.; Martin-Villar, E.; Flores, J. M.; Wenners, A.; Alkatout, I.; Klapper, W.; Rocken, C.; Bronsert, P.; Stickeler, E.; Staebler, A.; Bauer, M.; Arnold, N.; Soriano, J.; Perez-Martinez, M.; Megias, D.; Moreno-Bueno, G.; Ortega-Gutierrez, S.; Artola, M.; Vazquez-Villa, H.; Quintanilla, M.; Fernandez-Piqueras, J.; Canela, E. I.; McCormick, P. J.; Guzman, M.; Sanchez, C. Role of Cannabinoid Receptor CB2 in HER2 Pro-Oncogenic Signaling in Breast Cancer. *JNCI J. Natl. Cancer Inst.* **2015**, *107*, djv077.

(93) Ford, L. A.; Roelofs, A. J.; Anavi-Goffer, S.; Mowat, L.; Simpson, D. G.; Irving, A. J.; Rogers, M. J.; Rajnicek, A. M.; Ross, R. a. A Role for L-Alpha-Lysophosphatidylinositol and GPR55 in the Modulation of Migration, Orientation and Polarization of Human Breast Cancer Cells. *Br. J. Pharmacol.* **2010**, *160*, 762–771.

(94) Gomella, L. G.; Liu, X. S.; Trabulsi, E. J.; Kelly, W. K.; Myers, R.; Showalter, T.; Dicker, A.; Wender, R. Screening for Prostate Cancer: The Current Evidence and Guidelines Controversy. *Can. J. Urol.* **2011**, *18*, 5875–5883.

(95) Djulbegovic, M.; Beyth, R. J.; Neuberger, M. M.; Stoffs, T. L.; Vieweg, J.; Djulbegovic, B.; Dahm, P. Screening for Prostate Cancer: Systematic Review and Meta-Analysis of Randomised Controlled Trials. *BMJ* **2010**, *341*, c4543.

(96) Fu, W.; Madan, E.; Yee, M.; Zhang, H. Progress of Molecular Targeted Therapies for Prostate Cancers. *Biochim. Biophys. Acta* **2012**, *1825*, 140–152.

(97) Darwish, O. M.; Raj, G. V. Management of Biochemical Recurrence after Primary Localized Therapy for Prostate Cancer. *Front. Oncol.* **2012**, *2*, 1–6.

(98) Grossmann, M.; Zajac, J. D. Androgen Deprivation Therapy in Men with Prostate Cancer: How Should the Side Effects Be Monitored and Treated? *Clin. Endocrinol. (Oxf).* **2011**, *74*, 289–293.

(99) Czifra, G.; Varga, A.; Nyeste, K.; Marincsák, R.; Tóth, B. I.; Kovács, I.; Kovács, L.; Bíró, T. Increased Expressions of Cannabinoid Receptor-1 and Transient Receptor Potential Vanilloid-1 in Human Prostate Carcinoma. *J. Cancer Res. Clin. Oncol.* **2009**, *135*, 507–514.

(100) Chung, S. C.; Hammarsten, P.; Josefsson, A.; Stattin, P.; Granfors, T.; Egevad, L.; Mancini, G.; Lutz, B.; Bergh, A.; Fowler, C. J. A High Cannabinoid CB(1) Receptor Immunoreactivity Is Associated with Disease Severity and Outcome in Prostate Cancer. *Eur. J. Cancer* **2009**, *45*, 174–182.

(101) Piñeiro, R.; Maffucci, T.; Falasca, M. The Putative Cannabinoid Receptor GPR55 Defines a Novel Autocrine Loop in Cancer Cell Proliferation. *Oncogene* **2011**, *30*, 142–152.

(102) Hohmann, A. G.; Guindon, J. The Endocannabinoid System and Cancer: Therapeutic Implication. *Br. J. Pharmacol.* **2011**, *163*, 1447–1463.

(103) Díaz-Laviada, I. The Endocannabinoid System in Prostate Cancer. *Nat. Rev. Urol.* **2011**, *8*, 553–561.

(104) Orellana-Serradell, O.; Poblete, C. E.; Sanchez, C.; Castellón, E. A.; Gallegos, I.; Huidobro, C.; Llanos, M. N.; Contreras, H. R. Proapoptotic Effect of Endocannabinoids in Prostate Cancer Cells. *Oncol. Rep.* **2015**, 1599–1608.

(105) Abad Martínez, M. J.; Bermejo Benito, P. Biological Activity of Quinones. *Stud. Nat. Prod. Chem.* **2005**, *30*, 303–366.

(106) Asche, C. Antitumour Quinones. *Mini-Reviews Med. Chem.* **2005**, *5*, 449–467 449.

(107) Lu, J.-J.; Bao, J.-L.; Wu, G.-S.; Xu, W.-S.; Huang, M.-Q.; Chen, X.-P.; Wang, Y.-T. Quinones Derived from Plant Secondary Metabolites as Anti-Cancer Agents. *Anticancer. Agents Med. Chem.* **2013**, *13*, 456–463.

(108) Alcaín, F. J.; Villalba, J. M. NQO1-Directed Antitumour Quinones. *Expert Opin. Ther. Patents* **2007**, *17*, 649–665.

(109) El-Najjar, N.; Gali-Muhtasib, H.; Ketola, R. A.; Vuorela, P.; Urtti, A.; Vuorela, H. The Chemical and Biological Activities of Quinones: Overview and Implications in Analytical Detection. *Phytochem. Rev.* **2011**, *10*, 353–370.

(110) O'Brien, P. J. Molecular Mechanisms of Quinone Cytotoxicity. *Chem. Biol. Interact.* **1991**, *80*, 1–41.

(111) Vujčić, M. T.; Tufegdžić, S.; Novaković, I.; Djikanović, D.; Gašić, M. J.; Sladić, D. Studies on the Interactions of Bioactive Quinone Avarone and Its Methylamino Derivatives with Calf Thymus DNA. *Int. J. Biol. Macromol.* **2013**, *62*, 405–410.

(112) Wondrak, G. T. Redox-Directed Cancer Therapeutics: Molecular Mechanisms and Opportunities. *Antioxid. Redox Signal.* **2009**, *11*, 3013–3069.

(113) Cabello, C. M.; Bair, W. B.; Wondrak, G. T. Experimental Therapeutics: Targeting the Redox Achilles Heel of Cancer. *Curr. Opin. Investig. Drugs* **2007**, *8*, 1022–1037.

(114) Gehrmann, M. Drug Evaluation: STA-4783--Enhancing Taxane Efficacy by Induction of Hsp70. *Curr. Opin. Investig. Drugs* **2006**, *7*, 574–580.

(115) Gorrini, C.; Harris, I. S.; Mak, T. W. Modulation of Oxidative Stress as an Anticancer Strategy. *Nat. Rev. Drug Discov.* **2013**, *12*, 931–947.

(116) Tacar, O.; Sriamornsak, P.; Dass, C. R. Doxorubicin: An Update on Anticancer Molecular Action, Toxicity and Novel Drug Delivery Systems. *J. Pharm. Pharmacol.* **2013**, *65*, 157–170.

(117) Dunn, C. J.; Goa, K. L. Mitoxantrone: A Review of Its Pharmacological Properties and Use in Acute Nonlymphoblastic Leukaemia. *Drugs Aging* **1996**, *9*, 122–147.

(118) Siegel, D.; Gibson, N. W.; Preusch, P. C.; Ross, D. Metabolism of Mitomycin C by DT-Diaphorase: Role in Mitomycin C-Induced DNA Damage and Cytotoxicity in Human Colon Carcinoma Cells. *Cancer Res.* **1990**, *50*, 7483–7489.

(119) Cummings, J.; Spanswick, V. J.; Tomasz, M.; Smyth, J. F. Enzymology of Mitomycin C Metabolic Activation in Tumour Tissue: Implications for Enzyme-Directed Bioreductive Drug Development. *Biochem. Pharmacol.* **1998**, *56*, 405–414.

(120) Tareen, B.; Summers, J. L.; Jamison, J. M.; Neal, D. R.; McGuire, K.; Gerson, L.; Diokno, A. A 12 Week, Open Label, Phase I/IIa Study Using Apatone for the Treatment of Prostate Cancer Patients Who Have Failed Standard Therapy. *Int. J. Med. Sci.* **2008**, *5*, 62–67.

(121) Beck, R.; Pedrosa, R. C.; Dejeans, N.; Glorieux, C.; Levêque, P.; Gallez, B.; Taper, H.; Eeckhoudt, S.; Knoops, L.; Calderon, P. B.; Verrax, J. Ascorbate/menadione-Induced Oxidative Stress Kills Cancer Cells That Express Normal or Mutated Forms of the Oncogenic Protein Bcr-Abl. An in Vitro and in Vivo Mechanistic Study. *Invest. New Drugs* **2011**, *29*, 891–900.

(122) Kogan, N. M.; Rabinowitz, R.; Levi, P.; Gibson, D.; Sandor, P.; Schlesinger, M.; Mechoulam, R. Synthesis and Antitumor Activity of Quinonoid Derivatives of Cannabinoids. *J. Med. Chem.* **2004**, *47*, 3800–3806.

(123) Kogan, N. M.; Bl, C.; Alvarez, L.; Gallily, R.; Schlesinger, M.; Guzm, M.; Mechoulam, R. A Cannabinoid Quinone Inhibits Angiogenesis by Targeting Vascular Endothelial Cells. *Mol. Pharmacol.* **2006**, *70*, 51–59.

(124) Kogan, N. M.; Schlesinger, M.; Peters, M.; Marincheva, G.; Beeri, R.; Mechoulam, R. A Cannabinoid Anticancer Quinone, HU-331, Is More Potent and Less Cardiotoxic than Doxorubicin: A Comparative in Vivo Study. *J. Pharmacol. Exp. Ther.* **2007**, *322*, 646–653.

(125) Regal, K.; Mercer, S.; Deweese, J. Characterization of HU-331 as a Cannabinoid Quinone Inhibitor of Topoisomerase II (549.6). *FASEB J* **2014**, *28*.

(126) Anighoro, A.; Bajorath, J.; Rastelli, G. Polypharmacology: Challenges and Opportunities in Drug Discovery. *J. Med. Chem.* **2014**, *57*, 7874–7887.

(127) M. O'Boyle, N.; J. Meegan, M. Designed Multiple Ligands for Cancer Therapy. *Curr. Med. Chem.* **2011**, *18*, 4722–4737.

(128) Gediya, L. K.; Njar, V. C. Promise and Challenges in Drug Discovery and Development of Hybrid Anticancer Drugs. *Expert Opin. Drug Discov.* **2009**, *4*, 1099–1111.

(129) Cumella, J.; Hernández-Folgado, L.; Girón, R.; Sánchez, E.; Morales, P.; Hurst, D. P.; Gómez-Cañas, M.; Gómez-Ruiz, M.; Pinto, D. C. G. a; Goya, P.; Reggio, P. H.; Martin, M. I.; Fernández-Ruiz, J.; Silva, A. M. S.; Jagerovic, N. Chromenopyrazoles: Non-Psychoactive and Selective CB1 Cannabinoid Agonists with Peripheral Antinociceptive Properties. *ChemMedChem* **2012**, *7*, 452–463.

(130) Wu, A.; Duan, Y.; Xu, D.; Penning, T. M.; Harvey, R. G. Regiospecific Oxidation of Polycyclic Aromatic Phenols to Quinones by Hypervalent Iodine Reagents. *Tetrahedron* **2010**, *66*, 2111–2118.

(131) Akai, S.; Kita, Y. Recent Progress in the Synthesis of P-Quinones and P-Dihydro-Quinones through Oxidation of Phenol Derivatives. A Review. *Org. Prep. Proced. Int.* **1998**, *30*, 603–629.

(132) Barret, R.; Daudon, M. Oxidation of Phenols to Quinones by Bis(trifluoroacetoxy)iodobenzene. *Tetrahedron Lett.* **1990**, *31*, 4871–4872.

(133) Magdziak, D.; Rodriguez, A. A.; Water, R. W. Van De; Pettus, T. R. R. Regioselective Oxidation of Phenols to O -Quinones with O -Iodoxybenzoic Acid (IBX). *Org. Lett.* **2002**, 6669–6672.

(134) Harvey, R. G.; Dai, Q.; Ran, C.; Penning, T. M. Synthesis of the O-Quinones and Other Oxidized Metabolites of Polycyclic Aromatic Hydrocarbons Implicated in Carcinogenesis. *J. Org. Chem.* **2004**, *69*, 2024–2032.

(135) Barontini, M.; Bernini, R.; Crisante, F.; Fabrizi, G. Selective and Efficient Oxidative Modifications of Flavonoids with 2-Iodoxybenzoic Acid (IBX). *Tetrahedron* **2010**, *66*, 6047–6053.

(136) Ekins, S.; Waller, C. L.; Swaan, P. W.; Cruciani, G.; Wrighton, S. a; Wikel, J. H. Progress in Predicting Human ADME Parameters in Silico. *J. Pharmacol. Toxicol. Methods* **2001**, *44*, 251–272.

(137) Van de Waterbeemd, H.; Gifford, E. ADMET in Silico Modelling: Towards Prediction Paradise? *Nat. Rev. Drug Discov.* **2003**, *2*, 192–204.

(138) Jorgensen, W. L.; Duffy, E. M. Prediction of Drug Solubility from Structure. *Adv. Drug Deliv. Rev.* **2002**, *54*, 355–366.

(139) Lipinski, C. A. Drug-like Properties and the Causes of Poor Solubility and Poor Permeability. *J. Pharmacol. Toxicol. Methods* **2001**, *44*, 235–249.

(140) Metzger-Filho, O.; Tutt, A.; De Azambuja, E.; Saini, K. S.; Viale, G.; Loi, S.; Bradbury, I.; Bliss, J. M.; Azim, H. a.; Ellis, P.; Di Leo, A.; Baselga, J.; Sotiriou, C.; Piccart-Gebhart, M. Dissecting the Heterogeneity of Triple-Negative Breast Cancer. *J. Clin. Oncol.* **2012**, *30*, 1879–1887.

(141) Abramson, V. G.; Mayer, I. a. Molecular Heterogeneity of Triple-Negative Breast Cancer. *Curr. Breast Cancer Rep.* **2014**, 154–158.

(142) Lehmann, B. D. B.; Bauer, J. a J.; Chen, X.; Sanders, M. E.; Chakravarthy, a B.; Shyr, Y.; Pietenpol, J. a. Identification of Human Triple-Negative Breast Cancer Subtypes and Preclinical Models for Selection of Targeted Therapies. *J. Clin. Invest.* **2011**, *121*, 2750–2767.

(143) Caffarel, M. M.; Moreno-Bueno, G.; Cerutti, C.; Palacios, J.; Guzman, M.; Mechta-Grigoriou, F.; Sanchez, C. JunD Is Involved in the Antiproliferative Effect of Delta9-Tetrahydrocannabinol on Human Breast Cancer Cells. *Oncogene* **2008**, *27*, 5033–5044.

(144) Nogueira, V.; Hay, N. Molecular Pathways: Reactive Oxygen Species Homeostasis in Cancer Cells and Implications for Cancer Therapy. *Clin. Cancer Res.* **2013**, *19*, 4309–4314.

(145) Boulares, A. H.; Yakovlev, A. G.; Ivanova, V.; Stoica, B. A.; Wang, G.; Iyer, S.; Smulson, M. Role of poly(ADP-Ribose) Polymerase (PARP) Cleavage in Apoptosis. Caspase 3-Resistant PARP Mutant Increases Rates of Apoptosis in Transfected Cells. *J. Biol. Chem.* **1999**, *274*, 22932–22940.

(146) Sarfaraz, S.; Afaq, F.; Adhami, V. M.; Mukhtar, H. Cannabinoid Receptor as a Novel Target for the Treatment of Prostate Cancer. *Cancer Res.* **2005**, *65*, 1635–1641.

(147) Sarfaraz, S.; Afaq, F.; Adhami, V. M.; Malik, A.; Mukhtar, H. Cannabinoid Receptor Agonist-Induced Apoptosis of Human Prostate Cancer Cells LNCaP Proceeds through Sustained Activation of ERK1/2 Leading to G1 Cell Cycle Arrest. *J. Biol. Chem.* **2006**, *281*, 39480–39491.

(148) Vara, D.; Morell, C.; Rodríguez-Henche, N.; Diaz-Laviada, I. Involvement of PPARγ in the Antitumoral Action of Cannabinoids on Hepatocellular Carcinoma. *Cell Death Dis.* **2013**, *4*, e618.

(149) Van Dross, R.; Soliman, E.; Jha, S.; Johnson, T.; Mukhopadhyay, S. Receptor-Dependent and Receptor-Independent Endocannabinoid Signaling: A Therapeutic Target for Regulation of Cancer Growth. *Life Sci.* **2013**, *92*, 463–466.

(150) Rocha, F. C. M.; Dos Santos Júnior, J. G.; Stefano, S. C.; da Silveira, D. X. Systematic Review of the Literature on Clinical and Experimental Trials on the Antitumor Effects of Cannabinoids in Gliomas. *J. Neurooncol.* **2014**, *116*, 11–24.

(151) Ross, R. A. The Enigmatic Pharmacology of GPR55. *Trends Pharmacol. Sci.* **2009**, *30*, 156–163.

(152) Pertwee, R. G. GPR55: A New Member of the Cannabinoid Receptor Clan? *Br. J. Pharmacol.* **2007**, *152*, 984–986.

(153) Morales, P.; Blasco-Benito, S.; Andradas, C.; Gómez-Cañas, M.; Flores, J. M.; Goya, P.; Fernández-Ruiz, J.; Sánchez, C.; Jagerovic, N. A Selective, Non-Toxic CB2 Cannabinoid O-Quinone with in Vivo Activity against Triple Negative Breast Cancer. *J. Med. Chem.* **2015**, *58*, 2256–2264.

(154) Jagerovic, N.; Morales, P.; Goya, P.; Blasco-Benito, S.; Sánchez, C.; Gómez-Cañas, M.; Fernández-Ruiz, J. Nuevas Cromenoquinonas Moduladoras de Receptores Cannabinoides CB2 Con Actividad Antitumoral. ES P201430372, 2014.

(155) Xue, J.; Ding, W.; Liu, Y. Anti-Diabetic Effects of Emodin Involved in the Activation of PPARgamma on High-Fat Diet-Fed and Low Dose of Streptozotocin-Induced Diabetic Mice. *Fitoterapia* **2010**, *81*, 173–177.

(156) Woo, C. C.; Loo, S. Y.; Gee, V.; Yap, C. W.; Sethi, G.; Kumar, A. P.; Tan, K. H. B. Anticancer Activity of Thymoquinone in Breast Cancer Cells: Possible Involvement of PPAR-Γ Pathway. *Biochem. Pharmacol.* **2011**, *82*, 464–475.

(157) Kumagai, Y.; Shinkai, Y.; Miura, T.; Cho, A. K. The Chemical Biology of Naphthoquinones and Its Environmental Implications. *Annu. Rev. Pharmacol. Toxicol.* **2012**, *52*, 221–247.

(158) Morales, P.; Vara, D.; Goméz-Cañas, M.; Zúñiga, M. C.; Olea-Azar, C.; Goya, P.; Fernández-Ruiz, J.; Díaz-Laviada, I.; Jagerovic, N. Synthetic Cannabinoid Quinones: Preparation, in Vitro Antiproliferative Effects and in Vivo Prostate Antitumor Activity. *Eur. J. Med. Chem.* **2013**, *70*, 111–119.

(159) Jagerovic, N.; Morales, P.; Goya, P.; Diaz-Laviada, I.; Vara, D.; Fernanadez-Ruiz, J.; Gómez-Ruíz, M.; Gómez-Cañas, M. Chromenopyrazolediones as Cannabinoid Quinone Derivatives Having Anti-Tumour Activity. WO2014013117, 2014.

Chapter 3

Piperazinyl Chromenopyrazoles: Targeting GPR55

Contents

1. Introduction

CB_1 and CB_2 receptors have widely been confirmed as cannabinoid targets. However, the complex pharmacology of the endocannabinoid system points to the existence of other receptors playing important physiological roles. Recently, the G-protein coupled receptor, GPR55, was presented as one of the missing cannabinoid subtypes, but the validity of this categorization is being extensively discussed.[1,2]

GPR55 was cloned and identified in 1999 being firstly reported by Sawzdargo *et al.*[3] Few years later, screening assays carried out on cannabinoid libraries by AstraZeneca[4] and GlaxoSmithKline[5] revealed that endogenous, plant-derived and synthetic cannabinoid ligands were able to activate GPR55. This is one of the main reasons why GPR55 was proposed as a novel member of the endocannabinoid system. However, the classification of GPR55 is intricate due to its complex cellular signaling pathways and biological functions.[6] Despite its clear relation with the ECS, the International Union of Basic and Clinical Pharmacology (IUPHAR) does not classify GPR55 as a cannabinoid receptor so far.[7,8] Currently, much research is focused on the determination of its role in numerous pathophysiological processes to exhaustively explore the therapeutic potential of such a promising target.

1.1 GPR55 structure

GPR55 is a seven transmembrane receptor which belongs to the δ group of rhodopsin-like GPCRs (Class A). Its human gene maps to chromosome 2q37. This receptor is formed by 319 amino acids bearing 67% of homology with its rat homolog.[3] The human GPR55 (*h*GPR55) sequence shares low identity with the cannabinoid receptors described so far CB_1R and CB_2R (13.5% and 14.4% respectively). The GPCR proteins disclosing the highest percentages of homology with GPR55 are GPR35 (27%), P2Y (29%), GPR23 (30%), CCR4 (23%), LPA4 (30%) and LPA5 (30%).[3,9] A schematic representation of GPR55 structure is displayed in figure 1.[10]

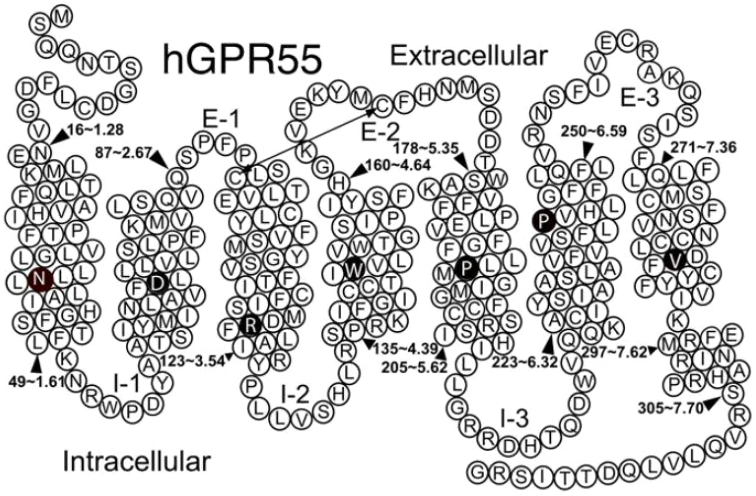

Figure 1. GPR55 structure.[10]

GPR55 preserves the highly conserved residues in TMH-1, 2, 4 and 5 of other rhodopsin-like sequence alignments (N1.50, D2.50, W4.50 and P5.50). Instead of the conserved E/DRY motif in TMH-3 of CBRs, GPR55 contains a DRF conservative substitution. In TMH-6 the conserved CWXP of the CBRs and rhodopsin receptors is substituted by SFLP in GPR55. The utmost variation appears in TMH-7 where GPR55 incorporates the non-conservative substitution DVFCY in place of the highly conserved motif NPXXY. This different sequence produces different hydration and local transmembrane flexibility, and consequently, a different conformation in this region.[10] Another difference with CBRs is the cysteine located on the second extracellular loop (EC-2) that can potentially form a disulfide bond with C3.25.[10,11] There are also changes in the number of residues of the EC-1 loop, being shorter in GPR55 (three amino acids versus six) than other rhodopsin-like receptors sequences. In contrast, the EC-3 loop is longer (fourteen residues versus six) than the Rho and CBRs sequences.

In what refers to the three-dimensional structure, as most of the GPCRs, no crystallographic data has been reported yet. However, homology models based on available GPCR crystal structures have been reported and will be discussed later in this chapter.[10,12]

1.2 Pharmacology

The pharmacology of GPR55 has been widely studied in the last years but it is still a very controversial issue. Its classification as a third cannabinoid receptor has generated strong debate. On the one hand, different cannabinoid ligands are able to stimulate GPR55 effects in several assays.[6,11,13,14] On the other hand, there is significant inconsistency between studies where cannabinoids are presented as agonists or antagonists or to exert no effect depending on the pharmacological outcome. In contrast, lysophosphatidylinositol (LPI) has been confirmed as agonist in all studies reported so far.[6]

While CBRs couple to G-proteins of the $G_{i/0}$ subfamily, as widely demonstrated in the literature,[15,16] GPR55 has been associated with different G-proteins such as $G_{\alpha 13}$,[17] $G_{\alpha q/11}$,[18] $G_{\alpha q}/G_{\alpha 12}$[19] or $G_{\alpha 12/13}$.[20,17] This G-protein coupling promiscuity depends on the ligand and the cell line. By engaging these G proteins, GPR55 activates a range of signaling pathways, including RhoA, MAPK cascades, actin filament formation or intracellular calcium release via the activity of phospholipase C (PLC). Extracellular signal-regulated kinase (ERK), RhoA activated kinase (ROCK) and phosphatidylinositol 3-kinase (PI3K) are ultimately activated in these pathways. Moreover, transcription factors such as NFAT or nuclear factor kappa-light-chain-enhancer of activated B cells (NFkB), that translocate to the nucleus and modulate the expression of different genes are induced following GPR55 activation.[17,20]

Subsequently, the evaluation of new potential GPR55 ligands has been intensely explored through different functional endpoints such as GTPγS binding,[1] analysis of intracellular calcium levels,[17,19] phosphorylation of ERK1/2,[21,22] and the activation of the small GTPase proteins Rac1, RhoA and Cdc42.[1,17,19] However, to date, GPR55 pharmacological assays have proven to be very problematic because of the lack of ligand specificity. Most of them modulate other targets (CBRs, transient receptor potential vanilloid channels (TRPVs), or peroxisome proliferator-activated receptors (PPARs) among others).[20,23] Furthermore, GPR55 discrepancies may rely on intrinsic properties of this GPCR such as the presence of different active conformation states,[24] the formation of

oligomers,[25–27] allosterism,[28,29] or the possible biased agonism[30] as well as the tissue or cell type evaluated.[8,25,31] These pharmacological inconsistencies have been under discussion in many recent reviews demonstrating the growing interest in this field.[6,11,13]

1.3 Biological relevance of GPR55

GPR55 is extensively expressed throughout the body; however, its physiological function remains to be fully established. GPR55 shows a co-localization with CB_1R and CB_2R. Indeed, GPR55 mRNA is expressed in peripheral tissues including the immune system (spleen, tonsil) as well as in the CNS (hippocampus, putamen, caudate, thalamic nuclei).[1,3,17,32,33] Recently, the relevance of GPR55 has been explored in diverse physiological and pathological processes.

There is increasing evidence of the implication of GPR55 in the modulation of inflammatory and neuropathic pain. GPR55 activation enhances neuronal excitability by increasing intracellular Ca^{2+} and suppressing the K^+ current acting on M-type channels suggesting a pro-nociceptive role of this receptor.[19] Moreover, Staton *et al.*[34] showed that GPR55 deficient mice did not display hyperalgesia upon inflammatory or neuropathic stimuli. Experiments in microglial cells[35] and neutrophils[36] further supported the role of GPR55 in inflammatory processes.

The contribution of GPR55 in metabolic regulation and energy homeostasis is now emerging.[37–39] For instance, a correlation between body weight and levels of GPR55 expression in visceral adipose tissue has been reported. It is clear that GPR55, as well as CB_1R, controls food intake, gut motility and insulin secretion.

Due to its expression in vascular endothelial cells, different research groups have studied the involvement of GPR55 in the regulation of vascular functions.[2,18,40–42]

Different indirect evidences indicate that GPR55 plays an important role in cancer physio-pathology. Increased levels of LPI, the putative GPR55 endogenous ligand, have been found in plasma and ascites from patients with this pathology.[43,44] Moreover, GPR55 expression is significantly increased in tumor tissues compared with their healthy counterparts. This fact

demonstrates that GPR55 expression may be used as potential biomarker in oncology associated to poor prognosis.[45,46] As detailed above, GPR55 signals through Rho GTPases, which control cytoskeleton organization, cell polarity and cell migration, are closely related to tumor progression.[47–49] Accordingly, activation of GPR55 triggers a number of signaling cascades that promote cancer cell proliferation, migration, and invasion. All these findings support the idea of GPR55 as a new potential target in oncology.

It has been suggested that GPR55 is implicated in bone physiology as well. Whyte *et al.*[50] reported that modulation of GPR55 may regulate osteoclast polarization and bone resorption activity. Therefore, GPR55 may represent a novel target for osteoporosis and bone loss associated with arthritis.

It is worthy to note that GPR55 is not involved in the regulation of CNS development, gross motor movement or learned behavior, however, it does play a role in motor coordination.[51]

The therapeutic potential of GPR55 modulation is schematically summarized in figure 2.

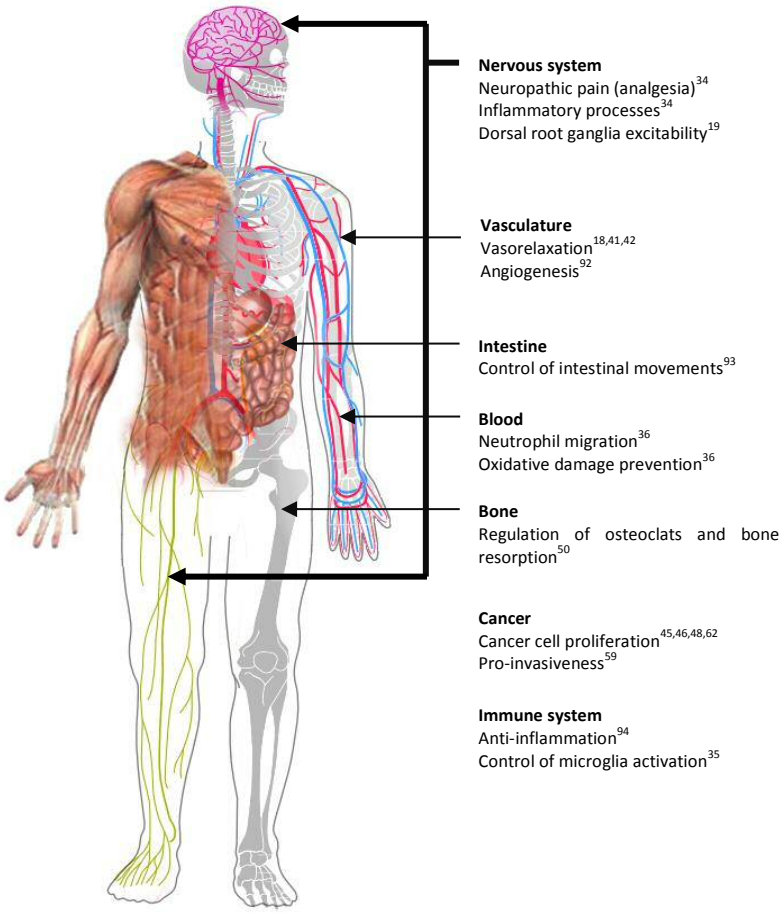

Figure 2. Biological relevance of GPR55. Different evidences reported so far suggest the involvement of GPR55 in a variety of pathophysiological functions. Adapted from Henstridge *et al* 2011.[52]

Even though the implication of GPR55 in the modulation of diverse physiopathological conditions has been evidenced, more investigations have to be performed, hopefully with more selective ligands, to determine GPR55 functions.

1.4 GPR55 ligands

In spite of the potential therapeutic interest of GPR55, the design of potent and selective GPR55 ligands remains a major challenge for medicinal chemists due to the lack of information on GPR55 three-dimensional structure and the complexity of the interpretation of GPR55 functionality assays. Herein, we categorize the different GPR55 modulators reported so far in the literature.

1.4.1 Endogenous ligands

Despite all the contradictory data reported for many GPR55 ligands, the bioactive lipid lysophosphatidylinositol has shown to be a GPR55 agonist in all the studies and functional assays reported so far.[20,32] These data led to propose LPI as an endogenous non-cannabinoid ligand of GPR55. Structurally, LPI contains a glycerol backbone esterified with a single fatty acid in sn-1 or sn-2 position and a phosphate group substituted with an inositol.[14,21] In a recent study performed by Oka *et al.*[22] to identify molecular species of LPI in rat brain, the most predominant fatty acyl moiety was stearic acid (50.5%) followed by arachidonic acid (22.1%). 2-Arachidonoyl-containing LPI species (2-AGPI) displayed the highest potency and efficacy of the LPI species published to date (figure 3). Consequently, 2-AGPI has been proposed as the natural LPI ligand for GPR55.[22,53]

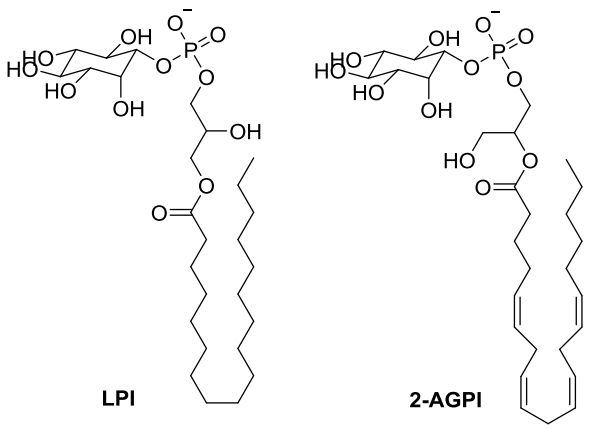

Figure 3. The structures of lysophosphatidylinositol (LPI) and its 2-arachidonoyl-derivative (2-AGPI).

The ability of LPI to activate GPR55 has been confirmed in various cellular systems and pharmacological outcomes. For instance, increase of LPI levels has been detected not only in diverse tumors but also in cancer cell proliferation and tumor progression processes.[54–56] In what concern the pharmacological outcomes, LPI induces phosphorylation of ERK and elicits a rapid Ca^{2+} transient in GPR55-expressing cells.[21] Further reports have supported these findings in HEK293 cells expressing GPR55 and in large-diameter DRG neurons[19] and endothelial cells.[18] Henstridge *et al.*[17] showed that LPI stimulates Ca^{2+} release that is dependent on $G_{\alpha 13}$ and RhoA activation. In the β-arrestin PathHunter™ assay, LPI also reveals to be a potent agonist.[57]

1.4.2 Cannabinoid-related GPR55 ligands

- Endocannabinoids and derivatives

Many endogenous cannabinoid ligands have been identified as GPR55 modulators (figure 4). Anandamide, the predominant endocannabinoid, displayed inconsistent results in different GPR55 assays. This lipid neurotransmitter stimulated [^{35}S]GTPγS binding in the nanomolar range and caused calcium mobilization in the micromolar range. Nevertheless, AEA did not affect phosphorylation of ERK, β-arrestin signaling and induction of receptor internalization. Another important endocannabinoid, 2-arachidonoylglycerol, showed agonist efficacy in [^{35}S]GTPγS binding assay but it was ineffective in β-arrestin recruitment and GPR55 internalization. These

inconsistencies may be due to the aforementioned discrepancies between functional assays or cell systems.[8] In accordance with IUPHAR, there is no irrefutable evidence that these eicosanoids are GPR55 agonists.

Other endocannabinoids such as noladin ether, palmitoylethanolamide, virodhamine and oleylethanolamide stimulated [^{35}S]GTPγS binding in transiently transfected *h*GPR55-HEK293 cells, with EC_{50} values of 10, 4, 12 and 440 nM respectively.[1] Similar results were previously reported by AstraZeneca in the same [^{35}S]GTPγS assay.[4] According to those GTPγS studies, anandamide activated GPR55 and CBRs with similar potencies while palmitoylethanolamide, virodhamine and 2-AG displayed selective action through GPR55.

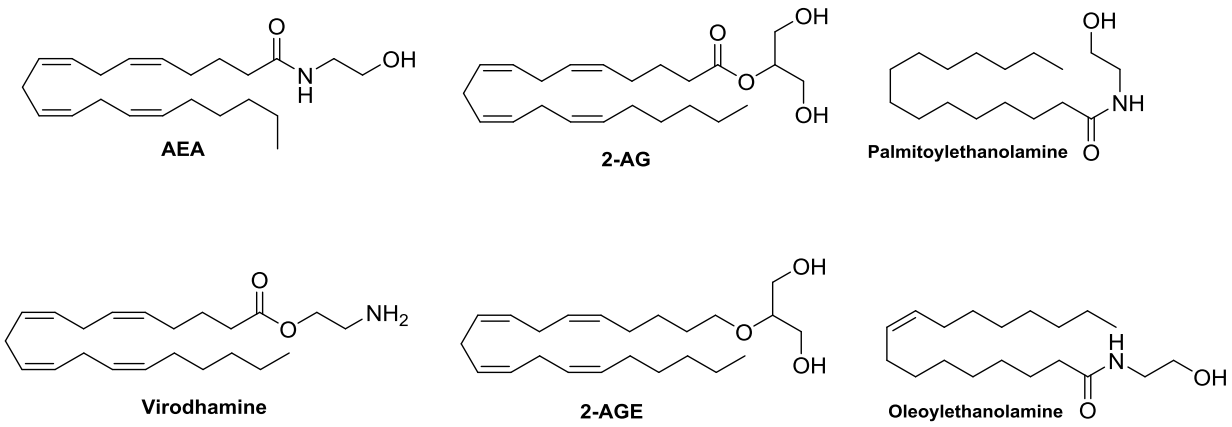

Figure 4. Endocannabinoids as GPR55 ligands.

- Phytocannabinoids and related molecules

Bioactive constituents from the plant *Cannabis Sativa* and synthetic analogues (figure 5) have also shown discrepant data regarding their GPR55 pharmacology. Δ^9-THC exhibits activation of GPR55 in [^{35}S]GTPγS binding, RhoA assays and intracellular calcium mobilization in transiently transfected *h*GPR55-HEK293 cells.[1,4,19] However, this phytocannabinoid was unable to stimulate ERK1/2 phosphorylation or β-arrestin recruitment.[21,57] It remains to be determined whether this is a consequence of experimental variability, differences in functional readouts or GPR55 intrinsic properties. HU210, a synthetic derivative of Δ^9-THC, also displayed activity as GPR55 agonist in

diverse assays being inactive in others.[1,4,57] Abnormal-cannabidiol (Abn-CBD) and its structurally related molecule O-1602 have been reported as GPR55 selective agonists in [^{35}S]GTPγS assays with EC_{50} values in the micromolar and nanomolar ranges respectively.[1,2,4] Conversely, other research groups reported lack of activity through different cellular systems or functional endpoints.[22,57]

The potent CB_1R/CB_2R agonist CP55,940 has also shown conflicting data, being GPR55 agonist in [^{35}S]GTPγS assays[1,4] and GPR55 antagonist[17,21,58] in β-arrestin, ERK phosphorylation and calcium mobilization tests.

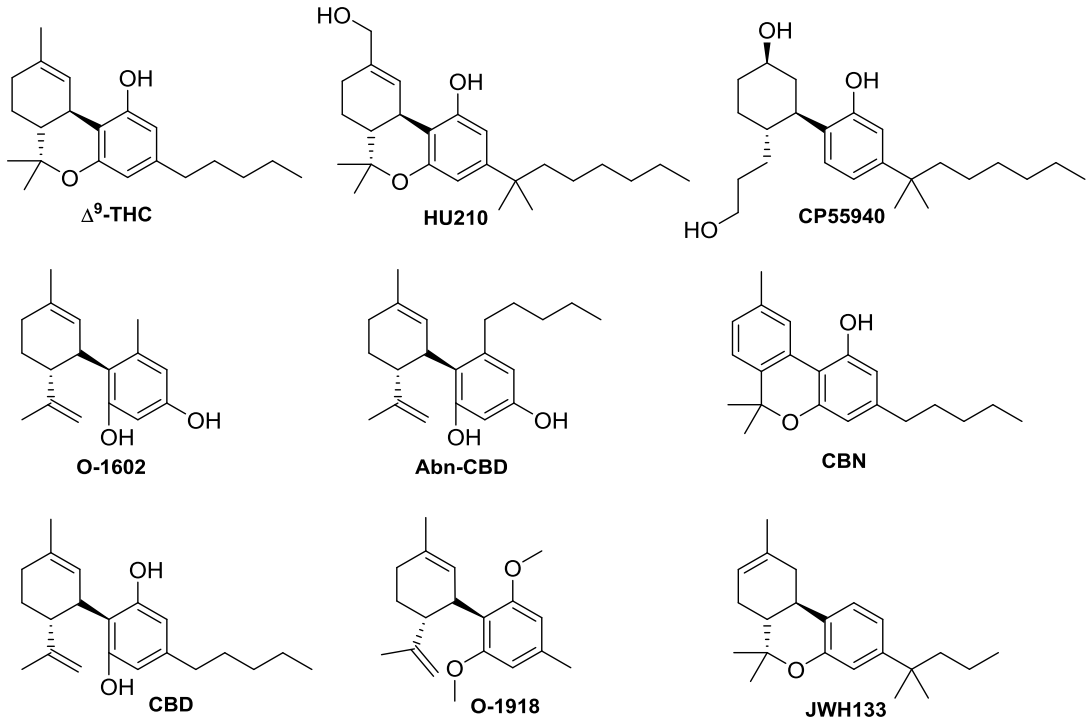

Figure 5. Structure of some phytocannabinoid and synthetic derivatives related to GPR55.

Regarding other compounds such as cannabinol and JWH133, different studies confirmed their inactivity towards GPR55.[8] However, a recent sensitive ERK assay, developed by Sharon Anavi-Goffer *et al.*,[28] determined that JWH133 could reduce basal pERK acting as GPR55 inverse agonist. From the same GPR55 readout, the phytocannabinoids Δ^9-tetrahydrocannabivarin, cannabidivarin and cannabigerovarin acted as potent inhibitors of LPI and may be novel GPR55 ligands.

CBD, whose cannabinoid mechanism of action has not been fully understood, has also shown inconsistent pharmacological data regarding its GPR55 activity. This non-psychoactive phytocannabinoid acted as GPR55 antagonist preventing [^{35}S]GTPγS binding and Rho activation,[1,50,59] but it was inactive in intracellular Ca^{2+} mobilization assays[19] and β-arrestin recruitment.[57] O-1918, a synthetic derivative of CBD that does not bind to CBRs[60] was able to act as GPR55 antagonist in the intracellular Ca^{2+} functional analysis using endothelial cells that express GPR55.[18]

- Synthetic cannabinoid ligands

Arylpyrazoles

The arylpyrazole scaffold has been widely explored in the cannabinoid system becoming very relevant in the design of CB_1R or CB_2R inverse agonists or antagonists (figure 6). Rimonabant (SR141716A), the well-known CB_1R arylpyrazole antagonist, has been found to behave as GPR55 agonist in some assays[4,20,57,61] but as GPR55 antagonist in others, [18,19,62] exerting no effect in an additional study.[21] In contrast, SR144528, a potent CB_2R antagonist, is inactive in all the GPR55 assays reported so far. It did not induce calcium rise in transiently transfected *h*GPR55-HEK293 cells nor in β-arrestin binding assays.[19,57] The GPR55 pharmacology of AM251 and AM281, CB_1R antagonists structurally related to SR141716A, was also extensively studied. AM251 behaved as GPR55 agonist in different biochemical assays,[1,5,17,20,32,57,58,61] whereas AM281 did not interact with this GPCR receptor[1] or displayed very weak agonist effects.[23,35]

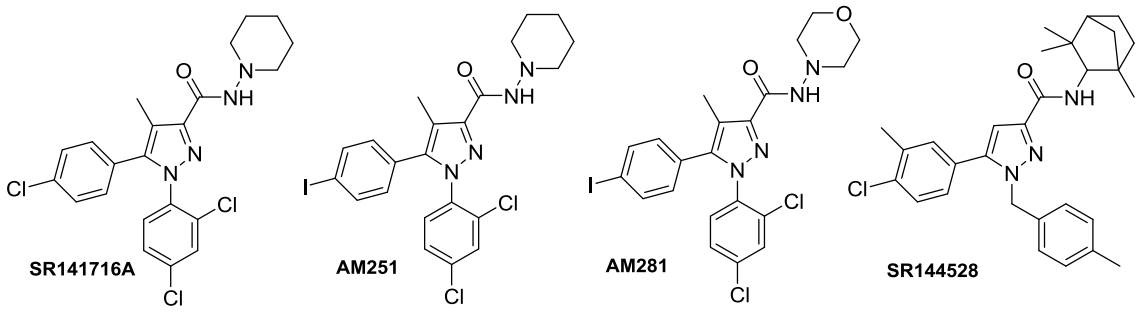

Figure 6. Arylpyrazoles SR141716A, AM251, AM281 and SR144528.

As shown by Anavi-Goffer *et al.*,[28] CB_1R antagonists (SR141716A, AM281 and AM251) can act as agonists by themselves and as inhibitors of LPI inducing activation of ERK phosphorylation under the same cellular model. These results may explain the disagreements surrounding GPR55 pharmacology of several cannabinoid ligands. They suggest that certain arylpyrazole ligands may act as bitopic ligands of GPR55.[63]

In 2010 Daly *et al.*[41] have reported the GPR55 pharmacology of the commercially available fluorescent ligand T1117. This molecule, structurally formed by the CB_1R ligand AM251 linked to a fluorescent tetramethylrhodamine group, showed weak or no affinity towards CB_1R but curiously activated GPR55 by promoting a characteristic oscillatory Ca^{2+} response in HEK293 cells stably expressing recombinant GPR55.

Aminoalkylindoles

The cannabinoid agonist WIN55,212-2 has been extensively used to investigate the endocannabinoid system (figure 7). This relevant aminoalkylindole does not display activity towards GPR55. Consistent data from various biological assays confirm that this potent CB_1R/CB_2R ligand does not bind GPR55 either as agonist or antagonist.[1,4,19] However, JWH015, a WIN55,212-2 analogue, was able to activate GPR55 in [^{35}S]GTPγS assay with EC_{50} value in the nanomolar range and JWH015 was effective at micromolar concentrations in calcium mobilization assays.[19]

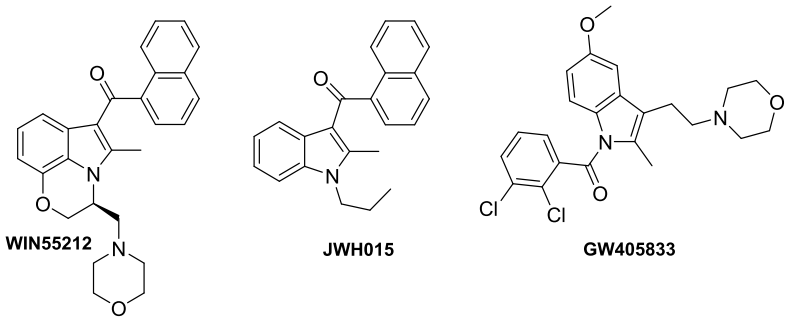

Figure 7. Synthetic cannabinoid ligands WIN55212, JWH015 and GW405833 .

Furthermore, data from an ERK1/2 phosphorylation assay suggest that the CB_2R agonist GW405833 is bitopic ligand of GPR55. It acts as a partial agonist of GPR55 alone or as an allosteric modulator enhancing LPI signaling.[28]

Coumarins

The coumarin scaffold has shown a great potential and versatility in the development of highly selective and potent CBRs ligands.[64] Exploring this scaffold, 3-substituted coumarins have been identified as novel GPR55 antagonists through β-arrestin recruitment assays.[29] Interaction with CBRs require lipophilic moiety in position 7 (PSB-SB-487, figure 8) while the methyl moiety in position 8 is favorable for GPR55 antagonism (PSB-SB-489, figure 8). Recently, Deng *et al.*[65] have developed computational QSAR models in order to design coumarin derivatives with improved potency.

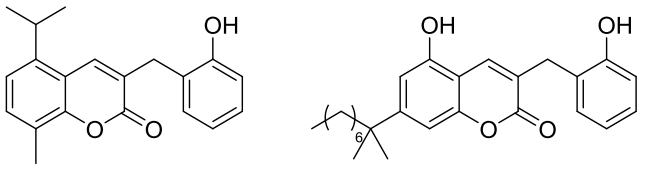

PSB-SB-489 PSB-SB-487

Figure 8. 3-(2-Hydroxybenzyl)-5-isopropyl-8-methyl-2*H*-chromen-2-one (PSB-SB-489) and 7-(1,1-dimethyloctyl)-5-hydroxy-3-(2-hydroxybenzyl)-2*H*-chromen-2- one (PSB-SB-487)

Magnolol derivatives

Magnolol (figure 9) is one of the main bioactive compounds identified in the bark of *Magnolia officinalis*.[66] This biphenylic compound and other related lignans are able to interact with cannabinoid receptors.[67] Magnolol is a partial CB_1R/CB_2R agonist whereas its major metabolite, tetrahydromagnolol, is a potent peripheral CB_2R agonist that behaves as a weak antagonist of GPR55.[68] In a remarkable investigation, Müller *et al.*[69] developed structure-activity relationships of new magnolol analogs varying the alkyl chains and the phenolic groups. As a result, they have demonstrated that methylation of one of the hydroxyl groups leads to an increase of the antagonistic

potency at GPR55 being 5´-hexyl-2´-methoxy-5-propylbiphenyl-2-ol the most potent of this series. This structure represents a potential lead compound in the development of new GPR55 antagonists.

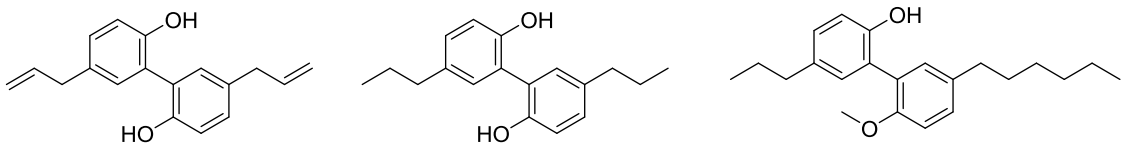

Figure 9. Magnolol and analogs.

1.4.3 Non-cannabinoid related GPR55 ligands

The growing interest of this therapeutic target has focused extensive research in the identification of new selective GPR55 ligands. Within this context, collaborative project between individual laboratories and the Sandford-Burnham screening center of the Molecular Libraries Probe Production Centers Network (MLPCN)[70,71] allowed the identification of six different GPR55 chemical scaffolds.[70,71] This study consisted in high-throughput screening of a library of compounds by β-arrestin assays in U2OS cells permanently expressing HA-GPR55E and βarr2-GFP.[58] Phenylpiperazine CID2440433, triazoloquinoline CID1172084 and morpholinesulfonylphenylamide CID15945391, represented in figure 10, exemplify the potent GPR55 agonists discovered in this study;[71] whereas piperadinyloxadiazolone CID23612552, thienopyrimidine CID1434953 and quinoline aryl sulfonamide CID1261822 of figure 10 are representative GPR55 antagonists.[70]

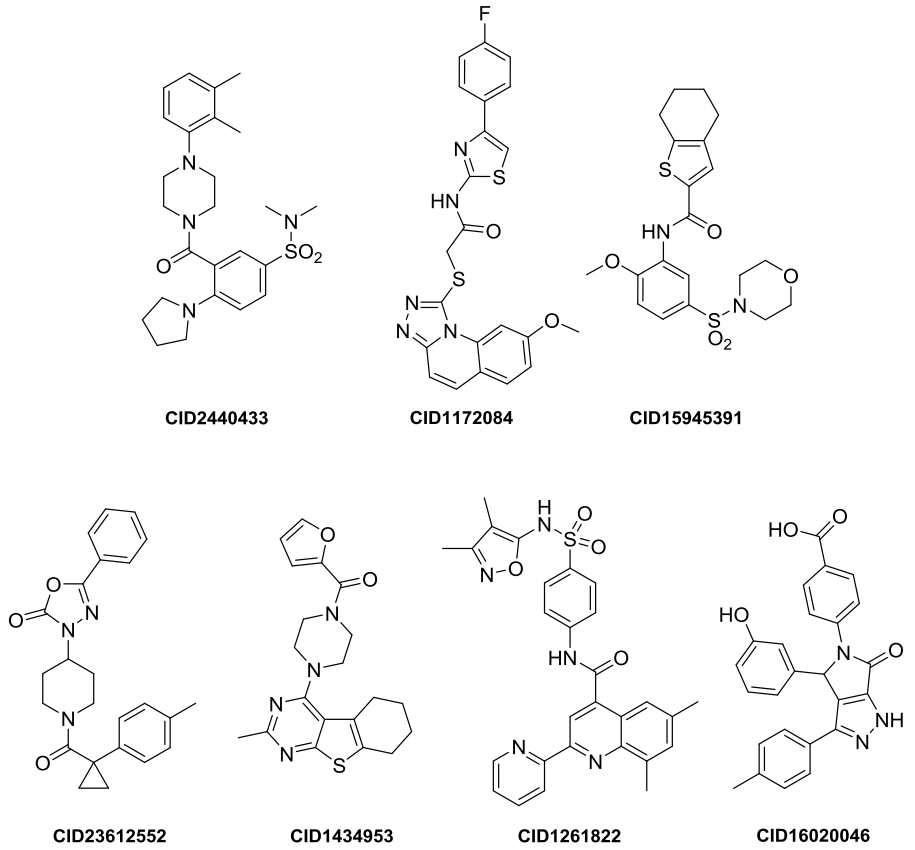

Figure 10. Hits of the identified GPR55 agonist scaffolds (CID2440433, CID1172084 and CID15945391) and GPR55 antagonist scaffolds (CID23612552, CID1434953 and CID1261822). CID16020046 is another GPR55 antagonist recently described by Kargl *et al.*[72]

Parallel studies[61] developed by the company GlaxoSmithKline in 2011 validated the abovementioned benzoylpiperazine as GPR55 agonists in *Saccharomyces cerevisiae* yeast and in HEK293 cells. GSK494581A, the most potent ligand, and GSK575594A, the most selective one, had been previously patented as glycine transporter subtype 1 inhibitors (being 60-fold selective for GPR55) (figure 11). It is noteworthy that these novel GPR55 selective ligands activate human but not rodent GPR55 pointing to differences in the binding pocket of the two orthologs.

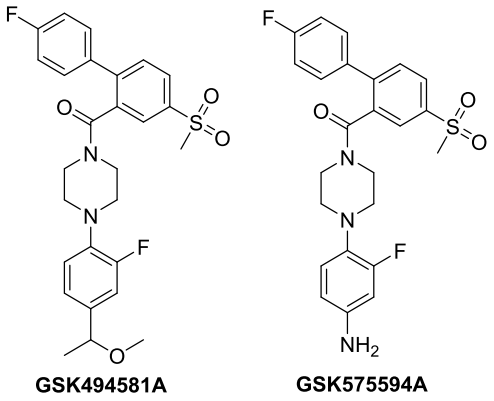

Figure 11. Benzoylpiperazines previously reported as glycine transporter inhibitors.

In 2013, Kargl *et al.*[72] identified CID16020046 (figure 10) as a selective GPR55 antagonist.[72] This compound was originated in the same MLSCN screening; however, it was not selected by those researchers for further development. This molecule antagonizes agonist-mediated GPR55 activation in yeast cells and inhibits GPR55-mediated intracellular Ca^{2+} release. CID16020046 reduces LPI signaling in primary human lung microvascular endothelial cells (HMVEC-L) and in human platelet suggesting novel therapeutic applications for GPR55.

A very recent research has demonstrated that (R,R´)-4´-methoxy-1-naphthylfenoterol (MNF, figure 12), an analog of (R,R´)-fenoterol (short-acting β2-adrenergic agonist) with a 573-fold greater selectivity for β2-AR than β1-AR, is able to reduce GPR55 agonist efficacy.[73] The compound exerts selective attenuation in GPR55 signaling as demostrated through different biological readouts such as ERK phosphorilation and cell motility. (R,R´)-MNF inhibits the pro-oncogenic activity of GPR55 revealing its therapeutic potential as an antitumor agent.

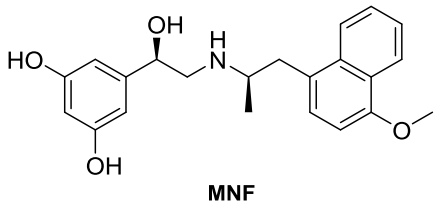

Figure 12. Naphthylfenoterol (MNF).

The analysis of the miscellaneous range of GPR55 scaffolds reported so far may help to deepen in the elucidation of the structural motifs involved in the interaction with the receptor. This knowledge may contribute to the rational design of new compounds able to selectively bind this promising target providing new therapeutic strategies.

1.5 Molecular modeling studies

Although no crystal structure is already available for GPR55, Reggio and coworkers[10,12,74] have developed an homology model based on previously crystallized GPRC structures. This model was refined according to sequence differences. It allows exploring the GPR55 ligand binding pocket and the key residues involved in the ligand-receptor interaction. However, different mutations on the receptor remain to be done in order to fully elucidate these interactions.

As reported by Reggio[10] in the LPI-GPR55* complex the endogenous ligand adopts an inverted-L shape conformation where the primary interaction site for LPI involves a salt bridge between its phosphate group and the residue K2.60. According to the aforementioned model, LPI inserts its fatty acid tail deep within the transmembrane bundle (TMH-2, 3, 5, 6 and 7). Molecular dynamics studies of the lipid-derived agonists of GPR55 showed that LPI and 2-AGPI sit much higher in the bilayer than anandamide. 2-AGPI and LPI can adopt a tilted head group orientation by hydrogen bonding to the phospholipid phosphate group.[74] These molecular modeling studies suggest that the binding site of the active state of the receptor may accommodate ligands with inverted-L or T shapes exposing their most electronegative region in the intersection and positioning their long part vertically deep in the receptor. The critical interaction for these agonists may occur between K2.60 and their highly electronegative moiety.

Molecular modeling studies of CID1172084, CID2440433 (figure 10) have been accomplished in the active GPR55 model described by Kotsikorou *et al.*[10] These agonists fit in the putative binding site of the receptor in the region of TMH 2-3-5-6-7 mirroring the bioactive conformation of LPI. Their broad head regions occupy a horizontal binding pocket opening near the EC loops. On the other

hand, docking studies of the thienopyrimidine derivative CID1434953 and other antagonists were performed in the inactive state of the GPR55 model.[12] This modeling suggests that GPR55 antagonists adopt a 7 or T shape with the electronegative region near the end of the central portion of the molecule. Their binding pocket is in the extracellular loop region and the top part to the transmembrane helixes.

These studies offer an insight into GPR55 modulation and pharmacophore.

2. Aims

As aforementioned, GPR55 pharmacology reveals serious inconsistencies between studies and functional outcomes.[6] Therefore, it becomes crucial to focus our efforts in the discovery of novel potent and selective GPR55 molecules that may enable the development of adequate research tools for the biological study of this putative cannabinoid receptor.

Within the context of exploring the chromenopyrazole scaffold this chapter includes the following specific aims leading to two new series of compounds:

- Design of novel potential GPR55 ligands.[a]
- Synthesis of the proposed molecules.[a]
- Analysis of *in silico* drug-like properties of the novel structures.[a]
- Evaluation of GPR55 activity.[b]
- Study their selectivity *vs* cannabinoid receptors CB_1R and CB_2R.[c]

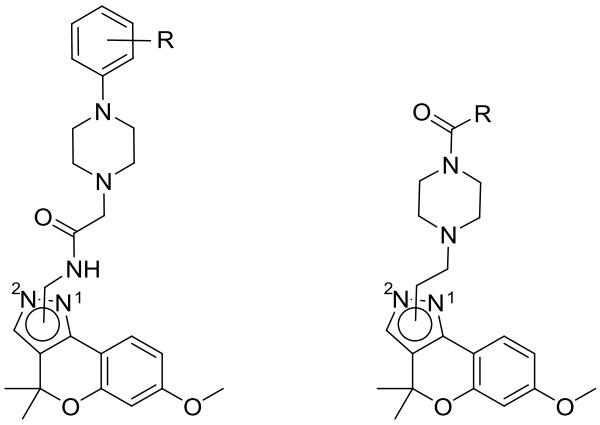

Figure 13. Proposed potential GPR55 structures.

a) Performed by PM at Instituto de Química Médica (CSIC).
b) Performed by PM hosted by Prof. Ruth Ross (School of Medicine, University of Toronto).
c) Performed by PM hosted by Prof. Javier Fernández-Ruiz (Facultad de Medicina, UCM).

3. Results

3.1 Design

Potent and selective GPR55 ligands have been unavailable principally because most of the known modulators of this receptor were identified from cannabinoid receptor or lipid compound libraries.[57,61] Recently, the Sanford-Burnham screening center of MLPCN performed a high-throughput, high-content screening identifying new GPR55 ligands as described in the introduction of this chapter.[70,71] These new scaffolds served us as a basis to design our novel potential GPR55 chemotypes. We particularly focused on the structural features highlighted in figure 14.

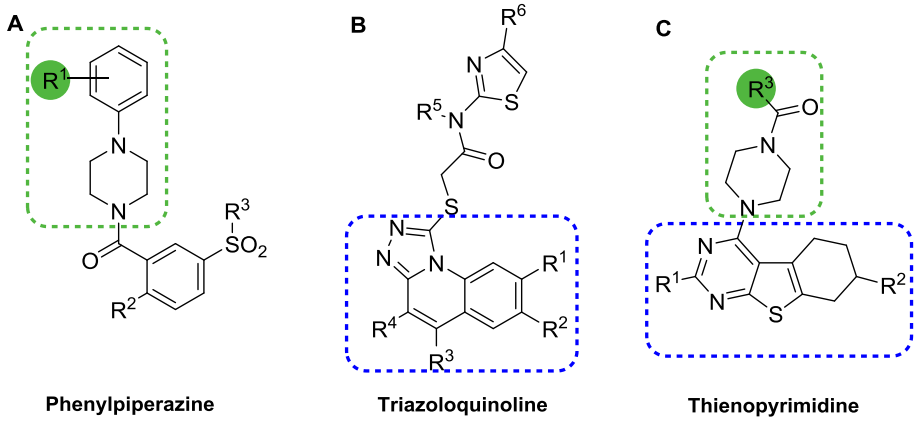

Figure 14. GPR55 scaffolds identified in the MLPCN screening. **A**) Phenylpiperazine **B**) Triazoquinoline **C**) Thienopyrimidine. Structural features retained for novel GPR55 structures are highlighted. Head region is boxed in blue and tail profiles in green.

Reported SAR studies and molecular modeling of the most potent molecules of these series allowed to determine the chemical requirements for GPR55 activity.[10,12,70,71] Scaffold **A** comprises a central phenylpiperazine core substituted by a 3-sulfonylphenone. The preferred R^1 substituents are hydrogen, halogens, methyl or methoxy groups. Other structural modifications such as nitro R^1 substituents caused a drastic loss of activity. The triazoloquinoline core of scaffold **B** accepted hydrogen and methoxy groups as R^1 and R^2 to modulate GPR55. R^3 and R^4 tolerate hydrogen or methyl groups to retain activity. Regarding scaffold **C**, unsubstituted or methylated thienopyrimidine cores were preferred in the active compounds. The acylated piperazine moiety is affected by alkyl R^3 substituents whereas furan derivatives were determinant for increased potency.

Based on these data, we designed novel potential GPR55 chromenopyrazole derivatives. Replacement of the triazoloquinoline or thienopyrimidine core by our tricyclic heterocyclic scaffold as head region is proposed (figure 15). Phenylpiperazine and acylated piperazine moieties, present in scaffolds **A** and **C**, were selected as pyrazole substituents.

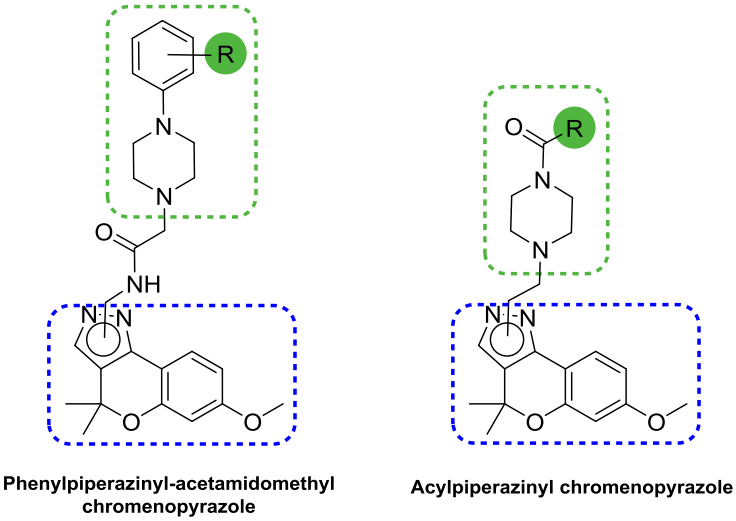

Figure 15. Designed chromenopyrazole scaffolds.

As previously commented, molecular modeling studies[10,12] suggested that GPR55 ligands should adopt an inverted-L or T shape with the presence of an electronegative region located close to the

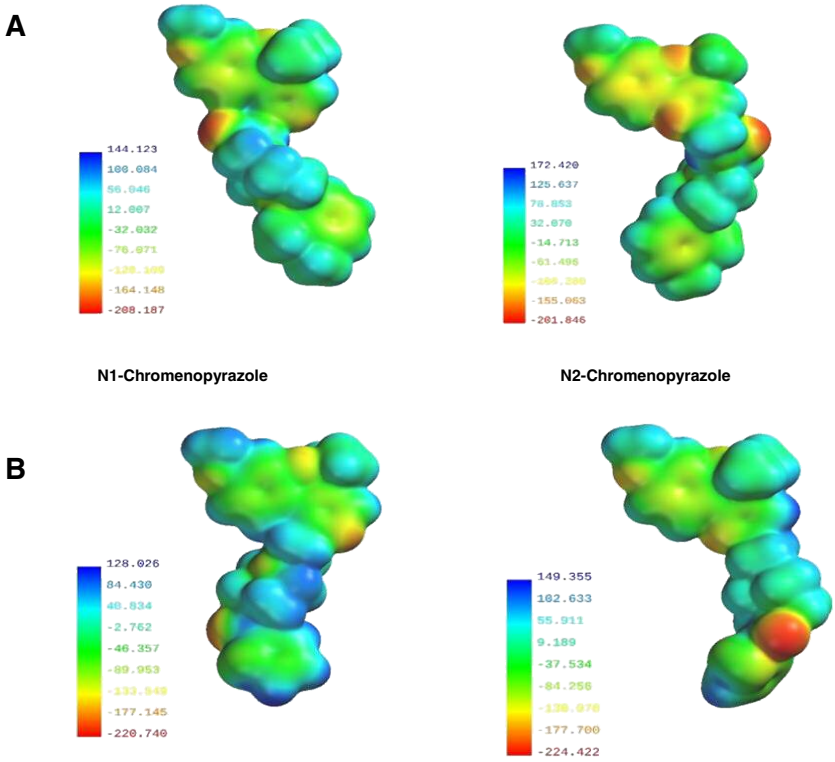

head region or in the central portion of the molecule. To appraise if the minimum energy conformers of these prototypes could adopt similar shapes, a conformational analysis of two pyrazole isomers from each proposed series was undertaken. The molecular electrostatic potential maps were calculated from the global minimum energy. Figure 16 illustrates the minimum energy conformer of *N*1 and *N*2-substituted chromenopyrazole derivatives. A noteworthy feature resulting from this study is the inverted-L shape adopted by the *N*2-substituted isomers from both series. This shape could mimic the bioactive conformation reported by Reggio.[10,12] The molecular electrostatic potential maps showed a high electronegative region nearby the chromenopyrazole head region (series I) and in the central area of the molecule (series II).

Figure 16. A) *N*1 and *N*2-(4-(2,3-dimethylphenyl)piperazinyl)acetamidomethyl-chromenopyrazole (Series I) electrostatic potential maps. **B**) *N*1 and *N*2-(4-(2-thenoyl)piperazinyl)ethyl-chromenopyrazole (Series II) electrostatic potential maps. . The electrostatic potential scale (in kJ/mol) is provided as a color scale. This scale is from blue (most electropositive) to red (most electronegative).

The different electronegative patterns of these two series along with the possible substitution of the pyrazole ring at *N*1 or *N*2 position may provide an overview of the scaffold versatility and chemical requirements for GPR55 activity.

3.2 Synthesis

The chromenopyrazole core of the new derivatives was prepared following the synthetic route depicted in scheme **1.** 7-Methoxy-2,2-dimethyl-2,3-dihydrochromen-4-one **3.1** was obtained by cyclization of 2-hydroxy-4-methoxyacetophenone with acetone. α-Formylation of **3.1** was achieved under microwave irradiation conditions as previously described in Chapter 1. 3-Hydroxymethylenechromen-4-one **3.2** tautomerizes to the corresponding β-keto aldehyde under the reaction conditions. Finally, condensation of the β-keto aldehyde with anhydrous hydrazine yielded the corresponding 7-methoxy-4,4-dimethyl-1,4-dihydrochromeno[4,3-*c*]pyrazole (**3.3**).

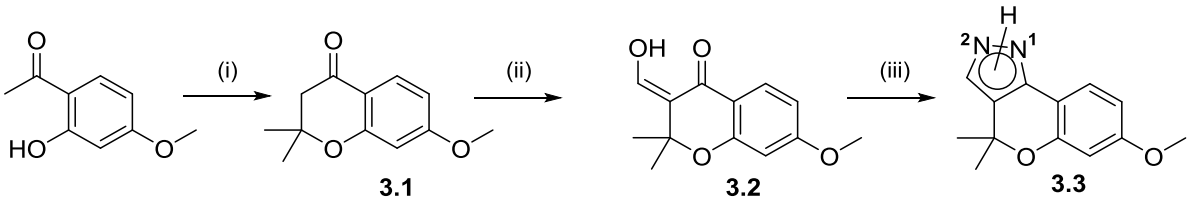

Scheme 1. Synthesis of 7-methoxy-4,4-dimethyl-1,4-dihydrochromeno[4,3-c]pyrazole **3.3**. Reaction conditions: **(i)** acetone, pyrrolidine, EtOH, 5 h, reflux, 82%; **(ii)** NaH, THF, MW, 45ºC, 25 min, then ethyl formate, THF, MW, 45ºC, 25 min, 52%; **(iii)** anhydrous hydrazine, EtOH, 2 h, 60ºC, 69%.

Then, arylpiperazines **3.4**–**3.7** were synthesized by N-alkylation of the suitable phenylpiperazine with 2-chloro-*N*-hydroxymethylacetamide. As displayed in scheme **2**, the final compounds **3.8a**–**3.11** were prepared by alkylation of 7-methoxy-1,4-dihydro-4,4-dimethylchromeno[4,3-*c*]pyrazole (**3.3**) with the corresponding phenylpiperazine derivative **3.4**–**3.7** under refluxing conditions.

Purification of the *N*1 and *N*2 regioisomers resulted difficult in most cases obtaining the desired compounds in low yields. Flash column chromatography followed by a semipreparative HPLC was required to separate both phenylpiperazinyl-acetamidomethyl chromenopyrazoles isomers. In order to improve the yield of this synthetic route, the hydroxyl group of **3.4**–**3.7** was mesylated or

tosylated with the respective sulfonyl chloride in order to improve the leaving group capacity. Unfortunately, the yields of pyrazole alkylation were not significantly enhanced.

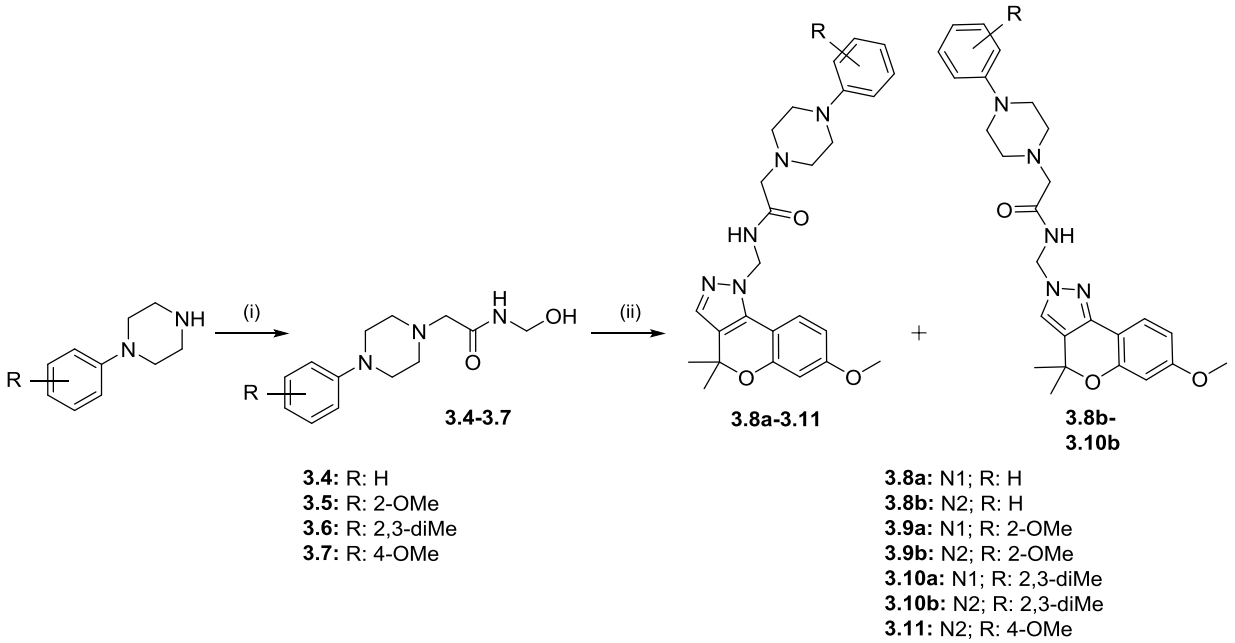

Scheme 2. Synthesis of phenylpiperazinyl-acetamidomethyl chromenopyrazoles **3.8a**-**3.11** (Series I). Reaction conditions: **(i)** 2-chloro-N-hydroxymethylacetamide, K_2CO_3, acetonitrile, 2-5 h, reflux (24-63%); **(ii)** compound **3.3**, NaH, THF, 12-72 h, reflux (2-14%).

In view of the difficulties to obtain the phenylpiperazinyl-acetamidomethyl chromenopyrazole derivatives, a different strategy was developed for the achievement of the second series of compounds. The synthesis of acylpiperazinyl chromenopyrazoles is shown in scheme **3**. Alkylation of compound **3.3** with 1,2-dibromoethane afforded the desired 2-bromoethyl-chromenopyrazoles **3.12a** and **3.12b**. In contrast to the above reaction, these regioisomers were easily separated by column chromatography. Finally, compounds **3.13**–**3.19** were obtained in good yields reacting the corresponding bromoethyl-chromenopyrazole with different acyl piperazines under refluxing conditions.

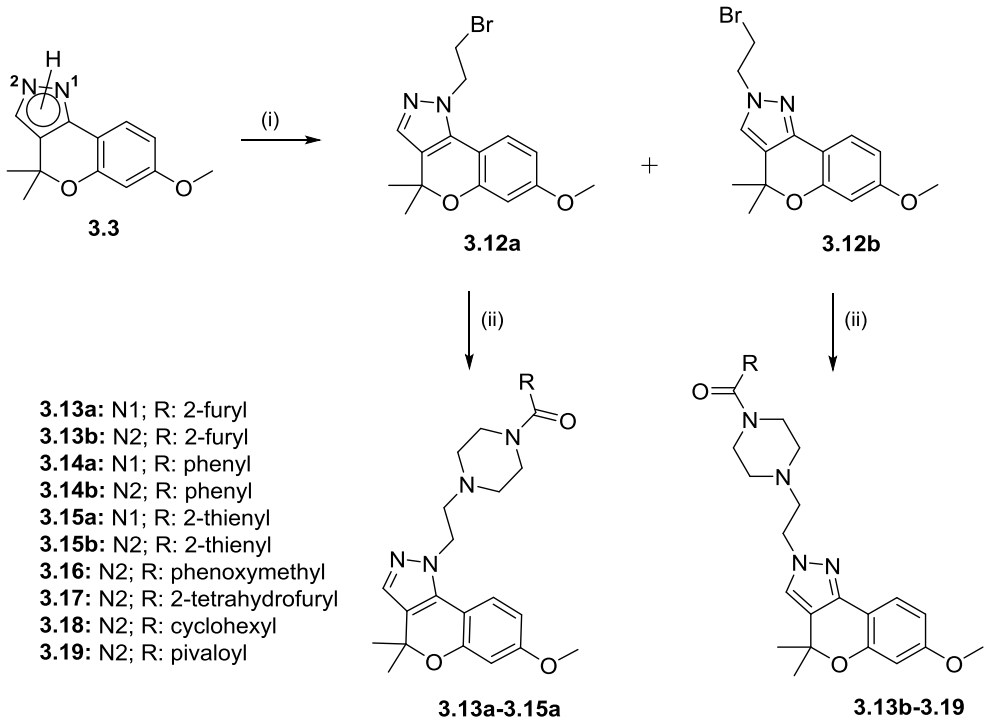

Scheme 3. Synthesis of acylpiperazinyl chromenopyrazoles **3.13**-**3.19** (Series II). Reaction conditions: **(i)** 1,2-dibromoethane, NaH, THF, 4 h, reflux, 21 and 40%; **(ii)** acyl piperazine, K_2CO_3, THF, overnight, reflux, 23-81%.

Most of the reactions were also performed by microwave heating conditions and despite the reaction time decrease, the yields were lower and more subproducts were obtained hindering the purifications.

3.3 *In silico* ADME properties

So far, the most potent known ligand for GPR55 is LPI. However, LPI is very unstable when exposed to air or sunshine; it oxidizes very easily. Due to these particularities, LPI is not suitable as therapeutic agent. Therefore, the druggability profile of the new compounds was predicted using a set of 34 physicochemical descriptors computed by QikProp. Selected pharmacokinetic properties of compounds **3.8**–**3.19** and the GPR55 agonist LPI are displayed in table 1. Lipinski rule of five as well as Jorgensen rule of three[75,76] are followed by all the new chromenopyrazole derivatives whereas LPI drug-likeness is quite poor. Several LPI parameters such as bioavailability, aqueous solubility, or blood-brain partition coefficient fall outside the optimum range of values for 95% of known drugs

showing an overall ADME-compliance score very low. The prediction of solubility, blood-brain barrier permeability, human oral absorption, gut-blood barrier permeability and metabolism suggests that chromenopyrazole derivatives **3.8**–**3.19** can be considered as suitable drug-like candidates. Moreover, their predicted parameters suggest a clear ADME improvement compared to LPI.

Table 1. Physicochemical descriptors calculated by QikProp 3.5 integrated in Maestro (Schrödinger, LLC, New York, USA)

Compd	QPlogS[a]	QlogBB[b]	QPlogHERG[c]	QPPCaco[d]	%Human oral absorption GI[e]
3.8a	-4.81	0.11	-5.80	529	100
3.8b	-4.75	0.10	-6.06	504	100
3.9a	-4.82	0.05	-5.59	529	100
3.9b	-4.74	0.04	-5.84	504	100
3.10a	-5.50	0.10	-5.54	529	100
3.10b	-5.52	0.09	-5.79	504	100
3.11	-4.56	0.06	-5.39	529	100
3.13a	-4.11	-0.05	-6.78	559	100
3.13b	-4.10	0.08	-7.05	774	100
3.14a	-4.73	0.01	-7.07	641	100
3.14b	-5.28	0.08	-7.52	796	100
3.15a	-4.83	0.12	-6.75	642	100
3.15b	-4.92	0.25	-7.08	880	100
3.16	-4.42	0.03	-6.33	589	100
3.17	-2.90	0.13	-5.03	512	89
3.18	-4.67	0.30	-5.13	832	100
3.19	-3.92	0.27	-5.04	750	100
LPI	-3.41	-4.84	-4.14	5	11

[a]Predicted aqueous solubility [-6.5/0.5]; [b]Predicted log of the brain/blood partition coefficient [-3.0/1.2]; [c]HERG K^+ Channel Blockage (log IC_{50}) [concern below -5]; [d]Apparent Caco-2 cell permeability in nm/s [<25 poor, >500 excellent]; [e]Human Oral Absorption in GI [<25% is poor]; [range of 95% of drugs].

3.4 GPR55 assays

As commented in the introduction of this chapter, the pharmacology of GPR55 is rather puzzling. In fact, activity of GPR55 ligands is completely influenced by the assay used to assess receptor-mediated downstream signaling.[20,28,58] Moreover, the paucity of structural data and selective potent modulators has also limited the development of accurate pharmacological assays.

Cellular impedance assay

The potential GPR55 activity of new chromenopyrazole derivatives was assessed using xCELLigence experiments.[77,78] This is a label-free methodology based on cellular impedance measurements on real time. The integrated readout of GPR55 function allowed by this assay may circumvent some of the abovementioned pharmacological problems. The xCELLigence assay has been optimized for GPR55 receptors by Ruth Ross´s research group.[79] They were able to detect agonist or antagonist activity of previously known GPR55 ligands such as LPI, 2-AGPI, or CID16020046 among others. These ligands were assessed through other functional assays demonstrating similar GPR55 activity profiles. Potency and efficacy differences depend on the sensitivity of the technique, assay formats and stable cell lines.

This assay is based on the detection of cellular morphological changes triggered by ligand-dependent GPCR activation and coupling to downstream pathways. These changes modulate the physical contact between cell and electrode which is reflected by changes in electrical impedance (converted to cell index units by the system). Recent studies have widely validated this impedance-based technology for monitoring GPCR activation and signaling in cells.[80–82]

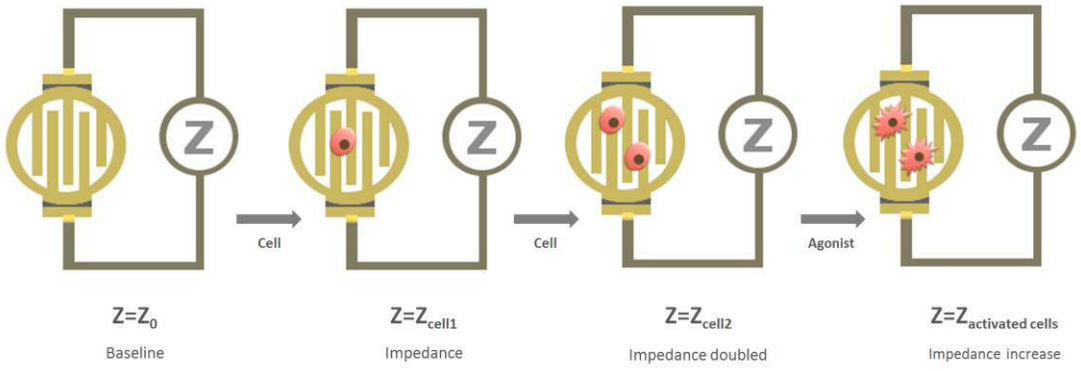

Figure 17. Schematic representation of microelectrodes and the principle of xCELLigence experiments. Cells are plated onto gold microelectrode arrays, which when stimulated with a low voltage generate an electric field sensitive to changes in the properties of a cell. The impedance increases as cells attach and spread or after cell shape changes induced by GPCR activation. In the absence of cells, the baseline impedance (Z_0) value is determined by the software. Addition of cells to the sensor microelectrodes leads to changes in impedance signal (Z_{cell}) that is directly proportional to the number of cells seeded on the sensors. Figure adapted from ACEA Biosciences.[83]

Results

Cellular impedance of increasing concentrations of LPI and chromenopyrazole derivatives **3.8–3.19** was monitored in a human embryonic kidney 293 cell line stably overexpressing recombinant human GPR55 (*h*GPR55-HEK293). Cells were seeded one day prior to stimulation with the compounds for attachment to the electrodes located in the bottom of the plate. Activation of the receptor by a GPR55 ligand causes changes in cellular impedance detected by the system. Agonistic effects of test compounds were compared to the activity of the GPR55 agonist LPI (LPI effect at 1 μM is set at 100%). Dose-response curves were obtained plotting the peak cell index response (five minutes after administration of the drugs), versus the logarithm of the concentration for each compound. Cell index values were normalized for each well to the time point immediately preceding agonist addition. EC_{50} values and the corresponding E_{max} of LPI and chromenopyrazole derivatives are displayed in table 2. The activity observed for LPI was consistent with published data in all the experiments.[79]

Table 2. Potencies of chromenopyrazole derivatives **3.8**-**3.19** for GPR55 receptor measured using xCELLigence system.

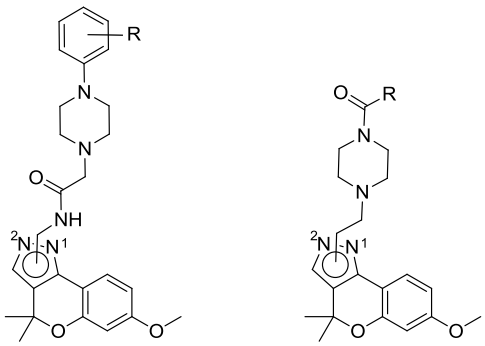

Compd	R	Pyrazole Substitution	GPR55 EC_{50} (nM)[a]	GPR55 E_{max} (%)[b]
3.8a	H	**N1**	-	NR
3.8b	H	**N2**	-	NR
3.9b	2-OMe	**N2**	6.36 (0.98-41.52)	51 (36-67)
3.10b	2,3-diMe	**N2**	-	NR
3.11	4-OMe	**N1**	-	NR

3.13a		**N1**	-	NR
3.13b		**N2**	0.88 (0.05-14.56)	43 (31-54)
3.14b		**N2**	0.60 (0.12-3.03)	51 (42-60)
3.15a		**N1**	-	NR
3.15b		**N2**	0.51 (0.06-4.22)	45 (36-54)
3.16	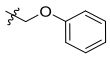	**N2**	1.28 (0.20-9.46)	52 (41-63)
3.17		**N2**	0.40 (0.03-4.61)	51 (40-62)
3.18		**N2**	8.67 (1.18-63.45)	47 (36-58)
3.19		**N2**	0.69 (0.06-7.63)	49 (37-62)
LPI	-	-	2.82 (0.64-12.30)	100 (81-118)

The data is presented as a percentage of the maximal LPI stimulation (at 1 μM, LPI displays off-target activity at 10 μM). [a]EC_{50} values were calculated using nonlinear regression analysis. Data represent the mean of at least four experiments performed in duplicate, and 95% confidence intervals (CI) for the EC_{50} values are given in parentheses. [b]E_{max}: Maximal agonist effect, determined using nonlinear regression analysis (95% CI). NR: No response at tested concentrations (E_{max} lower that 25% relative to LPI).

According to the ability to activate GPR55, there is a clear difference between both series of compounds [**3.8**–**3.11** (series I) and **3.13**–**3.19** (series II)]. All the tested acylpiperazinyl chromenopyrazoles (series II) exhibited agonistic GPR55 profile except **3.15a**. Conversely, excluding **3.9b** which partially activated the receptor, tested phenylpiperazinyl-acetamidomethyl chromenopyrazoles (series I) did not show capacity to activate GPR55 in this cell model.

Compounds **3.9b**, **3.13b**, **3.14b**, **3.15b**, **3.16**, **3.17**, **3.18** and **3.19** displayed partial agonism in GPR55-HEK293 cells when compared with LPI response. These compounds exhibit good potency with EC_{50} values in the nanomolar range. However, these chromenopyrazole derivatives displayed half of the maximal efficacy produced by the putative endogenous modulator LPI.

Interestingly, in the acylpiperazinyl series (II), the *N*1- or *N*2-pyrazole substitution influences the ability of the compounds to activate GPR55. Effectively, *N*2-regioisomers (**3.13b**, **3.14b**, **3.15b**, **3.16**, **3.17**, **3.18** and **3.19**) present the preferred substitution while substitution at *N*1-position (**3.13a** and

3.15a) exerts a negative impact on GPR55 activation. Figure 18 exemplifies the effects of both isomers, *N*1- (**3.13a**) and *N*2-substituted (**3.13b**), on dose-response curves in *h*GPR55-HEK293 cells.

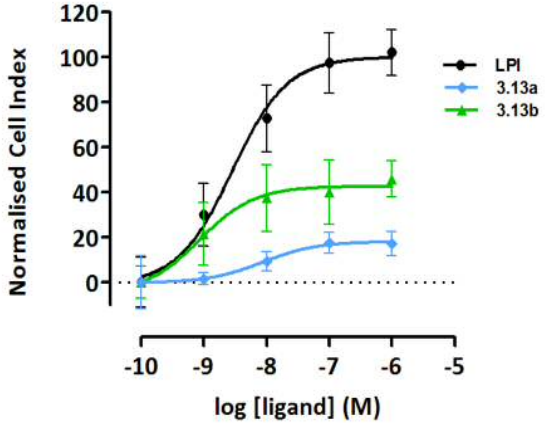

Figure 18. Concentration-response curves of LPI and representative chromenopyrazole derivatives **3.13a** and **3.13b** in *h*GPR55-HEK293 cells. Data points represent the mean ± SEM values of four independent experiments, performed in duplicate. The data is presented as a percentage of the maximal LPI stimulation (at 1 μM, LPI displays off-target activity at 10 μM).

After analyzing the ability of the compounds to activate GPR55, their potential antagonistic activity at the receptor was evaluated. The capacity of **3.8a–3.19** to inhibit LPI-mediated GPR55 stimulation was assessed at a concentration of 1 μM. Full concentration-response curves for LPI in presence and absence of the compounds were determined (table 3). A representative graph is displayed in figure 19. These experiments were performed by coincubation of the cells with the tested compounds (or vehicle) and different concentrations of the standard agonist LPI.

Table 3. Potencies and maximal effect of LPI in the presence and absence of chromenopyrazole derivatives **3.8–3.19** (1 μM) at GPR55.

Compd	R	Pyrazole Substitution	GPR55	
			EC_{50} (nM)[a]	E_{max} (%)[b]
LPI A+3.8a	H	**N1**	27.7 (8.9-86.1)	97 (80-115)
LPI A+3.8b	H	**N2**	31.5 (5.4-83.6)	94 (78-108)
LPI A+3.9b	2-OMe	**N2**	28.4 (4.7-96.1)	90 (71-104)

	LPI A+3.10b	2,3-diMe	**N2**	30.4 (10.1-91.5)	102 (90-115)
	LPI A+3.11	4-OMe	**N1**	27.3 (1.2-97.5)	80 (60-105)
	LPI A+3.13a		**N1**	19.6 (5.9-65.3)	97 (83-111)
As	**LPI B+3.13b**		**N2**	19.8 (3.9-76.1)	106 (92-120)
	LPI B+3.14b		**N2**	15.5 (3.8-54.6)	105 (96-113)
	LPI A+3.15a		**N1**	29.3 (8.4-79.2)	99 (82-116)
	LPI B+3.15b		**N2**	8.2 (2.5-26.4)	96 (87-106)
	LPI B+3.16*	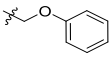	**N2**	18.2 (4.6-71.1)	100 (91-115)
	LPI B+3.17*		**N2**	24.6 (7.9-66.8)	102 (91-106)
	LPI B+3.18*		**N2**	25.4 (6.6-96.7)	99 (90-113)
	LPI B+3.19*		**N2**	21.9 (5.5-87.6)	100 (86-114)
	LPI A	-	-	4.1 (1.3-12.1)	104 (91-114)
	LPI B	-	-	1.6 (0.6-4.2)	99 (90-108)

[a]EC_{50} values were calculated using nonlinear regression analysis. Data represent the mean of at least four experiments performed in duplicate, and 95% confidence intervals (CI) for the EC_{50} values are given in parentheses. [b]E_{max}: Maximal agonist effect, determined using nonlinear regression analysis (95% CI). ***** Significantly different (nonoverlapping confidence intervals) from the corresponding LPI alone. The effect of each compound over LPI dose-response is related to their corresponding LPI (A or B) in absence of the potential antagonist.

showed in table 3, phenylpiperazinyl-acetamidomethyl chromenopyrazoles (series I) were not able to significantly inhibit LPI dose-dependent GPR55 activation. Nonetheless, among acylpiperazinyl chromenopyrazoles (series II), **3.16**, **3.17**, **3.18** and **3.19** exhibited a significant capacity to antagonize LPI effect at 1μM. As previously demonstrated, these compounds are also partial agonist of the receptor when administered alone what highlights their interesting pharmacological profile.

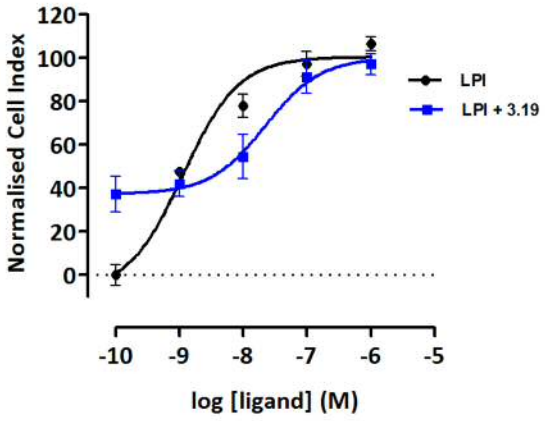

Figure 19. Concentration-response curves of LPI in the presence and absence of chromenopyrazole derivative **3.19** in *h*GPR55-HEK293 cells. Data points represent the mean ± SEM values of at least four

independent experiments, performed in duplicate. The data is presented as a percentage of the maximal LPI stimulation.

Taking into consideration the xCELLigence impedance assays presented so far, the most promising results come from series II. Three acylpiperazinyl chromenopyrazoles (**3.13b**, **3.14b** and **3.15b**) displayed capacity to partially activate GPR55, while **3.16**, **3.17**, **3.18** and **3.19** displayed both partial GPR55 agonism and GPR55 antagonism of LPI response. From series I, only one compound (**3.9b**) showed GPR55 partial agonism.

Selectivity towards GPR55

The activity of the compounds was evaluated in normal HEK293 cells to study if the response detected by cellular impedance was selectively GPR55-mediated. Full dose-response curves of all the new compounds and LPI were performed at concentrations from 1 nM to 10 μM in non-transfected HEK293 cells. Chromenopyrazoles derivatives **3.8**–**3.19** did not exhibit any response at doses up to 10 μM in normal cells confirming that the effects observed in over-expressed GPR55 cells were mediated by this receptor. However, LPI clearly displayed off-target stimulation at high concentrations (10 μM). Off-targets effects of LPI at doses over 1 μM have been observed through diverse functional endpoints.[84,85] Graphs of representative compounds and LPI are shown in figure 20 comparing their effect in GPR55 transfected and normal HEK293 cells.

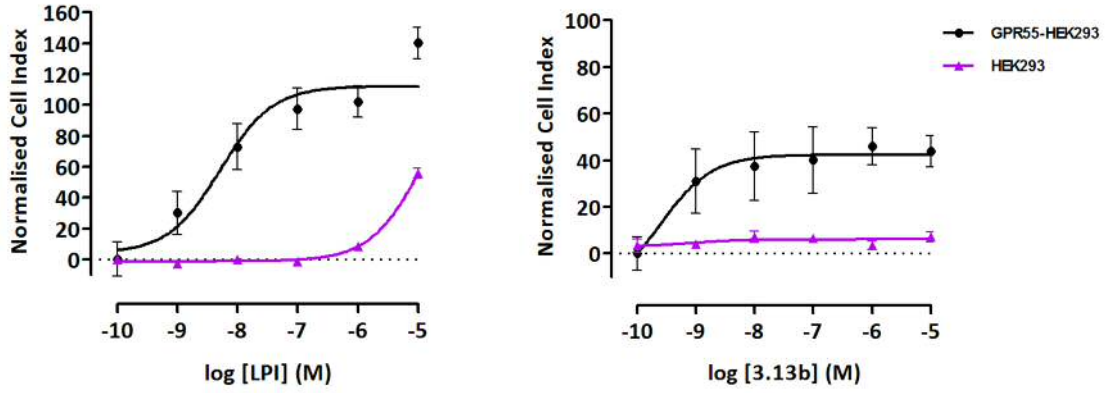

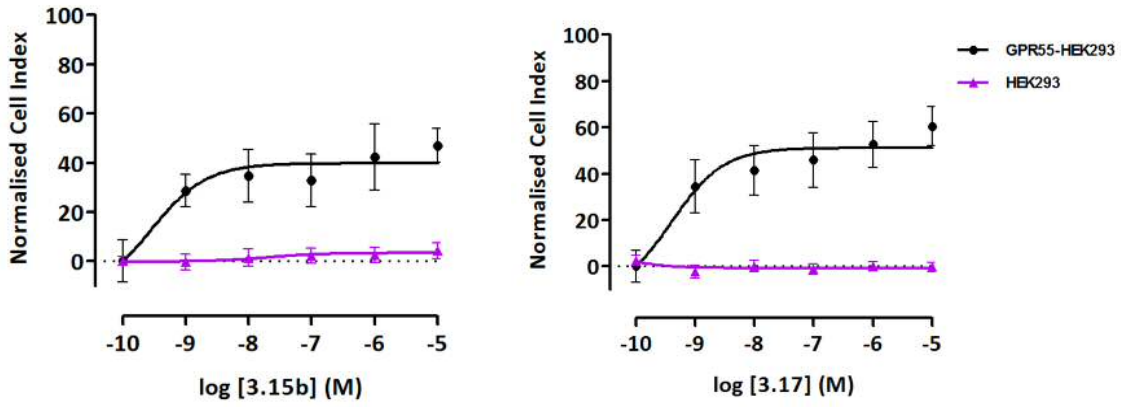

Figure 20. Concentration-response curves of LPI and representative chromenopyrazole derivatives in *h*GPR55-HEK293 and normal HEK293 cells. Data points represent the mean ± SEM values of four independent experiments, performed in duplicate. The data is presented as a percentage of the maximal LPI stimulation.

3.5 Cannabinoid binding studies

Most of the GPR55 ligands identified so far are also able to modulate CB_1 and/or CB_2 receptors. Indeed, in order to further investigate the selectivity of the new compounds, their capacity to interact with CB_1R and CB_2R was evaluated. The affinities of compounds **3.8–3.19** were determined by radioligand binding studies at human CB_1R and CB_2R using [^{3}H]CP55940 as cannabinoid receptor radioligand. As a source for human CB_1R and CB_2R, membrane preparations of HEK293 EBNA cells stably expressing the respective receptor subtype were utilized. Initially the compounds were screened at a concentration of 40 μM. In cases where inhibition of radioligand binding was at least about 70%, full concentration−effect curves were performed in order to calculate K_i values. The experimental binding affinities of **3.8–3.19** and WIN55,212-2 are reported in table 4.

As clearly shown by the affinity data, none of the compounds bind to CB_1R. From series I, chromenopyrazoles **3.9–3.11** did not bind either to CB_2R. However, when the phenyl group was not substituted (compounds **3.8a** and **3.8b**), a moderate CB_2R affinity was displayed. From this series, compound **9b,** which showed to be GPR55 partial agonist, stands out since it did not act on CBRs. Regarding series II, chromenopyrazoles **3.13–3.19** revealed moderate to high affinity towards CB_2R except compound **3.16** which lacked affinity for CBRs.

In conclusion, **3.16** can be considered a good lead compound for further development considering its GPR55 partial agonist/LPI antagonist properties and its GPR55 selectivity versus CBRs. This molecule bears a phenoxyacetyl piperazine which is the largest substituent assessed within this series. This fact may indicate that smaller substituents are preferred for CB_2R affinity.

Interestingly, the GPR55 partial agonist **3.15b**, is a selective and potent CB_2R agonist with affinity in the nanomolar range (GTPγS assays: EC_{50}: 331.0 ± 125.9 nM; E_{max}: 91.1 ± 7.5%). Even though our main purpose is the identification of GPR55 selective ligands, a dual GPR55-CB_2 drug may open novel therapeutic strategies due to the close relation of both GPCRs in different pathologies.[27,26]

Table 4. Binding affinity of compounds **3.8–3.19** and the reference cannabinoid WIN55,212-2 for hCB_1R and hCB_2R.

Compd	R	Pyrazole Substitution	CB_1R K_i (nM)[a]	CB_2R K_i (nM)[a]
3.8a	H	**N1**	>40000	4923 ± 349
3.8b	H	**N2**	>40000	1578 ± 461
3.9a	2-OMe	**N1**	>40000	>40000
3.9b	2-OMe	**N2**	>40000	>40000
3.10a	2,3-diMe	**N1**	>40000	>40000
3.10b	2,3-diMe	**N2**	>40000	>40000
3.11	4-OMe	**N1**	>40000	>40000
3.13a		**N1**	>40000	nd
3.13b		**N2**	>40000	698 ± 107
3.14a		**N1**	>40000	nd
3.14b		**N2**	>40000	3604 ± 941
3.15a		**N1**	>40000	nd
3.15b		**N2**	>40000	15.4 ± 7.8
3.16	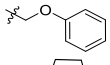	**N2**	>40000	>40000
3.17		**N2**	>40000	1073 ± 238
3.18		**N2**	>40000	523 ± 144
3.19		**N2**	>40000	6392 ± 327
WIN55,212-2	-	-	45.6 ± 8.6	3.7 ± 0.2

[a]Values obtained from competition curves using [^{3}H]CP55940 as radioligand for *h*CB_1R and *h*CB_2R cannabinoid receptors and are expressed as the mean ± SEM of at least three experiments. nd: not determined.

4. Discussion and conclusions

The first selective GPR55 ligands were discovered only a few years ago. Since then, few new structures have been reported. Regarding ligand-receptor interactions, there is also little information already available. In this context, the study developed in this chapter aims to identify a novel GPR55 chemotype. The two series presented here have been designed based on the chromenopyrazole scaffold and structural features of previously investigated GPR55 ligands. In the first series, the chromenopyrazole is *N*-substituted by a 2-(4-arylpiperazinyl)acetamidomethyl group. In the second series, 2-(4-acylpiperazinyl)ethyl group was selected as *N*-substituent of the same scaffold. The synthesis of these compounds showed some difficulties. The preparation of the derivatives of series I resulted in poor yields due to purification issues in the last step of the route (scheme 2). Nevertheless, the synthesis of the acylpiperazinyl chromenopyrazoles (series II) afforded the desired compounds with reasonable yields by a 5 steps synthetic procedure.

In what concerns the pharmacological evaluation, it is noteworthy to mention that it is the first time that a GPR55 screening to discover new ligands was performed by xCELLigence assays. Discrepancies reported in the literature regarding GPR55 pharmacology are mainly due to the inconsistent outcomes obtained from different functional assays. Therefore, appraisal of GPR55 activity of the new synthesized compounds was accomplished by using an innovative technology based on cell-impedance providing an integrative assessment of the cellular response to GPR55 stimulation. These assays take into account the different possible signaling pathways circumventing the individual functional outcome problems. The use of this novel label-free technology approach adds value to the drug discovery process considering the lack of available GPR55 radioligands.

The functional assays revealed that most chromenopyrazoles of series II showed GPR55-mediated effects. Compared to LPI efficacy, they are partial agonist of GPR55, however they have similar potency. The only two inactive derivatives correspond to the tested chromenopyrazoles substituted in *N*1-position. This finding highlights the *N*2-preferred substitution suggested by the electrostatic

potential maps studies obtained in the design of the novel potential GPR55 chemotypes. The experimental data are in agreement with a possible inversed-L or 7 shape adopted by the *N*2-substituted isomers. Upon antagonist treatment, four of these GPR55 partial agonists significantly inhibited GPR55-mediated LPI effect (**3.16**-**3.19**).

To ensure that this functionality was GPR55-mediated and considering that the impedance measurements are cell-based screening, control experiments with normal HEK293 cells were undertaken. It is noteworthy that the new compounds did not show any effect while off-targets effects of LPI was observed at 1 μM.

Since GPR55 was shown to be activated by cannabinoid ligands, it was of interest to evaluate the affinity of these novel compounds for CBRs in radioligand binding assays. The first observation concerns the lack of CB_1R binding for all compounds eliminating the possible psychotropic side-effects associated with the activation of the central CB_1R. One of GPR55 partial agonists/antagonists of LPI of series II was also devoid of CB_2R affinity. Therefore, this GRP55 selective compound (**3.16**) can be considered a good lead candidate for further development. From a structural point of view, this chromenopyrazole differs from the others of the series by the presence of a phenoxymethyl substituent on the piperazine.

Compound **3.15b** stands out because of its CB_2R affinity with EC_{50} value in the nanomolar range. This property, along with its ability to partially activate GPR55 suggests that it could be exploited as a dual GPR55-CB_2R drug. The recently reported relation of both receptors points to very interesting therapeutic opportunities, however, this is beyond the aim of the current work. From series I, we identified a partial agonist of GPR55 which lacks of CBRs affinity (**3.9**). This compound could represent a suitable lead structure, however, it would be necessary to look for an easier synthetic access to such compounds.

Despite the potential therapeutic interest of GPR55 agonists and antagonists in the treatment of diverse pathologies, it is essential to discover selective and potent ligands to develop adequate research tools for its biological study. Although LPI possess good activity and has demonstrated to

activate the receptor from different functional readouts, it is still prone to important disadvantages: poor "drug-like" properties and lack of selectivity. In this scenario, we have identified a novel GPR55 scaffold that may facilitate the characterization of this receptor. The GPR55 selective chromenopyrazoles discovered in this project[86,87] are potential candidates to generate helpful pharmacological tools or potential drugs for novel therapeutic strategies.

5. Experimental section

Chemistry.

General methods and materials. Reagents and solvents were purchased from Sigma-Aldrich Co., Fluorochem, Acros Organics, Manchester Organics and Lab-Scan and were used without further purification or drying. Microwave assisted organic synthesis was performed using the microwave reactor Biotage Initiator. Products were purified using flash column chromatography (Merck Silica gel 60, 230-400 mesh) or medium pressure chromatography using Biotage Isolera One with pre-packed silica gel columns (Biotage SNAP cartridges). Semipreparative HPLC purifications were performed on a Waters 2695 HPLC system equipped with a Photodiode Array 2998 coupled to a 3100 Mass Detector mass spectrometer, using a Sunfire^{TM} C18 column (19 mm x 150 mm) and 70 min gradient A: CH_3CN/0.1% formic acid, B: H_2O/0.1% formic acid monitoring at λ=254 nm. The flow rate was 24 mL/min. The compounds were characterized by combination of NMR experiments, HPLC-MS, high resolution mass spectrometry (HRMS) and elemental analysis. HPLC-MS analysis was performed on a Waters 2695 HPLC system equipped with a photodiode array 2996 coupled to Micromass ZQ 2000 mass spectrometer (ESI-MS), using a reverse-phase column SunFireTM (C-18, 4.6 x 50 mm, 3.5 μm) and 10 min gradient A: CH_3CN/0.1% formic acid, B: H_2O/0.1% formic acid visualizing at λ = 254 nm. Flow rate was 1 mL/min. Elemental analyses of the compounds were performed using a LECO CHNS-932 apparatus. Deviations of the elemental analysis results from the calculated are within ± 0.4%. The purity of compounds **3.8**-**3.19** was determined by LC coupled to HRMS. The experiments were performed in a LC-MS hybrid quadrupole/time of flight (QTOF) analyzer equipped with an Agilent 1100 LC coupled to an Agilent 6500 Accurate Mass (1-2 ppm mass accuracy) using electrospray ionization in the positive mode (ESI^+). ^1H, ^{13}C, HSQC and HMBC-NMR spectra were recorded on a Mercury 400 (400 and 101 MHz) or a Varian 500 (500 and 126 MHz) at 25 °C. Samples were prepared as solutions in deuterated solvent and referenced to internal non-deuterated solvent peak. Chemical shifts were

expressed in ppm (δ) downfield of tetramethylsilane. Coupling constants are given in hertzs (Hz). Melting points were measured on a MP 70 Mettler Toledo apparatus.

7-Methoxy-2,2-dimethylchroman-4-one (3.1).[88]

To a solution of 2-hydroxy-4-methoxyacetophenone (3.01 g, 18.05 mmol) in ethanol (30 mL) and acetone (13.24 mL, 180.53 mmol), pyrrolidine (4.52 mL, 54.16 mmol) was added in one portion. The mixture was refluxed for 6 h. After reaction completion, the solvent was removed under reduced pressure. The resultant crude was diluted by EtOAc and washed with aqueous NH_4Cl solution and brine. The aqueous layer was extracted with EtOAc three times. The combined organic layer was dried over anhydrous $MgSO_4$, filtered and the solvent was condensed under vacuum. Column chromatography on silica gel (hexane/ EtOAc, 3:1) provided the desired product as a yellow solid (3.04 g, 82%); mp: 81–83ºC (82-83ºC);[89] ^{1}H-NMR (400 MHz, $CDCl_3$) δ: 7.78 (d, *J* = 8.8 Hz, 1H, 5-H), 6.52 (dd, *J* = 8.8, 2.4 Hz, 1H, 6-H), 6.36 (d, *J* = 2.4 Hz, 1H, 8-H), 3.81 (s, 3H, OCH_3), 2.66 (s, 2H, 3-H), 1.44 ppm (s, 6H, $OC(CH_3)_2$); ^{13}C-NMR (101 MHz, $CDCl_3$) δ: 191.3 (4-C), 166.4 (7-C), 162.2 (8a-C), 128.4 (5-C), 114.3 (4a-C), 109.5 (8-C), 101.3 (6-C), 79.8 (2-C), 55.8 (OCH_3), 48.8 (3-C), 26.9 ppm ($OC(CH_3)_2$); HPLC-MS: [A, 15→95%], t_R: 4.55 min, (99%); MS (ES^+, *m/z*) 207 $[M + H]^+$.

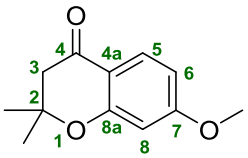

3-(Hydroxymethylene)-7-methoxy-2,2-dimethylchroman-4-one (3.2).[90]

A solution of **3.1** (2.80 g, 13.59 mmol) in anhydrous THF (15 mL) was added to a vial containing dry sodium hydride (1.30 g, 54.36 mmol) under N_2 atmosphere. The mixture was irradiated under microwave at 45ºC for 25 minutes. Subsequently, ethyl formate (5.48 mL, 67.96 mmol) was added to the sealed vial and it was irradiated under microwave at 45ºC for 25 minutes. Water was added and the product was extracted with EtOAc. The combined organic layers were dried over Mg_2SO_4 and the solvent was evaporated under reduced pressure. The crude was purified by column chromatography on silica gel (hexane/ EtOAc, 3:1) to afford the title product **3.2** (1.46 g, 52%) as a light yellow oil: ^{1}H-NMR (400 MHz, $CDCl_3$) δ: 7.82 (d, *J*=8.7 Hz, 1H, 5-H), 7.78 (d, *J* = 9.0 Hz, 1H, C*H*OH), 6.49 (dd, *J*= 8.7, 2.1 Hz,

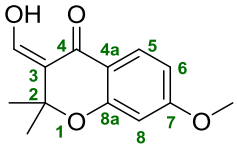

1H, 6-H), 6.26 (d, *J* = 2.1 Hz, 1H, 8-H), 3.37 (s, 3H, OCH_3), 1.45 ppm (s, 6H $OC(CH_3)_2$); ^{13}C-NMR (101 MHz, $CDCl_3$) δ: 189.6 (4-C), 167.4 (7-C), 164.2 (CHOH), 158.9 (8a-C), 126.8 (5-C), 115.1(4a-C), 110.3 (8-C), 105.8 (6-C), 87.1 (2-C), 64.5 (OCH_3), 50.9 (3-C), 25.8 ppm ($OC(CH_3)_2$); HPLC-MS: [A, 60→95%], t_R: 2.70 min, (98%); MS (ES^+, *m/z*) 235 $[M + H]^+$.

1,4-Dihydro-7-methoxy-4,4-dimethylchromeno[4,3-*c*]pyrazole (3.3).[91]

A solution of **3.2** (1.46 g, 6.27 mmol) and anhydrous hydrazine (0.58 mL, 18.83 mmol) in EtOH (20 mL) was stirred at 60ºC during 2 h. The solvent was removed under reduced pressure, and the crude residue was subjected to silica gel column chromatography (hexane/EtOAc, 1:1) to obtain **3.3** as a white solid (0.99 g, 69%); mp: 158–160ºC (167-169ºC);[91] ^{1}H-NMR (400 MHz, $CDCl_3$) δ: 7.98-7.96 (br s, 1H, NH), 7.57 (d, *J* = 7.8, Hz, 1H, 9-H), 7.33 (s, 1H, 3-H), 6.55 (d, *J* = 2.5 Hz, 1H, 6-H), 6.52 (dd, *J* = 7.8, 2.5 Hz, 1H, 8-H), 3.78 (s, 3H, OCH_3), 1.61 ppm (s, 6H, $OC(CH_3)_2$); ^{13}C-NMR (101 MHz, $CDCl_3$) δ: 161.3 (7-C), 154.6 (5a-C), 125.6 (9b-C), 123.7 (3-C), 123.1 (3a-C), 120.2 (9-C), 109.9 (8-C), 108.1 (6-C), 103.2 (9a-C), 76.2 ($OC(CH_3)_2$), 55.5 (OCH_3), 29.4 ppm ($OC(CH_3)_2$); HPLC-MS: [A, 15→95%], t_R: 4.09 min, (98%); MS (ES^+, *m/z*) 231 $[M + H]^+$.

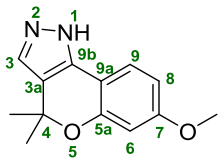

General procedure for the synthesis of phenylpiperazinyl-acetamides 3.4–3.7

To a mixture of the corresponding phenylpiperazine (1 eq) and K_2CO_3 (1.5 eq) in acetonitrile, a solution of 2-chloro-N-hydroxymethylacetamide (2 eq) in acetonitrile was added. The reaction was refluxed for 2-5 h. After reaction completion, the solvent was removed under reduced pressure. The resultant crude was diluted by EtOAc, washed with water and extracted three times with EtOAc. The combined organic layers were dried over $MgSO_4$, filtered and the solvent was evaporated under vacuum. The residue was purified by flash column chromatography performed on a Biotage Isolera One. The chromatography eluent and yield are indicated below for each reaction.

***N*-Hydroxymethyl-2-(4-phenylpiperazinyl)acetamide (3.4).**

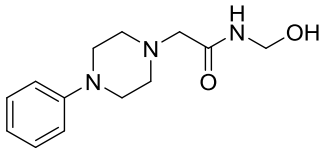

Prepared from 1-phenylpiperazine (0.62 mL, 4.05 mmol) and 2-chloro-*N*-(hydroxymethyl)acetamide (0.99 g, 8.11 mmol) and K_2CO_3 (0.83 g, 6.08 mmol) by following the above-mentioned procedure. Flash column chromatography (EtOAc) furnished **3.4** as a white solid (0.42 g, 41% yield); mp: 112–114ºC; ^{1}H-NMR (400 MHz, $CDCl_3$) δ: 8.10–8.02 (br s, 1H, NH), 7.39–7.22 (m, 2H, H_{Ph}), 7.06–6.85 (m, 3H, H_{Ph}), 4.82 (s, 2H, C*H*$_2$OH), 3.28–3.19 (m, 4H, piperazine), 3.13 (s, 2H, $COCH_2$), 2.90–2.57 ppm (m, 4H, piperazine); ^{13}C-NMR (101 MHz, $CDCl_3$) δ: 173.6 (CO), 151.5 (C_{Ph}-N), 129.8, 129.7, 120.5, 119.3 and 116.7 (C_{Ph}), 73.1(CH_2OH), 62.0 (CO*C*H$_2$), 54.1, 53.7, 50.9 and 49.8 ppm (piperazine); HPLC-MS: [A, 2% →95%], t_R: 2.46 min (93%), MS (ES$^+$, *m/z*) 250 [M+H]$^+$; Anal. Calcd. for $C_{13}H_{19}N_3O_2$: C 62.63%, H 7.68%, found: C 62.41%, H 7.83%.

_N_-Hydroxymethyl-2-[4-(2-methoxyphenyl)piperazinyl]acetamide (3.5).

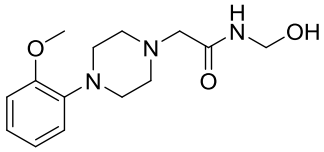

Prepared from 1-(2-methoxyphenyl)piperazine (1.17 g, 6.08 mmol) and 2-chloro-*N*-hydroxymethylacetamide (1.49 g, 12.18 mmol) and K_2CO_3 (1.26 g, 9.12 mmol) by following the general procedure. Flash column chromatography (EtOAc) afforded **3.5** as a white solid (1.06 g, 63% yield); mp: 134–136ºC; ^{1}H-NMR (400 MHz, $CDCl_3$) δ: 8.14–8.11 (br s, 1H, NH), 7.03–6.96 (m, 2H, H_{Ph}), 6.89–6.78 (m, 2H, H_{Ph}), 4.79 (s, 2H, C*H*$_2$OH), 3.94–3.64 (m, 5H, $COCH_2$ and OCH_3), 3.17–2.89 (m, 4H, piperazine), 2.84–2.66 ppm (m, 4H, piperazine); ^{13}C-NMR (101 MHz, $CDCl_3$) δ: 171.4 (CO), 151.7 (C_{Ph}-N), 140.4 (C_{Ph}- OCH_3), 122.6, 120.5, 117.6 and 110.8 (C_{Ph}), 63.0 (CH_2OH), 61.0 (CO*C*H$_2$), 54.8 (OCH_3), 53.6, 53.2, 51.0 and 50.1 ppm (piperazine); HPLC-MS: [A, 2% →95%], t_R: 3.24 min (92%), MS (ES$^+$, *m/z*) 280 [M+H]$^+$; Anal. Calcd. for $C_{14}H_{21}N_3O_3$: C 60.20%, H 7.58%, found: C 60.31%, H 7.72%.

2-[4-(2,3-Dimethylphenyl)piperazinyl]-_N_-hydroxymethylacetamide (3.6).

Prepared from 1-(2,3-dimethylphenyl)piperazine (0.29 mL, 1.57 mmol) and 2-chloro-*N*-

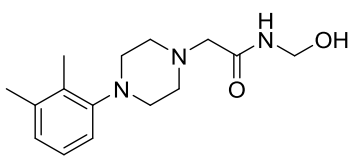

hydroxymethylacetamide (0.39 g, 3.15 mmol) and K_2CO_3 (0.32 g, 2.36

mmol) by following the general procedure. Flash column chromatography (EtOAc) yielded **3.6** as a white solid (0.11 g, 25% yield); mp: 126–127ºC; ^{1}H-NMR (400 MHz, $CDCl_3$) δ: 8.19–8.14 (br s, 1H, NH), 7.07 (t, J = 7.6 Hz, 1H, H_{Ph}), 6.98–6.90 (m, 2H, H_{Ph}), 5.59–5.57 (br s, 1H, OH), 4.82 (s, 2H, CH_2OH), 3.14 (s, 2H, $COCH_2$), 2.94–2.92 (m, 4H, piperazine), 2.77–2.73 (m, 4H, piperazine), 2.27 (s, 3H,CH_3), 2.21 ppm (s, 3H, CH_3); ^{13}C-NMR (101 MHz, $CDCl_3$) δ: 173.8 (CO), 172.0 (C_{Ph}-N), 151.2, 138.0, 131.3, 125.8 and 125.1 (C_{Ph}), 74.6 (CH_2OH), 67.3 (COCH_2), 63.7, 61.5, 54.1 and 52.2 (piperazine), 20.6 (CH_3), 13.9 ppm (CH_3); HPLC-MS: [A, 2%→95%], t_R: 3.99 min (90%), MS (ES^+, m/z) 278 $[M+H]^+$; Anal. Calcd. for $C_{15}H_{23}N_3O_2$: C 64.96%, H 8.36%, found: C 65.09%, H 8.03%.

***N*-Hydroxymethyl-2-[4-(4-methoxyphenyl)piperazinyl]acetamide (3.7).**

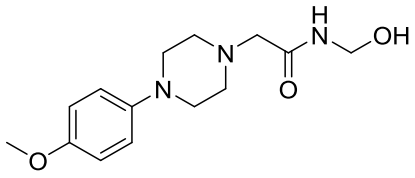

Prepared from 1-(4-methoxyphenyl)piperazine (0.39 g, 2.03 mmol) and 2-chloro-*N*-hydroxymethylacetamide (0.50 g, 4.05 mmol) and K_2CO_3 (0.42 mg, 3.04 mmol) by following the general procedure. Flash column chromatography (EtOAc) provided **3.7** as a white solid (0.14 g, 24% yield); mp: 140–143ºC; ^{1}H-NMR (400 MHz, $CDCl_3$) δ: 7.09–6.95 (m, 2H, H_{Ph}), 6.71–6.54 (m, 2H, H_{Ph}), 4.83 (s, 2H, CH_2OH), 3.78–3.60 (m, 5H, $COCH_2$ and OCH_3), 3.14–3.05 (m, 4H, piperazine), 2.77–2.71 ppm (m, 4H, piperazine); ^{13}C-NMR (101 MHz, $CDCl_3$) δ: 173.0 (CO), 152.4 (C_{Ph}-N), 143.6 (C_{Ph}-OCH_3), 123.4, 122.1, 118.6 and 112.3 (C_{Ph}), 65.7 (CH_2OH), 63.2 (COCH_2), 55.1 (OCH_3), 54.3, 53.8, 51.8 and 51.2 ppm (piperazine); HPLC-MS: [A, 2%→95%], t_R: 3.03 min (90%), MS (ES^+, m/z) 280 $[M+H]^+$; Anal. Calcd. for $C_{14}H_{21}N_3O_3$: C 60.20%, H 7.58%, found: C 60.56%, H 7.25%.

General procedure for the synthesis of phenylpiperazinyl-acetamidomethyl chromenopyrazoles 3.8–3.11

A solution of **3.3** (1 eq) in anhydrous THF (2-8 mL) was added dropwise to a precooled suspension of NaH (2.5-3 eq) in anhydrous THF (1-4 mL) under nitrogen atmosphere. The resulting mixture was stirred for 10 minutes at room temperature. The corresponding phenylpiperazinyl-acetamide (2

eq) was added and the reaction mixture was refluxed at room temperature 12-72 h. The solvent was removed under vacuum and the crude was diluted in EtOAc, washed with water and extracted three times with EtOAc. The combined organic layers were dried over $MgSO_4$ and the solvent was removed under vacuum. The residue was first purified by flash column chromatography (EtOAc as eluent) obtaining a mixture of the *N*1 and *N*2 regioisomers which was then purified by semipreparative HPLC.

1,4-Dihydro-7-methoxy-4,4-dimethyl-1-[2-(4-phenylpiperazinyl)acetamidomethyl]-chromeno[4,3-*c*]pyrazole (3.8a) and 2,4-dihydro-7-methoxy-4,4-dimethyl-2-[2-(4-phenylpiperazinyl)acetamidomethyl]-chromeno[4,3-*c*]pyrazole (3.8b).

The products were prepared according to the above described procedure from **3.3** (95 mg, 0.41 mmol) *N*-hydroxymethyl-2-(4-phenylpiperazinyl)acetamide **3.4** (0.21 g, 0.82 mmol) and NaH (24 mg, 1.03 mmol). Flash column chromatography and subsequent semipreparative HPLC (conditions previously indicated) afforded the regioisomers **3.8a** and **3.8b**. Compound **3.8a** was obtained as a white solid (25.0 mg, 13% yield); mp: 196–198ºC; ^{1}H-NMR (500 MHz, $CDCl_3$) δ: 8.02–7.97 (br t, *J* = 6.3 Hz, 1H, NH), 7.76 (d, *J* = 8.7 Hz, 1H, 9-H), 7.26 (s, 1H, 3-H), 6.85–6.74 (m, 2H, H_c and H_e), 6.55 (dd, *J* = 8.6, 2.6 Hz, 2H, H_b and H_f), 6.53–6.46 (m, 2H, 8-H and H_d), 6.45 (d, *J* = 2.5 Hz, 1H, 6-H), 5.73 (d, *J* = 6.3 Hz, 2H, CH_2NH), 3.71 (s, 3H, OCH_3), 3.13–3.07 (m, 4H, piperazine), 3.03 (s, 2H, $COCH_2$), 2.57–2.48 (m, 4H, piperazine), 1.52 ppm (s, 6H, $OC(CH_3)_2$); ^{13}C-NMR (126 MHz, $CDCl_3$) δ: 170.2 (CO), 165.1 (7-C), 161.0 (5a-C), 154.3 (C_a), 149.2(9b-C), 133.8 (C_c and C_e), 132.5 (3-C), 129.1 (9-C), 123.3 (3a-C), 121.4 (C_b and C_f), 120.0 (C_d), 116.2 (9a-C), 107.8 (8-C), 103.85 (6-C), 76.73 (O*C*$(CH_3)_2$), 61.3 (CO*C*H_2), 55.3 (OCH_3), 54.32 (CH_2NH), 53.4, 49.1 (piperazine), 28.24 ppm (OC(*C*$H_3)_2$); HPLC-MS: [A, 15%→40%], t_R: 8.01 min (97%), MS (ES^+, *m*/*z*) 462 $[M+H]^+$; HRMS calcd for $C_{26}H_{31}N_5O_3$: 461.2426, found: 461.2433.

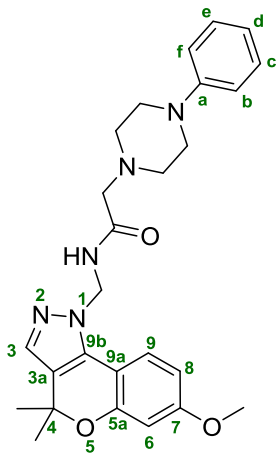

Compound **3.8b** was obtained as a white gummy solid (10.2 mg, 5% yield); ^{1}H-NMR (500 MHz, CD_3OD) δ: 8.44–8.40 (br s, 1H, NH), 7.51 (d, *J* = 8.5, 1H, 9-H), 7.44 (s, 1H, 3-H), 7.15–7.04 (m, 2H, H_c and H_e), 6.82 (dd, *J* = 7.4, 1.0 Hz, 2H, H_b and H_f), 6.72 (tt, *J* = 7.4, 1.0 Hz, 1H, H_d), 6.47 (dd, *J* = 8.5, 2.4 Hz, 1H, 8-H), 6.39 (d, *J* = 2.4 Hz, 1H, 6-H), 5.40 (s, 2H, CH_2NH), 3.69 (s, 3H, OCH_3), 3.10-3.07 (m, 4H, piperazine), 3.02 (s, 2H, $COCH_2$), 2.55-2.49 (m, 4H, piperazine), 1.46 ppm (s, 6H, $OC(CH_3)_2$); ^{13}C-NMR (126 MHz, CD_3OD) δ: 173.7 (CO), 162.7 (7-C), 156.1 (5a-C), 152.7 (C_a), 144.6 (9b-C), 130.0 (C_c and C_e), 126.6 (3-C), 123.9 (9-C), 122.4 (3a-C), 121.1 (C_b and C_f), 117.5 (C_d), 111.5 (9a-C), 108.8 (8-C), 104.2 (6-C), 77.6 (O*C*$(CH_3)_2$), 62.1 (CO*C*H_2), 55.8 (OCH_3), 55.4 (CH_2NH), 54.3, 54.2, 50.5, 50.4 (piperazine), 29.3 ppm (OC(*C*$H_3)_2$); HPLC-MS: [A, 15%→40%], t_R: 7.71 min (95%), MS (ES^+, *m/z*) 462 $[M+H]^+$; HRMS calcd for $C_{26}H_{31}N_5O_3$: 461.2426, found: 461.2421.

1,4-Dihydro-7-methoxy-1-{2-[4-(2-methoxyphenyl)piperazinyl)acetamidomethyl]}-4,4-dimethylchromeno[4,3-*c*]pyrazole (3.9a) and 2,4-dihydro-7-methoxy-2-{2-[4-(2-methoxyphenyl)piperazinyl]acetamidomethyl}-4,4-dimethylchromeno[4,3-*c*]pyrazole (3.9b).

The products were prepared according to the above described procedure from **3.3** (50 mg, 0.21 mmol) *N*-hydroxymethyl-2-[4-(2-methoxyphenyl)piperazinyl]acetamide **3.5** (0.12 g, 0.43 mmol) and NaH (15 mg, 0.65 mmol). Flash column chromatography and subsequent semipreparative HPLC furnished the regioisomers **3.9a** and **3.9b**. Compound **3.9a** was obtained as a white gummy solid (3.4 mg, 3% yield); ^{1}H-NMR (500 MHz, $CDCl_3$) δ: 7.35 (d, *J* = 8.1 Hz, 1H, 9-H), 7.16 (s, 1H, 3-H), 6.71–6.59 (m, 4H, H_c, H_d, H_e and H_f), 6.42 (dd, *J* = 8.1, 2.4 Hz, 1H, 8-H), 6.38 (d, *J* = 2.4 Hz, 1H, 6-H), 5.27 (s, 2H, CH_2NH), 3.59 (s, 3H, OCH_3), 3.54 (s, 3H, OCH_3), 3.29 (s, 2H, $COCH_2$), 3.10–3.03 (m, 4H, piperazine), 2.98–2.86 (m, 4H, piperazine), 1.69 ppm (s,

6H, $OC(CH_3)_2$); ^{13}C-NMR (126 MHz, $CDCl_3$) δ: 175.0 (CO), 160.4 (7-C), 155.6 (5a-C), 155.1 (C_a), 149.5 (C_b), 147.1 (9b-C), 130.2 (3-C), 127.5 (9-C), 124.9 (3a-C), 118.7, 116.9, 116.3, 113.3 (C_c, C_d, C_e and C_f), 111.4 (9a-C), 106.8 (8-C), 104.2 (6-C), 75.8 ($OC(CH_3)_2$), 61.4 ($COCH_2$), 55.9 (OCH_3), 55.1 (OCH_3), 54.0 (CH_2NH), 53.7, 51.3 (piperazine), 25.9 ppm ($OC(CH_3)_2$); HPLC-MS: [A, 15%→40%], t_R: 7.35 min (93%), MS (ES^+, *m/z*) 492 $[M+H]^+$; HRMS calcd for $C_{27}H_{33}N_5O_4$: 491.2532, found: 491.2528.

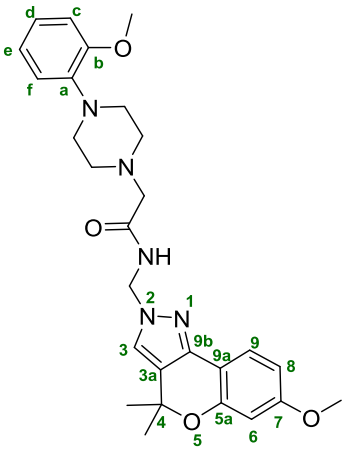

Compound **3.9b** was obtained as a yellow oil (9.1 mg, 8% yield); ^{1}H-NMR (500 MHz, $CDCl_3$) δ: 7.04 (d, J = 7.5 Hz, 1H, 9-H), 6.91 (s, 1H, 3-H), 6.69–6.51 (m, 5H, 8-H, H_c, H_d, H_e and H_f), 6.42 (d, J = 2.6 Hz, 1H, 6-H), 5.51 (s, 2H, CH_2NH), 3.64 (s, 3H, OCH_3), 3.59 (s, 3H, OCH_3), 3.16 (s, 2H, $COCH_2$), 2.92–2.89 (m, 4H, piperazine), 2.76–2.70 (m, 4H, piperazine), 1.54 ppm (s, 6H, $OC(CH_3)_2$); ^{13}C-NMR (126 MHz, $CDCl_3$) δ: 173.2 (CO), 163.1 (7-C), 156.7 (5a-C), 153.1 (C_a), 148.1 (C_b), 144.9 (9b-C), 132.6 (3-C), 126.1 (9-C), 125.6 (3a-C), 120.9, 118.2, 117.5, 114.0 (C_c, C_d, C_e and C_f), 110.6 (9a-C), 109.4 (8-C), 106.0 (6-C), 75.3 ($OC(CH_3)_2$), 60.2 ($COCH_2$), 56.8 (OCH_3), 56.1 (OCH_3), 54.6 (CH_2NH), 52.5, 50.7 (piperazine), 26.4 ppm ($OC(CH_3)_2$); HPLC-MS: [A, 15%→40%], t_R: 7.17 min (95%), MS (ES^+, *m/z*) 492 $[M+H]^+$; HRMS calcd for $C_{27}H_{33}N_5O_4$: 491.2532, found: 491.2540.

1-{2-[4-(2,3-Dimethylphenyl)piperazinyl]acetamidomethyl}-1,4-dihydro-7-methoxy-4,4-dimethylchromeno[4,3-*c*]pyrazole (3.10a) and 2-{2-[4-(2,3-dimethylphenyl)piperazinyl]acetamidomethyl}-2,4-dihydro-7-methoxy-4,4-dimethylchromeno[4,3-*c*]pyrazole (3.10b).

The products were prepared according to the above described procedure from **3.3** (90 mg, 0.39 mmol) *N*-hydroxymethyl-2-[4-(2,3-dimethylphenyl)piperazinyl]acetamide **3.6** (0.21 g, 0.78 mmol) and NaH (23 mg, 0.97 mmol). Flash column chromatography and subsequent semipreparative HPLC provided the regioisomers **3.10a** and **3.10b**. Compound **3.10a** was obtained as a yellow oil

(3.5 mg, 2% yield); ^{1}H-NMR (500 MHz, $CDCl_3$) δ: 8.08–8.02 (bt, *J* = 6.4 Hz, 1H, NH), 7.76 (d, *J* = 8.1 Hz, 1H, 9-H), 7.50 (s, 1H, 3-H), 6.94 (t, *J* = 7.5 Hz, 1H, H_e), 6.85 (d, *J* = 7.5 Hz, 1H, H_d or H_f),

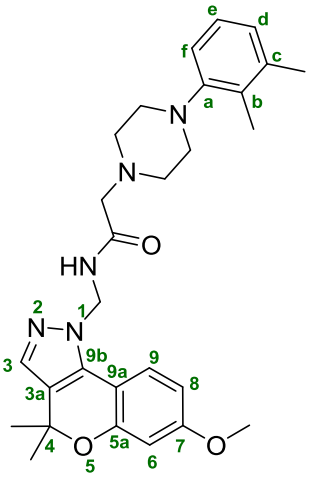

6.80 (d, *J* = 7.7 Hz, 1H, H_d or H_f), 6.61 (dd, *J* = 8.1, 2.6 Hz, 1H, 8-H), 6.48 (d, *J* = 2.6 Hz, 1H, 6-H), 5.61 (d, *J* = 6.4 Hz, 2H, C*H*$_2$NH), 3.84 (s, 3H, OCH_3), 3.08 (s, 2H, $COCH_2$), 2.77–2.69 (m, 4H, piperazine), 2.64–2.59 (m, 4H, piperazine), 2.31 (s, 3H, CH_3), 2.27 (s, 3H, CH_3), 1.48 ppm (s, 6H, $OC(CH_3)_2$); ^{13}C-NMR (126 MHz, $CDCl_3$) δ: 169.8 (CO), 162.4 (7-C), 156.0 (5a-C), 151.3 (C_a), 144.2 (9b-C), 140.3 (C_c), 132.5 (3-C), 126.1 (9-C), 125.0 (C_e), 123.9 (C_d), 123.1 (C_b), 121.8 (3a-C), 117.2 (C_f), 109.8 (9a-C), 108.4 (8-C), 104.9 (6-C), 75.7 (O*C*$(CH_3)_2$), 61.3 (CO*C*H_2), 56.0 (OCH_3), 54.7 (CH_2NH), 53.3, 51.9 (piperazine), 28.8 (OC(*C*$H_3)_2$), 19.7 (CH_3), 14.1 ppm (CH_3); HPLC-MS: [A, 15%→40%], t_R: 9.47 min (92%), MS (ES^+, *m*/*z*) 490 $[M+H]^+$; HRMS calcd for $C_{28}H_{35}N_5O_3$: 489.2739, found: 489.2746.

Compound **3.10b** was obtained as a white solid (8.3 mg, 4% yield); mp: 199–201°C; ^{1}H-NMR (500 MHz, $CDCl_3$) δ: 8.22–8.17 (br t, *J* = 6.9 Hz, 1H, NH), 7.62 (d, *J* = 8.5 Hz, 1H, 9-H), 7.42 (s, 1H, 3-H), 7.08 (t, *J* = 7.7 Hz, 1H, H_e), 6.91 (d, *J* = 7.7 Hz, 1H, H_d or H_f),

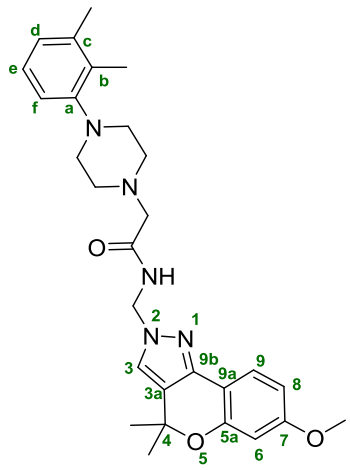

6.87 (d, *J* = 7.7 Hz, 1H, H_d or H_f), 6.57 (dd, *J* = 8.5, 2.5 Hz, 1H, 8-H), 6.51 (d, *J* = 2.5 Hz, 1H, H-6), 5.54 (d, *J* = 6.9 Hz, 2H, C*H*$_2$NH), 3.79 (s, 3H, OCH_3), 3.11 (s, 2H, $COCH_2$), 2.87 (t, *J* = 4.8 Hz, 4H, piperazine), 2.63 (t, *J* = 4.8 Hz, 4H, piperazine), 2.25 (s, 3H, CH_3), 2.18 (s, 3H, CH_3), 1.58 ppm (s, 6H, $OC(CH_3)_2$); ^{13}C-NMR (126 MHz, $CDCl_3$) δ: 171.5 (CO), 161.0 (7-C), 154.6 (5a-C), 151.1 (C_a), 143.5 (9b-C), 138.0 (C_c), 131.2 (3-C), 125.8 (9-C), 125.2 (C_e), 124.7 (C_d), 122.8(C_b), 121.5 (3a-C), 116.6 (C_f), 110.4 (9a-C), 108.0 (8-C), 103.0 (6-C), 76.5 (O*C*$(CH_3)_2$), 61.4 (CO*C*H_2), 55.3 (OCH_3), 54.2 (CH_2NH), 53.9, 52.0 (piperazine), 29.1 (OC(*C*$H_3)_2$), 20.6 (CH_3), 13.8 ppm (CH_3); HPLC-MS: [A,

15%→40%], t_R: 9.11 min (95%), MS (ES^+, m/z) 490 $[M+H]^+$; HRMS calcd for $C_{28}H_{35}N_5O_3$: 489.2739, found: 489.2750.

1,4-Dihydro-7-methoxy-1-{2-[4-(4-methoxyphenyl)piperazinyl]acetamidomethyl}-4,4-dimethylchromeno[4,3-*c*]pyrazole (3.11).

The compound was prepared according to the above described procedure from **3.3** (52 mg, 0.22 mmol) N-(hydroxymethyl)-2-(4-(4-methoxyphenyl)piperazinyl)acetamide **3.7** (0.13 g, 0.45 mmol) and NaH (13 mg, 0.56 mmol). Flash column chromatography furnished **3.11** as a yellow oil (15 mg, 14% yield); ^{1}H-NMR (500 MHz, $CDCl_3$) δ: 7.50–7.48 (br t, J = 5.1 Hz, 1H, NH), 6.81–6.76 (m, 4H, 9-H, 3-H, H_c and H_e), 6.76–6.68 (m, 2H, H_b and H_f), 6.47 (dd, J = 8.5, 2.5 Hz, 1H, 8-H), 6.39 (d, J = 2.5 Hz, 1H, 6-H), 5.39 (d, J = 5.1 Hz, 2H, CH_2NH), 3.68 (s, 3H, OCH_3), 3.63 (s, 3H, OCH_3), 3.01 (s, 2H, $COCH_2$), 2.97–2.94 (m, 4H, piperazine), 2.55–2.47 (m, 4H, piperazine), 1.46 ppm (s, 6H, $OC(CH_3)_2$); ^{13}C-NMR (126 MHz, $CDCl_3$) δ: 172.2 (CO), 161.2 (7-C), 154.6 (5a-C), 154.2 (C_a), 145.2 (9b-C), 143.2 (C_d), 125.1 (3-C), 122.4 (9-C), 120.9 (3a-C), 118.7 (C_b and C_f), 113.8 (C_c and C_e), 110.0 (9a-C), 107.3 (8-C), 102.7 (6-C), 76.1 (O*C*$(CH_3)_2$), 60.6 (CO*C*H_2), 54.4 (OCH_3), 54.3 (OCH_3), 53.9 (CH_2NH), 52.9, 50.4 (piperazine), 27.8 ppm ($OC(CH_3)_2$); HPLC-MS: [A, 15%→40%], t_R: 7.35 min (93%), MS (ES^+, m/z) 492 $[M+H]^+$; HRMS calcd for $C_{27}H_{33}N_5O_4$: 491.2532, found: 491.2524.

1-(2-Bromoethyl)-1,4-dihydro-7-methoxy-4,4-dimethylchromeno[4,3-*c*]pyrazole (3.12a) and 2-(2-bromoethyl)-2,4-dihydro-7-methoxy-4,4-dimethylchromeno[4,3-*c*]pyrazole (3.12b).

A solution of **3.3** (0.23 g, 0.99 mmol) in anhydrous THF (8 mL) was added dropwise to a precooled suspension of sodium hydride (28 mg, 1.19 mmol) in anhydrous THF (1 mL) under nitrogen atmosphere. The resulting mixture was stirred for 10 minutes at room temperature. 1,2-Dibromoethane (0.42 mL, 4.97 mmol) was added and the reaction mixture was refluxed for 4 h. The solvent was removed under vacuum and the crude was diluted in EtOAc, washed with water and extracted three times with EtOAc. The combined organic layers were dried over $MgSO_4$ and the

solvent was removed under vacuum. Column chromatography on silica gel (hexane/EtOAc, 1:1) afforded the two isomers **3.12a** and **3.12b**. Compound **3.12a** was obtained as a yellow oil (75 mg, 20%); ^{1}H NMR (400 MHz, $CDCl_3$) δ: 7.34 (d, *J* = 7.9 Hz, 1H, 9-H), 7.22 (s, 1H, 3-H), 6.50 (dd, *J* = 7.9, 2.4 Hz, 1H, 8-H), 6.43 (d, *J* = 2.4 Hz, 1H, 6-H), 4.61 (t, *J* = 6.6 Hz, 2H, 1´-H), 4.09 (t, *J* = 6.6 Hz, 2H, 2´-H), 3.92 (s, 3H, OCH_3), 1.45 ppm (s, 6H, $OC(CH_3)_2$); ^{13}C-NMR (101 MHz, $CDCl_3$) δ: 161.7 (7-C), 155.3 (5a-C), 144.7 (9b-C), 133.4 (3-C), 123.9 (9-C), 121.9 (3a -C), 108.5 (8-C), 103.4 (6-C), 101.8 (9a-C), 76.7 ($OC(CH_3)_2$), 59.3 (OCH_3), 55.8 (1´-C), 29.6 ($OC(CH_3)_2$); 28.5 ppm (2´-C); HPLC-MS: [A, 30→95%], t_R: 4.66 min, (94%); MS (ES^+, *m/z*) 337 $[M + H]^+$; HRMS calcd for $C_{15}H_{17}BrN_2O_2$: 336.0473, found: 336.0478.

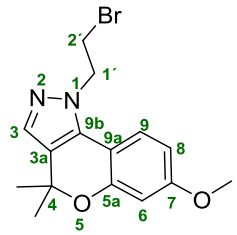

12b was obtained as a yellow oil (0.19 g, 51%); ^{1}H-NMR (400 MHz, $CDCl_3$) δ: 7.68 (d, *J* = 8.4 Hz, 1H, 9-H), 7.32 (s, 1H, 3-H), 6.63 (dd, *J* = 8.4, 2.5 Hz, 1H, 8-H), 6.58 (d, *J* = 2.5 Hz, 1H, 6-H), 4.54 (t, *J* = 6.5 Hz, 2H, 1´-H), 3.86 (s, 3H, OCH_3), 3.80 (t, *J* = 6.5 Hz, 2H, 2´-H), 1.66 ppm (s, 6H, $OC(CH_3)_2$). ^{13}C-NMR (101 MHz, $CDCl_3$) δ: 161.1 (7-C), 154.7 (5a-C), 143.8 (9b-C), 124.6 (3-C), 123.2 (9-C), 120.9 (3a -C), 110.9 (8-C), 108.1 (6-C), 103.2 (9a-C), 76.6 ($OC(CH_3)_2$), 55.5 (OCH_3), 53.8 (1´-C), 30.7 (2´-C), 29.4 ppm ($OC(CH_3)_2$); HPLC-MS: [A, 30→95%], t_R: 4.54 min, (96%); MS (ES^+, *m/z*) 337 $[M + H]^+$; HRMS calcd for $C_{15}H_{17}BrN_2O_2$: 336.0473, found: 336.0470.

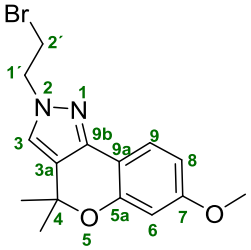

General procedure for the synthesis of acylpiperazinyl chromenopyrazoles 3.13–3.19

A mixture of the corresponding acyl piperazine (1 eq) and K_2CO_3 (3 eq) was stirred 10 minutes at room temperature in THF (1-3 mL). Then, the corresponding 2-bromoethyl-dihydro-7-methoxy-4,4-dimethyl-chromeno[4,3-*d*]pyrazole **3.12a** or **3.12b** (1 eq) dissolved in THF (1-3 mL) was added. The resulting mixture was refluxed overnight. The solvent was evaporated, the crude was dissolved in EtOAc, washed with water and extracted three times with EtOAc. The organic layers were combined and dried over $MgSO_4$, filtered and the solvent was evaporated under reduced pressure.

The residue was purified by flash column chromatography performed on a Biotage Isolera One. The chromatography eluents and yields are indicated below for each reaction.

1-{2-[4-(2-Furoyl)piperazinyl]ethyl}-1,4-dihydro-7-methoxy-4,4-dimethylchromeno[4,3-*c*] pyrazole (3.13a).

Prepared from **3.12a** (22 mg, 0.06 mmol), 1-(2-furoyl)piperazine (12 mg, 0.06 mmol) and K_2CO_3 (27 mg, 0.19 mmol) by following the general procedure. Flash column chromatography (hexane/EtOAc, 1:1) afforded **3.13a** as a white oil (7 mg, 25% yield); ^{1}H-NMR (400 MHz, $CDCl_3$) δ: 7.57 (d, *J* = 8.5 Hz, 1H, 9-H), 7.33–7.28 (m, 1H, H_c), 7.11 (s, 1H, 3-H), 6.96–6.92 (m, 1H, H_e), 6.60 (dd, *J* = 8.5, 2.5 Hz, 1H, 8-H), 6.53 (d, *J* = 2.5 Hz, 1H, 6-H), 6.39–6.36 (m, 1H, H_d), 4.22 (t, *J* = 6.6 Hz, 2H, 1´-H), 3.78 (s, 3H, OCH_3), 3.39–3.21 (m, 4H, piperazine), 2.83 (t, *J* = 6.6 Hz, 2H, 2´-H), 2.72-2.64 (m, 4H, piperazine), 1.52 ppm (s, 6H, $OC(CH_3)_2$); ^{13}C-NMR (101 MHz, $CDCl_3$) δ: 162.0 (CO), 155.6 (7-C), 153.1 (5a-C), 145.3 (9b-C), 142.6 (C_a), 141.8 (C_c), 124.1 (3-C), 123.2 (9-C), 121.3 (3a-C), 117.0, 112.2 (C_d and C_e), 109.2 (9a -C), 108.4 (8-C), 103.2 (6-C), 76.1 ($OC(CH_3)_2$), 57.5 (OCH_3), 55.1 (2´-C), 54.1, 50.7 (piperazine), 49.5 (1´-C), 28.9 ppm ($OC(CH_3)_2$); HPLC-MS: [A, 15%→95%], t_R: 2.88 min (94%), MS (ES^+, *m/z*) 437 $[M+H]^+$; HRMS calcd for $C_{24}H_{28}N_4O_4$: 436.2110, found: 436.2107.

2-{2-[4-(2-Furoyl)piperazinyl]ethyl}-2,4-dihydro-7-methoxy-4,4-dimethylchromeno[4,3-*c*]pyrazole (3.13b).

Prepared from **3.12b** (20 mg, 0.06 mmol), 1-(2-furoyl)piperazine (11 mg, 0.06 mmol) and K_2CO_3 (25 mg, 0.18 mmol) by following the general procedure. Flash column chromatography (EtOAc/MeOH, 98:2) afforded **3.13b** as a pale yellow oil (6 mg, 24 % yield); ^{1}H-NMR (400 MHz, $CDCl_3$) δ: 7.61 (d, *J* = 8.4 Hz, 1H, 9-H), 7.48–7.45 (m, 1H, H_c), 7.18 (s, 1H, 3-H), 7.00–6.94 (m, 1H, H_e), 6.54 (dd, *J* = 8.4, 2.5 Hz, 1H, 8-H), 6.50 (d, *J* = 2.5 Hz, 1H, 6-H), 6.46–6.44 (m, 1H, H_d), 4.23 (t, *J* = 6.5 Hz, 2H,

1´-H), 3.76–3.62 (br s, 7H, OCH_3, piperazine), 2.86 (t, *J* = 6.5 Hz, 2H, 2´-H), 2.70–2.66 (m, 4H, piperazine), 1.58 ppm (s, 6H, $OC(CH_3)_2$); ^{13}C-NMR (101 MHz, $CDCl_3$) δ: 160.9 (CO), 159.3 (7-C), 154.5 (5a-C), 148.0 (9b-C), 143.9 (C_a), 142.9 (C_c), 124.2 (3-C), 123.1 (9-C), 121.0 (3a-C), 116.7, 111.5 (C_d and C_e), 111.2 (9a -C), 108.0 (8-C), 103.2 (6-C), 76.7 ($OC(CH_3)_2$), 58.0 (OCH_3), 55.5 (2´-C), 53.6, 51.3 (piperazine), 50.4 (1´-C), 29.5 ppm ($OC(CH_3)_2$); HPLC-MS: [A, 15%→95%], t_R: 2.91 min (99%), MS (ES^+, *m/z*) 437 $[M+H]^+$; HRMS calcd for $C_{24}H_{28}N_4O_4$: 436.2110, found: 436.2121.

1-[2-(4-Benzoylpiperazinyl)ethyl]-1,4-dihydro-7-methoxy-4,4-dimethylchromeno[4,3-*c*]pyrazole (3.14a).

Prepared from **3.12a** (20 mg, 0.06 mmol), 1-benzoylpiperazine (11 mg, 0.06 mmol) and K_2CO_3 (25 mg, 0.18 mmol) by following the general procedure. Flash column chromatography (hexane/EtOAc, 1:1) yielded **3.14a** as a yellow gummy solid (8 mg, 30 % yield); ^{1}H-RMN (400 MHz, $CDCl_3$) δ: 7.55 (d, *J* = 8.4 Hz, 1H, 9-H), 7.38–7.29 (m, 5H, H_b, H_c, H_d, H_e and H_f), 7.13 (s, 1H, 3-H), 6.49 (dd, *J* = 8.4, 2.5 Hz, 1H, 8-H), 6.44 (d, *J* = 2.5 Hz, 1H, 6-H), 4.41 (t, *J* = 6.7 Hz, 2H, 1´-H), 3.73 (s, 3H, OCH_3), 3.41–3.26 (m, 4H, piperazine), 2.81 (t, *J* = 6.7 Hz, 2H, 2´-H), 2.59–2.37 (m, 4H, piperazine), 1.52 ppm (s, 6H, $OC(CH_3)_2$); ^{13}C-NMR (101 MHz, $CDCl_3$) δ: 170.3 (CO), 165.1 (7-C), 160.7 (5a-C), 154.3 (9b-C), 130.2 (C_a), 129.7 (C_d), 128.5, 127.1 (C_b, C_c, , C_e and C_f), 124.4 (3-C), 123.9 (9-C), 122.8 (3a-C), 107.9 (9a -C), 107.6 (8-C), 103.0 (6-C), 76.4 ($OC(CH_3)_2$), 57.8 (OCH_3), 55.4 (2´-C), 55.3, 53.6 (piperazine), 50.1 (1´-C), 29.2. ppm ($OC(CH_3)_2$); HPLC-MS: [A, 15%→95%], t_R: 3.05 min (97%), MS (ES^+, *m/z*) 447 $[M+H]^+$; HRMS calcd for $C_{26}H_{30}N_4O_3$: 446.2317, found: 446.2324.

2-[2-(4-Benzoyl-piperazinyl)ethyl]-2,4-dihydro-7-methoxy-4,4-dimethylchromeno[4,3-*c*]pyrazole (3.14b).

Prepared from **3.12b** (28 mg, 0.08 mmol), 1-benzoylpiperazine (16 mg, 0.08 mmol) and K_2CO_3 (34 mg, 0.25 mmol) by following the general procedure. Flash column chromatography (EtOAc/MeOH, 95:5) furnished **3.14b** as a yellow solid (30 mg, 81 % yield); mp: 161–162ºC; ^{1}H-

NMR (400 MHz, $CDCl_3$) δ: 7.62 (d, *J* = 8.4 Hz, 1H, 9-H), 7.46–7.32 (m, 5H, H_b, H_c, H_d, H_e and H_f),

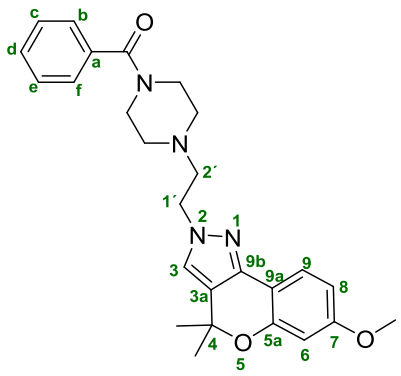

7.17 (s, 1H, 3-H), 6.55 (dd, *J* = 8.4, 2.5 Hz, 1H, 8-H), 6.50 (d, *J* = 2.5 Hz, 1H, 6-H), 4.23 (t, *J* = 6.6 Hz, 2H, 1´-H), 3.79 (s, 3H, OCH_3), 3.41–3.20 (m, 4H, piperazine), 2.87 (t, *J* = 6.6 Hz, 2H, 2´-H), 2.73–2.60 (m, 4H, piperazine), 1.58 ppm (s, 6H, $OC(CH_3)_2$); ^{13}C-NMR (101 MHz, $CDCl_3$) δ: 170.4 (CO), 160.8 (7-C), 154.5 (5a-C), 142.9 (9b-C), 135.8 (C_a), 129.9 (C_d), 128.6, 127.1 (C_b, C_c, C_e and C_f), 124.1 (3-C), 123.0 (9-C), 120.9 (3a-C), 111.1 (9a -C), 107.9 (8-C), 103.1 (6-C), 76.6 ($OC(CH_3)_2$), 57.9 (OCH_3), 55.4 (2´-C), 53.7, 50.2 (piperazine), 47.9 (1´-C), 29.4 ppm ($OC(CH_3)_2$); HPLC-MS: [A, 15%→95%], t_R: 3.08 min (100%), MS (ES^+, *m/z*) 447 $[M+H]^+$; HRMS calcd for $C_{26}H_{30}N_4O_3$: 446.2317, found: 446.2311.

1,4-Dihydro-7-methoxy-4,4-dimethyl-1-{2-[4-(2-thenoyl)piperazinyl]ethyl}-chromeno[4,3-*c*]pyrazole (3.15a).

Prepared from **3.12a** (20 mg, 0.06 mmol), 1-(2-thenoyl)piperazine trifluoroacetate (18 mg, 0.06 mmol) and K_2CO_3 (25 mg, 0.18 mmol) by following the general procedure. Flash column chromatography (hexane/EtOAc, 1:9) yielded **3.15a** as a yellow gummy solid (6 mg, 23 % yield); ^{1}H-NMR (400 MHz, $CDCl_3$) δ: 7.49 (d, *J* = 8.8 Hz, 1H, 9-H), 7.44 (dd, *J* = 5.0, 1.2 Hz, 1H, H_c), 7.28 (s, 1H, 3-H), 7.23-7.21 (m, 1H, H_e), 7.03 (dd, *J* = 5.0, 3.6 Hz, 1H, H_d), 6.61–6.58 (m, 1H, 8-H), 6.57 (d, *J* = 2.6 Hz, 1H, 6-H), 4.54 (t, *J* = 7.1 Hz, 2H, 1´-H), 3.82 (s, 3H, OCH_3), 3.77–3.64 (m, 4H, piperazine), 2.93–2.87 (m, 2H, 2´-H), 2.67–2.43 (m, 4H, piperazine), 1.58 ppm (s, 6H, $OC(CH_3)_2$); ^{13}C-NMR (101 MHz, $CDCl_3$) δ: 163.7 (CO), 161.0 (7-C), 154.6 (5a-C), 150.3 (9b-C), 137.1 (C_a), 132.8, 129.1, 128.9 (C_c, C_d and C_e), 126.9 (3-C), 122.7 (9-C), 121.4 (3a-C), 109.1 (9a -C), 107.9 (8-C), 104.1 (6-C), 76.4 ($OC(CH_3)_2$), 57.4 (OCH_3), 55.6 (2´-C), 53.6, 51.3 (piperazine), 49.5 (1´-C), 28.6 ppm ($OC(CH_3)_2$); HPLC-MS: [A, 15%→95%], t_R: 3.22 min (97%), MS (ES^+, *m/z*) 453 $[M+H]^+$; HRMS calcd for $C_{24}H_{28}N_4O_3S$: 452.1882, found: 452.1891.

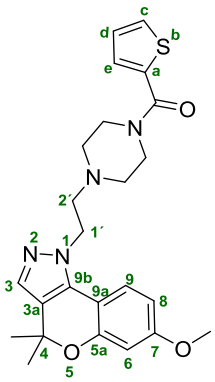

2,4-Dihydro-7-methoxy-4,4-dimethyl-2-{2-[4-(2-thenoyl)piperazinyl]ethyl}-chromeno[4,3-*c*]pyrazole (3.15b).

Prepared from **3.12b** (30 mg, 0.09 mmol), 1-(2-thenoyl)piperazine trifluoroacetate (28 mg, 0.09 mmol) and K_2CO_3 (37 mg, 0.27 mmol) by following the general procedure. Flash column chromatography (EtOAc/MeOH, 98:2) afforded **3.15b** as a yellow solid (22 mg, 55 % yield); mp: 163–165ºC; ^{1}H-NMR (400 MHz, $CDCl_3$) δ: 7.62 (d, J = 8.4 Hz, 1H, 9-H), 7.44 (dd, J = 5.0, 1.2 Hz, 1H, H_c), 7.25–7.23 (m, 1H, H_e), 7.20 (s, 1H, 3-H), 7.03 (dd, J = 5.0, 3.6 Hz, 1H, H_d), 6.55 (dd, J = 8.4, 2.5 Hz, 1H, 8-H), 6.51 (d, J = 2.5 Hz, 1H, 6-H), 4.27 (t, J = 6.5 Hz, 2H, 1´-H), 3.79 (s, 3H, OCH_3), 3.78–3.72 (m, 4H, piperazine), 3.01–2.91 (m, 2H, 2´-H), 2.63–2.43 (m, 4H, piperazine), 1.59 ppm (s, 6H, $OC(CH_3)_2$); ^{13}C-NMR (101 MHz, $CDCl_3$) δ: 163.8 (CO), 161.0 (7-C), 154.6 (5a-C), 143.1 (9b-C), 137.0 (C_a), 129.1, 128.9, 126.9 (C_c, C_d and C_e), 124.3 (3-C), 123.1 (9-C), 121.0 (3a-C), 111.1 (9a -C), 108.0 (8-C), 103.2 (6-C), 76.7 ($OC(CH_3)_2$), 57.9 (OCH_3), 55.5 (2´-C), 53.5, 50.2 (piperazine), 46.1 (1´-C), 29.5 ppm ($OC(CH_3)_2$); HPLC-MS: [A, 15%→95%], t_R: 3.03 min (100%), MS (ES^+, m/z) 453 $[M+H]^+$; HRMS calcd for $C_{24}H_{28}N_4O_3S$: 452.1882, found: 452.1889.

2,4-Dihydro-7-methoxy-4,4-dimethyl-2-[2-(4-phenoxyacetylpiperazinyl)ethyl]-chromeno[4,3-*c*]pyrazole (3.16).

Prepared from **3.12b** (30 mg, 0.09 mmol), 1-(phenoxyacetyl)piperazine (20 mg, 0.09 mmol) and K_2CO_3 (37 mg, 0.27 mmol) by following the general procedure. Flash column chromatography (EtOAc/MeOH, 95:5) afforded **3.16** as an orange solid (16 mg, 38 % yield); mp: 177–179ºC; ^{1}H-NMR (500 MHz, CD_3OD) δ: 7.56 (d, J = 8.5 Hz, 1H, 9-H), 7.52 (s, 1H, 3-H), 7.31–7.21 (m, 2H, H_c and H_e), 7.00–6.90 (m, 3H, H_b, H_d and H_f), 6.56 (dd, J = 8.5, 2.5 Hz, 1H, 8-H), 6.48 (d, J = 2.5 Hz, 1H, 6-H), 4.76 (s, 2H, OCH_2), 4.26 (t, J = 6.4 Hz, 2H, 1´-H), 3.77 (s, 3H, OCH_3), 3.63-3.50 (m, 4H, piperazine), 2.84 (t, J =

6.4 Hz, 2H, 2´-H), 2.56-2.46 (m, 4H, piperazine), 1.56 ppm (s, 6H, $OC(CH_3)_2$); ^{13}C-NMR (126 MHz, CD_3OD) δ: 167.4 (CO), 161.1 (7-C), 158.0 (C_a), 154.5 (5a-C), 142.5 (9b-C), 129.1 (C_c and C_e), 125.4 (3-C), 122.3 (9-C), 121.1 (C_d), 120.5 (9-C), 114.3 (C_b and C_f), 110.4 (9a-C), 107.2 (8-C), 102.8 (6-C), 76.2 ($OC(CH_3)_2$), 66.1 (OCH_2), 57.2 (OCH_3), 54.3 (2´-C), 52.8, 52.3 (piperazine), 49.1 (1´-C), 44.7, 43.7 (piperazine), 28.0 ppm ($OC(CH_3)_2$); HPLC-MS: [A, 15%→95%], t_R: 3.24 min (100%), MS (ES^+, *m/z*) 477 $[M+H]^+$; HRMS calcd for $C_{27}H_{32}N_4O_4$: 476.2423, found: 476.2427.

2,4-Dihydro-7-methoxy-4,4-dimethyl-2-{2-[4-(2-tetrahydrofuroyl)piperazinyl]ethyl}-chromeno[4,3-*c*]pyrazole (3.17).

Prepared from **3.12b** (30 mg, 0.09 mmol), 1-(2-tetrahydrofuroyl)piperazine (16 mg, 0.09 mmol) and K_2CO_3 (37 mg, 0.27 mmol) by following the general procedure. Flash column chromatography (EtOAc/MeOH, 98:2) furnished **3.17** as a yellow solid (14 mg, 36 % yield); mp: 158–160ºC; ^{1}H-NMR (500 MHz, CD_3OD) δ: 7.46 (d, *J* = 8.5 Hz, 1H, 9-H), 7.43 (s, 1H, 3-H), 6.46 (dd, *J* = 8.5, 2.5 Hz, 1H, 8-H), 6.38 (d, *J* = 2.5 Hz, 1H, 6-H), 4.67–4.54 (m, 1H, H_a), 4.17 (t, *J* = 6.5 Hz, 2H, 1´-H), 3.83–3.81 (m, 1H, H_c), 3.76–3.70 (m, 1H, $H_{c'}$), 3.68 (s, 3H, OCH_3), 3.55–3.39 (m, 4H, piperazine), 2.76 (t, *J* = 6.5 Hz, 2H, 2´-H), 2.46–2.33 (m, 4H, piperazine), 2.12–1.99 (m, 1H, H_e), 1.95–1.86 (m, 1H, $H_{e'}$), 1.85–1.75 (m, 2H, H_d and $H_{d'}$), 1.47 ppm (s, 6H, $OC(CH_3)_2$); ^{13}C-NMR (126 MHz, CD_3OD) δ: 171.3 (CO), 161.1 (7-C), 154.5 (5a-C), 142.5 (9b-C), 125.4 (3-C), 122.3 (9-C), 120.5 (3a-C), 110.4 (9a-C), 107.2 (8-C), 102.8 (6-C), 76.2 (C_a), 75.2 ($OC(CH_3)_2$), 68.7 (C_c), 57.2 (OCH_3), 54.3 (2´-C), 52.9, 52.3 (piperazine), 47.5 (1´-C), 44.9, 43.7 (piperazine), 28.8 (C_e), 28.0 ($OC(CH_3)_2$), 25.1 ppm (C_d); HPLC-MS: [A, 15%→95%], t_R: 2.98 min (95%), MS (ES^+, *m/z*) 441 $[M+H]^+$; HRMS calcd for $C_{24}H_{32}N_4O_4$: 440.2423, found: 440.2436.

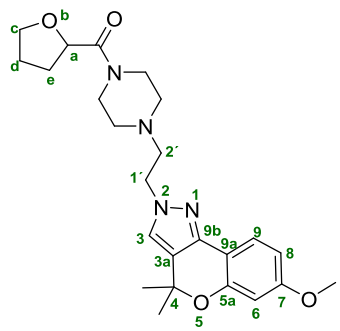

2-[2-(4-Cyclohexylcarbonylpiperazinyl)ethyl]-2,4-dihydro-7-methoxy-4,4-dimethylchromeno[4,3-*c*]pyrazole (3.18).

Prepared from **3.12b** (30 mg, 0.09 mmol), 1-(cyclohexylcarbonyl)piperazine (17 mg, 0.09 mmol) and K_2CO_3 (37 mg, 0.27 mmol) by following the general procedure. Flash column chromatography (EtOAc/MeOH, 95:5) yielded **3.18** as a yellow solid (25 mg, 62 % yield); mp: 151–152ºC; ^{1}H-NMR (400 MHz, $CDCl_3$) δ: 7.63 (d, *J* = 8.5 Hz, 1H, 9-H), 7.18 (s, 1H, 3-H), 6.56 (dd, *J* = 8.5, 2.5 Hz, 1H, 8-H), 6.51 (d, *J* = 2.4 Hz, 1H, 6-H), 4.23 (t, *J* = 6.6 Hz, 2H, 1´-H), 3.79 (s, 3H, OCH_3), 3.66–3.39 (m, 4H, piperazine), 2.85 (t, *J* = 6.6 Hz, 2H, 2´-H), 2.54–2.35 (m, 4H, piperazine), 1.82–1.75 (m, 1H, H_a), 1.73–1.61 (m, 4H, H_b and H_f), 1.59 (s, 6H, $OC(CH_3)_2$), 1.57–1.42 ppm (m, 6H, H_c, H_d and H_e); ^{13}C-NMR (101 MHz, $CDCl_3$) δ: 174.8 (CO), 160.9 (7-C), 154.6 (5a-C), 143.0 (9b-C), 124.2 (3-C), 123.1 (9-C), 121.0 (3a-C), 111.2 (9a -C), 108.0 (8-C), 103.2 (6-C), 76.7 ($OC(CH_3)_2$), 58.0 (OCH_3), 55.5 (2´-C), 53.2, 50.3 (piperazine), 45.6 (1´-C), 41.7 (C_a), 30.6 (C_b and C_f), 29.6 ($OC(CH_3)_2$), 26.1 ppm (C_c, C_d and C_e); HPLC-MS: [A, 15%→95%], t_R: 3.19 min (100%), MS (ES^+, *m/z*) 453 $[M+H]^+$; HRMS calcd for $C_{26}H_{36}N_4O_3$: 452.2787, found: 452.2773.

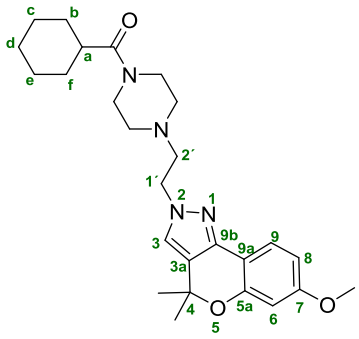

2,4-Dihydro-7-methoxy-4,4-dimethyl-2-[2-(4-pivaloyl-piperazinyl)ethyl]-chromeno[4,3-*c*]pyrazole (3.19).

Prepared from **3.12b** (20 mg, 0.06 mmol), 1-(pivaloyl)piperazine (10 mg, 0.09 mmol) and K_2CO_3 (25 mg, 0.18 mmol) by following the general procedure. Flash column chromatography (EtOAc/MeOH, 95:5) gave **3.19** as a yellow gummy solid (8 mg, 32 % yield); ^{1}H-NMR (400 MHz, $CDCl_3$) δ: 7.62 (d, *J* = 8.4 Hz, 1H, 9-H), 7.18 (s, 1H, 3-H), 6.55 (dd, *J* = 8.4, 2.5 Hz, 1H, 8-H), 6.51 (d, *J* = 2.5 Hz, 1H, 6-H), 4.23 (t, *J* = 6.6 Hz, 2H, 1´-H), 3.79 (s, 3H, OCH_3), 3.63 (t, *J* = 5.0 Hz, 4H, piperazine), 2.84 (t, *J* = 6.6 Hz, 2H, 2´-H), 2.46 (t, *J* = 5.0 Hz, 4H, piperazine), 1.59 (s, 6H, $OC(CH_3)_2$), 1.26 ppm (s, 9H, $C(CH_3)_3$); ^{13}C-NMR (101 MHz, $CDCl_3$) δ: 176.5 (CO), 160.9 (7-C), 154.6 (5a-C), 142.9 (9b-C), 124.2 (3-C), 123.1 (9-C), 121.0 (3a-C), 111.2 (9a -C), 108.0 (8-C), 103.2 (6-C), 76.7 ($OC(CH_3)_2$), 58.0 (OCH_3),

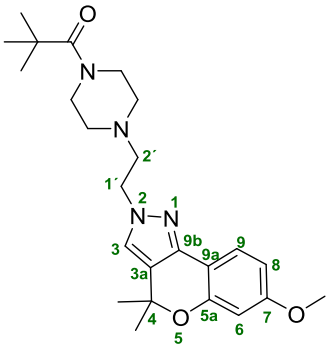

55.5 (2´-C), 53.6, 50.2 (piperazine), 45.3 (1´-C), 38.8 ($C(CH_3)_3$), 29.5 ($OC(CH_3)_2$), 28.6 ppm ($C(CH_3)_3$); HPLC-MS: [A, 15%→95%], t_R: 2.99 min (99%), MS (ES^+, m/z) 427 $[M+H]^+$; HRMS calcd for $C_{24}H_{34}N_4O_3$: 426.2630, found: 426.2618.

Conformational analysis and electrostatic potential map calculation. Global minimum energy analysis of the compounds was performed using *ab initio* Hartree-Fock (HF) calculations at the 6-31G* level, within the Spartan '08 (Wave function, Inc., Irvine, CA). A conformational search was next implemented using Molecular Mechanics (Monte Carlo method). Local energy minima was identified by rotation of a subject torsion angle through 360 in 60 increments (6-fold search), followed by HF 6-31G* energy minimization of each rotamer generated. The electrostatic potential of the global minimum energy conformer was calculated using the Hatree-Fock method at the 6-31G* level of theory and was mapped on the 0.002 isodensity surface of each molecule. The surface was color-coded according to the potential, with electron rich regions colored red and electron poor regions colored blue.

***In silico* ADME calculations.** A set of 34 physico-chemical descriptors was computed using QikProp version 3.5 integrated in Maestro (Schrödinger, LLC, New York, USA). The QikProp descriptors are shown in table 1. The 3D conformations used in the calculation of QikProp descriptors were generated using the program Spartan ´08 (Wave function, Inc., Irvine CA) as follows: the structure of each molecule was built from the fragment library available in the program. Then, *ab initio* energy minimizations of each structure at the Hartree-Fock 6-31G* level were performed. A conformational search was next implemented using Molecular Mechanics (Monte Carlo method) followed by a minimization of the energy of each conformer calculated at the Hartree-Fock 6-31G* level. The global minimum energy conformer of each compound was used as input for ADME studies with QikProp.

Pharmacological assays.

Cannabinoid binding experiments. Membranes from transfected cells with human CB_1 or CB_2 expressed cannabinoid receptors (RBHCB1M400UA and RBXCB2M400UA) were supplied by Perkin-Elmer Life and Analytical Sciences (Boston, MA). The protein concentration for the CB_1R membranes was 8.0 mg/mL, whereas for the CB_2R membranes was 4.0 mg/mL or 3.6 mg/mL depending on the batch. The commercial membranes were diluted (approximatively 1:20) with the binding buffer (50 mM TrisCl, 5 mM $MgCl_2.H_2O$, 2.5 mM EDTA, 0.5 mg/mL BSA and pH = 7.4 for CB_1 binding; 50 mM TrisCl, 5 mM $MgCl_2.H_2O$, 2.5 mM EGTA, 1 mg/mL BSA and pH = 7.5 for CB_2 binding). The final membrane protein concentration was 0.4 mg/mL of incubation volume and 0.2 mg/mL of incubation volume for the CB_1R and the CB_2R assays, respectively. The radioligand used was [^{3}H]-CP55940 (PerkinElmer) at a concentration of membrane K_D x 0.8 nm, and the final volume was 200 μL for CB_1 binding and was 600 μL for CB_2R binding. 96-Well plates and the tubes necessary for the experiment were previously siliconized with Sigmacote (Sigma).
Membranes were resuspended in the corresponding buffer and were incubated with the radioligand and each compound (10^{-4}-10^{-11} M) for 90 min at 30ºC. Non-specific binding was determined with 10 μM WIN55212-2 and 100 % binding of the radioligand to the membrane was determined by its incubation with membrane without any compound. Filtration was performed by a Harvester® filtermate (Perkin-Elmer) with Filtermat A GF/C filters pretreated with polyethylenimine 0.05%. After filtering, the filter was washed nine times with binding buffer, dried and a melt-on scintillation sheet (Meltilex™ A, Perkin Elmer) was melted onto it. Then, radioactivity was quantified by a liquid scintillation spectrophotometer (Wallac MicroBeta Trilux, Perkin-Elmer). Competition binding data were analyzed by using GraphPad Prism program and K_i values are expressed as mean ± SD of at least three experiments performed in triplicate for each point.

[^{35}S]-GTPγS Binding analysis. [^{35}S]-GTPγS binding analysis of compound **3.15b** was performed using CB_2R-containing membranes (HTS020M2, Eurofins Discovery Services). For this purpose, membranes (5 μg/well) were permeabilized by addition of saponin (Sigma-Aldrich), then mixed with

0.3 nM [^{35}S]-GTPγS (Perkin-Elmer) and 10 μM GDP (Sigma-Aldrich) in 20 mM HEPES (Sigma-Aldrich) buffer containing 100 mM NaCl (Merck) and 10 mM MgCl2 (Merck), at pH 7.4. 30 nM CP55,940 (Sigma-Aldrich) and increasing concentrations of compound **3.15b** (from 10^{-11} to 10^{-4} M) were added in a final volume of 100 μl and incubated for 30 min at 30 °C. The non-specific signal was measured with 10 μM GTPγS (Sigma-Aldrich). All 96-well plates and the tubes necessary for the experiment were previously silanized with Sigmacote (Sigma-Aldrich). The reaction was terminated by rapid vacuum filtration with a filtermate Harvester apparatus (Perkin-Elmer) through Filtermat A GF/C filters. The filters were rinsed nine times with washing buffer (10 mM sodium phosphate, pH 7.4), and left to dry, and melt-on scintillation pads (Meltilex A, Perkin Elmer) were melted onto them. The bound radioactivity was quantified by liquid scintillation spectrophotometer (Wallac MicroBeta Trilux, PerkinElmer). Data were analyzed by nonlinear regression analysis of sigmoidal dose- response curves using GraphPad Prism 5.02 (GraphPad, San Diego, CA). EC_{50} and E_{max} values are expressed as mean ± SEM of at least three independent experiments performed in triplicate.

GPR55 functionality: xCELLigence assays. Untransfected HEK293 and *h*GPR55-HEK293[17] cells were maintained at 37 °C with 5% CO_2 in α-MEM supplemented with 10% FBS, 100 IU/mL Penicillin, 100ug/mL Streptomycin and 2 mM Glutamine. The xCELLigence RTCA instrument (ACEA Biosciences; San Diego, CA) is housed within the incubator at all times allowing all experiments to be performed at 37 °C with 5% CO_2. E-plates (ACEA Biosciences; San Diego, CA) with microelectrodes integrated into the bottom of the wells to allow measurement of impedance at the electrode-cell interface, were used. In preparation for the experiment, cells were grown to 80% confluence in flasks, harvested by trypsinisation and then seeded into 96 well E-plates at a density of $5x10^4$ cells per well in duplicate. Before the addition of cells to the plate, a background reading was obtained by adding 100 μl of serum free media to each well in order to adjust for any discrepancies between wells (wells with a cell index reading above or below 0.01 were not used for experiments).

Cellular impedance was measured every 30 minutes overnight in order to monitor cell attachment and subsequent proliferation. The following day the cells were switched to serum free media (100 μl α-MEM without FBS) for 5 hours, the time taken for cellular impedance to re-stabilise in HEK293 and GPR55-HEK293 cells. All ligands were prepared in serum free media with a final concentration of DMSO at 0.1% (agonist studies) or 0.2% (antagonist studies). Compounds were tested at concentrations from 1 nM to 10 μM. The experiment is started immediately after the addition of test compounds to the wells (10 μl per well). To ensure consistency within the analysis, all experiments were normalised to the point directly before the addition of test compounds. Once normalised, the minimum cell index (dose dependant decrease found to be 5 minutes for all the compounds) was obtained and converted to a percentage decrease in cellular impedance. Dose response curves were generated using GraphPad PRISM software in order to calculate EC_{50} and E_{max} values. Full concentration−response curves for LPI in presence and absence of the compounds were determined by coadministration of the test compounds at 1 μM (or vehicle) and different concentrations of the standard agonist.

6. References

(1) Ryberg, E.; Larsson, N.; Sjögren, S.; Hjorth, S.; Hermansson, N.-O.; Leonova, J.; Elebring, T.; Nilsson, K.; Drmota, T.; Greasley, P. J. The Orphan Receptor GPR55 Is a Novel Cannabinoid Receptor. *Br. J. Pharmacol.* **2007**, *152*, 1092–1101.

(2) Johns, D. G.; Behm, D. J.; Walker, D. J.; Ao, Z.; Shapland, E. M.; Daniels, D. A.; Riddick, M.; Dowell, S.; Staton, P. C.; Green, P.; Shabon, U.; Bao, W.; Aiyar, N.; Yue, T.-L.; Brown, A. J.; Morrison, A. D.; Douglas, S. A. The Novel Endocannabinoid Receptor GPR55 Is Activated by Atypical Cannabinoids but Does Not Mediate Their Vasodilator Effects. *Br. J. Pharmacol.* **2007**, *152*, 825–831.

(3) Sawzdargo, M.; Nguyen, T.; Lee, D. K.; Lynch, K. R.; Cheng, R.; Heng, H. H.; George, S. R.; O'Dowd, B. F. Identification and Cloning of Three Novel Human G Protein-Coupled Receptor Genes GPR52, PsiGPR53 and GPR55: GPR55 Is Extensively Expressed in Human Brain. *Brain Res. Mol. Brain Res.* **1999**, *64*, 193–198.

(4) Drmota, P.; Greasley, P.; Groblewski, T. Screening Assays for Cannabinoid- Ligand Type Modulators. AstraZeneca, 2004.

(5) Brown, A. J.; Wise, A. Identification of Modulators of GPR55 Activity. GlaxoSmithKline, 2001, Patent WO00186305.

(6) Ross, R. A. The Enigmatic Pharmacology of GPR55. *Trends Pharmacol. Sci.* **2009**, *30*, 156–163.

(7) GPR18, GPR55 and GPR119: GPR55. IUPHAR/BPS Guide to Pharmacology http://www.guidetopharmacology.org/GRAC/ObjectDisplayForward?objectId=109. (accessed Aug 17, 2015).

(8) Pertwee, R. G.; Howlett, A. C.; Abood, M. E.; Alexander, S. P. H.; Marzo, V. Di; Elphick, M. R.; Greasley, P. J.; Hansen, H. S.; Kunos, G. International Union of Basic and Clinical Pharmacology. LXXIX. Cannabinoid Receptors and Their Ligands: Beyond CB1 and CB2. *Pharmacol. Rev.* **2010**, *62*, 588–631.

(9) Elbegdorj, O.; Westkaemper, R. B.; Zhang, Y. A Homology Modeling Study toward the Understanding of Three-Dimensional Structure and Putative Pharmacological Profile of the G-Protein Coupled Receptor GPR55. *J. Mol. Graph. Model.* **2013**, *39*, 50–60.

(10) Kotsikorou, E.; Madrigal, K. E.; Hurst, D. P.; Sharir, H.; Lynch, D. L.; Heynen-Genel, S.; Milan, L. B.; Chung, T. D. Y.; Seltzman, H. H.; Bai, Y.; Caron, M. G.; Barak, L.; Abood, M. E.; Reggio, P. H. Identification of the GPR55 Agonist Binding Site Using a Novel Set of High-Potency GPR55 Selective Ligands. *Biochemistry* **2011**, *50*, 5633–5647.

(11) Sharir, H.; Abood, M. E. Pharmacological Characterization of GPR55, a Putative Cannabinoid Receptor. *Pharmacol. Ther.* **2010**, *126*, 301–313.

(12) Kotsikorou, E.; Sharir, H.; Shore, D.; Hurst, D. P.; Lynch, D. L.; Madrigal, K. E.; Heynen-Genel, S.; Milan, L. B.; Chung, T. D. Y.; Seltzman, H. H.; Bai, Y.; Caron, M. G.; Barak, L.; Croatt, M. P.; Abood, M. E.; Reggio, P. H. Identification of the GPR55 Antagonist Binding Site Using a Novel Set of High-Potency GPR55 Selective Ligands. *Biochemistry* **2013**, *52*, 9456–9469.

(13) Moriconi, A.; Cerbara, I.; Maccarrone, M.; Topai, A. GPR55: Current Knowledge and Future Perspectives of a Purported "Type-3" Cannabinoid Receptor. *Curr. Med. Chem.* **2010**, *17*, 1411–1429.

(14) Nevalainen, T.; Irving, A. J. GPR55 , a Lysophosphatidylinositol Receptor with Cannabinoid Sensitivity? *Curr. Top. Med. Chem.* **2010**, *1*, 799–813.

(15) Childers, S. R.; Deadwyler, S. A. Role of Cyclic AMP in the Actions of Cannabinoid Receptors. *Biochem. Pharmacol.* **1996**, *52*, 819–827.

(16) Bonhaus, D. W.; Chang, L. K.; Kwan, J.; Martin, G. R. Dual Activation and Inhibition of Adenylyl Cyclase by Cannabinoid Receptor Agonists: Evidence for Agonist-Specific Trafficking of Intracellular Responses. *J. Pharmacol. Exp. Ther.* **1998**, *287*, 884–888.

(17) Henstridge, C. M.; Balenga, N. A. B.; Ford, L. A.; Ross, R. A.; Waldhoer, M.; Irving, A. J. The GPR55 Ligand L-Alpha-Lysophosphatidylinositol Promotes RhoA-Dependent Ca2+ Signaling and NFAT Activation. *FASEB J.* **2009**, *23*, 183–193.

(18) Waldeck-Weiermair, M.; Zoratti, C.; Osibow, K.; Balenga, N.; Goessnitzer, E.; Waldhoer, M.; Malli, R.; Graier, W. F. Integrin Clustering Enables Anandamide-Induced Ca2+ Signaling in Endothelial Cells via GPR55 by Protection against CB1-Receptor-Triggered Repression. *J. Cell Sci.* **2008**, *121*, 1704–1717.

(19) Lauckner, J. E.; Jensen, J. B.; Chen, H.-Y.; Lu, H.-C.; Hille, B.; Mackie, K. GPR55 Is a Cannabinoid Receptor That Increases Intracellular Calcium and Inhibits M Current. *Proc. Natl. Acad. Sci. U. S. A.* **2008**, *105*, 2699–2704.

(20) Henstridge, C. M.; Balenga, N. A.; Schröder, R.; Kargl, J. K.; Platzer, W.; Martini, L.; Arthur, S.; Penman, J.; Whistler, J. L.; Kostenis, E.; Waldhoer, M.; Irving, A. J. GPR55 Ligands Promote Receptor Coupling to Multiple Signalling Pathways. *Br. J. Pharmacol.* **2010**, *160*, 604–614.

(21) Oka, S.; Nakajima, K.; Yamashita, A.; Kishimoto, S.; Sugiura, T. Identification of GPR55 as a Lysophosphatidylinositol Receptor. *Biochem. Biophys. Res. Commun.* **2007**, *362*, 928–934.

(22) Oka, S.; Toshida, T.; Maruyama, K.; Nakajima, K.; Yamashita, A.; Sugiura, T. 2-Arachidonoyl-Sn-Glycero-3-Phosphoinositol: A Possible Natural Ligand for GPR55. *J. Biochem.* **2009**, *145*, 13–20.

(23) Henstridge, C. M. Off-Target Cannabinoid Effects Mediated by GPR55. *Pharmacology* **2012**, *89*, 179–187.

(24) Park, P. S.-H. Ensemble of G Protein-Coupled Receptor Active States. *Curr. Med. Chem.* **2012**, *19*, 1146–1154.

(25) Audet, M.; Bouvier, M. Restructuring G-Protein- Coupled Receptor Activation. *Cell* **2012**, *151*, 14–23.

(26) Moreno, E.; Andradas, C.; Medrano, M.; Caffarel, M. M.; Pérez-Gómez, E.; Blasco-Benito, S.; Gómez-Cañas, M.; Pazos, M. R.; Irving, A. J.; Lluís, C.; Canela, E. I.; Fernández-Ruiz, J.; Guzmán, M.; McCormick, P. J.; Sánchez, C. Targeting CB2-GPR55 Receptor Heteromers Modulates Cancer Cell Signaling. *J. Biol. Chem.* **2014**, *289*, 21960–21972.

(27) Balenga, N. A.; Martínez-Pinilla, E.; Kargl, J.; Schröder, R.; Peinhaupt, M.; Platzer, W.; Bálint, Z.; Zamarbide, M.; Dopeso-Reyes, I.; Ricobaraza, A.; Pérez-Ortiz, J. M.; Kostenis, E.; Waldhoer, M.; Heinemann, A.; Franco, R. Heteromerization of GPR55 and Cannabinoid CB2 Receptors Modulates Signaling. *Br. J. Pharmacol.* **2014**, *171*, 5387–5406.

(28) Anavi-Goffer, S.; Baillie, G.; Irving, A. J.; Gertsch, J.; Greig, I. R.; Pertwee, R. G.; Ross, R. A. Modulation of L-A-lysophosphatidylinositol/GPR55 Mitogen-Activated Protein Kinase (MAPK) Signaling by Cannabinoids. *J. Biol. Chem.* **2012**, *287*, 91–104.

(29) Rempel, V.; Volz, N.; Gläser, F.; Nieger, M.; Bräse, S.; Müller, C. E. Antagonists for the Orphan G-Protein-Coupled Receptor GPR55 Based on a Coumarin Scaffold. *J. Med. Chem.* **2013**, *56*, 4798–4810.

(30) Kenakin, T. P. Cellular Assays as Portals to Seven-Transmembrane Receptor-Based Drug Discovery. *Nat. Rev. Drug Discov.* **2009**, *8*, 617–626.

(31) Venkatakrishnan, A. J.; Deupi, X.; Lebon, G.; Tate, C. G.; Schertler, G. F.; Babu, M. M. Molecular Signatures of G-Protein-Coupled Receptors. *Nature* **2013**, *494*, 185–194.

(32) Balenga, N. A. B.; Henstridge, C. M.; Kargl, J.; Waldhoer, M. *Pharmacology, Signaling and Physiological Relevance of the G Protein-Coupled Receptor 55.*; 1st ed.; Elsevier Inc., 2011; Vol. 62.

(33) Sylantyev, S.; Jensen, T. P.; Ross, R. a; Rusakov, D. a. Cannabinoid- and Lysophosphatidylinositol-Sensitive Receptor GPR55 Boosts Neurotransmitter Release at Central Synapses. *Proc. Natl. Acad. Sci. U. S. A.* **2013**, *110*, 5193–5198.

(34) Staton, P. C.; Hatcher, J. P.; Walker, D. J.; Morrison, A. D.; Shapland, E. M.; Hughes, J. P.; Chong, E.; Mander, P. K.; Green, P. J.; Billinton, A.; Fulleylove, M.; Lancaster, H. C.; Smith, J. C.; Bailey, L. T.; Wise, A.; Brown, A. J.; Richardson, J. C.; Chessell, I. P. The Putative Cannabinoid Receptor GPR55 Plays a Role in Mechanical Hyperalgesia Associated with Inflammatory and Neuropathic Pain. *Pain* **2008**, *139*, 225–236.

(35) Pietr, M.; Kozela, E.; Levy, R.; Rimmerman, N.; Lin, Y. H.; Stella, N.; Vogel, Z.; Juknat, A. Differential Changes in GPR55 during Microglial Cell Activation. *FEBS Lett.* **2009**, *583*, 2071–2076.

(36) Balenga, N. A. B.; Aflaki, E.; Kargl, J.; Platzer, W.; Schröder, R.; Blättermann, S.; Kostenis, E.; Brown, A. J.; Heinemann, A.; Waldhoer, M. GPR55 Regulates Cannabinoid 2 Receptor-Mediated Responses in Human Neutrophils. *Cell Res.* **2011**, *21*, 1452–1469.

(37) Liu, B.; Song, S.; Jones, P. M.; Persaud, S. J. GPR55: From Orphan to Metabolic Regulator? *Pharmacol. Ther.* **2015**, *145*, 35–42.

(38) Jenkin, K. a; McAinch, A. J.; Zhang, Y.; Kelly, D. J.; Hryciw, D. H. Elevated Cannabinoid Receptor 1 and G Protein-Coupled Receptor 55 Expression in Proximal Tubule Cells and Whole Kidney Exposed to Diabetic Conditions. *Clin. Exp. Pharmacol. Physiol.* **2015**, *42*, 256–262.

(39) Lanuti, M.; Talamonti, E.; Maccarrone, M.; Chiurchiù, V. Activation of GPR55 Receptors Exacerbates oxLDL-Induced Lipid Accumulation and Inflammatory Responses, While Reducing Cholesterol Efflux from Human Macrophages. *PLoS One* **2015**, *10*, e0126839.

(40) Bondarenko, A.; Waldeck-Weiermair, M.; Naghdi, S.; Poteser, M.; Malli, R.; Graier, W. F. GPR55-Dependent and -Independent Ion Signalling in Response to Lysophosphatidylinositol in Endothelial Cells. *Br. J. Pharmacol.* **2010**, *161*, 308–320.

(41) Daly, C. J.; Ross, R. a; Whyte, J.; Henstridge, C. M.; Irving, a J.; McGrath, J. C. Fluorescent Ligand Binding Reveals Heterogeneous Distribution of Adrenoceptors and "Cannabinoid-like" Receptors in Small Arteries. *Br. J. Pharmacol.* **2010**, *159*, 787–796.

(42) AlSuleimani, Y. M.; Hiley, C. R. The GPR55 Agonist Lysophosphatidylinositol Relaxes Rat Mesenteric Resistance Artery and Induces Calcium Release in Rat Mesenteric Artery Endothelial Cells. *Br. J. Pharmacol.* **2015**, *172*, 3043–3057.

(43) Xiao, Y. J.; Schwartz, B.; Washington, M.; Kennedy, A.; Webster, K.; Belinson, J.; Xu, Y. Electrospray Ionization Mass Spectrometry Analysis of Lysophospholipids in Human Ascitic Fluids: Comparison

of the Lysophospholipid Contents in Malignant vs Nonmalignant Ascitic Fluids. *Anal. Biochem.* **2001**, *290*, 302–313.

(44) Sutphen, R.; Xu, Y.; Wilbanks, G. D.; Fiorica, J.; Grendys, E. C.; LaPolla, J. P.; Arango, H.; Hoffman, M. S.; Martino, M.; Wakeley, K.; Griffin, D.; Blanco, R. W.; Cantor, A. B.; Xiao, Y.; Krischer, J. P. Lysophospholipids Are Potential Biomarkers of Ovarian Cancer. *Cancer Epidemiol. Biomarkers Prev.* **2004**, *13*, 1185–1191.

(45) Andradas, C.; Caffarel, M. M.; Pérez-Gómez, E.; Salazar, M.; Lorente, M.; Velasco, G.; Guzmán, M.; Sánchez, C. The Orphan G Protein-Coupled Receptor GPR55 Promotes Cancer Cell Proliferation via ERK. *Oncogene* **2011**, *30*, 245–252.

(46) Pérez-Gómez, E.; Andradas, C.; Flores, J. M.; Quintanilla, M.; Paramio, J. M.; Guzmán, M.; Sánchez, C. The Orphan Receptor GPR55 Drives Skin Carcinogenesis and Is Upregulated in Human Squamous Cell Carcinomas. *Oncogene* **2013**, *32*, 2534–2542.

(47) Karlsson, R.; Pedersen, E. D.; Wang, Z.; Brakebusch, C. Rho GTPase Function in Tumorigenesis. *Biochim. Biophys. Acta* **2009**, *1796*, 91–98.

(48) He, D.; Wang, J.; Zhang, C.; Shan, B.; Deng, X.; Li, B.; Zhou, Y.; Chen, W.; Hong, J.; Gao, Y.; Chen, Z.; Duan, C. Down-Regulation of miR-675-5p Contributes to Tumor Progression and Development by Targeting pro-Tumorigenic GPR55 in Non-Small Cell Lung Cancer. *Mol. Cancer* **2015**, *14*, 1–14.

(49) Hofmann, N. a; Yang, J.; Trauger, S. a; Nakayama, H.; Huang, L.; Strunk, D.; Moses, M. a; Klagsbrun, M.; Bischoff, J.; Graier, W. F. The GPR 55 Agonist, L-A-Lysophosphatidylinositol, Mediates Ovarian Carcinoma Cell-Induced Angiogenesis. *Br. J. Pharmacol.* **2015**, 4107–4118.

(50) Whyte, L. S.; Ryberg, E.; Sims, N. A.; Ridge, S. A.; Mackie, K.; Greasley, P. J.; Ross, R. A.; Rogers, M. J. The Putative Cannabinoid Receptor GPR55 Affects Osteoclast Function in Vitro and Bone Mass in Vivo. *Proc. Natl. Acad. Sci. U. S. A.* **2009**, *106*, 16511–16516.

(51) Wu, C.-S.; Chen, H.; Sun, H.; Zhu, J.; Jew, C. P.; Wager-Miller, J.; Straiker, A.; Spencer, C.; Bradshaw, H.; Mackie, K.; Lu, H.-C. GPR55, a G-Protein Coupled Receptor for Lysophosphatidylinositol, Plays a Role in Motor Coordination. *PLoS One* **2013**, *8*, e60314.

(52) Henstridge, C. M.; Balenga, N. a B.; Kargl, J.; Andradas, C.; Brown, A. J.; Irving, A.; Sanchez, C.; Waldhoer, M. Minireview: Recent Developments in the Physiology and Pathology of the Lysophosphatidylinositol-Sensitive Receptor GPR55. *Mol. Endocrinol.* **2011**, *25*, 1835–1848.

(53) Okuno, T.; Yokomizo, T. What Is the Natural Ligand of GPR55? *J. Biochem.* **2011**, *149*, 495–497.

(54) Dorsam, R. T.; Gutkind, J. S. G-Protein-Coupled Receptors and Cancer. *Nat. Rev. Cancer* **2007**, *7*, 79–94.

(55) Lin, M.-E.; Herr, D. R.; Chun, J. Lysophosphatidic Acid (LPA) Receptors: Signaling Properties and Disease Relevance. *Prostaglandins Other Lipid Mediat.* **2010**, *91*, 130–138.

(56) Pyne, N. J.; Pyne, S. Sphingosine 1-Phosphate and Cancer. *Nat. Rev. Cancer* **2010**, *10*, 489–503.

(57) Yin, H.; Chu, A.; Li, W.; Wang, B.; Shelton, F.; Otero, F.; Nguyen, D. G.; Caldwell, J. S.; Chen, Y. A. Lipid G Protein-Coupled Receptor Ligand Identification Using Beta-Arrestin PathHunter Assay. *J. Biol. Chem.* **2009**, *284*, 12328–12338.

(58) Kapur, A.; Zhao, P.; Sharir, H.; Bai, Y.; Caron, M. G.; Barak, L. S.; Abood, M. E. Atypical Responsiveness of the Orphan Receptor GPR55 to Cannabinoid Ligands. *J. Biol. Chem.* **2009**, *284*, 29817–29827.

(59) Ford, L. A.; Roelofs, A. J.; Anavi-Goffer, S.; Mowat, L.; Simpson, D. G.; Irving, A. J.; Rogers, M. J.; Rajnicek, A. M.; Ross, R. a. A Role for L-Alpha-Lysophosphatidylinositol and GPR55 in the Modulation of Migration, Orientation and Polarization of Human Breast Cancer Cells. *Br. J. Pharmacol.* **2010**, *160*, 762–771.

(60) Offertáler, L.; Mo, F.-M.; Bátkai, S.; Liu, J.; Begg, M.; Razdan, R. K.; Martin, B. R.; Bukoski, R. D.; Kunos, G. Selective Ligands and Cellular Effectors of a G Protein-Coupled Endothelial Cannabinoid Receptor. *Mol. Pharmacol.* **2003**, *63*, 699–705.

(61) Brown, A. J.; Daniels, D. a; Kassim, M.; Brown, S.; Haslam, C. P.; Terrell, V. R.; Brown, J.; Nichols, P. L.; Staton, P. C.; Wise, A.; Dowell, S. J. Pharmacology of GPR55 in Yeast and Identification of GSK494581A as a Mixed-Activity Glycine Transporter Subtype 1 Inhibitor and GPR55 Agonist. *J. Pharmacol. Exp. Ther.* **2011**, *337*, 236–246.

(62) Piñeiro, R.; Maffucci, T.; Falasca, M. The Putative Cannabinoid Receptor GPR55 Defines a Novel Autocrine Loop in Cancer Cell Proliferation. *Oncogene* **2011**, *30*, 142–152.

(63) Valant, C.; Sexton, P. M.; Christopoulos, A. Orthosteric/AllostericBitopic Ligands: Going Hybrid at GPCRs. **2009**, *9*, 125–135.

(64) Rempel, V.; Volz, N.; Hinz, S.; Karcz, T.; Meliciani, I.; Nieger, M.; Wenzel, W.; Bräse, S.; Müller, C. E. 7-Alkyl-3-Benzylcoumarins: A Versatile Scaffold for the Development of Potent and Selective Cannabinoid Receptor Agonists and Antagonists. *J. Med. Chem.* **2012**, *55*, 7967–7977.

(65) Deng, F.-F.; Xie, M.-H.; Li, P.-Z.; Tian, Y.-L.; Zhang, X.-Y.; Zhai, H.-L. Study on the Antagonists for the Orphan G Protein-Coupled Receptor GPR55 by Quantitative Structure–activity Relationship. *Chemom. Intell. Lab. Syst.* **2014**, *131*, 51–60.

(66) Lee, Y.-J.; Lee, Y. M.; Lee, C.-K.; Jung, J. K.; Han, S. B.; Hong, J. T. Therapeutic Applications of Compounds in the Magnolia Family. *Pharmacol. Ther.* **2011**, *130*, 157–176.

(67) Schuehly, W.; Paredes, J. M. V.; Kleyer, J.; Huefner, A.; Anavi-Goffer, S.; Raduner, S.; Altmann, K.-H.; Gertsch, J. Mechanisms of Osteoclastogenesis Inhibition by a Novel Class of Biphenyl-Type Cannabinoid CB(2) Receptor Inverse Agonists. *Chem. Biol.* **2011**, *18*, 1053–1064.

(68) Rempel, V.; Fuchs, A.; Hinz, S.; Karcz, T.; Lehr, M.; Koetter, U.; Müller, C. E. Magnolia Extract, Magnolol, and Metabolites: Activation of Cannabinoid CB2 Receptors and Blockade of the Related GPR55. *ACS Med. Chem. Lett.* **2013**, *4*, 41–45.

(69) Fuchs, A.; Rempel, V.; Müller, C. E. The Natural Product Magnolol as a Lead Structure for the Development of Potent Cannabinoid Receptor Agonists. *PLoS One* **2013**, *8*, e77739.

(70) Heynen-genel, S.; Dahl, R.; Shi, S.; Milan, L.; Sergienko, E.; Hedrick, M.; Dad, S.; Stonich, D.; Su, Y.; Chung, T. D. Y.; Sharir, H.; Caron, M. G.; Barak, L. S.; Abood, M. E. Screening for Selective Ligands for GPR55-Antagonists. Probe Reports from the NIH Molecular Libraries Program; National Center for Biotechnology Information (U.S.): Bethesda, MD, 2010; Http://www.ncbi.nlm.nih.gov/books/NBK66153/.

(71) Heynen-genel, S.; Dahl, R.; Shi, S.; Milan, L.; Bravo, Y.; Sergienko, E.; Hedrick, M.; Dad, S.; Stonich, D.; Su, Y.; Chung, T. D. Y.; Sharir, H.; Barak, L. S.; Abood, M. E. Screening for Selective Ligands for

GPR55-Agonists. Probe Reports from the NIH Molecular Libraries Program; National Center for Biotechnology Information (U.S.): Bethesda, MD, 2010; Http://www.ncbi.nlm.nih.gov/books/NBK66152/.

(72) Kargl, J.; Brown, A. J.; Andersen, L.; Dorn, G.; Schicho, R.; Waldhoer, M.; Heinemann, A. A Selective Antagonist Reveals a Potential Role of G Protein-Coupled Receptor 55 in Platelet and Endothelial Cell Function. *J. Pharmacol. Exp. Ther.* **2013**, *346*, 54–66.

(73) Paul, R. K.; Wnorowski, A.; Gonzalez-Mariscal, I.; Nayak, S. K.; Pajak, K.; Moaddel, R.; Indig, F. E.; Bernier, M.; Wainer, I. W. (R,R')-4'-Methoxy-1-Naphthylfenoterol Targets GPR55-Mediated Ligand Internalization and Impairs Cancer Cell Motility. *Biochem. Pharmacol.* **2014**, *87*, 547–561.

(74) Kotsikorou, E.; Lynch, D. L.; Abood, M. E.; Reggio, P. H. Lipid Bilayer Molecular Dynamics Study of Lipid-Derived Agonists of the Putative Cannabinoid Receptor, GPR55. *Chem. Phys. Lipids* **2011**, *164*, 131–143.

(75) Jorgensen, W. L.; Duffy, E. M. Prediction of Drug Solubility from Structure. *Adv. Drug Deliv. Rev.* **2002**, *54*, 355–366.

(76) Lipinski, C. A. Drug-like Properties and the Causes of Poor Solubility and Poor Permeability. *J. Pharmacol. Toxicol. Methods* **2001**, *44*, 235–249.

(77) Scott, C. W.; Peters, M. F. Label-Free Whole-Cell Assays: Expanding the Scope of GPCR Screening. *Drug Discov. Today* **2010**, *15*, 704–716.

(78) *Label-Free Technologies for Drug Discovery*; Cooper, M.; Mayr, L. M., Eds.; John Wiley & Sons, Ltd: Chichester, UK, 2011.

(79) Whyte, L.; Irving, A.; Ross, R. A. Pharmacological Profiling of GPR55 Ligands Using Cellular Impedance Analysis. In *25th Annual Symposium of the International Cannabinoid Research Society*; 2015; p. 97.

(80) Yu, N.; Atienza, J. M.; Bernard, J.; Blanc, S.; Zhu, J.; Wang, X.; Xu, X.; Abassi, Y. a. Real-Time Monitoring of Morphological Changes in Living Cells by Electronic Cell Sensor Arrays: An Approach to Study G Protein-Coupled Receptors. *Anal. Chem.* **2006**, *78*, 35–43.

(81) Stallaert, W.; Dorn, J. F.; van der Westhuizen, E.; Audet, M.; Bouvier, M. Impedance Responses Reveal β2-Adrenergic Receptor Signaling Pluridimensionality and Allow Classification of Ligands with Distinct Signaling Profiles. *PLoS One* **2012**, *7*, e29420.

(82) Scandroglio, P.; Brusa, R.; Lozza, G.; Mancini, I.; Petrò, R.; Reggiani, A.; Beltramo, M. Evaluation of Cannabinoid Receptor 2 and Metabotropic Glutamate Receptor 1 Functional Responses Using a Cell Impedance-Based Technology. *J. Biomol. Screen. Off. J. Soc. Biomol. Screen.* **2010**, *15*, 1238–1247.

(83) ACEA Biosciences-xCELLigence System http://www.aceabio.com/theory.aspx?cateid=277 (accessed Feb 12, 2015).

(84) Yamashita, A.; Oka, S.; Tanikawa, T.; Hayashi, Y.; Nemoto-Sasaki, Y.; Sugiura, T. The Actions and Metabolism of Lysophosphatidylinositol, an Endogenous Agonist for GPR55. *Prostaglandins Other Lipid Mediat.* **2013**, *107*, 103–116.

(85) Piñeiro, R.; Falasca, M. Lysophosphatidylinositol Signalling: New Wine from an Old Bottle. *Biochim. Biophys. Acta - Mol. Cell Biol. Lipids* **2012**, *1821*, 694–705.

(86) Jagerovic, N.; Morales, P.; Ross, R. A.; Whyte, L. S. Selective Modulators of GPR55 Activity: Chromenopyrazole Derivatives. ES P201530608, 2015.

(87) Morales, P.; Whyte, L. S.; Chicharro, R.; Gómez-Cañas, M.; Pazos, M. R.; Goya, P.; Irving, A. J.; Fernandez-Ruiz, J.; Ross, R. A.; Jagerovic, N. Identification of Novel GPR55 Modulators Using Cell-Impedance-Based Label-Free Technology. **2015**, Submitted to J. Med Chem.

(88) Zhu, M.; Kim, M. H.; Lee, S.; Bae, S. J.; Kim, S. H.; Park, S. B. Discovery of Novel Benzopyranyl Tetracycles That Act as Inhibitors of Osteoclastogenesis Induced by Receptor Activator of NF-κB Ligand. *J. Med. Chem.* **2010**, *53*, 8760–8764.

(89) Camps, F.; Coll, J.; Messeguer, A.; Pericás, M. A.; Ricart, S.; Bowers, W. S.; Soderlund, D. M. An Improved Procedure for the Preparation of 2,2-Dimethyl-4-Chromanones. *Synthesis (Stuttg).* **1980**, *1980*, 725–727.

(90) An, H.; Eum, S.-J.; Koh, M.; Lee, S. K.; Park, S. B. Diversity-Oriented Synthesis of Privileged Benzopyranyl Heterocycles from S-Cis-Enones. *J. Org. Chem.* **2008**, *73*, 1752–1761.

(91) Brown, R. E.; Shavel, J. J. Substituted Benzopyranopyrazoles. Patent US19690826656, 1971.

(92) Zhang, X.; Maor, Y.; Wang, J. F.; Kunos, G.; Groopman, J. E. Endocannabinoid-like N-Arachidonoyl Serine Is a Novel pro-Angiogenic Mediator. *Br. J. Pharmacol.* **2010**, *160*, 1583–1594.

(93) Ross, G. R.; Lichtman, A.; Dewey, W. L.; Akbarali, H. I. Evidence for the Putative Cannabinoid Receptor (GPR55)-Mediated Inhibitory Effects on Intestinal Contractility in Mice. *Pharmacology* **2012**, *90*, 55–65.

(94) Cantarella, G.; Scollo, M.; Lempereur, L.; Saccani-Jotti, G.; Basile, F.; Bernardini, R. Endocannabinoids Inhibit Release of Nerve Growth Factor by Inflammation-Activated Mast Cells. *Biochem. Pharmacol.* **2011**, *82*, 380–388.

General Conclusions

General conclusions

In this dissertation several drug discovery approaches targeting the ECS have been developed. For that purpose, the chromenopyrazole scaffold was intensively explored by following different strategies. Structural modifications have been performed on the tricyclic core mainly focusing on the pyrazole and the phenol moieties leading to novel compounds able to modulate the cannabinoid receptors or/and the putative cannabinoid receptor GPR55.

The results obtained in this dissertation allow us to conclude that:

Chapter 1

The design and the synthesis of alcoxychromeno-pyrazoles and -isoxazoles led to selective CB_2 cannabinoid receptor ligands in agreement with molecular modeling data. These new lead compounds could afford a great therapeutic opportunity in various disease states where CB_2 cannabinoid receptors are physiologically relevant.

The bivalent ligand approach targeting CB_2R dimers provided bisalcoxychromenopyrazoles as the first CB_2R fully selective homobivalent ligands. Since dimerization plays an essential role in the regulation of receptor processing and trafficking, these new ligands are considered attractive tools for selective targeting of CB_2R dimers.

Chapter 2

The reported chromenopyrazolediones, designed by merging the cannabinoid scaffold with a quinone feature, resulted in multifunctional agents for cancer therapy as tested *in vitro* and *in vivo*. Selected compounds reduced prostate tumor through activation of the cannabinoid receptor CB_1, PPARγ receptors and through oxidative stress. Other compounds were active against triple-negative breast cancer through a mechanism involving the cannabinoid receptor CB_2 and redox properties. Another additional fact that needs to be taken into consideration for these new

antitumor agents is their lack of cytotoxicity confirmed *in vitro* and *in vivo*. Therefore, the use of both types of chromenopyrazolediones represents a promising canabinoid-quinone anticancer approach. The CB_2R acting antitumor agents would have the advantage of lacking psychotropic effects giving them high potential for further preclinical development in the management of neoplasms.

Chapter 3

Targeting the new potential drug target GPR55, acylpiperazinyl chromenopyrazoles have been identified as partial agonists and antagonists of this putative cannabinoid receptor. The novelty in this area lies on i) the selectivity of some of these compounds *vs* cannabinoid receptor CB_1R and CB_2R activity, ii) the use of an innovative label-free cell impedance assay that resolved the problems resulting from the complex signaling pathways generated by GPR55 modulation, iii) the improved druggable properties of the new compounds compared to the endogenous ligand LPI. Therefore, these compounds can serve as pharmacological tools for mechanistic studies of GPR55 as well as radioligands for binding screening assays.

In summary, the results reported in this dissertation uncover the chromenopyrazole as a privileged scaffold in drug discovery and especially in the cannabinoid field.

Conclusiones generales

Conclusiones generales

A lo largo de esta tesis se han desarrollado distintas estrategias para la obtención de nuevos moduladores del sistema endocannabinoide. Para ello, se ha profundizado en la estructura del esqueleto de cromenopirazol realizando diversas modificaciones sobre el fenol y el pirazol que constituyen en esqueleto tricíclico central. Estos cambios estructurales han sido diseñados en base a distintas aproximaciones farmacológicas que han permitido desglosar este trabajo de investigación en tres capítulos. Concretamente, los resultados obtenidos en esta tesis doctoral nos permiten obtener las siguientes conclusiones:

Capítulo 1

El diseño y síntesis de una serie de alcoxicromenopirazoles y alcoxicromenoisoxazoles dio lugar a la identificación de ligandos potentes y selectivos para el receptor CB_2. Dada la relevancia terapéutica de este receptor en procesos patológicos, estos nuevos compuestos presentan un gran potencial para el tratamiento de numerosas enfermedades.

A continuación, con el fin de profundizar en la homodimerización del receptor CB_2, se sintetizó una serie de bis-alcoxicromenopirazoles que resultaron ser los primeros ligandos bivalentes CB_2 selectivos. Puesto que los procesos de dimerización juegan un papel esencial en la regulación funcional de los receptores acoplados a proteínas G, estas nuevas moléculas podrían constituir interesantes herramientas para el estudio de homodímeros CB_2.

Capítulo 2

Las cromenopirazoldionas descritas en el segundo capítulo de esta tesis resultaron ser prometedores agentes multifuncionales con propiedades antitumorales *in vitro* e *in vivo*. Determinados compuestos de esta serie fueron capaces de reducir el crecimiento de tumores de próstata mediante la activación de receptores CB_1 y PPARγ y mediante la inducción de estrés

oxidativo. Otras cromenopirazoldionas mostraron propiedades antitumorales en modelos de cáncer de mama triple negativo generando apoptosis mediante la activación de receptores CB_2 e induciendo estrés oxidativo. Ensayos *in vitro* e *in vivo*, demostraron que estas nuevas moléculas no generan cititoxicidad en células normales. Por tanto, las cromenopirazoldionas representan una prometedora aproximación antitumoral quinona-cannabinoide con potencial aplicación para el tratamiento del cáncer de mama triple negativo y el cáncer de próstata. Los compuestos CB_2 selectivos presentan la ventaja de carecer de propiedades psicoactivas teniendo por ende un mayor potencial para el desarrollo preclínico de estos compuestos en el tratamiento de neoplasias.

Capítulo 3

Con el fin de desarrollar nuevas moléculas capaces de unirse al receptor GPR55, se diseñó y sintetizó una serie de acilpiperazinil cromenopirazoles. Entre estos derivados se identificaron agonistas parciales y antagonistas de GPR55. Dentro de este trabajo de investigación cabe destacar los siguientes aportes novedosos: i) el descubrimiento de compuestos selectivos por el receptor GPR55 frente a CB_1 y CB_2; ii) el empleo de una novedosa técnica para la evaluación de la actividad GPR55 mediante el análisis de la impedancia celular en tiempo real; iii) el perfil fisicoquímico y farmacocinético mejorado de los nuevos compuestos con respecto al agonista endógeno LPI. Por tanto, estos compuestos tienen potencial para el desarrollo de herramientas farmacológicas que permitan continuar con la caracterización funcional de GPR55.

En resumen, los resultados obtenidos en esa tesis doctoral ponen de manifiesto el potencial de la estructura de cromenopirazol siendo un esqueleto privilegiado y versátil para el desarrollo de moduladores del sistema endocannabinoide.

Appendix 1

Chromanones: A Synthetic Issue

Appendix 2

Chromenopyrazoledione-Porphyrin Conjugate for Cancer Therapy

Introduction

Cancer is a multifactorial disease that involves numerous pathological processes. Therefore, the combination of different therapies represents a promising strategy in the treatment of malignant neoplams. In this scenario, photodynamic therapy (PDT) appears as a minimally invasive alternative.[1,2] PDT has already been clinically approved for the treatment of various types of malignant disorders such as bladder, lung or esophageal cancer.[3] This technique involves the administration of a tumor localizing photosensitizer (PS) followed by its activation with irradiation at a wavelength corresponding to an absorbance band of the PS (figure 1). In the presence of tissue oxygen, the photoactive sensitizer triggers a series of photochemical processes that lead to direct cancer cell death and tumor microvascular damage.[4] Different cell death pathways such as apoptosis, necrosis and autophagy may be evoked by PDT.[5] Furthermore, the preferential accumulation of the photosensitizer by malignant cells and the focused light delivery confer to this procedure certain selectivity toward cancer cells.[6]

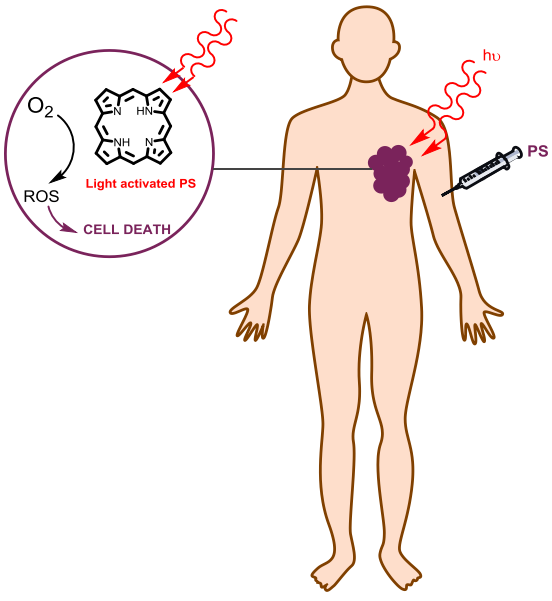

Figure 1. PDT destroys neoplastic lesions with reactive oxygen species (ROS), which are produced by using light of specific wavelengths to irradiate the PS. In the first step of PDT for cancer treatment, the PS is injected into the bloodstream. The agent is absorbed by cells all over the body but stays in cancer cells longer than in normal cells.

Porphyrin-based photosensitizers

The critical step in PDT is the election of an appropriate photosensitizer. The efficacy of this agent depends on its efficient insertion into cellular membranes and specific delivery into tumor cells. An optimal photosensitizing agent should have a high absorption peak between 600 and 800 nm (red to deep red) in order to form a substantial yield of reactive oxygen species upon irradiation. Higher is the wavelength deeper is the penetration in tissues. Consequently, agents with strong absorbance like porphycenes, porphyrin derivatives, chlorins, and phthalocyanines are suitable for PDT.[7] Most of the photosensitizers used in cancer therapy are based on a tetrapyrrole structure, similar to that of the protoporphyrin contained in hemoglobin.

Porphyrins can localize in tumor tissue and have been widely investigated as sensitizing drugs for application in PDT.[8] In fact, the first PS to be clinically employed for cancer treatment was a water-soluble mixture of porphyrins called hematoporphyrin derivative (HpD).[9,10] A partial purification of this mixture later became the commercial product porfimer sodium known as Photofrin®, which was approved in several countries in the 1990s. Even though Photofrin® still is the most widely used photosensitizer, it has some disadvantages including a long-lasting skin photosensitivity.

The second generation photosensitizer 5-aminolevulanic acid (ALA, (Levulan®), a biosynthetic precursor of protoporphyrin IX, offers different advantages such as rapid clearance along with oral or topical administration. It is approved in certain countries for the treatment of actinic keratosis and basal cell carcinoma.[11] Many research efforts are currently focused on the development of improved porphyrin-based photosensitizers with less normal tissue photosensitivity and with better tumor specificity.

Porphyrins conjugated to biomolecules

In spite of the promising results obtained in the cancer treatment using PDT, most current phototherapy agents have serious side effects as they damage healthy tissue.[12] To overcome these limitations novel strategies are emerging.[13] These last years, it has increased the development of studies in which porphyrins are conjugated to molecules showing preferential accumulation on

specific tumors.[3] Most intensive efforts have been generated for the use of carriers such as nanoparticles,[14–16] liposomes,[17] polymers,[18] translocator protein,[19] glycoproteins,[20] antibodies,[21] or cyclodextrins[22] to enhance the efficiency of the photosensitizers. Another challenging strategy is the conjugation of a therapeutic drug to a porphyrin that could conduce to two different approaches: combining a photosensitizer with a chemotherapy agent or using porphyrins as carriers due to their ability to accumulate in cancer tissues as compared to normal tissues.[23] For instance, the photosensitizer temoporfin has been conjugated to non-steroidal anti-inflammatory compounds to improve the post-PDT treatment tumor regrowth.[24] The cytotoxic agent trilobolide, a sesquiterpene lactone inductor of nitroxic oxide, has been lately conjugated to porphyrin to increase its taking up by cancer cells.[25] The use of porphyrins as translocation vectors has also been examined with the anticancer agent doxorubicin that has been conjugated to porphyrazine through an acid-labile oxime linker.[26]

Aims and background

One of the challenges going forward in our research[27,28] is to design an antitumor agent selectively delivered. Since porphyrins possess selectivity toward tumor tissues, conjugating such macrocycles with CB_1 or CB_2 cannabinoids could be a strategy for specific drug delivery to tumor cells. Another therapeutic approach could be the use of combined PDT and cannabinoid therapies in a single entity.

Many types of cannabinoid receptors positive cancers are superficial or can be reached by endoscopy, consequently, cannabinoids have great potential for target-selective phototherapy. The aim of the current study is to develop a novel cannabinoid photosensitizer based on porphyrin-chromenopyrazoledione conjugation as displayed in figure 2. During the course of this research, Bai *et al.* reported the first CB_2R-targeted photosensitizer (IR700DX-mbc94).[29] Phototherapy treatment using IR700DX-mbc94 greatly inhibited the growth of CB_2 positive tumors but not CB_2 negative tumors.[30,31]

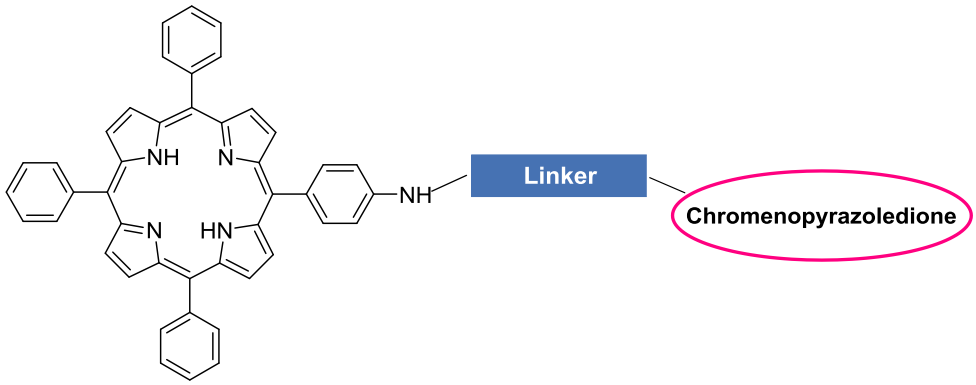

Figure 2. Schematic design of the porphyrin-chromenopyrazoledione conjugate.

Tetraphenylporphyrin (TPP), an intense chromophore with strong Soret band and medium Q-band absorption, has been chosen as the photosensitizer of our novel conjugates. As other porphyrin photosensitizers, it generates effectively singlet-oxygen upon excitation with a far-red irradiation (650 nm).[32]

Furthermore, chromenopyrazoledione **2.1** described in Chapter 2 was selected for this study because of biological and chemical reasons. On the one hand, this compound exhibited promising antiproliferative effects in prostate cancer mediated by generation of ROS and CB_1 receptors.[28] This cannabinoid-quinone displays affinity towards both cannabinoid receptors in the submicromolar range. On the other hand, its non-substituted pyrazole moiety enables different organic reactions that may ease the synthesis of the conjugate.

Results

Synthesis

Preparation of the porphyrin moiety started from the commercially available *meso*-tetraphenylporphyrin which was regioselectively *para*-nitrated to 5-(*p*-nitrophenyl)-10,15,20-triphenylporphyrin (**1**). The mononitro functionality was introduced using 1.8 equiv of sodium nitrite in the presence of TFA. This regiospecific mild procedure for electrophilic nitration at the *para* position of the phenyl groups in TPP was previously reported by Kevin Smith and coworkers.[33] This approach provides selective control in the number of phenyl groups nitrated by varying the

amount of sodium nitrite and the duration of the reaction. Nitroporphyrin **1** was then easily reduced with tin (II) chloride to obtain 5-(*p*-aminophenyl)-10,15,20-triphenylporphyrin **2** (scheme 1).

The conversion of the amino group of porphyrin **2** to the carboxylic acid **3**, was achieved by reaction with diglycolic anhydride in DMF.[34] Unfortunately, the coupling of porphyrin **3** with chromenopyrazoledione **2.1** that was attempted through diverse procedures was not achieved in our hands.

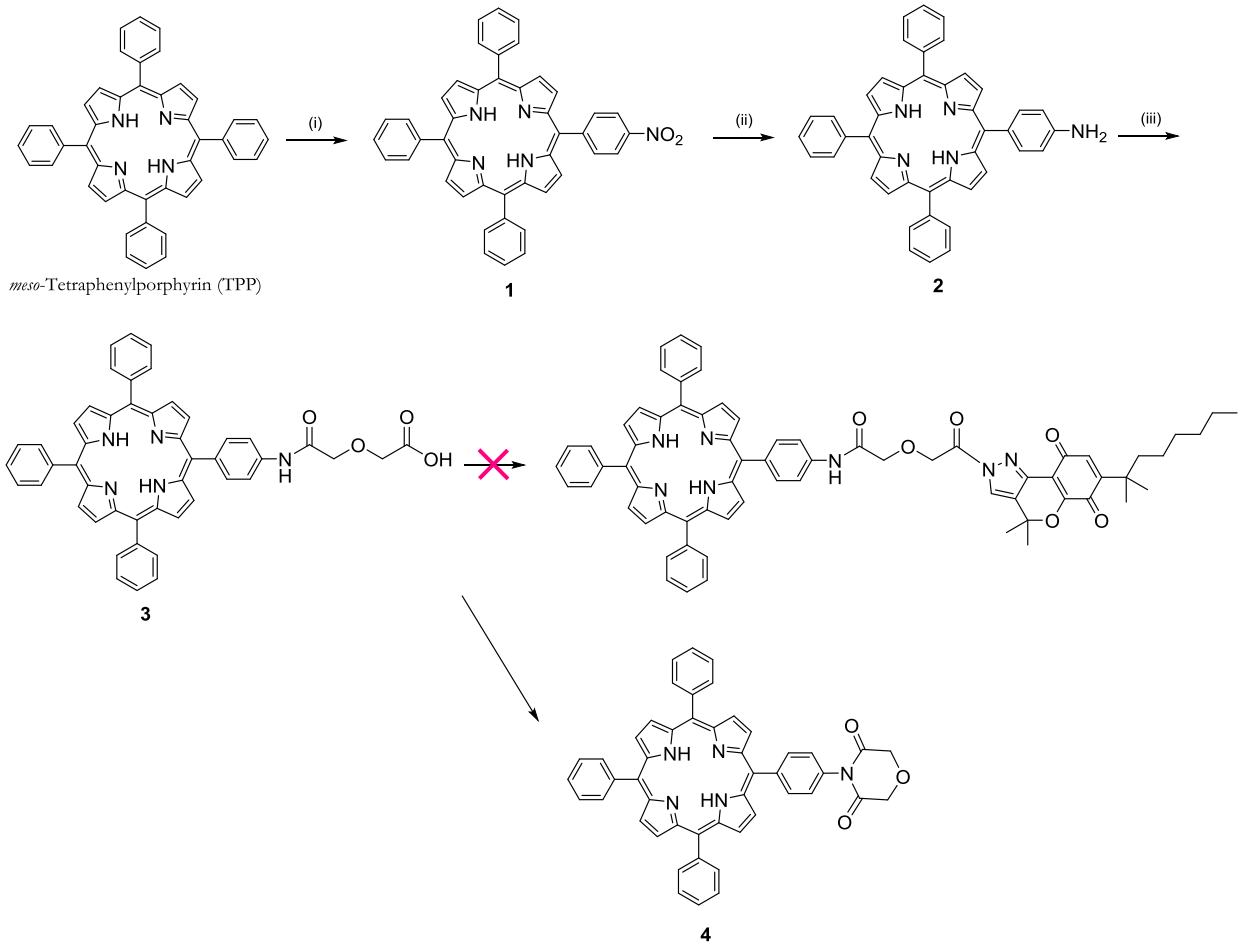

Scheme 1: Synthesis of porphyrin derivatives. Reaction conditions: **(i)** $NaNO_2$ (1.8 equiv), TFA, 25 °C, 3 min (49%); **(ii)** $SnCl_2$, conc. HCl, 65 °C, 1 h (99%); **(iii)** Diglycolic anhydride, DMF, rt, 24 h (89%).

Conversion of the carboxylic acid **3** to the corresponding acid chloride reacting with thionyl chloride followed by reaction with **2.1** failed to give the desired amide. Similarly, different coupling reagents such as carbodiimides [carbonyldiimidazole (CDI)] or more potent coupling reagents such as phosphonium-[(benzotriazol-1-yloxy)-tris[pyrrolidino] phosphonium hexafluorophosphate

(PyBOP)] or uronium salts [hexafluorophosphate salt of the O-(7-azabenzotriazolyl)tetra-methyl uranium (HATU)] in the presence of a base and dry DMF as solvent were unsuccessfully employed in independent reactions.

In some of these reactions, intramolecular cyclation of the (amino-2-oxoethoxy)-acetic acid group of compound **3** to the corresponding morpholine-3,5-dione porphyrin **4** was observed. Curiously, this porphyrin has never been described so far in the literature.

To avoid this intramolecular cyclation, the same synthetic approach was followed using the malonyl derivative **6** prepared by reaction of aminoporphyrin **2** with malonyl chloride and hydrolyzing with sodium hydroxide afterwards. However, the desired final coupling did not afford the expected conjugate (scheme 2).

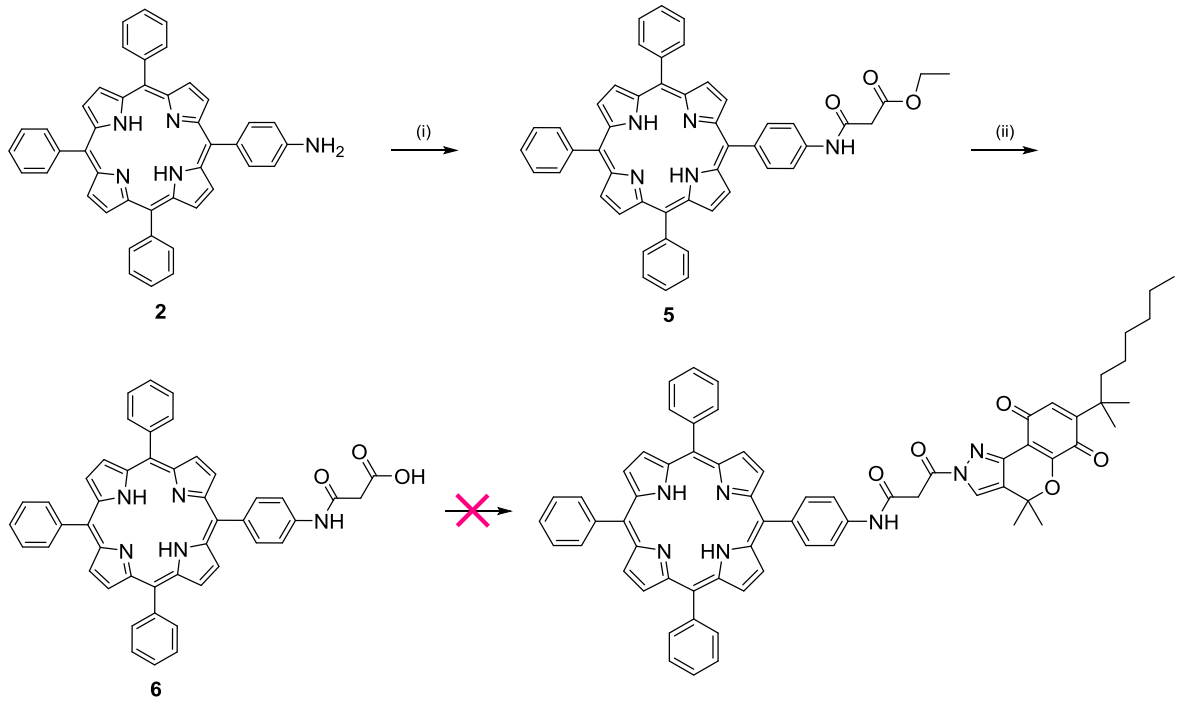

Scheme 2: Synthesis of porphyrin derivatives. Reaction conditions: **(i)** Malonyl chloride, Et_3N, DCM, rt, 1 h (74%); **(ii)** NaOH, rt, 4 h (91%).

After these synthetic failures, we decided to use the piperazine derivative **7** as starting material for the coupling with the chromenopyrazoles. This porphyrin (**7**) was previously decribed by Masson and colleagues[35] to tether tetraphenylporphyrin to glucosamines. Following their procedure, in order to convert aminoporphyrin **2** into a more potent nucleophile, the photosensitizer derivative was

firstly acylated using bromoacetyl bromide to give 5-(4α-bromoacetylamidophenyl)-10,15,20-triphenylporphyrin (**7**). Then, a nucleophilic substitution with piperazine afforded the nucleophilic porphyrin intermediate 5-(4α-piperazineacetylamidophenyl)-10,15,20-triphenylporphyrin (**8**) (scheme 3). Interestingly, the piperazine moiety is an appropriate linker because of its low toxicity and biotransformation that involves several well-known metabolic reactions.[36]

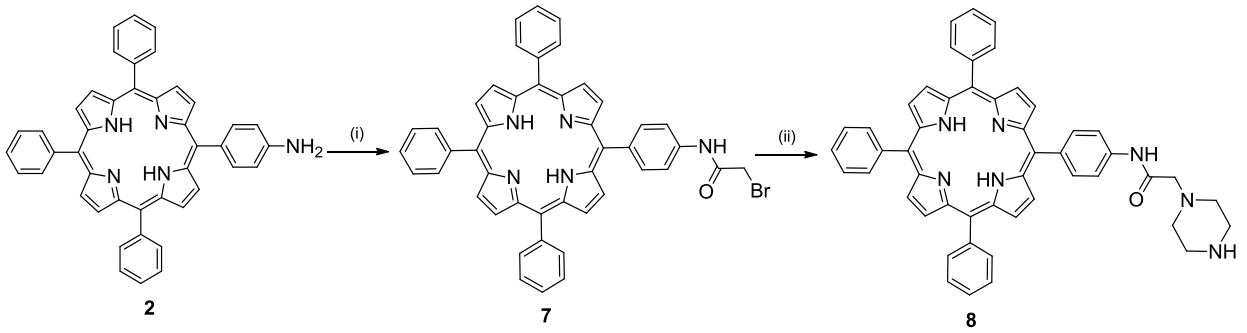

Scheme 3: Synthesis of the porphyrin-piperazine intermediate. Reaction conditions: **(i)** Bromoacetyl bromide, Et_3N, CH_2Cl_2, 25 °C, 1 h (31%); **(ii)** Piperazine, CH_2Cl_2, 25 °C, 45 min (96%).

Finally, the porphyrin-cannabinoid conjugate **10** was achieved as depicted in scheme 4. Acylation of chromenopyrazoledione **2.1** using bromoacetyl bromide afforded the substituted chromenopyrazole **9** that was then allowed to alkylate the piperazine intermediate **8**.

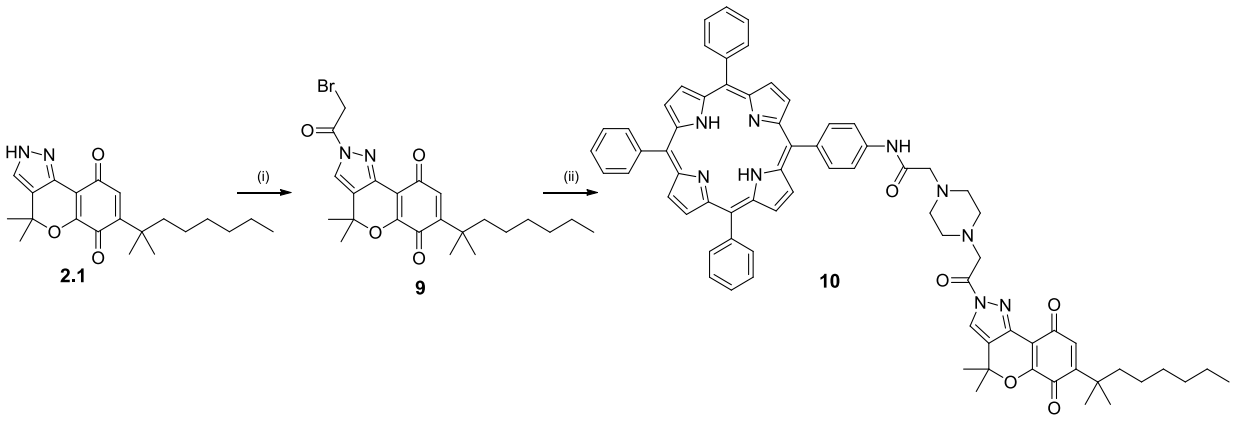

Scheme 4: Synthesis of the porphyrin-chromenopyrazoledione conjugate. Reaction conditions: **(i)** Bromoacetyl bromide, Et_3N, CH_2Cl_2, 25 °C, 1 h (58 %); **(ii)** Porphyrin**8**, Et_3N, CH_2Cl_2, 25 °C, 24 h (7 %).

It is interesting to note that attempts to directly link the aminoporphyrin **2** to compound **9** did not give the porphyrin-chromenopyrazoledione conjugate in our experiments. This fact may be due to the weak nucleophilicity of the aminoporphyrin.[37]

Conformational analysis of the porphyrin-chromenopyrazoledione conjugate

A complete conformational analysis of the novel conjugate (**10**) was performed using *ab initio* Hartre-Fock calculations at the 6-31G* level as encoded in Spartan ´08 (Wave function, Inc., Irvine CA). As displayed in figure **2** the global minimum energy conformer of conjugate **10** adopts an expanded spatial conformation whereas folded conformers (Figure 2B) exert higher relative energy values. Nonetheless, these theoretical values are calculated for vacuum conditions, the polarity of the solvent should determine the lowest energy conformer in solution. Under physiological conditions the aggregation of porphyrins should influence their conformation.

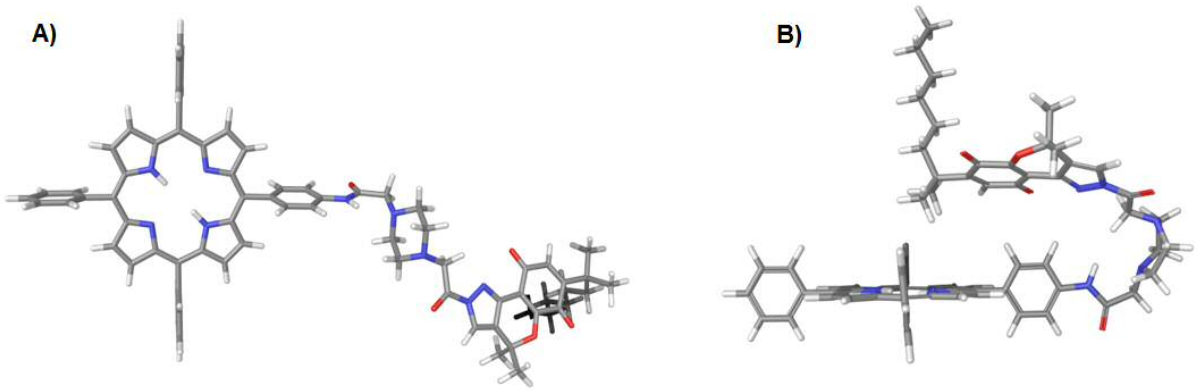

Figure 2. A) Global minimum energy conformer of compound **10** (ΔE: -0.11 Kcal/mol). B) Higher energy conformer of compound **10** showed for comparison (ΔE: 4.55 Kcal/mol).

Photophysicochemical properties

The UV−vis spectra of the porphyrin-chromenopyrazoledione conjugate **10** and the free *meso*-tetraphenylporphyrin were recorded. A Soret band with absorption maxima near 420 nm and medium Q-bands at 500-700 nm were observed for both porphyrins (figure 3). Even though the

shape of the absorption spectrum of **10** is quite similar to that of TPP in water/DMSO, slight bathochromic shifts are displayed. As clearly depicted in figure 3, compound **10** shows stronger absorption intensity relative to free TPP in both Soret and Q-bands exhibiting higher molecular extinction coefficients (table 2). In what concerns organic solvents, the Soret peak of **10** became gradually sharper and slightly shifted in dioxane and dichloromethane being broader in water solution. This fact could be due to either porphyrin–solvent interactions or self-aggregation of the TPP moiety. In conclusion, the molecular extinction coefficients of the new conjugate **10** are higher from those of TPP what highlights its appropriate absorption pattern. Absorption maxima and molecular extinction coefficients are summarized in table 2.

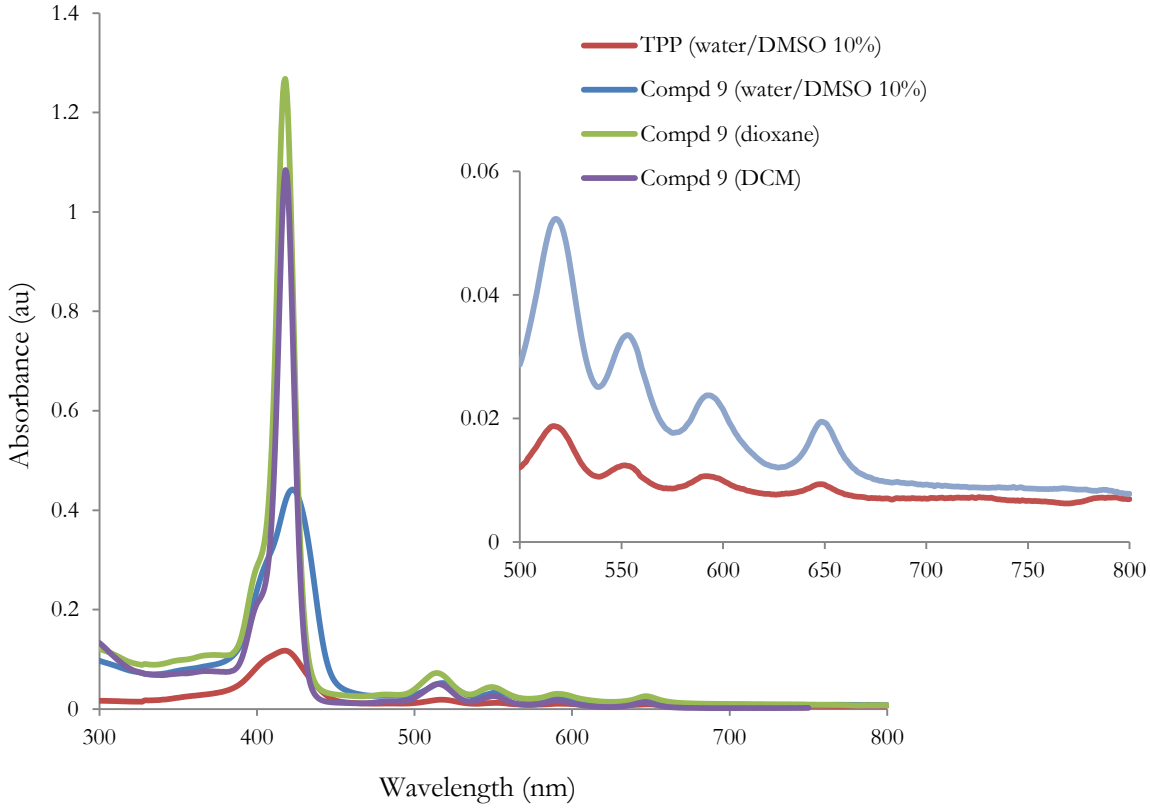

Figure 3. UV−vis absorption spectra of **10** and tetraphenylporphyrin (TPP) at constant concentration (0.1 mM) in different solvents at room temperature.

Table 2. Absorption maxima and molecular extinction coefficients of **10** and tetraphenylporphyrin (TPP) in different solvents at room temperature.

Absorption Band	TPP (water/DMSO)		Compd 10 (water/DMSO)		Compd 10 (dioxane)		Compd 10 (DCM)	
	λ_{max}(nm)	ε($M^{-1}cm^{-1}$)	λ_{max}(nm)	ε($M^{-1}cm^{-1}$)	λ_{max}(nm)	ε($M^{-1}cm^{-1}$)	λ_{max}(nm)	ε($M^{-1}cm^{-1}$)
Soret Band	418	17763.2	423	69244.8	418	201449.6	418	173102.4
Q-Band	517	1984.0	518	6985.6	514	10276.6	515	7721.6
	552	968.1	553	3979.2	549	5752.0	550	3782.4
	591	688.0	592	2417.6	591	3564.8	590	2300.8
	648	479.9	648	1731.2	647	2809.6	646	1795.2

A suitable PS should absorb light in the red or far-red wavelengths in order to penetrate tissue. Absorption bands at shorter wavelengths have less tissue penetration and are more likely to trigger skin photosensitivity. Consequently, these absorption studies qualify the novel cannabinoid-TPP conjugate **10** as a potential photosensitizer with applicability to PDT.

At the same concentration, the fluorescence intensity of the TPP or compound **10** in aqueous solution showed practically no emission (fluorescence is almost fully quenched). This absence of fluorescence may be caused by porphyrin–solvent interactions promoting non-radiative decay or self-aggregation of porphyrin molecules. Excitation of compound dissolved in DCM at 418 nm resulted in the fluorescence spectrum displayed in figure 4.

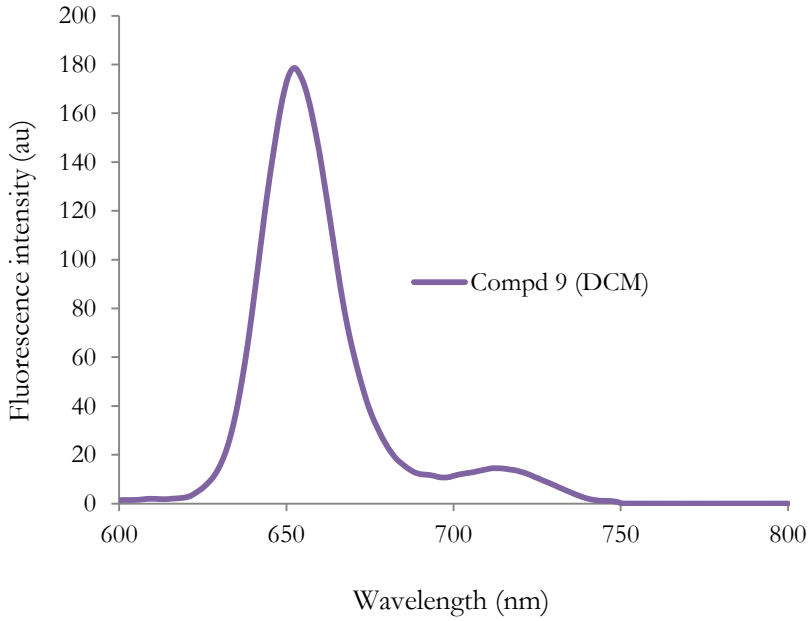

Figure 4. Fluorescence spectrum of compd **9** under excitation with light of 418 nm in dichloromethane (slit width: 15−15 nm, and 1 cm path length).

Cannabinoid receptors affinity

The cannabinoid binding affinity of the porphyrin-chromenopyrazoledione conjugate **10** was determined through radioligand competition experiments. The porphyrin-piperazine intermediate **8** was also appraised in order to check if the potential affinity is due to interaction of the receptors with the TPP or the piperazine moieties. As depicted in table 1, the new conjugate did not retain the affinity of its chromenopyrazole precursor **2.1**. Compound **10** did not bind to CB_1 receptors but displayed moderate affinity towards CB_2 in the micromolar range. The TPP intermediate did not show binding affinity for these targets.

Table 1. Binding affinity of the porphyrin-chromenopyrazoledione conjugate **10**, the porphyrin intermediate **8** and the reference cannabinoid WIN55,212-2 for *h*CB_1 and *h*CB_2 cannabinoid receptors.

Compd	CB_1 K_i (μM)[a]	CB_2 K_i (μM)[a]
2.1	0.32 ± 0.23	0.13 ± 0.02
8	> 40	> 40
10	> 40	13.79 ± 0.20
WIN55,212-2	0.04 ± 0.08	0.003 ± 0.002

[a]Values obtained from competition curves using [^{3}H]CP55940 as radioligand for *h*CB_1 and *h*CB_2 cannabinoid receptors and are expressed as the mean ± SEM of at least three experiments.

The tetraphenylporphyrin macrocycle may difficult the entrance of the molecule in the receptor and therefore, its binding to CB_1 or CB_2 receptors. The synthesized conjugate is probably too bulky to fit into the binding site. Likewise, the physicochemical properties of the conjugate have been completely modified compared to the chromenopyrazoldione contributing to the drastic loss of affinity.

Conclusions and future perspectives

With the purpose of developing an improved antitumor agent, chromenopyrazoledione **2.1** was conjugated to a tetraphenylporphyrin derivative. This macrocycle may confer to our cannabinoid a more specific tumor tissue delivery and may enable the development of target-selective phototherapy approaches.

The novel conjugate **10** binds moderately but selectively to CB_2R. Further antiproliferative experiments will be performed on tumor cell lines to appraise its antitumor capacity. Photophysicochemical properties of the new chromenopyrazoledione conjugate **10** are consistent with those of well-known porphyrins and therefore, completely appropriate for the development of near-infrared photosensitizers. In view of that, antiproliferative experiments will be also performed under light exposure conditions regarding the possibility of combining antitumor cannabinoid effects with PDT. Another aspect that needs to be taking into account is the metabolism process of this porphyrin-chromenopyrazoledione. Therefore, metabolism assays will be carried out to check if the conjugate is stable under physiological conditions or if it acts as a prodrug.

The results presented in this appendix are very preliminary, for that reason, optimization of the ligand, the linker, and the macrocycle will be further explored.

References

(1) Benov, L. Photodynamic Therapy: Current Status and Future Directions. *Med. Princ. Pract.* **2015**, *24*, 14–28.

(2) Allison, R. R.; Moghissi, K. Oncologic Photodynamic Therapy: Clinical Strategies That Modulate Mechanisms of Action. *Photodiagnosis Photodyn. Ther.* **2013**, *10*, 331–341.

(3) Agostinis, P.; Berg, K.; Cengel, K. a; Foster, T. H.; Girotti, a W.; Gollnick, S. O.; Hahn, S. M.; Hamblin, M. R.; Juzeniene, A.; Kessel, D.; Koberlik, M.; Moan, J.; Mroz, P.; Nowis, D.; Piette, J.; Wilson, B.; Golab, J. Photodynamic Therapy of Cancer: An Update. *CA Cancer J Clin* **2011**, *61*, 250–281.

(4) Kushibiki, T.; Hirasawa, T.; Okawa, S.; Ishihara, M. Responses of Cancer Cells Induced by Photodynamic Therapy. *J. Healthc. Eng.* **2013**, *4*, 87–108.

(5) Skupin-Mrugalska, P.; Sobotta, L.; Kucinska, M.; Murias, M.; Mielcarek, J.; Duzgunes, N. Cellular Changes, Molecular Pathways and the Immune System Following Photodynamic Treatment. *Curr. Med. Chem.* **2014**, *21*, 4059–4073.

(6) Castano, A. P.; Demidova, T. N.; Hamblin, M. R. Mechanisms in Photodynamic Therapy: Part One - Photosensitizers, Photochemistry and Cellular Localization. *Photodiagnosis Photodyn. Ther.* **2004**, *1*, 279–293.

(7) De Rosa, F. S.; Bentley, M. V. Photodynamic Therapy of Skin Cancers: Sensitizers, Clinical Studies and Future Directives. *Pharm. Res.* **2000**, *17*, 1447–1455.

(8) Dougherty, T. J.; Gomer, C. J.; Henderson, B. W.; Jori, G.; Kessel, D.; Korbelik, M.; Moan, J.; Peng, Q. Photodynamic Therapy. *J. Natl. Cancer Inst.* **1998**, *90*, 889–905.

(9) Dougherty, T. J.; Potter, W. R.; Weishaupt, K. R. The Structure of the Active Component of Hematoporphyrin Derivative. *Prog. Clin. Biol. Res.* **1984**, *170*, 301–314.

(10) Dougherty, T. J. Hematoporphyrin as a Photosensitizer of Tumors. *Photochem. Photobiol.* **1983**, *38*, 377–379.

(11) Triesscheijn, M.; Baas, P.; Schellens, J. H. M.; Stewart, F. a. Photodynamic Therapy in Oncology. *Oncologist* **2006**, *11*, 1034–1044.

(12) Tong, R.; Kohane, D. S. Shedding Light on Nanomedicine. *Wiley Interdiscip. Rev. Nanomed. Nanobiotechnol.* **2012**, *4*, 638–662.

(13) Schmitt, F.; Juillerat-Jeanneret, L. Drug Targeting Strategies for Photodynamic Therapy. *Anticancer. Agents Med. Chem.* **2012**, *12*, 500–525.

(14) Lin, L.; Xiong, L.; Wen, Y.; Lei, S.; Deng, X.; Liu, Z.; Chen, W.; Miao, X. Active Targeting of Nano-Photosensitizer Delivery Systems for Photodynamic Therapy of Cancer Stem Cells. *J. Biomed. Nanotechnol.* **2015**, *11*, 531–554.

(15) Lucky, S. S.; Soo, K. C. Nanoparticles in Photodynamic Therapy. *Chem. Rev.* **2015**, *115*, 1990–2042.

(16) Savarimuthu, W. P.; Gananathan, P.; Rao, A. P.; Manickam, E.; Singaravelu, G. Protoporphyrin IX-Gold Nanoparticle Conjugates for Targeted Photodynamic Therapy–An <I>In-Vitro</I> Study. *J. Nanosci. Nanotechnol.* **2015**, *15*, 5577–5584.

(17) Weijer, R.; Broekgaarden, M.; Kos, M.; Vught, R. Van; Rauws, E. a. J.; Breukink, E.; Gulik, T. M. va.; Storm, G.; Heger, M. Enhancing Photodynamic Therapy of Refractory Solid Cancers: Combining Second-Generation Photosensitizers with Multi-Targeted Liposomal Delivery. *J. Photochem. Photobiol. C Photochem. Rev.* **2015**, *23*, 103–131.

(18) Saboktakin, M. R.; Tabatabaee, R. M. The Novel Polymeric Systems for Photodynamic Therapy Technique. *Int. J. Biol. Macromol.* **2014**, *65*, 398–414.

(19) Rogers, L.; Senge, M. O. The Translocator Protein as a Potential Molecular Target for Improved Treatment Efficacy in Photodynamic Therapy. *Future Med. Chem.* **2014**, *6*, 775–792.

(20) Titov, D. V; Gening, M. L.; Tsvetkov, Y. E.; Nifantiev, N. E. Glycoconjugates of Porphyrins with Carbohydrates: Methods of Synthesis and Biological Activity. *Russ. Chem. Rev.* **2014**, *83*, 523–554.

(21) Pereira, P. M. R.; Korsak, B.; Sarmento, B.; Schneider, R. J.; Fernandes, R.; Tomé, J. P. C. Antibodies Armed with Photosensitizers: From Chemical Synthesis to Photobiological Applications. *Org. Biomol. Chem.* **2015**, *13*, 2518–2529.

(22) Králová, J.; Kejík, Z.; Bříza, T.; Poučková, P.; Král, A.; Martásek, P.; Král, V. Porphyrin - Cyclodextrin Conjugates as a Nanosystem for Versatile Drug Delivery and Multimodal Cancer Therapy. *J. Med. Chem.* **2010**, *53*, 128–138.

(23) Lamberti, M. J. Breast Cancer as Photodynamic Therapy Target: Enhanced Therapeutic Efficiency by Overview of Tumor Complexity. *World J. Clin. Oncol.* **2014**, *5*, 901.

(24) Rogers, L.; Sergeeva, N. N.; Paszko, E.; Vaz, G. M. F.; Senge, M. O. Lead Structures for Applications in Photodynamic Therapy. 6. Temoporfin Anti-Inflammatory Conjugates to Target the Tumor Microenvironment for In Vitro PDT. *PLoS One* **2015**, *10*, e0125372.

(25) Tomanová, P.; Rimpelová, S.; Jurášek, M.; Buděšínský, M.; Vejvodová, L.; Ruml, T.; Kmoníčková, E.; Drašar, P. B. Trilobolide–porphyrin Conjugates: On Synthesis and Biological Effects Evaluation. *Steroids* **2015**, *97*, 8–12.

(26) Trivedi, E. R.; Blumenfeld, C. M.; Wielgos, T.; Pokropinski, S.; Dande, P.; Hai, T. T.; Barrett, A. G. M.; Hoffman, B. M. Multi-Gram Synthesis of a Porphyrazine Platform for Cellular Translocation, Conjugation to Doxorubicin, and Cellular Uptake. *Tetrahedron Lett.* **2012**, *53*, 5475–5478.

(27) Morales, P.; Blasco-Benito, S.; Andradas, C.; Gómez-Cañas, M.; Flores, J. M.; Goya, P.; Fernández-Ruiz, J.; Sánchez, C.; Jagerovic, N. A Selective, Non-Toxic CB2 Cannabinoid O-Quinone with in Vivo Activity against Triple Negative Breast Cancer. *J. Med. Chem.* **2015**.

(28) Morales, P.; Vara, D.; Goméz-Cañas, M.; Zúñiga, M. C.; Olea-Azar, C.; Goya, P.; Fernández-Ruiz, J.; Díaz-Laviada, I.; Jagerovic, N. Synthetic Cannabinoid Quinones: Preparation, in Vitro Antiproliferative Effects and in Vivo Prostate Antitumor Activity. *Eur. J. Med. Chem.* **2013**, *70*, 111–119.

(29) Bai, M.; Sexton, M.; Stella, N.; Bornhop, D. J. MBC94, a Conjugable Ligand for Cannabinoid CB 2 Receptor Imaging. *Bioconjug. Chem.* **2008**, *19*, 988–992.

(30) Jia, N.; Zhang, S.; Shao, P.; Bagia, C.; Janjic, J. M.; Ding, Y.; Bai, M. Cannabinoid CB2 Receptor as a New Phototherapy Target for the Inhibition of Tumor Growth. *Mol. Pharm.* **2014**, *11*, 1919–1929.

(31) Zhang, S.; Jia, N.; Shao, P.; Tong, Q.; Xie, X.-Q.; Bai, M. Target-Selective Phototherapy Using a Ligand-Based Photosensitizer for Type 2 Cannabinoid Receptor. *Chem. Biol.* **2014**, *21*, 338–344.

(32) Ormond, A. B.; Freeman, H. S. Dye Sensitizers for Photodynamic Therapy. *Materials (Basel).* **2013**, *6*, 817–840.

(33) Luguya, R.; Jaquinod, L.; Fronczek, F. R.; Vicente, M. G. H.; Smith, K. M. Synthesis and Reactions of Meso-(p-Nitrophenyl)porphyrins. *Tetrahedron* **2004**, *60*, 2757–2763.

(34) Sibrian-Vazquez, M.; Jensen, T. J.; Hammer, R. P.; Vicente, M. G. H. Peptide-Mediated Cell Transport of Water Soluble Porphyrin Conjugates. *J. Med. Chem.* **2006**, *49*, 1364–1372.

(35) Gaware, V. S.; Håkerud, M.; Leósson, K.; Jónsdóttir, S.; Høgset, A.; Berg, K.; Másson, M. Tetraphenylporphyrin Tethered Chitosan Based Carriers for Photochemical Transfection. *J. Med. Chem.* **2013**, *56*, 807–819.

(36) Button, W. G.; Judson, P. N.; Long, A.; Vessey, J. D. Using Absolute and Relative Reasoning in the Prediction of the Potential Metabolism of Xenobiotics. *J. Chem. Inf. Comput. Sci.* **2003**, *43*, 1371–1377.

(37) Matthews, S. E.; Pouton, C. W.; Threadgill, M. D. Monofunctional Electrophilic and Nucleophilic Derivatives of Rneso-Tetraphenylporphyrin for Attachment to Peptides. *J Chem Soc Chem Commun* **1995**, 1809–1811.

Appendix 3

Publications and Patents arising from this Dissertation

List of publications and patents

The present doctoral dissertation is based on the following original publications and patents:

Peer reviewed publications

- Morales, P.; Gómez-Cañas, M.; Navarro, G.; Lagartera, L.; Hurst, D. P.; Pazos, R.; Goya, P.; Reggio, H. P.; Franco, R.; Fernández-Ruiz, J.; Jagerovic, N. Chromenopyrazole as Versatile Cannabinoid Scaffold: from CB_1 towards CB_2 Selectivity. *Under preparation*

- Morales, P.; Whyte, L.; Chicharro, R.; Gómez-Cañas, M.; Pazos, R.; Goya, P.; Irving, A.; Fernández-Ruiz, J.; Ross, R. A.; Jagerovic, N. Identification of novel GPR55 modulators using cell-impedance-based label-free technology. *J. Med. Chem. (accepted under major revision).*

- Morales, P.; Blasco-Benito, S.; Andradas, C.; Gómez-Cañas, M.; Goya, P.; Fernández-Ruiz, J.; Sanchez, C.; Jagerovic, N. Selective, non-toxic CB_2 cannabinoid o-quinones with in vivo activity against triple negative breast cancer. *J. Med. Chem.* **2015**, *58*, 2256-2264.

- Morales, P.; Azofra, L. M.; Cumella, J.; Hernandez-Folgado, L.; Roldán, M.; Alkorta, I.; Jagerovic, N. Preparation of 2,2-dimethylchroman-4-ones from 5-alkyl-substituted resorcinols: microwave-assisted synthesis and theoretical calculations. *Arkivoc* **2014**, ii, 319-322.

- **Morales, P.**; Vara, D.; Gómez-Cañas, M.; Zúñiga, M. C.; Olea-Azar, C.; Goya, P.; Fernández-Ruiz, J.; Diaz-Laviada, I.; Jagerovic, N. Synthetic cannabinoid quinones: Preparation, in vitro antiproliferative effects and *in vivo* prostate antitumor activity. *Eu. J. Med. Chem.* **2013**, 70, 111-119.

- Cumella, J.; Hernández-Folgado, L.; Giron, R.; Sánchez, E.; **Morales, P.**; Hurst, D. W.; Gómez-Cañas, M.; Gómez-Ruiz, M.; Goya, P.; Reggio, P. H.; Martin, M. I.; Fernández-Ruiz, J.; Silva, A. M. S.; Jagerovic, N. Chromenopyrazoles: non-psychoactive and selective CB_1 cannabinoid agonist with peripheral antinociceptive properties. *ChemMedChem*, **2012**, 7, 452-463.

- Hernandez-Folgado, L.; Cumella, J. M.; **Morales, P**.; Alkorta, I.; Elguero,J.; Jagerovic, N. Tautomerism of hydroxychromenopyrazoles. *Journal of Molecular Structure,* **2012**, 1015, 162-165.

Patents

- Patent: **ES P201530608.** Selective modulators of GPR55 activity: Chromenopyrazole derivatives.
Priority Date: 05-05-2015
Inventor Name(s): Jagerovic, N.; **Morales, P**.; Ross, R.; Whyte, L
Patent Assignee Name(s) and Code(s): CSIC; University of Toronto.

- Patent: **PCT/ES2015/070184**; **ES P201430372.** Nuevas cromenoquinonas moduladoras de receptores cannabinoides CB_2 con actividad antitumoral.
Priority Date: 03-18-2014

Inventor Name(s): Jagerovic, N.; **Morales, P**.; Goya, P.; Blasco-Benito, S.; Sánchez, C.; Gómez-Cañas, M; Fernández-Ruiz, J.
Patent Assignee Name(s) and Code(s): CSIC; Universidad Complutense de Madrid.

- Patent: **WO2014013117**; **ES P201231126**; **PCT/ES2013/070499**. Chromenopyrazolediones as cannabinoid-quinone derivatives having antitumor activity.
Publication Date: 01-23-2014; Priority Date: 07-18-2012
Inventor Name(s): Jagerovic, N.; **Morales, P**.; Goya, P.; Diaz-Laviada, I.; Vara, D.; Fernández-Ruiz, J.; Gómez-Ruiz, M.; Gómez-Cañas M.
Patent Assignee Name(s) and Code(s): CSIC; Universidad de Alcalá; Universidad Complutense de Madrid.

Participation of the opponent in the following publications:

- Ragusa, G.;* Gómez-Cañas, M.;* **Morales, P**.;* Hurst, D. P.; Deligia, F.; Pinna, G.; Fernández-Ruiz, J.; Goya, P.; Reggio, P.; Jagerovic, N. ; García-Arencibia, M.; Murineddu, G. Synthesis, pharmacological evaluation and docking studies of pyrrole structure-based CB_2 receptor antagonists. *Eu. J. Med. Chem.* **2015**, *101*, 651-667. *These three authors share the first position within the authorship.

- Fernández-Fernández, C.; Callado L. F.; Girón, R.; Sánchez, E.; Erdozain, A. M.; **Morales, P**.; López-Moreno, J. A.; Rodríguez de Fonseca, F.; Fernández-Ruiz, J.; Goya, P.; Meana, J. J.; Martín, M. I.; Jagerovic, N. Combining Rimonabant and Fentanyl Pharmacophores as Cannabinoid/Opioid Ligands: Synthesis, in vitro and in vivo Evaluation. *Drug Des. Devel. Ther.* **2014***, 8*, 263-277.

- Fernández-Fernández, C.; Decara, J.; Bermúdez-Silva, F. J.; Sánchez, E.; **Morales, P.;** Gómez-Cañas, M.; Gómez-Ruiz, M.; Callado, L. F.; Goya, P.; Rodríguez de Fonseca, F.; Martín, M. I.; Fernández-Ruíz, J.; Meana, J. J.; Jagerovic, N. Description of a Bivalent Cannabinoid Ligand with Hypophagic Properties *Arch. Pharm. Chem. Life Sci.* **2013**, 346, 171-179.

- Vanthuyne, N.; Roussel, C.; Naubron, J.; Jagerovic, N.; **Morales-Lázaro, P**.; Alkorta, I.; Elguero, J. Determination of the absolute configuration of 1,3,5-triphenyl-4,5-dihydropyrazole enantiomers by a combination of VCD, ECD measurements, and theoretical calculations. *Tetrahedron: Asymmetry*, **2011**, 22, 1120-1124.